# Utilising Yeast as a Model Organism to Deconstruct the Regulation of Tumour Associated Lipogenesis

By

**Kerry Ann Rostron Bsc (Hons), MSc**

A thesis submitted in partial fulfilment of the requirements for the degree of:

**Doctor of Philosophy (PhD)**

University of Central Lancashire

May 2015

# Student declaration form

**Concurrent registration for two or more academic awards**

*I declare that while registered as a candidate for the research degree, I have not been a registered candidate or enrolled student for another award of the University or other academic or professional institution.

**Material submitted for another award**

*I declare that no material contained in the thesis has been used in any other submission for an academic award and is solely my own work

**Collaboration**

Where a candidate's research programme is part of a collaboration project, the thesis must indicate in addition clearly the candidate's individual contribution and the extent of the collaboration. Please state below: N/A.

**Signature of candidate**_____

**Type of award: Doctor of Philosophy (PhD)**

**School: Pharmacy and Biomedical Sciences.**

*For Jay Lynchehaun and Inbetweenears*

# Abstract

It is important for cells to respond to external signals. Central to these responses are the sensing and signalling pathways that communicate with the nucleus and facilitate necessary changes in gene expression. Of particular importance are the mitogen-activated protein kinase (MAPK) and the mammalian target of rapamycin (mTOR) pathways. Both of these pathways have been shown to be involved in cell growth, proliferation, motility and survival. They are under intensive investigation in connection with cancer with recent evidence suggests their role in mediating lipogenesis. Lipogenesis accompanies a variety of disease states, including the formation of brain tumours. Malignant brain tumours are rapidly growing and often invade surrounding healthy tissue, resulting in poor prognosis for the patient. The ability to limit tumour growth and reduce invasion through a better understanding of tumour associated lipid formation may offer targets for the development of new therapies.

Yeast is frequently used as a paradimic organism for the study of human diseases. In this study a Nile red assay has been developed, optimised and validated to measure levels of both polar and neutral lipids within yeast cells. This method has been utilised in the yeast species, *Saccharomyces cerevisiae* and *Schizosaccharomyces pombe*, to study the role of the MAPK pathways in regulating lipid accumulation. Data in this thesis demonstrates that stress-activated protein kinase pathways (SAPK) play a key role in regulating lipid accumulation upon nitrogen limitation, as cells enter the stationary phase of growth. Evidence from *S. cerevisiae* proposes that the lipogenic switch occurs in two phases, with the central MAPK (Hog1) activated in both a MAPKK (Pbs2) independent and dependent manner. Analysis of Hog1 phosphorylation during various growth phases, suggests that there are previously uncharacterised sites on Hog1 which are potentially phosphorylated during phase one by the protein kinase Sch9, a target of the Tor1 complex. The second phase results in Hog1 being dually phosphorylated by the canonical pathway, via Pbs2p. It is proposed that Hog1 may have a number of downstream cytoplasmic and nuclear targets, including lipid related enzymes (Dga1) and transcription factors (Msn2/4). Data also suggests that lipid accumulation in *S. pombe* is also regulated in a similar manner.

The oleaginous yeast *Lipomyces starkeyi* is able to accumulate high levels of lipid and has similarity to lipid enzymes found in mammalian cells. As such, it was proposed that *L. starkeyi* may be utilised as a model organism to further characterise the role of MAPK in lipid accumulation. Information from stress response studies and bioinformatics suggests the MAPK pathway in *L. starkeyi* is highly conserved. However, the application of yeast molecular tools to *L. starkeyi* was unsuccessful, demonstrating that further work is required to develop its use as a model organism.

Data in this thesis has shown a novel role for the SAPK pathways in regulating lipid accumulation in yeast. It has also demonstrated cross talk between the MAPK and TOR pathways, resulting in an integrated cellular response. The high level of conservation of these pathways across species, suggests that directly targeting these pathways in cancer cells may reduce tumour associated lipogenesis, therefore inhibiting growth of glioma. With current treatments only delivering limited results, this could help extend patient survival.

# Contents

# List of Figures

# List of Tables

## Acknowledgements

I would like to take this opportunity to thank all that have provided me with the support needed allowing me to complete this project.

Firstly I would like to thank my supervisor, Dr. Clare Lawrence, for giving me the opportunity to work on such an interesting and challenging project. Your help, support, guidance and above all patience, over the last 3 years have not only helped me to grow as a research scientist, but also as an individual. Thank you for making me realise with most issues I have encountered that, "in the grand scheme of things" it didn't really matter.

I would also like to thank my second supervisor, Dr. Carole Rolph, for feedback and assistance with lipid related aspects of the project.

Further thanks go to Christine Hughes (micro-mummy) for taking me under her wing on the 3rd floor when I first started. I would also like to thank the science family, Tony Dickson, Gill Ward, Chrissy Woodcock, Steve Kirby and Carly Chandler for technical support and much needed humour at times.

Thank you to Dr. Vicky Jones and Dr. Gail Welsby for help and support with microscopy, and also to Dr. Christopher Smith for support with statistical analysis.

To Charlotte Tumilson, my best friend and partner in crime, it has been a pleasure riding the PhD rollercoaster with you. Thank you to Aaron Tetley for his continuous support and reassurance that "everything will be ok". I would also like to thank Karl Norris for his IT assistance and invaluable help with figure making.

Finally I extend special thanks to my friends and family, especially my parents, for their continual support, encouragement and advice, without which I undoubtedly would not have been able to reach where I am today.

## Abbreviations

| | |
|---|---|
| 4E-BPs | 4E-binding proteins |
| 5-FOA | 5-Fluoroorotic Acid |
| Abs | Absorbance |
| ACAT | Acyl-Coenzyme A: cholesterol acyltransferase |
| ACC | Acetyl-coenzyme A carboxylase |
| AcCoA | Acetyl Coenzyme A |
| AceAcCoA | Acetacetyl Coenzyme A |
| Akt | Protein kinase B |
| AMPK | Adenosine monophosphate-activated protein kinase |
| AMPKK | Adenosine monophosphate-activated protein kinase kinase |
| ANOVA | Analysis of variance |
| Atf1 | Activating transcription factor 1 |
| ATF-2 | Activating transcription factor 2 |
| ATP | Adenosine triphosphate |
| Bcl-2 | B-cell lymphoma 2 |
| BODIPY | Boron-dipyrromethene |
| cDNA | Complementary deoxyribonucleic acid |
| CDP-choline | Cytadine diphosphate-choline |
| CDP-DAG | Cytidine diphosphate-diacylglycerol |
| CDP-ethanolamine | Cytadine diphosphate-ethanolamine |
| ChIP | Chromatin immunoprecipitation |
| CLM | Carbon limiting media |
| *CLN1* | Ceroid lipofuscinosis-1 |
| CNS | Central nervous system |
| CREB | Cyclic adenosine monophosphate response element binding protein |
| CTP | Cytadine triphosphate |
| DAG | 1,2 diacylglycerol |
| Deptor | DEP domain-containing mTOR-interacting protein |
| DGA1 | Diacylglycerol acyltransferase |
| DGAT | 1,2 diacylglycerol acyltransferase |
| DMSO | Dimethyl Sulfoxide |

| | |
|---|---|
| DNA | Deoxyribonucleic acid |
| dNTPs | Deoxyribonucleotide triphosphates |
| DOE | Department of energy |
| EBI | European Bioinformatics Institute |
| ECL | Enhanced chemiluminescence |
| EDTA | Ethylenediaminetetraacetic acid |
| EGF | Epidermal growth factor |
| EGFR | Epidermal growth factor receptor |
| EGFRvIII | Epidermal growth factor receptor variant III |
| ELK-1 | ETS domain-containing protein |
| EMM | Edinburgh minimal medium |
| ER | Endoplasmic reticulum |
| ERK | Extracellular signal-regulated kinase |
| EtOH | Ethanol |
| Euroscarf | European *Saccharomyces cerevisiae* Archive for Functional Analysis |
| $FADH_2$ | Flavin adenine dinucleotide |
| FAMES | Fatty acid methyl esters |
| FAs | Fatty acids |
| FAS | Fatty acid synthase |
| FASN | Fatty acid synthase N |
| FBase | Fructose 1,6-biphosphatase |
| FK506 | FK506 binding protein |
| FKBP12 | Immunophilin, FK506 binding protein |
| FRB | FKBP12-rapamycin-binding domain |
| G3P | Glycerol-3-phosphate |
| GBM | Glioblastoma multiforme |
| GC | Gas chromatography |
| GC-MS | Gas chromatography-mass spectrometry |
| GDP | Guanine diphosphate |
| GFP | Green fluorescent protein |
| GLUT-1 | Glucose transporter 1 |
| GPAT | Glycerol-3-phosphate-acyltransferase |
| GPLs | Glycerophospholipids |

| | |
|---|---|
| Grb2 | Growth factor receptor bound protein-2 |
| GTP | Guanine triphosphate |
| HIF1-α | Hypoxia-inducible factor 1-alpha |
| HOG | High osmolarity glycerol |
| JGI | Joint genome institute |
| JNK | c-Jun $NH_2$-terminal kinase |
| *L. starkeyi* | *Lipomyces starkeyi* |
| LBK1 | Liver kinase B1 |
| LCAT | Lecithin:cholesterol acyltransferase |
| LC-MS | Liquid chromatography-mass spectrometry |
| LDA | Lactate dehydrogenase-A |
| LDs | Lipid droplets |
| LiAc | Lithium acetate |
| LPA | Lysophosphatidic acid |
| LRO1 | Phospholipid diacylglycerol acyltransferase |
| Mal CoA | Malonyl Coenzyme A |
| MAPK | Mitogen-activated protein kinase |
| MAPKK/MAP2K/MEK | Mitogen-activated protein kinase kinase |
| MAPKKK/MAP3K/MEKK | Mitogen-activated protein kinase kinase kinase |
| MAPKKKK | Mitogen-activated protein kinase kinase kinase kinase |
| MKK3 | Mitogen-activated protein kinase kinase 3 |
| MKK4 | Mitogen-activated protein kinase kinase 4 |
| MKK6 | Mitogen-activated protein kinase kinase 6 |
| MKK7 | Mitogen-activated protein kinase kinase 7 |
| mLST8 | Mammalian lethal with SEC13 protein 8 |
| MNK | Mitogen activated protein kinase interacting kinase |
| mRNA | Messenger ribonucleic acid |
| MS | Mass spectrometry |
| MSA | Multiple sequence alignment |
| MSKs | Mitogen and stress activated protein kinases |
| Msn2 | Multicopy suppressors of the snf1 defect 2 |
| Msn4 | Multicopy suppressors of the snf1 defect 4 |
| mTOR | Mammalian target of rapamycin |
| mTORC1 | Mammalian target of rapamycin complex 1 |

| | |
|---|---|
| mTORC2 | Mammalian target of rapamycin complex 2 |
| *MUC-1* | *Mucin 1* |
| Myc | c-Myc transcription factor |
| NADH | Nicotinamide adenine dinucleotide |
| NADPH | Nicotinamide adenine dinucleotide phosphate |
| NaOH | Sodium hydroxide |
| NF-$_{\kappa}$B | Nuclear factor kappa-light-chain-enhancer of activated B cells |
| Nile red | 9-diethylamino-5H-benzo[a]phenoxazine-5-one |
| NLM | Nitrogen limiting media |
| OD | Optical density |
| ORF | Open reading frame |
| OXPHOS | Oxidative phosphorylation |
| PA | Phosphatidic acid |
| PAK | p21 activated kinases |
| PAPs | Phosphatidic acid phosphorylases |
| PBS | Phosphate buffered saline |
| PC | Phosphatidylcholine |
| PCR | Polymerase chain reaction |
| PDK1 | Phosphoinositide-dependent kinase-1 |
| PDME | Phosphatidyldimethylethanolamine |
| PDS | Post-diauxic shift |
| PE | Phosphatidylethanolamine |
| PEG | Polyethylene glycol |
| PET | Positron emission topography |
| PHAs | Polyhydroxyalkanoates |
| PI | Phosphatidylinositol |
| PI3K | Phosphoinositide 3-kinase |
| PIP2 | Phosphatidylinositol 4,5-biphosphate |
| PIP3 | Phosphatidylinositol (3,4,5)-triphosphate |
| PIPs | Phosphatidylinositol phosphates |
| PKCα | Protein kinase Cα |
| PKM2 | Pyruvate kinase M2 isoform |
| PL | Phospholipid |
| PMME | Phosphatidylmonomethylethanolamine |

| | |
|---|---|
| Protor-1 | Protein observed with Rictor-1 |
| PS | Phosphatidylserine |
| PSS1 | Phosphatidylserine synthase 1 |
| PSS2 | Phosphatidylserine synthase 2 |
| PTEN | Phosphatase and tensin homolog |
| PVDF | Polyvinylidine fluoride |
| RFU | Relative fluorescence unit |
| Rictor | Rapamycin-insensitive companion of mTOR |
| RNA | Ribonucleic acid |
| ROS | Reactive oxygen species |
| Rpm | Revolutions per minute |
| *S. cerevisiae* | *Saccharomyces cerevisiae* |
| *S. pombe* | *Schizosaccharomyces pombe* |
| S6Ks | S6 kinases |
| SAPK | Stress-activated protein kinase |
| SCAP | Sterol regulatory element binding protein cleavage activating protein |
| SD | Standard deviation |
| SDS | Sodium dodecyl sulphate |
| SDS-PAGE | Sodium dodecyl sulphate polyacrylamide electrophoresis |
| Ser | Serine |
| SEs | Sterol esters |
| SGK1 | Serum and glucocorticoid-induced protein kinase 1 |
| SILAC | Stable isotope labelling by amino acids in cell culture |
| Sin1 | SAPK-interacting protein 1 |
| SLs | Sphingolipids |
| SOS | Son of Sevenless |
| *SREBF1* | *Sterol regulatory element binding transcription factor 1* |
| *SREBF2* | *Sterol regulatory element binding transcription factor 2* |
| SREBP-1 | Sterol regulatory element-binding protein 1 |
| SREBPs | Sterol regulatory element binding proteins |
| SRM-MS | Selective reaction monitoring mass spectrometry |
| STAT1 | Signal transducer and activator of transcription 1 |
| STAT3 | Signal transducer and activator of transcription 3 |

| | |
|---|---|
| STRE | Stress response elements |
| TAGs | Triacylglycerol's |
| TBST | Tris buffered saline tween |
| TCA | Tricarboxylic acid |
| TFs | Transcription factors |
| TGX | Tris-glycine eXtended |
| Thr | Threonine |
| TLC | Thin layer chromatography |
| TOR | Target of rapamycin |
| TORC1 | Target of rapamycin complex 1 |
| TORC2 | Target of rapamycin complex 2 |
| Tris-HCl | Tris-hydrachloride |
| TSC2 | Tuberous sclerosis complex 2 |
| Tyr | Tyrosine |
| URA | Uracil |
| VLCFA | Very long chain fatty acids |
| WEs | Wax esters |
| WHO | World Health Organisation |
| *Y. lipolytica* | *Yarrowia lipolytica* |
| YES | Yeast extract sucrose |
| YNB | Yeast nitrogen base |
| YPD | Yeast extract peptone dextrose |

# Chapter I Introduction

# 1. Introduction

## 1.1 Cancer – The problem and ultimate aims

Cancer is, at a functional level, both a genomic and proteomic disease (Wulfkuhle *et al.* 2004) that is vastly complex and heterogeneous (Roukos 2011). Cancer is one of the major causes of death worldwide with predictions, that by 2030, approximately 26 million new cases of cancer will be diagnosed resulting in an estimated 17 million deaths per year (Thun *et al.* 2010). Alterations occurring in cellular DNA, which may lead to cancer, can result from a combination of many factors including immune responses to infectious agents (Karin *et al.* 2006), environmental factors such as poor diet, smoking as well as exposure to pollution (Colditz 2009) and indeed genetic factors.

Modifications in the DNA may be present as amplifications, deletions, insertions, rearrangements, translocations and epigenetic changes. These changes have the potential to disrupt normal functioning of proto-oncogenes, tumour suppressor genes and cellular communications which may contribute to the conversion of non-cancerous cells into those that are proliferative and cancerous in nature, thus forming tumours (Martinkova *et al.* 2009).

Although uncontrolled proliferation leading to tumourigenesis has been known for many decades, the biological mechanisms which underpinned the conversion of cells and progression of tumours remained largely unknown. Due to this surgery was often the only form of treatment until radiotherapy, which still could not combat metastatic cancer completely (Chabner and Roberts 2005).

Even centuries later with improved understanding of molecular cancer biology along with current cancer treatments including surgery, radiotherapy and chemotherapy complete success is limited. Relapse often occurs as a result of micrometatases of dormant tumour cells (Zitvogel *et al.* 2008) or resistance of cancer to drugs after a period of time. Along with this treatments are often not discriminative which may lead to a number of deleterious side effects for the patient (Feyer *et al.* 2008), with further problems arising in cases of cancer where tumours are difficult to treat or inoperable, such as with brain tumours (gliomas) (Jiang and Wang 2010).

For clinicians the ability to detect cancer type, identify treatments that will be beneficial to the patient and successfully predict disease outcome will help in tailoring patient treatment. This will help avoid unnecessary treatment and toxic side effects resulting from the aforementioned adjuvant therapies (Goodison *et al.* 2010). In order to avoid subjective, flawed prediction based on demographic data and unreliable clinical observations, the identification of individual novel molecular targets is ultimately required for precise assessment of effective treatment and improved clinical outcome (Weigelt *et al.* 2010). The importance of this is further increased as, although tumours from patient to patient may exhibit similar histology, they can encompass differing mutations and therefore different signalling behaviours, which in turn means potentially different responses to therapeutic intervention.

The aim, therefore, is to further improve understanding of the molecular basis of cancer, leading to treatment for patients on an individual level through the identification and analysis of novel molecular targets (Weigelt *et al.* 2010). The ultimate goal of anti-cancer therapy would be development of tailored therapeutic strategies targeted at specific types of cancers and tumours where the molecular profile has been defined. Such treatment will serve to reduce cancer-related mortality whilst conserving quality of life for patients and reducing costs by avoiding use of treatment plans with little or no efficacy (Goodison *et al.* 2010).

## 1.2 Glioma

Malignant gliomas are the most common form of primary central nervous system (CNS) neoplasm (Lim *et al.* 2011). Gliomas are a set of invasive, heterogeneous tumours which are derived from and display histological similarity to glial cells. They incorporate astrocytes, ependyma and oligodendrocytes (Lim *et al.* 2011, Wen and Kesari 2008) with gliomas being broadly classified based on which cell type they hold the closest resemblance. Of all the glioma subtypes, glioblastoma (also known as glioblastoma multiforme (GBM)), accounts for approximately 60-70% of malignancies. Astrocytomas account for 10-15%, oligodendrogliomas and oligoastrocytomas (mixed glioma) for 10%, with less prevalent tumours such as gangliogliomas and ependymomas accounting for the remainder (Louis *et al.* 2007). Although in absolute numbers the overall incidence of gliomas accounts for only a small proportion of total cancers diagnosed (fewer than 2% in England and Wales), it is important to note that a disproportionately high rate of morbidity and mortality is associated with glial tumours (Yoon *et al.* 2010).

### 1.2.1 Classification and Tumour types

The World Health Organisation (WHO) grading of CNS tumours establishes a malignancy scale which is based on the histological features of tumours ranging from grade I to IV. This grading is also utilised to predict neoplasm behaviour and it clinically influences the choice of therapy for the patient. See Table 1.1 for tumour types and classification.

**Table 1.1: Main tumour types and their sub-types with corresponding graded classifications based on histological features (WHO criteria).** Adapted from Louis *at al.* (2007).

| Tumour type | Grade I | Grade II | Grade III | Grade IV |
|---|---|---|---|---|
| **Astrocytomas** | | | | |
| Pilocytic | ✔ | | | |
| Diffuse | | ✔ | | |
| Anaplastic | | | ✔ | |
| Glioblastoma | | | | ✔ |
| **Oligodendrogliomas** | | | | |
| Oligodendroglioma | | ✔ | | |
| Anaplastic | | | ✔ | |
| **Mixed gliomas** | | | | |
| Oligoastrocytomas | | ✔ | | |
| Anaplastic Oligoastrocytoma | | | ✔ | |
| **Ependymoma** | | | | |
| Subependymoma | ✔ | | | |
| Ependymoma | | ✔ | | |
| Anaplastic | | | ✔ | |

Under this classification system, low grade tumours (I and II) are classified as benign and high grade tumours (III and IV) classified as malignant. WHO grade I lesions are characterised by low proliferative potential. Grade II lesions are usually infiltrating in spite of low levels of proliferation and often recur with some tumour types progressing to those of greater malignancy (Louis *et al.* 2007). Grade III lesions encompass histological evidence of malignancy, usually in the form of mitotic activity with infiltrative capability, nuclear atypica and anaplasia. Finally grade IV lesions are characterised as being mitotically active, prone to necrosis and are usually associated with a rapid pre and post-operative evolution of disease state (Louis *et al.* 2007).

#### 1.2.1.1 Astrocytic tumours

Tumours of astrocytic origin form the majority of gliomas in adults (Lim *et al.* 2011), however, pilocytic astrocytomas (WHO grade I) occur mainly in children or young adults but are slow growing and rarely fatal (Burger *et al.* 2000).

Diffuse astrocytomas are classified under the WHO system as grade II, they are well differentiated and, again, slow growing tumours (Lim *et al.* 2011). They are, however, infiltrative in nature with increased cellularity and cytological atypica (Louis *et al.* 2007). As a result they harbour the ability to recur after surgical resection and may transform to more malignant forms, WHO grade III and IV (Ohgaki and Kleihues 2009).

Anaplastic astrocytomas are grade III lesions that may arise *de novo* or from a diffuse astrocytoma (Kleihues *et al.* 2000b). They exhibit increased cellularity, distinct nuclear atypica and heightened mitotic activity in comparison to their diffuse counterparts (Louis *et al.* 2007) whilst also possessing an intrinsic tendency to develop into GBM.

#### 1.2.1.2 Glioblastoma multiforme (GBM)

GBM is the most common and malignant CNS neoplasm that most often develops *de novo* with no evidence of a less malignant precursor lesion (primary GBM), or less commonly from a diffuse or anaplastic astrocytoma (secondary GBM) (Kleihues *et al.* 2000a). GBM is highly malignant, highly proliferative and often results in fatality within 15 months of diagnosis (Lim *et al.* 2011). Although secondary GBM exhibits a better median survival it otherwise differs very little histologically from that of a primary malignancy, with the two forms often only distinguishable by differing genetic aberrations present (Ohgaki *et al.* 2004, Ohgaki and Kleihues 2007).

Characteristics of GBM include increased intratumoral heterogeneity, invasive pattern of growth, high mitotic activity and resistance to therapeutic intervention (Furnari *et al.* 2007, Holland 2000, Maher *et al.* 2001, Wen and Kesari 2008) with cells often being pleomorphic in nature and exhibiting nuclear aplasia (Louis *et al.* 2007). Also, widespread central necrosis is often observed with a “halo” of viable cells (pseudopalisading) (Lim *et al.* 2011, Louis *et al.* 2007, Wen and Kesari 2008). Along with this vascular thrombosis with microvascular proliferation may also be observed (Lacob and Dinca 2009) (Figure 1.1). This central necrosis observed in GBM is illustrative of the aggressiveness of the cancerous cells as they outgrow their blood supply (Lacob and Dinca 2009).

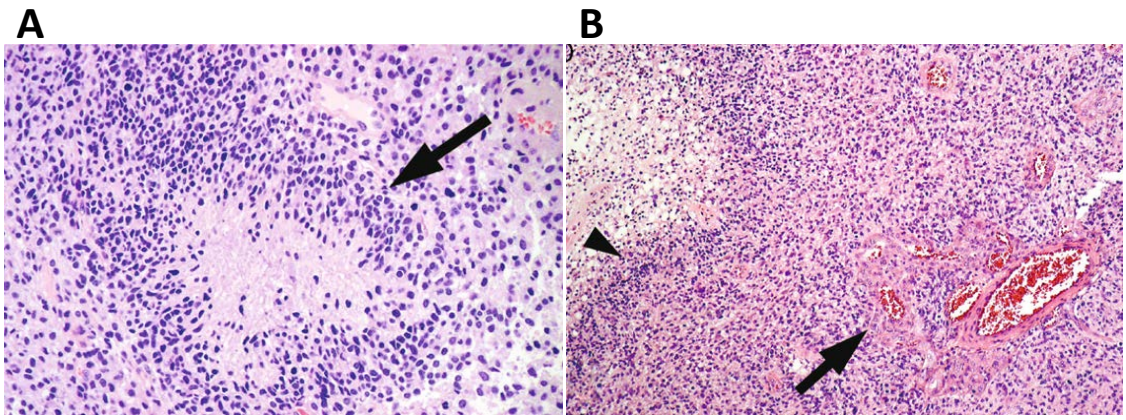


**Figure 1.1: Histological features of glioblastoma A:** Pseudopalisades are indicated by the black arrow and show tumour cells aggregating around a clear zone with some apoptotic cells. **B:** Low magnification image showing pseudopalisading (arrowhead). Microvascular hyperplasia, a form of angiogenesis induced by pseudopalisading hypoxic cells is shown by the black arrow. Taken from Rong *et al.* (2006).

### 1.2.1.3 Oligodendroglial tumours

Occurring less frequently and exhibiting a better prognosis than astrocytomas of similar grading, oligodendroglial grade II tumours are well differentiated, slow growing and diffusely infiltrating (Louis *et al.* 2007).

Accounting for 50% of oligodendroglial tumours, anaplastic subtypes are classified as grade III neoplasms, which in contrast to grade II tumours hold a less favourable prognosis. They possess characteristics similar to those of grade II tumours, but in addition often contain focal or diffuse features of malignancy (Louis *et al.* 2007) obvious microvascular proliferation and/or necrosis as well as marked mitotic activity (Engelhard *et al.* 2003). Both subtypes of oligodendroglial tumours may also be found to exhibit perinuclear halos along with a branching blood vessel network (Wen and Kesari 2008).

#### 1.2.1.4 Mixed gliomas - Oligoastrocytomas

Oligoastrocytomas are tumours which are composed of two distinct neoplastic cell types, which resemble cells found in both oligodendrogliomas and diffuse astrocytomas (Louis *et al.* 2007). WHO grade II oligoastrocytomas exhibit some cellularity and cytologic atypica with occasional mitotic figures.

In contrast, WHO grade III anaplastic oligoastrocytomas are poorly differentiated tumours with histological features of malignancy (Ohgaki and Kleihues 2009). Anaplastic tumours are characterised by the presence of pleomorphic cells, high cellularity and mitotic activity with nuclear atypica, necrotic sites and microvascular proliferation (Reifenberger *et al.* 2000).

#### 1.2.1.5 Ependymal Tumours

Ependymal tumours occur less frequently than astrocytomas and exhibit relatively better prognosis. Ependymomas are usually well delineated tumours, subependymoma (WHO grade I) lesions are slow growing neoplasms with good prognosis following surgical resection (Godfraind 2009).

WHO grade II lesions (ependymomas) are also slow growing tumours that have four histological variants; cellular, papillary, clear cell, and tanycytic ependymoma. Anaplastic ependymomas (WHO grade III) are characterised by accelerated growth, increased cellularity and mitotic activity and often exhibit signs of microvascular proliferation with pseudopalisading necrosis, all of which are exempt from grade II neoplasms in accordance with WHO classification guidelines (Godfraind 2009).

The WHO criteria as described above, however, are only one component of the array of criteria utilised to predict response to therapy and disease outcome. Other criteria that are required to make accurate assessments include: the age of the patient, location of the tumour, extent of surgical resection and genetic alterations present (Louis *et al.* 2007).

### 1.2.2 Diagnosis

Gliomas often produce no deleterious symptoms until the tumour reaches a certain mass. Clinical history is generally short in duration with symptoms developing abruptly due to increased intracranial pressure with infiltration of surrounding brain structures and compression (Lacob and Dinca 2009, Ohgaki and Kleihues 2009). Symptoms experienced are largely dependent on the location of the tumour and may include: headaches, seizures, sensory disturbance, personality changes and visual defects (Lacob and Dinca 2009).

Diagnosis of gliomas is achieved based upon findings of neuroradiological imaging, with Magnetic Resonance Imaging (MRI) with and without contrast being the current method of choice (Chishty *et al.* 2010). To assist diagnosis further positron emission topography (PET), which uses consumption of radioactively labelled glucose (Lacob and Dinca 2009), may be used to distinguish between low and high grade gliomas by assessing whether tumours are hypo or hyper-metabolic (Cavaliere *et al.* 2005). Nevertheless, the aforementioned tests are not utilised in place of histological analysis, and so a tissue sample obtained via stereotactic biopsy or from tissue removed during surgery is needed for definitive diagnosis.

### 1.2.3 Prognosis and treatment

As previously mentioned, WHO grade I lesions exhibit low proliferative potential and have a good possibility of cure following surgical resection without the need for adjuvant therapy, whereas grade II and III tumours often recur with the potential to develop into more malignant forms. The most malignant grade IV tumours hold poor prognosis for the patient with rapid reoccurrence, evolution of disease state and ultimately fatality (Louis *et al.* 2007). However, due to the heterogeneity of gliomas, prognosis is often made on a case by case basis relying on the age of the patient, location of the tumour, molecular profile and how amenable the neoplasm is to surgery and further adjuvant treatments if required (Wen and Kesari 2008).

The first step in the treatment of all glioma types is usually gross surgical resection (Welch and Lai 2009) followed by eradication of potential residual cancerous cells irremovable by surgery alone with six weeks of radiotherapy treatment concomitant with chemotherapy (Yoon *et al.* 2010). The most common form of chemotherapy administered is the oral

alkylating agent temozolomide (Lim *et al.* 2011) and following on from radiotherapy/chemotherapy an additional six monthly cycles of maintenance by treatment with temozolomide may be required (Stupp *et al.* 2005).

In spite of the fact that full treatment has the ability to increase significantly the 1-3 month median survival of even the most aggressive glioma forms, inevitably more needs to be done (Yoon *et al.* 2010). The inability to extend GBM patient survival beyond 12 months is due, primarily, to the non-specificity of both radiotherapy and chemotherapy coupled with intrinsic resistance of cancerous cells to treatment thus allowing the tumour to recur (Hou *et al.* 2006). Although treatment with radiotherapy and cytostatic drugs dominates first line adjuvant therapy for gliomas at present, targeted intervention is becoming increasingly investigated and trialled in an attempt to combat gliomas (Ohgaki and Kleihues 2009).

Due to the poor prognosis of patients diagnosed with malignant glioma, there is a requirement for improved treatment strategies. Understanding the molecular mechanisms underlying cancer would ultimately help with the development of new treatments. As previously mentioned signalling pathways are often de-regulated in cancer and, although some mechanisms of this deregulation are known, much is left to be elucidated.

## 1.3 Signal Transduction Pathways

It is fundamentally important that cells are able to detect and respond to external signals from the environment. Central to such responses are the sensing and signalling pathways that communicate with cytoplasmic and nuclear targets (Lawrence C.L. *et al.* 2007). Signal transduction pathways relay information via a variety of stimuli from the cells exterior through protein interactions and finally to transcription factors. These transcription factors then go on to regulate multiple cellular responses including the expression of genes (Bebek and Yang 2007).

Normal cellular responses and behaviour are controlled by a complex network of highly-regulated signalling pathways (Downward 2003); consequentially they have received vast attention as when this normal regulation is disrupted a range of disease phenotypes may result (Downward 2003, Wilkinson and Millar 2000).

Of key importance are the mitogen activated protein kinase (MAPK) and mammalian target of rapamycin (mTOR) signalling pathways, which are involved in cell growth, motility, proliferation and survival (Hsu *et al.* 2011, Ihermann-Hella *et al.* 2014). Misregulation of both pathways is currently under investigation in connection with initiation and progression of numerous cancers, including gliomas (Masui *et al.* 2011). Such deregulation can disrupt the activation and or deactivation of genes enabling cells to possess limitless replicative potential, as well as avoidance of cellular death mechanisms (Hanahan and Weinberg 2011).

### 1.3.1 mTOR signalling

mTOR is a serine threonine protein kinase conserved in all eukaryotes which comprises of two discrete multi-protein complexes, mTORC1 and mTORC2. mTOR belongs to the phosphoinositide 3-kinase (PI3K) related kinase family and is activated in response to a plethora of external signals including cellular stress, growth factors, energy status and the availability of nutrients (Laplante and Sabatini 2009a). mTOR consists of two separate complexes mTORC1/mTORC2 with the PI3K/Akt/mTOR signal transduction pathway serving as a central regulator of cell growth, proliferation, metabolism and survival. The mTORC1 complex comprises of mTOR, Deptor and mLST8 (gβL) and is sensitive to rapamycin, whilst mTORC2 is composed of mTOR, Rictor, mLST8, Sin1, Protor-1 and Deptor and is largely rapamycin insensitive (Akhavan *et al.* 2010). Much of the knowledge on mTORC1 function comes from studies utilising the inhibitor rapamycin. Upon entry to cells rapamycin binds to the rapamycin-binding protein FKBP12 via the immunophilin FK506. The rapamycin-FKBP12 then binds to the FKBP12-rapamycin-binding domain (FRB) inhibiting the function of mTORC1 (Ma and Blenis 2009).

Engagement of a growth factor with its receptor is the typical route for PI3K activation. As shown in Figure 1.2 activated PI3K then converts its substrate phosphatidylinositol 4,5-biphosphate (PIP2) into phosphatidylinositol (3,4,5)-triphosphate (PIP3) which brings Akt and phosphoinositide-dependent kinase-1 (PDK1) into close proximity. PDK1 is then able to phosphorylate and activate Akt at threonine 308; however, for full Akt activation mTORC2 is also required to phosphorylate Akt at serine 473. Once fully activated Akt can activate mTORC1 via inhibitory phosphorylation of tuberous sclerosis complex 2 (TSC2). Active mTORC1 can then go on to phosphorylate and activate downstream substrates to initiate processes such as cell growth and proliferation (Hay and Sonenberg 2004).

The best characterised direct downstream targets of mTORC1 are proteins involved in controlling the translation of mRNA including S6 kinases (S6Ks) and the 4E-BPs (Hara *et al.* 1998). Other targets of mTORC1 include the transcription factor, hypoxia-inducible factor 1-alpha (HIF1-α), a regulator of cellular response to hypoxia (Land and Tee 2007), and signal transducer and activator of transcription-3 (STAT3) which promotes cell survival (Haidinger *et al.* 2010). Further mTORC1 targets include Lipin-1 and the transcription factor SREBP-1 which both influence signalling events involved in the synthesis of cellular lipids (Peterson *et al.* 2011).

Targets of the mTORC2 complex include Akt, which upon activation promotes cell survival. mTORC2 also regulates growth via activation of serum and glucocorticoid-induced protein kinase 1 (SGK1) and regulates processes involved in cytoskeletal dynamics via protein kinase Cα (PKCα) (Huang *et al.* 2009).

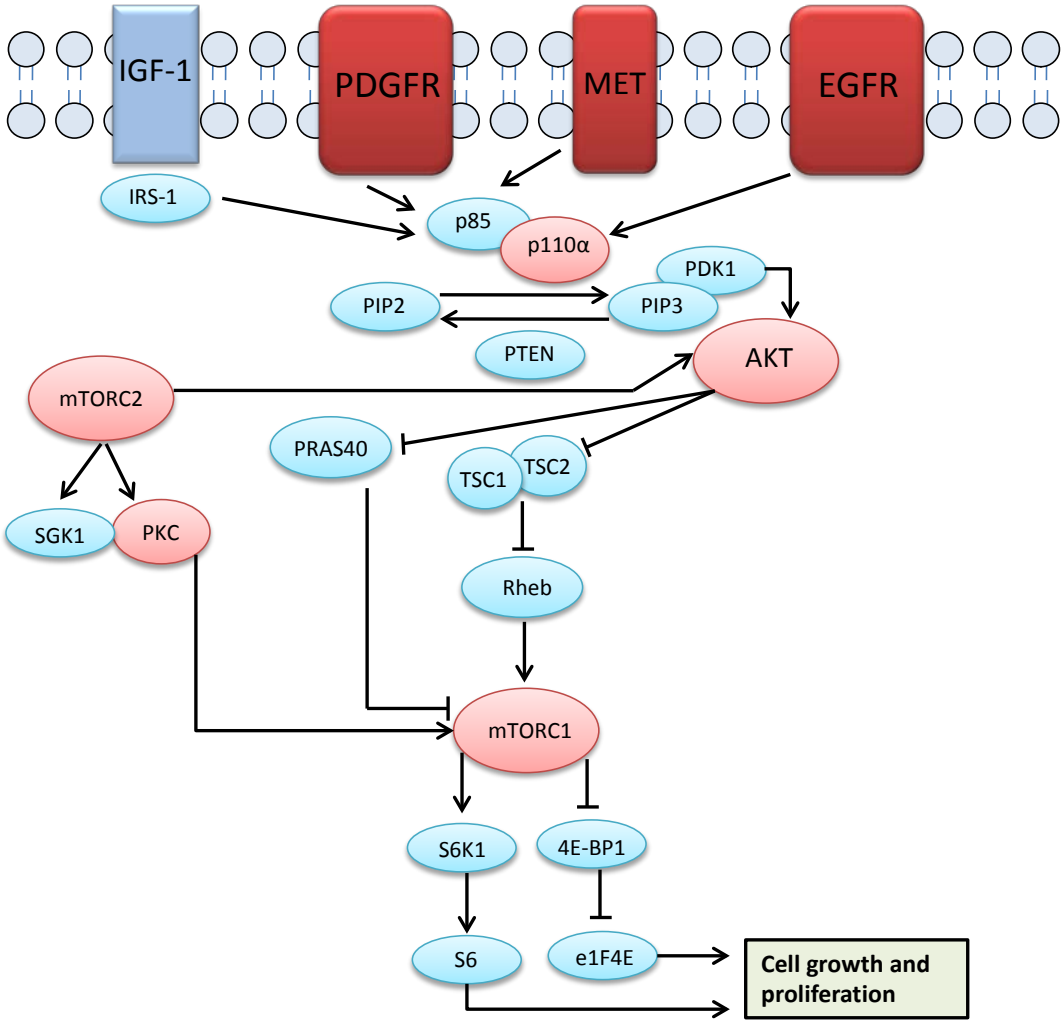


**Figure 1.2: mTOR signalling regulation in mammalian cells.** Engagement of growth factors including insulin-like growth factor receptor-1 (IGF-1), platelet derived growth factor receptor (PDGRF) and epidermal growth factor receptor (EGFR) are the canonical route of mTOR activation via phosphoinositide 3-kinase (PI3K) which is depicted on the diagram by its p85 and p110α subunits. Active PI3K is able to indirectly activate Akt via phosphorylation by phosphoinositide-dependent kinase-1 (PDK1). Akt then activates mTORC1 by inhibitory phosphorylation of tuberous sclerosis complex 2 (TSC2). Active mTOR then has the ability to activate downstream targets to regulate cellular growth. Adpated from Hay and Sonenberg (2004).

Genetic alterations such as loss and gain of function occurring in tumour suppressor and proto-oncogenes respectively within the TOR signalling pathway, have been implicated in initiation of cellular transformation resulting in cancer. Specifically in glioblastoma, amplification of the cell surface receptor epidermal growth factor receptor (EGFR) occurs in approximately 44% of cases (Ohgaki *et al.* 2004), which is often associated with deletion mutations. One of the most commonly occurring molecular aberrations of EGFR, is the truncation of the protein resulting in the loss of exons 2-7, EGFRvIII. This variant comprises 75% of those co-expressing EGFR amplification and results constitutive expression of EGFR (Sugawa *et al.* 1990). This constitutive activation drives activation of PI3K/Akt mediated signalling events and in turn activation of mTOR (Yoshimoto *et al.* 2008).

Further, in up to 50% of glioblastoma cases a mutation in the phosphatase and tensin homolog (PTEN), which negatively regulates PI3K signalling via PIP3 dephosphorylation, is observed. The mutation results in loss of function of PTEN, thus allowing PI3K/Akt/mTOR mediated signalling to persist (Choe *et al.* 2003).

### 1.3.2 MAPK Signalling

Mitogen-activated protein kinases (MAPKs) are serine-threonine protein kinases that mediate intracellular signalling associated with numerous cellular activities including cell proliferation, differentiation, survival, transformation, migration and apoptosis (Dhillon 2007, Kim 2010). MAPK pathways are evolutionary conserved and consist of a three tier protein kinase module which is activated sequentially (Figure 1.3).

MAPK pathways are activated in response to numerous stimuli including growth factors, stress and via G-protein coupled receptors (Kyriakis and Avruch 2012). In order for a MAPK to be activated, phosphorylation on conserved tyrosine and threonine residues by a mitogen-activated protein kinase kinase (MAPKK/MAP2K/MEK) is required. The MAPKK itself is activated by phosphorylation of conserved serine and threonine residues by a mitogen-activated protein kinase kinase kinase (MAPKKK/ MAP3K/MEKK). Additionally to phosphorylation of cytoplasmic targets, activation of MAP kinases promotes their nuclear translocation and subsequent modulation of transcription factors resulting in altered expression of genes (Wilkinson 2000).

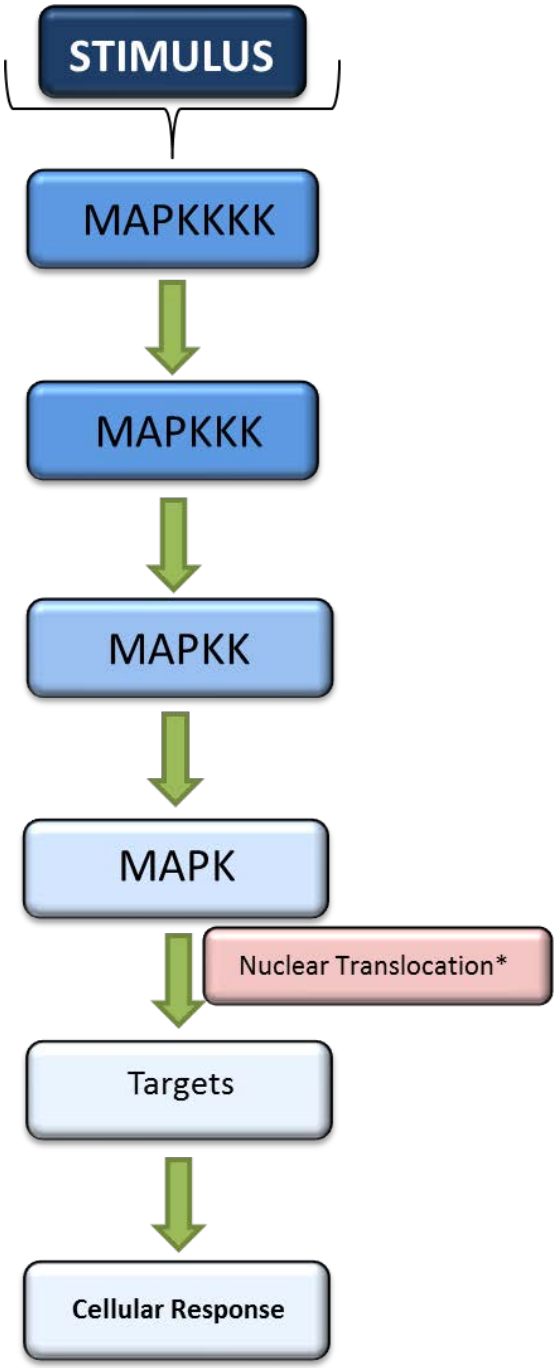


**Figure 1.3: Protein kinase module that makes up the MAPK cascade.** A mitogen activated kinase kinase kinase kinase (MAPKKKK) is activated in response to external stimulus which then phosphorylates and activates a mitogen activated protein kinase kinase kinase (MAPKKK). Active MAPKKKs phosphorylate and activate mitogen activates protein kinase kinases (MAPKKs) on conserved serine and threonine residues. This then leads to activation of the mitogen activated protein kinase (MAPK) which is phosphorylated on conserved tyrosine and threonine residues by a MAPKK, resulting in the MAPKs translocation to the nucleus* to activate/inhibit target proteins and genes. *phosphorylation is not always sufficient for exclusive nuclear translocation of MAPK. Adapted from Roberts *et al.* (2007).

The best studied mammalian MAP kinases are the extracellular signal-regulated kinase (ERK) of the ERK-MAPK pathway, c-Jun $NH_2$-terminal kinase (JNK) and p38 of the JNK/p38 pathways as shown in Figure 1.4. In general JNK and p38 pathways are activated via stress and growth factors, whereas the ERK pathway is usually activated by growth factor stimulated cellular surface receptors (Roberts and Der 2007).

#### 1.3.2.1 ERK MAPK

The ERK-MAPK pathway, shown in Figure 1.4, is most commonly activated by binding of growth factors, such as epidermal growth factor (EGF), to transmembrane receptor tyrosine kinases, in this case EGFR, and serves to regulate processes including cellular proliferation, differentiation and survival.

Upon ligand binding to the extracellular domain, the receptors dimerize resulting in autophosphorylation on tyrosine residues on the intracellular domain. This leads to the recruitment of adapter proteins, such as growth factor receptor bound protein-2 (Grb2), followed by guanine nucleotide exchange factors such as son of sevenless (SOS). Once in close proximity to the membrane bound Ras proteins (Schulze *et al.* 2005, Zarich *et al.* 2006), SOS results in the removal of guanine diphosphate (GDP) from Ras which is then subsequently activated by guanine triphosphate (GTP) binding. Once activated, Ras then interacts with protein kinase Raf (MAPKKK) which initiates the phosphorylation of the ERK cascade (Avruch *et al.* 2001).

Cytosolic targets of ERKs include ribosomal S6 kinases (S6Ks) which, once activated, may translocate to the nucleus and phosphorylate transcription factors such as c-Fos (a proto-oncogene) and cAMP response element binding protein (CREB). In the nucleus ERKs phosphorylate numerous other targets such as mitogen and stress activated protein kinases (MSKs) and the transcription factor Elk1. ERK may also directly phosphorylate the c-Jun and c-Fos components of the transcription factor AP-1, although there are many other nuclear targets including Myc (c-Myc) and nuclear factor kappa-light-chain-enhancer of activated B cells (NF-$_K$B), which are both frequently deregulated in cancer (Krauss 2008).

### 1.3.2.2 JNK MAPK

The JNK MAPK pathway is activated in response to a range of cellular stresses and inflammatory cytokines. It may also be stimulated via growth factor mechanisms. The JNK cascade holds important roles in the production of cytokines, metabolism, inflammation and apoptosis (Morrison 2012).

Mammalian cells harbour 3 *JNK* genes, *JNK1*, *JNK2* and *JNK3*, which are alternatively spliced producing at least 10 isoforms, with JNKs 1 and 2 being ubiquitously expressed. After activation of the MAPKKKs (AAK1, MEKK1 and MLK3), JNK kinases are activated by the MAPKKs, MKK4 and MKK7, via phosphorylation on conserved threonine and tyrosine residues. The activation of MKK4 is triggered mainly by environmental stress and MKK7 by cytokines (Davis 2000). Activated JNK MAPK is then able to phosphorylate transcription factors, including Jun, ATF-2, Elk1, p53, STAT1/3, numerous nuclear hormone receptors as well as transcription factors regulating the synthesis of ribosomes (Figure 1.4) (Krauss 2008).

### 1.3.2.3 p38 MAPK

The p38 MAPK cascade is involved primarily in the cellular response to stress and is activated by growth factors and a range of environmental stresses including cytokine stimulation, osmotic shock, heat shock and ultraviolet irradiation. Once activated it regulates a range of processes including autophagy, apoptosis and proliferation. Mammalian p38 MAPKs comprise four isoforms p38α, p38β, p38γ and p38δ, with the p38α isoform ubiquitously expressed in most cell types. Activation of upstream MAP3Ks is complex and involves phosphorylation by p21 activated kinases (PAK) and binding of Rho GTP-binding proteins (Cuadrado and Nebreda 2010).

As shown in Figure 1.4, p38 MAPK kinases are mainly activated by the MAPKKs, MKK3 and MKK6, on conserved Thr-Gly-Tyr residues. Additionally the α isoform may be activated via MKK4, which also activates JNK MAPK. Activated p38 has the ability to phosphorylate transcription factors STAT-1, activating transcription factor 2 (ATF-2) and p53 (Thornton and Rincon 2009), as well as protein kinases MSK1, MNK, cell cycle control factors such as cyclin D1 and death/survival modulators including Bcl-2 and caspases (Cargnello and Roux 2011). p38 is another kinase that is frequently deregulated in a range of cancers, with the up regulation being implicated in promoting proliferation, angiogenesis and metastasis of

cancerous cells (Leelahavanichkul *et al.* 2014, Mao *et al.* 2010). However, the role of p38 in cancer remains controversial as both cell survival, through Bcl2 upregulation, and anti-proliferative functions, via cell cycle inhibition have been noted. The inhibition of cell cycle progression however could serve to promote cancer cell drug resistance rather than to inhibit growth (Liu Liang *et al.* 2014).

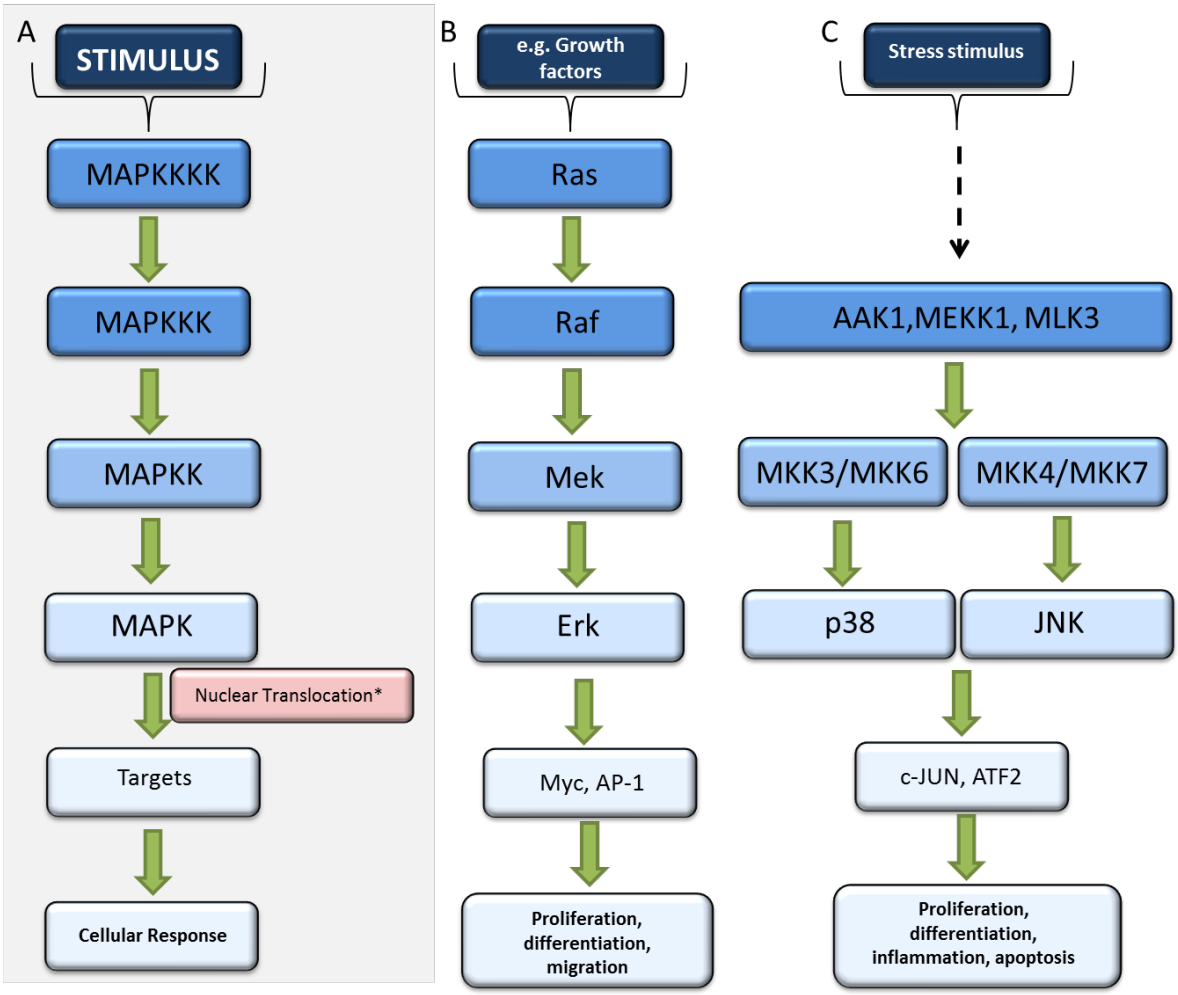


**Figure 1.4: Well characterised MAP Kinase signalling pathways in mammalian cells.** A: Overview of the construction of MAP Kinase pathways. B: Ras/Raf/MEK/ERK signalling pathway C: p38 and JNK MAP Kinase pathways. Adapted from Roberts *et al.* (2007).

As discussed in the previous sections mTOR and MAPK pathways are both frequently deregulated in the initiation and progression of numerous cancer types. In the case of solid tumours, lipid homeostasis is also often perturbed and has been linked to upstream oncogenic signalling (Santos CR. and Schulze 2012).

## 1.4 Lipids

Lipids are key constituents of eukaryotic cells; their metabolism is complex and involves numerous metabolic reaction steps which produce an array of lipid types. Lipids may be broadly classified into neutral and polar lipid subtypes which include fatty acids (FAs), triacylglycerols (TAGs), wax esters (WEs), sterol esters (SEs), phospholipids (PLs), lysolipids and sphingolipids (SLs) (Nielsen 2009, Rajakumari S *et al.* 2008). The major biological functions of lipids include roles as structural components of cellular membranes (mainly PLs), serving as central energy stores (mainly TAGs and SEs). Furthermore, they have been shown to be important signalling molecules.

The regulation of lipid metabolism and its impact on human disease is under intense investigation. Defects in lipid metabolism have been linked to several disease states including Alzheimer's, cancer, diabetes and Niemann-Pick disease (Di Paolo and Kim 2011, Oresic *et al.* 2008, Zech *et al.* 2013, Zhang F. and Du 2012). Therefore an increased understanding of the mechanisms underlying regulation of lipid metabolism in proliferating tumour cells, through the analysis of signal transduction pathways, could allow the identification of novel targets for therapeutic intervention.

### 1.4.1 Lipogenesis

Lipogenesis is defined as the metabolic formation of fat and is the process whereby acetyl CoA is converted to fatty acids. The *de novo* synthesis of fatty acids (FAs), which mainly serve as intermediaries in lipid biosynthesis, begins with the carboxylation of acetyl-CoA to malonyl-CoA both of which are utilised by fatty acid synthase (FAS) to synthesise the long carbon chains of FAs. The majority of synthesised FAs are either incorporated into TAGs for metabolic energy storage, or assimilated into the membranes as phospholipid components (Figure 1.5) (Nelson and Cox 2008).

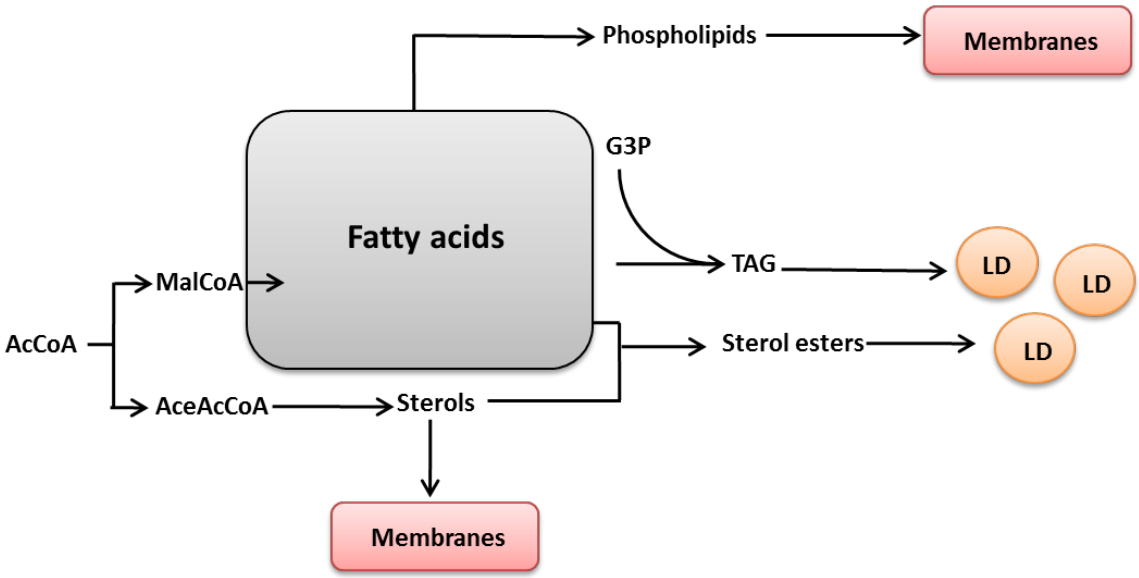


**Figure 1.5: Simplified overview of lipid synthesis from acetyl-CoA.** Acetyl CoA (AcCoA) is converted to malonyl CoA (MalCoA) or acetoacetyl CoA (AceAcCoA) for fatty acid and sterol synthesis for formation of traicylglycerol (TAG) and sterol esters (SEs), respectively. TAGs and SEs can then be stored as a cellular energy reserve in intracellular lipid droplets (LD). Adapted from Nielsen (2009).

### 1.4.2 Neutral lipids

Neutral lipids, comprising TAGs, WEs and SEs are molecules which lack charged groups conferring their inability to incorporate into membrane bilayers in significant quantities (Athenstaedt and Daum 2006). TAGs and SEs hold central roles in the storage of sterols, diacylglycerols and free fatty acids for cellular energy (Hutchins *et al.* 2008). As such, neutral lipids within cells are stored within cytosolic lipid droplets (LDs) with neutral lipids forming the core of the droplet which is surrounded by a monolayer of phospholipids. The fatty acids that are encased in LDs can be used for both phospholipid synthesis and for cellular energy production via the process of β-oxidation (Athenstaedt and Daum 2006).

#### 1.4.2.1 Triacylglycerol and sterol ester synthesis

The synthesis of TAGs can occur via the glycerol-3-phosphate pathway. Glycerol-3-phosphate (G3P) is obtained primarily from glycolysis and is esterified by glycerol-3-phosphate acyltransferases to produce lysophosphatidic acid (LPA) which is further esterified to form phosphatidic acid (PA). Phosphatidic acid is then dephosphorylated by phosphatidic acid phosphorylases (PAPs) to yield 1,2 diacylglycerol (DAG), which can then be utilised in the production of TAG or phospholipids (Coleman and Lee 2004). The terminal step of TAG synthesis is the formation of an ester bond between a fatty acid and

the hydroxyl group of DAG synthesised by 1,2 diacylglycerol acyltransferase (DGAT) (Figure 1.6) (Yen *et al.* 2005).

Sterol esters can be synthesised by a acyl-CoA independent reaction whereby lecithin:cholesterol acyltransferase (LCAT) catalyses the transfer of a FA from a glycerophospholipid to a hydroxyl group of an acceptor sterol. Secondly sterol esters can be produced via an acyl CoA dependent process catalysed by acyl-CoA: cholesterol acyltransferase (ACAT) (Athenstaedt and Daum 2006).

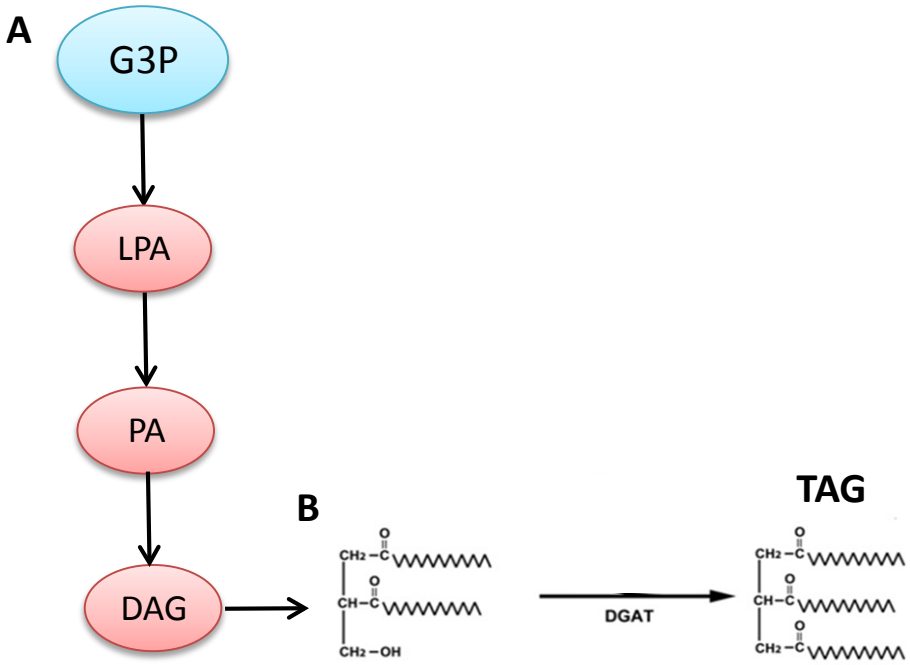


**Figure 1.6: Key steps facilitating the synthesis of triacylglycerols.** A:Glycerol 3-phosphate (G3P) is esterified to produce lysophosphatidic acid (LPA). LPA is further esterified to form phosphatidic acid (PA). PA is dephosphorylated to form 1,2-diacylglycerol (DAG). B: Triacylglycerol (TAG) is then synthesised from DAG by 1,2 diacylglycerol acyltransferase (DGAT).

### 1.4.2.2 Formation of lipid droplets

Intracellular LDs, as described previously, were long considered to be inert molecules for the storage of cellular energy. Due to recent advances, driven by the pandemic rise of lipid dysregulation in human disease, it is now understood that LDs are in fact dynamic organelles with diverse functions in the production of both energy and metabolism of lipids (Beller *et al.* 2010). In spite of such advances the specific functions and molecular details of lipid droplet processes are largely unknown with several models proposed for their intracellular formation (Beller *et al.* 2010) (Figure 1.7).

The most prominent and widely cited model put forward for LD biogenesis is the "lensing" model whereby neutral lipids are deposited between endoplasmic reticulum (ER) membrane leaflets. Once a crucial size is accumulated the neutral lipid core formed protrudes outwards and the LD is formed, with the surrounding monolayer derived from the ER membranes cytosolic leaflet. The formed LD may completely bud away from the ER membrane or remain attached (Martin and Parton 2006) (Figure 1.7A).

Other models for LD biogenesis that have been proposed include the "bicelle" and "vesicle-budding" models, both of which have little direct evidence to support them (Wilfling *et al.* 2013).

In the bicelle model the notion of neutral lipid accumulation between ER leaflets is mutual with that of the lensing model, however rather than the resultant monolayer surrounding the neutral lipid core comprising completely of ER cytosolic leaflet both membranes of the ER contribute to vesicle formation and the surface monolayer of the final LD (Ploegh 2007) (Figure 1.7B). The major flaw of the bicelle model is that the integrity of the ER membrane would be severely compromised by the excision of completed LDs (Walther and Farese Jr 2009).

Conversely the vesicle-budding model proposes that droplets are formed within a small bilayer vesicle which remains attached to the membrane of the ER and that these vesicles act as a platform for LD synthesis (Figure 1.7C). Lipids accumulated within the vesicle bilayer fill the space between the membranes which squeezes the lumen of the vesicle such that it either becomes a small inclusion within the LDs or fuses with the outer leaflet of the droplet (Walther and Farese Jr 2009).

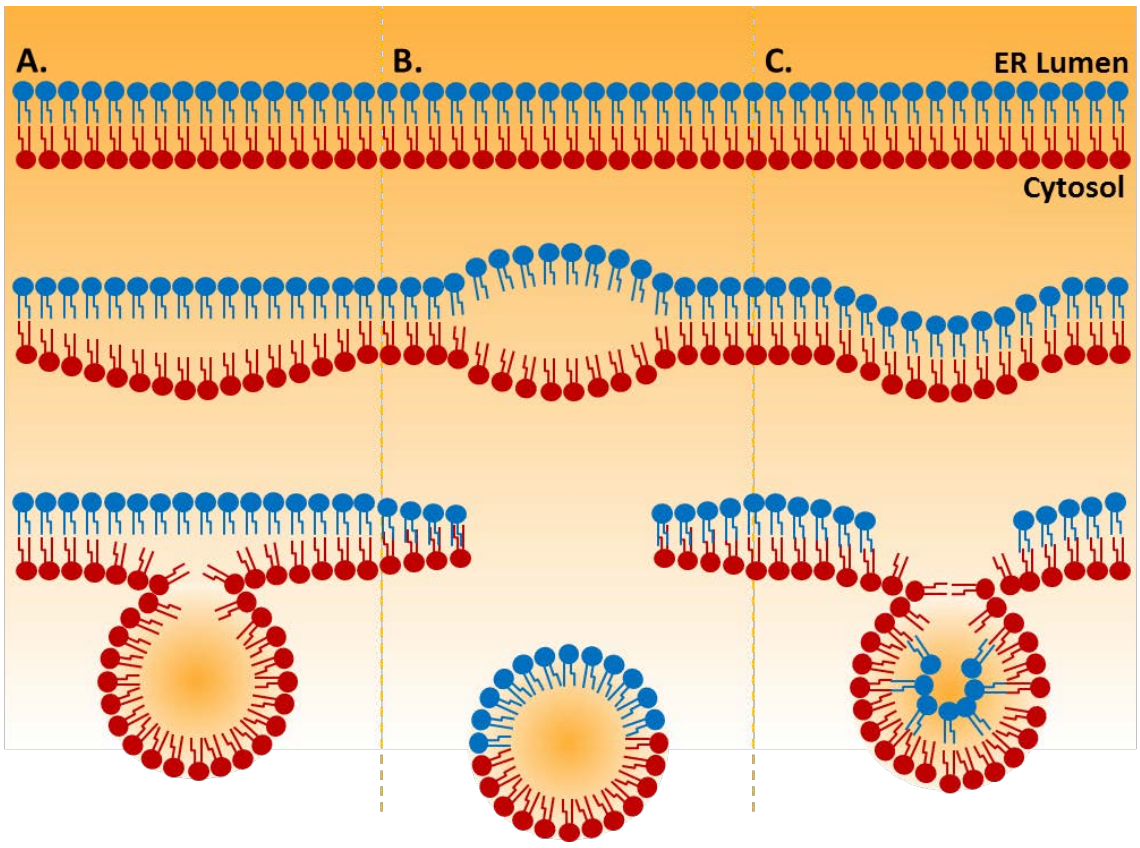


**Figure 1.7: Proposed models of lipid droplet formation at the endoplasmic reticulum. A:** The lensing model. Neutral lipids are accumulated between the membrane leaflets of the endoplasmic reticulum (ER) until a critical size is reached. Lipid droplets may either remain attached to the ER or "bud" off from the membrane. **B:** The bicelle model. Lipid droplets comprise of both membranes of the ER **C:** The vesicle budding model. Droplets are formed within a small bi-layer vesicle, the resultant lipid droplet forms from one membrane of the ER, with the membrane contributing to the vesicle potentially forming a small inclusion. Adapted from Kohlwein *et al.* (2013).

In response to cellular biosynthetic requirements, neutral lipids accumulated within LDs are mobilised by lipases (lipolysis) to provide substrates for production of lipids for membrane synthesis or cellular energy in the form of ATP, yielded via fatty acid oxidation (Guo Yi *et al.* 2009b). After cytoplasmic activation, oxidation of fatty acids occurs in the mitochondria and peroxisomes of cells in a process known as β-oxidation. This process results in the sequential removal of two carbon units with each cycle involving four steps.

The first is dehydrogenation of and acyl-CoA ester to produce trans-2-enoyl-CoA followed by hydration of the double bond. This is then followed by dehydrogenation of the resultant L-3-hydoxy-acyl-CoA to 3-keto-acyl-CoA before finally, thiolytic cleavage of to yield an acetyl CoA and acyl-CoA shortened by two carbons (Houten and Wanders 2010). Each β-oxidation cycle yields both of the aforementioned thiolytic cleavage products as

well as one flavin adenine dinucleotide ($FADH_2$) and one nicotinamide adenine dinucleotide (NADH). The resultant acetyl-CoA may enter the tricarboxylic acid (TCA) cycle and is further oxidised producing more $FADH_2$ and NADH which is then transferred, along with those produced in β-oxidation, to the electron transport chain yielding ATP (Houten and Wanders 2010).

### 1.4.3 Polar lipids

Glycerophospholipids (GPLs) are the most abundant lipids present in eukaryotic membranes and are derived from phosphatidic acid (PA) (Figure 1.8). The major classes present are phosphatidylcholine (PC) phosphatidylethanolamine (PE), phosphatidylinositol (PI) and phosphatidylserine (PS). GPLs are instrumental molecules not only for the structural maintenance of biological membranes, but also in mediating cellular regulatory functions due to their capacity to be converted into lipid second messengers such as LPA and DAG (Vance 2008).

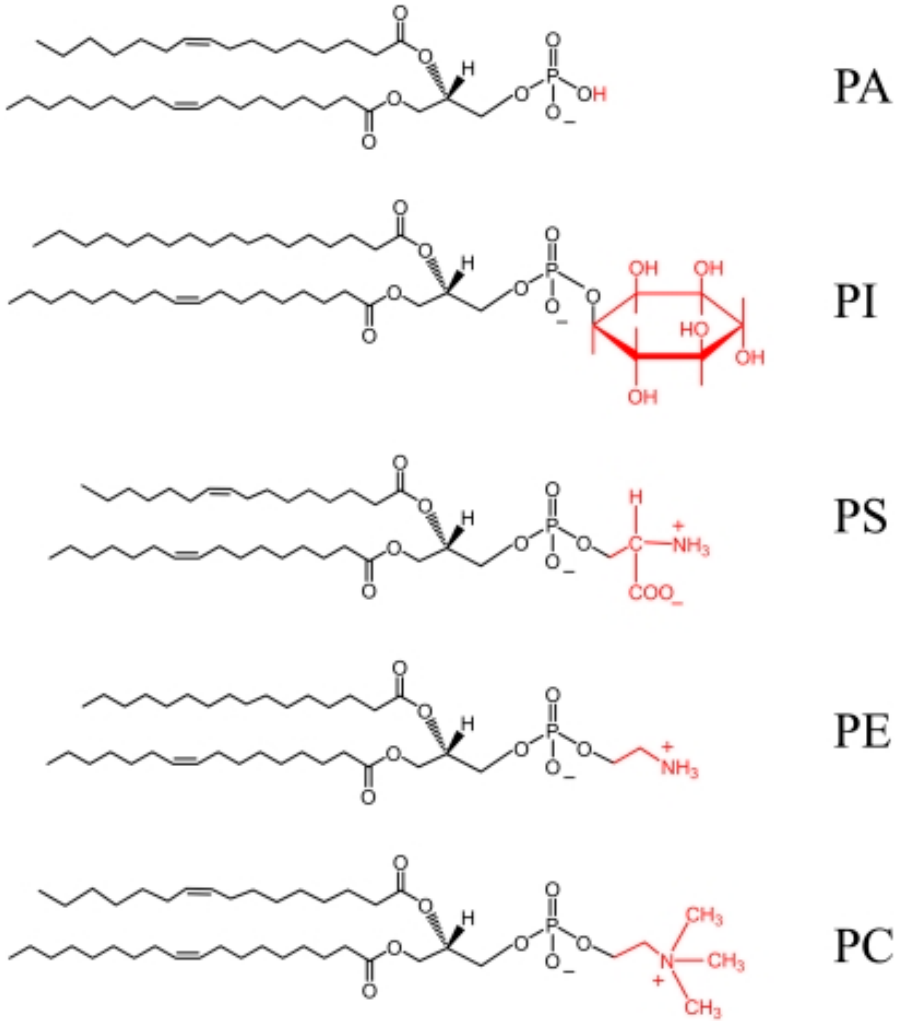


**Figure 1.8: Major classes of Glycerophospholipids derived from phosphatidic acid.** The major classes of glycerophospholipids derived from phosphatidic acid (PA) along with their structures. The major phospholipids are: phosphatidylinositol (PI), phosphatidylserine (PS), phosphatidylethanolamine (PE) and phosphatidylcholine (PC). Shown in red are the hydrophilic head groups (inositol, serine, ethanolamine and choline). Taken from Henry *et al.* (2012).

### 1.4.4 Phospholipid synthesis

The precursor for the synthesis of all glycerophospholipids is PA which can be generated *de novo* from G3P (as seen with TAG synthesis) or via the phosphorylation of DAG (Hermansson *et al.* 2011, Hishikawa *et al.* 2014). The resultant PA can be utilised in the synthesis of PLs via two different pathways. The first involves production of DAG which can then be utilised in the synthesis of PE, PC, PS or TAG. In the second pathway PA is utilised to produce PL classes by the creation of CDP-DAG molecules (Henry *et al.* 2012). An overview of the pathways contributing to synthesis of major phospholipid classes is depicted in Figure 1.9.

#### 1.4.4.1 Phosphatidylcholine synthesis

Phosphatidylcholine (PC) may be produced via two pathways. In the first pathway PC is synthesised via the CDP-choline (Kennedy) pathway. Firstly choline is phosphorylated to phosphocholine by choline kinase before it is further activated using CTP to produce CDP-choline. The phosphocholine moiety is then transferred to DAG from CDP-choline to form PC. Secondly PC can be produced as the end product of the CDP-DAG pathway, whereby CDP-DAG is initially converted by PS synthase to PS. The resultant PS is then decarboxylated to PE which is in turn methylated sequentially to yield PC (Rajakumari S. *et al.* 2010).

#### 1.4.4.2 Phosphatidylethanolamine synthesis

The synthesis of PE via the Kennedy pathway is produced by ethanolamine kinase phosphorylating ethanolamine forming phosphoethanolamine. Phosphoethanolamine is then further activated by CTP yielding CDP-ethanolamine with the final step involving transfer of ethanolamine to DAG yielding PE. Via the CDP-DAG pathway, CDP-DAG is converted to PS primarily which is then decarboxylated to form PE (Hermansson *et al.* 2011).

#### 1.4.4.3 Phosphatidylserine synthesis

Phosphatidylserine is a minor lipid component of cellular membranes. L-serine is an amino acid which is actively synthesised and produced in almost all cell types. The synthesis of PS occurs via base-exchange from PC or PE by PS synthase. Phosphatidylserine synthase 1 (PSS1) replaces the head group of PC with L-serine yielding phosphatidylserine and choline, whereas phosphatidylserine synthase 2 (PSS2) catalyses the same reaction replaces the head group of PE with L-serine yielding phosphatidylserine and ethanolamine.

#### 1.4.4.4 Phosphatidylinositol synthesis

A class of GPL that serve as important lipid signalling molecules are phosphatidylinositols. PI is formed from PA by the production of CDP-DAG which is condensated with *myo-inositol* by PI synthase. The head group of PI can also be phosphorylated to produce phosphatidylinositol phosphates (PIPs). In addition to roles in maintaining structural cellular integrity, PI and its metabolites are involved in the regulation of numerous cellular processes including signal transduction, actin cytoskeleton organisation, protein anchoring, mRNA export and vesicle mediated membrane trafficking (Gardocki *et al.* 2005, Kim Sung-Kuk *et al.* 2011).

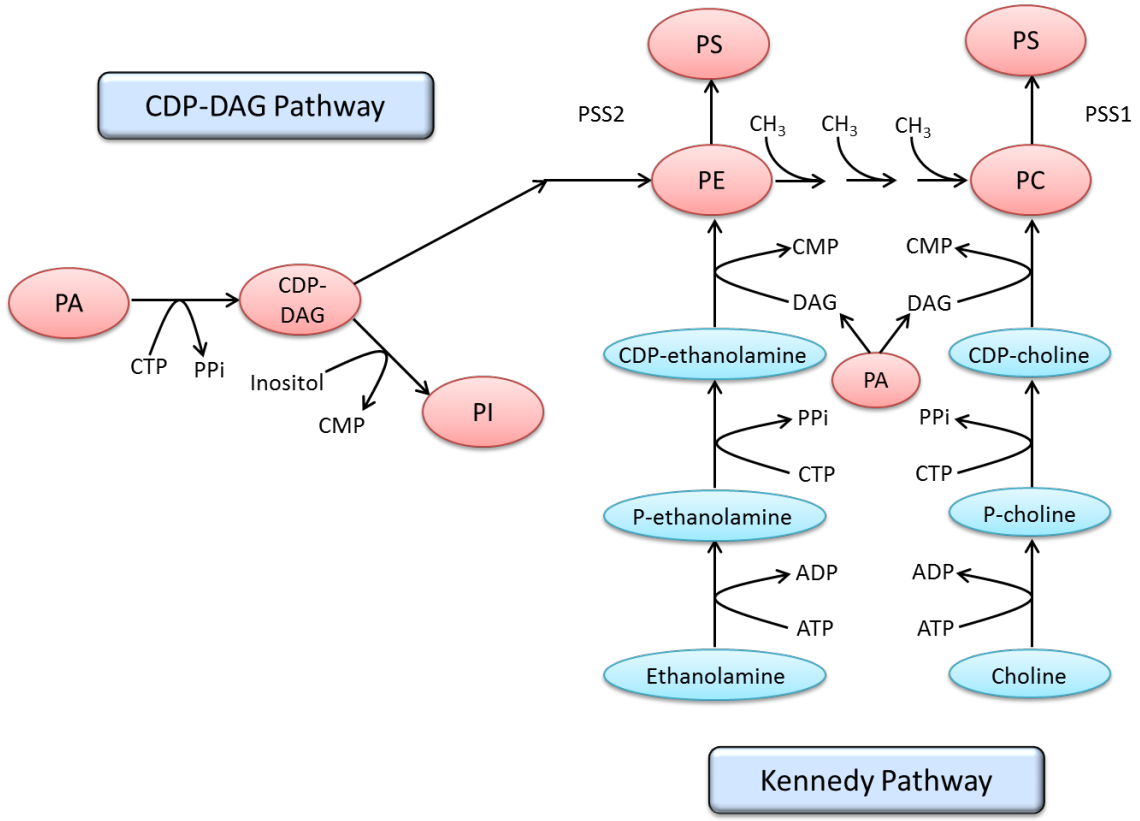


**Figure 1.9: Overview of phospholipid biosynthetic pathways.** Phospholipid biosynthetic pathways, left: CDP-DAG pathway and right: Kennedy pathway. PA: Phosphatidic acid, PSS1: phosphatidylserine synthase 1, PSS2: phosphatidylserine synthase 2, PS: Phosphatidylserine, PE: Phosphatidylethanolamine, PI: Phosphatidylinositol, PC: Phosphatidylcholine, DAG: Diacylglycerol, P-ethanolamine: phosphoethanolamine, P-choline: phosphocholine, ATP: Adenosine triphosphate, ADP: Adenosine diphosphate. Adapted from Choi Hyeon-Son *et al.* (2004).

## 1.5 Metabolic switch of cancerous cells

The uncontrolled potential of cancerous cells to proliferate requires an enhanced nutrient supply along with biomass synthesis and subsequently energy consumption. Aberrant metabolism of human cancer cells was first recognised in the 1920s when Otto Warburg noted that rapidly proliferating tumour cells consume glucose at an accelerated rate compared to non-cancerous cells (Warburg O. 1925, Warburg O 1956).

Accompanying the high glycolytic characteristic of tumour cells, heightened rates of anabolic processes are also displayed resulting in elevated amino acid and lipid synthesis. Various types of tumours have been found to undergo increased *de novo* endogenous fatty acid synthesis irrespective of existing extracellular lipid levels (Esechie and Du 2009). This phenomenon occurs downstream from oncogenic signalling and is directly linked to increased glycolysis associated with solid tumours (Swinnen *et al.* 2006).

As depicted in Figure 1.10, in quiescent cells there is a basal rate of glycolysis whereby glucose is converted to pyruvate and enters the TCA cycle where it is oxidised. Alongside this process cells are also able to oxidise substrates including fatty acids and amino acids from degradation of macromolecules or simply from their environment. Conversely in proliferating cells there is a marked increase in glycolytic flux which generates large amounts of ATP within the cytoplasm. Most of the resultant pyruvate from glycolysis is converted via lactate dehydrogenase-A (LDA) to lactate allowing glycolysis to continue. Some resultant pyruvate is converted to acetyl-CoA and enters the TCA cycle where it is converted to intermediates (DeBerardinis R J. *et al.* 2008b). One such intermediate is citrate which may be exported from the mitochondria to the cytoplasm and cleaved to produce substrates including oxaloacetate and notably acetyl-CoA which is then processed by fatty acid synthase (FASN) for the synthesis of lipids (Bauer DE. *et al.* 2005).

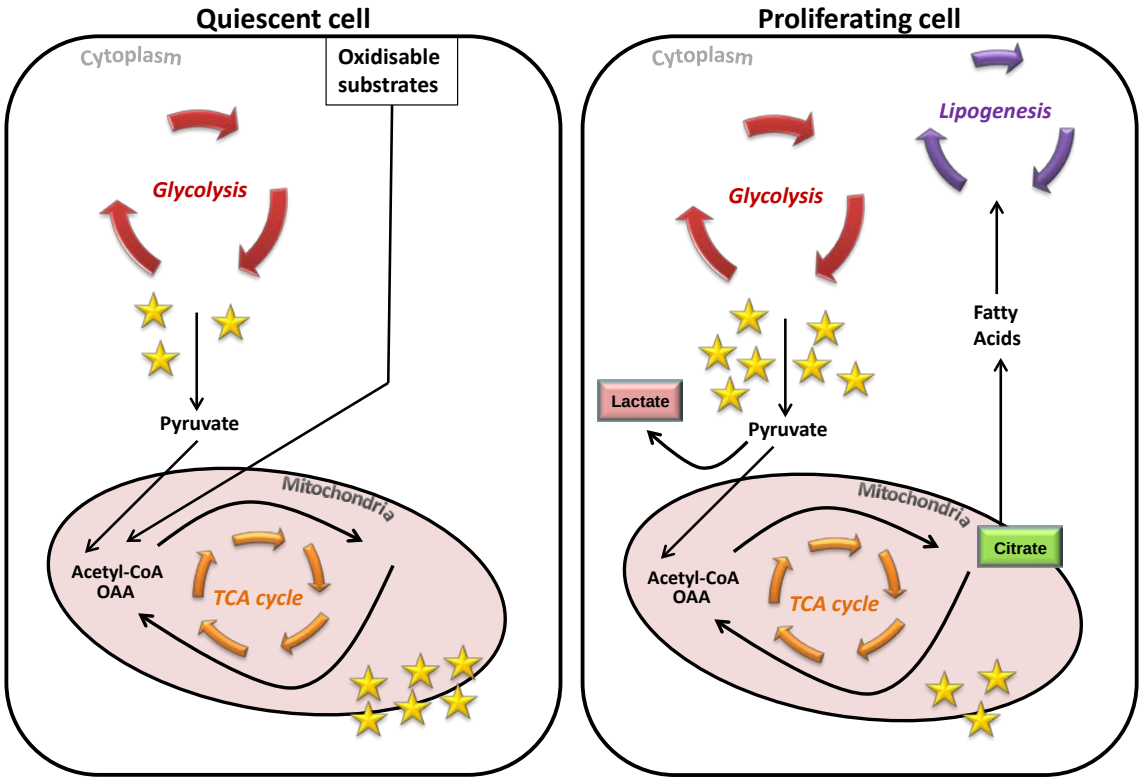


**Figure 1.10: Differences in carbon flux between non-proliferating and proliferating cells.** In quiescent cells (left) there is a basal rate of glycolysis whereas proliferating cells in comparison (right) have a larger glycolytic flux which generates cytoplasmic ATP readily (stars). Most of the resulting pyruvate is converted to lactate which, due to NAD+, allows glycolysis to continue. Some of the resulting pyruvate is converted to Acetyl-CoA before entry into the TCA cycle. After entry into the TCA cycle, intermediates, such as citrate is formed. Citrate is one of the requirements for the synthesis of fatty acids and cholesterol which is used to generate lipid membranes required for proliferating cells. Adapted from DeBerardinis RJ. *et al.* (2008a).

The process of increased glycolysis compared to energy generation by oxidative phosphorylation is energetically unfavourable to cells. For example, the conversion of glucose to lactate only produces 2 ATPs per molecule of glucose, whereas oxidative phosphorylation (OXPHOS) may generate up to 36 ATPs per glucose molecule. However for cancerous cells which require rapid growth and proliferative potential, this switch harbours many advantages. Firstly, if glycolytic flux is markedly increased then the percentage of ATP generated from glycolysis can exceed that of OXPHOS due to its higher rate (Pfeiffer *et al.* 2001). Secondly the metabolic requirements of cancerous cells extend beyond that of mere ATP production and the process of glycolysis also yields intermediates for the production of lipids, amino acids and nucleotides (Vander Heiden *et al.* 2009). Along with this the high lactate production resulting from increased glycolysis serves to produce NADPH for anabolic reactions as well as serving to assist cancerous cells

in evading immune responses and promoting cellular migration (Hirschhaeuser *et al.* 2011).

More recently it has been shown that cancerous cells residing in solid tumours may have dual metabolism for the generation of ATP in a more economical fashion which allows effective adaptation to the tumour microenvironment. This study suggests that once cancerous cells consume glucose and produce lactate resulting in lactic acidosis, a common feature of solid tumours, the cells switch to OXPHOS to generate ATP in a more energetically favourable fashion whilst glucose levels are low (Xie *et al.* 2014). It is postulated that the Warburg effect has the advantage when glucose supply is sufficient for supplying metabolic requirements for rapid proliferation, whereas in non-glycolytic circumstances under conditions of lactic acidosis the cancer cells are able to adapt to a limited glucose metabolic environment (Xie *et al.* 2014).

Although the changes governing the regulation of increased *de novo* lipogenesis are not fully understood, it is postulated that the high rate of *de novo* lipogenesis occurring in rapidly proliferating tumour cells not only creates a supply of phospholipids for membrane biogenesis but also a readily available store of energy (Jackowski *et al.* 2000).

### 1.5.1 Pathways involved in the metabolic switch

Over the last decade a plethora of information has accumulated on the signalling components involved in the accelerated glycolytic and lipogenic rates observed in cancerous cells. As depicted in Figure 1.11, oncogenic gain of function and loss of tumour suppressors may both contribute to stimulating the transcription of genes encoding proteins mediating glycolysis.

For example, as described earlier, PI3K/Akt is deregulated via both EGFR mutation and loss of PTEN resulting in constitutive activation. The overexpression of Akt can lead to increased LDA fuelling lactate and $NAD^+$ production, increased activity of glucose transporter-1 (GLUT-1) which will in turn enhance cellular glucose influx to feed glycolysis and phosphofructokinase 2 (PFK2) another positive regulator of glycolysis. Furthermore constitutive activation of Akt suppresses β-oxidation processes supporting anabolic metabolism of lipids and therefore proliferation (DeBerardinis RJ. *et al.* 2006). Downstream from enhanced PI3K/Akt signalling, consequent mTOR activation contributes

to S6K and HIF-1α up regulation which contribute to enhanced GLUT-1 expression (Buller *et al.* 2008).

AMP-activated protein kinase (AMPK) is a critical regulator of both glucose and lipid metabolism. Upon activation of AMPK by its major upstream AMPKK, processes that generate ATP are enhanced, such as β-oxidation, whilst energy consuming processes including fatty acid synthesis are downregulated. Although often classed as a tumour suppressor, AMPK has also been implicated in contributing to promoting cell survival and adaptation (Liang and Mills 2013). Loss of function of LBK1 in many human cancers means that the activation of AMPK is perturbed resulting in heightened proliferative potential occurring from the inability to supress downstream targets such as mTORC1 and HIF-1α (Faubert *et al.* 2013, Lisi *et al.* 2014).

Activation of sterol regulatory element binding proteins (SREBPs) is also implicated in facilitating cancer progression. SREBPs are membrane bound helix-loop-helix leucine zipper transcription factors, with three isoforms SREBP-1a, SREBP-1c and SREBP-2 encoded by *SREBPF1* and *SREBPF2* found in mammalian cells. SREBP-1a regulates all SREBP-responsive genes whereas SREBP-1c and SREBP-2 regulates genes involved in fatty acid and cholesterol synthesis, respectively. Control of SREBP isoform activity is controlled by the binding protein, SREBP cleavage activating protein (SCAP) (Espenshade and Hughes 2007, Shao and Espenshade 2014).

It has been demonstrated that mTOR promotes the activation of SREBP-1a, a master regulator of fatty acid synthesis (Porstmann *et al.* 2008). The active, cleaved form of SREBP-1a translocates to the nucleus where it promotes activation of SREBP responsive genes holding roles in the synthesis of cholesterol, FAs and TAGs. Targets of SREBP-1a/c include fatty acid synthase (FASN), acetyl-CoA carboxylase (ACC) and glycerol-3-phosphate-acyltransferase (GPAT) (Laplante and Sabatini 2009b).

Additionally, numerous common oncogenes, including c-Myc and H-ras, contribute to oncogenic signalling fuelling anabolic reactions. Specifically the transcription factor c-Myc, a regulator of cell growth, targets glycolytic enzymes such as well as regulating nucleotide, amino acid and carbon metabolism.

Tumour suppressors can also aid in regulating cellular metabolism. For instance, activation of p53 results in enhancement of β-oxidation processes as well as favouring cellular energy production via OXPHOS. Due to the loss of p53 in many solid tumours, a significant growth advantage is given to cancerous cells as they are able to engage in glycolysis with a gain of anti-angiogenic function (Jones and Thompson 2009).

Links between upregulation of MAPK signalling via the Ras/Raf/MEK/ERK pathway have also been implicated in increased expression and activation of FASN via SREBP-1, leading to enhanced lipogenesis in cancerous cells (Yang Yu-An *et al.* 2002). As with PI3K/Akt signalling, ERK pathway activation also causes increased HIF1α levels, which as previously described, serves to upregulate the expression of GLUT-1. It has also been demonstrated that ERK is required for nuclear translocation of the glucose metaboliser pyruvate kinase M2 (PKM2) which promotes the Warburg effect observed in cancerous cells and also serves as a regulator of Myc (Yang W *et al.* 2012).

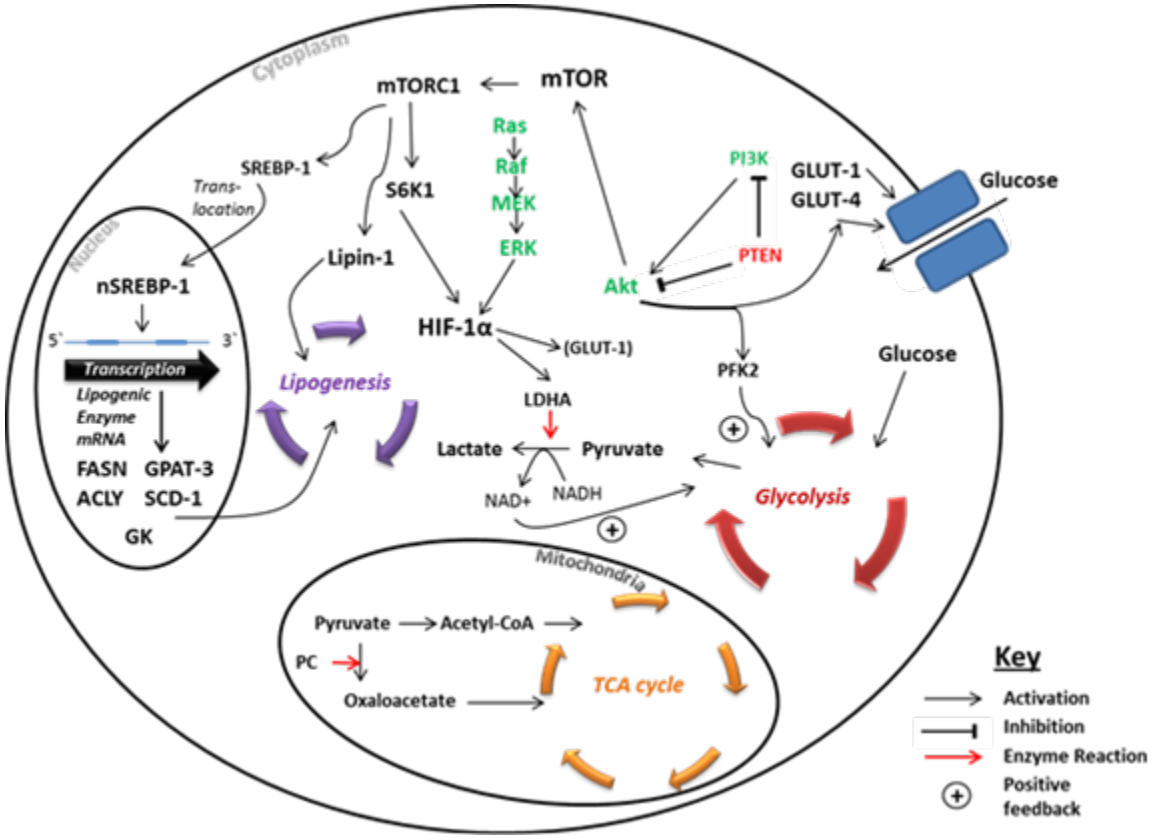


**Figure 1.11: Overview of metabolic reprogramming occurring via oncogenic signalling.** Downstream from growth factor expression, gain of function in proto-oncogenes (green) or loss of function in tumour suppressor genes (red) can lead to de-regulated lipid metabolism. PI3K/Akt/mTOR upregulation activates SREBP-1 transcription factors which drives expression of lipid metabolism genes whilst also activating Lipin-1 to drive lipogenesis. Overactive Ras/Raf/MEK/ERK serves to upregulate HIF-1α, contributing to GLUT-1 activation to increase glycolytic flux. PC: Pyruvate carboxylase. LDHA: Lactate dehydrogenase A.

Numerous upstream oncogenic signalling components, as described above, have been described to fuel the lipogenic phenotype. However, further understanding and dissection of the underlying mechanisms that allow metabolic transformation is still required in order to develop targeted therapeutic strategies. Much of the understanding of signalling and lipid biosynthetic regulatory mechanisms has been derived from studies utilising the budding yeast *Saccharomyces cerevisiae* (*S. cerevisiae*) as a model organism (Athenstaedt 2010, Dann and Thomas 2006, Schmidt *et al.* 2013). It is postulated that further studies using simple eukaryotic model organisms will accelerate understanding further of the upstream events that regulate lipid biosynthesis.

## 1.6 Yeast as a model organism

Approximately a quarter of a century ago it was predicted that yeast could be utilised as the ideal model organism for eukaryotic biology (Botstein D and Fink 1988). Following on from this, studies utilising the budding yeast *Saccharomyces cerevisiae* (*S. cerevisiae*) and fission yeast *Schizosaccharomyces pombe* (*S. pombe*), have enabled major biological breakthroughs in understanding a plethora of cellular and molecular processes (Mager and Winderickx 2005). Today, yeast are still intensively employed as an excellent genetically well-defined model for studying eukaryotic biology.

The attractiveness for the utilisation of yeast in research stems from their simplistic nature, especially with respect to elucidation of genotype/phenotype relationship, ease of culture in low cost media and genetic tractability. In this sense yeast cells hold an advantage over their mammalian counterparts as it is easier, in comparison, to identify the biochemical function of a gene as well as to study the biological consequences of inactivation or overexpression (Botstein D. and Fink 2011, Mager and Winderickx 2005). Along with this a more detailed molecular analysis may be carried out when utilising yeast than can be undertaken in the clinic or with human primary cell culture (Petranovic *et al.* 2010).

Although phylogenetically distant from the cells of humans and other mammals, a number of key processes and regulatory elements are highly evolutionarily conserved. Therefore gene functions, gene/protein interactions and indeed signalling networks can be compared with other eukaryotes including those of *Homo sapiens* (Botstein D. and Fink 2011, Petranovic *et al.* 2010). A comparison of genes in 1997 showed that 30% of known

genes involved in human diseases also have orthologues in yeast and that hundreds of additional yeast genes exhibit links to such genes (Françoise 1997). Additionally as the fission yeast *S. pombe* is only distantly related to budding yeast, a valuable complementary model system is provided.

It is therefore not surprising that both MAPK and mTOR pathways are highly conserved between yeast and mammalian cells. In addition, regulation of cellular energy metabolism is also highly similar between yeast and mammalian cells with increasing evidence that the metabolism of lipids is also conserved (Petranovic *et al.* 2010).

### 1.6.1 mTOR signalling in yeast

As previously described and depicted in Figure 1.12, mTOR complexes are structurally and functionally conserved in yeast and mammalian cells. Multiple advances in the elucidation of cellular growth processes in mammalian cells were initially described utilising yeast, including the roles of TOR signalling (Dann and Thomas 2006). Pioneering work in yeast in 1991 led to the discovery of the two isoforms of TOR in *S. cerevisiae* through analysis of resistance to the antifungal agent rapamycin (Heitman *et al.* 1991).

Since then TOR protein complexes and signalling behaviours have been under intensive investigation in the progression of many human cancers and more recently in the regulation of lipid metabolism. As with mammalian cells, the TOR pathway residing in yeast cells regulates cell growth in response to cellular stresses and nutrient availability (Loewith 2011). Activation of TOR complexes modulates responses to processes including protein synthesis, autophagy, cell cycle and activation of gene transcription (Hay and Sonenberg 2004).

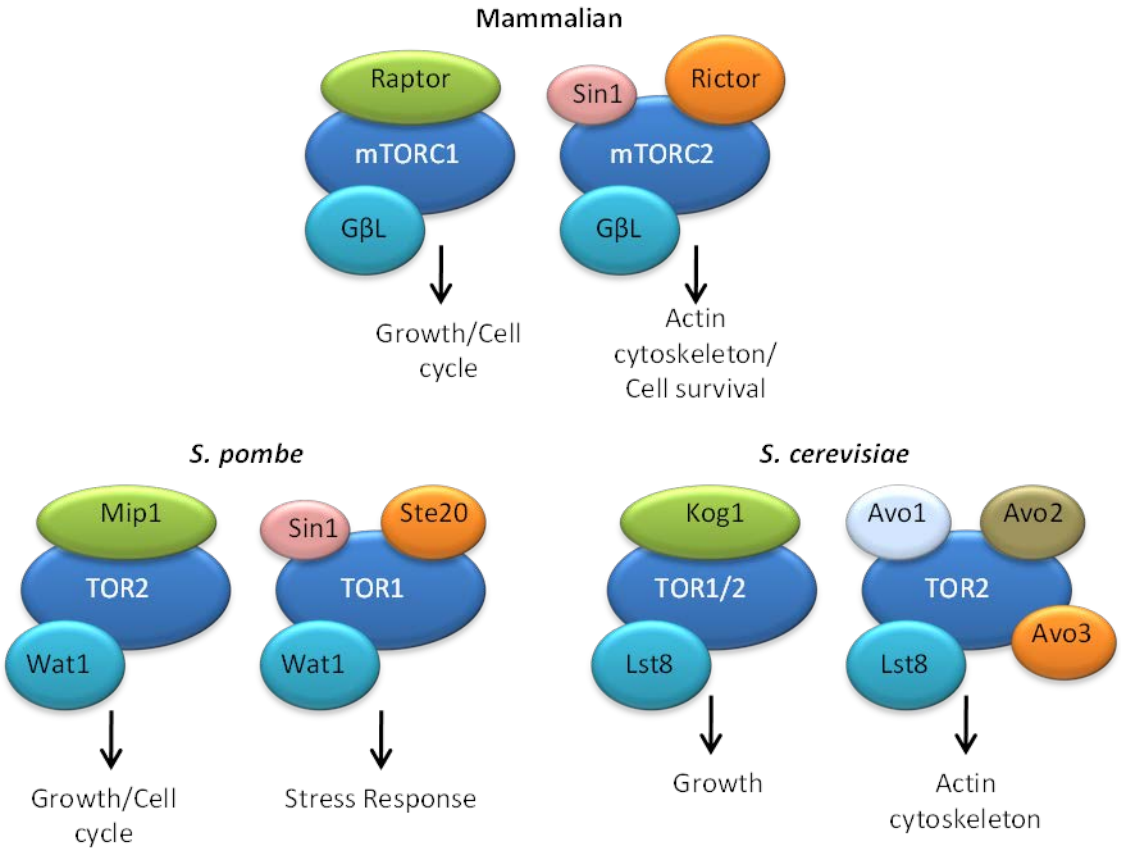


**Figure 1.12: Conservation of TOR complex components between mammalian, *S. cerevisiae* and *S. pombe* cells.** TOR complexes are highly conserved between mammalian and yeast cells. Homology of key complex components including GβL/Lst8/Wat1 and Raptor/Kog1/Mip is indicated by colour.

In *S. cerevisiae* the TOR complex 1 (TORC1) comprises of either Tor1p or Tor2p along with Kog1p, Lst8p and Tco89p and is sensitive to the drug rapamycin. Conversely TOR complex 2 (TORC2) is insensitive to rapamycin and comprises of TOR2 accompanied by Avo1p, Avo2p, Lst8p, Bit61p, Slm2p, Slm1p and Tsc11p (Loewith *et al.* 2002). In budding yeast the regulatory mechanisms upstream of TORC1 are not as well described as the downstream effects. In favourable conditions with a plentiful nutrient supply, TOR1 inhibits transcriptional activators involved in a range of processes including the retrograde response (Rtg1, Rtg3) and stress response (Msn2p, Msn4p) (Crespo JL. *et al.* 2002) by sequestering them within the cytoplasm. Simultaneously, activation of transcription factors with roles in the biogenesis of ribosomes (Spf1, Flh1) is initiated (Bandhakavi *et al.* 2008). Conversely, under conditions of nitrogen starvation TOR1 activity is inhibited resulting in the elevated activity of such transcriptional activators (Rødkær and Færgeman 2014). As mTORC1 activates S6Ks in mammalian cells, TOR1 has been found to directly

phosphorylate *S. cerevisiae* Sch9, a regulator of translation initiation and ribosome biogenesis (Urban *et al.* 2007b).

Analysis of TOR in fission yeast remained largely incomplete until approximately 2009, which is remarkable as fission yeast have been found to be more highly conserved to mammalian systems in aspects such as cell cycle regulation and response to stress (Cromie and Smith 2008, Papadakis and Workman 2004). In *S. pombe* there are also two distinct TOR homologues, Tor1 and Tor2. However, it is important to note that budding and fission yeast TOR complexes are numbered in opposing ways. The equivalent to budding yeast TORC1 is therefore TORC2 in *S. pombe* and *S. cerevisiae* TORC2 is analogous to the fission yeast TORC1 complex.

*S. pombe* TORC2 consists of Tor1, Ste20, Wat1, Bit61 and Sin1. TORC1 is comprised of Tor2, Wat1, Mip1, Toc1 and Tco89 (Otsubo and Yamamato 2008). Interestingly it was found, in contravention with budding yeast and mammalian systems, that rapamycin treatment did not arrest growth in fission yeast but rather inhibited sexual development (Weisman 2004). Regardless, it has been shown that both fission yeast TOR complexes contain a conserved domain which could interact with FKBP12-rapamycin (Kawai *et al.* 2001, Weisman *et al.* 2001). Further to this it is reported that amino acid uptake, which is dependent on Tor1 is rapamycin sensitive, being rescued with replacement of wild type *tor1* containing a defective rapamycin binding allele. (Weisman *et al.* 2005)

Upstream of the TOR complexes in fission yeast, functional orthologues of mammalian Rheb as well as orthologues of Tsc1/2 components regulate Tor2 activation (Yang W. *et al.* 2001). However, very few direct targets of fission yeast TOR complexes have been elucidated. It is known that Tor1 directly regulates the AGC kinase, Gad8, by phosphorylation (Du *et al.* 2012). Direct downstream targets of Tor2 include the AGC kinase orthologue, Psk1 which is required for phosphorylation of ribosomal protein S6 (Nakashima *et al.* 2012a). Along with this potential interactions with other AGC kinases Sck1/2 have also been noted (Nakashima *et al.* 2012a), thus showing conserved mechanisms between mammalian and *S. pombe* mediated TOR signalling events.

### 1.6.2 MAPK pathways in the budding yeast S. cerevisiae

In *S. cerevisiae* five MAP Kinase pathways have been identified. Four of the MAPK pathways present, filamentation-invasion, mating-pheromone response, cell wall integrity and high osmolarity growth have been well characterised (Figure 1.13), with the fifth believed to hold roles in spore wall assembly (Chen R. and Thorner 2007).

#### 1.6.2.1 Invasive growth and pheromone response MAPK pathways

The invasive growth and pheromone response pathways of *S. cerevisiae* are activated by common MAPKKKs and MAPKKs Ste11 and Ste7. The invasive growth pathway is stimulated in response to nutrient limitation in haploid cells (Bauer F. and Pretorius 2002) resulting in activation of Ras2p. The MAP kinase of this cascade is Kss1p, which is activated via phosphorylation by the MAPKK Ste7p. This phosphorylation then results in activation of the transcription factors Tec1p-Ste12p to control cell adhesion and induce expression of target genes including and *MUC1* which is a glycoprotein required for invasive growth (Chen R. and Thorner 2007).

The pheromone response pathway mediates cellular response to mating pheromones. Stimulation by pheromones results in activation of Fus3 via the MAPKK Ste7. Once activated Fus3 regulates mating specific genes through Ste12 transcription factor activation (Chou *et al.* 2006).

#### 1.6.2.2 Cell wall integrity pathway

Activation of the cell wall integrity pathway occurs via Wsc1, Wsc2, Wsc3, Mid2 and Mtl1 cell surface sensors. Once activated nucleotide exchange on the Rho1 G-protein is stimulated (Levin 2005). Rho1 in its GTP bound state activates Pkc1 which then activates the MAKKK Bck1 which phosphorylates Mkk1/2 MAPKKs (Levin 2005). Downstream of the MAPK Mpk1 transcriptional responses are facilitated via Swi4/6, also known as the SBF complex, and Rlm1 which regulates the expression of genes involved in cell wall biogenesis (Jung *et al.* 2002, Truman *et al.* 2009). Additionally transcription factors Hsf1, Skn7 and Msn2/4 are also regulated downstream of Mpk1 mediating responses to cell wall stress (Garcia *et al.* 2004, Jung and Levin 1999, Li S. *et al.* 1998).

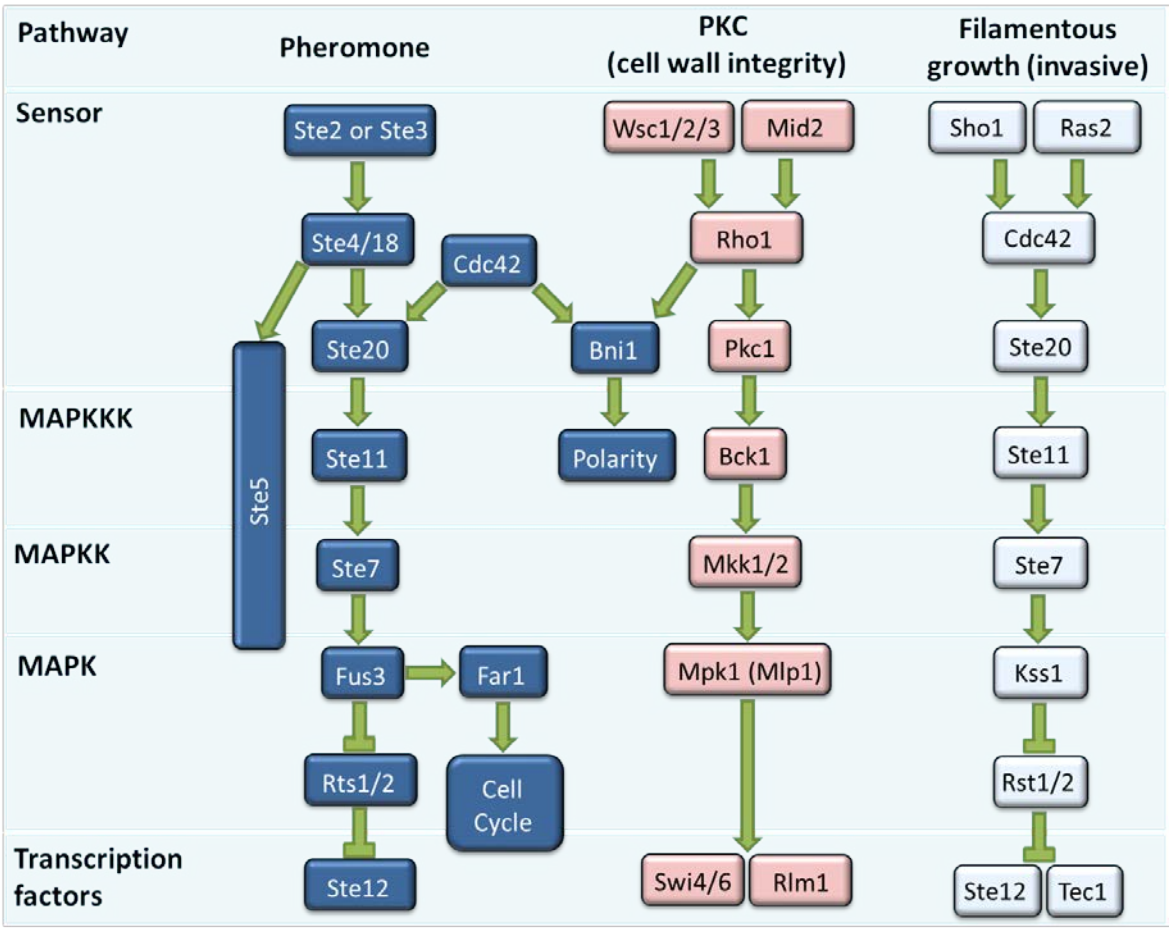


**Figure 1.13: MAP Kinase signalling pathways in the budding yeast *S. cerevisiae.*** **A:** Pheromone response pathway mediates cellular response to mating pheromones for activation of mating specific genes via the MAPK Fus3 **B:** Filamentous growth pathway controls cell adhesion and invasive growth via its MAPK Kss1 **C:** Cell wall integrity pathway MAPK Mpk1, regulates the expression of genes involved in cell wall biogenesis via transcription factors such as Swi4/6. Adapted from Thomas and Limper (2007).

### 1.6.3 MAPK pathways in the fission yeast S. pombe

In the fission yeast *S. pombe* three distinct MAP Kinase pathways have been identified: the pheromone pathway, the stress response pathway and the cellular integrity pathway, (Figure 1.14).

The pheromone MAPK cascade has two pheromone receptors encoded by Mam2 and Map3. When pheromones are bound, Ras1 activates the MAPK module which comprises Byr2, Byr1 and the MAPK Spk1 (Tamanoi 2011). Activated Spk1 is responsible for regulation of conjugation and sporulation and triggers sexual differentiation via activation of the transcription factor Ste11 (Kim Lila *et al.* 2012).

The cell integrity pathway in *S. pombe* serves to regulate processes including construction and maintenance of the cell wall, morphogenesis and cytokinesis. The cascade comprises the MAPKKK Mkh1, MAPKK Pek1 and MAPK Pmk1 (Madrid *et al.* 2006). A major downstream target of Pmk1 includes the transcription factor Atf1, which is phosphorylated by Pmk1 under cell wall damage (Takada *et al.* 2007).

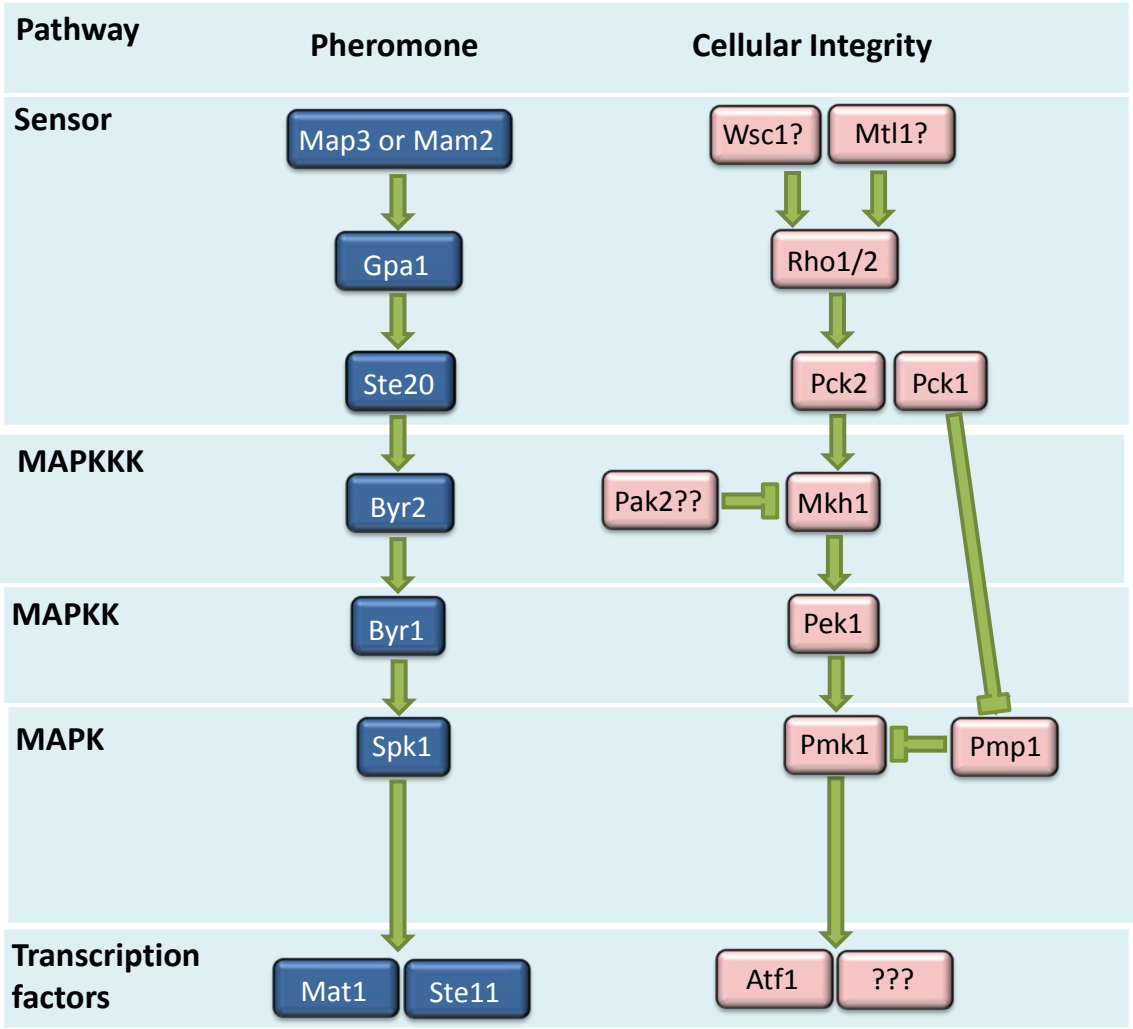


**Figure 1.14: *S. pombe* MAPK pathways. A:** The pheromone response pathway is activated when pheromone signals are received. The activation is relayed to the MAPKKK Byr2 by the upstream Ste20 Kinase, which then phosphorylates the MAPKK Byr1. Phosphorylated Byr1 then phosphorylates the MAPK Spk1. Spk1 modulates the expression of transcription factors including Ste11 and Mat1 to regulate sexual differentiation, conjugation and sporulation. **B:** The Cellular integrity pathway is activated under conditions of cell wall stress, little is known concerning the targets of this pathway that are related to cell wall biogenesis. It is known that Pmk1 can phosphorylate Atf1, which is a common transcription factor with the stress activated protein kinase pathway of *S. pombe.*

### 1.6.4 Mammalian p38 MAPK orthologues in yeast

As demonstrated in the previous section, MAPK pathways in *S. cerevisiae* and *S. pombe* are composed of a three kinase module that is conserved in MAPK cascades of mammalian cells. Mammalian p38 MAPK pathways are structurally and functionally conserved in yeast via Hog1 (*S. cerevisiae)* and Sty1 (*S. pombe*) stress response pathways (Banuett 1998), (Figure 1.15).

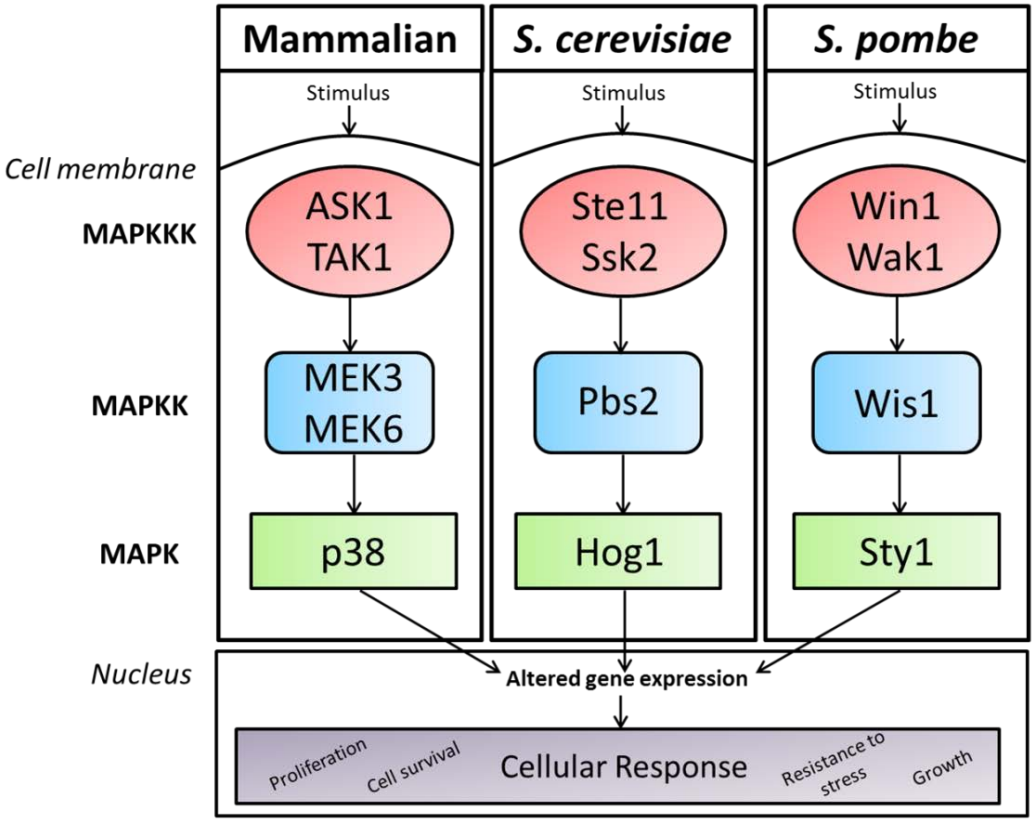


**Figure 1.15: Conservation of eukaryotic p38 pathways.** The MAPK pathways of mammalian and yeast cells are highly structurally and functionally conserved. Left: mammalian p38 MAP Kinase pathway. Centre: *S. cerevisiae* HOG pathway. Right: *S. pombe* Sty1 pathway.

### 1.6.4.1 The high osmolarity glycerol (HOG) pathway in S. cerevisiae

The HOG pathway of *S. cerevisiae* is activated in response to high osmolarity, citric acid and pH (Kapteyn *et al.* 2001, Lawrence C. L. *et al.* 2004, Saito and Posas 2012). Upon activation an adaptive response of cells is mounted. Responses include transient cell cycle arrest and global readjustment of the expression of genes (Saito and Posas 2012).

As demonstrated by Figure 1.16, the HOG cascade can be activated via two distinct branches, Sln1 and Sho1, both of which converge to a common MAPKK, Pbs2 (O'Rourke *et al.* 2002).

The Sln1 branch is controlled via a phosphorelay system comprising the Sln1 membrane sensor, and proteins Ypd1 and Ssk1 (Kaserer *et al.* 2009). After autophosphorylation of Sln1 in iso-osmotic conditions, Ypd1 is phosphorylated which then subsequently phosphorylates Ssk1 (Chen Ming-Tang and Weiss 2005). The phosphorylated form of Ssk1 is unable to bind MAPKKKs Ssk2 and Ssk22. Once under conditions of hyperosmotic stress Ssk1 is dephosphorylated and binds Ssk2/Ssk22 leading to autophosphorylation and in turn phosphorylation of the MAPKK Pbs2 (Horie *et al.* 2008).

The Sho1 branch is controlled by two transmembrane sensors, Hkr1 and Msb2 which are stimulated under hyperosmotic shock (Tatebayashi *et al.* 2007). Stimulation of the transmembrane sensors promotes Cla4 and Ste20 to bind Cdc42, a membrane bound G-protein, and become activated. This activation results in phosphorylation of the MAPKKK Ste11, which goes on to activate the MAPKK Pbs2 via phosphorylation (Lamson *et al.* 2002).

Once Pbs2 is active, it goes on to activate the MAPK Hog1 by dual phosphorylation of residues which are common to other MAPKs, Thr174 and Ty176 (Maayan *et al.* 2012). Under non-stressed conditions Hog1 is distributed evenly between the nucleus and cytoplasm. Rapid accumulation of Hog1 in the nucleus is observed under conditions of hyperosmotic stress allowing Hog1 to control gene expression via DNA binding proteins including Msn2/4 and Hot1 (Alepuz *et al.* 2001).

Hog1 can also control transcriptional initiation via direct phosphorylation; however phosphorylation is not essential for regulating transcription factors which include Hot1. In

this case Hog1 can interact with RNA Polymerase II and other transcriptional machinery components recruiting them to the coding regions of genes (Alepuz *et al.* 2003).

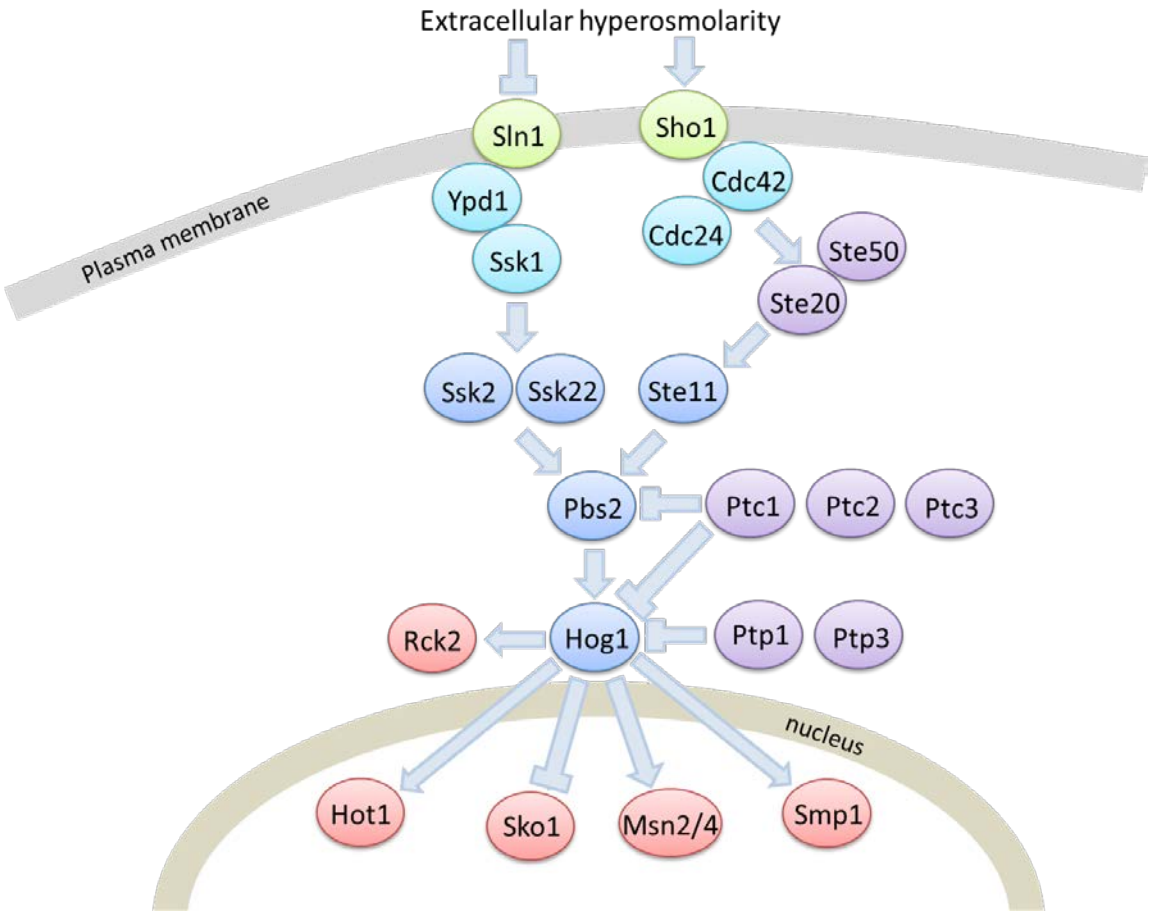


**Figure 1.16: The Hog MAPK pathway of *S. cerevisiae.*** The stress activated protein kinase pathway in *S. cerevisiae* is activated by external stresses, including osmotic stress. There are two distinct branches of this pathway that converge at the point of the common MAPKK Pbs2. Active Pbs2 phosphorylates Hog1 on conserved tyrosine and threonine residues. Hog1 is then able to translocate to the nucleus and activate transcription factors, including Msn2/4 and Hot1, to drive expression of stress responsive genes. Hog1 activity is downregulated by the activity of phosphatases to prevent lethality caused by overexpression of Hog1.

Due to the inhibitory effect of Hog1 on progression of the cell cycle, constitutive activation of Hog1 is lethal to *S. cerevisiae* cells (Clotet and Posas 2007). Hog1 kinase activity is controlled, in part, by dephosphorylation of the phosphorylated threonine 174 and threonine 176 residues. This is controlled by tyrosine phosphatases Ptp2 and Ptp3 along with serine/threonine phosphatases Ptc1, Ptc2 and Ptc3 (Warmka *et al.* 2001, Wurgler-Murphy *et al.* 1997). Ptp2 dephosphorylates tyrosine in the nucleus whereas Ptp3 dephosphorylates tyrosine in the cytoplasm (Mattison and Ota 2000, Wurgler-Murphy *et al.* 1997). The serine/threonine phosphatases dephosphorylate the threonine residue with Ptc1 holding the greatest role over Ptc2 and Ptc3 (Warmka *et al.* 2001).

Phosphorylated Hog1p can also phosphorylate upstream targets such as Ste50 in order to down-regulate the HOG cascade (Hao *et al.* 2008). Phosphorylation of Ste50 acts as a negative feedback loop by reducing the affinity of Ste50 to interact with Opy2, which is required for Hog1 activation (Yamamoto *et al.* 2010).

#### 1.6.4.2 Sty1 stress response pathway in S. pombe

The Sty1 MAPK pathway is also activated in response to a range of external stressors including heat stress, oxidative stress, osmotic stress and nutrient stress. Sty1p is activated on the conserved tyrosine and threonine residues by Wis1 (MAPKK), which is activated by upstream Wis4 and Win1 (MAPKKK) (Figure 1.17) (Zhou *et al.* 2010).

Under moderate oxidative stress conditions Sty1 is regulated by Mak2 and Mak3 histidine kinases, along with Mpr1 and Mcs4 (Quinn *et al.* 2002). Under high oxidative stress Sty1 activation is independent of Mak2/3 (Quinn *et al.* 2002). As with the Hog1p, overexpression of Sty1p is lethal to *S. pombe* cells, as such, the dual phosphatases Pyp1 and Pyp2 are key regulators in Sty1p dephosphorylation (Shiozaki and Russell 1996).

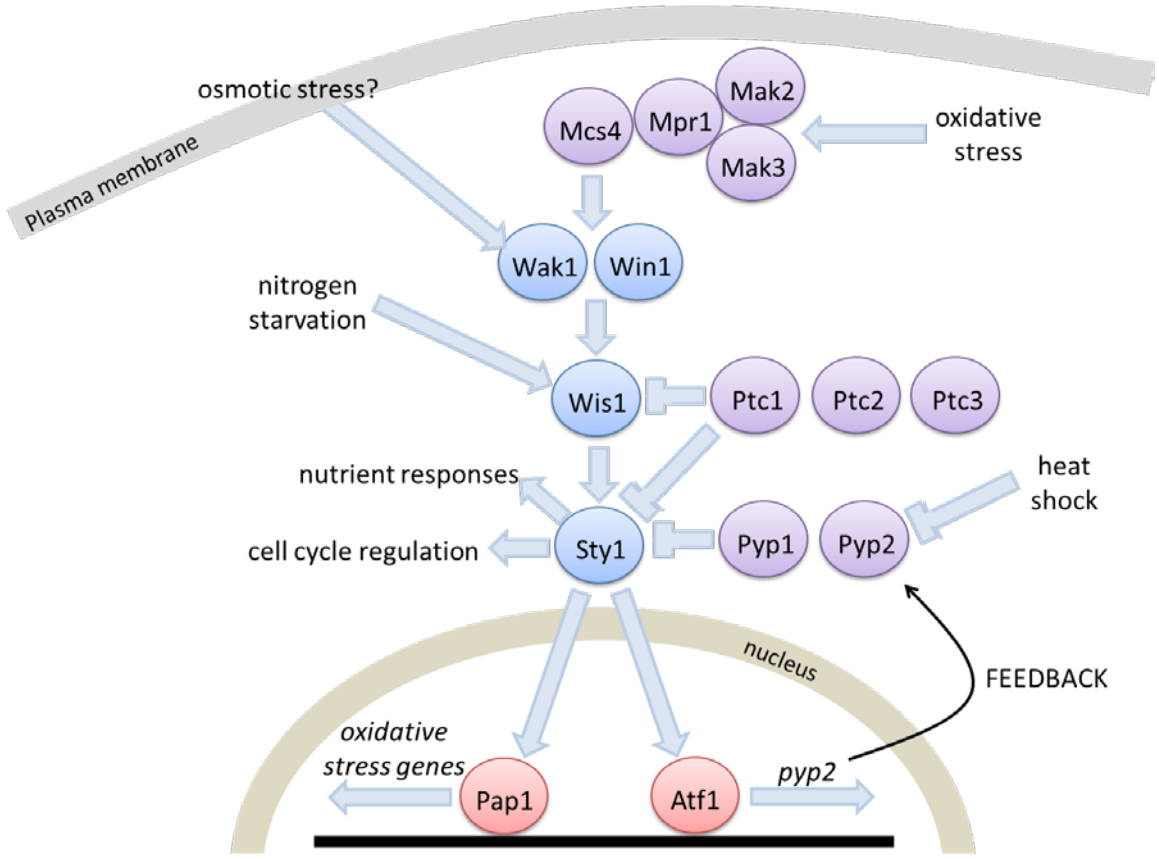


**Figure 1.17: The Sty MAPK pathway of *S. pombe*.** The stress activated protein kinase pathway in *S. pombe* is activated by external stresses including oxidative and osmotic stress. After activation of MAPKKKs the pathway converges at the common MAPKK Wis1. Active Wis1 phosphorylates Sty1 on conserved tyrosine and threonine residues. Sty1 is then able to translocate to the nucleus and activate transcription factors, including Aft1 and Pap1, to drive expression of stress responsive genes.

Downstream of Sty1 the regulation of genes in response to stress occurs via Atf1p, a bZIP transcription factor. Although not critical for its function, Atf1 is phosphorylated and stabilised by Sty1 (Lawrence C.L. *et al.* 2007). Atf1 is important in the cellular response to high oxidative stress, whereas activation of the transcription factor Pap1 is required under conditions of low oxidative stress (Chen D. *et al.* 2008).

### 1.6.5 Lipid synthesis in yeast

As with MAPK signalling, the regulation of lipid metabolism is very well conserved from humans to yeast. *S. cerevisiae* has proved the model of choice in understanding regulatory mechanisms underlying lipid metabolism over the last decade (Henry *et al.* 2012).

*S. cerevisiae* cells synthesise the same general classes of lipids found in higher eukaryotic cells and furthermore the synthesis is via pathways with high structural homology to that of mammalian systems (Figure 1.18). Although largely conserved there are some slight differences in both lipid composition and biosynthetic routes, including the fact the yeast synthesis ergosterol rather than cholesterol and have simpler fatty acid compositions (van Meer *et al.* 2008). For polar lipids the route of phospholipid synthesis also differs slightly to that of mammalian cells (Carman and Henry 2007).

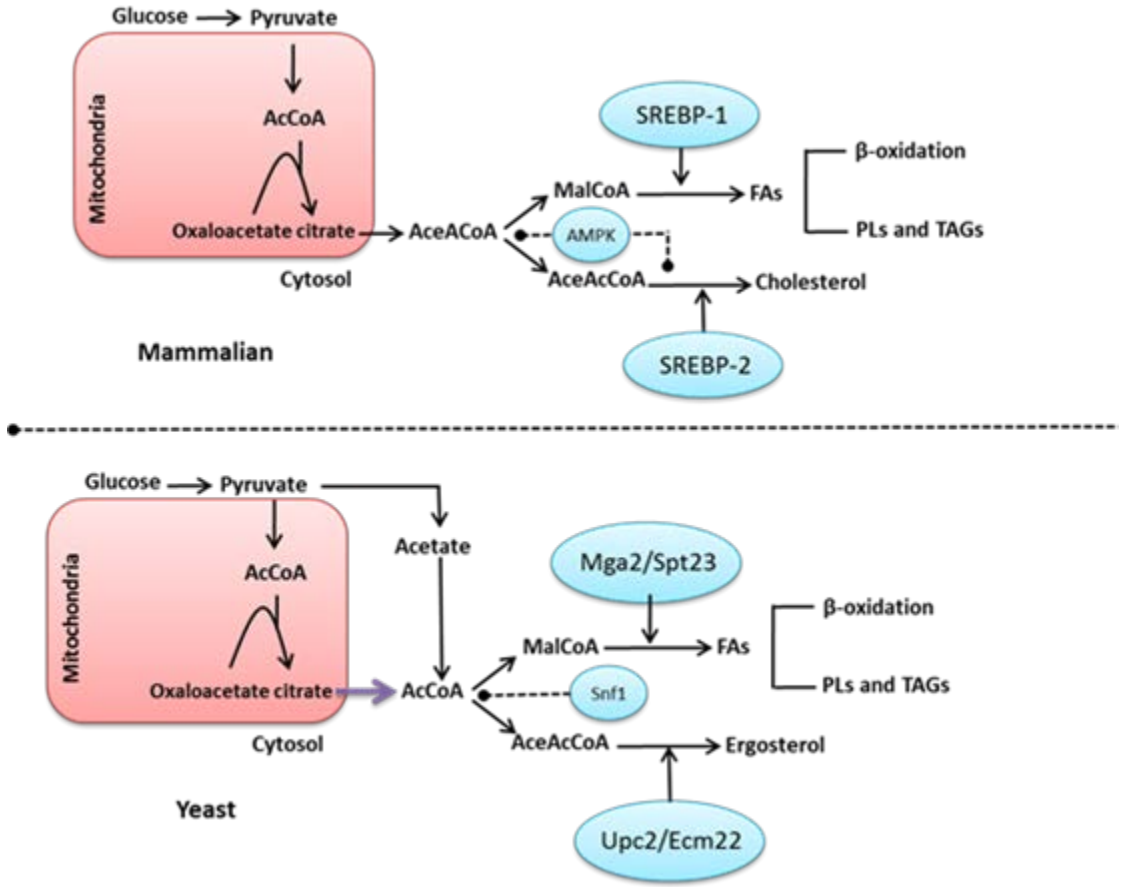


**Figure 1.18: Conservation of the mechanisms of lipid synthesis between mammalian and yeast cells.** Lipids are synthesised via conserved mechanisms in mammalian and yeast cells. AcetylCoA (AcCoA) is converted to malonyl CoA (MalCoA) via a different mechanism and yeast synthesise ergosterol instead of cholesterol. However the regulation downstream from this including the synthesis of fatty via SREBP like proteins and β-oxidation are largely conserved. Furthermore, oleaginous yeast species, such as *L. starkeyi,* have the ability to convert citrate to AcCoA (indicated by the purple arrow) due to the presence of ATP citrate lyase activity. Adapted from Nielsen (2009).

#### 1.6.5.1 Neutral lipids

As with mammalian systems, synthesis of TAGs in yeast can occur via the glycerol-3-phosphate pathway. In *S. cerevisiae,* analogous to that of mammals, glycerol-3-phosphate is acylated by G3P acyltransferase (*SCT1*) forming LPA which is then acylated by LPA acyltransferase (*SLC1*) to yield PA. PA is then dephosphorylated by PA phosphohydrolase (PAP) releasing DAG. In the terminal step of TAG synthesis DAG is acylated by either DAG acyltransferase (*DGA1*) or alternatively by phospholipid DAG acyltransferase (*LRO1*) (Beopoulos *et al.* 2008).

#### 1.6.5.2 Phospholipids

Yeast synthesise phospholipids via both the Kennedy pathway and CDP-DAG pathway described earlier in Section 1.4.4, which are principally identical to mammalian pathways. The Kennedy pathway is the dominant route for both PE and PC synthesis in mammalian cells, whereas the CDP-DAG pathway is the dominant route for synthesis in *S. cerevisiae.* However, the components and routes involved for synthesis via each pathway are largely conserved (Dowd *et al.* 2001).

With respect to PS synthesis, in mammalian cells this occurs via base-exchange facilitated by PSS1 and PSS2 which replace the head groups of PE and PC respectively with L-serine. In contrast yeast Cho1 facilitates the addition of L-serine to CPD-DAG to form PS (Vance and Tasseva 2013).

At the transcriptional level regarding SREBP proteins, although no orthologues exist in *S. cerevisiae* the proteins Upc2 and Ecm22 are considered functional orthologues. Additionally two further SREBP like proteins in *S. cerevisiae,* Spt23 and Mga2 have been identified to have roles in regulating fatty acid synthesis (Nielsen 2009). Conversely *S. pombe* contains orthologues to mammalian SREBP-1a (Sre1 and Sre2) as well as mammalian SCAP (Scp1) (Bien and Espenshade 2010). Some other key lipid regulatory elements conserved between all three systems are listed in Table 1.2.

In comparison to the plethora of information available regarding *S. cerevisiae* lipid metabolism, very little work has been done to date in the regulation of lipid metabolism in the fission yeast species *S. pombe* (Yazawa *et al.* 2012). However, *S. pombe* is becoming

increasingly investigated as a biotechnologically relevant yeast species due to valuable lipid products that it is able to produce, such as oleic acid, a ricinoleic acid precursor (Yazawa *et al.* 2012). Furthermore, phosphatidylinositol (3,4,5)-triphosphate has not yet been identified in *S. cerevisiae* but has been detected in *S. pombe*. Also *S. pombe* has, as mentioned previously, been demonstrated to confer greater similarity to mammalian systems in aspects of the stress response and cell cycle regulatory mechanisms than *S. cerevisiae*, as such greater insight may be yielded from the study of lipid metabolism in *S. pombe*.

**Table 1.2: Key energy/lipid regulatory components conserved between mammalian and yeast cells.** Key regulatory elements in mammalian and yeast cells for energy production and the synthesis of lipids have homologues in both *S. cerevisiae* and *S. pombe* yeast species.

| Mammalian | *S. cerevisiae* | *S. pombe* | Role |
|---|---|---|---|
| DGAT | Dga1 | Dga1 | Catalyses terminal step of TAG synthesis. |
| PDAT | Lro1 | Plh1 | TAG synthesis |
| SREBPs | Upc2/Ecm22<br>SPt23/Mga2 | Sre1/Sre2 | Cholesterol/Ergosterol synthesis<br>Fatty acid synthesis |
| FASN | FAS | Fas1/2 | Catalyses fatty acid synthesis |
| AMPK | Snf1 | Ssp2 | Cellular energy homesostasis |
| PSS1 | Cho1 | Pps1 | Phosphatidylserine synthase |

The oleaginous yeast species *Lipomyces starkeyi* (*L. starkeyi*) is a prominent yeast species employed in the biotechnology industry for lipid production. It is extensively employed for lipid production as it has the ability to accumulate up to 70% of its dry cell mass as lipid, in comparison *S. cerevisiae* is only able to accumulate approximately 11% of its cell mass as lipids. Although little is known on the regulatory mechanisms governing lipid metabolism in this non-conventional yeast species, coupled with a lack of molecular tools available for its genetic manipulation, it is expected that they will be largely conserved to that of *S. cerevisiae* and *S. pombe,* as detailed in Table 1.2. Additionally oleaginous

yeasts, in agreement with mammalian cells, contain ATP: citrate lyase activity, and so the synthesis of lipids may be more similar to that observed in mammalian cells. As such, oleaginous yeast species, such as *L. starkeyi,* may prove to be valuable metabolic models in deconstructing the regulatory mechanisms involved in lipogenesis. The usefulness of non-conventional yeasts to study human disease has been demonstrated by the employment of *Yarrowia lipolytica* (*Y. lipolytica*), which has been utilised to investigate mitochondrial disorders (Kerscher *et al.* 2004).

## 1.7 Aims

In the last decade, lipid metabolism regulatory pathways have been under intense investigation with respect to human disease research. The mTOR pathway has already been identified as a major player in promoting lipid metabolism in cancer by elevation of SREBP-1 activity.

The aim of this thesis is to study the regulation of lipogenesis and to elucidate whether the p38 MAP kinase pathway of eukaryotes is involved in the regulation of cellular lipid homeostasis. *Saccharomyces cerevisiae* and *Schizosaccharomyces pombe* are ideal model organisms in which to study the regulation of lipid accumulation. Due to the similarity of major signalling pathways including p38 MAP Kinase, with the Hog1 and Sty1 pathways in yeast, coupled with conservation of the regulation of lipid metabolism, it is hoped that yeast will help further knowledge of the regulation of lipid accumulation accompanying solid tumours. A further aim was to develop the oleaginous yeast species *L. starkeyi* as a complementary model organism for investigating the regulation of lipid accumulation.

Chapter 3 describes the development of suitable methodology for determination of lipid accumulation profiles and lipid quantitation in oleaginous and non-oleaginous budding and fission yeast species. Chapter 4 studies the involvement of the Hog1 and Sty1 MAP kinase signal transduction pathways in the regulation of lipid accumulation. Finally, chapter 5 assesses the suitability of utilising the oleaginous yeast species *L. starkeyi* as a potential model organism which could subsequently be used as a metabolic model for cancer.

Data within this thesis describes how the regulation of lipid accumulation is impacted through the deletion of components within the MAP Kinase pathway. The influence of MAPK mediated signalling events on lipogenesis may allow further insight not only into the regulation of lipid metabolism, but also anti-lipogenic targets which may be modulated in the treatment of highly lipogenic tumour types.

# Chapter II Materials and Methods

# 2. Materials and methods

## 2.1 Yeast strains

Details of the yeast species and strains utilised are detailed in Table 2.1.

All strains were maintained on agar plates, either yeast extract peptone dextrose (YPD) (*S. cerevisiae*) or yeast extract sucrose (YES) (*S. pombe*), containing 2% agar. Antibiotics were added to agar as appropriate (100 µg/ml G418 from 1000x stock in water). For genes deleted by incorporation of sequences encoding amino acids, strains were maintained on defined medium agar plates, either yeast nitrogen base (YNB) (*S. cerevisiae*) or Edinburgh minimal medium (EMM) (*S. pombe*) lacking the appropriate amino acids. See Section 2.1.1 for media composition.

**Table 2.1: Yeast species and strains utilised in the present study.** Strain information for wild type and deletion (Δ) yeast species and strains used in the present study. NBRP: National BioResource Project (Japan). Euroscarf: European *Saccharomyces cerevisiae* Archive for Functional Analysis (Germany).

| Yeast species | Strain | Genotype | Reference |
|---|---|---|---|
| *S. cerevisiae* wild type | BY4741a (derivative of S288C) | *MAT*a *his3*Δ1 *leu2*Δ0 *met15*Δ0 *ura3*Δ0 | Brachmann *et al.* (1998) |
| *S. pombe* wild type | NJ1 | *h⁺ura4-D18 leu1-32 ade6-M210 his7-366* | Lawrence *et al.* (2007) |
| *S. pombe* wild type | NJ2 | *h⁻ura4-D18 leu1-32 ade6-M210 his7-366* | Lawrence *et al.* (2007) |
| *L. starkeyi* wild type | NCYC2710 | No details available. | Lodder & Kreger-van Rij (1952) |
| *S. cerevisiae hog1Δ* | BY23209 | MATα *hog1::URA3 leu2 his3 trp1 ura3* | NBRP of the MEXT, Japan |
| *S. cerevisiae msn2/4Δ* | BYP23752 | MATa *msn2::HIS3 msn4::URA3 ade2-1 his3-11,15 leu2-3,112 trp1-1 ura3-1 can1-100* | NBRP of the MEXT, Japan |
| *S. cerevisiae sho1Δ* | Y06116 | BY4741; MATa; *his3Δ1; leu2Δ0; met15Δ0; ura3Δ0; sho1::kanMX4* | Euroscarf, Germany |
| *S. cerevisiae fat1Δ* | BYP5648 | MATa *fat1::HIS3 ade2-1 leu2-1,112 ura3-1 trp1-1 his3-11,15 can1-100 ssd1-d2 rad3-535* | NBRP of the MEXT, Japan |
| *S. cerevisiae tor1Δ* | Y06864 | BY4741; MATa; *his3Δ1; leu2Δ0; met15Δ0; ura3Δ0; tor1::kanMX4* | Euroscarf |

| | | | |
|---|---|---|---|
| *S. cerevisiae pbs2Δ* | Y07101 | BY4741; MATa; *his3Δ1; leu2Δ0; met15Δ0; ura3Δ0; pbs2::kanMX4* | Euroscarf |
| *S. cerevisiae dga1Δ* | Y02501 | BY4741; MATa; *his3Δ1; leu2Δ0; met15Δ0; ura3Δ0; dga1::kanMX4* | Euroscarf |
| *S. cerevisiae ste11Δ* | Y05271 | BY4741; MATa; *his3Δ1; leu2Δ0; met15Δ0; ura3Δ0; ste11::kanMX4* | Euroscarf |
| *S. cerevisiae lro1Δ* | Y05383 | BY4741; MATa; *his3Δ1; leu2Δ0; met15Δ0; ura3Δ0; lro1::kanMX4* | Euroscarf |
| *S. cerevisiae tco89Δ* | Y02072 | BY4741; MATa; *his3Δ1; leu2Δ0; met15Δ0; ura3Δ0; tco89::kanMX4* | Euroscarf |
| *S. cerevisiae hot1Δ* | Y06957 | BY4741; MATa; *his3Δ1; leu2Δ0; met15Δ0; ura3Δ0YMR172w::kanMX4* | Euroscarf |
| *S. cerevisiae ecm22Δ* | Y05137 | BY4741; MATa; *his3Δ1; leu2Δ0; met15Δ0; ura3Δ0YLR228c::kanMX4* | Euroscarf |
| *S. cerevisiae upc2Δ* | Y03572 | BY4741; MATa; *his3Δ1; leu2Δ0; met15Δ0; ura3Δ0YDR213w::kanMX4* | Euroscarf |
| *S. cerevisiae spt23Δ* | Y04869 | BY4741; MATa; *his3Δ1; leu2Δ0; met15Δ0; ura3Δ0; YKL020c::kanMX4* | Euroscarf |
| *S. cerevisiae mga2Δ* | Y05968 | BY4741; MATa; *his3Δ1; leu2Δ0; met15Δ0; ura3Δ0; YIR033w::kanMX4* | Euroscarf |
| *S. cerevisiae pip2Δ* | Y01660 | BY4741; MATa; *his3Δ1; leu2Δ0; met15Δ0; ura3Δ0; YOR363c::kanMX4* | Euroscarf |
| *S. cerevisiae oaf1Δ* | Y00355 | BY4741; MATa; *his3Δ1; leu2Δ0; met15Δ0; ura3Δ0*; *YAL051w::kanMX4* | Euroscarf |
| *S. cerevisiae fld1Δ* | Y05313 | BY4741; MATa; *his3Δ1; leu2Δ0; met15Δ0; ura3Δ0*; *YLR404w::kanMX4* | Euroscarf |
| *S. cerevisiae ino2Δ* | Y04057 | BY4741; MATa; *his3Δ1; leu2Δ0; met15Δ0; ura3Δ0*; *YDR123c::kanMX4* | Euroscarf |
| *S. cerevisiae ino4Δ* | Y06258 | BY4741; MATa; *his3Δ1; leu2Δ0; met15Δ0; ura3Δ0*; *YOL108c::kanMX4* | Euroscarf |
| *S. cerevisiae opi1Δ* | Y00943 | BY4741; MATa; *his3Δ1; leu2Δ0; met15Δ0; ura3Δ0*;; *YHL020c::kanMX4* | Euroscarf |
| *S. cerevisiae avo2Δ* | Y06201 | BY4741; MATa; *his3Δ1; leu2Δ0; met15Δ0; ura3Δ0*; *YMR068w::kanMX4* | Euroscarf |
| *S. cerevisiae* W303 wild type | W303-1a | *MATa ade2-1 leu2-3,112 his3-1 ura3-52 trp1-100 can1-100* | J. Rine |
| *S. cerevisiae ecm22Δ* | JRY7180 | W303-1a *ecm22Δ::TRP1* | J. Rine |
| *S. cerevisiae* | JRY7181 | W303-1a *ecm22Δ::TRP1 upc2Δ::HIS3* | J. Rine |

| | | | |
|---|---|---|---|
| *ecm22Δupc2Δ* | | | |
| *S. pombe wis1Δ* | FY19955 | h- *leu1 ura4 wis1::his7+ spc1-12myc-ura4+* | NBRP of the MEXT, Japan |
| *S. pombe sty1Δ* | FY19932 | h- *leu1 ura4 spc1::ura4+* | NBRP of the MEXT, Japan |
| *S. pombe* sty1 kinase dead | FY20578 | h- LU *spc1*-kinaseDead | NBRP of the MEXT, Japan |
| *S. pombe pap1Δ* | FY9748 | h- *leu1 ura4 pap1::ura4+* | NBRP of the MEXT, Japan |
| *S. pombe atf1Δ* | FY13438 | h- *ade6-M216 leu1 ura4-D18 gad7::ura4+* | NBRP of the MEXT, Japan |
| *S. pombe ptl3Δ* | BG_H1649 | *ptl3Δ:*kanMX4 *ade6*-M210 *URA4*-d18 *leu1*-32 | Bioneer corporation |
| *S. pombe dga1Δ* | BG_H4437 | *dga1Δ:*kanMX4 *ade6*-M210 *URA4*-d18 *leu1*-32 | Bioneer corporation |
| *S. pombe sre1Δ* | ----- | h⁻, his3-Δ1,leu1-32, ura4 Δ 18, ade6-M210; sre1::KanMX6 | P. Epenshade 2005 |
| *S. pombe sre2Δ* | ------- | h⁻, his3-Δ1,leu1-32, ura4 Δ 18, ade6-M210; sre2::KanMX6 | P. Epenshade 2005 |
| *S. pombe scp1Δ* | ------- | h⁻, his3-Δ1,leu1-32, ura4 Δ 18, ade6-M210; scp1::KanMX6 | P. Epenshade 2005 |

### 2.1.1 Growth Media

All growth media, including agar for strain maintenance, were prepared in distilled water before autoclaving for 15 minutes at 121 $^{o}$C and 15 pounds per square inch (psi) of pressure. Unless otherwise stated all strains were cultured in an orbital shaking incubator at 30 $^{o}$C, duplicate.

*Lipomyces starkeyi* (*L. starkeyi*), *Saccharomyces cerevisiae* (*S. cerevisiae*) and *Schizosaccharomyces pombe* (*S. pombe*) strains utilised in this study, listed in Table 2.1, were pre-cultured in appropriate complex media. Either YPD [2% glucose, 1% peptone, 1% yeast extract] (*S. cerevisiae* and *L. starkeyi*) or YES [3% glucose, 0.5% yeast extract, 0.005% amino acids leucine, lysine, adenine, histidine and uracil] (*S. pombe*) (ForMedium™, UK) were used.

Limiting growth media were prepared according to Rolph, Moreton and Harwood (1989). Nitrogen limiting media (NLM) contained: 0.7% $KH_2PO_4$, 0.2% $Na_2HPO_4$, 0.15%

$MgSO_4.7H_2O$, 0.01% $CaCl_2.2H_2O$, 0.0008% $FeCl_3.6H_2O$, 0.0001% $ZnSO_4.7H_2O$ 0.15% yeast extract, 0.05% $NH_4Cl$, 3% glucose. Carbon limiting media (CLM) was as NLM except that $NH_4Cl$ and glucose were added at 0.3% and 1% respectively.

Defined minimal medium was either Yeast Nitrogen Base (YNB) (*S. cerevisiae* and *L. starkeyi*) [0.67% yeast nitrogen base without amino acids (ForMedium™, UK), 2% glucose and 0.002% of appropriate amino acids except for threonine, uracil, tyrosine, lysine at 0.001% and 0.005% leucine] or Edinburgh Minimal Media (EMM) (*S. pombe*) [1.2% EMM without added dextrose and amino acids (ForMedium™ UK), 2% glucose and 0.0225% appropriate amino acids].

Unless otherwise stated all experiments for *S. cerevisiae* were undertaken utilising the wild type strain BY4741a and *S. pombe* utilising wild type strain NJ1 or NJ2. NJ1 and NJ2 comprise the same genotype, only differing by mating type ($h^+/ h^-$).

For *Escherichia coli* (*E. coli)*, (genotype: *fhuA2 Δ(argF-lacZ)U169 phoA glnV44 Φ80 Δ(lacZ)M15 gyrA96 recA1 relA1 endA1 thi-1 hsdR17*), Luria Broth (LB) [10% tryptone, 5% yeast extract, 0.5% NaCl] was utilised for shake flask growth. Cultures were grown at 37 $^oC$ with shaking, 200 rpm. For selection of cells containing vectors and plasmids in liquid culture, LB was supplemented with 100 µg/ml Ampicillin. LB containing 2% agar and 100 µg/ml Ampicillin was utilised after cell transformation for selection of cells containing vectors and plasmids.

### 2.1.2 Growth curves and doubling times

Mid-exponential cultures of *S. cerevisiae*, *S. pombe* and *L. starkeyi* were diluted in the appropriate media and allowed to grow for 15 hours (or until stationary phase was achieved) at 30 $^oC$, duplicate. Growth of all three yeast species was monitored at hourly intervals using a spectrophotometer at a wavelength of 595 nm. For growth curves conducted in limiting and defined minimal media, cells were pre-cultured in appropriate complex medium (YPD or YES) at 30 $^oC$, duplicate overnight, before resuspending to a density of ~2.0 x $10^6$ cells/ml for *S. cerevisiae* and *S. pombe* and ~4.0 x $10^6$ cells/ml for *L. starkeyi* ($OD_{595}$ approximately 0.1). Cell counts were conducted using a haemocytometer to determine cell number at a given absorbance reading.

## 2.2 Extraction of cellular lipids for gravimetric analyses

Extraction of cellular lipids was carried out using a modified Bligh and Dyer method described by (Rolph *et al.* 1989). Cultures of 50 ml volume were harvested by centrifugation for 2 minutes at 492 x g. The resultant cell pellet was resuspended in 10 ml of media and transferred to 10 ml of methanol, pre-warmed to 70 $^{o}$C (Fisher, UK). Samples were heated for 30 mins at 70 $^{o}$C, cooled and 20 ml chloroform (Fisher, UK) was added giving a chloroform/methanol ratio of 2:1 (v/v). A 10 ml aliquot of 5% NaCl (w/v) was then added to the extraction mixture prior to stirring for 1 hr at room temperature, allowing a two phase system to develop. The lower chloroform phases were removed using a glass pipette into pre-weighed aluminium boats. Lipid extracts were then evaporated to complete dryness under nitrogen gas ($N_2$) at 40 $^{o}$C. Aluminium boats were allowed to equilibrate before weighing and recording mass differences on an Ohaus Pioneer precision balance with an accuracy of 0.001g. Lipid mass data was expressed as mg of lipid per 50 ml of culture harvested.

### 2.2.1 FAME analysis Gas Chromatography

Fatty acid methyl esters (FAMES) were prepared from total lipid extracts, as described by Rolph and Goad (1991). Lipid samples were extracted as per Section 2.2. Aliquots of 200 µl lipid extract dissolved in chloroform were spiked with 40 µg of diheptadecyl phosphatidylcholine in chloroform as the internal standard. The mixture was evaporated to complete dryness under $N_2$ at 40 $^{o}$C, and mixed with 2 ml of methylating solution (2.5% (v/v) $H_2SO_4$ in anhydrous methanol) before heating at 70 $^{o}$C for 2 hours. The methylated sample was then cooled and mixed with 5ml 5% (w/v) NaCl solution and stored at 4 $^{o}$C.

Prior to FAME extraction, 2 ml petroleum ether was added, and quickly vortex mixed three times at highest speed setting, creating a top layer of petroleum ether containing FAMEs which was extracted using Pasteur pipettes into a tapered glass tube. This was repeated twice more, extracting into the same tube. The extracted solution was evaporated to complete dryness under $N_2$ at 40 $^{o}$C, and 50 µl petroleum ether added to the dried sample using a Hamilton syringe. The sample was kept at 4 $^{o}$C prior to GC analysis. 1µl of sample was loaded into the GC sampler (ATI unicam 610 series). The oven was ramped to 250 $^{o}$C over a 30 minute period from 50 $^{o}$C. FAMES were identified by comparison with the relative retention times of authentic standards. The area under the

peaks and retention times were calculated using Azur software at the following settings: PW: 50, TH: 125, WA: 25.

### 2.2.2 Thin Layer Chromatography (TLC) of extracted yeast lipids

Aliquots (50 µl) of each prepared lipid sample and standards were applied to TLC plates (Analtech) in 1 cm bands using microcapillary pipettes. Standards utilised were triacylglycerols (TAGs), oleic acid (for FFAs), sterol esters (SEs), and cholesterol (for sterols) at a stock concentration of 5 mg/ml (Sigma Aldrich, UK). The solvent system consisted of petroleum ether/diethyl ether/glacial acetic acid (80/20/2, v/v) (Thermo Fisher Scientific, UK).

After equilibration of the tank for 1 hour, the plate was run for 40 minutes until the solvent front was 1 cm from the top of the plate. Lipid classes on the completed TLC plate were visualised utilising iodine vapour (Sigma Aldrich, UK). Strength of resultant lipid classes on the TLC plate was assessed semi-quantitatively by visual inspection.

## 2.3 Nile red 96-well plate assay

A modified version of the screening method described by Sitepu *et al.* (2012) was used. Briefly, cells were harvested by centrifugation at 492 x g for 2 mins. The resultant cell pellet was washed twice in phosphate buffered saline (PBS) [8% NaCl, 0.2% KCl, 1.44% $Na_2HPO_4$, 0.24% $KH_2PO_4$] (Fisher, UK), in order to remove the high background fluorescence of the medium, before being resuspended in (PBS) at a density of 2 x $10^7$ cells/ml (*S. cerevisiae* and *S. pombe*) and 4 x $10^7$ cells/ml (*L. starkeyi*) ($OD_{595}$~1.0). The optical density at 595 nm was recorded again after final resuspension and ~5 x $10^6$ (*S. cerevisiae* and *S. pombe*) or ~10 x $10^6$ (*L. starkeyi*) cells were plated into the wells of a black, clear bottomed 96-well plate (Krystal 2000, Porvair Sciences) in triplicate. A 25µl volume of DMSO/PBS (1:1 v/v) solution was added to each well before addition of a final concentration 5 µg/ml Nile red in acetone. The wavelengths excitation 485 nm and emission 535 nm were utilised to determine the amount of neutral lipid in yeast cell suspensions. Conversely wavelengths excitation 535 nm and emission 590 nm were utilised to determine the amount of polar lipid.

The number of plate reader cycles for each wavelength was previously optimised by reading samples plated out onto separate plates on a kinetic reading for 20 mins, with a 60 second interval. The cycle before saturation point of the Nile red dye was determined for the three yeast species for each wavelength and subsequently used for further screens in all cases.

Plates were read immediately after addition of Nile red firstly for polar lipids and then for neutral lipids using the determined kinetic cycle on a Tecan Genios Pro platereader using the top 50% mirror setting. The gain settings for each wavelength of individual experiments was set to optimal and recorded after the initial screen before setting the gain manually to the same values for further screens within the triplicate.

Data was corrected against PBS containing 1/10 volume DMSO/PBS (1:1 v/v) and 5 μg/ml Nile red in acetone and further corrected for optical density of each sample. In order to plot data together for triplicates, all data was adjusted to the screen with the highest background fluorescence by multiplying relative fluorescence averages for each sample by the determined ratio. To determine total lipid levels, fluorescence RFU values from neutral and polar lipids were combined.

### 2.3.1 Methylene blue viability staining of yeast cells

Methylene blue stains non-viable cells dark blue but is de-colourised by mitochondrial dehydrogenase activity of viable yeast cells and was used to determine the viability of yeast cells. Citrate methylene blue [0.01% (w/v) methylene blue (Sigma, UK) 2% sodium citrate] was added to an equal volume of cell culture and mixed by vortexing. After incubation at room temperature for 5 minutes samples were viewed on a Zeiss Axio upright microscope, using the bright phase setting at 100x magnification. Yeast cells that were stained blue were counted as non-viable whilst unstained cells were counted as viable. Percentage viability was determined by the following equation:

% Viability = (Total cells counted – total blue cells counted) / total cells counted x 100

### 2.3.2 Nile red fluorescence microscopy

Cells for microscopy were stained by addition of a final concentration of 5 μg/ml Nile red in acetone per 250 μl of yeast culture before incubation for 5 minutes in the dark at room temperature. Stained cultures were then centrifuged for 2 mins at 492 x g before washing twice in phosphate buffered saline (PBS) (Fisher, UK). Cells were resuspended in 10% (v/v) formalin and fixed for 15 mins in the dark at room temperature before centrifugation and a further 2 washes with PBS. Cell pellets were resuspended in SlowFade (Invitrogen, UK) to prevent loss of cellular fluorescence exhibited when viewing cells with 590 nm emission.

Nile red stained cells were viewed on a Zeiss Axio upright microscope using an AxioCam MRm camera at 100 x magnification. Excitation and emission wavelengths utilised for visualisation of neutral and polar lipids were 485nm/535nm and 535nm/590nm, respectively.

## 2.4 Yeast genomic DNA extraction

Genomic DNA extractions were carried out according to Lõoke *et al.* (2011). Aliquots (200μl) of exponentially growing culture (~2.4 x $10^7$ cells/ml *S. cerevisiae* and *S. pombe* and ~1.6 x$10^7$ cells/ml *L. starkeyi*), were harvested and centrifuged at 14 000 x g for 2 minutes before being resuspended in 100 μl 0.2M LiAc, 1% SDS solution and incubated for 5 minutes at 70 $^{o}$C. An equal volume of 96-100% EtOH was added and samples vortexed before centrifuging at 16 000 x g for 3 minutes. The resultant pellet was then washed with 70% EtOH and allowed to air dry for 3 minutes before being resuspended in 50 μl of sterile water.

### 2.4.1 Polymerase chain reaction

Primers utilised in this study are listed in Table 2.2. All primers were synthesised by integrated DNA technologies (IDT, UK).

### 2.4.1.1 Amplification of p38 orthologues

Primers CLL001-002 and CLL021-022 (Table 2.2) were used to amplify *S. cerevisiae hog1*, CLL005-006 and CLL026-27 (Table 2.2) for *L. starkeyi* p38 orthologue and CLL023-024 (Table 2.2) for *S. pombe sty1*. Each PCR reaction contained 0.25µM of each primer (IDT), 200µM dNTP mix, 1mM $MgCl_2$, 1x GoTaq Flexi buffer and 1.25units of GoTaq Flexi Polymerase (Promega). PCR parameters used for amplification were:

**1.** Initial denaturation – 94°C, 5 minutes

**2.** Denaturation – 94°C, 1 minute
**3.** Annealing – 45°C, 1 minute
**4.** Extension – 72°C, 1 minute
} 30 cycles

**5.** Final Extension – 72°C, 7 minutes

**Table 2.2: Table of primers designed and utilised for PCR reactions.**

| Primer | Sequence | Restriction sites |
|---|---|---|
| CLL001 SC *hog1* F | 5'- TGG TAC GGA TCC GAC CAC TAA CGA GGA AAT C -3' | *Bam*HI |
| CLL002 SC *hog1* R | 5'- GGC ATT CCA TGG GGA ACT CAT TAG CGT ACT G -3' | *Bam*HI |
| CLL003 conserved *hog1/sty1* F | 5'- CAT GGA GGA TCC GAC ACA GAT ATT CGG TAC AG -3' | *Bam*HI |
| CLL004 conserved *hog1/sty1* R | 5'- CGC AAT CCA TGG CTG AGT ACA TCA TAA CAC GC -3' | *Bam*HI |
| CLL005 LS MAPK F | 5’ TTG TAC GGA TCC ATG GCA GAA TTT ATT CGT ACA C 3’ | *Bam*HI |
| CLL006 LS MAPK R | 5’ GGC ATT CCA TGG TTA GGA TTG CAG TTC ATT ATC C 3’ | *Bam*HI |
| CLL007 SP *sty1* F | 5'- TTG TAC GGA TCC ATG GCC GAT TTC ATC AGG TAT -3' | *Bam*HI |
| CLL008 SP *sty1* R | 5'- GGC ATT CCA TGG TTA TTC CGG TGA AAC TAC TCC -3' | *Bam*HI |
| CLL009 LS deletion G418 F | 5'- CTT CTA CGG CTC GCT CTG TCC CAT CCA TCA ACA CAG TAT CTG TCT GCT CAG CAA CCG TCG TCA GTG CTA TTT AGT GAT CTG CTA ACA CCA CGG ATC CCC GGG TTA ATT AA -3' | NA |
| CLL010 LS deletion G418 R | 5'- AGT AGC AGG GTT TAG CTG CCC ACC TTT CCG TGA CGT AGC AGT TGA GAC CTT CCG GCA ATT TCT TCT TCT TTT TCT CTC CGG CCG GCC TCT GAA TTC GAG CTC GTT TAA AC -3' | NA |
| CLL015 LS deletion URA F | 5'- CTT CTA CGG CTC GCT CTG TCC CAT CCA TCA ACA CAG TAT CTG TCT GCT CAG CAA CCG TCG TCA GTG CTA TTT AGT GAT CTG CTA ACA CCA CGC CAG GGT TTT CCC AGT CAC GAC -3 | NA |
| CLL016 LS deletion URA R | 5'- AGT AGC AGG GTT TAG CTG CCC ACC TTT CCG TGA CGTAGC AGT TGA GAC CTT CCG GCA ATT TCT TCT TCT TTT TCT CTC CGG CCG GCC TCT AGC GGA TAA CAA TTT CAC ACA GGA -3' | NA |
| CLL021 SC *hog1* + 1kb promoter F | 5' TTG TAC TCT AGA TGG CTG GCT CCA GAT AC 3' | *Xba*I |

| | | |
|---|---|---|
| CLL022 SC *hog1* R | 5' GGC ATT GAG CTC TTA CTG TTG GAA CTC ATT AGC 3' | *Sac*I |
| CLL026 LS MAPK + 1Kb promoter | 5' TTG TAC TCT AGA GTT CCA AGT GCA AGT GAA TTC 3' | *Xba*I |
| CLL028 LS MAPK R | 5' GGC ATT GAG CTC TTA TTC CGG TGA AAC TAC TCC 3' | *Sac*I |

### 2.4.1.2 Amplification of deletion cassettes by PCR

PCR was performed using Phusion polymerase (Fisher, UK) with 200 µM dNTPs, 2.5 mM $MgCl_2$, 1 x HF buffer and 2 µM each of forward and reverse primers (CLL009-010: G418 and CLL015-016: URA) with the following PCR parameters:

**1.** Initial denaturation – 94°C, 5 minutes

**2.** Denaturation – 94°C, 1 minute

**3.** Annealing – 55°C, 1 minute } 35 cycles

**4.** Extension – 72°C, 2 minutes

**5.** Final Extension – 72°C, 3 minutes

The products of ten PCR reactions were pooled prior to extraction using phenol chloroform isoamyl alcohol (25:24:1) (Fisher, UK) and ethanol precipitation.

## 2.5 Cloning for yeast phenotype recovery and heterologous protein expression

Details of plasmids used in this study are given in Table 2.3. Corresponding plasmid maps are shown in Appendix I.

**Table 2.3: Plasmids utilised in the present study** Plasmids constructed for complementation in *S. cerevisiae* and heterologous protein expression in *L. starkeyi*.

| Plasmid name | Base vector | Selectable markers/promoter | Construction | Source |
|---|---|---|---|---|
| CLLp001 | pRS315 | Amp/*LEU2* gene under its own promoter | *HOG1* + 1Kb upstream of ATG cloned into *Xba*I and *Sac*I sites of pRS315 | This study |
| CLLp002 | pRS315 | Amp/*LEU2* gene under its own promoter | *MAPK* + 1Kb upstream of ATG cloned into *Xba*I and *Sac*I sites of pRS315 | This study |
| CLLp004 | pRS313 | Amp/*HIS3* gene under its own promoter | *HOG1*+ 1Kb upstream of ATG cloned into *Xba*I and *Sac*I sites of pRS313 | This study |
| CLLp006 | pFA6a-KanMX6 | Amp/*KanMX* | n/a | Lab stock |
| CLLp008 | pFA6a-natMX6 | Amp/*NatMX* | n/a | Lab stock |

For routine transformation of vectors and of ligation products to obtain constructed plasmids *Escherichia coli* (*E.* coli) DH5α cells were utilised. Briefly for transformation of *E. coli*, 100 µl of cells were incubated on ice with 100 ng of plasmid DNA for 30 minutes. Cells were then heat shocked for 90 seconds at 42 $^{o}$C before placing back onto ice for 2 minutes before addition of 1 ml room temperature LB. Cells were incubated with shaking at 37 $^{o}$C, 200 rpm for 1 hour before plating out onto LB plates containing 100 µg/ml Ampicillin.

*S. cerevisiae HOG1* (under the control of its own promoter) was initially cloned into pRS315 (CLLp001), a pBluescript based centromere vector containing the yeast selectable marker *LEU2*. The *HOG1* open reading frame was amplified from *S. cerevisiae* genomic DNA utilising primers CLL021 and CLL022. Both purified PCR product and vector were digested with *Xba*I and *Sac*I (Thermo Scientific) before ligation and transformation into *E. coli* DH5α cells. Resultant colonies were screened for insert using primers CLL021 and CLL022 by colony PCR. Positive colonies were cultured overnight in LB medium at 37$^{o}$C, 200 rpm before extracting plasmid DNA using a GeneJET plasmid mini prep kit (Thermo Scientific).

For cloning of *S. cerevisiae HOG1* into pRS313, CLLp001 was digested with *Xba*I and *Sac*I before running on a 0.8% agarose gel for 30 minutes at 100V. Gel extraction was performed using GeneJET gel extraction kit (Thermo Scientific) before ligation with digested pRS313 (*Xba*I and *Sac*I).

*L. starkeyi MAPK* plus 1 kb upstream of the ATG was cloned into pRS315 on *Sac*I and *Xba*I sites in the same way as *S. cerevisiae* HOG1 using primers CLL026 and CLL028 to amplify the insert.

PCR parameters for all inserts and colony PCR screens were as described in Section 2.3.1.1.

### 2.5.1 Plasmid transformation in S. cerevisiae

Preparation and transformation of *S. cerevisiae* competent cells was carried out according to Knop *et al.* (1999). Mid exponentially growing cells were harvested by centrifugation at 492 x g for 5 minutes and washed once with 0.5 volumes of sterile water and once with 0.2 volumes of SORB [100mM LiAc, 10mM Tris-HCl pH 8, 1mM EDTA/NaOH pH 8.0, 1M sorbitol] adjusted to pH 8 with dilute acetic acid.

SORB was removed by aspiration and cells resuspended in 360 µl SORB per 50 ml culture and 1 mg/ml salmon sperm carrier DNA added (Invitrogen, UK). 50 µl of prepared competent cells were added to 4 µg plasmid DNA and mixed well before addition of a six-fold volume of PEG [100mM LiAc, 10mM Tris-HCl pH 8, 1mM EDTA/NaOH pH 8, 40% PEG 4000 (Fisher, UK)]. The suspension was incubated for 30 minutes at room temperature, mixing throughout. 10% DMSO was added before heat shocking the cells at 42 $^{o}$C for 15

minutes. Cells were pelleted by centrifugation for 2 minutes at 300 x g, the supernatant removed and cells resuspended in 200 µl of liquid medium before plating onto selective medium (YNB lacking the appropriate amino acid).

### 2.5.2 Plasmid transformation in S. pombe

*S. pombe* transformations were carried out as described in the modified acetate procedure of Moreno *et al.* (1998). 1 x $10^7$ cells/ml of mid exponentially growing cells were harvested at 492 x g for 2 minutes and washed once in water before being resuspended at 1 x $10^9$ cells/ml in 0.1M lithium acetate (pH 4.9). Cells were divided into 100 µl aliquots and incubated for 1 hour at room temperature. 1 µg of plasmid DNA and 50 µg salmon sperm carrier DNA (Invitrogen, UK) was added to the cells before mixing thoroughly and addition of a 3.6 fold volume of 50% PEG and 10% DMSO. The reaction mixture was then subjected to heat shock at 42 $^oC$ for 15 minutes before centrifuging at 300 x g for 2 minutes. Cells were resuspended in 200 µl of liquid medium before plating onto selective medium.

#### 2.5.2.1 Sensitivity testing S. cerevisiae and S. pombe

Cultures were grown in YPD/YES or YNB/EMM medium lacking the relevant amino acid supplement at 30 $^oC$, duplicate for 2 days. Cell densities of cultures were adjusted to ~2 x $10^7$ ($OD_{595}$ ~1.0) before making a 1:10 serial dilution generating aliquots with optical densities down to 0.0001. 10 µl of each serial dilution (corresponding to 200 000, 20 000, 2 000, 200, 20 and 4 cells respectively) were then spotted onto the relevant solid medium and solid medium containing the stress inducing agent, either sodium chloride or hydrogen peroxide. Plates were left face up at room temperature to allow absorption of the culture before inversion of the plates and incubation at 30 $^oC$ for 2-3 days.

#### 2.5.2.2 Sensitivity testing L. starkeyi

Cultures were grown in YPD medium at 30 $^oC$, duplicate. Cell densities of cultures were adjusted to ~2 x $10^7$ ($OD_{595}$ ~0.5) before making a 1:10 dilution series generating aliquots with optical densities down to 0.0001. 10 µl of each serial dilution (corresponding to 200 000, 20 000, 2 000, 200, 20 and 4 cells respectively) were then spotted onto the relevant solid medium and solid medium containing various stress inducing agents, such as sodium chloride and hydrogen peroxide. Plates were incubated at 30 $^oC$ for 1 week.

## 2.6 SDS-PAGE and Western blotting

### 2.6.1 Denatured protein extraction

Denatured protein extractions were carried out as described by Lawrence *et al.* (2007). Cells were harvested at 492 g before resuspension in 1 ml of 0.3M NaOH. 150 µl of trichloroacetic acid 55% (w/v) was added before vortexing and incubation on ice for 10 minutes. Samples were centrifuged at 4 $^{o}$C at 17000 x g for 10 minutes before removal of the supernatant by aspiration. The pellet was then resuspended in 30 µl SDS sample buffer [50 mm Tris-Cl (pH 6.8), 2% SDS (w/v), 0.1% bromophenol blue, 10% (v/v) glycerol, 10 mm dithiothreitol] per Abs $0.1_{595}$ of cells. Proteins were denatured at 100 $^{o}$C for 10 minutes and spun briefly prior to loading onto pre-cast 12% TGX polyacrylamide gels (Biorad, UK). Gels were run using Tris/Glycine/SDS buffer [25 mM Tris, 192 mM glycine, 0.1% SDS] at a constant 20 mA per gel.

### 2.6.2 Phos-tag gels of protein extracts

Protein extractions were carried out as described in Section 2.5.1. 12% polyacrylamide gels were prepared with 200 µM manganese chloride ($MnCl_2$) and 5.0 mmol/L Phos-tag (Wako chemicals Ltd), added. Gels were run at a constant 20 mA per gel and washed for 10 minutes in transfer buffer containing 1.0 mM EDTA before protein transfer was performed as described in Section 2.5.3.

### 2.6.3 Western blotting

For Western blotting proteins were transferred to polyvinylidene fluoride (PVDF) membrane (Millipore, UK) by electroblotting for 1 hour at constant voltage, 100 V. Membranes were blocked for 1 hour in 10% milk solution (Marvel) before washing 3 times in Tris buffered saline tween (TBST) [50 mM Tris HCl, pH 7.4, 150 mM NaCl, 0.1% Tween 20] for 10 minutes each. Primary antibodies were applied at 1:1000 dilution in TBST and incubated overnight on a shaking platform at 4 $^{o}$C. Membranes were then washed 3 times in TBST as described above before application of the secondary antibody diluted 1:10000 in TBST. PVDF membranes were incubated for 45 minutes at room temperature in secondary antibody before a further three 10 minute washes prior to detection.

For detection a 1:1 ratio of Enhanced chemiluminescence (ECL) prime solutions (GE Healthcare) were incubated with membranes for 5 minutes. The membrane was then exposed to X-ray film (Fisher, UK) in the dark for 1 minute before placing into developer solution (Sigma, UK) for 30 seconds. X-ray films were then rinsed in distilled water and fixed with fixer solution (Sigma, UK).

Antibodies utilised in the present study were: primary antibody α-Hog1p to detect total amounts of Hog1p (Santa Cruz Biotechnology). Primary antibody α-P-p38 to detect dually phosphorylated Hog1p (Cell Signalling Technology). ECL Rabbit IgG, HRP-linked secondary antibody (from donkey) (GE Healthcare).

## 2.7 Statistical analysis

All data is displayed as means of triplicate experiments +/- SD. Where relevant, statistical analyses were performed by means of one way ANOVA with Tukey *post hoc* comparisons using GraphPad Prism 5.0 software. A significant result was determined to have a p value of $<0.05$.

# Chapter III Development of methodology to evaluate lipid accumulation in both oleaginous and non-oleaginous yeast species

## 3.1 Introduction

As outlined previously in Section 1.4, lipids are important molecules that play a wide range of roles supporting living processes within both prokaryotic and eukaryotic cells. They may be broadly classified into neutral and polar lipid subtypes. Unlike their more dynamic polar counterparts (e.g. phospholipids) that support a range of cellular functions, neutral lipids (mainly triacylglycerols (TAGs) and sterol esters (SEs)) are almost exclusively synthesised to facilitate the storage of cellular energy within phospholipid and protein monolayer vesicles known as lipid droplets (LDs) (Hutchins *et al.* 2008).

In humans, the ectopic production of triacylglycerols has been shown to be a characteristic feature of several prominent pathological states of global significance, including cancer (Di Paolo and Kim 2011, Zhang F. and Du 2012). The understanding of the mechanisms involved in the regulation of ectopic lipid metabolism constitutes an interesting focus for the development of future therapeutic strategies. The study described within this thesis utilises several yeast paradigms of human disease to further knowledge of the aforementioned regulatory strategies.

The currently utilised methods to quantify lipids such as gravimetric, gas or liquid chromatography are time consuming and laborious, often involving several steps from extraction to determination of lipid amounts (Bligh and Dyer 1959, Folch *et al.* 1957, Santamauro *et al.* 2014, Shahidi 2001). Therefore, screening large numbers of samples is complex requiring the need for multiple extractions, which often necessitate the use of large quantities of environmentally challenging organic solvents (Poli *et al.* 2014). Increased throughput methods allowing rapid screening of multiple samples, such as Nile red, have been developed but lack specificity and sensitivity with regards to identification of molecular species and limits of detection.

In this chapter it has been demonstrated that gravimetric analyses were difficult to perform with the low lipid producing non-oleaginous species *S. cerevisiae.* Furthermore the gravimetric, gas chromatography (GC) and thin layer chromatography (TLC) methods were time consuming and labour intensive and so not conducive to analysing large numbers of samples, as is required by the present study. It has also been shown in this chapter that total Nile red fluorescence was a reliable measure of total lipid in *L. starkeyi* when compared to gravimetric analyses undertaken. Additionally, it has been

demonstrated that utilising different excitation and emission wavelengths of Nile red can separate fluorescence due neutral and polar lipid types.

Furthermore use of Nile red may be utilised in an assay screening format to distinguish between neutral and polar lipid phenotypes in the non-oleaginous budding yeast, *S. cerevisiae* and, for the first time, the non-oleaginous fission yeast *S. pombe.*

## 3.2 Results

### 3.2.1 Lipomyces starkeyi growth and characterisation of lipid accumulation

It is widely reported in the literature that oleaginous yeast species accumulate large quantities of neutral lipids when grown under nitrogen-limiting conditions. Meanwhile, growth under carbon-limiting conditions is characterised by relatively little neutral lipid production. This lipid accumulation occurs maximally when the cells enter the stationary phase of growth (Ratledge 1982, Seip *et al.* 2013).

*L. starkeyi* is one of several species of yeast which can accumulate up to 70% of its dry cell mass as lipid (Tapia *et al.* 2012) and, as such, it is an excellent model to validate methods for monitoring lipid accumulation.

Preliminary evaluation of *L. starkeyi* growth to determine where stationary phase occurs in limiting medium was conducted by inoculation of single colonies into nitrogen limiting media (NLM) and carbon limiting media (CLM). Growth was then monitored via optical density and cell number over a period of 120 hours (hrs). The growth of this yeast species was found to be extremely slow in both limiting media with an initial lag phase of approximately 60 hrs before stationary phase was achieved at ~90 hrs, as indicated by plateaued growth, (Figures 3.1, 3.2 and Table 3.1).

Nitrogen limiting cultures typically entered the stationary phase of growth at an optical density (595 nm) of 10, whereas cells grown in CLM accumulated less cell mass, entering stationary phase with an optical density of 2.4. Although the exponential doubling time of this species is ~4 hrs, due to the long lag phase an increased culturing period would be required before stationary phase samples could be obtained, which would impact on time taken to execute experiments.

To determine if time taken for *L. starkeyi* to reach stationary phase could be reduced by pre-culturing in complex medium, colonies were inoculated in rich medium (YPD). Exponentially growing cells, as determined from Figure 3.3, were then transferred to limiting medium at a density of ~4.0 x $10^6$ cells/ml (corresponding to an $OD_{595}$ 0.1). Cell growth was then monitored by optical density until plateaued growth, indicating stationary phase, was observed.

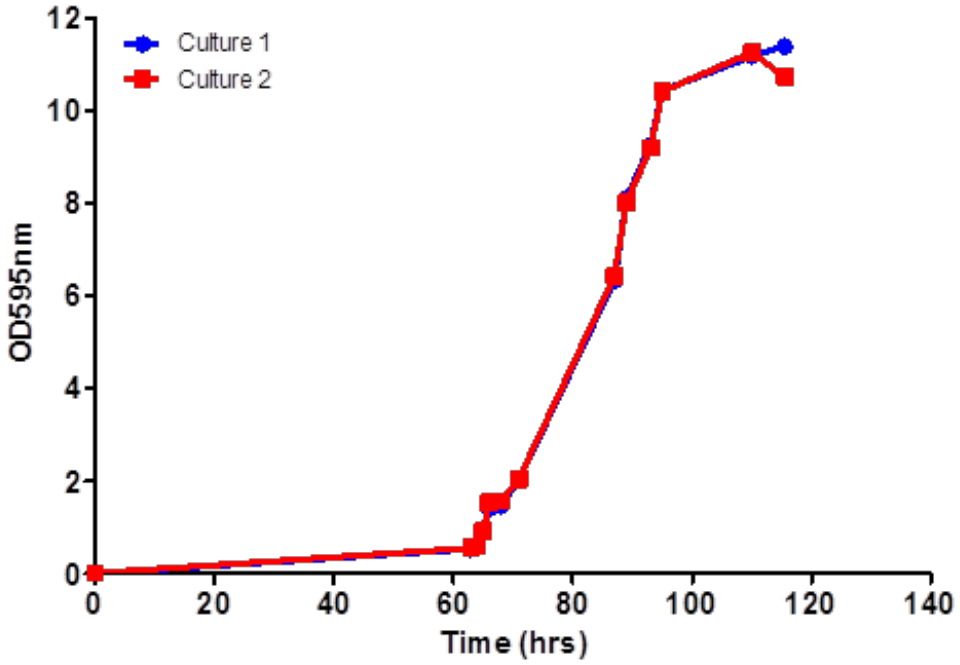


**Figure 3.1: Growth analysis of *L. starkeyi* in nitrogen limiting medium (NLM).** In order to determine stationary phase. *L. starkeyi* colonies were inoculated directly into the medium and cultures were allowed to grow with shaking at 180rpm, 30°C. Readings were taken as appropriate until stationary phase was reached, as indicated by plateaued growth. Growth curves were conducted in duplicate with blue and red lines denoting growth pattern observed from two distinct colonies.

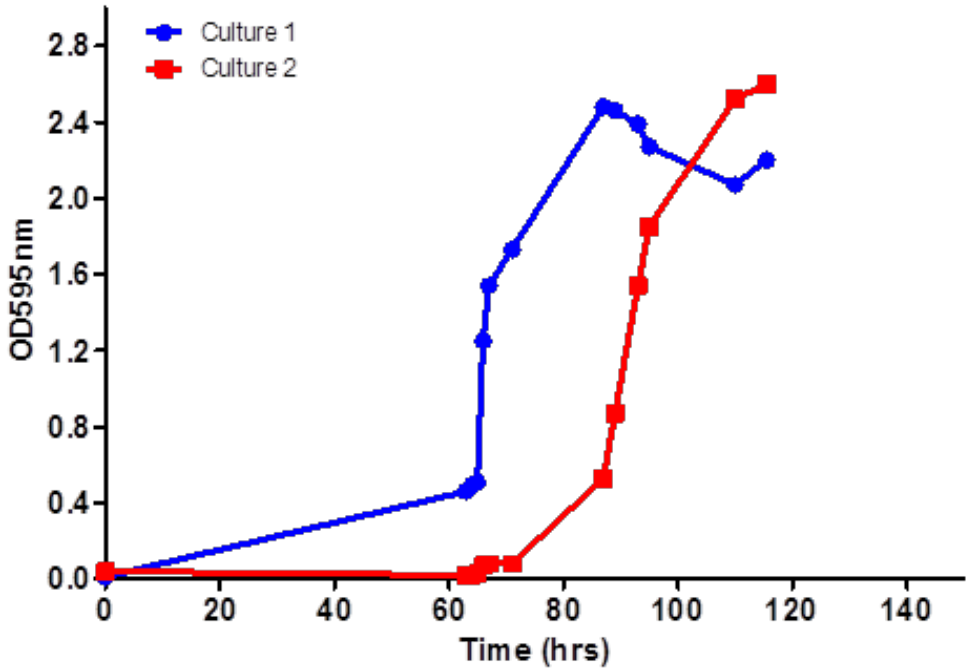


**Figure 3.2: Growth analysis of *L. starkeyi* in carbon limiting medium (CLM).** In order to determine stationary phase. *L. starkeyi* colonies were inoculated directly into the medium and cultures were allowed to grow with shaking at 180rpm, 30°C. Readings were taken as seen appropriate until stationary phase was reached, as indicated by plateaued growth. Growth curves were conducted in duplicate with blue and red lines denoting growth pattern observed from two distinct colonies.

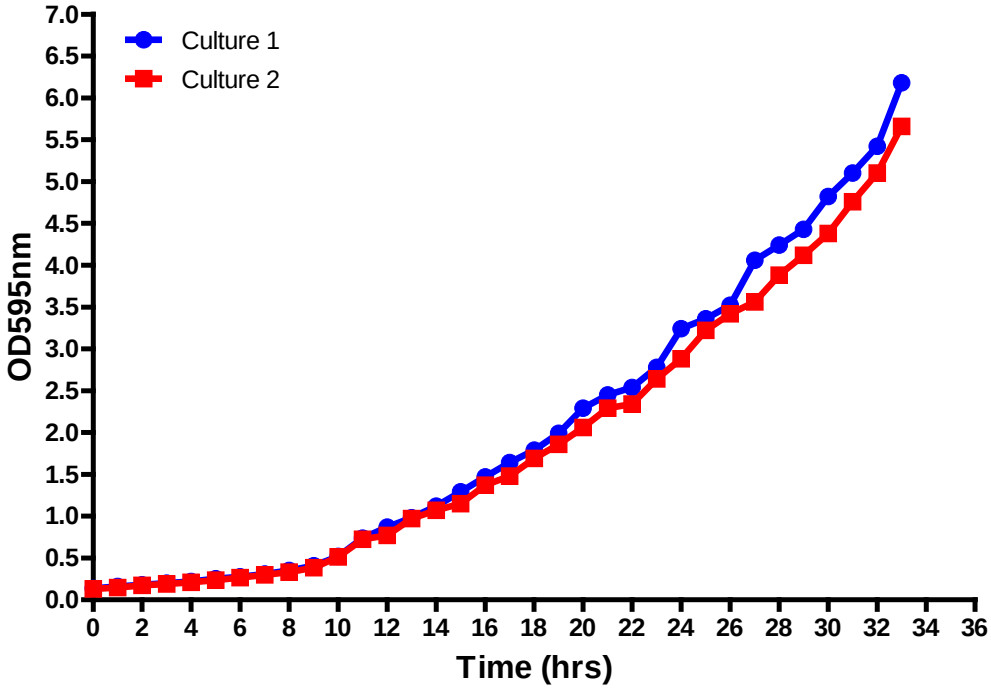


**Figure 3.3: Growth of *L. starkeyi* in YPD medium.** Cultures were diluted in YPD medium to a density of 4 x $10^6$ cells/ml. Cultures were incubated with shaking at duplicate, 30$^o$C and optical density readings taken each hour to determine the exponential growth phase of *L. starkeyi*. Growth curves were conducted in duplicate with blue and red lines denoting growth pattern observed from two distinct colonies.

As shown in Figures 3.4 and 3.5, the time required for *L. starkeyi* to enter early stationary phase of growth was reduced from ~110hrs to ~40hrs in NLM and from ~85-110 hrs to ~17 hrs in CLM by firstly acquiring cell mass in rich medium (Table 1). Optical density measurements obtained by this method on entry of the cells into stationary phase were concurrent with cultures from direct inoculation. As previously described, NLM cultures entered early stationary phase at an optical density of approximately 10, and CLM cultures at an optical density of 2.5.

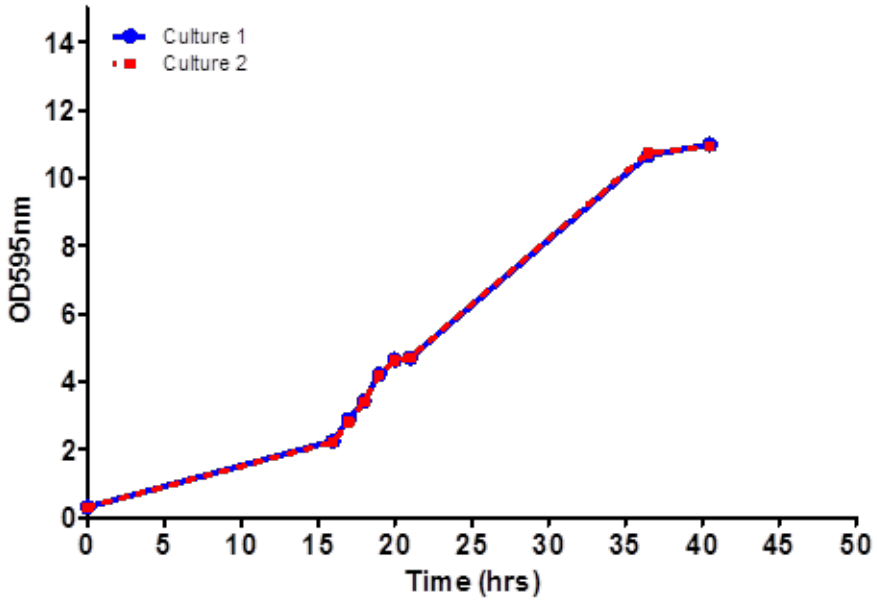


**Figure 3.4: Growth analysis of *L. starkeyi* whereby cell mass was accumulated in YPD before re-suspension in nitrogen limiting medium (NLM) in order to determine stationary phase.** Cells from log phase YPD cultures were resuspended in limiting medium to give a starting optical density half that of the original YPD culture. Cultures were allowed to grow, with shaking at 180rpm, 30°C and readings taken as appropriate until stationary phase was reached, as indicated by plateaued growth. Growth curves were conducted in duplicate with blue and red lines denoting growth pattern observed from two distinct colonies.

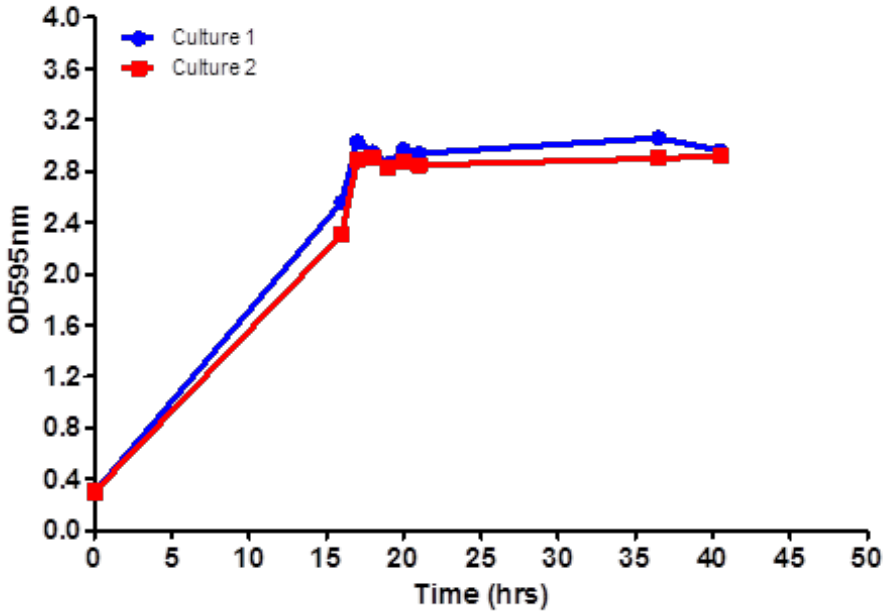


**Figure 3.5: Growth analysis of *L. starkeyi* whereby cell mass was accumulated in YPD before re-suspension in carbon limiting medium (CLM) in order to determine stationary phase.** Cells from log phase YPD cultures were resuspended in limiting medium to give a starting optical density half that of the original YPD culture. Cultures were allowed to grow, with shaking at 180rpm 30°C and readings taken as appropriate until stationary phase was reached, as indicated by plateaued growth. Growth curves were conducted in duplicate with blue and red lines denoting growth pattern observed from two distinct colonies.

**Table 3.1: Time (hrs) taken to reach stationary phase of growth for *L. starkeyi.*** Comparison of cultures inoculated directly into limiting medium (NLM/CLM) and for *L. starkeyi* grown in rich medium before re-suspension of cellular mass in limiting medium (YNLM/YCLM).

| Culture | NLM | YNLM | CLM | YCLM |
|---|---|---|---|---|
| **Time to stationary phase** | ~110 hours | ~40 hours | ~85-110 hours | ~17 hours |
| **Difference in time taken to reach stationary phase (hrs)** | 70 hours | | 68-93 hours | |

In order to elucidate whether the re-suspension of YPD pre-cultured cells into limiting medium affected lipid production in *L. starkeyi*, samples were taken for lipid extractions during exponential and stationary phases of growth, as determined from the growth curves. The amount of lipid was then quantified via the gravimetric method detailed in Chapter 2, Section 2.2. As Figure 3.6 shows, the ability of *L. starkeyi* to accumulate lipid in both limiting media, by utilising the method whereby cell mass is firstly accumulated in YPD, was not affected.

For carbon limiting cultures, consistently low levels of lipid mass ranging between 1 mg and 3 mg per 50 ml culture were obtained from both directly inoculated and resuspended cultures irrespective of the phase of growth. For cells inoculated directly in NLM lipid masses of 9 mg and 13 mg per 50 ml culture were obtained at 96 hrs and 17 mg per 50 ml culture was obtained for both 120 hr cultures. Cells pre-cultured in YPD before re-suspension in NLM accumulated raw lipid masses of 4 mg and 6 mg per 50 ml culture at 48 hrs and 16 mg and 17mg per 50 ml culture for stationary phase at 72 hrs.

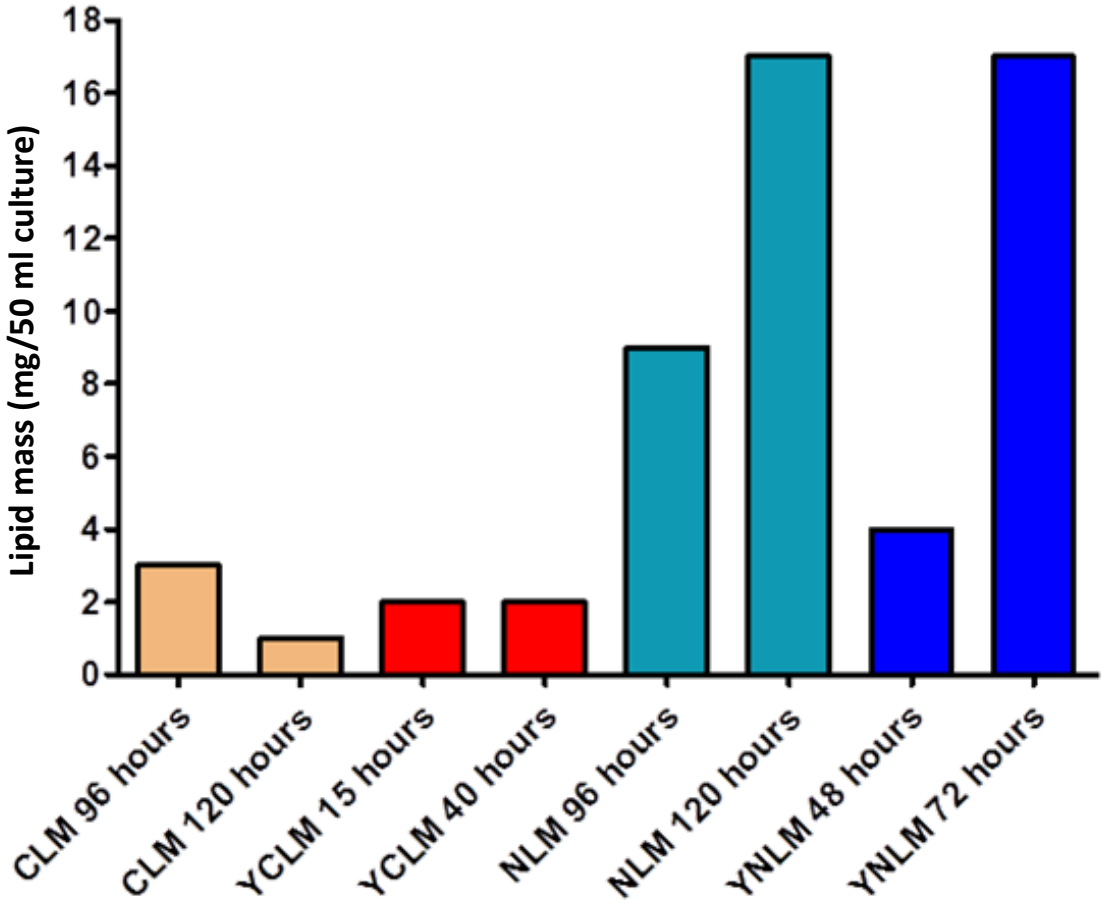


**Figure 3.6: Graph showing total mass of lipids accumulated is not affected between direct inoculation and re-suspension from YPD pre-cultures.** Total cellular lipids were analysed utilising the gravimetric method. Data is presented as the average lipid mass of extractions carried out in duplicate. CLM: carbon limiting medium, YCLM: carbon limiting cultures from YPD pre-cultures, NLM: nitrogen limiting medium, YNLM: nitrogen limiting cultures from YPD pre-cultures.

As a result, re-suspending *L. starkeyi* cells into limiting medium from YPD pre-cultures was the optimum culturing method allowing cell mass production and lipid accumulation. The technique did not affect the amount of lipids that are accumulated by this yeast species in stationary phase and drastically reduced the time in which stationary phase of growth was achieved.

### 3.2.2 Detailed growth and lipid accumulation of L. starkeyi

Having identified the optimum method for determining lipid accumulation in *L. starkeyi*, a full growth and lipid characterisation of the wild type strain was conducted. Growth of the cultures was monitored every 2 hrs, (Figure 3.7), and lipid extractions were conducted in duplicate every 24 hrs up to 144 hrs, (Figure 3.8). These time points were chosen so that data on the amount of lipid accumulated could be obtained for each growth phase from early exponential to late stationary phase.

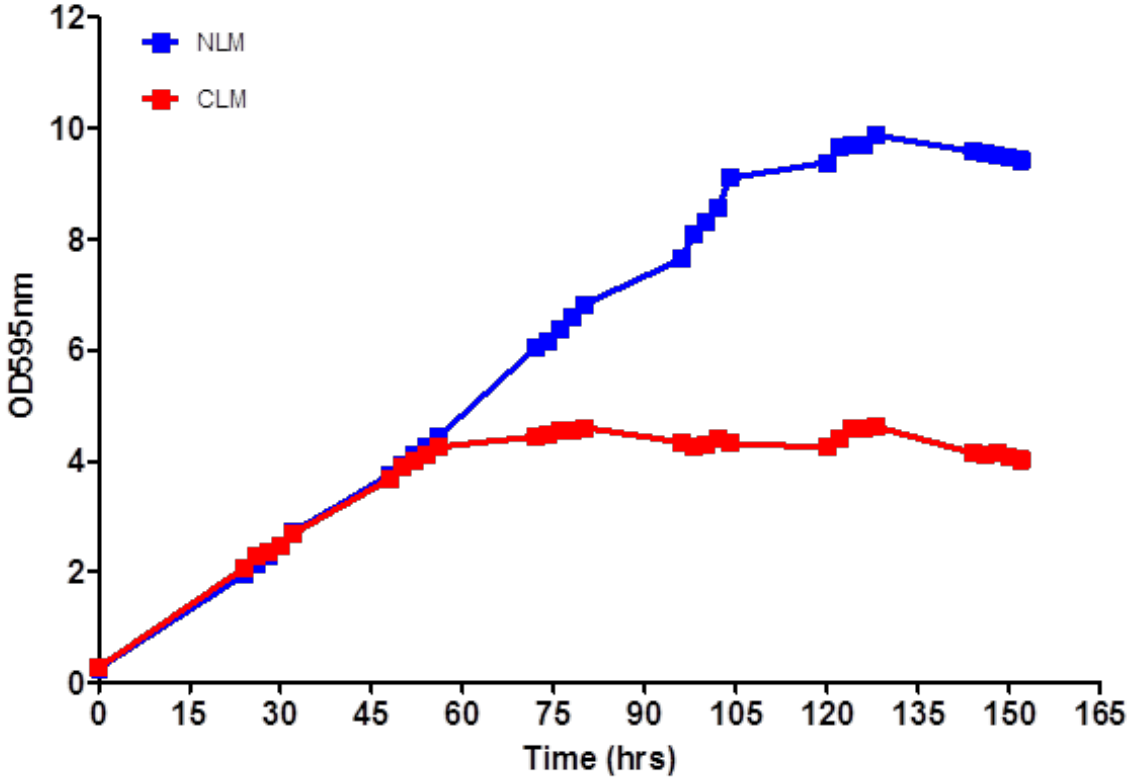


**Figure 3.7: Detailed growth analyses of *L. starkeyi* after re-suspension of YPD pre-culture into limiting medium.** After re-suspension in either nitrogen limiting (NLM) or carbon limiting (CLM) media, cultures were allowed to grow with shaking at duplicate, 30°C. Optical density readings were taken 5 times per day at regularly spaced intervals to construct the curve.

It is important to note that the time taken to reach stationary phase has increased 2 fold for *L. starkeyi* in both nitrogen and carbon limiting medium compared to the initial characterisation detailed in Section 3.2.1. This was due to the larger culture volumes that were required in order to harvest 50ml samples for lipid extractions at each point of the time course. This highlights that growth curves should be conducted alongside experiments where the culture volume has been subsequently altered.

As shown in Figure 3.8 similar levels of lipid were observed in exponential phase cultures for both NLM and CLM at 24 and 48 hrs. At 72 hrs lipid accumulation began to increase in NLM cultures until late stationary phase at 144 hrs. Raw lipid amounts and final adjusted lipid amounts were consistent within each duplicate.

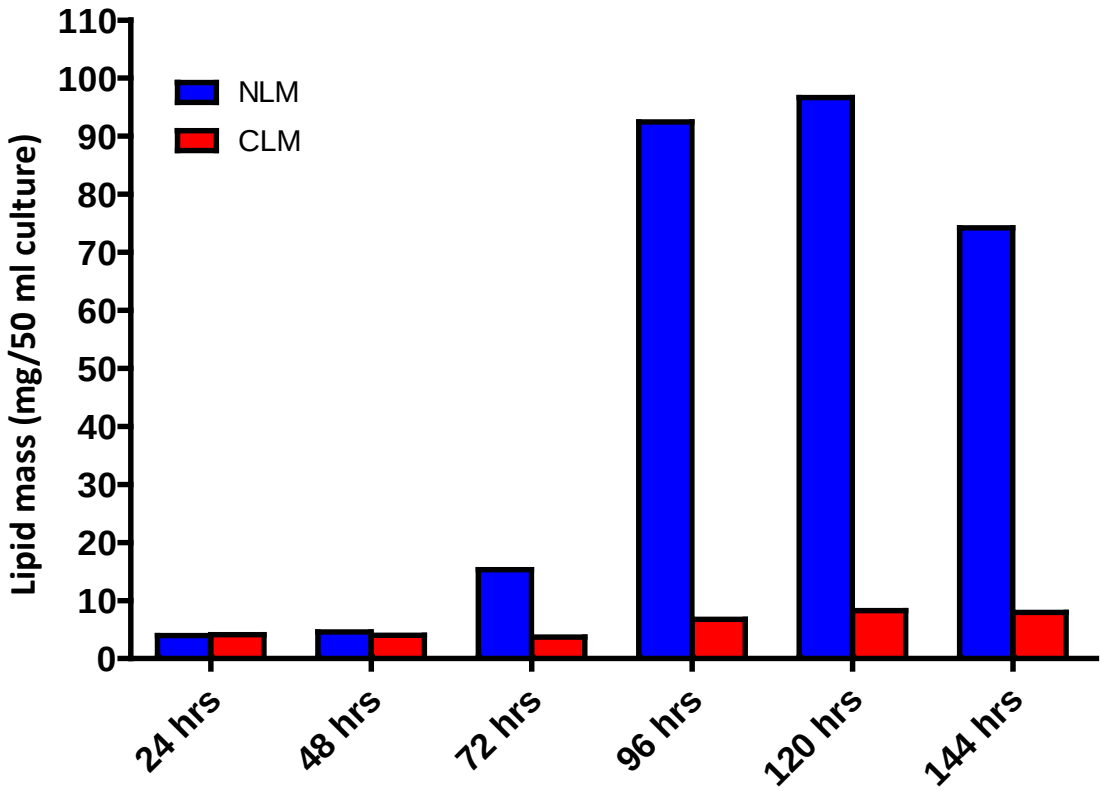


**Figure 3.8: Characterisation of *L. starkeyi* lipid accumulation in nitrogen limiting (NLM) and carbon limiting media (CLM).** Every 24 hrs samples were harvested from the cultures used to construct the growth curve in Figure 3.7. Lipid extractions were carried out as detailed in the Section 2.2. Raw lipid mass was normalised to account for differences in cell number, all data adjusted to an $OD_{595}$ of 10, and the adjusted data plotted. Data presented as means of duplicate experiments.

By combining the two data sets, lipid accumulation relative to growth phase of the *L. starkeyi* species was determined. As depicted in Figure 3.9, under nitrogen limiting conditions, lipid begins to accumulate in mid exponential phase (~72 hrs) with a mass of 15.3 mg/50ml culture and then increases 6.3 fold to 96.7 mg/50 ml culture in mid-stationary phase (~120 hrs). After this point, at late stationary phase (~144 hrs), where the cells would no longer be dividing, there is a 1.3 fold decrease in total lipid amount to 74.2 mg/50 ml culture. From this it is concluded that the methodology utilised is appropriate for the gravimetric measurement of lipid from *L. starkeyi*.

After optimisation in *L. starkeyi* this methodology was used to determine if it was also appropriate for use in *S. cerevisiae* and *S. pombe* for monitoring lipid accumulation.

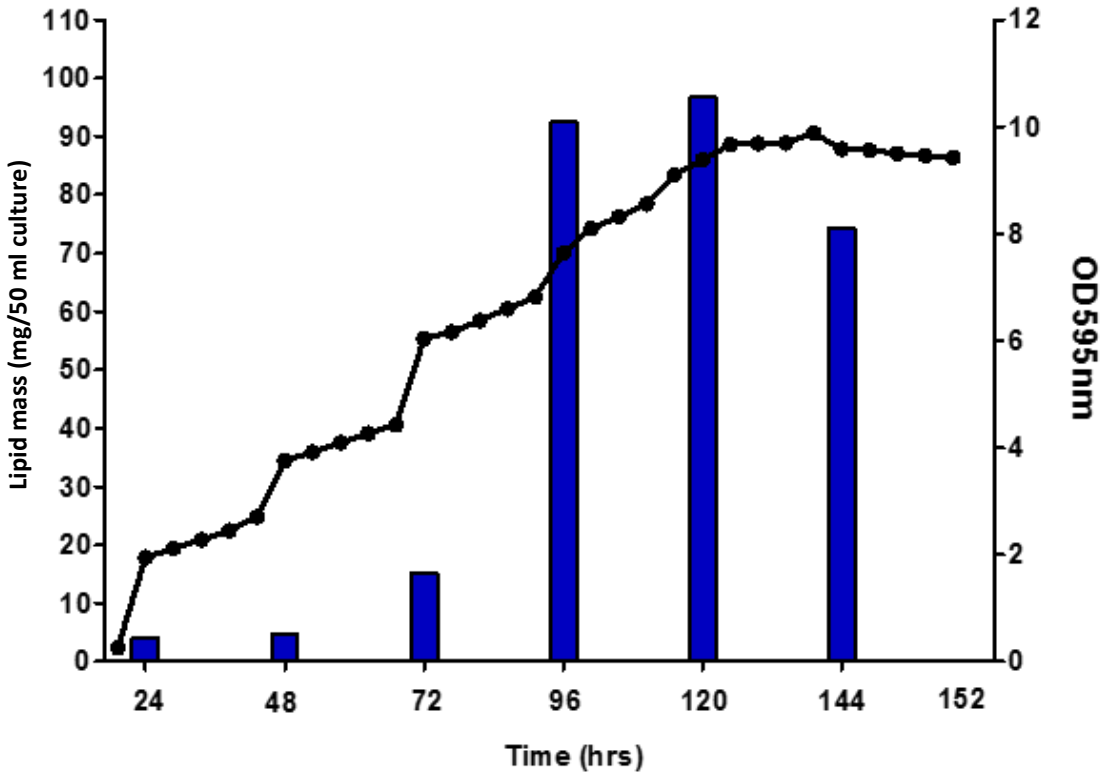


**Figure 3.9: Characterisation of lipid accumulation in nitrogen limiting media (NLM) relative to growth phase of *L. starkeyi.*** As depicted by the graph in log phase (exponential growth ~48-72hrs) limited amounts of lipid are produced. A sharp increase is seen in late exponential/early stationary phase (~96 hrs) and a slight further increase in mid stationary phase (~120 hrs). After this point the amount of total lipid decreases in late stationary phase (~144 hrs). Lipid data are presented as mean mg mass of duplicate 50ml cultures.

## 3.3 Characterisation of growth and lipid accumulation in S. cerevisiae

Due to the availability of tools allowing genetic modification and the high conservation of many signalling pathways to that of mammalian cells, *S. cerevisiae* is an excellent model organism for use in elucidating components involved in lipid accumulation.

*S. cerevisiae* also accumulates lipid as it enters stationary phase as a result of nutrient limitation. However, as a non-oleaginous yeast it accumulates approximately 11% total lipid (Sitepu *et al.* 2012) compared to *L. starkeyi* which accumulates approximately 70% of total lipid in stationary phase. The previously devised methodology was applied in the elucidation of whether the gravimetric method could be applied to the non-oleaginous yeast *S. cerevisiae*. In order to assess when cells enter stationary phase growth, where maximal lipid accumulation would occur, *S. cerevisiae* cultures were monitored and optical density readings taken over the course of 2 days.

Upon inoculating *S. cerevisiae* directly into limiting medium, and monitoring growth for the 48 hr period, limited growth was observed (data not shown). Therefore, as in Section 3.2.1, cell mass was firstly accumulated in rich medium before transferring mid exponentially growing cells (8 x $10^6$ cells/ml) into limiting media. Exponentially growing cells (7 hrs) were transferred to limiting media as determined by monitoring growth of *S. cerevisiae* in YPD, Figure 3.10. Exponential growth was shown to begin ~5 hrs after inoculation into YPD. Growth of *S. cerevisiae* after re-suspension in limiting medium is detailed in Figure 3.11.

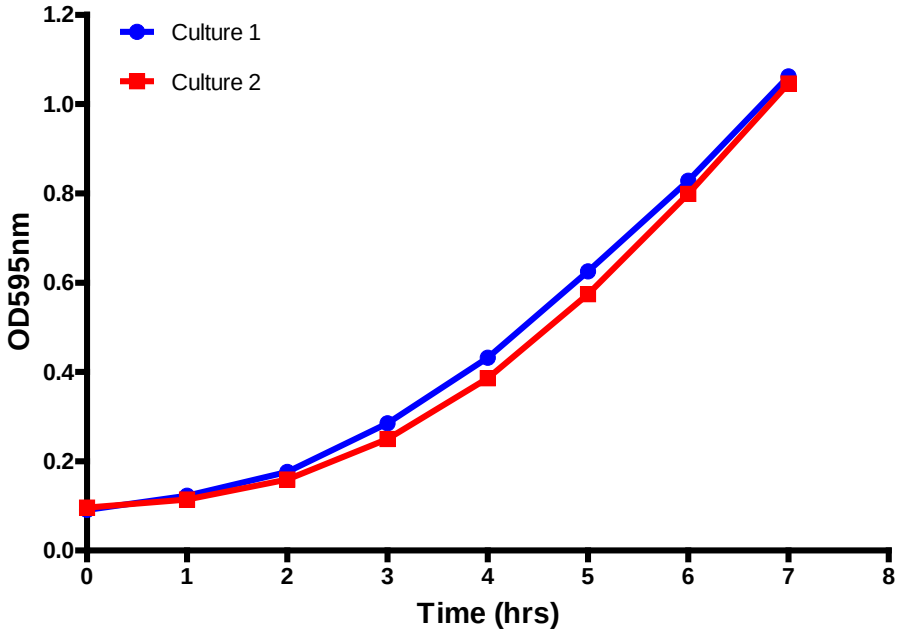


**Figure 3.10: Growth of *S. cerevisiae* in YPD medium** Cultures were diluted in YPD medium to a density of 2 x $10^6$ cells/ml. Cultures were incubated with shaking at duplicate, 30°C and optical density readings taken each hour to determine the exponential growth phase of *S. cerevisiae*. Growth curves were conducted in duplicate with blue and red lines denoting growth pattern observed from two distinct colonies.

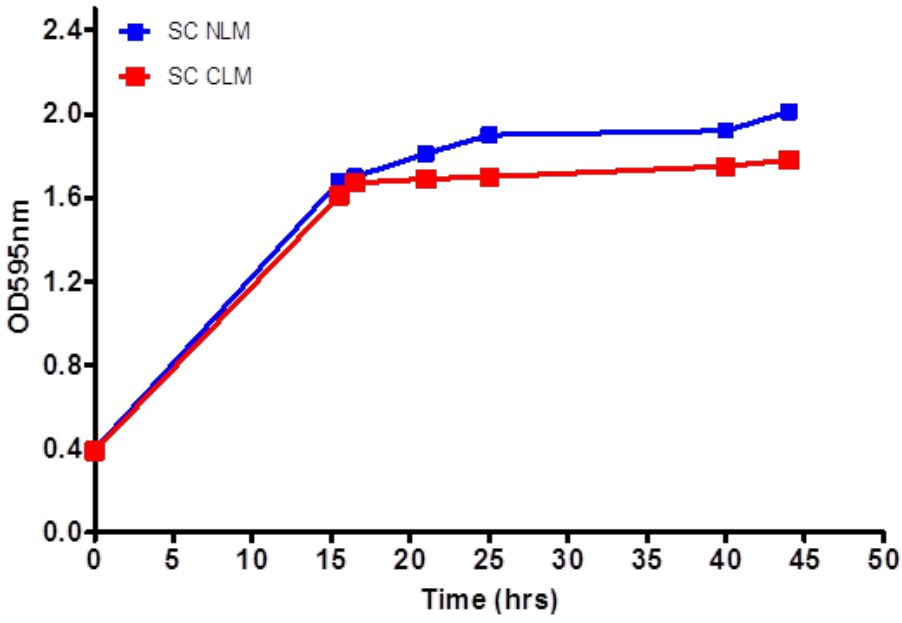


**Figure 3.11: Growth analysis of *S. cerevisiae* whereby cell mass was accumulated in YPD before re-suspension in limiting medium in order to determine stationary phase.** Cells from log phase YPD cultures were resuspended in either nitrogen limiting (NLM) or carbon limiting (CLM) media to give a starting optical density half that of the original YPD culture. Cultures were allowed to grow, with shaking at 180rpm, 30°C and readings taken as appropriate until stationary phase was reached, as indicated by plateaued growth.

As Figure 3.11 shows *S. cerevisiae* stationary phase was achieved within approximately 15 hrs of inoculation in both CLM and NLM.

Following on from the data derived from initial growth experiments, a more detailed analysis of *S. cerevisiae* was undertaken; along with this the lipid accumulation was also investigated. Growth and lipid analyses were conducted, as previously described in Section 3.2, using wild type *S. cerevisiae*. Growth of the cultures was monitored via optical density; (Figure 3.12), and lipid extractions carried out at 0, 15, 23, 39 and 67 hrs to align with and a range of points in stationary phase (15 hrs onwards), (Figure 3.13). These time points were chosen so that samples could be obtained largely from the stationary phase of growth, where maximal lipid accumulation was expected to occur in order to allow the assessment of the suitability of gravimetric measurement.

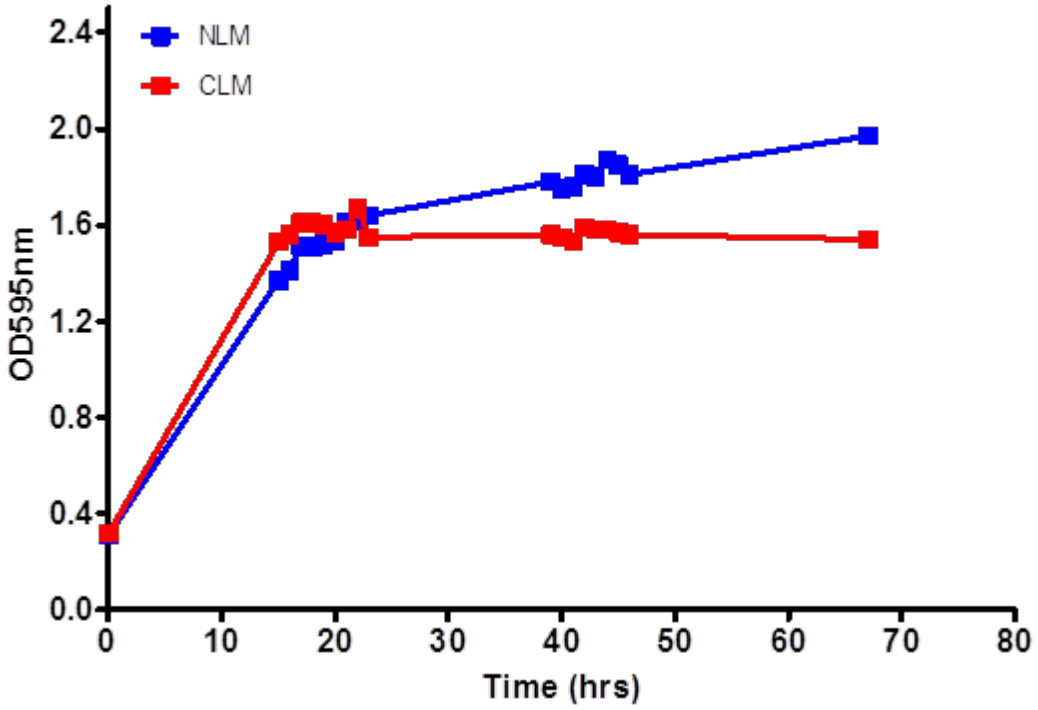


**Figure 3.12: Growth analyses of *S. cerevisiae* after re-suspension of YPD pre-culture into limiting medium.** After re-suspension in either nitrogen limiting (NLM) or carbon limiting (CLM) media, cultures were allowed to grow with shaking at 180rpm, 30°C. Optical density readings were taken hourly each day to construct the curve. As the growth curve shows cultures are reaching early stationary phase at ~20 hrs follow by mid stationary ~40 hrs and late stationary at ~60 hrs.

Lipid extractions from 50 ml of culture, analysed by gravimetric means, yielded little lipid mass over the full course of growth analysed (minimum 0.2 mg and maximum 1.7mg). This was not accurately measurable by using the methodology for *L. starkeyi* and weighing on an analytical balance. As shown by the raw lipid mass data, the amount of lipid measured did not exceed 2 mg total weight per 50 ml culture, (Figure 3.13). The amount of lipid increased 4.5 fold from 0 to 15 hrs (0.22 mg to 1 mg/50 ml culture), with a further increase of 1.4 fold from 15 to 23 hrs (1 mg to 1.4 mg/50 ml culture). Although due to high error in measurements from 0 and 15 hr samples it was deemed that the gravimetric method is inappropriate for use with *S. cerevisiae*.

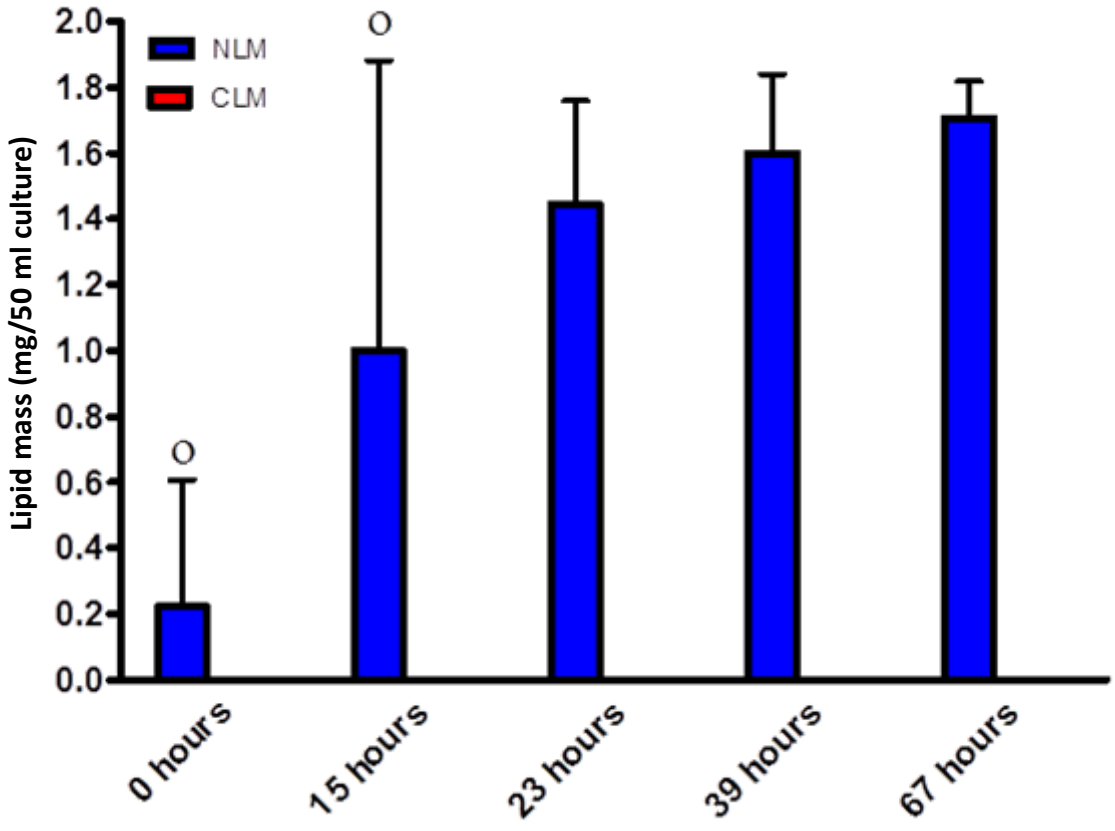


**Figure 3.13: Characterisation of *S. cerevisiae* lipid accumulation in nitrogen limiting (NLM) and carbon limiting (CLM) media.** At the time points indicated on the graph samples were harvested from the cultures used to construct the growth curve in Figure 11. Raw lipid mass data is plotted (see Figure 13 for adjusted lipid mass). As the graph shows there little lipid produced by *S. cerevisiae* of the course of different growth phases, with the maximum being ~1.7 mg. As the amounts are so small it is difficult to accurately quantify lipid mass by standard weight measurement (as indicated by the error observed at 0 and 15 hrs). Data are presented as means of triplicates ± SD per 50ml culture. o indicates an outlier was present within the triplicate.

### 3.3.2 Growth characterisation of S. pombe in limiting medium

As with *S. cerevisiae* there are also numerous genetic tools that can be utilised to deconstruct the regulation of lipid accumulation in *S. pombe*. *S. pombe* was cultured in complex medium (YES) prior to re-suspension in NLM and CLM. Growth curves were conducted by transferring exponentially growing cells from YES into NLM and CLM at a density of 8 x $10^6$ cells/ml. Growth was then monitored via optical density (OD) at 595nm for 48 hrs. The results are shown in Figure 3.14.

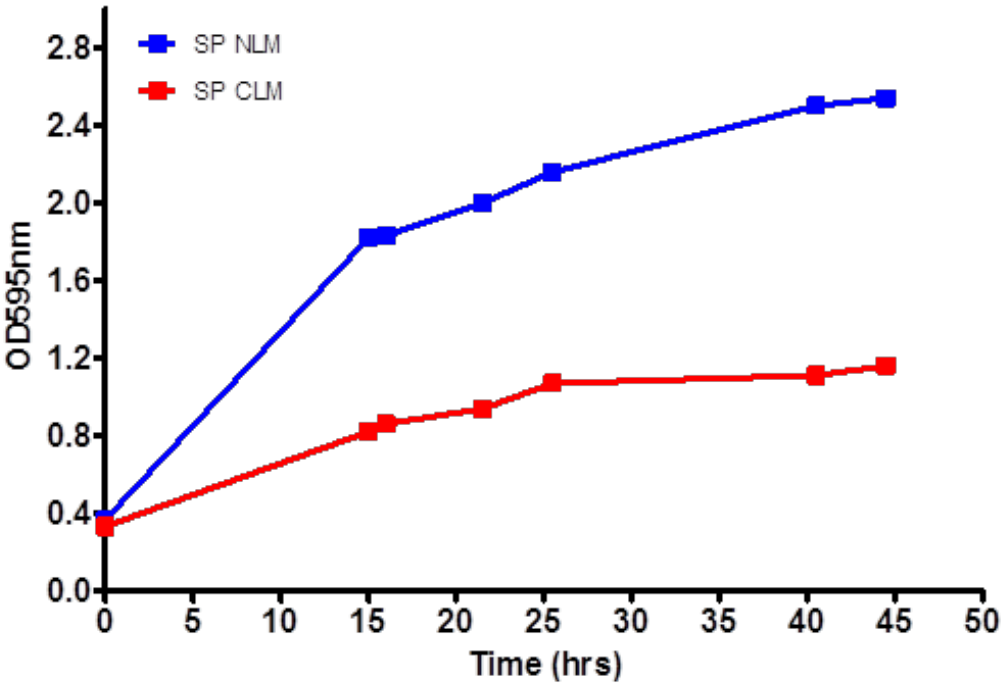


**Figure 3.14: Growth analysis of *S. pombe* whereby cell mass was accumulated in YES before re-suspension in limiting medium in order to determine stationary phase.** Cells from log phase YPD cultures were resuspended in in either nitrogen limiting (NLM) or carbon limiting (CLM) media to give a starting optical density half that of the original YES culture. Cultures were allowed to grow, with shaking at 180rpm, 30°C and readings taken as appropriate until stationary phase was reached, as indicated by plateaued growth.

As shown by the growth curve, *S. pombe* growth in limiting medium was analogous to that of *S. cerevisiae* producing a slow growth phenotype, with growth plateauing within 15-20 hrs post re-suspension in limiting medium (Figure 3.14). Based on the gravimetric results obtained with *S. cerevisiae* it was postulated that a measurable amount of lipid would not be obtained by gravimetric means in *S. pombe,* as it is also a non-oleaginous yeast species.

### 3.3.3 Growth analysis of the three yeast species in minimal medium

Following on from the experiments conducted within this chapter it was found that growth in limiting medium potentially causes an autophagic, mitophagic and stress response in both *S. cerevisiae* and *S. pombe* (Crespo J. L. and Hall 2002, Mukaiyama *et al.* 2009). As a result, growth and lipid accumulation was monitored using defined minimal medium instead. *L. starkeyi* and *S. cerevisiae* were cultured in yeast nitrogen base (YNB) and *S. pombe* in Edinburgh minimal medium (EMM) supplemented with relevant amino acids. This strategy was based on data from several published papers that employed minimal medium in lipid accumulation analyses (Park *et al.* 2009, Shin *et al.* 2012) and investigated responses of lipid production to genetic manipulation (Kamisaka *et al.* 2006, Shi *et al.* 2012).

Furthermore, these defined media were chosen as others have utilised YNB and EMM to investigate the stress response via MAP Kinase and mTOR pathways as well as the activation of these pathways in response to external stimuli (Berlanga *et al.* 2010, Maayan *et al.* 2012, Valbuena *et al.* 2012). Figures 3.15, 3.16 and 3.17 show detailed growth of *L. starkeyi, S. cerevisiae* and *S. pombe*, in minimal medium.

#### 3.3.3.1 Growth of L. starkeyi in yeast nitrogen base medium

Growth curves were conducted for wild type *L. starkeyi* by firstly accumulating cell mass in YPD before transferring exponentially growing cells to YNB medium, giving a cell density of 4 x $10^6$ cells/ml. Growth was monitored via optical density for a period of 72 hrs until stationary phase was reached (Figure 3.15).

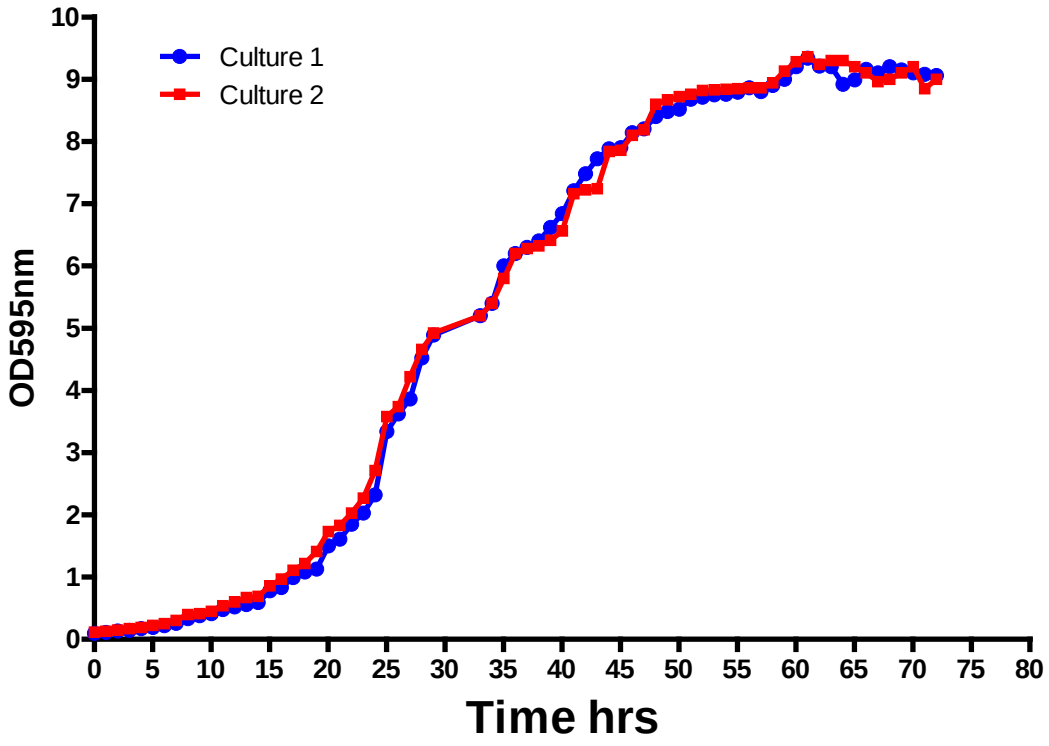


**Figure 3.15: Growth curve of *L. starkeyi* in YNB medium.** Cells from log phase YPD cultures were resuspended in minimal medium to give a starting optical density half that of the original YPD culture, 0.1. Cultures were allowed to grow, with shaking at 180rpm 30°C and readings taken as seen appropriate until stationary phase was reached, as indicated by plateaued growth. Growth curves were conducted in duplicate with blue and red lines denoting growth pattern observed from two distinct colonies.

As shown by Figure 3.15, *L. starkeyi* cells remained in lag phase for 15 hrs post re-suspension in YNB medium before exponential growth is observed. Cells then entered early stationary phase after approximately 48 hrs.

### 3.3.3.2 Growth of S. cerevisiae in yeast nitrogen base medium

Growth curves were conducted for wild type *S. cerevisiae* by firstly accumulating cell mass in YPD before transferring mid exponentially growing cells to give a cell density of 2 x $10^6$ cells/ml in YNB medium. Growth was monitored via optical density for a period of 21 hrs, (Figure 3.16), until growth plateaued, indicative of cells in stationary phase.

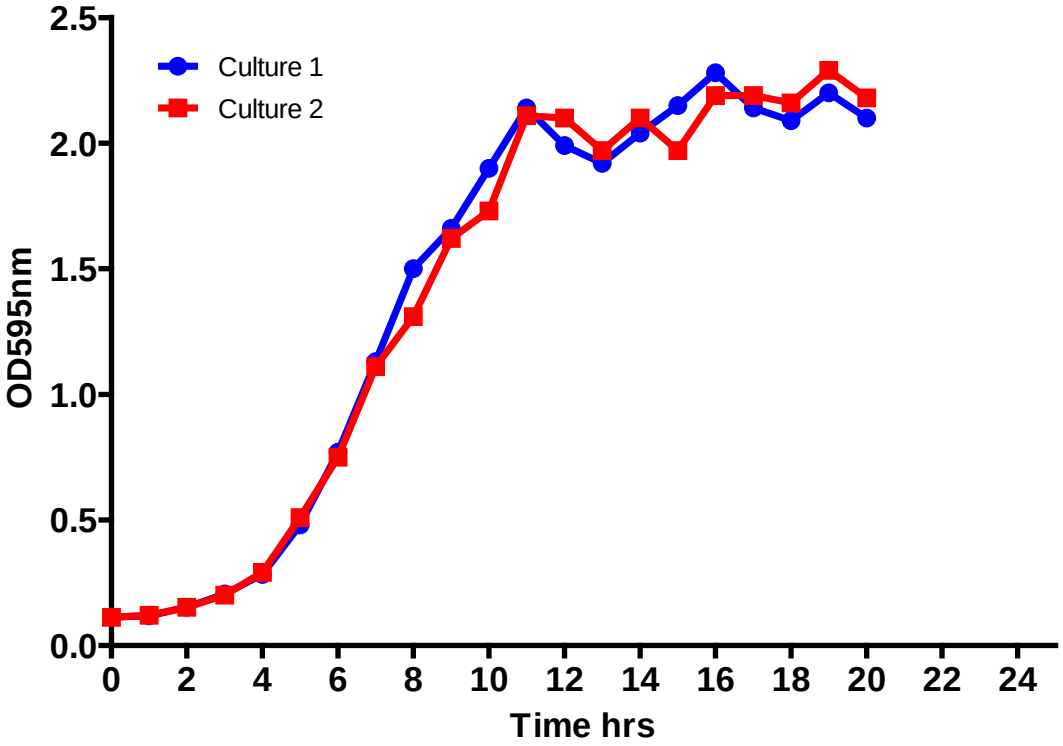


**Figure 3.16: Growth curve of *S. cerevisiae* in YNB medium.** Cells from log phase YPD cultures were resuspended in minimal medium to give a starting optical density half that of the original YPD culture, 0.1. Cultures were allowed to grow, with shaking at 180rpm, 30°C and readings taken as appropriate until stationary phase was reached, as indicated by plateaued growth. Growth curves were conducted in duplicate with blue and red lines denoting growth pattern observed from two distinct colonies.

As depicted by Figure 3.16, the lag phase of *S. cerevisiae* continued for 5 hrs after re-suspension of cells in YNB medium before exponential phase of growth was entered. Early stationary phase occurred at approximately 12 hrs post re-suspension.

### 3.3.3.3 Growth of S. pombe in Edinburgh minimal medium

Growth curves were conducted for wild type *S. pombe* utilising the same procedure as that given for *S. cerevisiae* (Section 3.3.3.2) Growth was monitored via optical density for a period of 32 hours until stationary phase was reached (Figure 3.17).

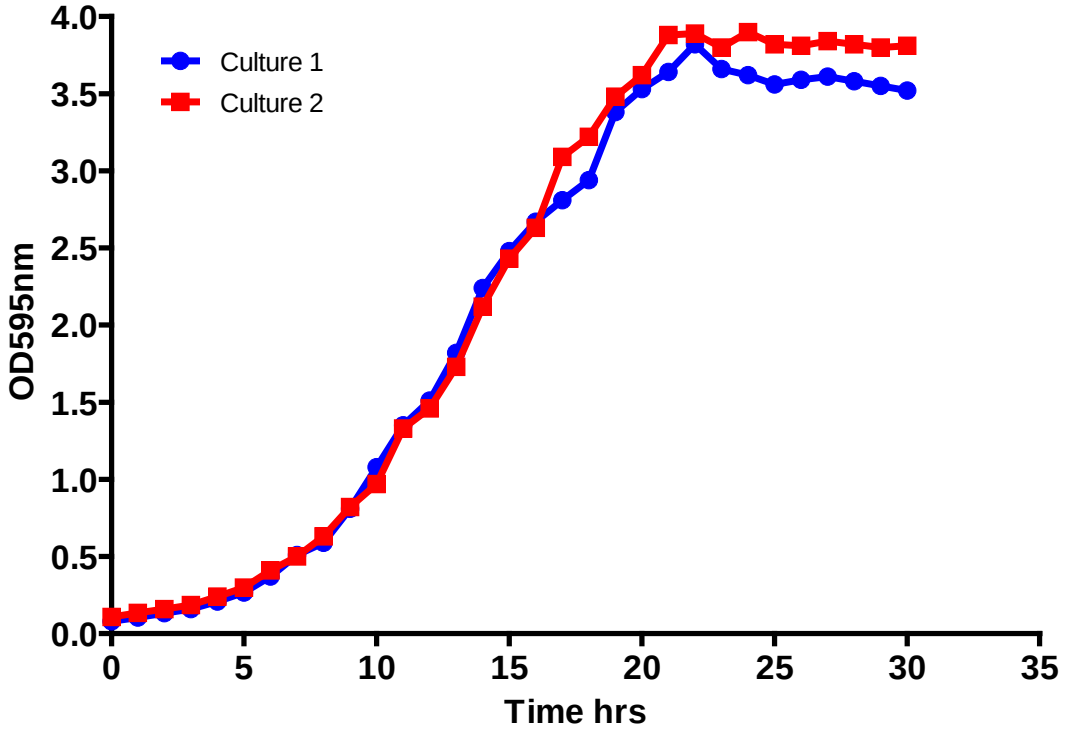


**Figure 3.17: Growth curve of *S. pombe* in Edinburgh minimal media (EMM) medium.** Cells from log phase YES cultures were resuspended in minimal medium to give a starting optical density half that of the original YES culture, 0.1. Cultures were allowed to grow, with shaking at 180rpm 30°C and readings taken as seen appropriate until stationary phase was reached, as indicated by plateaued growth. Growth curves were conducted in duplicate with blue and red lines denoting growth pattern observed from two distinct colonies.

As shown by Figure 3.17, *S. pombe* cells remained in lag phase for 8 hrs post re-suspension in EMM medium before exponential growth was observed. Cells then entered early stationary phase after approximately 20 hrs.

Having determined the growth phases for all three yeast species in minimal medium, a lipid accumulation profile of each yeast species was then required to identify optimal time points for assessing the accumulation of lipids. This was accomplished utilising a Nile red microplate assay.

## 3.4 Development of a Nile red screening method for accumulation of lipids

Following the results of gravimetric analyses conducted in the non-oleaginous yeast *S. cerevisiae*, other methodologies were trialled to identify a suitable method to detect and quantify lipid accumulation in low lipid yeasts. Thin layer and gas chromatographic methods were initially employed as qualitative and quantitative techniques respectively to investigate the accumulation of neutral lipids in wild type *S. cerevisiae*. Nevertheless, these methods were deemed inappropriate for the current investigation as the methodology proved to be time consuming and labour intensive. This study demanded an increased throughput method of semi-quantitative analysis due to the numerous deletion strains that would require screening in order to distinguish phenotypes.

Nile red (9-diethylamino-5H-benzo[a]phenoxazine-5-one), is a lipophilic dye that has been used extensively to visualise lipids in a range of organisms. In a study by Sitepu *et al.* (2012), Nile red was utilised to quantify lipids in numerous oleaginous species and was also demonstrated to have the ability determine lipid content in non-oleaginous yeast species, including *S. cerevisiae* (Sitepu *et al.* 2012).

### 3.4.1 Optimisation of Nile red methodology

Based on the gravimetric data obtained for *S. cerevisiae* and the labour intensive, low throughput nature of gas and thin layer chromatography, Nile red was trialled in a modified microplate assay. The Nile red assay used was adapted from a method by Sitepu *et al.* (2012) with a number of modifications. To undertake screening, Krystal 2000 96-well plates were chosen over plates utilised in the previous study (Costar microplates product #3370), due to the plates consisting of individually moulded wells.

Although Nile red has varying fluorescence properties in a range of media types (Sitepu *et al.* 2012), the fluorescence properties of spent culture media may differ. As such, all cells were washed twice in phosphate buffered saline (PBS) to reduce background fluorescence resulting from culture medium; this was carried out for all three yeast species. In addition, fluorescence data obtained was corrected against not only cell density but additionally background fluorescence resulting from PBS. This improved the accuracy of the method by eliminating fluorescence occurring from the background medium, PBS in this case, thus

ensuring that RFU values obtained are a measure of fluorescence pertaining to cellular lipid content alone.

#### 3.4.1.2 The Nile red fluorescence method showed comparable trends to the gravimetric measurement of total lipids in the oleaginous yeast, L. starkeyi

To develop and optimise the use of the Nile red method for high throughput screening of lipid content in yeast, we first validated the method using the oleaginous yeast *L. starkeyi.*

As lipids accumulated in oleaginous yeast species have the ability to be determined gravimetrically, the sum of relative fluorescence intensities from each wavelength obtained over a range of growth points of *L. starkeyi* were compared to absolute lipid content determined gravimetrically. Figure 3.18 shows the results. The time points chosen were the same as those utilised in the initial lipid characterisation of *L. starkeyi* in Section 3.2.2.

As shown in Figure 3.18, the same trend of lipid accumulation was observed for both gravimetric and fluorescence determination of total lipids with increasing amounts of lipid until the point of late stationary phase (96 hrs) before a decrease at 120 and 144 hrs. This data demonstrated the Nile red method gave trends equivalent to the well-established gravimetric method, and so was appropriate to use for further studies.

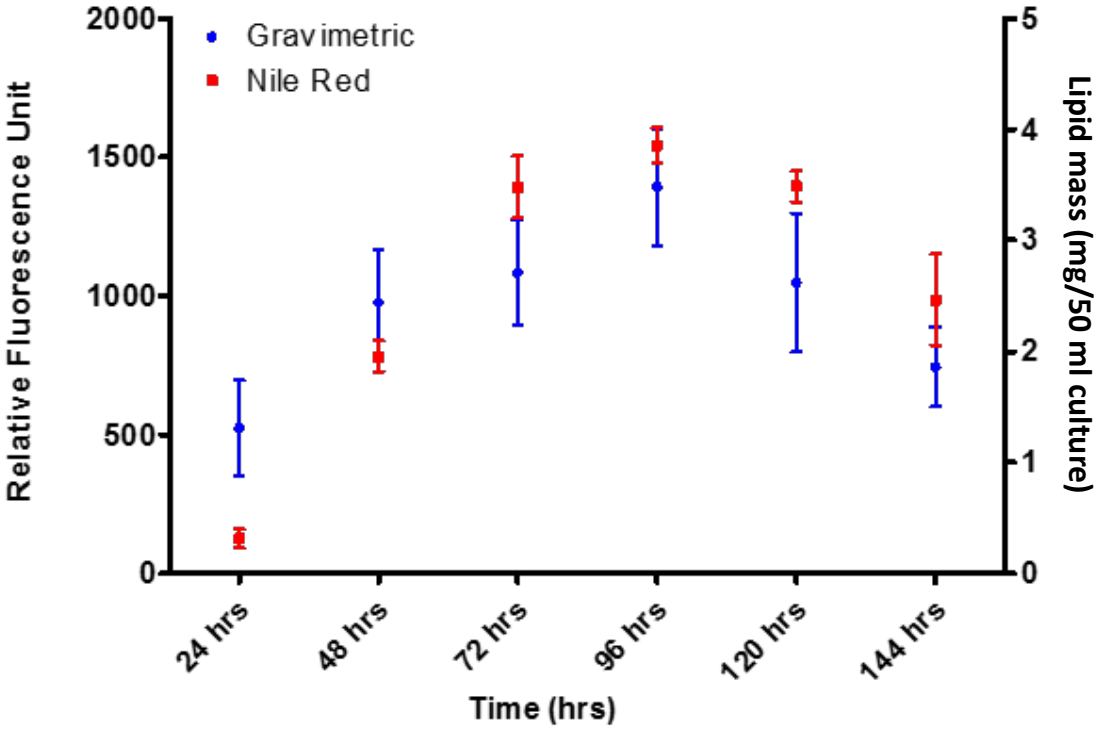


**Figure 3.18: Comparison of total lipid determination by Nile red and gravimetric assessment in *L. starkeyi* cells.** Cells were harvested at 24 hourly intervals until 144 hrs post resuspension in YNB. For Nile red cells were washed twice in PBS before adjusting to a cell density of 4 x $10^7$ cells/ml. 10 x $10^6$ cells were transferred to the wells of black 96-well plates in triplicate. 25µl PBS/DMSO (1:1 v/v) and 5µg/ml Nile red were added to each sample. Plates were screened using the wavelengths: excitation 485 nm, emission 535 nm (neutral lipids) and excitation 535 nm, emission 590 nm (polar lipids). Total lipids were extracted and measured by gravimetric means as describe in Section 2.2. Results of gravimetric analyses were compared to combined relative fluorescence values obtained for both neutral and polar lipids. All values are normalised to a cell density of 4 x $10^7$ cells, corresponding to $OD_{595}$ of 1.0. Data are shown as means of triplicate experiments ± SD.

### 3.4.2 Nile red for use as a selective lipophilic dye

One feature of the Nile Red dye, identified by Greenspan *et al.* (1985), but seldom used experimentally, is that it can select between different lipid subtypes present within cells. Depending on the hydrophobicity of the lipid type with which Nile red is associated, a shift in the emission spectra from red to yellow is observed (Diaz *et al.* 2008).

Polar lipids, such as phospholipids (PLs), are stained red and mainly found to be present in cellular membranes. Conversely neutral lipids, such as TAGs and SEs, found to be present in intracellular lipid droplets, are stained yellow (Greenspan *et al.* 1985).

To determine the specificity of Nile red at the two emission wavelengths, fluorescence microscopy was used to visualize neutral and polar lipids within cells (Figure 3.19). Samples of *L. starkeyi* cultures were taken at mid stationary phase (72 hrs) and stained with Nile red, before being visualised. Polar, membranous lipids and those associated with intracellular lipid droplets could be readily distinguished via fluorescence microscopy using the two wavelengths described. (Figure 3.19).

Characteristic of a number of oleaginous yeast species, a large lipid filled vacuole (neutral lipids visualised at an emission wavelength of 535 nm) was observed in *L. starkeyi* cells viewed during stationary phase (Certik *et al.* 1999). This can be distinguished easily from the more polar membranous structures (polar lipids, visualised at an emission wavelength of 590 nm).

To determine if Nile red could distinguish between polar and neutral lipids in the non-oleaginous yeast, *S. cerevisiae* and *S. pombe*, cells were stained and viewed using fluorescent microscopy. Samples for *S. cerevisiae* were harvested at mid stationary phase (18 hrs) for Nile red staining. Viewed under yellow-gold fluorescence the stationary phase Nile red stained cells exhibited discrete fluorescent bodies, of varying sizes, throughout the cytoplasm of the cell. This pattern of fluorescence was similar across the population of *S. cerevisiae* cells observed and indicated the presence of intracellular lipid droplets. However, under red fluorescence the cells showed consistent staining across the cell, with limited appearance of fluorescent bodies within the cytoplasm.

As with *S. cerevisiae,* fluorescence microscopy of Nile red stained *S. pombe* cells in stationary phase (24 hrs) at 535 nm showed varying numbers of distinct fluorescent bodies throughout the cytoplasm of the cell, indicative of intracellular neutral lipid droplets. At 590 nm, there was consistent staining across the cell suggesting staining of the polar lipids in the cell membrane with some appearance of polar lipid monolayer surrounding the lipid droplets.

Green fluorescence observed in colour images results from the merging of images containing both red and yellow fluorescence.

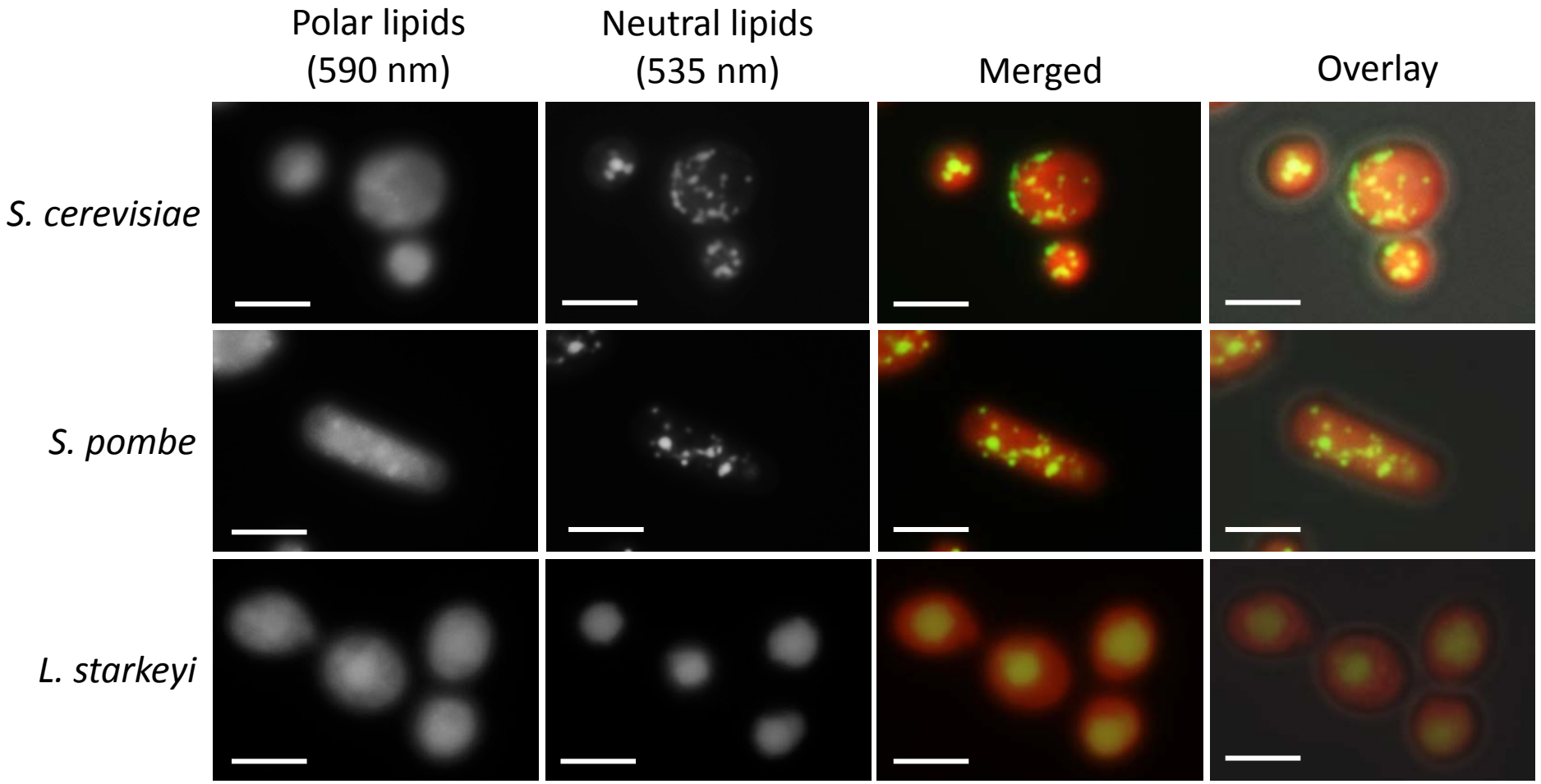


**Figure 3.19: Fluorescence microscopy highlighting emission properties of Nile Red stained yeast cells.** *S. cerevisiae, S. pombe* and *L. starkeyi* stationary phase cells were stained with Nile Red and visualised for both polar (590 nm emission) and neutral (535 nm emission) lipids. Scale bar 5µM.

Nile red, via microscopic means, appears to have the ability to distinguish between the two main subtypes of lipids present in cells. Can it also be used to distinguish the levels of each class of lipids?

### 3.4.2.2 Using dual wavelengths, the Nile red fluorescence method can distinguish levels of neutral and polar lipids in L. starkeyi

To further test the ability of Nile red to distinguish between neutral and polar lipid pools, the dual wavelengths for Nile red fluorescence were used to assess amounts of fluorescence pertaining to cellular lipid amounts during growth. Figures 3.20 and 3.21, show fluorescence intensity values obtained for *L. starkeyi* when screened for lipid molecules at each emission wavelength, neutral and polar lipids, across the growth series. As expected for neutral lipids, fluorescence intensity increased gradually yet sharply at each time point from 48 hrs until cells approached stationary phase at 72 – 96 hrs, before a marked decrease was observed at 144 hrs.

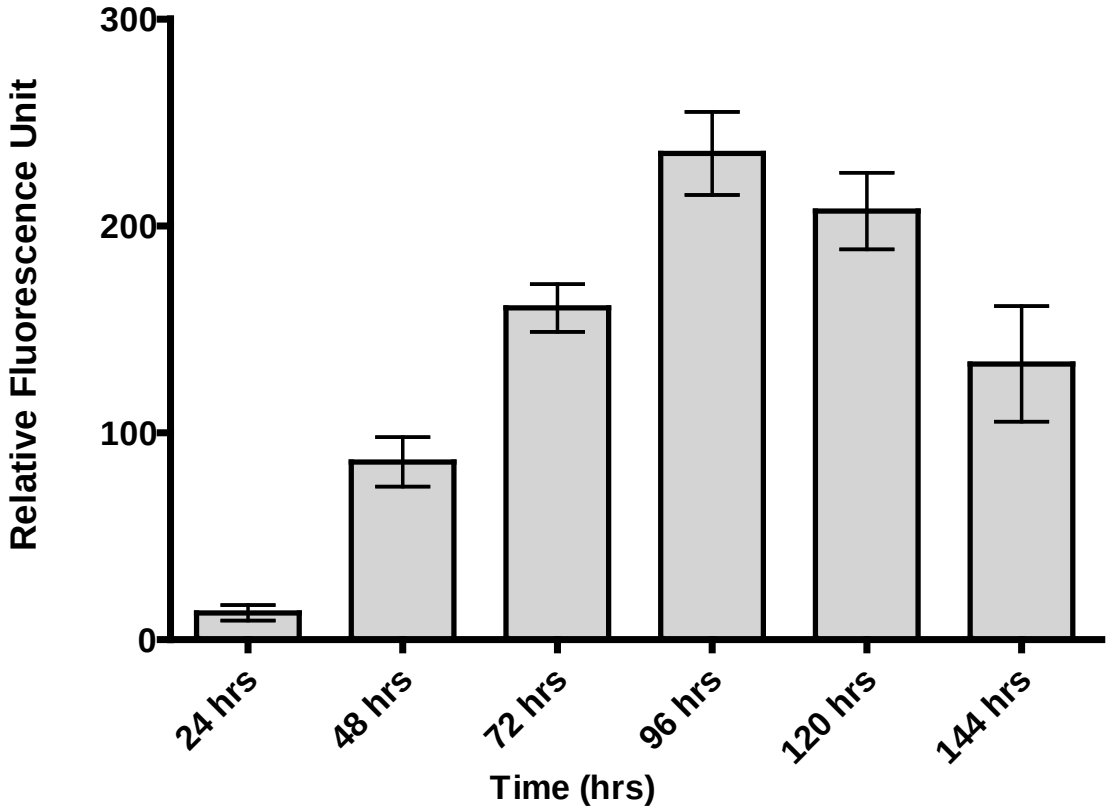


**Figure 3.20: Neutral lipid fluorescence intensity of Nile red stained *L. starkeyi* over a range of growth phases.** Cells were harvested at 24 hourly intervals until 144 hrs post resuspension in YNB. For Nile red analysis, cells were washed twice in PBS before adjusting to a cell density of 4 x $10^7$ cells/ml. 10 x $10^6$ cells were transferred to the wells of black 96-well plates in triplicate. 25µl PBS/DMSO (1:1 v/v) and 5µg/ml Nile red were added to each sample. Fluorescence intensity was measured using an excitation wavelength of 485 nm and an emission wavelength of 535 nm. All values are normalised to a cell density of 4 x $10^7$ cells, corresponding to $OD_{595}$ of 1.0. Data are shown as means of triplicate experiments ± SD.

As expected for more polar lipids (Figure 3.21) after an initial increase post 48 hrs, fluorescence levels remained relatively constant until late stationary phase (Becker and Lester 1977).

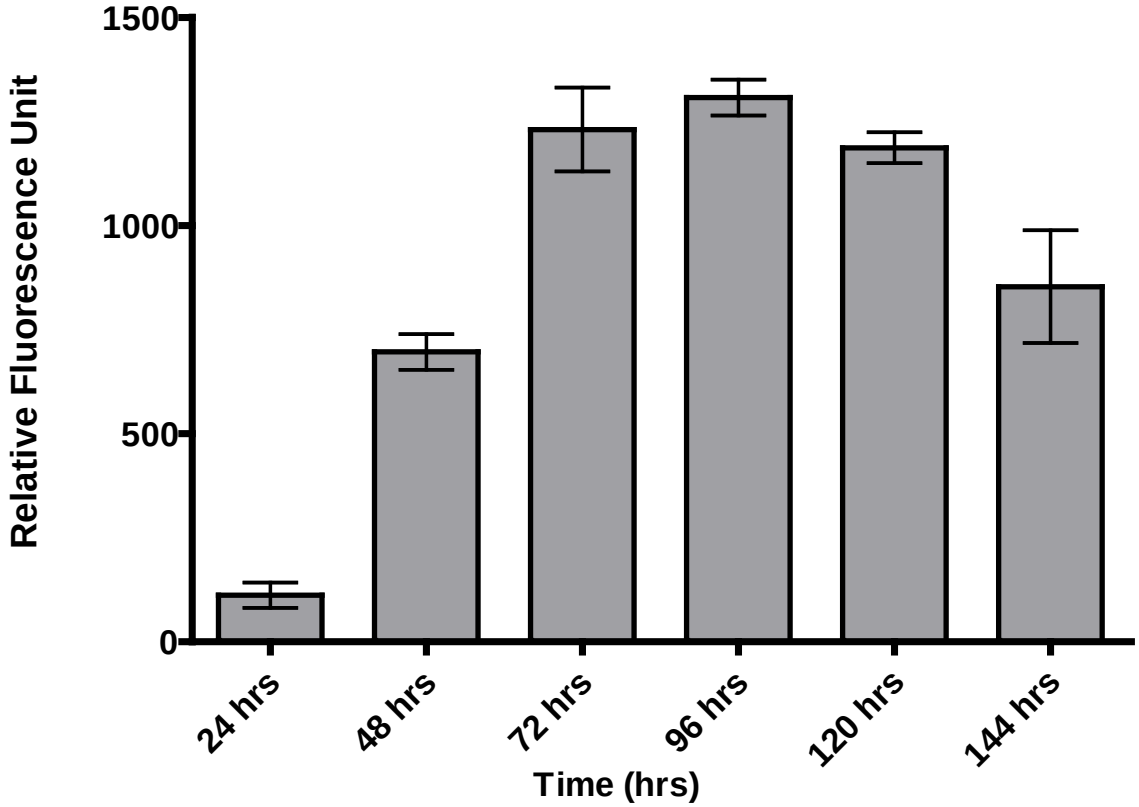


**Figure 3.21: Polar lipid fluorescence intensity of Nile red stained *L. starkeyi* over a range of growth phases.** Cells were harvested at 24 hourly intervals until 144 hrs post resuspension in YNB. For Nile red analysis, cells were washed twice in PBS before adjusting to a cell density of 4 x $10^7$ cells/ml. 10 x $10^6$ cells were transferred to the wells of black 96-well plates in triplicate. 25µl PBS/DMSO (1:1 v/v) and 5µg/ml Nile red were added to each sample. Fluorescence intensity was measured using an excitation wavelength of 535 nm and an emission wavelength of 590 nm. All values are normalised to a cell density of 4 x $10^7$ cells, corresponding to $OD_{595}$ of 1.0. Data are shown as means of triplicate experiments ± SD.

These results indicated the dual wavelength Nile red method was a viable increased throughput screening method for determination of neutral and polar lipid content in oleaginous yeast cells.

## 3.5 Determination of lipid content in the non-oleaginous budding yeast, S. cerevisiae using the Nile red fluorescence assay

As previously demonstrated in Section 3.3, the low lipid content of *S. cerevisiae* cells means accurate measurement by gravimetric means was difficult, therefore alternative methods are required.

Growth phases on which to conduct Nile red screening were determined from the growth curve described in Section 3.3.3.2 (Figure 3.16) and reflected each growth phase of *S. cerevisiae* cells in YNB, ranging from exponential through to late stationary phase.

Figure 3.22 shows neutral and Figure 3.23 polar lipid levels. Fluorescence levels pertaining to cellular lipid content increased over time from exponential growth leading into mid stationary phase (18 hrs) before decreasing at late stationary phase, (48hrs) in a similar manner to that observed for *L. starkeyi.*

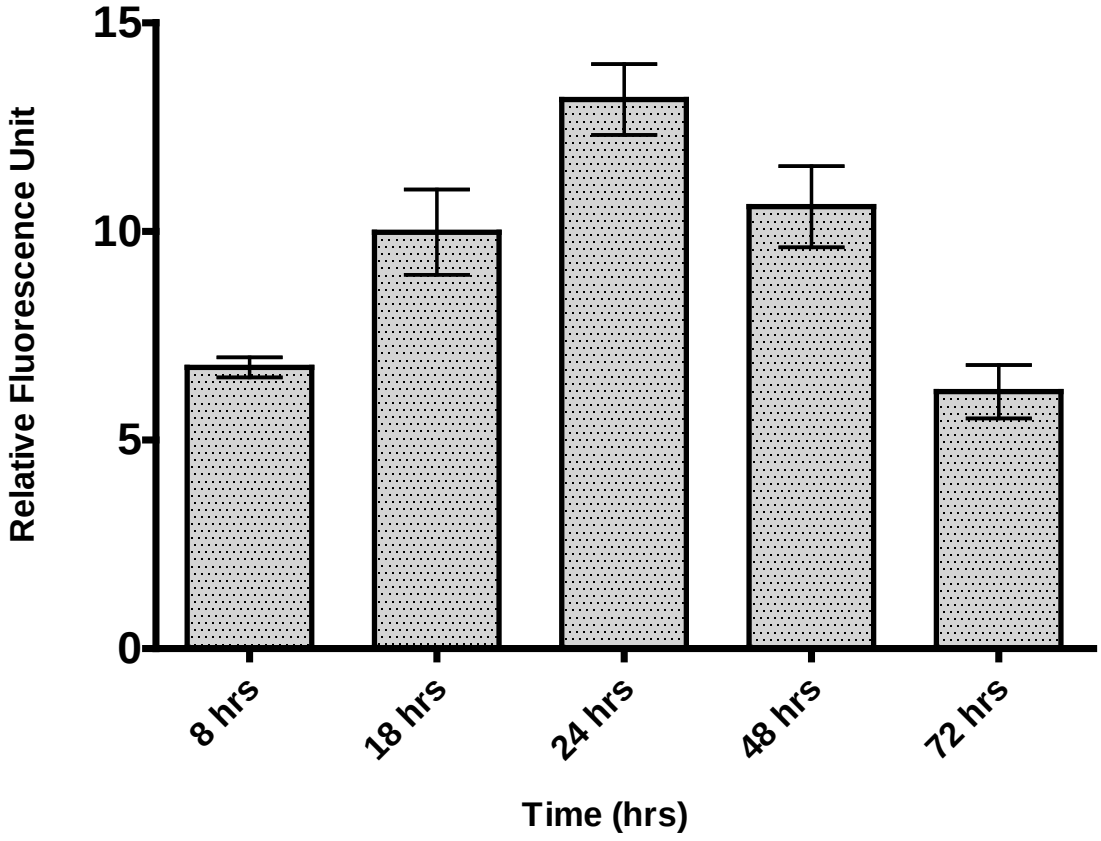


**Figure 3.22: Neutral lipid fluorescence intensity of Nile red stained *S. cerevisiae* over a range of growth phases.** Cells were harvested at 8, 18, 24, 48 and 72 hrs post resuspension in YNB. For Nile red analysis cells were washed twice in PBS before adjusting to a cell density of $2 \times 10^7$ cells/ml. $5 \times 10^6$ cells were transferred to the wells of black 96-well plates in triplicate. 25µl PBS/DMSO (1:1 v/v) and 5µg/ml Nile red were added to each sample. Fluorescence intensity was measured using an excitation wavelength of 485 nm and an emission wavelength of 535 nm. All values are normalised to a cell density of $2 \times 10^7$ cells, corresponding to $OD_{595}$ of 1.0. Data are shown as means of triplicate experiments ± SD.

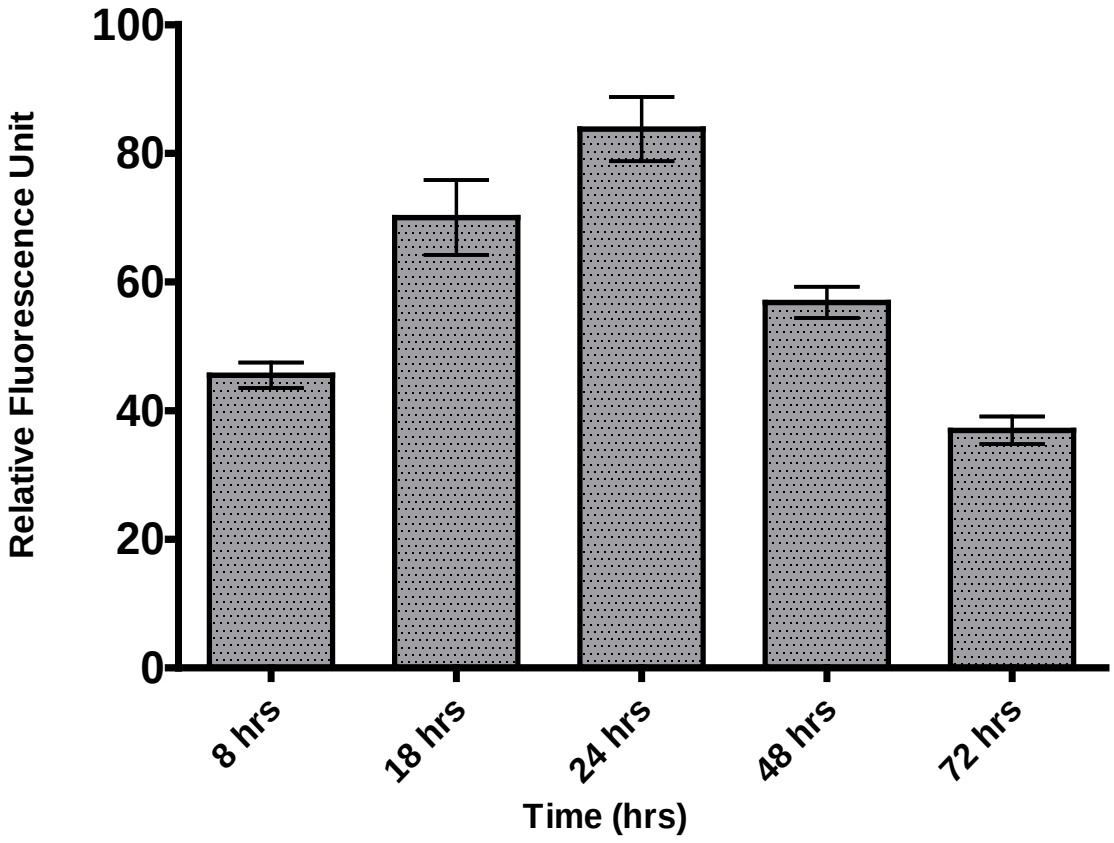


**Figure 3.23: Polar lipid fluorescence intensity of Nile red stained *S. cerevisiae* over a range of growth phases.** Cells were harvested at 8, 18, 24, 48 and 72 hrs post resuspension in YNB. For Nile red analysis cells were washed twice in PBS before adjusting to a cell density of 2 x $10^7$ cells/ml. 5 x $10^6$ cells were transferred to the wells of black 96-well plates in triplicate. 25µl PBS/DMSO (1:1 v/v) and 5µg/ml Nile red were added to each sample. Fluorescence intensity was measured using an excitation wavelength of 535 nm and an emission wavelength of 590 nm. All values are normalised to a cell density of 2 x $10^7$ cells, corresponding to $OD_{595}$ of 1.0. Data are shown as means of triplicate experiments ± SD.

### 3.5.1 The dual wavelength Nile red fluorescence assay can distinguish between polar and neutral lipid phenotypes in S. cerevisiae deletion strains

In order to test the sensitivity and selectivity of the dual wavelength Nile red method, a screen was undertaken with *S. cerevisiae* gene deletions known to produce a neutral lipid phenotype at stationary phase. The deletions used were *dga1, lro1* and *fat1.* The genes *DGA1* and *IRO1* encode enzymes involved in triacylglycerol synthesis with Dga1p (Diacylglycerol acyl transferase) catalysing the terminal step by acylating diacylglycerol using acyl-CoA as an acyl donor (Oelkers Peter *et al.* 2002). Lro1p is an acyltransferase that catalyses diacylglycerol esterification utilising phospholipid as the acyl donor (Oelkers P. *et al.* 2000). In *S. cerevisiae*, Dga1p and Lro1p catalyse 96% of TAG synthesis (Sandager *et al.* 2002), and so cells deleted for these genes would be expected to display a decreased neutral lipid phenotype compared with wild type cells. *FAT1* encodes a protein, which functions as a fatty acid transporter and a very long chain acyl-CoA synthetase (Choi J. Y. and Martin 1999); its deletion could be expected to result in an increased intracellular (neutral) lipid phenotype (Watkins *et al.* 1998).

Growth curves were carried out for all strains to ensure growth was similar between the mutant and wild type cells. No observed growth defects were seen with the deletions tested apart from a slightly increased lag phase coupled with a greater cell mass for the *fat1*Δ, as shown in Figures 3.24, 3.25 and 3.26.

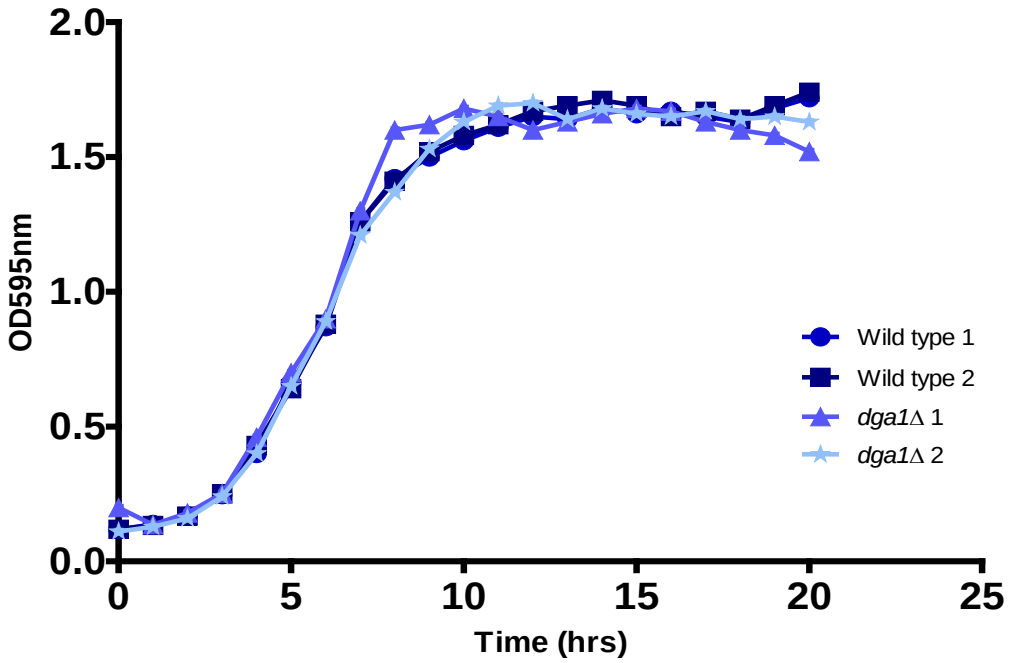


**Figure 3.24: Growth curves of *S. cerevisiae* wild type and *dga1Δ* under normal conditions in yeast nitrogen base medium (YNB).** Cultures were diluted to 2 x $10^6$ cells ($OD_{595}$ ~0.1) and incubated with shaking, 180rpm, at 30°C. Optical density readings were taken hourly until mid to late stationary phase was reached. Growth curves were conducted in duplicate (culture 1 and culture 2 for both WT and deletion strain) showing growth patterns observed for two distinct colonies of the same strain.

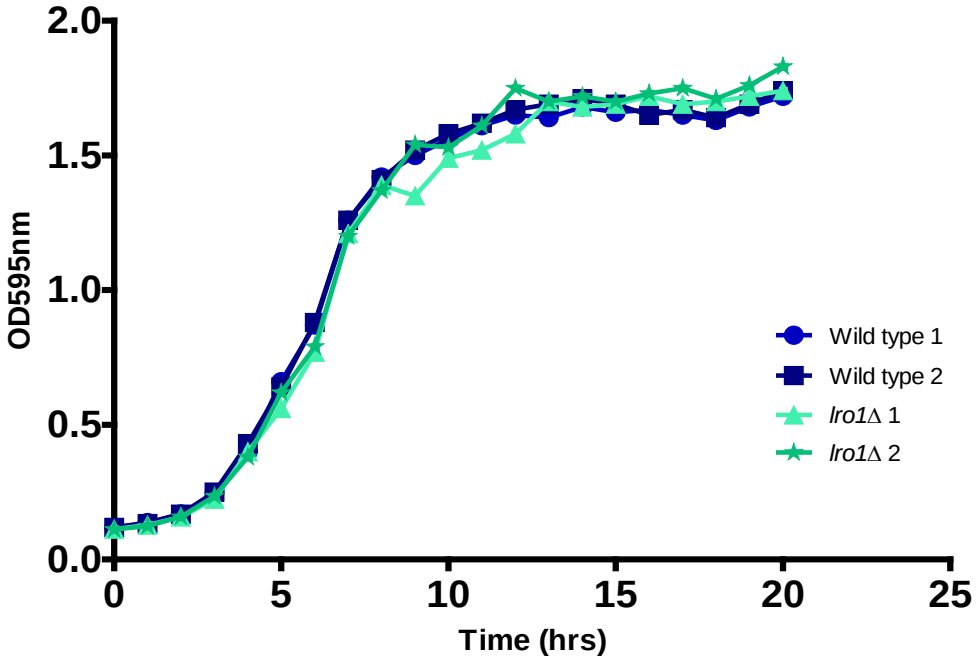


**Figure 3.25: Growth curves of *S. cerevisiae* wild type and *lro1Δ* under normal conditions in yeast nitrogen base medium (YNB).** Cultures were diluted to 2 x $10^6$ cells ($OD_{595}$ ~0.1) and incubated with shaking, 180rpm, at 30°C. Optical density readings were taken hourly until mid to late stationary phase was reached. Growth curves were conducted in duplicate (culture 1 and culture 2 for both WT and deletion strain) showing growth patterns observed for two distinct colonies of the same strain.

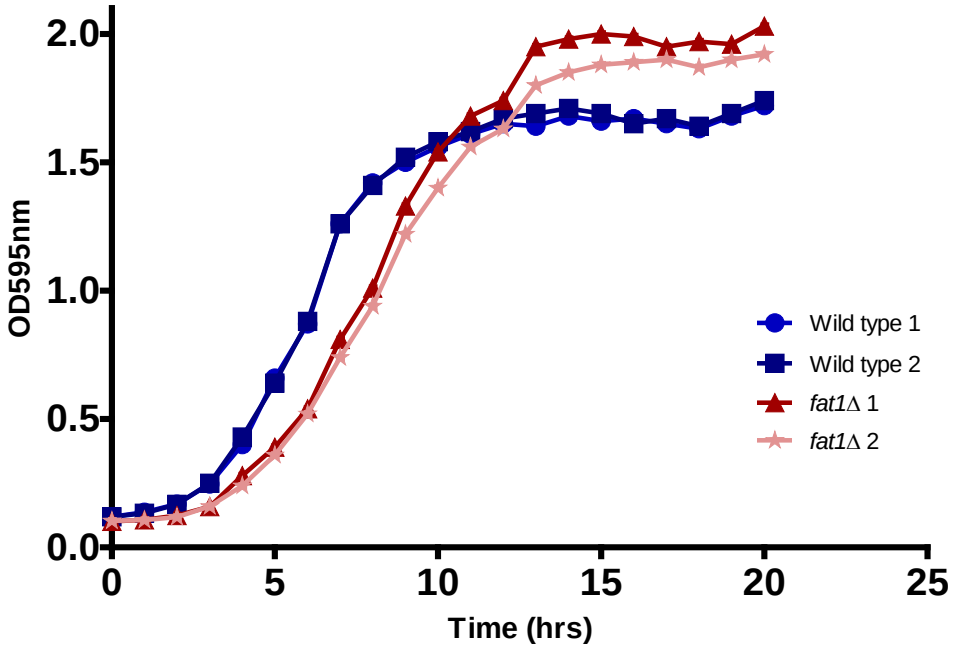


**Figure 3.26: Growth curves of *S. cerevisiae* wild type and *fat1Δ* under normal conditions in yeast nitrogen base medium (YNB).** Cultures were diluted to 2 x $10^6$ cells ($OD_{595}$ ~0.1) and incubated with shaking, 180rpm, at 30°C. Optical density readings were taken hourly until mid to late stationary phase was reached. Growth curves were conducted in duplicate (culture 1 and culture 2 for both WT and deletion strain) showing growth patterns observed for two distinct colonies of the same strain.

The Nile red assay was carried out in stationary phase wild type and deletion cells to infer phenotype, along with cells about to exit lag phase as an additional low lipid control. Figures 3.27 and 3.28 show the results of the neutral lipid and polar lipid fluorescence intensity of wild type and deletion strains, respectively, in both early exponential and stationary phases of growth. Figure 3.27 shows stationary phase cells deficient in *DGA1* exhibited a significant reduction in fluorescence attributable to neutral lipids compared to that of wild type cells with a 1.4 fold decrease. Cells lacking *lro1* showed a slight decrease in neutral lipids in stationary phase, although to a lesser extent than that of the *dga1Δ*, which failed to reach significance. Cells deleted for *FAT1* on the other hand, as expected, exhibited a significant increase compared to wild type cells of 1.2 fold.

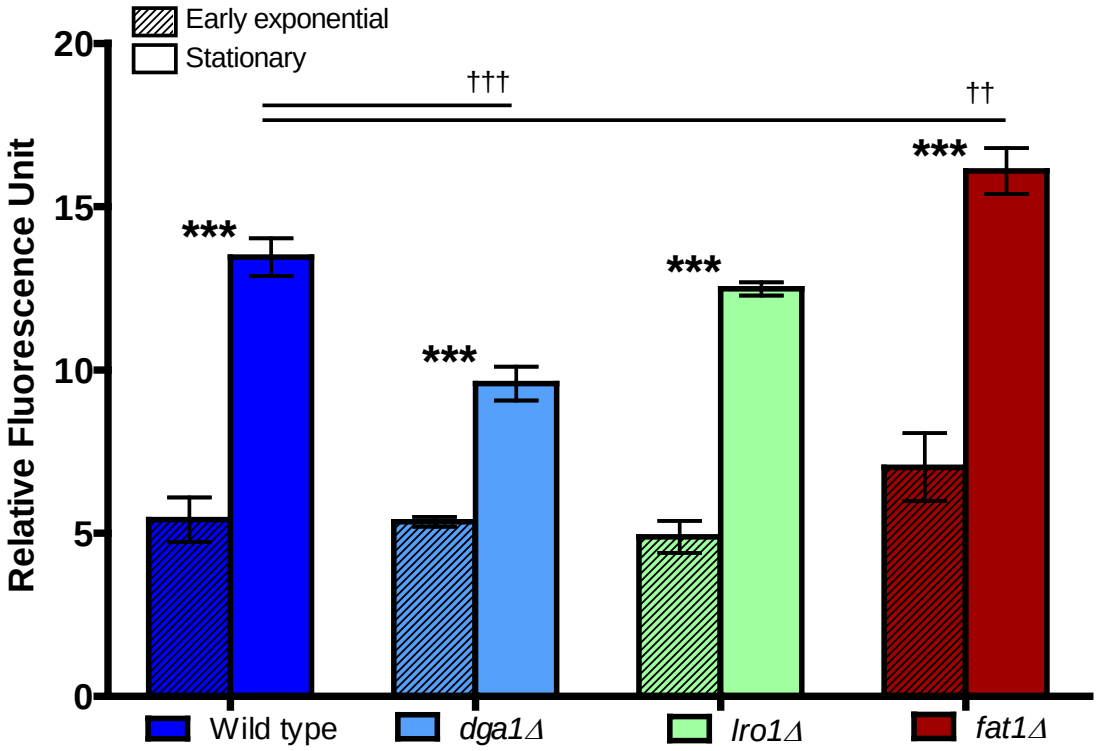


**Figure 3.27: Neutral lipid fluorescence intensity of Nile red stained *S. cerevisiae* wild type and deletions known to produce a neutral lipid phenotype.** Cells were harvested at 5 and 18 hrs post resuspension in YNB for early exponential and stationary phase samples respectively. Cells were washed twice in PBS before adjusting to a cell density of 2 x $10^7$ cells/ml. 5 x $10^6$ cells were transferred to the wells of black 96-well plates in triplicate. 25µl PBS/DMSO (1:1 v/v) and 5µg/ml Nile red were added to each sample. Plates were screened using the wavelengths: excitation 485 nm, emission 535 nm. Data shown as means of triplicates ±SD. Significance indicated between early exponential and stationary phases ***p≤0.001 and difference in stationary phases between cells indicated by solid black lines ††p≤0.01, ††† p≤0.001. Data analysed by one way ANOVA with Tukey *post hoc* test.

Conversely, when yeast samples were screened using the wavelength to identify more polar lipid classes no significant difference was observed (Figure 3.28).

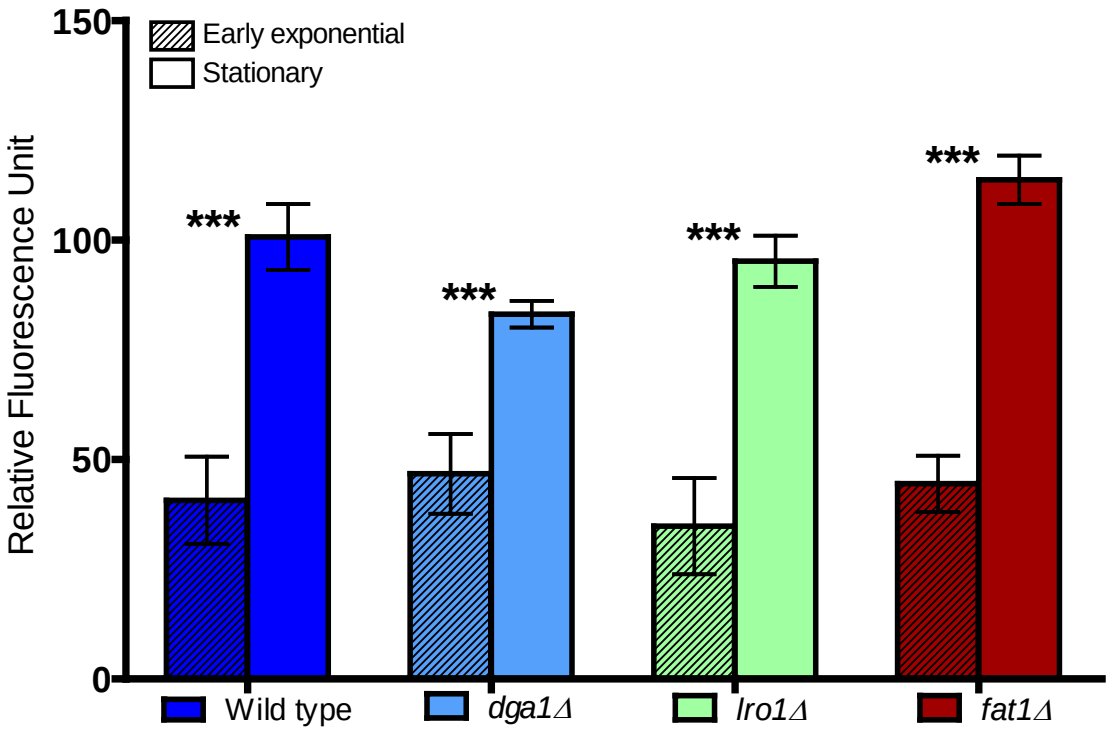


**Figure 3.28: Polar lipid fluorescence intensity of Nile Red stained *S. cerevisiae* wild type and deletions known to produce a neutral lipid phenotype.** Cells were harvested at 5 and 18 hrs post resuspension in YNB for early exponential and stationary phase samples respectively. Cells were washed twice in PBS before adjusting to a cell density of 2 x $10^7$ cells/ml. 5 x $10^6$ cells were transferred to the wells of black 96-well plates in triplicate. 25µl PBS/DMSO (1:1 v/v) and 5µg/ml Nile red were added to each sample. Plates were screened using the wavelengths: excitation 535 nm, emission 590 nm. Data shown as means of triplicates ±SD. Significance indicated between exponential and stationary phases ***p≤0.001. Data analysed by one way ANOVA with Tukey *post hoc* test.

These results demonstrated that the dual wavelength Nile red fluorescence method was sensitive enough to detect differences between polar and neutral lipids in *S. cerevisiae*, a non-oleaginous yeast.

### 3.5.1.1 Nile Red screening in S. cerevisiae utilising deletion strains known to regulate polar lipid production

In order to further test the sensitivity of the dual wavelength capabilities of Nile red, transcription factor mutants known to be involved in the regulation of phospholipid metabolism *ino2Δ, ino4Δ* and *opi1Δ* were screened for both polar and neutral lipids. Ino2p and Ino4p are basic helix-loop-helix transcription factors, which are required in response to inositol depletion for de-repression of phospholipid biosynthetic genes.

Opi1p is a negative regulator of the Ino2p/Ino4p complex and therefore negatively regulates transcription of phospholipid biosynthetic genes. Growth curves were conducted to ensure that all strains were in a comparable phase of growth before screening via Nile red, (Figures 3.29, 3.30 and 3.31).

As shown in Figures 3.29 and 3.30, both the *ino2Δ* and *ino4Δ* strains reached a lower cell density than wild type cells. However, time taken to exit lag phase (5hrs) and enter early stationary phase (12 hrs) were consistent between the deletion strains and wild type cells. The *opi1Δ* had comparable growth phases whilst also reaching a cell density equivalent to that of wild type cells (Figure 3.31).

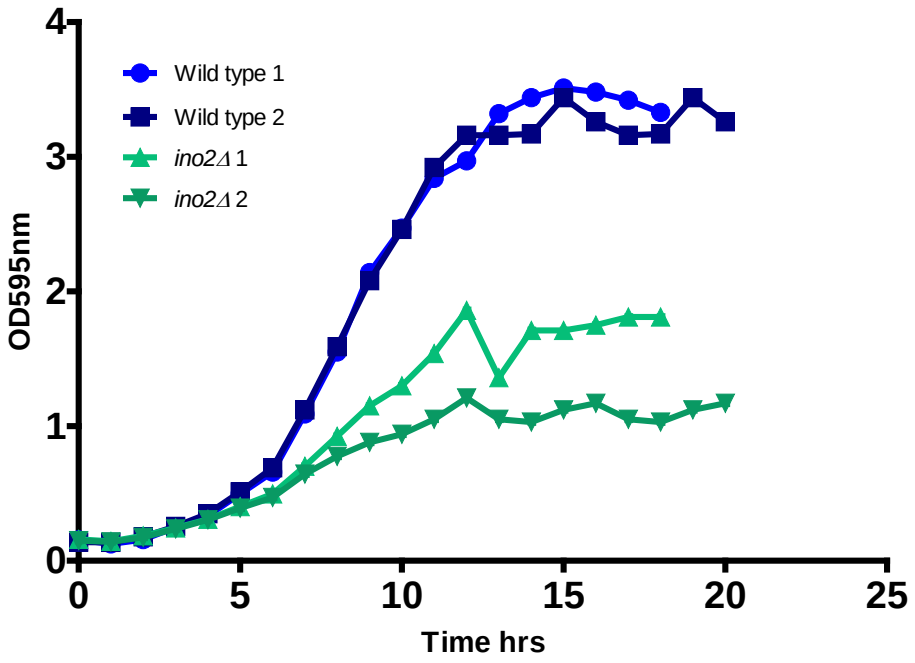


**Figure 3.29: Growth curves of *S. cerevisiae* wild type and *ino2Δ* under normal conditions in yeast nitrogen base medium (YNB).** Cultures were diluted to 2 x $10^6$ cells ($OD_{595}$ ~0.1) and incubated with shaking, 180rpm, at 30°C. Optical density readings were taken hourly until mid to late stationary phase was reached. Growth curves were conducted in duplicate (culture 1 and culture 2 for both WT and deletion strain) showing growth patterns observed for two distinct colonies of the same strain.

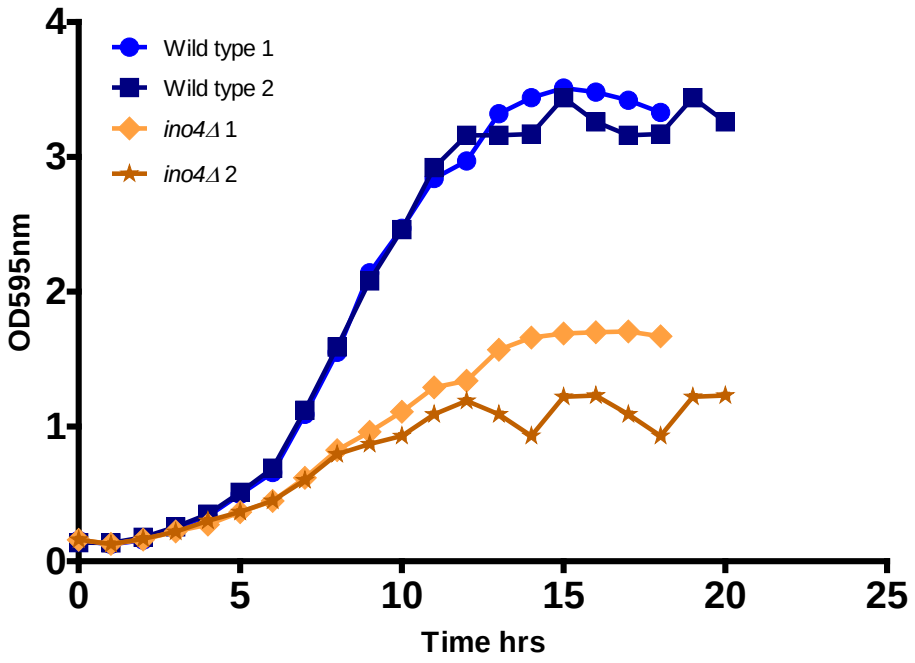


**Figure 3.30: Growth curves of *S. cerevisiae* wild type and *ino4Δ* under normal conditions in yeast nitrogen base medium (YNB).** Cultures were diluted to 2 x $10^6$ cells ($OD_{595}$ ~0.1) and incubated with shaking, 180rpm, at 30°C. Optical density readings were taken hourly until mid to late stationary phase was reached. Growth curves were conducted in duplicate (culture 1 and culture 2 for both WT and deletion strain) showing growth patterns observed for two distinct colonies of the same strain.

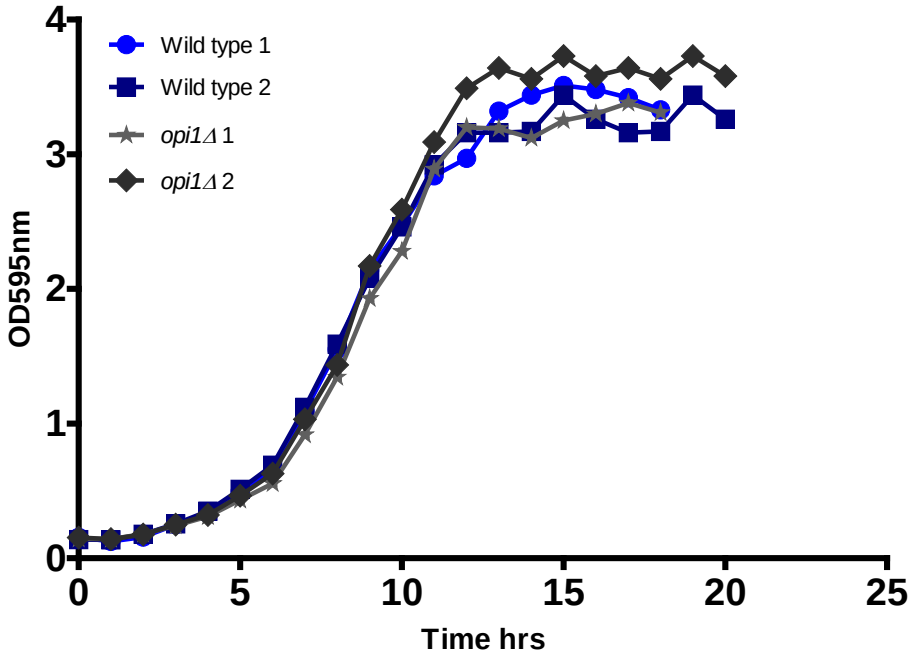


**Figure 3.31: Growth curves of *S. cerevisiae* wild type and *opi1Δ* under normal conditions in yeast nitrogen base medium (YNB).** Cultures were diluted to 2 x $10^6$ cells ($OD_{595}$~0.1) and incubated with shaking, 180rpm, at 30°C. Optical density readings were taken hourly until mid to late stationary phase was reached. Growth curves were conducted in duplicate (culture 1 and culture 2 for both WT and deletion strain) showing growth patterns observed for two distinct colonies of the same strain.

Figures 3.32 and 3.33 show results of neutral and polar lipid fluorescence obtained from the Nile red assay. For cells deficient in *INO2* and *INO4* increases of 2.7 and 2.6 fold respectively, were observed for neutral lipids. Cells deleted for *OPI1* displayed a neutral lipid phenotype comparable to that of wild type cells.

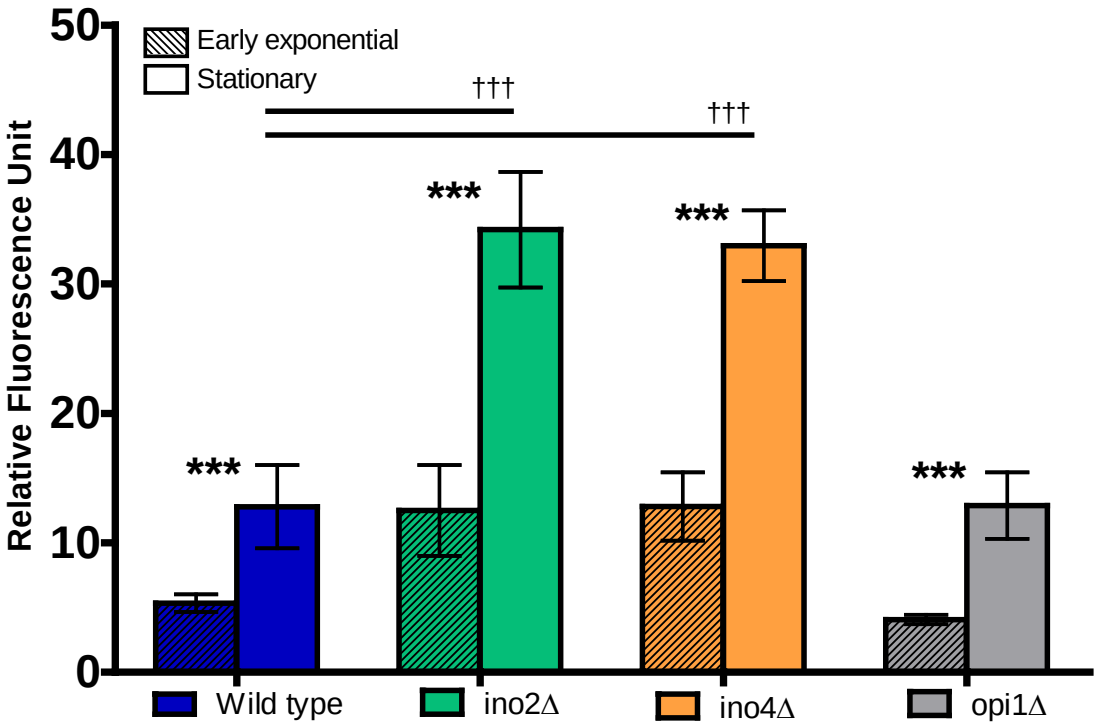


**Figure 3.32: Neutral lipid fluorescence intensity of Nile Red stained *S. cerevisiae* wild type and deletion strains involved in phospholipid biosynthesis.** Cells were harvested at 5 and 18 hrs post resuspension in YNB for early exponential and stationary phase samples respectively. Cells were washed twice in PBS before adjusting to a cell density of 2 x $10^7$ cells/ml. 5 x $10^6$ cells were transferred to the wells of black 96-well plates in triplicate. 25µl PBS/DMSO (1:1 v/v) and 5µg/ml Nile red were added to each sample. Plates were screened using the wavelengths: excitation 485 nm, emission 535 nm. Data shown as means of triplicates ±SD. Significance indicated between early exponential and stationary phases ***p≤0.001 and difference in stationary phases between cells indicated by solid black lines ††† p≤0.001. Data analysed by one way ANOVA with Tukey *post hoc* test.

In the case of the screen conducted to infer more polar lipid species significant increases were also seen for the *ino2Δ* and *ino4Δ* of 2.6 and 2.5 fold, respectively. Concurrent with neutral lipid status, the *opi1Δ* did not significantly differ in fluorescence level from that of the wild type strain (Figure 3.33).

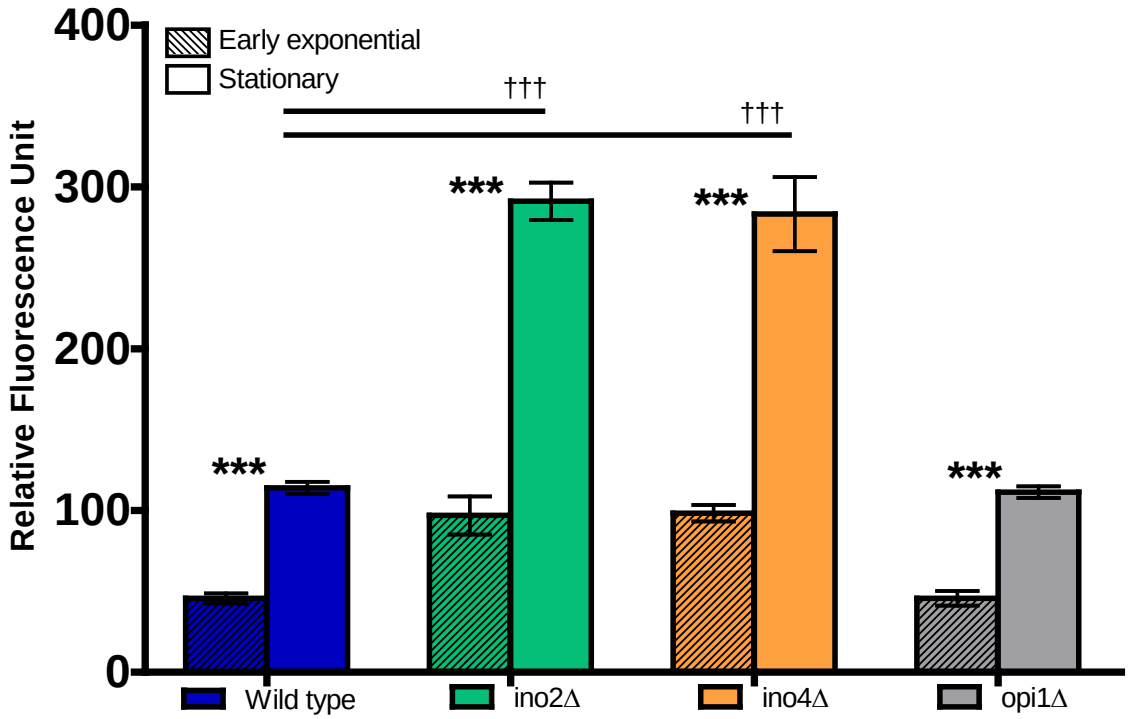


**Figure 3.33: Polar lipid fluorescence intensity of Nile Red stained *S. cerevisiae* wild type and deletion strains involved in phospholipid biosynthesis.** Cells were harvested at 5 and 18 hrs post resuspension in YNB for early exponential and stationary phase samples respectively. Cells were washed twice in PBS before adjusting to a cell density of 2 x $10^7$ cells/ml. 5 x $10^6$ cells were transferred to the wells of black 96-well plates in triplicate. 25µl PBS/DMSO (1:1 v/v) and 5µg/ml Nile red were added to each sample. Plates were screened using the wavelengths: excitation 535 nm, emission 590 nm. Data shown as means of triplicates ±SD. Significance indicated between early exponential and stationary phases ***p≤0.001 and difference in stationary phases between cells indicated by solid black lines ††† p≤0.001. Data analysed by one way ANOVA with Tukey *post hoc* test.

### 3.5.1.2 Nile red screening of S. cerevisiae mutants involved in lipid droplet morphology and β-oxidation

Other *S. cerevisiae* deletion strains involved in lipid droplet morphology, *fld1Δ* and transcription factors involved in β-oxidation, *oaf1Δ* and *pip2Δ,* were also screened via Nile red to elucidate whether a phenotype could be shown. Growth curves of the deletion strains were conducted, Figures 3.34, 3.35 and 3.36, alongside *S. cerevisiae* wild type cultures to ensure that no growth defects were present and to ensure cells were in a comparable growth phase prior to screening. As shown in Figures 3.34, 3.35 and 3.36 exponential growth routinely began 5 hrs post re-suspension in YNB medium before cells reached early stationary phase after 12 hrs of incubation.

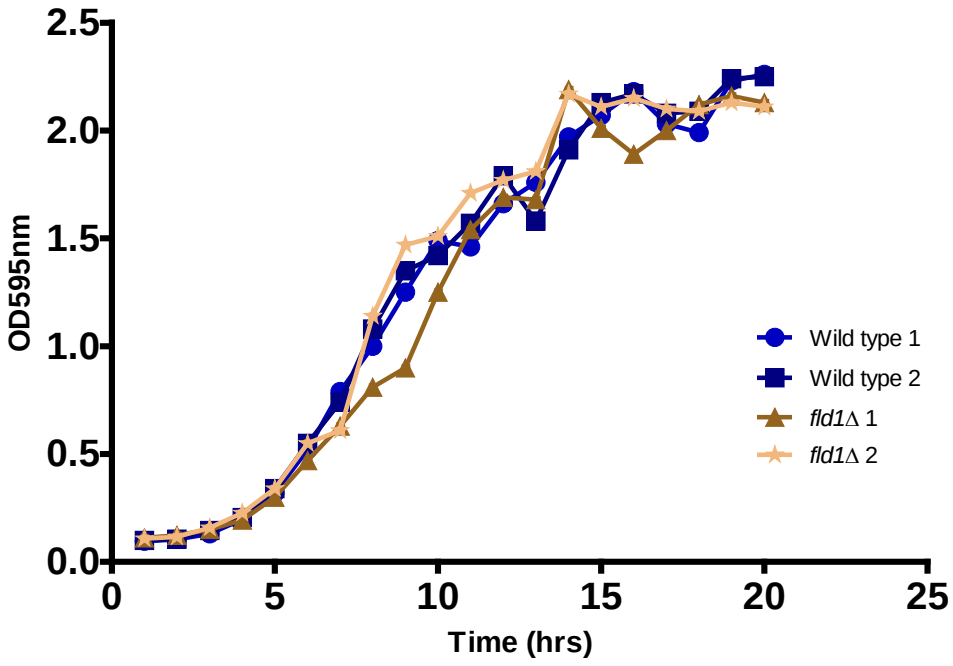


**Figure 3.34: Growth curves of *S. cerevisiae* wild type and *fld1Δ* under normal conditions in yeast nitrogen base medium (YNB).** Cultures were diluted to 2 x $10^6$ cells ($OD_{595}$ ~0.1) and incubated with shaking, 180rpm, at 30°C. Optical density readings were taken hourly until mid to late stationary phase was reached. Growth curves were conducted in duplicate (culture 1 and culture 2 for both WT and deletion strain) showing growth patterns observed for two distinct colonies of the same strain.

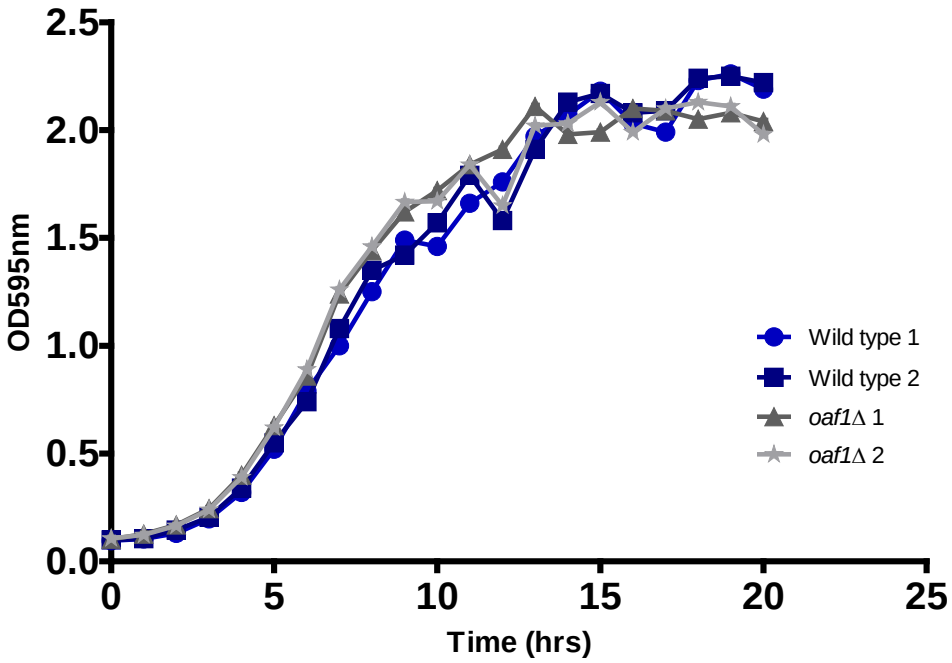


**Figure 3.35: Growth curves of *S. cerevisiae* wild type and *oaf1Δ* under normal conditions in yeast nitrogen base medium (YNB).** Cultures were diluted to 2 x $10^6$ cells ($OD_{595}$ ~0.1) and incubated with shaking, 180rpm, at 30°C. Optical density readings were taken hourly until mid to late stationary phase was reached. Growth curves were conducted in duplicate (culture 1 and culture 2 for both WT and deletion strain) showing growth patterns observed for two distinct colonies of the same strain.

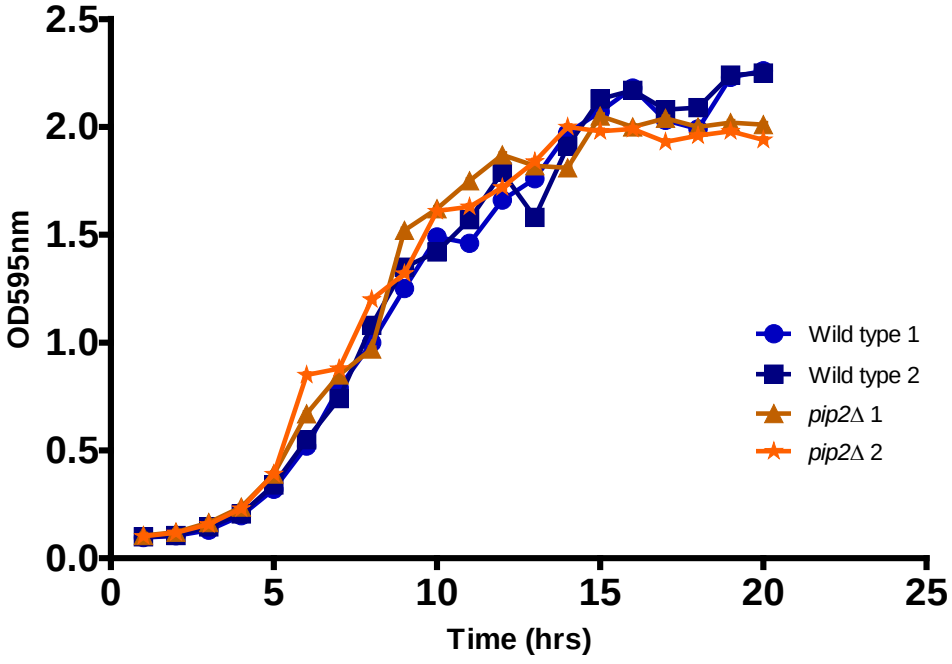


**Figure 3.36: Growth curves of *S. cerevisiae* wild type and *pip2Δ* under normal conditions in yeast nitrogen base medium (YNB).** Cultures were diluted to 2 x $10^6$ cells ($OD_{595}$ ~0.1) and incubated with shaking, 180rpm, at 30°C. Optical density readings were taken hourly until mid to late stationary phase was reached. Growth curves were conducted in duplicate (culture 1 and culture 2 for both WT and deletion strain) showing growth patterns observed for two distinct colonies of the same strain.

As shown in Figure 3.37, at stationary phase, the amounts of neutral lipid in all three deletion strains did not differ significantly from that of the wild type. The *fld1Δ* exhibited a slight increase whilst deletion of *OAF1* and *PIP2* resulted in decreases of 1.1 fold.

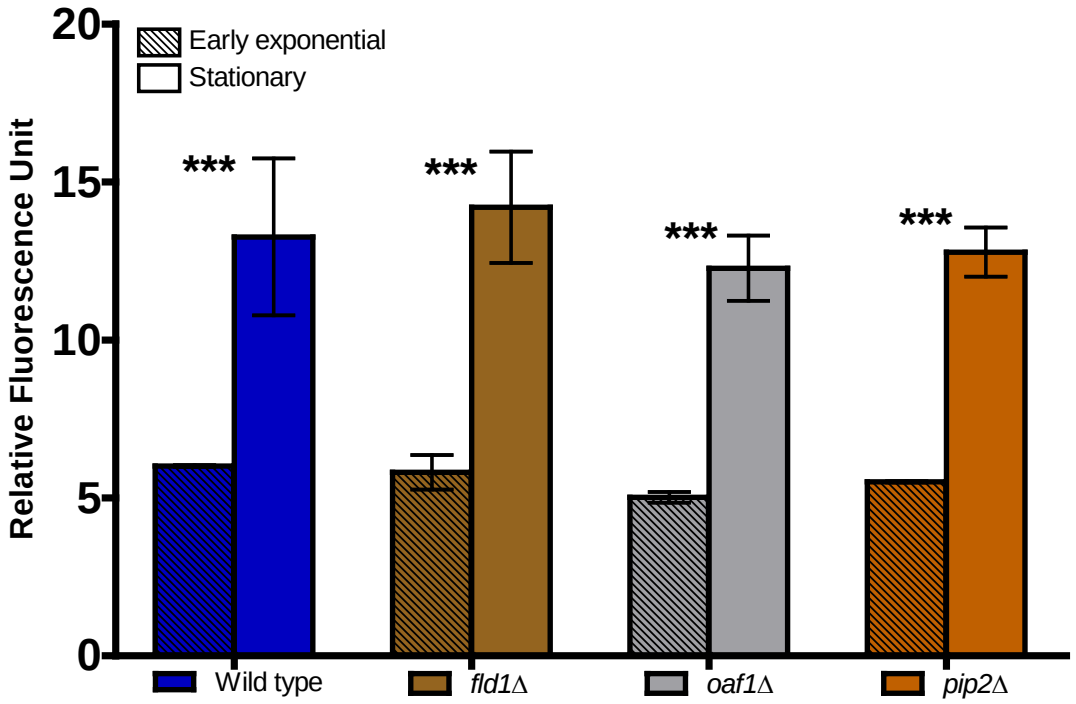


**Figure 3.37: Neutral lipid fluorescence intensity of Nile Red stained *S. cerevisiae* wild type and deletion strains involved in lipid droplet morphology and β-oxidation.** Cells were harvested at 5 and 18 hrs post resuspension in YNB for early exponential and stationary phase samples respectively. Cells were washed twice in PBS before adjusting to a cell density of 2 x $10^7$ cells/ml. 5 x $10^6$ cells were transferred to the wells of black 96-well plates in triplicate. 25µl PBS/DMSO (1:1 v/v) and 5µg/ml Nile red were added to each sample. Plates were screened using the wavelengths: excitation 485 nm, emission 535 nm. Data shown as means of triplicates ±SD. Significance indicated between early exponential and stationary phases ***p≤0.001. Data analysed by one way ANOVA with Tukey *post hoc* test.

For polar lipids in stationary phase deletion strains did not display a significantly different phenotype from that of wild type cells (Figure 3.38).

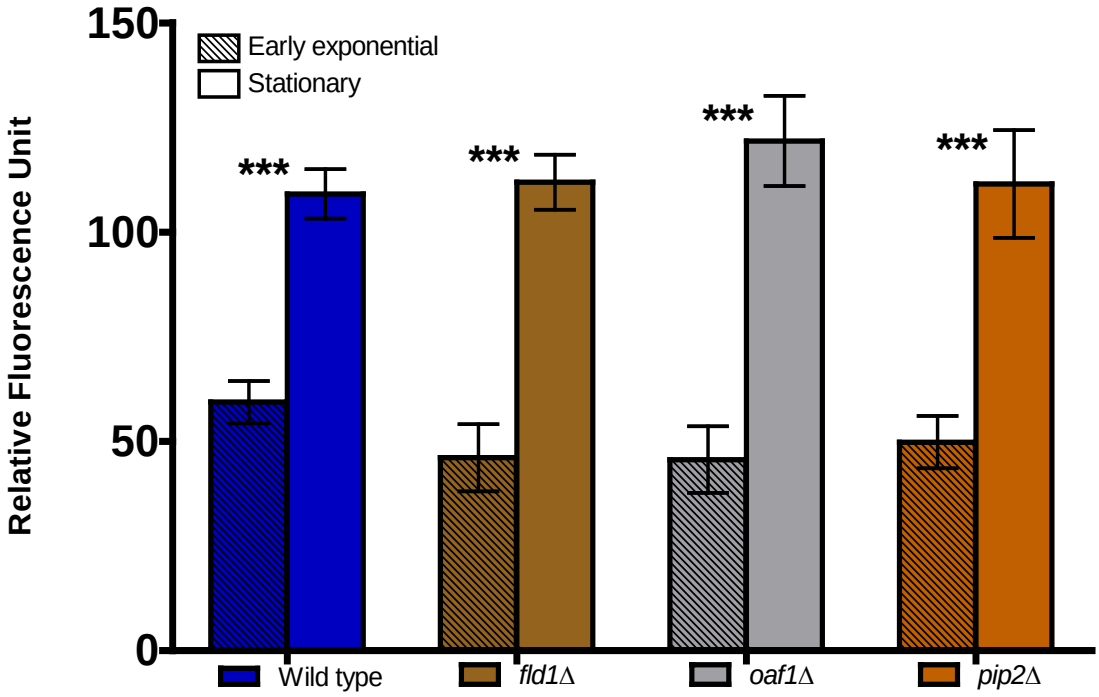


**Figure 3.38: Polar lipid fluorescence intensity of Nile Red stained *S. cerevisiae* wild type and deletion strains involved in lipid droplet morphology and β-oxidation.** Cells were harvested at 5 and 18 hrs post resuspension in YNB for early exponential and stationary phase samples respectively. Cells were washed twice in PBS before adjusting to a cell density of 2 x $10^7$ cells/ml. 5 x $10^6$ cells were transferred to the wells of black 96-well plates in triplicate. 25µl PBS/DMSO (1:1 v/v) and 5µg/ml Nile red were added to each sample. Plates were screened using the wavelengths: excitation 535 nm, emission 590 nm. Data shown as means of triplicates ±SD. Significance indicated between early exponential and stationary phases ***p≤0.001. Data analysed by one way ANOVA with Tukey *post hoc* test.

### 3.5.1.3 Nile red screening of S. cerevisiae SREBP-like transcription factors

Although *S. cerevisiae* cells do not contain SREBP orthologues, the proteins Upc2 and Ecm22 are classified as functional orthologues to mammalian SREBP-2. Upc2 and Ecm22 are involved in the production of ergosterol, a component of yeast cellular membranes (Valachovic *et al.* 2006), whereas SREBP-2 in mammalian systems is involved in regulation of cholesterol synthesis. Similarly, as the *S. cerevisiae* proteins Spt23 and Mga2 function in the regulation of fatty acid synthesis and therefore TAG synthesis, they are functionally related to mammalian SREBP-1 (Rice *et al.* 2010).

Nile red screening was conducted for single deletion strains of genes encoding each SREBP like proteins to assess if a phenotype could be detected. Growth curves were conducted prior to screening to ensure no growth defects were present and additionally that screening was conducted at comparable growth phases.

As shown by Figures 3.39 and 3.40, no growth defects were observed for *ecm22Δ* or *upc2Δ* with growth rates comparable to that of wild type cells.

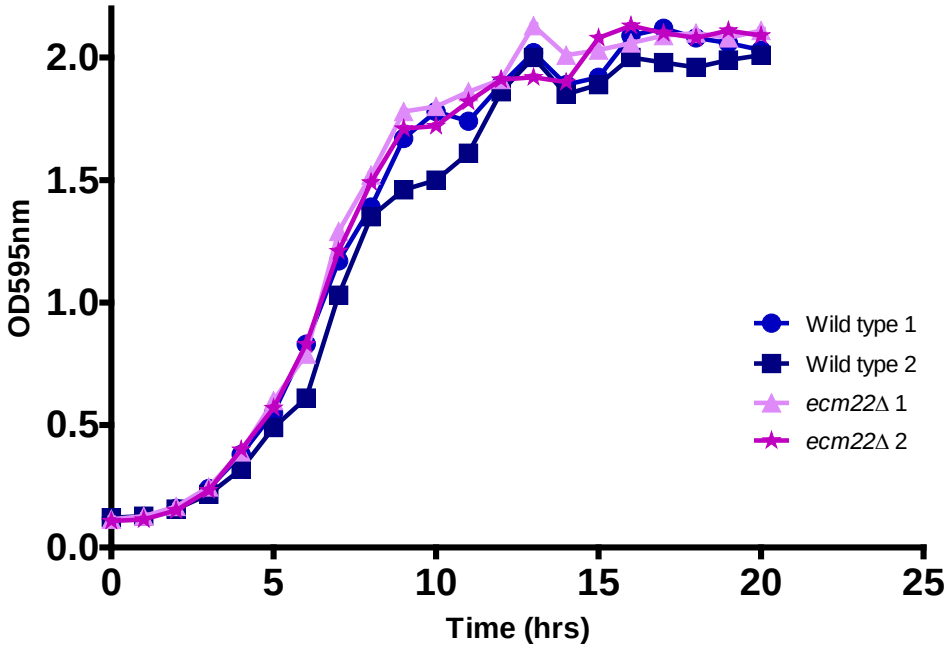


**Figure 3.39: Growth curves of *S. cerevisiae* wild type and *ecm22Δ* under normal conditions in yeast nitrogen base medium (YNB).** Cultures were diluted to 2 x 106 cells (OD595 ~0.1) and incubated with shaking, 180rpm, at 30oC. Optical density readings were taken hourly until mid to late stationary phase was reached. Growth curves were conducted in duplicate (culture 1 and culture 2 for both WT and deletion strain) showing growth patterns observed for two distinct colonies of the same strain.

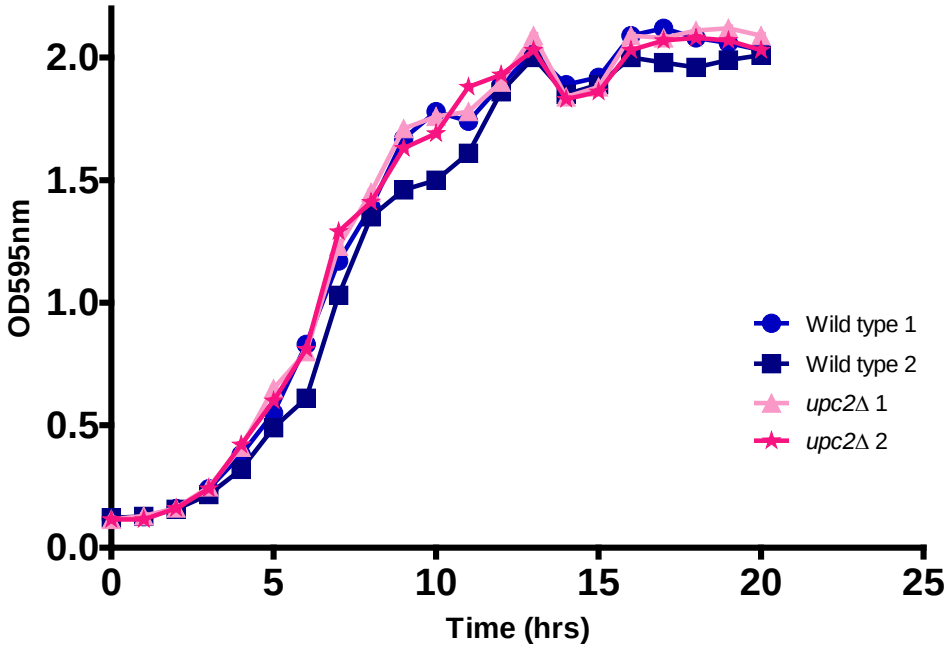


**Figure 3.40: Growth curves of *S. cerevisiae* wild type and *upc2Δ* under normal conditions in yeast nitrogen base medium (YNB).** Cultures were diluted to 2 x $10^6$ cells ($OD_{595}$ ~0.1) and incubated with shaking, 180rpm, at 30°C. Optical density readings were taken hourly until mid to late stationary phase was reached. Growth curves were conducted in duplicate (culture 1 and culture 2 for both WT and deletion strain) showing growth patterns observed for two distinct colonies of the same strain.

As depicted in Figures 3.41 and 3.42, growth profiles consistent to that of wild type cells were also obtained from the *spt23* and *mga2* single deletion strains.

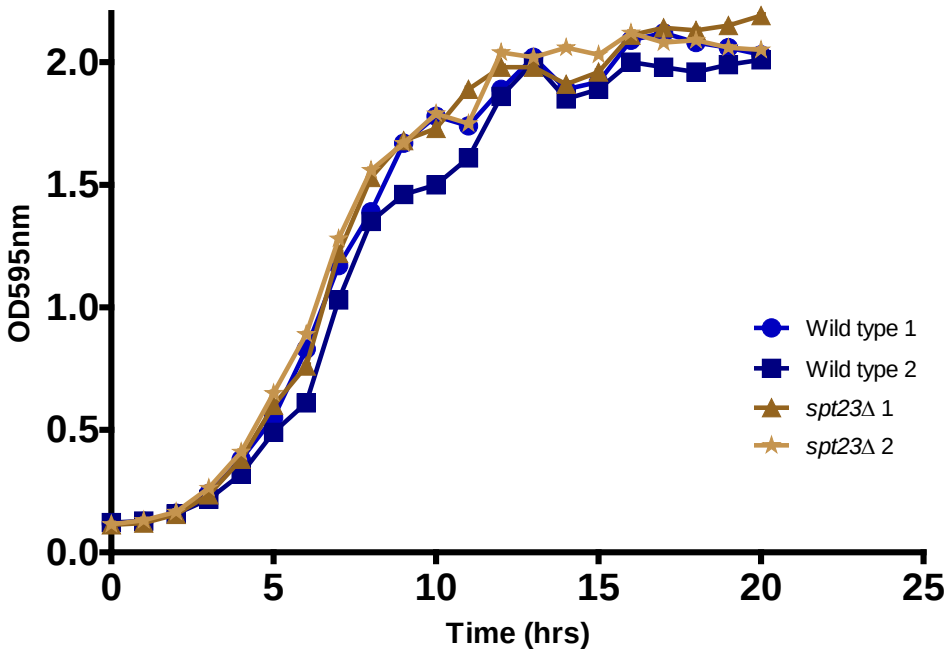


**Figure 3.41: Growth curves of *S. cerevisiae* wild type and *spt23Δ* under normal conditions in yeast nitrogen base medium (YNB).** Cultures were diluted to 2 x $10^6$ cells ($OD_{595}$ ~0.1) and incubated with shaking, 180rpm, at 30°C. Optical density readings were taken hourly until mid to late stationary phase was reached. Growth curves were conducted in duplicate (culture 1 and culture 2 for both WT and deletion strain) showing growth patterns observed for two distinct colonies of the same strain.

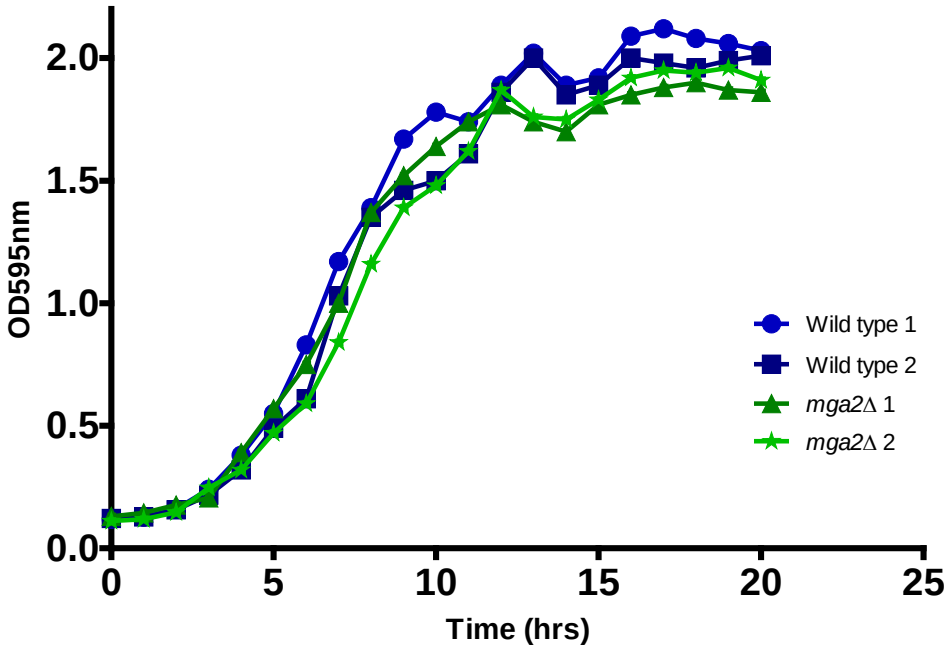


**Figure 3.42: Growth curves of *S. cerevisiae* wild type and *mga2Δ* under normal conditions in yeast nitrogen base medium (YNB).** Cultures were diluted to 2 x $10^6$ cells ($OD_{595}$ ~0.1) and incubated with shaking, 180rpm, at 30°C. Optical density readings were taken hourly until mid to late stationary phase was reached. Growth curves were conducted in duplicate (culture 1 and culture 2 for both WT and deletion strain) showing growth patterns observed for two distinct colonies of the same strain.

When single deletions were screened using the wavelength to infer neutral lipid status the deletion of *ECM22* and *UPC2* resulted in 1.1 fold and 1.2 fold decreases respectively. Cells deleted for *SPT23* showed a 1.2 fold reduction in fluorescence attributable to neutral lipids, with the *mga2Δ* giving the largest decrease of 1.3 fold compared to wild type cells (Figure 3.43).

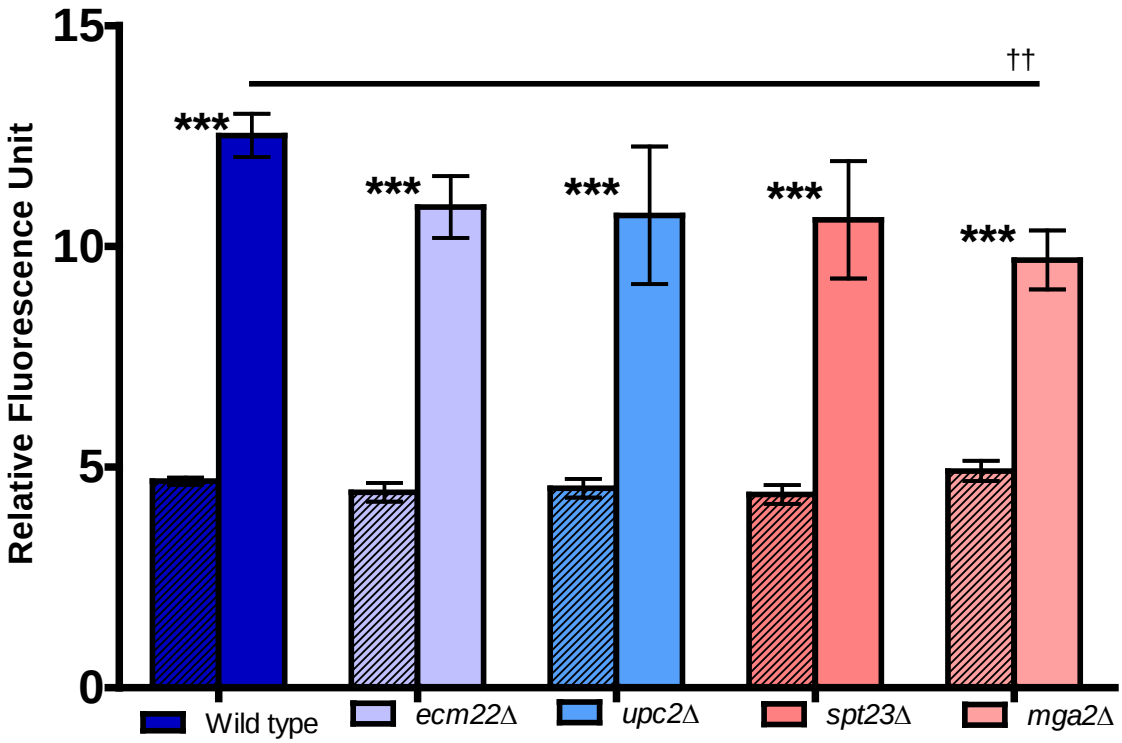


**Figure 3.43: Neutral lipid fluorescence intensity of Nile Red stained *S. cerevisiae* wild type and SREBP like component deletions.** Cells were harvested at 5 and 18 hrs post resuspension in YNB for early exponential and stationary phase samples respectively. Cells were washed twice in PBS before adjusting to a cell density of 2 x $10^7$ cells/ml. 5 x $10^6$ cells were transferred to the wells of black 96-well plates in triplicate. 25µl PBS/DMSO (1:1 v/v) and 5µg/ml Nile red were added to each sample. Plates were screened using the wavelengths: excitation 485 nm, emission 535 nm. Data shown as means of triplicates ±SD. Significance indicated between early exponential and stationary phases ***p≤0.001 and difference in stationary phases between cells indicated by solid black lines ǂp≤0.01. Data analysed by one way ANOVA with Tukey *post hoc* test.

Nile red screening using the wavelength to identify more polar lipids showed no significant differences compared to wild type cells. Cells deleted for *ECM22* and *UPC2* resulted in a 1.1 fold decrease and cells deficient in *MGA2* and *SPT23* exhibited a 1.2 fold decrease in fluorescence intensity (Figure 3.44).

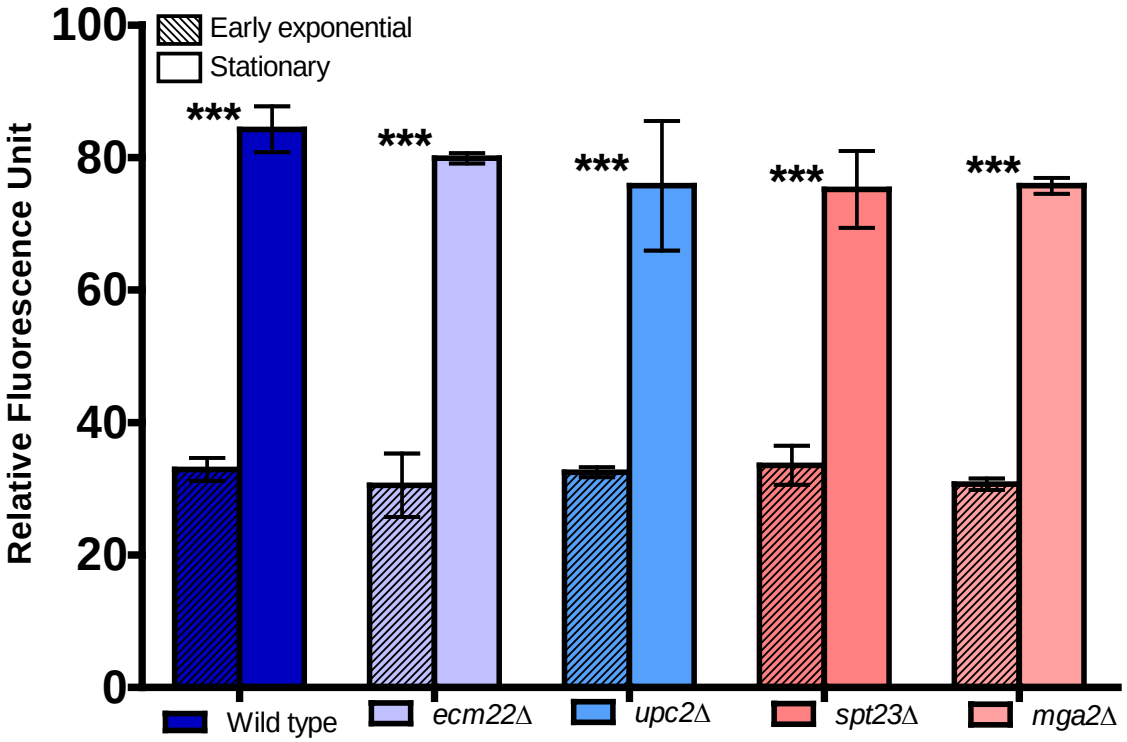


**Figure 3.44: Polar lipid fluorescence intensity of Nile Red stained *S. cerevisiae* wild type and SREBP like component deletions.** Cells were harvested at 5 and 18 hrs post resuspension in YNB for early exponential and stationary phase samples respectively. Cells were washed twice in PBS before adjusting to a cell density of 2 x $10^7$ cells/ml. 5 x $10^6$ cells were transferred to the wells of black 96-well plates in triplicate. 25µl PBS/DMSO (1:1 v/v) and 5µg/ml Nile red were added to each sample. Plates were screened using the wavelengths: excitation 535 nm, emission 590 nm. Data shown as means of triplicates ±SD. Significance indicated between early exponential and stationary phases ***p≤0.001. Data analysed by one way ANOVA with Tukey *post hoc* test.

### 3.5.1.4 ecm22/upc2 double deletion is viable in the W303 S. cerevisiae genetic background

Although deletion of single SREBP like components results in viable cells, double mutants of SREBP functional orthologues *ECM22/UPC2* or *SPT23/MGA2* are non-viable in the S288C background. However, the double deletion of *ECM22/UPC2* is viable in the W303 genetic background of *S. cerevisiae*.

This is due to W303 cells having functional *HAP1,* whereas the S288C cells contain a mutated *HAP1* allele (Davies and Rine 2006). Nile red screening was conducted to elucidate whether the double deletion of *ECM22* and *UPC2* would result in the detection of a more severe phenotype than was observed with the single deletions in Section 3.5.1.3.

Growth curves were conducted for W303 wild type cells along with cells containing the single deletion of *ecm22* and double deletion of *ecm22/upc2.* As shown by Figures 3.45 and 3.46, no growth defects were observed from either mutant strain.

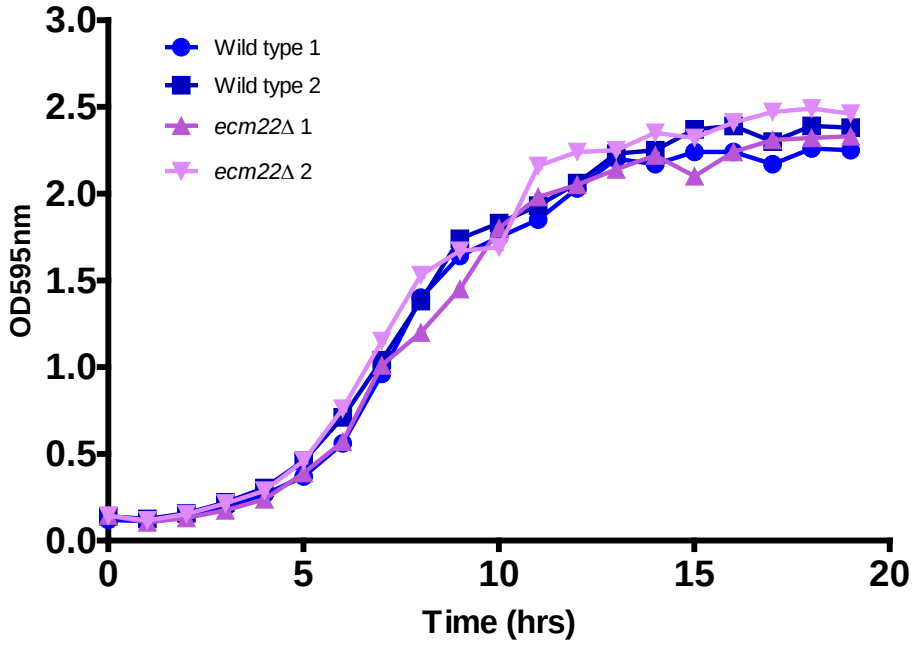


**Figure 3.45: Growth curves of *S. cerevisiae* wild type and *ecm22Δ* (W303 background) under normal conditions in yeast nitrogen base medium (YNB).** Cultures were diluted to 2 x $10^6$ cells ($OD_{595}$ ~0.1) and incubated with shaking, 180rpm, at 30°C. Optical density readings were taken hourly until mid to late stationary phase was reached. Growth curves were conducted in duplicate (culture 1 and culture 2 for both WT and deletion strain) showing growth patterns observed for two distinct colonies of the same strain.

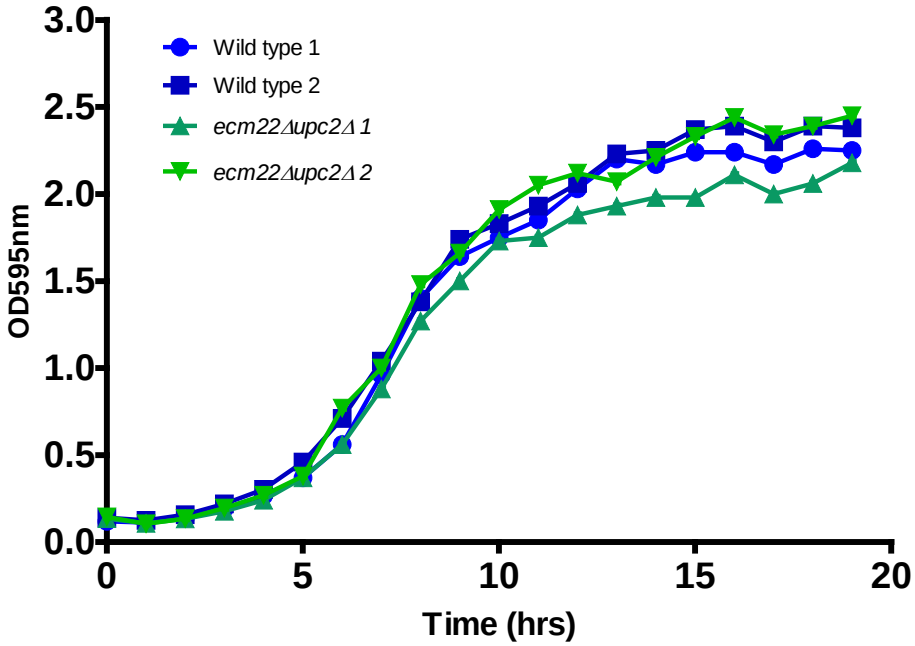


**Figure 3.46: Growth curves of *S. cerevisiae* wild type and *ecm22Δupc2Δ* (W303 background) under normal conditions in yeast nitrogen base medium (YNB).** Cultures were diluted to 2 x $10^6$ cells ($OD_{595}$ ~0.1) and incubated with shaking, 180rpm, at 30°C. Optical density readings were taken hourly until mid to late stationary phase was reached. Growth curves were conducted in duplicate (culture 1 and culture 2 for both WT and deletion strain) showing growth patterns observed for two distinct colonies of the same strain.

As previously demonstrated with the deletion of *ECM22* in the S288C background, the levels of neutral lipids were not significantly different to that of wild type cells in the W303 genetic background. The double deletion of *ecm22* and *upc2* resulted in a 1.2 fold decrease in the levels of fluorescence pertaining to neutral lipids, although this failed to reach significance (Figure 3.47).

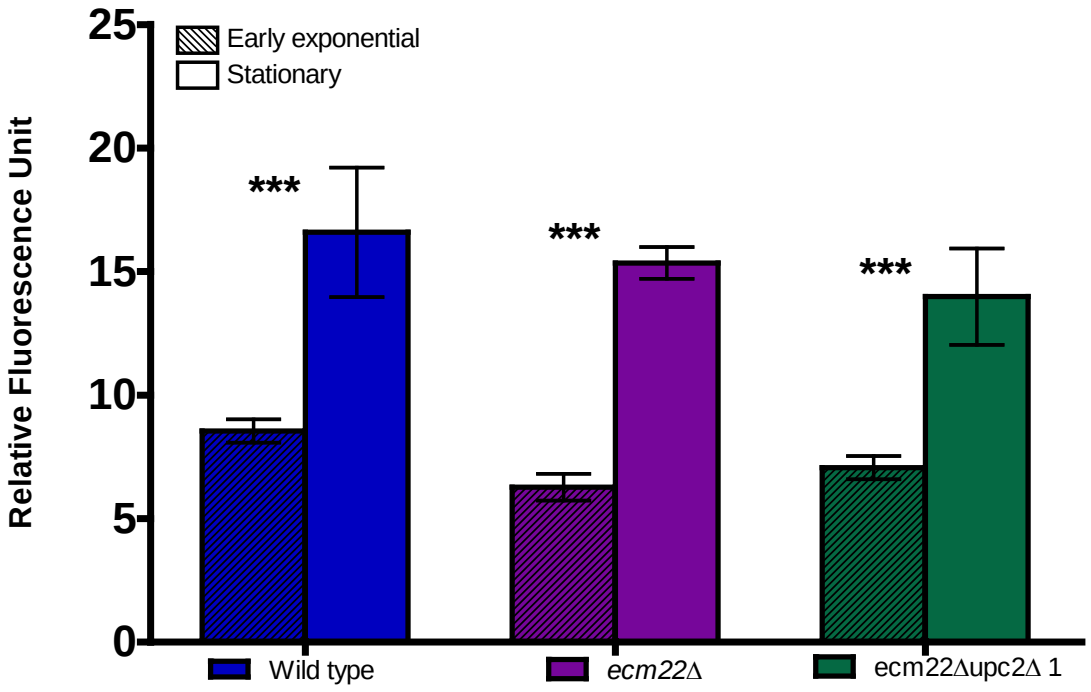


**Figure 3.47: Neutral lipid fluorescence intensity of Nile Red stained *S. cerevisiae* wild type and SREBP like component deletions in the W303 genetic background.** Cells were harvested at 5 and 18 hrs post resuspension in YNB for early exponential and stationary phase samples respectively. Cells were washed twice in PBS before adjusting to a cell density of 2 x $10^7$ cells/ml. 5 x $10^6$ cells were transferred to the wells of black 96-well plates in triplicate. 25µl PBS/DMSO (1:1 v/v) and 5µg/ml Nile red were added to each sample. Plates were screened using the wavelengths: excitation 485 nm, emission 535 nm. Data shown as means of triplicates ±SD. Significance indicated between exponential and stationary phases ***p≤0.001. Data analysed by one way ANOVA with Tukey *post hoc* test.

After analysis of fluorescence values for more polar lipid classes, again no significant difference was observed for the single deletion or double deletion strains (Figure 3.48).

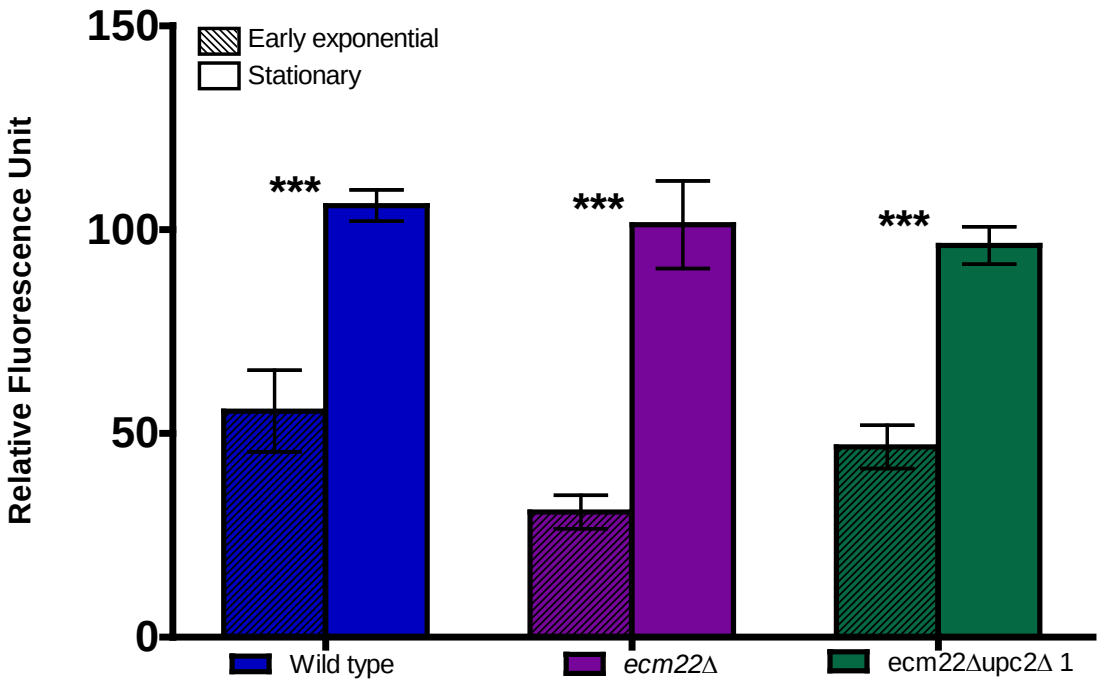


**Figure 3.48: Polar lipid fluorescence intensity of Nile Red stained *S. cerevisiae* wild type and SREBP like component deletions in the W303 genetic background.** Cells were harvested at 5 and 18 hrs post resuspension in YNB for early exponential and stationary phase samples respectively. Cells were washed twice in PBS before adjusting to a cell density of 2 x $10^7$ cells/ml. 5 x $10^6$ cells were transferred to the wells of black 96-well plates in triplicate. 25µl PBS/DMSO (1:1 v/v) and 5µg/ml Nile red were added to each sample. Plates were screened using the wavelengths: excitation 535 nm, emission 590 nm. Data shown as means of triplicates ±SD. Significance indicated between exponential and stationary phases ***p≤0.001. Data analysed by one way ANOVA with Tukey *post hoc* test.

## 3.6 Determination of lipid content in the non-oleaginous fission yeast, S. pombe using the Nile red fluorescence assay

At present, a published rapid screening method for lipid accumulation in *S. pombe* has yet to be developed and validated. Such platforms would aid in the rapid identification of superior culture conditions and relevant metabolism regulatory components, which can then be investigated more in depth.

Little research has been undertaken on lipid accumulation in the fission yeast, *S. pombe*. Due to the importance of *S. pombe* in the study of human diseases, we tested whether the dual wavelength Nile red assay could be used to examine the lipid content of *S. pombe* cells.

As Limited previous work has been published which describes lipid accumulation in *S. pombe* cells, growth phases in which to undertake a time course for Nile red screening of total lipid amounts were established from the growth curve shown in Section 3.3.3.3., Figure 3.17. Interestingly, unlike *L. starkeyi* and *S. cerevisiae*, we found a higher lipid content existed in *S. pombe* exponentially growing cells (8 hrs) compared to those in stationary phase (24 hrs) (Figures 3.49 and 3.50). As such, an exponentially growing culture of *S. pombe* could not be used as a low lipid control for screening stationary phase samples.

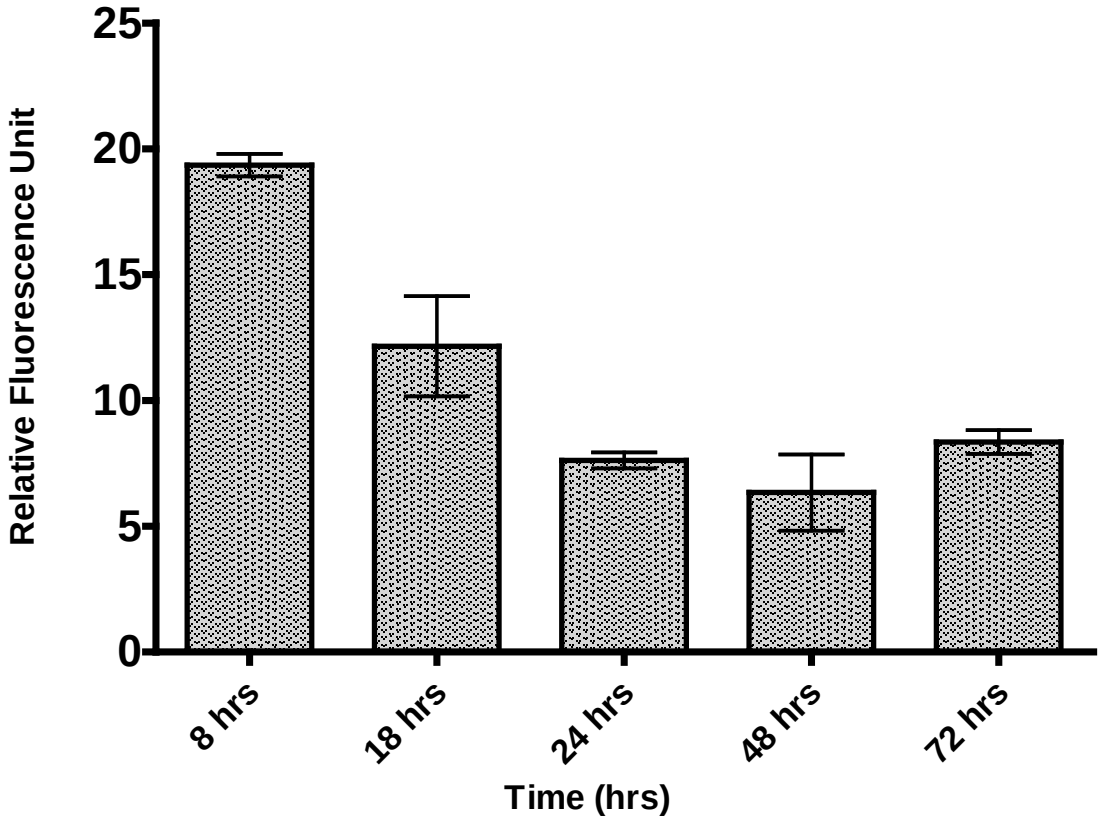


**Figure 3.49: Neutral lipid fluorescence intensity of Nile red stained *S. pombe* over a range of growth phases.** Cells were harvested at 8, 18, 24, 48 and 72 hrs post resuspension in EMM. For Nile red cells were washed twice in PBS before adjusting to a cell density of 2 x $10^7$ cells/ml. 5 x $10^6$ cells were transferred to the wells of black 96-well plates in triplicate. 25µl PBS/DMSO (1:1 v/v) and 5µg/ml Nile red were added to each sample. Fluorescence intensity was measured using an excitation wavelength of 485 nm and an emission wavelength of 535 nm. All values are normalised to a cell density of 2 x $10^7$ cells, corresponding to $OD_{595}$ of 1.0. Data are shown as means of triplicate experiments ± SD.

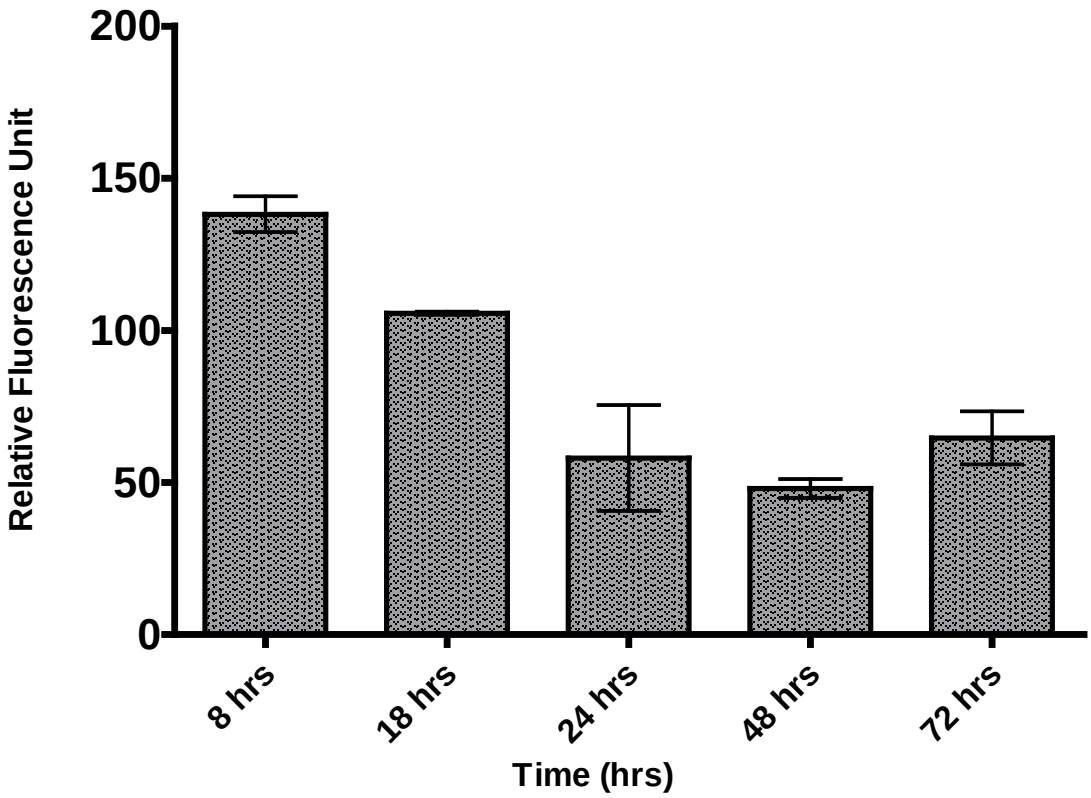


**Figure 3.50: Polar lipid fluorescence intensity of Nile red stained *S. pombe* over a range of growth phases.** Cells were harvested at 8, 18, 24, 48 and 72 hrs post resuspension in EMM. For Nile red cells were washed twice in PBS before adjusting to a cell density of 2 x $10^7$ cells/ml. 5 x $10^6$ cells were transferred to the wells of black 96-well plates in triplicate. 25µl PBS/DMSO (1:1 v/v) and 5µg/ml Nile red were added to each sample. Fluorescence intensity was measured using an excitation wavelength of 535 nm and an emission wavelength of 590 nm. All values are normalised to a cell density of 2 x $10^7$ cells, corresponding to $OD_{595}$ of 1.0. Data are shown as means of triplicate experiments ± SD.

### 3.6.1 The dual wavelength Nile red fluorescence assay can distinguish between polar and neutral lipids in S. pombe deletion strains

To assess whether the Nile red assay could be applied to *S. pombe* to deliver reliable lipid phenotype data, screening was conducted utilising *S. pombe* deletion strains expected to deliver a predominantly neutral lipid phenotype. The *S. pombe dga1Δ* mutant, analogous to its *S. cerevisiae* counterpart, is expected to show a significant decrease in neutral but not polar lipid amount. The deletion of *PTL3*, a predicted triacylglycerol lipase, is expected to demonstrate an increased quantity of neutral lipid. Growth curves of deletion strains alongside wild type cultures were conducted prior to screening, Figures 3.51 and 3.52, in order to ensure the mutant strains did not display any growth defects and that samples for Nile red screening were obtained with cells in comparable phases of growth.

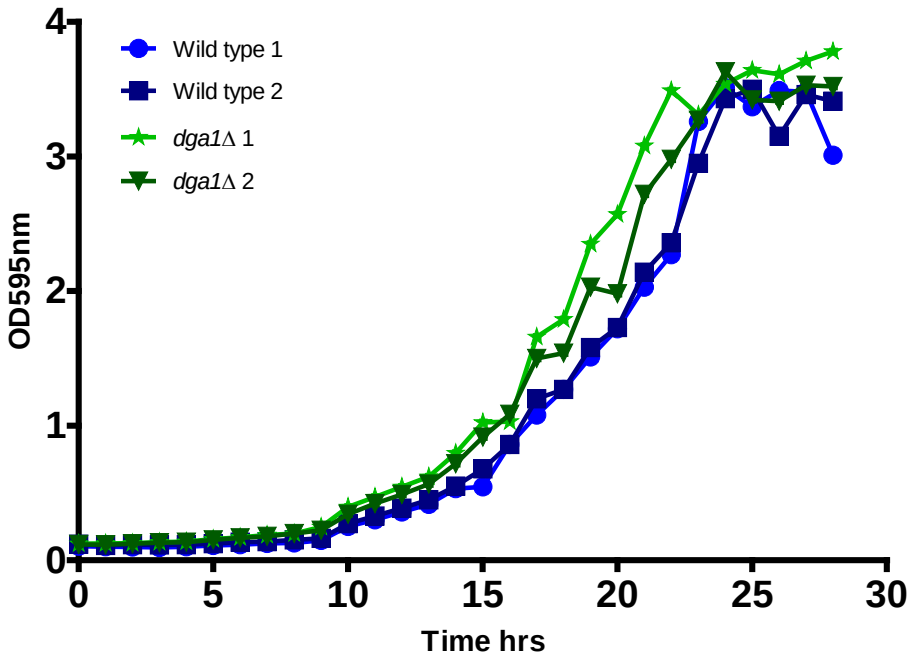


**Figure 3.51: Growth curves of *S. pombe* wild type and *dga1Δ* under normal conditions in yeast Edinburgh minimal medium (EMM).** Cultures were diluted to 2 x $10^6$ cells ($OD_{595}$ ~0.1) and incubated with shaking, 180rpm, at 30°C. Optical density readings were taken hourly until mid to late stationary phase was reached. Experiments were conducted in duplicate (culture 1 and culture 2 for both WT and deletion strain) showing growth patterns observed for two distinct colonies of the same strain.

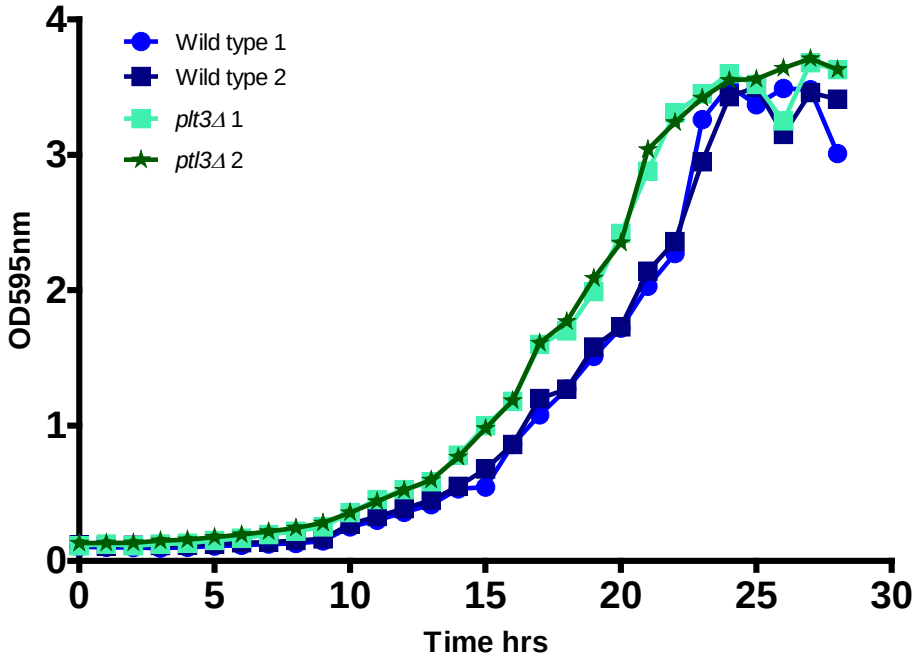


**Figure 3.52: Growth curves of *S. pombe* wild type and *ptl3Δ* under normal conditions in yeast Edinburgh minimal medium (EMM).** Cultures were diluted to 2 x $10^6$ cells ($OD_{595}$ ~0.1) and incubated with shaking, 180rpm, at 30°C. Optical density readings were taken hourly until mid to late stationary phase was reached. Experiments were conducted in duplicate (culture 1 and culture 2 for both WT and deletion strain) showing growth patterns observed for two distinct colonies of the same strain.

Unlike *S. cerevisiae*, a low lipid exponentially growing control could not be employed for *S. pombe* screening; as such *S. pombe* mutant cells were screened once early stationary phase had been achieved at 24 hrs and compared against wild type cells for both neutral lipids, Figure 3.53 and polar lipids, Figure 3.54.

Cells deleted for *DGA1* exhibited a 1.5 fold decrease in fluorescence attributed to neutral lipids when compared to the wild type, similar to the impact on neutral lipid amounts of the *dga1* deletion in *S. cerevisiae*. Cells lacking *PTL3* displayed a 1.4 fold increase in neutral lipid fluorescence compared to wild type (Figure 3.53).

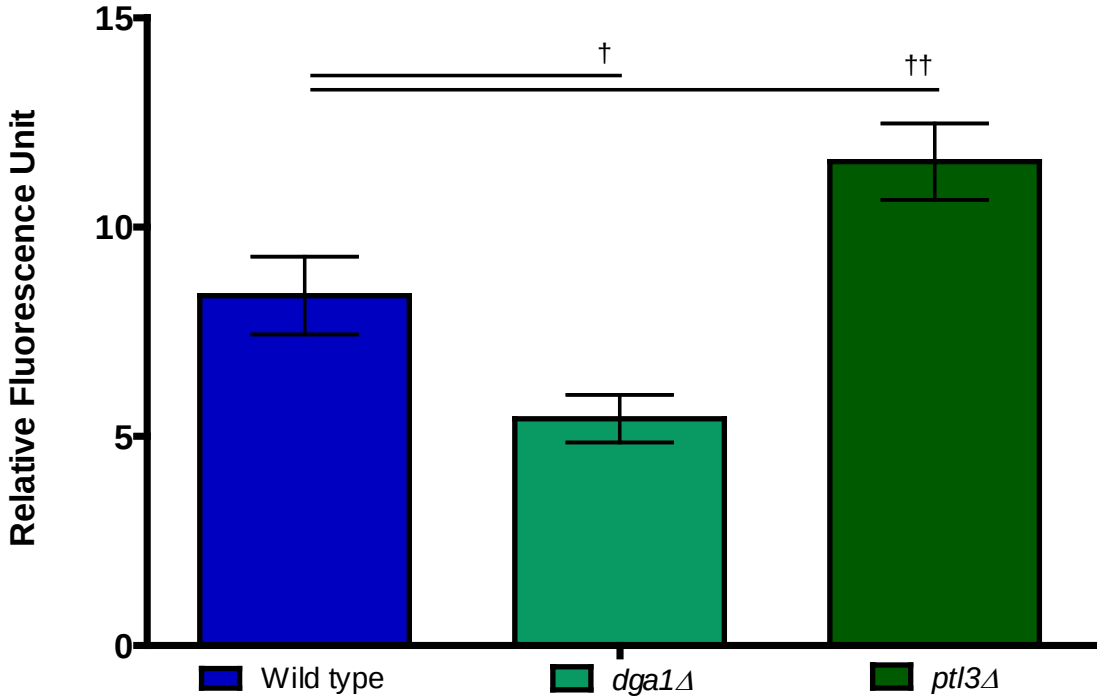


**Figure 3.53: Neutral lipid fluorescence intensity of Nile red stained *S. pombe* wild type, *dga1Δ* and *ptl3Δ* mutants.** Cells were harvested 24 hrs post resuspension in EMM. Cells were washed twice in PBS before adjusting to a cell density of 2 x $10^7$ cells/ml. 5 x $10^6$ cells were transferred to the wells of black 96-well plates in triplicate. 25µl PBS/DMSO (1:1 v/v) and 5µg/ml Nile red were added to each sample. Plates were screened using the wavelengths: excitation 485 nm, emission 535 nm. Data shown as means of triplicates ±SD. Significance indicated between strains indicated by solid black lines ŧ<0.05, ŧŧp≤0.01. Data analysed by one way ANOVA with Tukey *post hoc* test.

As expected for polar lipids no significant difference in fluorescence was observed in the *dga1* mutant. However, a significant increase of fluorescence pertaining to polar lipid amounts was observed in cells deficient in *PTL3* (Figure 3.54).

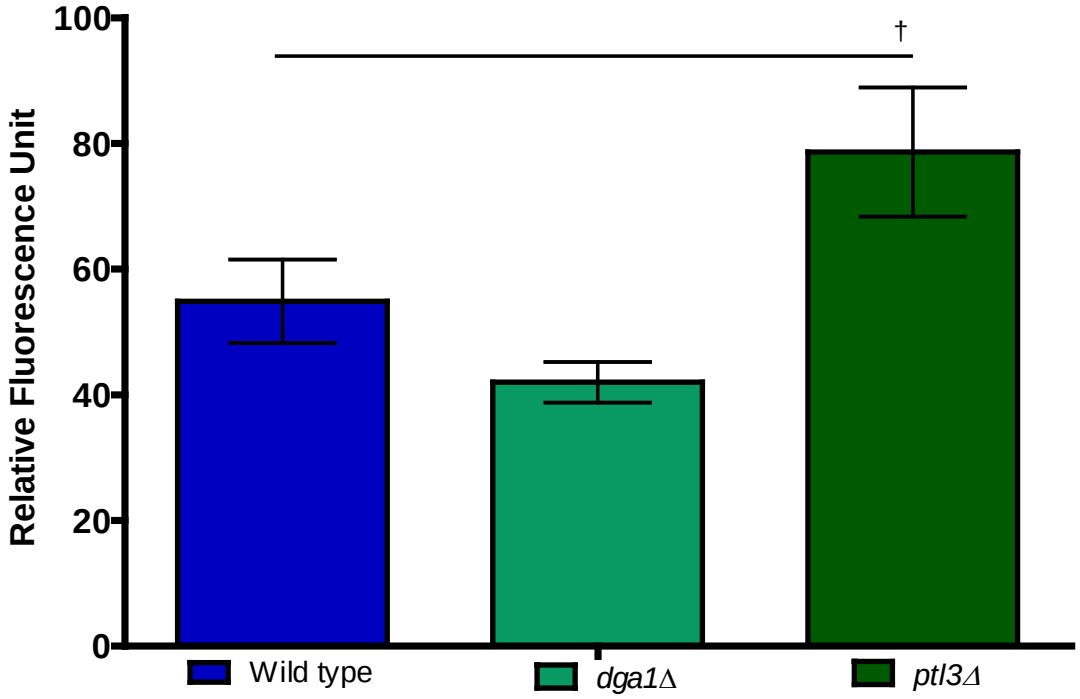


**Figure 3.54: Polar lipid fluorescence intensity of Nile red stained *S. pombe* wild type, *dga1Δ* and *ptl3Δ* mutants.** Cells were harvested 24 hrs post resuspension in EMM. Cells were washed twice in PBS before adjusting to a cell density of 2 x $10^7$ cells/ml. 5 x $10^6$ cells were transferred to the wells of black 96-well plates in triplicate. 25µl PBS/DMSO (1:1 v/v) and 5µg/ml Nile red were added to each sample. Plates were screened using the wavelengths: excitation 535nm, emission 590 nm. Data shown as means of triplicates ±SD. Significance indicated between strains indicated by solid black lines ŧ<0.05, ŧŧp≤0.01. Data analysed by one way ANOVA with Tukey *post hoc* test.

### 3.6.1.2 Nile red screening of S. pombe SREBP transcription factor homologues

*S. pombe*, unlike *S. cerevisiae*, contains orthologues to human SREBP-1a, Sre1 and Sre2, along with mammalian SCAP, Scp1. Sre1 is proteolytically cleaved in response to low sterol conditions and is dependent on interaction with Scp1, concurrent with the route of activation of its mammalian counterpart. The less well described Sre2 however, does not bind Scp1 and is constitutively cleaved (Bien and Espenshade 2010, Hughes Adam L. *et al.* 2005).

Growth curves of wild type *S. pombe* were conducted prior to Nile red screening to ensure mutant cells had comparable growth rate to that of wild type (Figures 3.55, 3.56 and 3.57).

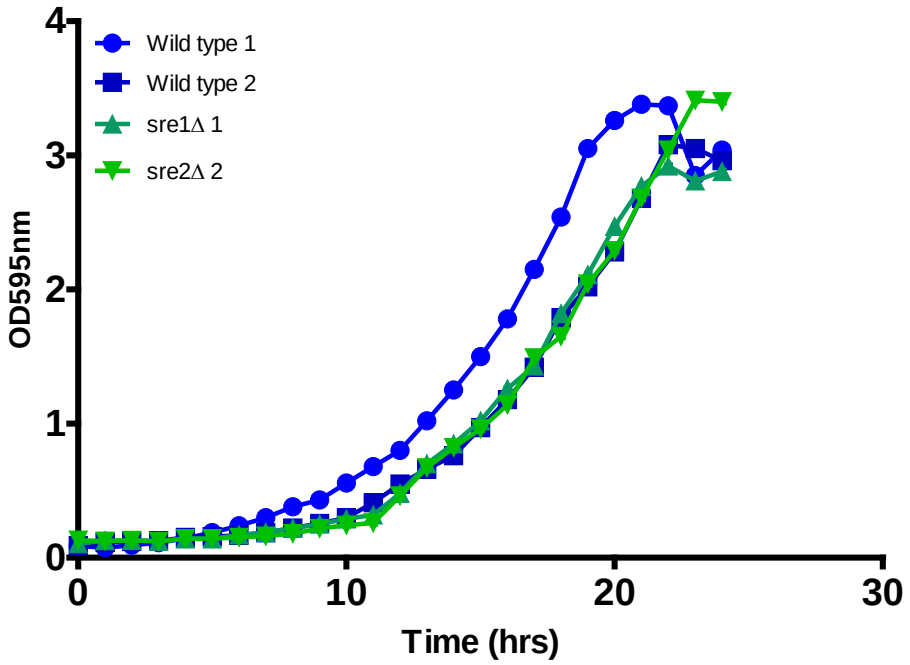


**Figure 3.55: Growth curves of *S. pombe* wild type and *sre1Δ* under normal conditions in yeast Edinburgh minimal medium (EMM).** Cultures were diluted to 2 x $10^6$ cells ($OD_{595}$ ~0.1) and incubated with shaking, 180rpm, at 30°C. Optical density readings were taken hourly until mid to late stationary phase was reached. Growth curves were conducted in duplicate (culture 1 and culture 2 for both WT and deletion strain) showing growth patterns observed for two distinct colonies of the same strain.

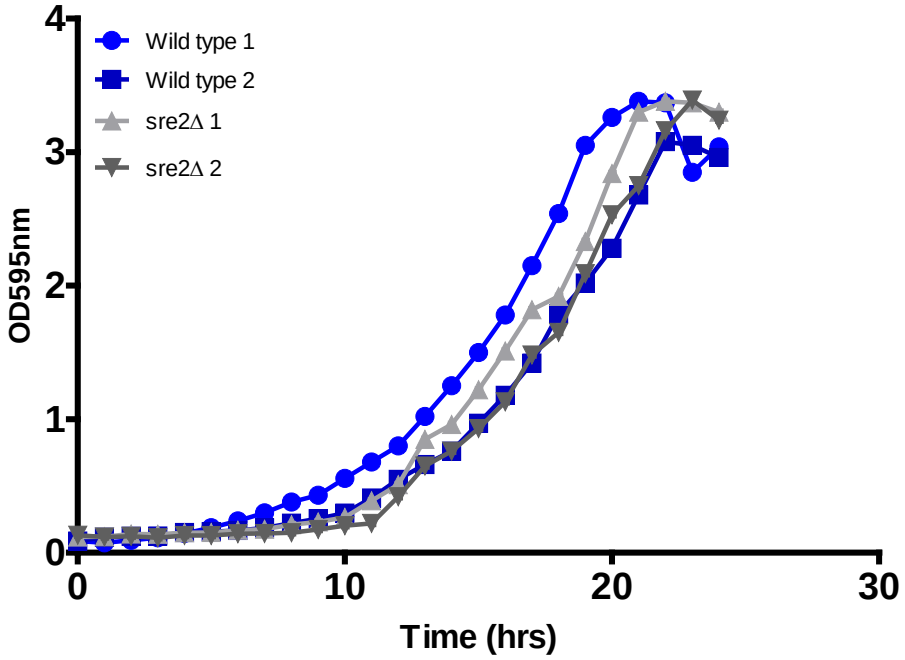


**Figure 3.56: Growth curves of *S. pombe* wild type and *sre2Δ* under normal conditions in yeast Edinburgh minimal medium (EMM).** Cultures were diluted to 2 x $10^6$ cells ($OD_{595}$ ~0.1) and incubated with shaking, 180rpm, at 30°C. Optical density readings were taken hourly until mid to late stationary phase was reached. Growth curves were conducted in duplicate (culture 1 and culture 2 for both WT and deletion strain) showing growth patterns observed for two distinct colonies of the same strain.

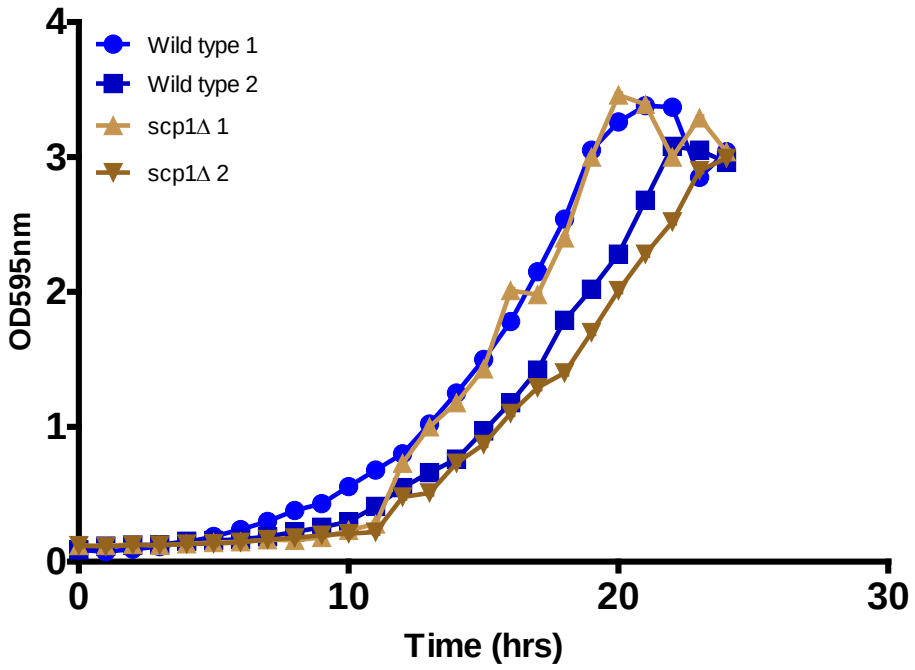


**Figure 3.57: Growth curves of *S. pombe* wild type and *scp1Δ* under normal conditions in yeast Edinburgh minimal medium (EMM).** Cultures were diluted to 2 x $10^6$ cells ($OD_{595}$ ~0.1) and incubated with shaking, 180rpm, at 30°C. Optical density readings were taken hourly until mid to late stationary phase was reached. Growth curves were conducted in duplicate (culture 1 and culture 2 for both WT and deletion strain) showing growth patterns observed for two distinct colonies of the same strain.

Data obtained from the neutral lipid screen indicated that levels of lipids in all SREBP component deletion strains did not differ significantly from that of wild type cells (Figure 3.58).

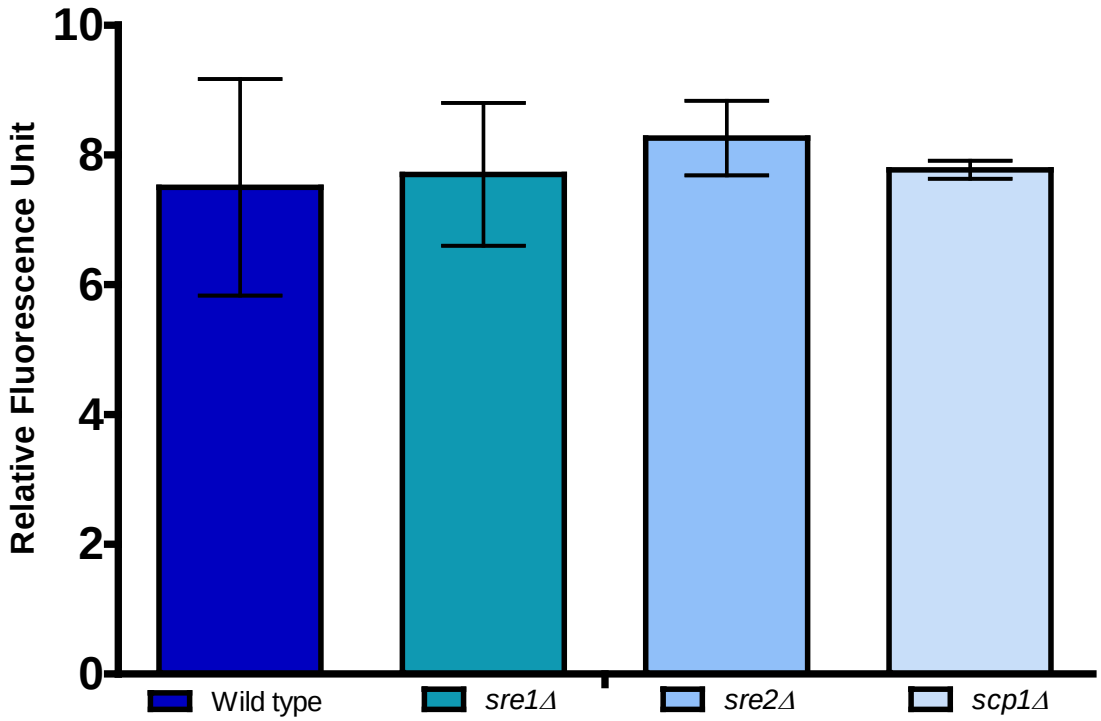


**Figure 3.58: Neutral lipid fluorescence intensity of Nile Red stained *S. pombe* wild type and SREBP component deletions *sre1, sre2* and *scp1*.** Cells were harvested 24 hrs post resuspension in EMM. Cells were washed twice in PBS before adjusting to a cell density of 2 x $10^7$ cells/ml. 5 x $10^6$ cells were transferred to the wells of black 96-well plates in triplicate. 25µl PBS/DMSO (1:1 v/v) and 5µg/ml Nile red were added to each sample. Plates were screened using the wavelengths: excitation 485nm, emission 535 nm. Data shown as means of triplicates ±SD. Data analysed by one way ANOVA with Tukey *post hoc* test.

For more polar lipid classes, no significant differences in fluorescence were observed for *sre1, sre2* or *scp1* deletion strains compared to wild type cells (Figure 3.59).

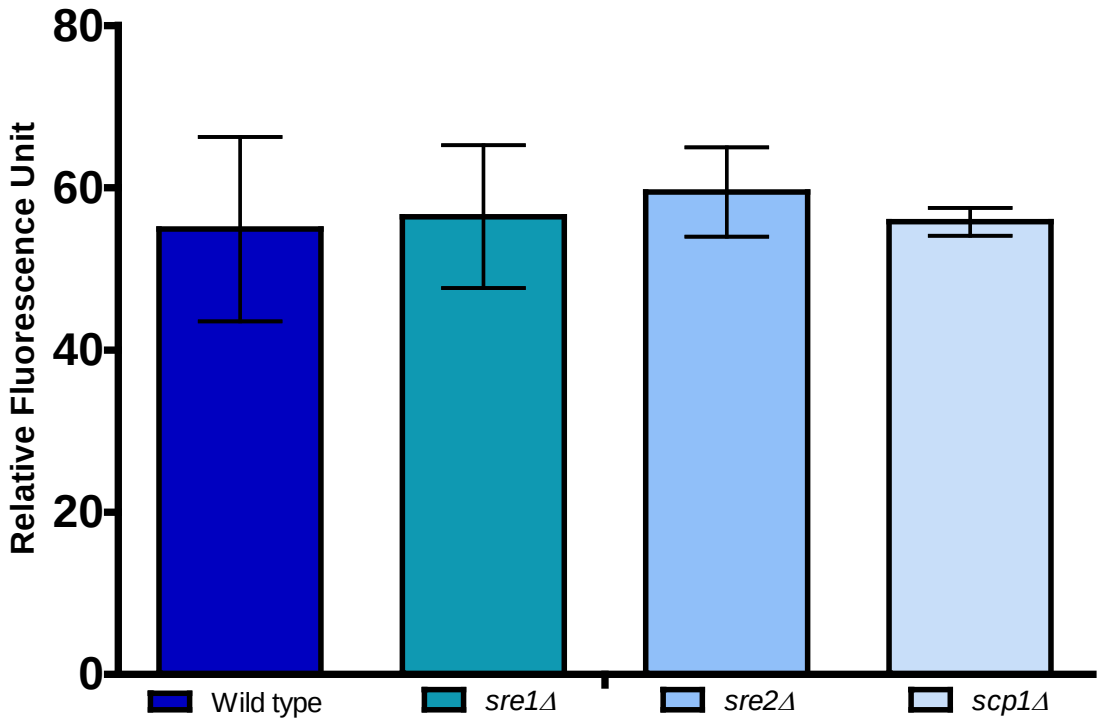


**Figure 3.59: Polar lipid fluorescence intensity of Nile Red stained *S. pombe* wild type and SREBP component deletions *sre1, sre2* and *scp*.** Cells were harvested 24 hrs post resuspension in EMM. Cells were washed twice in PBS before adjusting to a cell density of 2 x $10^7$ cells/ml. 5 x $10^6$ cells were transferred to the wells of black 96-well plates in triplicate. 25µl PBS/DMSO (1:1 v/v) and 5µg/ml Nile red were added to each sample. Plates were screened using the wavelengths: excitation 535nm, emission 590 nm. Data shown as means of triplicates ±SD. Data analysed by one way ANOVA with Tukey *post hoc* test.

## 3.7 Discussion

In this study the aim was to develop suitable methodology to assess lipid content in the oleaginous yeast species *L. starkeyi* as well as the non-oleaginous yeasts *S. cerevisiae* and *S. pombe*.

For oleaginous yeasts, such as *L. starkeyi,* cells are cultured in nitrogen limiting medium in order to achieve maximal lipid production via the assimilation of the excess carbon source (Tanimura *et al.* 2014). In this chapter, nitrogen limiting media (NLM) was utilised for lipid production and carbon limiting media (CLM) utilised as a medium that would produce cells to act as a low lipid controls (Wild *et al.* 2010). It was shown that the growth of *L. starkeyi* inoculated directly into limiting medium took an approximately 90-100 hrs to reach stationary phase in limiting media (Table 3.1). To reduce the time taken for cells to reach stationary phase, YPD pre-cultures were subsequently used as inoculum for nitrogen and carbon limiting culture conditions which did not have an effect of lipid production compared to direct inoculation (Figure 3.6).

Gravimetric assessment of the lipid accumulation profile of *L. starkeyi* in a range of growth phases showed that in NLM, lipid began to accumulate at 72 hrs and sharply increased at 96-120 hrs (Figure 3.8). The sharp increase observed at 96 hrs is consistent with cells entering early stationary phase of growth (Figure 3.7). The maximal lipid accumulation for this time course occurred at 120 hrs which is concurrent with cells in mid stationary phase, a reduction in lipid mass was then observed at 144hrs (Figure 3.8). The observed reduction is suggested to be as a consequence of lipase activity and subsequent β-oxidation (Beopoulos *et al.* 2011).

After optimisation in *L. starkeyi,* the methodology for culturing and assessing lipid accumulation was transferred to the non-oleaginous yeasts *S. cerevisiae* and *S. pombe*. Upon culturing cells in limiting medium a poor growth rate was observed for both species which could be attributed to an autophagic and/or mitophagic response (Crespo J. L. and Hall 2002, Mukaiyama *et al.* 2009). Further to this, both nitrogen and carbon limitation exert stress on both *S. cerevisiae* and *S. pombe* (Aoki Y. *et al.* 2011, Smith *et al.* 2002, Zuin *et al.* 2010a) which could have affected further work as it would have been difficult to separate the cellular response to stress from that of lipid accumulation.

Additionally, lipid amounts could not be accurately assessed in *S. cerevisiae* via gravimetric means (Figure 3.13). This is as a consequence of this species only being able to accumulate approximately 11% of its total mass as lipid (Sitepu *et al.* 2012).

The culture medium was changed from nitrogen and carbon limiting to a defined minimal medium, YNB for *L. starkeyi* and *S. cerevisiae* and EMM for *S. pombe.* By culturing in YNB, using 2% glucose as the carbon source, *de novo* lipid formation could be followed which is analogous to the route of lipid production in cancerous cells. Additionally, defined minimal medium has been utilised in studies investigating both lipid production and the stress response in *S. cerevisiae* (Kamisaka *et al.* 2007, Marques *et al.* 2006, Ruiz-Roig *et al.* 2012). Along with this a limiting nutrient source would occur as a natural consequence of growth rather than being limited throughout the culturing process, allowing a more accurate assessment of lipid production.

The use of gas chromatography in order analyse fatty acid composition of wild type cells was trialled initially after gravimetric means were deemed inappropriate. Although GC analysis proved to display enough sensitivity for low lipid quantification in *S. cerevisiae,* the labour intensive and low throughput nature of this analytical technology meant that it was time consuming and logistically incompatible with screening a large number of deletion strains. Moreover, it also meant that further work utilising a separate column and use of a solvent system would be required to infer the phospholipid status of the samples by liquid chromatography. Similarly analysis of samples by thin layer chromatography was equally labour and time intensive, whilst also being limited to sample space available on TLC plates. Further, after development and visualisation of the plates, assessment of lipid amounts would have been subjective unless plates were analysed via densitometry.

The Nile red assay for analysis of lipid amounts was adapted from a method by Sitepu *et al.* (2012). In optimisation of the methodology, a number of modifications were made to the method. Firstly Krystal 2000 plates were employed instead of Costar plates utilised in the study by Sitepu *et al.* (2012). As the wells of Krystal 2000 plates are individually moulded, each well is separate from the next, whereas Costar plates comprise of a single sheet of plastic running along the bottom of the plate. Plates comprising of individually moulded wells serve to increase the specificity of well fluorescence readings by avoidance of lateral piping of light underneath the wells.

Dual wavelengths were also utilised in the present study to distinguish polar and neutral lipid classes simultaneously, which has been seldom used in lipid analyses utilising Nile red assays. As described previously in this chapter, cells were washed in PBS twice prior to screening to reduce background fluorescence from spent culture medium. This is especially important with culture media such as YNB as it produces high levels of background fluorescence in the presence of Nile red.

Finally, as with the previous study, fluorescence data was corrected for cell density but then was also further corrected for background fluorescence resulting from Nile red in PBS. This further improved the accuracy of the method by eliminating fluorescence occurring from the background medium, PBS in this case, thus ensuring any changes in RFU values were the result of cellular lipid content alone.

The method was initially validated using the biotechnologically relevant oleaginous yeast, *Lipomyces starkeyi*. Lipid accumulation in yeast is affected by altering culture conditions. In this study 2% glucose is utilized as the carbon source in YNB medium for monitoring *de novo* lipid formation (Kamisaka *et al.* 2006). In *L. starkeyi*, the same trend of lipid accumulation was observed for both gravimetric and fluorescence determination of total lipids (Figure 3.18). As the cells enter stationary phase and exhaust the available nitrogen, lipids are stored for cellular energy resulting in maximum lipid accumulation (Beopoulos *et al.* 2011).

In late stationary phase a decrease in lipids is seen, which may occur as a consequence of triacylglycerol depletion as the acyl chains are released for β oxidation in a similar manner to that suggested by (Beopoulos *et al.* 2011). It is important to note that as cells approach mid stationary phase of growth, 72 hrs onwards, there was less total lipid detected by gravimetric analysis than Nile red. This is suggested to result from a common problem encountered with lipids extracted using the method of Bligh and Dyer whereby significant underestimates of lipid content, mainly neutral lipids, occurs in samples comprising in excess of 2% lipid content (Iverson *et al.* 2001). This data also suggested that Nile red is a more reliable and repeatable means of assessing cellular lipid due to the reduced standard deviation compared to the results of the gravimetric analyses (Figure 3.18).

Excitation of Nile red at two different wavelengths enables the microscopic detection of polar and neutral lipids. Fluorescence microscopy of Nile red stained *L. starkeyi* cells allowed visualization of specific structures related to neutral and polar lipids (Figure 3.19). Limited overlap in fluorescence signal was observed between the two wavelengths, indicating the selectivity of Nile red dye for neutral and polar lipids. This study also demonstrated that Nile red assays only utilising the wavelength for more polar lipids (590 nm), as described by Sitepu *et al.* (2012), would mainly detect lipids within membranous structures rather than the intracellular lipid content of the cells. Further to this our data indicated the dual wavelength Nile red method may be a viable microplate screening method for determining neutral and polar lipid content of oleaginous yeast cells.

It has also been demonstrated that the Nile red method is sensitive and specific enough to determine polar and neutral lipid levels within the non-oleaginous yeast, *S. cerevisiae*. Using neutral lipid mutants, it has been presented that the optimized Nile red fluorescence assay confers similar sensitivity to more advanced methodologies, such as gas chromatography, when a severe lipid phenotype results (Figures 3.27 and 3.28).

The validation mutant set for *S. cerevisiae* Nile red screening comprised of cells deficient in *DGA1, LRO1* and *FAT1.* Diacylglycerol acyltransferases in *S. cerevisiae* are encoded by *DGA1* in *S. cerevisiae,* a functional mammalian *DGAT2* homologue, and *LRO1*, which is homologous to mammalian *LCAT*. Both contribute substantially to the synthesis of neutral storage lipids by acylation of DAG to produce the end product TAG. Using the Nile red method, the data showed that cells deficient for *DGA1* exhibited a 1.4 fold decrease in neutral lipids compared to wild type cells (Figure 3.27). This supports findings by Oelkers *et al.*., who demonstrated a decrease (1.9 fold) in the amount of triacylglycerol synthesis via metabolic labelling (Oelkers Peter *et al.* 2002). Also consistent with the findings of Oelkers *et al.* (2002), cells lacking *LRO1* showed a slight decrease in neutral lipids in stationary phase, (Figure 3.27), which may indicate that Dga1 activity is greater in stationary phase.

The phenotypic differences between cells deleted for *DGA1* and *LRO1* may be explained by their activity in different growth phases. It has been demonstrated that Lro1 is more active in the synthesis of TAG in exponentially growing cells (Athenstaedt 2011) and so would not be expected to display a severe phenotype at stationary phase. Conversely,

Dga1 may be more active during later phases of growth and so may contribute to TAG formation more significantly in stationary phase cells (Oelkers Peter *et al.* 2002).

The *FAT1* gene of *S. cerevisiae* encodes an acyl-CoA synthetase required for activation of very long chain fatty acids (VLCFA). Work undertaken by Watkins *et al.* (1998) demonstrated that the *fat1Δ* accumulated markedly increased VLCFA when compared to wild type cells (Watkins *et al.* 1998). When cells deleted for *FAT1* were screened using Nile red they exhibited a significant increase in neutral lipids compared to wild type cells (Figure 3.27). Therefore, the observed increase could be as a result of its accumulation of hydrophobic very long chain fatty acids (Watkins *et al.* 1998).

For polar lipids, although slight changes in fluorescence values were observed in the deletion strains (Figure 3.28), this is believed to be due to amounts of the phospholipid monolayer encasing the lipid droplets (Grillitsch *et al.* 2011). These results demonstrated that the dual wavelength Nile red fluorescence method was able to detect changes to neutral lipids from that of polar lipids in *S. cerevisiae*, a non-oleaginous yeast.

For screening conducted utilising components known to be involved in phospholipid synthesis, an increased neutral lipid phenotype was observed for deletions in *INO2* (2.7 fold) and *INO4* (2.6 fold). This is suggested to be as a result of these strains harbouring "supersized" lipid droplets, which may increase fluorescence signal when using the wavelength for more neutral lipid subtypes (Wang *et al.* 2014). It was recently reported that components involved in β-oxidation, including Oaf1 and Pip2, are downregulated in *INO2* and *INO4* deletion strains, which would serve to increase the free fatty acid content of the cell. From looking at combined SE and TAG contents determined by gas chromatography in a study by Chumnanpuen *et al.* (2013), a 2.1 fold and 2 fold increase in neutral lipids resulted from deletion of *INO2* and *INO4* respectively (Chumnanpuen *et al.* 2013). These results are consistent with the data in this study using the Nile red method (Figure 3.32).

Interestingly an increase in phospholipid levels was also seen in both the *ino2Δ* and the *ino4Δ* (Figure 3.33). It is therefore suggested that these deletions, in normal culture conditions, may have up-regulated phospholipid synthesis via the CDP-DAG pathway, which has been described as being independent from the Ino2, Ino4, Opi1 regulatory circuit (Su and Dowhan 2006). Alternatively, the inability of these mutants to de-repress

enzymes which convert phosphatidylethanolamine (PE) to phosphatidylcholine (PC) may provide a further explanation. It was demonstrated that although mutations of *INO2* and INO4 resulted in reduced cellular PC, increased levels of PE, phosphatidylinositol and the phospholipid intermediates phosphatidylmonomethylethanolamine (PMME) and phosphatidyldimethylethanolamine (PDME) along with neutral lipids were observed compared to wild type cells (Fei Weihua *et al.* 2011, Loewy and Henry 1984). This demonstrated that the levels of polar lipids observed by Nile red in the present study may have resulted from increased levels of other polar lipid classes (Figure 3.33).

In the case of the *opiΔ,* it is expected that an increased level of phospholipids would result as Opi1 functions to repress transcriptional activity of Ino2/Ino4. Previous analysis by Klig *et al.* (1985) of phospholipid fractions in cells deleted for *OPI1* in YNB medium, demonstrated that levels of PI were increased 1.5 fold but both PS and PC levels were decreased 1.7 and 1.2 fold respectively (Klig *et al.* 1985). No significantly different phenotype from that of wild type cells was observed via Nile red screening for the *opi1Δ* in the present study (Figure 3.33). This, taken together with the work of Klig *et al.* (1985) suggested that the phospholipid phenotype does not severely affect the overall levels of the phospholipid pool.

In the screening of deletion strains involved in lipid droplet morphology and β-oxidation, no significant lipid phenotypes were determined using the Nile red assay (Figures 3.37 and 3.38). Fld1p is a functional homologue of mammalian seipin. It has been described that cells lacking *FLD1* contain "supersized" lipid droplets which demonstrate enhanced fusion activity compared to LDs in wild type cells (Fei W. *et al.* 2008). Although this would be expected to increase fluorescence intensity pertaining to neutral lipids, it is suggested that as cells lacking *FLD1* contain fewer lipid droplets (Fei W. *et al.* 2008). Therefore, the fluorescence intensity yielded from Nile red may be equivalent to that of wild type cells which contain an increased number of smaller LDs in comparison. In order to verify this fluorescence microscopy of Nile red stained wild type cells and those lacking *FLD1* could be employed.

Oaf1p and Pip2p are both components involved in β-oxidation. They are paralogues of each other and form a heterodimer to induce transcription of β-oxidation genes. Strains lacking components in β-oxidation processes may be expected to have increase neutral lipids in comparison to wild type cells, as components of β-oxidation serve to regulate the

breakdown of cellular fatty acids. It must be remembered that both growth phase and access to key nutrients also impact upon fatty acid catabolism. No significant differences were observed for neutral or polar lipid classes using Nile red screening (Figures 3.37 and 3.38). However, the Nile red method may not be sensitive enough to detect significance when only a slight lipid phenotype results.

Alternately, Oaf1 and Pip2 are paralogues of each other, meaning the phenotype of a single deletion may be rescued by activity of the other. It has been demonstrated that in the absence of Pip2, Oaf1 can homodimerise to induce gene expression of some oleate responsive genes (Trzcinska-Danielewicz *et al.* 2008). It has also been shown that expression of key peroxisomal β-oxidation genes are identical in cells lacking *OAF1* and *PIP2* to wild type cells growing in glucose medium. Although these observations support the Nile red data in the present study, it is not known what contribution TAGs and SEs are making to the neutral lipid pool. This could be further investigated by analysis of samples utilising gas chromatography.

The SREBP-like proteins of *S. cerevisiae* are key activators of genes which encode enzymes such as Erg2 and Erg3 in the late stages of ergosterol synthesis. They regulate transcription by binding of the sterol binding element in the promoters of target genes. Under normal culture conditions Ecm22p is more abundant at the *ERG* promoter regions. In contrast when sterols are depleted, Ecm22p decreases and is replaced at the *ERG* promoters by Upc2p (Davies *et al.* 2005). However, no significantly different phenotypes of cells lacking *ECM22* or *UPC2* were observed by the Nile red assay when compared to wild type cells (Figures 3.43 and 3.44). This result can be explained as Upc2 and Ecm22 are paralogues of each other, therefore deletion of one may result in the phenotype being rescued by the other. This is supported by the description that induction of *ERG* genes catalysing the final steps of ergosterol synthesis can be mediated by both Ecm22 and Upc2 (Davies *et al.* 2005).

For Mga2 and Spt23, which are involved in the regulation of fatty acid synthesis and regulate the expression of the FA desaturase *OLE1*, no significant lipid phenotype was observed for cells lacking *SPT23.* As with Ecm22 and Upc2, the deletion of Spt23 may be compensated by the presence of Mga2. It has been demonstrated that under normoxic growth conditions in glucose medium that Spt23 and Mga2 perform overlapping functions with little differences in *OLE1* expression (Chellappa *et al.* 2001). In cells lacking *MGA2* a

significantly reduced lipid phenotype was observed. This suggests that Mga2p is one of the dominant transcription factors for driving expression of lipid biosynthetic genes.

It has been further demonstrated that Mga2 function becomes critical for the expression of *OLE1* when there is an increased demand for *de novo* lipid synthesis (Surma *et al.* 2013). Additionally, it has been shown that Mga2 holds an additional role in the stabilisation of the *OLE1* transcript, therefore in the absence of Mga2 *OLE1* stability is perturbed which may result disturbed translation efficiency (Kandasamy *et al.* 2004). Taken together, the observations made in previous studies support the observations in the present study, whereby cells deficient for *MGA2* displayed a decreased neutral lipid phenotype compared to cells deleted for *SPT23* (Figure 3.43).

If the SREBP-like proteins are compensating for each other, it would be expected that a double deletion would show a further phenotype. In the W303 *S. cerevisiae* genetic background, the *ecm22Δ* did not result in a significantly altered neutral nor polar lipid phenotype. In cells lacking both *ECM22* and *UPC2* a slight reduction in the neutral lipid pool occurred, although this was not found to be significantly different from that of wild type cells (Figure3.47). This could be due to the presence of functional Hap1, which is both a transcriptional repressor and activator of *ERG* genes. As *ERG* gene transcription is activated by Hap1 in aerobic conditions (Hickman MJ. and Winston 2007) this suggests that Hap1 could compensate, to some level, for the loss of *ECM22* and *UPC2* in the W303 genetic background.

In addition to *S. cerevisiae*, the use of the Nile red fluorescence assay in the fission yeast, *S. pombe* has also been examined. As described previously little work has been undertaken on lipid accumulation in this yeast species, but due to its potential importance in human disease research the study was extended to fission yeast.

Unlike *L. starkeyi* and *S. cerevisiae*, the fission yeast *S. pombe* does not gradually accumulate lipid over time. Instead, maximal levels of lipid are seen during exponential growth with lower levels as cell progress into stationary phase (Figures 3.49 and 3.50). It has been previously demonstrated that *S. pombe* accumulates greater levels of certain lipid species in exponential phase, including TAG, PE and PS, than is seen in *S. cerevisiae* cells (Shui *et al.* 2010). Two observations could explain why the total lipid content of *S. pombe* would be significantly more during exponential growth than in stationary phase.

Firstly, as *S. pombe* has a polarized manner of growth, dividing via medial fission, increased levels of sterols are present at the tips during exponential growth before accumulating at the completed septum closer to cell division (Wachtler *et al.* 2003). Secondly, intracellular lipid droplets in *S. pombe* are increased in the G2 phase of the cell cycle (Long *et al.* 2012). As a result of this, when quantifying the lipid in *S. pombe* cells, an exponentially growing low lipid control could not be used. Instead, as we were interested in lipid accumulation as a result of assimilation of carbon, stationary phase cultures only were analysed and compared to wild type cultures.

The microscopy data demonstrated that in *S. pombe,* using the dual wavelengths of Nile red, neutral and polar lipids may be distinguished (Figure 3.19). The *S. pombe* validation set for high throughput screening via Nile red contained cells deficient for *dga1* and *ptl3.*

Dga1 in *S. pombe* is analogous to *S. cerevisiae* Dga1 and is responsible for the majority of TAG synthesis along with Plh1 (Lro1 homologue). Similar to the impact on neutral lipid amounts of the *DGA1* deletion in *S. cerevisiae*, *S. pombe* cells deleted for *dga1* also showed a 1.5 fold decrease in neutral lipids (Figure 3.53). This is suggested to be due to the inability of substantial TAG formation via esterification of DAG (Zhang Qian *et al.* 2003). As in *S. cerevisiae* the activity of *S. pombe* Plh1 has been found to be higher in logarithmic phase cells (Zhang Qian *et al.* 2003), showing a conserved mechanism of TAG synthesis between Lro1/Plh1. The phenotype observed by Nile red, for cells deficient in *dga1* also supports the hypothesis that *S. pombe* Dga1p may function to produce TAG mainly in stationary phase cells (Zhang Qian *et al.* 2003).

*S. pombe* contains three intracellular lipases; Ptl1, Ptl2 and Ptl3, with Ptl2 and Ptl3 conferring significant homology to *S. cerevisiae* lipases Tgl3, Tgl4 and Tgl5. It has been demonstrated upon deletion of triacylglycerol lipases in *S. cerevisiae* that intracellular TAG levels are increased (Athenstaedt and Daum 2005), and so it was expected an increased neutral lipid phenotype would have been observed in cells deleted for TAG lipases in *S. pombe*. The results for cells lacking *ptl3* (1.4 fold increase in neutral lipid), yielded data consistent with more recently published gas chromatography data where a 1.7 fold increase in average cellular TAG amounts was observed upon deletion of *ptl3* in *S. pombe* (Yazawa *et al.* 2012). This increase is observed as cells have a reduced ability to mobilise TAG stored in LDs when lipase activity is reduced (Figure 3.53).

For polar lipids, a significant change was only observed in the *ptl3* mutant (Figure 3.54). This result could be due to the level of increased neutral lipid observed, which in turn would mean more polar lipids due to the phospholipid monolayers encasing the droplets (Grillitsch *et al.* 2011). Alternatively, Ptl3p may also have a role in regulating phospholipid levels in addition to maintaining neutral lipid homeostasis, which has been shown with *S. cerevisiae* Tgl3 and Tgl5 (Rajakumari S. and Daum 2010a). A further possibility may be that, due to the deletion of *ptl3*, increased phospholipid synthesis/remodelling results, which has also been demonstrated to occur in *S. cerevisiae* triacylglycerol deleted strains (Mora *et al.* 2012, Rajakumari S. and Daum 2010b).

Nile red screening of *S. pombe* SREBP (*sre1, sre2*) and SCAP (*scp1*) deletions did not reveal significantly different lipid phenotypes to that of wild type cells (Figures 3.58 and 3.59). As the cleaved active form of Sre1 regulates transcription of genes in response to low oxygen and sterol levels (Hughes B. and Espenshade 2008), it is possible that cultures contained either sufficient levels of sterols or a sufficient oxygen supply to synthesise sterols without requiring the presence of active Sre1 (Hughes A. L. *et al.* 2008). In cells lacking Scp1, Sre1 activity is abolished and so it is suggested that oxygen levels within the cultures were sufficient to not require Sre1 activity via cleavage by Scp1 (Hughes A. L. *et al.* 2008). In the case of the less well characterised Sre2, which is constitutively cleaved irrespective of oxygen levels (Cheung and Espenshade 2013), it is suggested that the presence of Sre1 and Scp1 would be sufficient to maintain lipid homeostasis if a decrease in sterols occurred.

It has been established by utilising the dual emission properties of Nile red in a microplate assay that more informative phenotypic data may be obtained on lipid content of both oleaginous and non-oleaginous yeast cells. Knowledge of the effect of cellular components impacting neutral and polar lipid levels is of particular importance in human diseases, such as cancer, in order to understand the regulation of lipid metabolism and how components involved could be modulated for subsequent phenotype amelioration. Unlike most non-conventional yeast species, including *L. starkeyi*, genetic tools are available for use with *S. cerevisiae* and *S. pombe.* Additionally due to their extensive characterisation, both *S. cerevisiae* and *S. pombe* serve as excellent model organisms in eukaryotic biology. This coupled with a plethora of available genetically modified strains

means that novel lipogenic regulatory elements can be identified to provide further insight into aberrant metabolism in human disease processes.

For the first time, it has been shown, that a Nile red assay can be applied to the fission yeast *S. pombe*. This is of particular importance due to growing interest and research in the area of *S. pombe* lipid metabolism.

This method is however, not without its limitations especially with regards to dye bleaching when observing red emission and that neutral and polar fluorescence cannot be directly compared due to differences in optimal gain parameters. This is due to the gain for each wavelength comprising of different optimal values. The gain adjusts the voltage across the photomultiplier tube of the plate reader making it either more or less responsive to the intensity of the signal generated by the sample and so samples with a higher intensity of fluorescence will have a lower optimal gain setting. Therefore neutral and polar lipids can be compared within each class but not directly to one another. The method is also limited to general pools of lipids, therefore further analysis to determine changes in molecular species, which may not impact on overall lipid levels, would need to be conducted by other means.

However, the rapid nature, reproducibility and potential scalability of this methodology means that interesting yeast strains, species and indeed culture conditions, that have significant impact on lipid amounts, can be readily segregated for further analysis by modern hyphenated chromatographic technologies, including liquid chromatography-mass spectrometry (LC-MS) and gas chromatography-mass spectrometry (GC-MS). The employment of Nile red ultimately means avoidance of time consuming, labour intensive analyses of samples that may not yield a lipid phenotype.

# Chapter IV: The role of Mitogen Activated Protein Kinase signalling in lipogenesis

## 4.1 Introduction

As previously described in Chapter 1, upstream signalling has been found to contribute to the initiation of lipogenesis in solid tumours, resulting from oncogenic gain of function and loss of tumour suppressors. These aberrations serve to fuel a heightened glycolytic rate resulting in increased production and accumulation of cellular lipids which drive cellular proliferation. It has been well documented in mammalian models that the mTOR pathway has significant involvement in the regulation of lipid metabolism (Soliman 2011). However, a potential role for the p38 MAP Kinase pathway in lipogenesis has not yet been subject to in depth investigation.

The yeasts *S. cerevisiae* and *S. pombe* have been utilised extensively as eukaryotic model organisms in order to increase understanding of key cellular and molecular processes (Botstein D and Fink 1988). Although phylogenetically distant from mammalian cells, numerous processes, regulatory elements and key pathways are highly conserved. Both mTOR complexes and signalling are conserved between mammalian and yeast systems. Additionally the p38 MAPK pathway is structurally and functionally conserved to the yeast Hog1 and Sty1 pathways of *S. cerevisiae* and *S. pombe* respectively (Bahn 2008).

The HOG pathway in *S. cerevisiae* responds to a wide range of external stimuli including high osmolarity, pH, endoplasmic reticulum (ER) stress, cell wall stress and citric acid stress (Bicknell *et al.* 2010, Garcia *et al.* 2009, Hohmann 2002, Kapteyn *et al.* 2001, Lawrence C. L. *et al.* 2004). Hog1p may be activated via two distinct signalling branches which both converge at the point of the common MAPKK Pbs2 (O'Rourke *et al.* 2002). Pbs2 phosphorylates Hog1p dually on conserved Thr174 and Tyr176 residues (Maayan *et al.* 2012). The response of Hog1 to phosphorylation can vary widely and is dependent on the stimulus to which it is responding. Under osmotic stress, activation of Hog1 precedes a rapid nuclear translocation where it may induce DNA transcription through recruitment of DNA binding proteins (Msn2/4) or interaction with RNA Polymerase II (Alepuz *et al.* 2001). Conversely under conditions of cell wall stress, Hog1 remains in the cytoplasm, indicating that it additionally activates cytoplasmic targets to regulate cellular processes (Garcia *et al.* 2004).

Msn2/4 are zinc finger transcription factors that operate downstream of Hog1 and are involved in the regulation of the general stress response (Alepuz *et al.* 2001). Msn2/4 are responsible for the regulation of ~200 genes in response to a number of stresses which include osmotic stress, glucose limitation, oxidative stress and heat shock (Martinez-Pastor *et al.* 1996). Msn2/4 can be localised either in the cytoplasm or nucleus. Under normal conditions, Msn2/4 are tethered in the cytoplasm, a localisation that is in part regulated by Tor1 (Beck and Hall 1999). Upon exposure of the cells to stress Msn2/4 become hyperphosphorylated before translocating to the nucleus to induce the expression of target genes. After activation and translocation to the nucleus, Msn2/4 are observed to shuttle between the nucleus and cytoplasm, a periodic behaviour of the proteins that corresponds to an intermediate level of stress (Jacquet *et al.* 2003).

The fission yeast species *S. pombe* also contains a conserved MAPK pathway to that of the mammalian p38 pathway (Bahn 2008). The Sty1 pathway, as in *S. cerevisiae*, is also activated under a range of stress conditions. Sty1p is activated by its upstream MAPKK Wis1 on residues conserved in p38 and Hog1 (Zhou *et al.* 2010). The downstream targets of Sty1 are less well characterised than those of Hog1 in *S. cerevisiae*, the most well understood being the transcription factors Pap1, which is required under low levels of stress, and Atf1 which is required in high levels of stress (Chen D. *et al.* 2008).

The work presented within this chapter describes deletions of components within the high osmolarity glycerol (HOG) MAPK pathway in *S. cerevisiae* and their effect on the production of both neutral and polar lipids in stationary phase. Further to this the study was extended to look at regulation of lipid accumulation via the Sty1 pathway in *S. pombe*.

In this chapter it has been demonstrated that Hog1p may play a key role in neutral lipid synthesis and additionally may hold a role in the synthesis of phospholipids. It has been further demonstrated that downstream targets of Hog1p, Msn2/4 may also be involved in the regulation of neutral lipid homeostasis. Additionally, the role of the MAPK pathway in accumulation of lipid appears to be conserved in *S. pombe*.

## 4.2 Results

### 4.2.1 S. cerevisiae TOR1 component deletions display an altered lipid phenotype to that of wild type cells

The mTOR pathway has been shown to be involved in regulating lipid biosynthesis in mammalian cells, and displays high homology to yeast Tor proteins. As mammalian mTORC1 has been shown to play a definite role in lipid synthesis, deletion of *S. cerevisiae* Tor1 components, *tco89Δ* and *tor1*Δ were screened using the Nile red assay along with a component of the Tor2 complex *avo2Δ*, as a negative control.

The role of mTORC2 in lipogenesis is less clear than that of mTORC1 in mammalian cells. It has been suggested that the role of mTORC2 may be more subtle than that of mTORC1, although it has been observed that mTORC2 signalling drives lipogenesis in hepatic tissues (Hagiwara *et al.* 2012). This highlights that mTOR2 activity, in respect to lipid metabolism in mammals, may likely be cell type specific. In *S. cerevisiae* it has been reported that Tor2 is involved in ceramide and sphingolipids synthesis, through the essential protein component Avo3 (Aronova *et al.* 2008). The Tor2 component Avo2 is involved, as in higher eukaryotes, in regulating the actin cytoskeleton during progression of the cell cycle, and so is not expected to exhibit an altered lipid phenotype. As previously described, the Tor1 protein complex regulates cellular growth in response to nutrient availability. Additionally one of the subunits of Tor1, Tco89, has been implicated in degradation of vacuole proteins including fructose 1,6-biphosphatase (FBPase) (Alibhoy and Chiang 2011). Nile red screening was carried out on yeast TOR protein component deletions to assess whether a distinguishable lipid phenotype resulted before going onto screening components of the HOG MAPK pathway.

Growth curves were conducted prior to screening to ensure deletion strains did not convey any growth defects and to ensure that cells were harvested at comparable growth phases. As shown by Figures 4.1, 4.2 and 4.3 exponential growth began ~4 hrs post resuspension in YNB medium before stationary phase of growth was reached at ~ 12hrs in all cases.

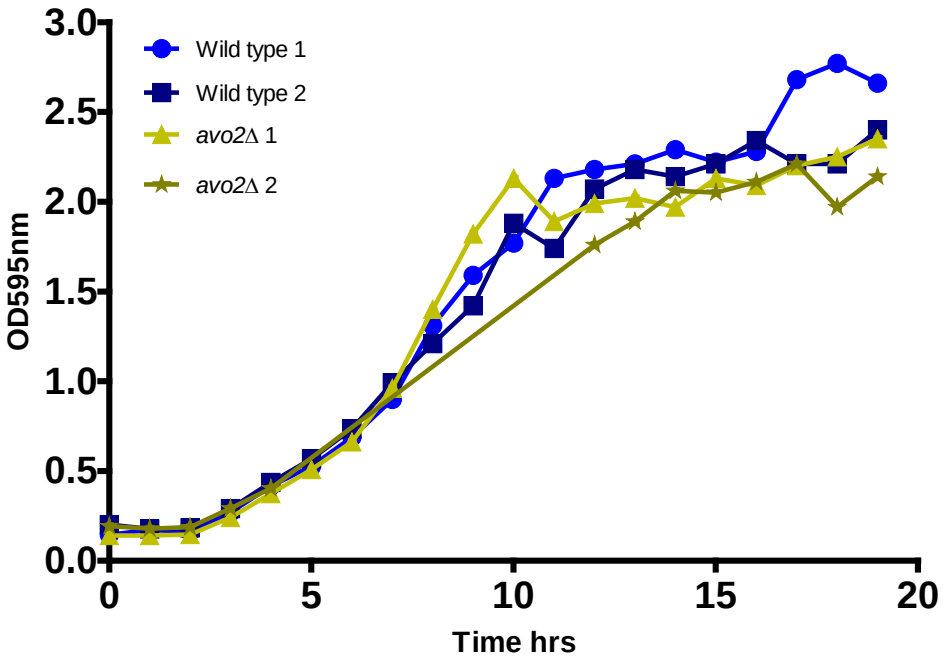


**Figure 4.1: Growth curve of *S. cerevisiae* wild type and *avo2Δ* under normal conditions in yeast nitrogen base medium (YNB).** Cultures were diluted to 2 x $10^6$ cells ($OD_{595}$ ~0.1) and incubated with shaking, duplicate, at 30°C. Optical density readings were taken hourly until mid to late stationary phase was reached. Growth curves were conducted in duplicate (culture 1 and culture 2 for both WT and deletion strain) showing growth patterns observed for two distinct colonies of the same strain.

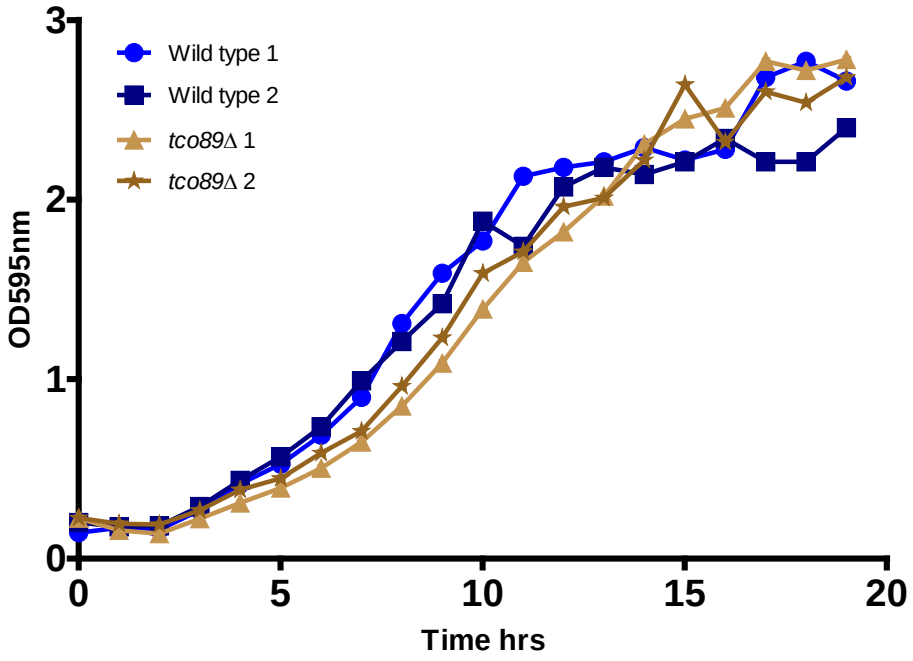


**Figure 4.2: Growth curve of *S. cerevisiae* wild type and *tco89Δ* under normal conditions in yeast nitrogen base medium (YNB).** Cultures were diluted to 2 x $10^6$ cells ($OD_{595}$ ~0.1) and incubated with shaking, duplicate, at 30°C. Optical density readings were taken hourly until mid to late stationary phase was reached. Growth curves were conducted in duplicate (culture 1 and culture 2 for both WT and deletion strain) showing growth patterns observed for two distinct colonies of the same strain.

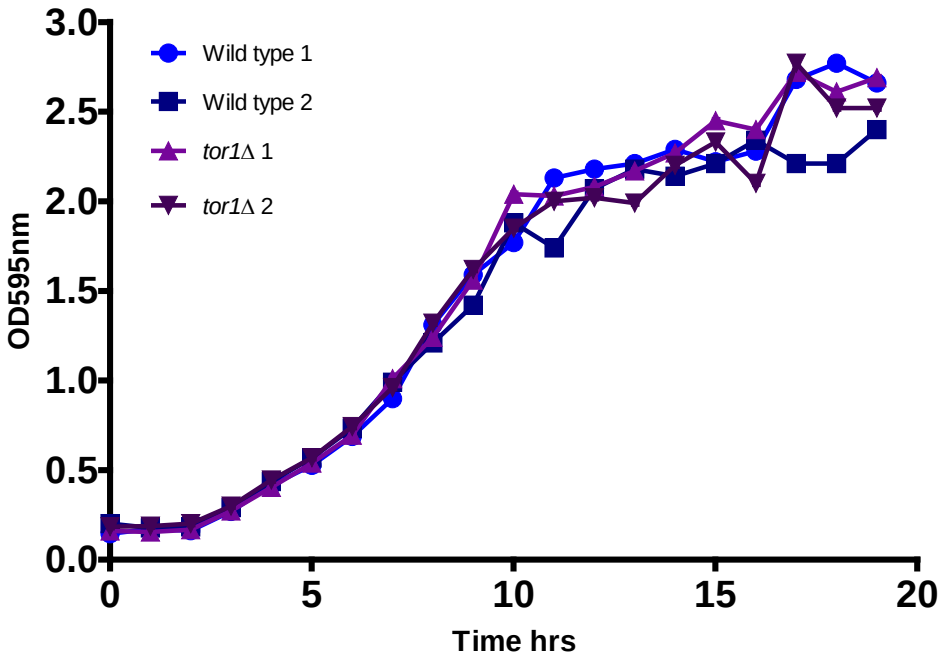


**Figure 4.3: Growth curve of *S. cerevisiae* wild type and *tor1Δ* under normal conditions in yeast nitrogen base medium (YNB).** Cultures were diluted to 2 x $10^6$ cells ($OD_{595}$ ~0.1) and incubated with shaking, duplicate, at 30°C. Optical density readings were taken hourly until mid to late stationary phase was reached. Growth curves were conducted in duplicate (culture 1 and culture 2 for both WT and deletion strain) showing growth patterns observed for two distinct colonies of the same strain.

Samples were harvested at 5 hrs and 18 hrs post resuspension in YNB for early exponential and mid stationary phases respectively, before processing and screening using the Nile red assay as described in Chapter 2, Section 2.3.

The results of both neutral and polar lipid accumulation, Figures 4.4 and 4.5 respectively, showed no significant difference between the strains when in early exponential stages of growth.

In stationary phase no significant difference was detected for neutral lipids in the *avo2Δ* compared to wild type cells. The deletion of *TCO89* resulted in a 1.1 fold increase in neutral lipids compared to wild type, although this failed to reach significance. For the *tor1Δ* a significant decrease in neutral lipids was observed, with a 1.3 fold decrease compared to the wild type strain (Figure 4.4).

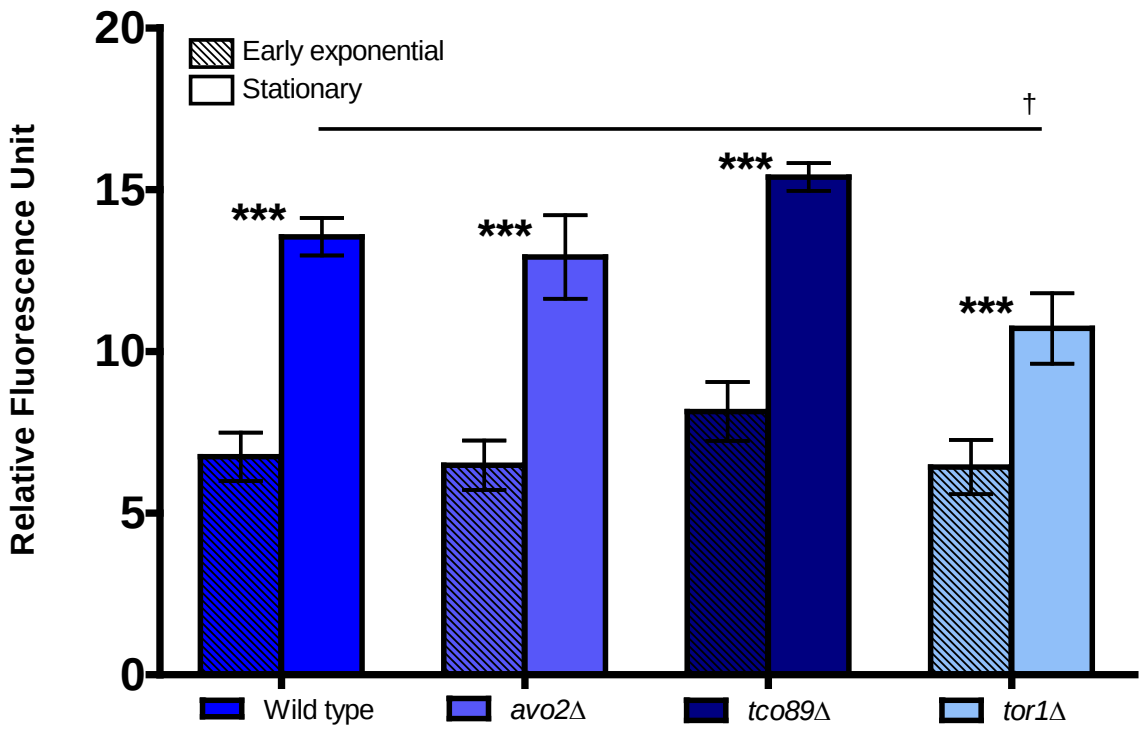


**Figure 4.4: Neutral lipid fluorescence intensity of Nile Red stained *S. cerevisiae* wild type and TOR component mutants.** Cells were harvested at 5 and 18 hrs post resuspension in YNB for early exponential and stationary phase samples respectively. Cells were washed twice in PBS before adjusting to a cell density of 2 x $10^7$ cells/ml. 5 x $10^6$ cells were transferred to the wells of black 96-well plates in triplicate. 25µl PBS/DMSO (1:1 v/v) and 5µg/ml Nile red were added to each sample. Plates were screened using the wavelengths: excitation 485nm, emission 535nm. Data shown as means of triplicates ±SD. Significance indicated between exponential and stationary phases ***p≤0.001 and difference in stationary phases between cells indicated by solid black lines ł p≤0.05. Data analysed by one way ANOVA with Tukey *post hoc* test.

Compared with wild type cells, the screen conducted for more polar lipid subtypes showed a decrease in polar lipids for the *avo2Δ,* an increase for *tco89Δ* and a 1.2 fold decrease for the *tor1Δ.* However these differences were not significantly different from the levels observed in wild type cells (Figure 4.5).

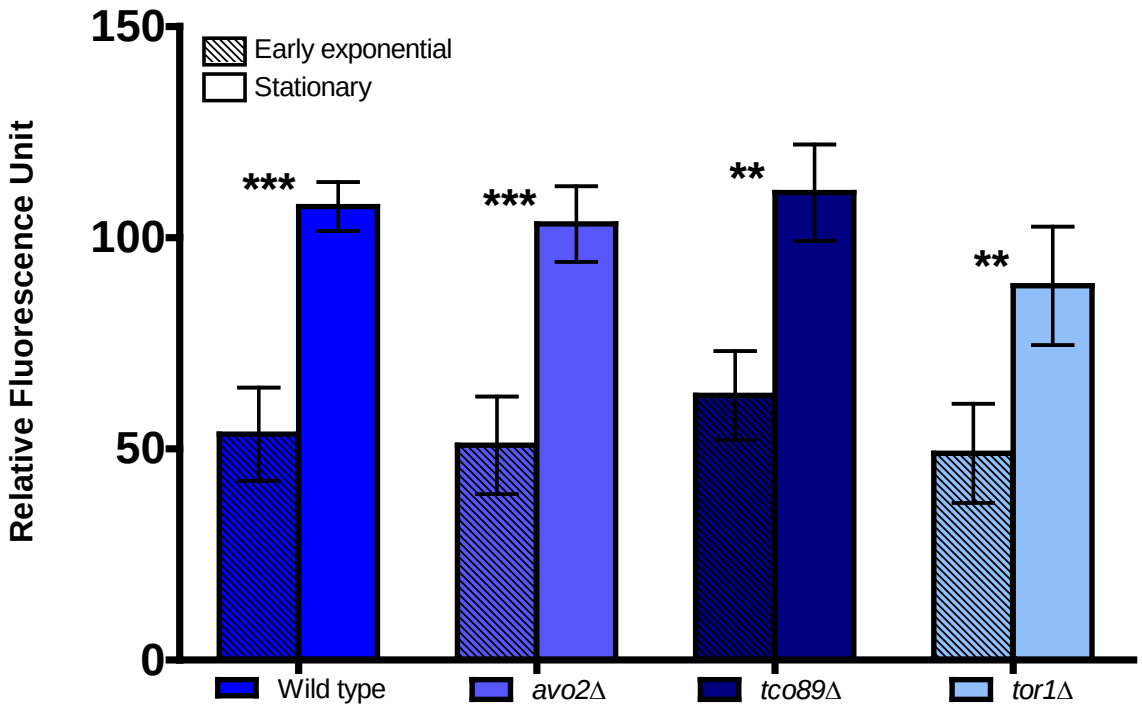


**Figure 4.5: Polar lipid fluorescence intensity of Nile Red stained *S. cerevisiae* wild type and TOR component mutants.** Cells were harvested at 5 and 18 hrs post resuspension in YNB for early exponential and stationary phase samples respectively. Cells were washed twice in PBS before adjusting to a cell density of 2 x $10^7$ cells/ml. 5 x $10^6$ cells were transferred to the wells of black 96-well plates in triplicate. 25µl PBS/DMSO (1:1 v/v) and 5µg/ml Nile red were added to each sample. Plates were screened using the wavelengths: excitation 535nm, emission 590nm. Data shown as means of triplicates ±SD. Significance indicated between exponential and stationary phases **p≤0.01 ***p≤0.001. Data analysed by one way ANOVA with Tukey *post hoc* test.

These results demonstrated that the Nile red method was able to detect a neutral lipid specific phenotype in cells deleted for *TOR1*, highlighting that possible phenotypes arising from MAPK component deletions may be confidently elucidated.

### 4.2.2 Neutral and polar lipid accumulation in S. cerevisiae hog1Δ cells is reduced in stationary phase

The PI3K/Akt/mTOR and MAP Kinase pathways are central to numerous signalling cascades and are involved in regulating a plethora of cellular processes. Along with this, their normal regulation is frequently disrupted in many cancer types.

Both mTOR and ERK MAPK signalling contributes to the initiation of increased lipid synthesis in cancer (Laplante and Sabatini 2009b, Yang W *et al.* 2012). Therefore it is postulated that the p38 MAPK pathway may also play a role in cancer related lipid synthesis due to its frequent upregulation. The *S. cerevisiae* MAPK Hog1p has been extensively characterised and demonstrated to be well conserved to mammalian p38 MAP kinase. As such, to determine if the HOG MAPK pathway in *S. cerevisiae* has a role in lipid accumulation, neutral and polar lipid levels were examined in a *HOG1* deletion strain using the Nile red method.

Firstly, growth curves were conducted to ensure samples from both wild type and *hog1Δ* strains had comparable growth phases for both exponential and stationary phases, with early exponential samples acting as the low lipid control. As shown in Figure 4.6, exponential growth routinely began for both wild type and *hog1Δ* cells at ~5hrs post resuspension in YNB before stationary phase was achieved at ~12hrs.

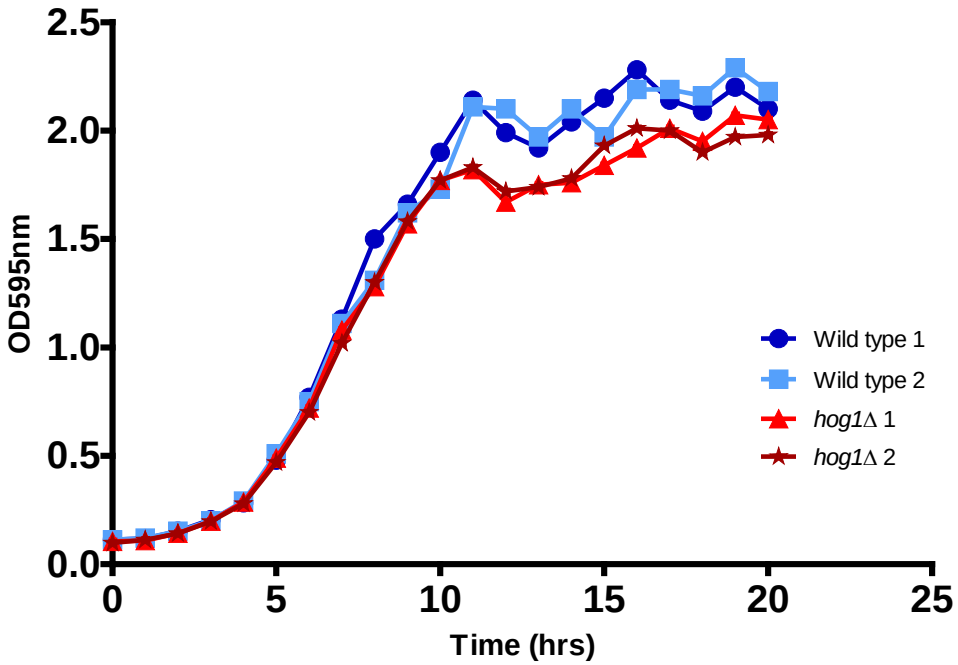


**Figure 4.6: Growth curves of *S. cerevisiae* wild type and *hog1Δ* under normal conditions in yeast nitrogen base medium (YNB).** Cultures were diluted to 2 x $10^6$ cells/ml ($OD_{595}$ ~0.1) and incubated with shaking, duplicate, at 30°C. Optical density readings were taken hourly until mid to late stationary phase was reached. Growth curves were conducted in duplicate (culture 1 and culture 2 for both WT and deletion strain) showing growth patterns observed for two distinct colonies of the same strain.

Samples were harvested at 5 hrs and 18 hrs post resuspension in YNB, representing early exponential and stationary phases of growth, before screening using the Nile red assay.

Results showed that accumulation of both neutral and polar lipids in stationary phase was decreased significantly in the *hog1Δ* strain compared to wild type. For neutral lipids the *hog1Δ* mutant showed a 1.4 fold decrease and for polar lipids a significant decrease of 1.7 fold was observed (Figures 4.7 and 4.8).

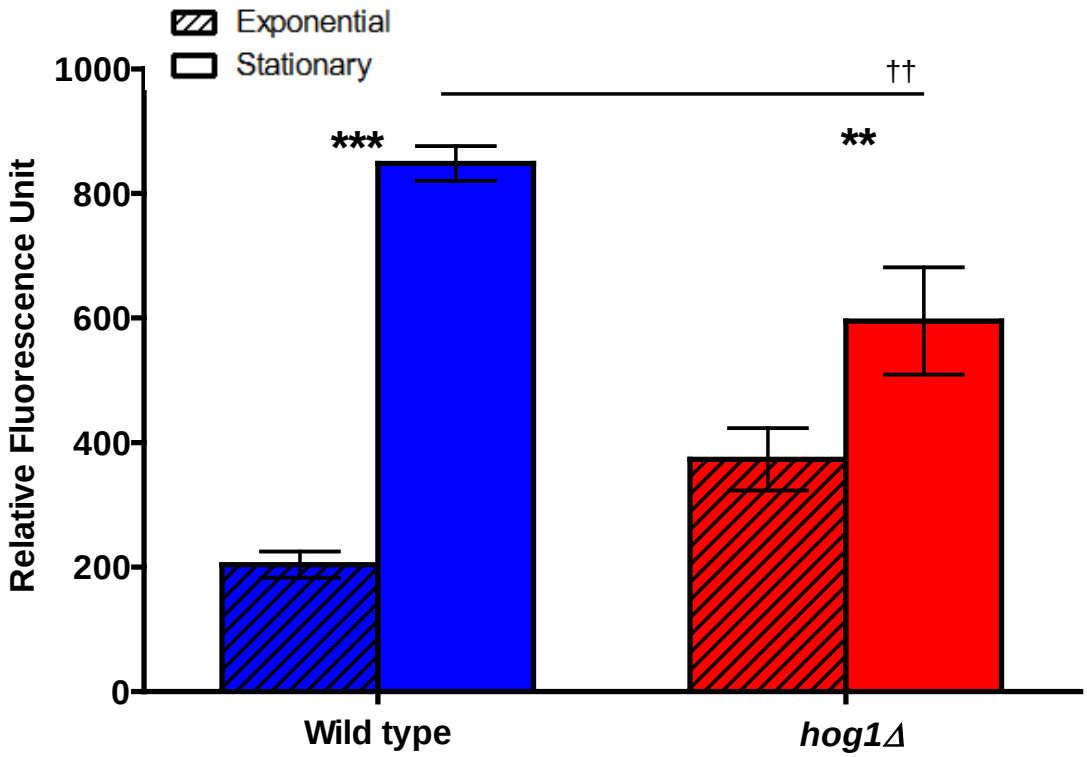


**Figure 4.7: Neutral lipid fluorescence intensity of Nile red stained *S. cerevisiae* wild type and *hog1Δ* cultures.** Cells were harvested at 5 and 18 hrs post resuspension in YNB for early exponential and stationary phase samples respectively. Cells were washed twice in PBS before adjusting to a cell density of 2 x $10^7$ cells/ml. 5 x $10^6$ cells were transferred to the wells of black 96-well plates in triplicate. 25µl PBS/DMSO (1:1 v/v) and 5µg/ml Nile red were added to each sample. Plates were screened using the wavelengths: excitation 485nm, emission 535nm. Data shown as means of triplicates ± SD. Significance indicated between wild type and hog1Δ cultures **p≤0.01 ***p≤0.001 and change from exponential to stationary phase indicated by solid black lines ǂp≤0.01. Data analysed by one way ANOVA with Tukey *post hoc* test.

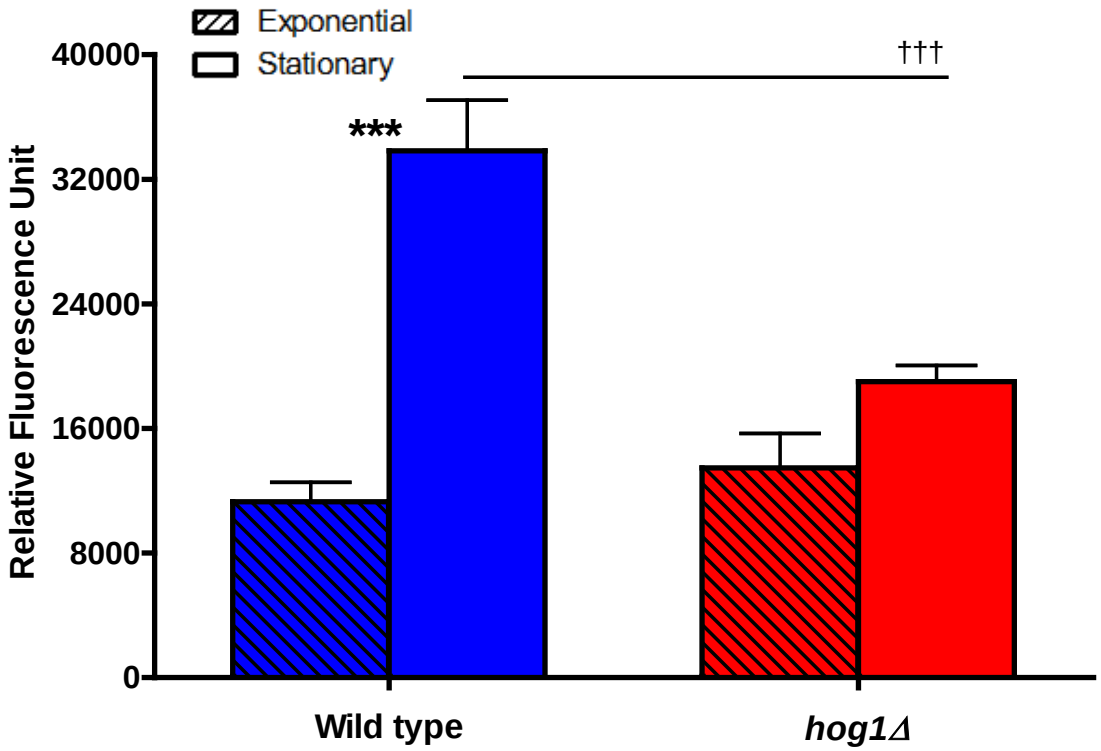


**Figure 4.8: Polar lipid fluorescence intensity of Nile red stained *S. cerevisiae* wild type and *hog1Δ* cultures.** Cells were harvested at 5 and 18 hrs post resuspension in YNB for early exponential and stationary phase samples respectively. Cells were washed twice in PBS before adjusting to a cell density of 2 x $10^7$ cells/ml. 5 x $10^6$ cells were transferred to the wells of black 96-well plates in triplicate. 25µl PBS/DMSO (1:1 v/v) and 5µg/ml Nile red were added to each sample. Plates were screened using the wavelengths: excitation 535nm, emission 590nm. Data shown as means of triplicates ± SD. Significance indicated between wild type and hog1Δ cultures ***p≤0.001 and change from exponential to stationary phase indicated by solid black lines ŧŧŧ≤0.001. Data analysed by one way ANOVA with Tukey *post hoc* test.

### 4.2.3 Transformation with pRS315 impacts on lipid accumulation in S. cerevisiae

In order to confirm that deletion of *HOG1* attenuated lipid accumulation, a complementation experiment was performed, whereby *HOG1* was introduced into the deletion strain using a single copy plasmid pRS315*HOG1* (CLLp001) under the control of its own promoter.

To assess whether complementation had been successful wild type and *hog1Δ* strains transformed either with pRS315 or pRS315 containing *HOG1* were spotted onto YNB agar, minus leucine and YNB agar minus leucine supplemented with 0.4 M NaCl was utilised to determine if sensitivity of the *hog1Δ* to NaCl had been recovered. As shown in Figure 4.9, NaCl sensitivity of *hog1Δ* cells was rescued upon transformation with pRS315 expressing *HOG1.*

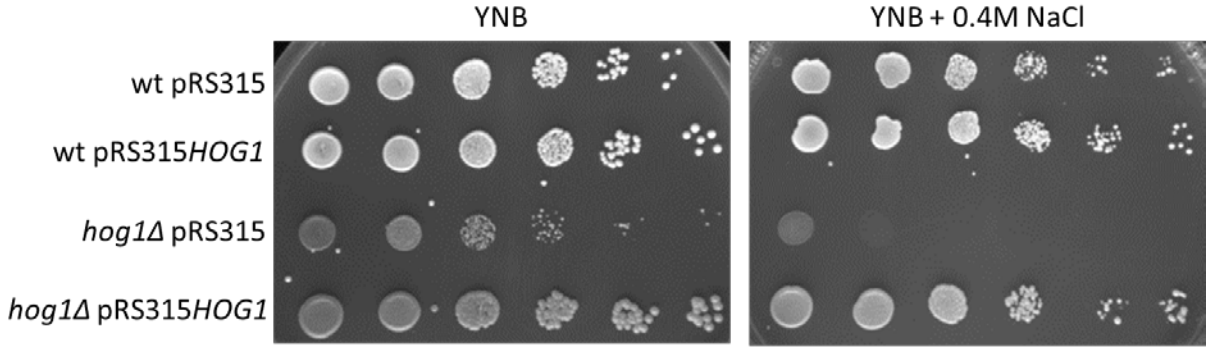


**Figure 4.9: Spot plates of *S. cerevisiae* wild type and *hog1Δ* with pRS315 and pRS315::*HOG1* exposed to osmotic stress.** Control plates (YNB) and osmotic stress plates, YNB supplemented with 0.4M NaCl. Starting cell densities were ~2.3 x $10^7$ cells/ml before being serially diluted 1:10 across the plate to 2.3 x $10^2$ cells/ml.

Transformed cells were then assessed using the Nile red method to determine their lipid phenotype in stationary phase. Cells were resuspended at a cell density of 2 x $10^6$ cells/ml in YNB minus leucine, and allowed to grow until early exponential at 5 hrs and stationary phase, 18 hrs, as described previously.

As demonstrated in Figure 4.10, cells deleted for *HOG1* containing the empty vector pRS315, exhibited an increase in fluorescence intensity, reaching levels comparable to wild type in both exponential and stationary phases of growth. This suggested an increase in neutral lipids within the yeast cells transformed with the empty vector.

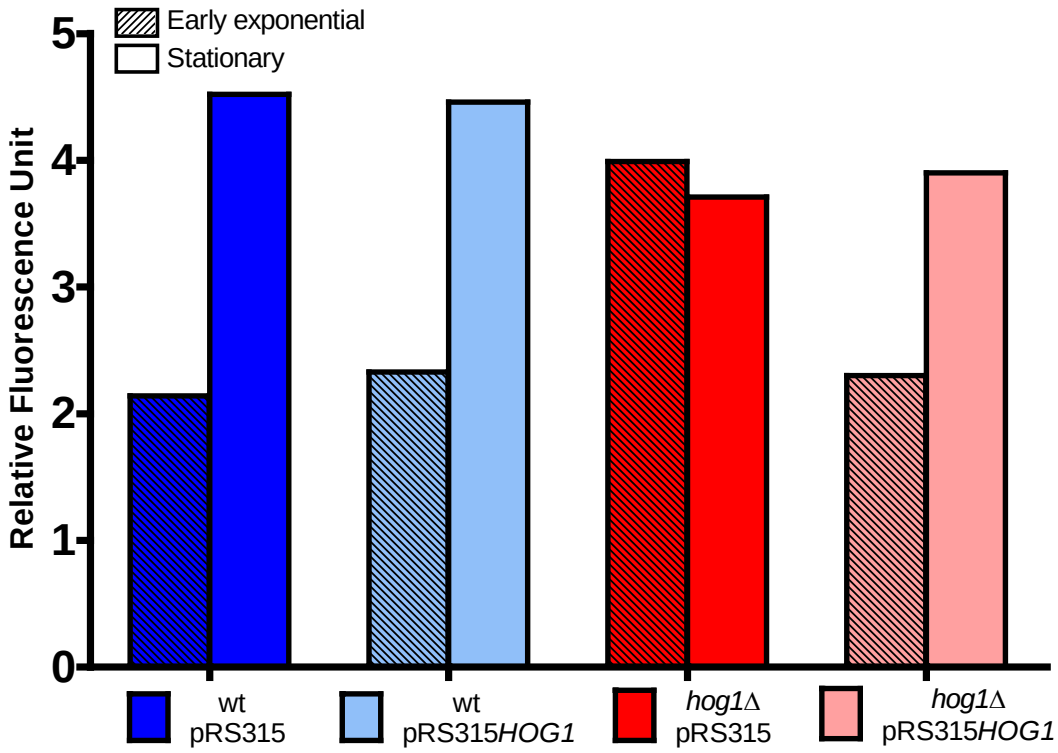


**Figure 4.10: Neutral lipid fluorescence intensity of Nile red stained *S. cerevisiae* wild type and *hog1Δ* containing pRS315 and pRS315*HOG1*** Cells were harvested at 5 and 18 hrs post resuspension in YNB for early exponential and stationary phase samples respectively. Cells were washed twice in PBS before adjusting to a cell density of 2 x $10^7$ cells/ml. 5 x $10^6$ cells were transferred to the wells of black 96-well plates in triplicate. 25µl PBS/DMSO (1:1 v/v) and 5µg/ml Nile red were added to each sample. Plates were screened using the wavelengths: excitation 485nm, emission 535nm. Fluorescence intensities of wild type cells containing pRS315 and pRS315*HOG1* compared to *hog1Δ* cells containing pRS315 and pRS315*HOG1*. Data displayed as means of duplicate experiments.

For more polar lipids, Figure 4.11, levels of fluorescence remained lower than that of wild type in *hog1* deleted cells regardless of whether they were transformed with vector pRS315 or pRS315*HOG1*.

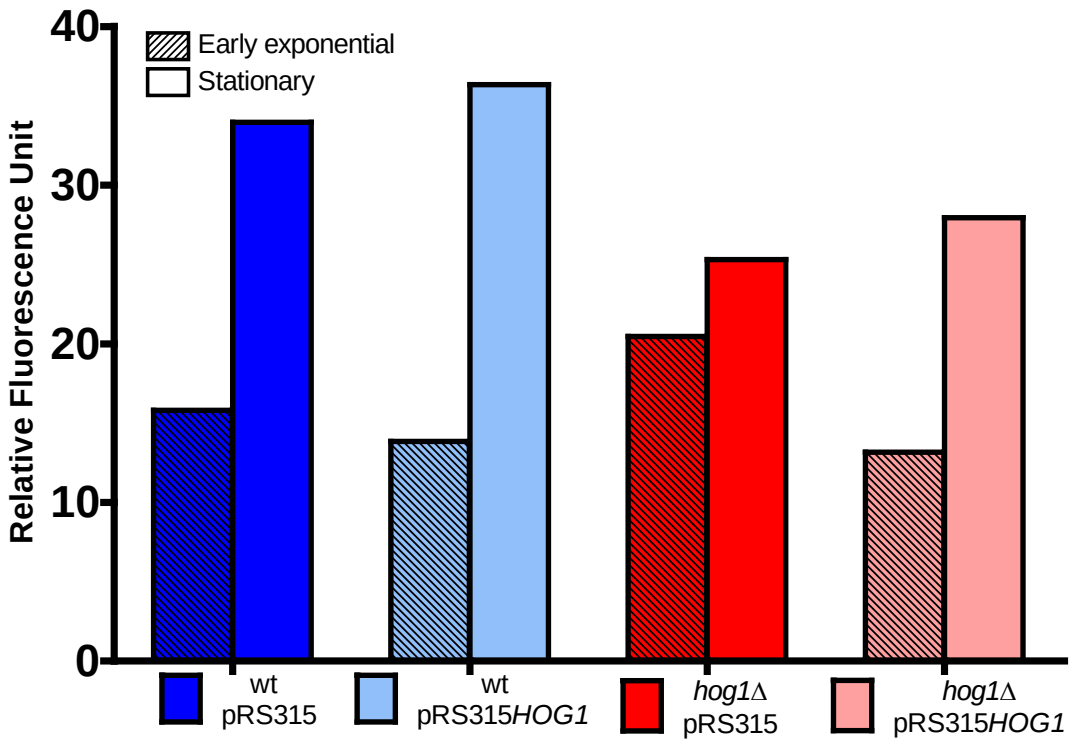


**Figure 4.11: Polar lipid fluorescence intensity of Nile red stained *S. cerevisiae* wild type and *hog1Δ* containing pRS315 and pRS315*HOG1*** Cells were harvested at 5 and 18 hrs post resuspension in YNB for early exponential and stationary phase samples respectively. Cells were washed twice in PBS before adjusting to a cell density of 2 x $10^7$ cells/ml. 5 x $10^6$ cells were transferred to the wells of black 96-well plates in triplicate. 25µl PBS/DMSO (1:1 v/v) and 5µg/ml Nile red were added to each sample. Plates were screened using the wavelengths: excitation 535nm, emission 590nm. Fluorescence intensities of wild type cells containing pRS315 and pRS315*HOG1* compared to *hog1Δ* cells containing pRS315 and pRS315*HOG1*. Data displayed as means of duplicate experiments.

As a result of the data derived from the Nile red assay, both wild type and *hog1Δ* strains were re-transformed with pRS315 and pRS315*HOG1*. Again the stress sensitive phenotype of cells deleted for *hog1* was recovered following transformation with pRS315*HOG1* on solid medium.

Consistent with the previous Nile red data obtained, cells deleted for *HOG1* containing empty pRS315 displayed an increased neutral lipid phenotype in stationary phase which on this occasion exceeded levels seen in wild type cells. Conversely in exponential phase the levels of fluorescence remained similar across all strains screened (Figure 4.12).

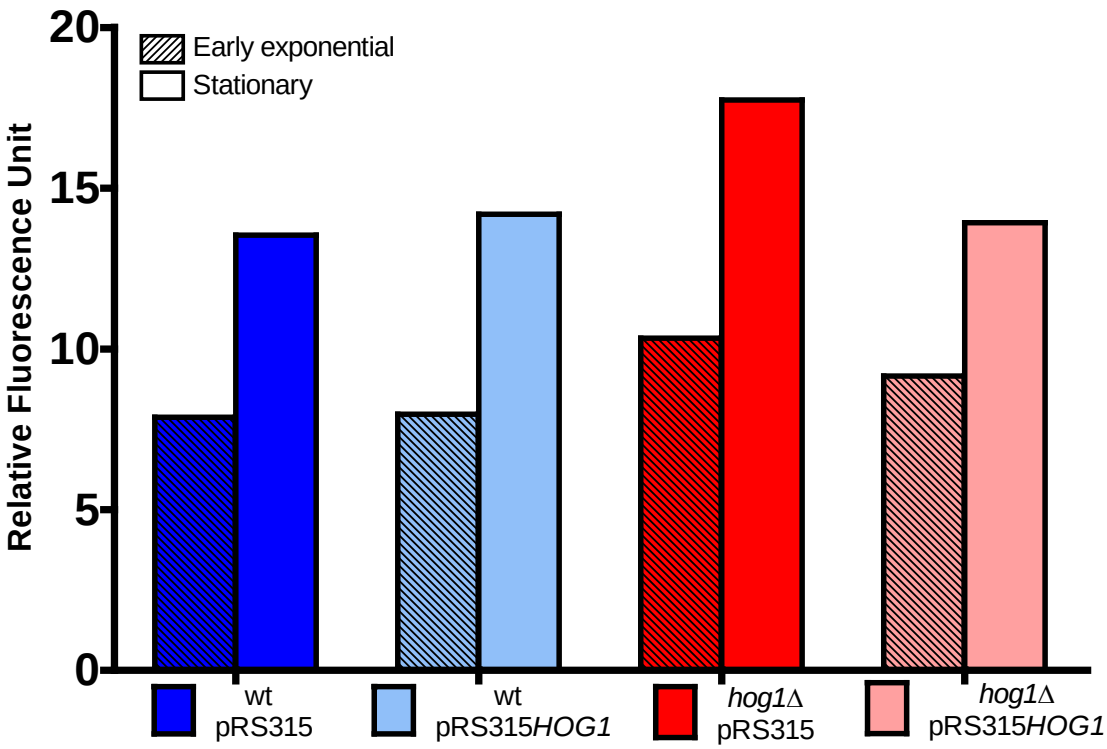


**Figure 4.12: Neutral lipid fluorescence intensity of Nile red stained *S. cerevisiae* wild type and *hog1Δ* containing pRS315 and pRS315*HOG1*** Cells were harvested at 5 and 18 hrs post resuspension in YNB for early exponential and stationary phase samples respectively. Cells were washed twice in PBS before adjusting to a cell density of 2 x $10^7$ cells/ml. 5 x $10^6$ cells were transferred to the wells of black 96-well plates in triplicate. 25µl PBS/DMSO (1:1 v/v) and 5µg/ml Nile red were added to each sample. Plates were screened using the wavelengths: excitation 485nm, emission 535nm. Fluorescence intensities of wild type cells containing pRS315 and pRS315*HOG1* compared to *hog1Δ* cells containing pRS315 and pRS315*HOG1*. Data displayed as means of duplicate experiments.

When screening was conducted for more polar lipids, again a decreased level of fluorescence was observed for the *hog1Δ* containing pRS315*HOG1*. In contrast to the previous experiment an increased level of fluorescence, which reached levels comparable to wild type, was seen in *hog1* deleted cells containing pRS315 (Figure 4.13).

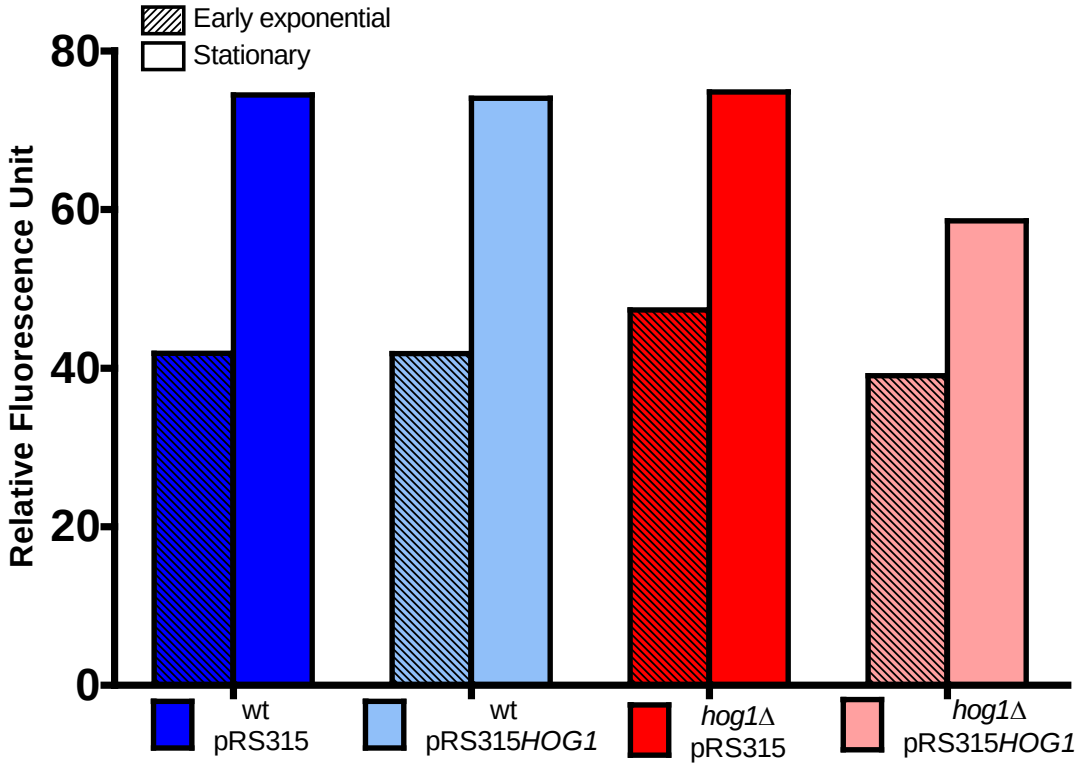


**Figure 4.13: Polar lipid fluorescence intensity of Nile red stained *S. cerevisiae* wild type and *hog1Δ* containing pRS315 and pRS315*HOG1*** Cells were harvested at 5 and 18 hrs post resuspension in YNB for early exponential and stationary phase samples respectively. Cells were washed twice in PBS before adjusting to a cell density of 2 x $10^7$ cells/ml. 5 x $10^6$ cells were transferred to the wells of black 96-well plates in triplicate. 25µl PBS/DMSO (1:1 v/v) and 5µg/ml Nile red were added to each sample. Plates were screened using the wavelengths: excitation 535nm, emission 590nm. Fluorescence intensities of wild type cells containing pRS315 and pRS315*HOG1* compared to *hog1Δ* cells containing pRS315 and pRS315*HOG1*. Data displayed as means of duplicate experiments.

The data derived from these two individual sets of transformations utilising pRS315 was inconsistent. It is suggested that utilisation of pRS315 may have affected the lipid phenotype. Due to this, *HOG1* was cloned into another single copy vector, pRS313, which contains *HIS3* as the selectable marker.

### 4.2.4 Complementation of HOG1 restores lipid accumulation to wild type levels

As previously described in Section 4.2.2, to ascertain that complementation had been successful wild type and *hog1Δ* strains were transformed with plasmid pRS313 and pRS313 containing *HOG1* (CLLp004). These cells were spotted onto YNB agar, minus histidine and YNB agar minus histidine supplemented with 0.4 M NaCl. As demonstrated by Figure 4.14, NaCl sensitivity of *hog1Δ* cells was abolished upon transformation with pRS313 expressing *HOG1* (CLLp004) and not with the pRS313 vector alone.

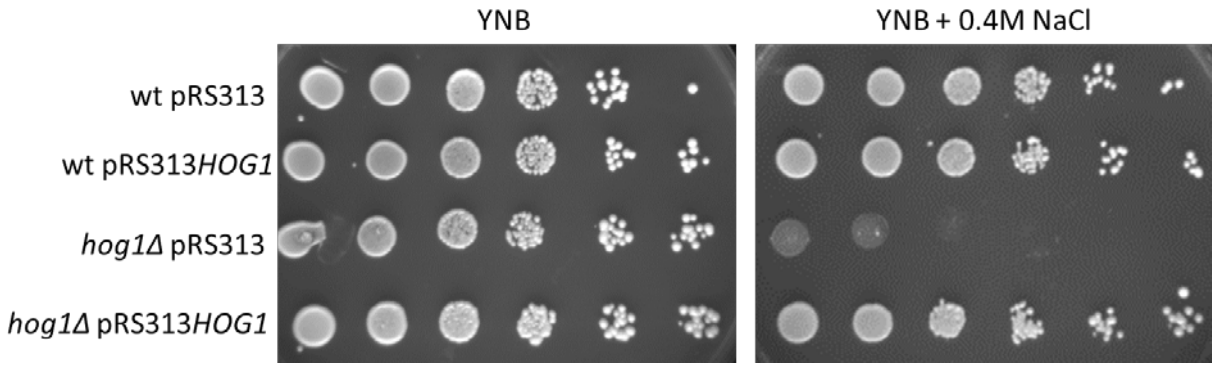


**Figure 4.14: Spot plates of *S. cerevisiae* wild type and *hog1Δ* with pRS315 and pRS315::*HOG1* exposed to osmotic stress.** Control plates (YNB) and osmotic stress plates, YNB supplemented with 0.4M NaCl. Starting cell densities were ~2.3 x $10^7$ cells/ml before being serially diluted 1:10 across the plate down to 2.3 x $10^2$ cells/ml.

Protein extracts from wild type cells containing pRS313 and *hog1Δ* cells containing pRS313 and pRS313*HOG1* were analysed by Western blotting using α-Hog1 antibody. This was carried out to ensure that *HOG1* expression was absent for the *hog1Δ* and that expression had been successfully restored in *hog1Δ* cells containing pRS313*HOG1.* As demonstrated by Figure 4.15 a band was observed corresponding to Hog1p at 50 kDa for wild type cells containing pRS313. A band corresponding to the 50 kDa Hog1p was also observed for the *hog1Δ* containing pRS313*HOG1* and no band was observed in *HOG1* deleted cells containing empty vector.

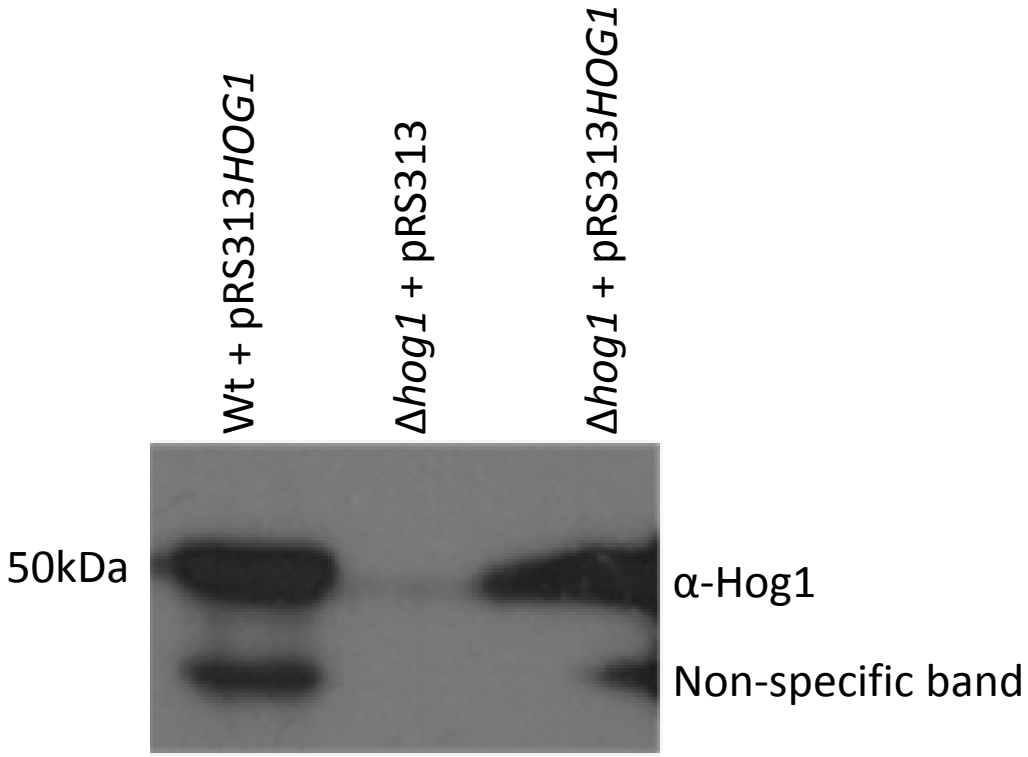


**Figure 4.15: Western blot showing restoration of Hog1p expression in *HOG1* deleted cells.** TCA extracted protein samples were prepared from wild type and *HOG1* deleted cells containing pRS313 and *HOG1* deleted cells containing pRS313*HOG1*. Proteins on Western blot were reacted with antibody specific for Hog1 to confirm complementation of Hog1 in the *hog1Δ.*

To determine if the *hog1Δ* lipid accumulation phenotype had been recovered, transformed cells were transferred to YNB medium lacking histidine before resuspending at a cell density of 2 x $10^6$ cells/ml in YNB minus histidine. Cultures were allowed to growth before harvesting as described in Section 4.2.3.

Figures 4.16 and 4.17 show the results of neutral and polar lipid fluorescence intensity of wild type and *hog1Δ* strains transformed with either empty vector, pRS313, or pRS313*HOG1* in both exponential and stationary phases of growth. Consistent with data shown in Section 4.2.2, the *hog1Δ* strain transformed with the empty vector displayed a significant reduction in fluorescence attributed to neutral lipids with a 1.6 fold decrease compared to wild type cells.

Upon transformation with pRS313*HOG1* levels of fluorescence attributable to neutral lipids was restored to that of wild type, increasing 1.7 fold from that of the *hog1Δ*. Wild type cells transformed with pRS313*HOG1* did not exhibit any significant difference in fluorescence intensity when compared to wild type cells.

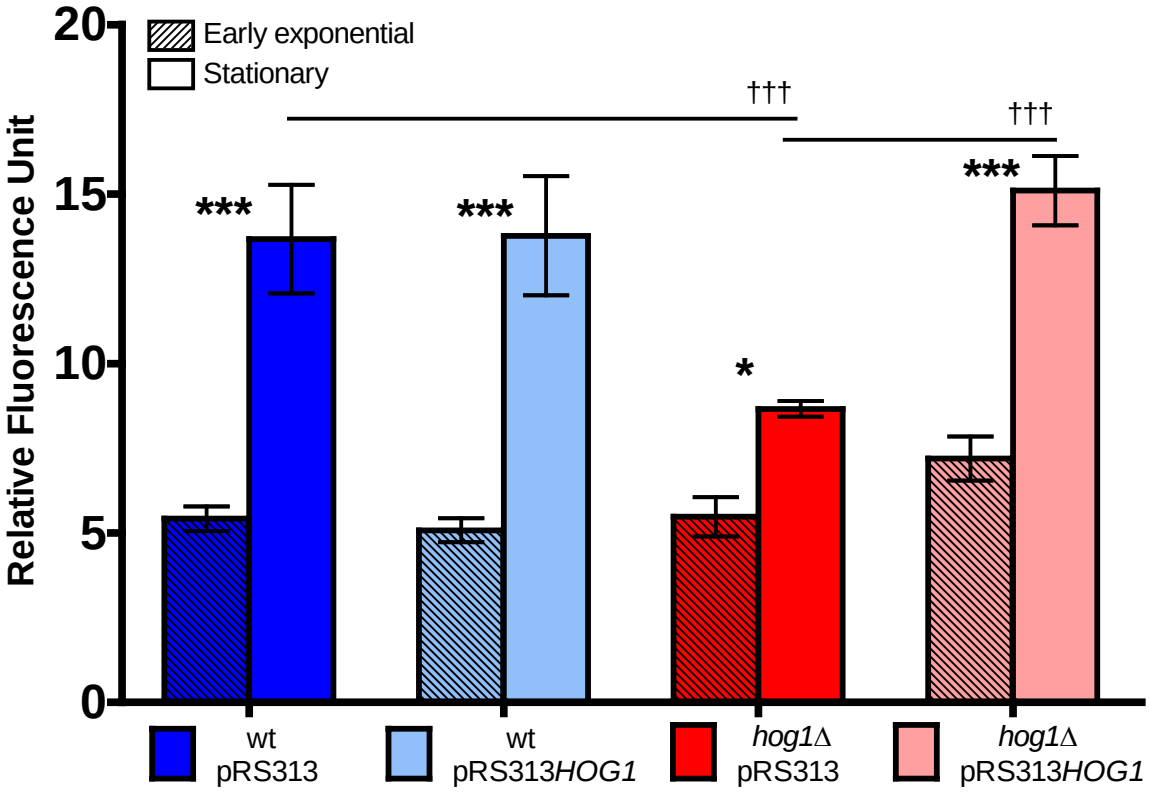


**Figure 4.16: Neutral lipid fluorescence intensity of Nile red stained retransformed *S. cerevisiae* wild type pRS313 and wild type pRS313::*HOG1* compared to *hog1Δ* pRS313 and *hog1* pRS313::*HOG1*.** Cells were harvested at 5 and 18 hrs post resuspension in YNB for early exponential and stationary phase samples respectively. Cells were washed twice in PBS before adjusting to a cell density of 2 x $10^7$ cells/ml. 5 x $10^6$ cells were transferred to the wells of black 96-well plates in triplicate. 25µl PBS/DMSO (1:1 v/v) and 5µg/ml Nile red were added to each sample. Plates were screened using the wavelengths: excitation 485nm, emission 535nm. Data shown as means of triplicates ±SD. Significance indicated between exponential and stationary phases * $p<0.05$ *** $p\leq0.001$ and difference in stationary phases between cells indicated by solid black lines ††† $p\leq0.001$. Data analysed by one way ANOVA with Tukey *post hoc* test.

When screened utilising the wavelength attributed to more polar lipid types (Figure 4.17), a significant reduction of 1.4 fold was observed in *hog1Δ* cells compared to wild type consistent with results from section 4.2.2. This was then restored with a 1.4 fold increase upon transformation with pRS313*HOG1* to wild type levels. Again, no significant

difference to that of wild type was observed for wild type cells transformed with pRS313*HOG1.*

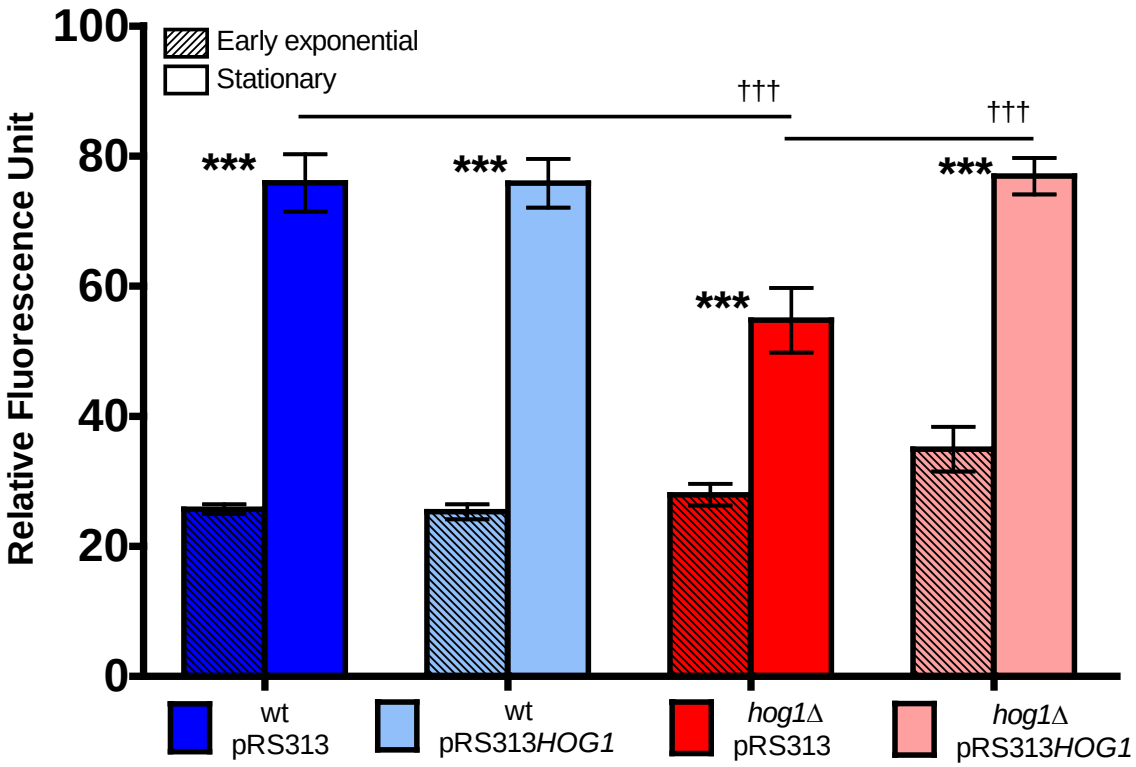


**Figure 4.17: Polar lipid fluorescence intensity of Nile Red stained retransformed *S. cerevisiae* wild type pRS313 and wild type pRS313::*HOG1* compared to *hog1Δ* pRS313 and *hog1* pRS313::*HOG1*.** Cells were harvested at 5 and 18 hrs post resuspension in YNB for early exponential and stationary phase samples respectively. Cells were washed twice in PBS before adjusting to a cell density of 2 x $10^7$ cells/ml. 5 x $10^6$ cells were transferred to the wells of black 96-well plates in triplicate. 25µl PBS/DMSO (1:1 v/v) and 5µg/ml Nile red were added to each sample. Plates were screened using the wavelengths: excitation 535nm, emission 590nm. Data shown as means of triplicates ±SD. Significance indicated between exponential and stationary phases ***p≤0.001 and difference in stationary phases between cells indicated by solid black lines ††† p≤0.001. Data analysed by one way ANOVA with Tukey *post hoc* test.

These results show *hog1* deleted cells display an altered lipid accumulation phenotype; and suggested the involvement of Hog1p in the regulation of lipid accumulation.

To further investigate this Nile red screening was conducted on other deletions within the HOG MAPK pathway to elucidate whether other components of the pathway are involved in regulating the accumulation of lipids.

### 4.2.5 Deletions upstream of HOG1 MAP Kinase do not display altered lipid phenotypes

In order to elucidate whether the accumulation of lipids is regulated by components upstream of the MAPK Hog1, Nile red screening was conducted on single deletion mutants of upstream components of the MAPK cascade *sho1Δ, ste11Δ* and *pbs2Δ* (see Chapter 1, Figure 1.16). Growth curves were conducted for each strain to ensure samples from wild type and deletion strains were in the same phase of growth for the assay (Figures 4.18, 4.19 and 4.20).

As shown in the growth curves, for all deletion strains and wild type cells, exponential phase growth typically began 5 hrs post resuspension in YNB medium before early stationary phase was reached at 12 hrs in both wild type and deletion strains.

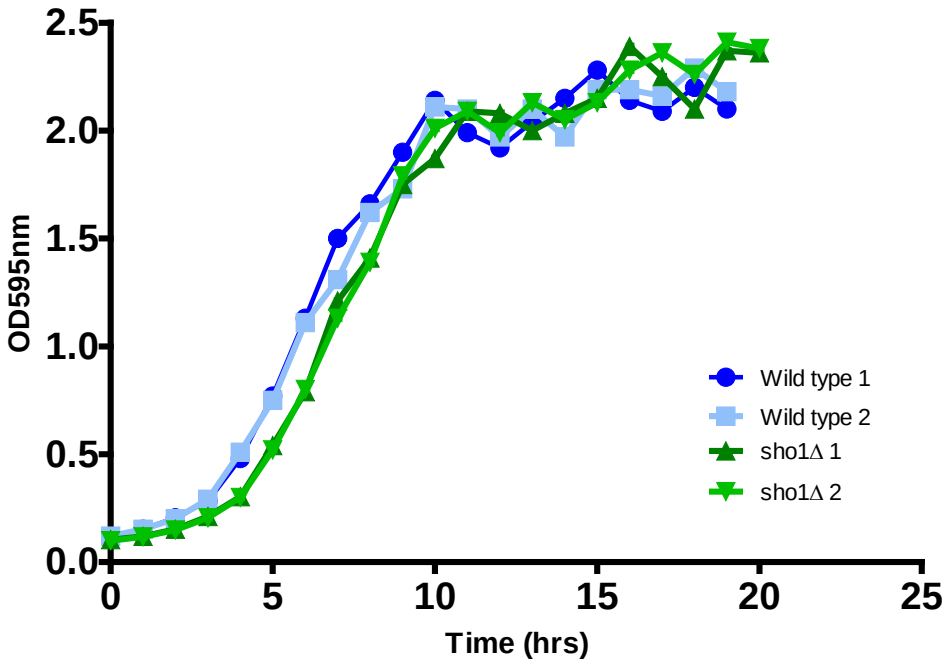


**Figure 4.18: Growth curve of *S. cerevisiae* wild type and *sho1Δ* under normal conditions in yeast nitrogen base medium (YNB).** Cultures were diluted to 2 x $10^6$ cells ($OD_{595}$ ~0.1) and incubated with shaking, duplicate, at 30°C. Optical density readings were taken hourly until mid to late stationary phase was reached. Growth curves were conducted in duplicate (culture 1 and culture 2 for both WT and deletion strain) showing growth patterns observed for two distinct colonies of the same strain.

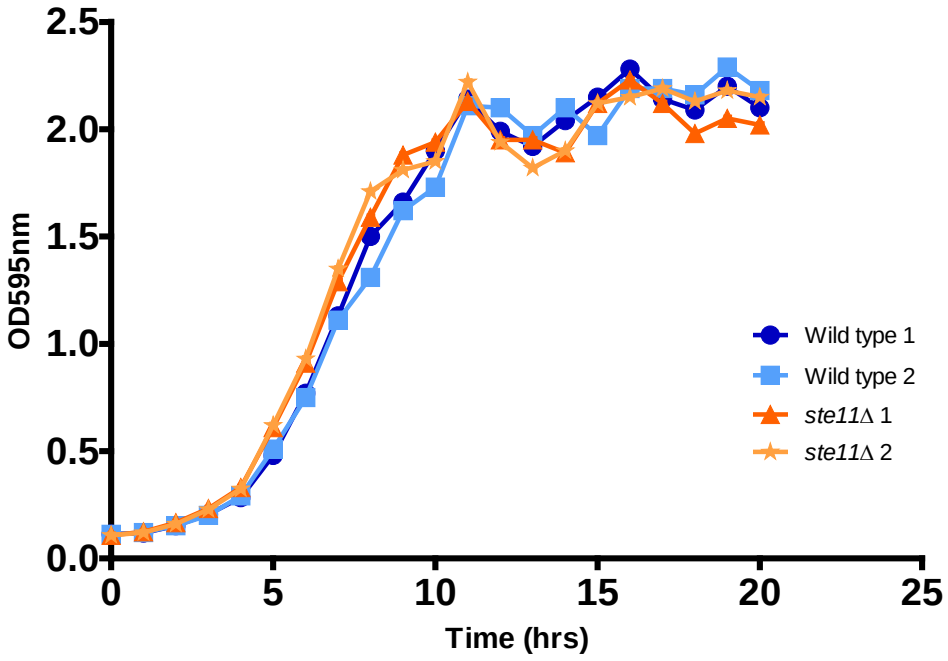


**Figure 4.19: Growth curve of *S. cerevisiae* wild type and *ste11Δ* under normal conditions in yeast nitrogen base medium (YNB).** Cultures were diluted to 2 x $10^6$ cells ($OD_{595}$ ~0.1) and incubated with shaking, duplicate, at 30°C. Optical density readings were taken hourly until mid to late stationary phase was reached. Growth curves were conducted in duplicate (culture 1 and culture 2 for both WT and deletion strain) showing growth patterns observed for two distinct colonies of the same strain.

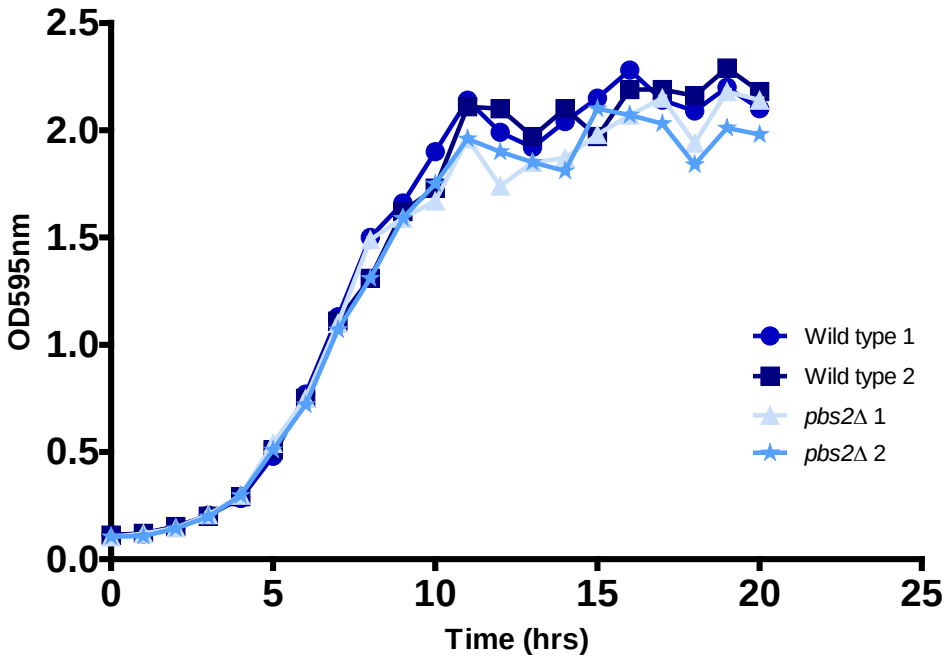


**Figure 4.20: Growth curve of *S. cerevisiae* wild type and *pbs2Δ* under normal conditions in yeast nitrogen base medium (YNB).** Cultures were diluted to 2 x $10^6$ cells ($OD_{595}$ ~0.1) and incubated with shaking, duplicate, at 30°C. Optical density readings were taken hourly until mid to late stationary phase was reached. Growth curves were conducted in duplicate (culture 1 and culture 2 for both WT and deletion strain) showing growth patterns observed for two distinct colonies of the same strain.

Samples from wild type, *sho1Δ*, *ste11Δ*, and *pbs2*Δ cultures were harvested and screened using Nile red as described in Section 4.2.1. The *hog1Δ* was also included as a control for low lipid accumulation in stationary phase.

Figures 4.19 and 4.20 show neutral and polar lipid fluorescence intensities of wild type and MAP kinase deletion strains in both early exponential and mid stationary phases of growth. Deletions in the upstream components of the HOG pathway had no effect on the accumulation of neutral or polar lipids, with all displaying comparable levels and no significant changes to that of the wild type strain. As previously demonstrated in Section 4.2.2, cells containing the *hog1* deletion displayed significantly attenuated lipid accumulation with a 1.7 fold decrease in neutral lipids and 1.4 fold decrease in polar lipids compared to wild type.

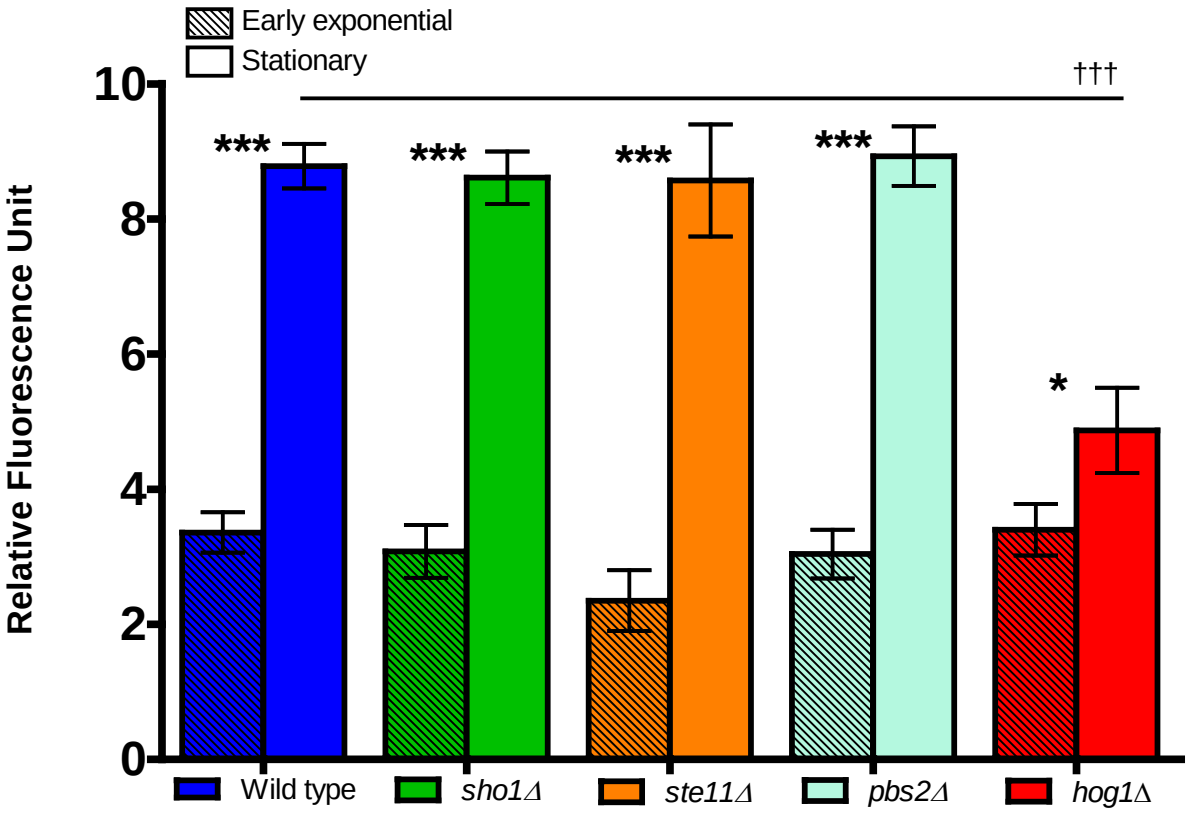


**Figure 4.21: Neutral lipid fluorescence intensity of Nile Red stained *S. cerevisiae* wild type and MAP Kinase pathway mutants.** Cells were harvested at 5 and 18 hrs post resuspension in YNB for early exponential and stationary phase samples respectively. Cells were washed twice in PBS before adjusting to a cell density of 2 x $10^7$ cells/ml. 5 x $10^6$ cells were transferred to the wells of black 96-well plates in triplicate. 25µl PBS/DMSO (1:1 v/v) and 5µg/ml Nile red were added to each sample. Plates were screened using the wavelengths: excitation 485nm, emission 535nm. Data shown as means of triplicates ±SD. Significance indicated between exponential and stationary phases *p<0.05 ***p≤0.001 and difference in stationary phases between cells indicated by solid black lines ††† p≤0.001. Data analysed by one way ANOVA with Tukey *post hoc* test.

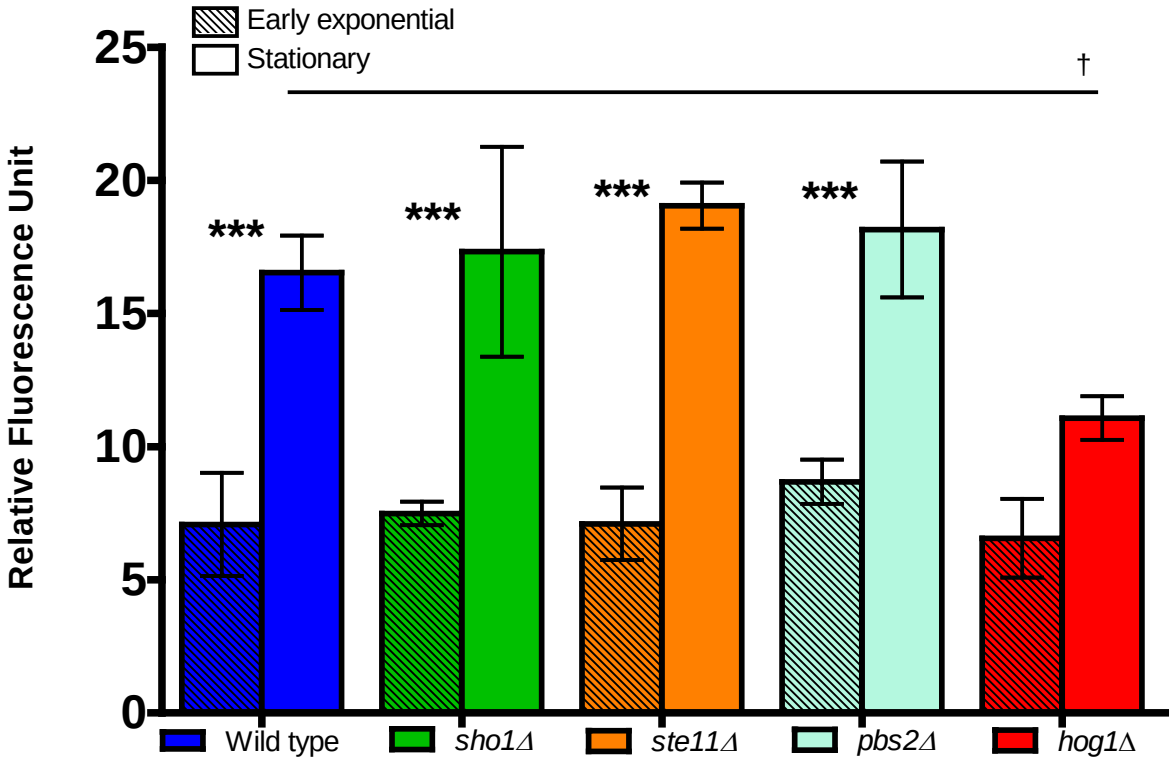


**Figure 4.22: Polar lipid fluorescence intensity of Nile Red stained *S. cerevisiae* wild type and MAP Kinase pathway mutants.** Cells were harvested at 5 and 18 hrs post resuspension in YNB for early exponential and stationary phase samples respectively. Cells were washed twice in PBS before adjusting to a cell density of 2 x $10^7$ cells/ml. 5 x $10^6$ cells were transferred to the wells of black 96-well plates in triplicate. 25µl PBS/DMSO (1:1 v/v) and 5µg/ml Nile red were added to each sample. Plates were screened using the wavelengths: excitation 435nm, emission 590nm. Data shown as means of triplicates ±SD. Significance indicated between exponential and stationary phases ***p≤0.001 and difference in stationary phases between cells indicated by solid black lines ł p<0.05. Data analysed by one way ANOVA with Tukey *post hoc* test.

This data demonstrated that components upstream of Hog1p in the MAPK cascade did not appear to be involved in the regulation of lipid accumulation. As such, the study was extended to screen components of the HOG pathway downstream from the MAPK Hog1p to elucidate if altered lipid phenotypes were displayed.

### 4.2.6 Neutral lipid accumulation is attenuated on deletion of Msn2/4, a downstream target of Hog1p

As the results from Section 4.2.5 show, lipid accumulation is only significantly reduced at the point of the MAPK Hog1p. To further characterise the role of this pathway in lipid regulation the Nile red assay was performed on a number of downstream targets of Hog1p to assess whether the transcription factors Msn2/4 and Hot1 contributed to the accumulation of lipids. Growth curves are shown in Figures 4.23 and 4.24, and the Nile Red assays were conducted as described previously, using *hog1Δ* cells as a low lipid control for stationary phase cultures.

As demonstrated by Figures 4.23 and 4.24, after an initial lag phase of 5 hrs the deletion strains and wild type cells entered exponential growth until early stationary phase is achieved at 12 hrs.

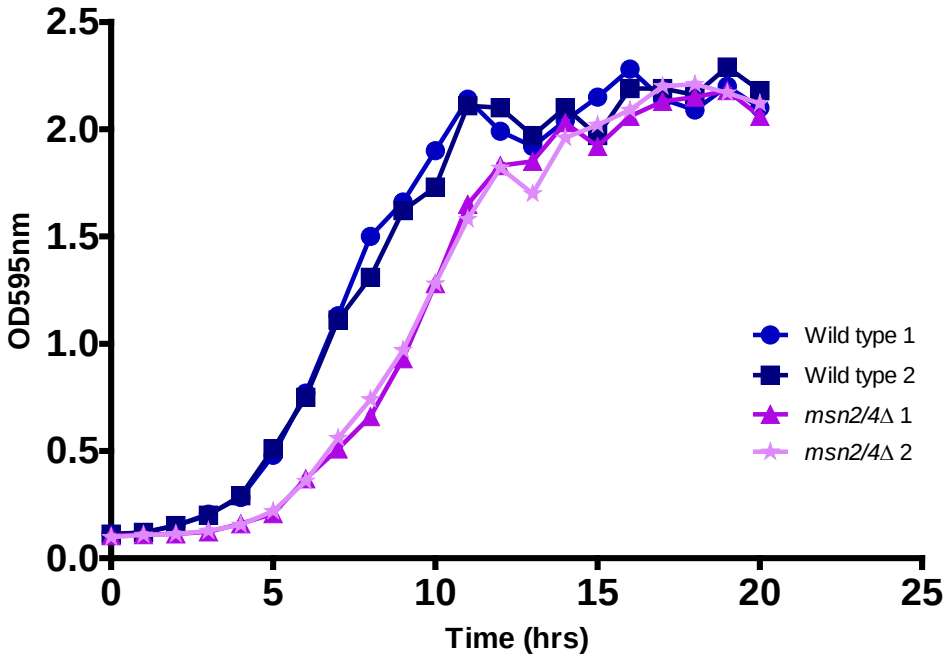


**Figure 4.23: Growth curve of *S. cerevisiae* wild type and *msn2/4Δ* under normal conditions in yeast nitrogen base medium (YNB).** Cultures were diluted to 2 x $10^6$ cells ($OD_{595}$~0.1) and incubated with shaking, duplicate, at 30°C. Optical density readings were taken hourly until mid to late stationary phase was reached. Growth curves were conducted in duplicate (culture 1 and culture 2 for both WT and deletion strain) showing growth patterns observed for two distinct colonies of the same strain.

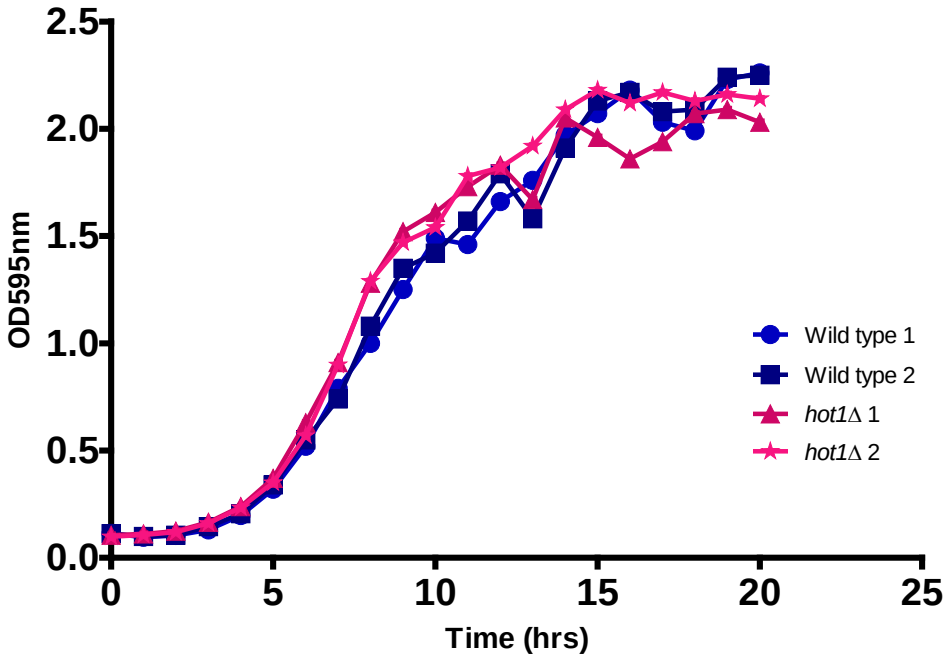


**Figure 4.24: Growth curve of *S. cerevisiae* wild type and *hot1Δ* under normal conditions in yeast nitrogen base medium (YNB).** Cultures were diluted to 2 x $10^6$ cells ($OD_{595}$ ~0.1) and incubated with shaking, duplicate, at 30°C. Optical density readings were taken hourly until mid to late stationary phase was reached. Growth curves were conducted in duplicate (culture 1 and culture 2 for both WT and deletion strain) showing growth patterns observed for two distinct colonies of the same strain.

Analysis of the Nile red fluorescence data for neutral lipids showed *hot1Δ* cells had wild type levels of neutral lipids. However, in the *msn2/4Δ* strain a significant decrease of 1.6 fold in neutral lipids compared to wild type was observed (Figure 4.25).

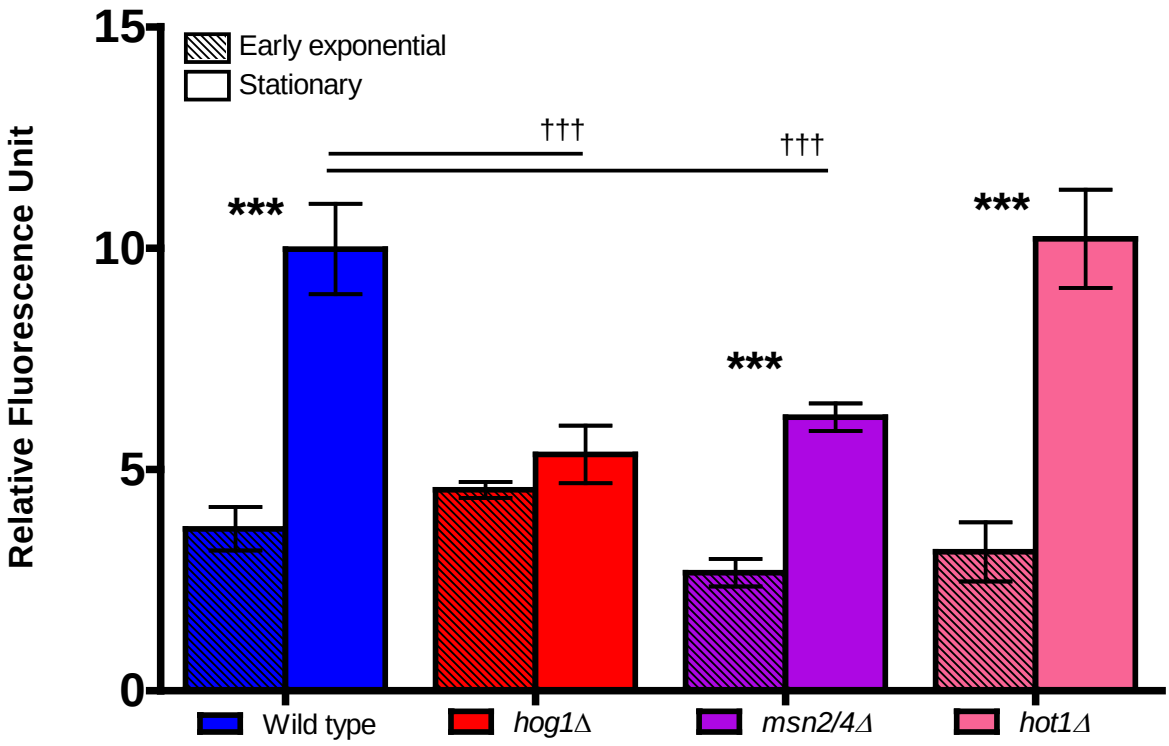


**Figure 4.25: Neutral lipid fluorescence intensity of Nile red stained *S. cerevisiae* wild type and transcription factor mutants.** Cells were harvested at 5 and 18 hrs post resuspension in YNB for early exponential and stationary phase samples respectively. Cells were washed twice in PBS before adjusting to a cell density of 2 x $10^7$ cells/ml. 5 x $10^6$ cells were transferred to the wells of black 96-well plates in triplicate. 25µl PBS/DMSO (1:1 v/v) and 5µg/ml Nile red were added to each sample. Plates were screened using the wavelengths: excitation 485nm, emission 535nm. Data shown as means of triplicates ±SD. Significance indicated between exponential and stationary phases ***p≤0.001 and difference in stationary phases between cells indicated by solid black lines ††† p≤0.001. Data analysed by one way ANOVA with Tukey *post hoc* test.

For polar lipids again *hot1Δ* cells showed no significant difference from wild type. For the *msn2/4*Δ strain, there was no significant difference in polar lipids compared with the wild type strain, with only a slight decrease in fluorescence of 1.1 fold (Figure 4.26).

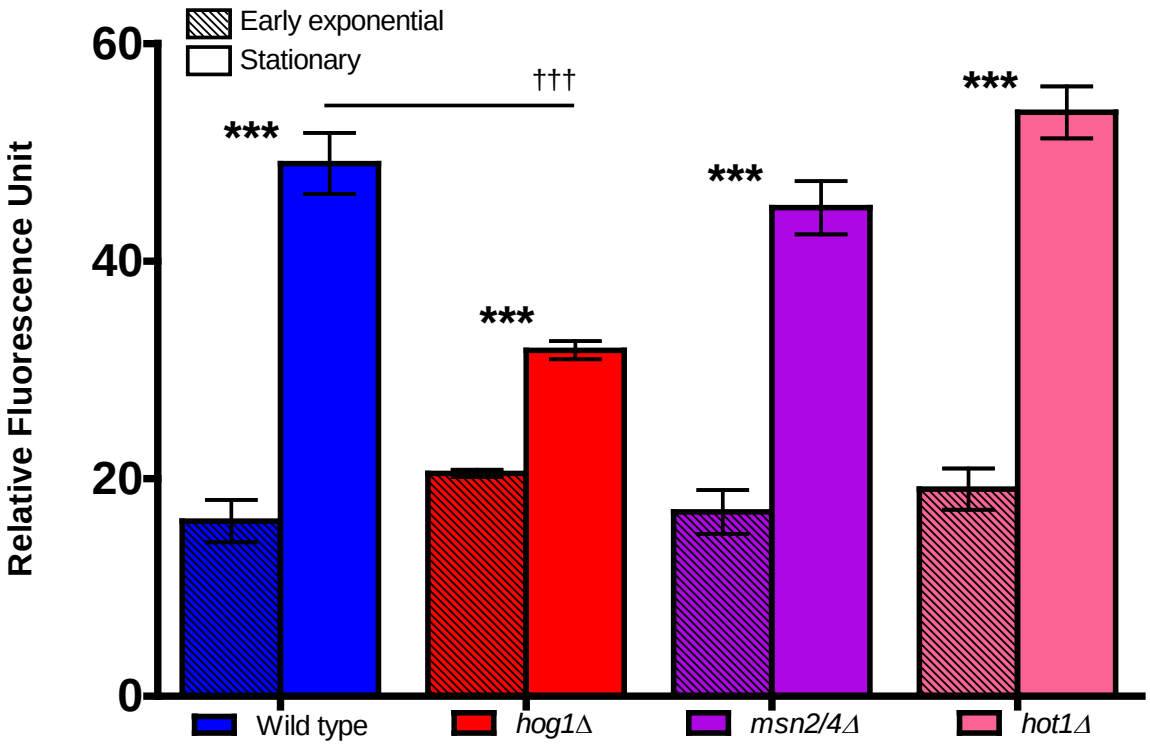


**Figure 4.26: Polar lipid fluorescence intensity of Nile red stained *S. cerevisiae* wild type and transcription factor mutants.** Cells were harvested at 5 and 18 hrs post resuspension in YNB for early exponential and stationary phase samples respectively. Cells were washed twice in PBS before adjusting to a cell density of 2 x $10^7$ cells/ml. 5 x $10^6$ cells were transferred to the wells of black 96-well plates in triplicate. 25µl PBS/DMSO (1:1 v/v) and 5µg/ml Nile red were added to each sample. Plates were screened using the wavelengths: excitation 535nm, emission 590nm. Data shown as means of triplicates ±SD. Significance indicated between exponential and stationary phases ***p≤0.001 and difference in stationary phases between cells indicated by solid black lines ††† p≤0.001. Data analysed by one way ANOVA with Tukey *post hoc* test.

### 4.2.7 Stress sensitivity of HOG pathway deletion strains does not align with observed lipid accumulation phenotypes

As the (HOG) MAPK pathway is involved in the response of cells to conditions of osmotic stress, a stress experiment was conducted for all tested deletion strains of the MAPK pathway. This was undertaken to assess whether the lipid phenotypes of cells deleted for *HOG1* and *MSN2/4* could potentially have resulted as a consequence of the stress response.

Figure 4.27 shows that cells lacking *SHO1* and *STE11* were no more sensitive to salt stress than wild type cells. Cells lacking *HOG1* and *PBS2,* when compared to wild type, showed limited growth in the presence of NaCl indicating similar stress sensitivities. In the case of the *msn2/4* deletion strain, cells displayed slight sensitivity to salt stress compared to wild type but markedly increased growth compared to cells deleted for *HOG1* and *PBS2*. This data indicated that stress sensitivity of the deletion strains did not align with the lipid accumulation phenotypes observed in the Nile red screen.

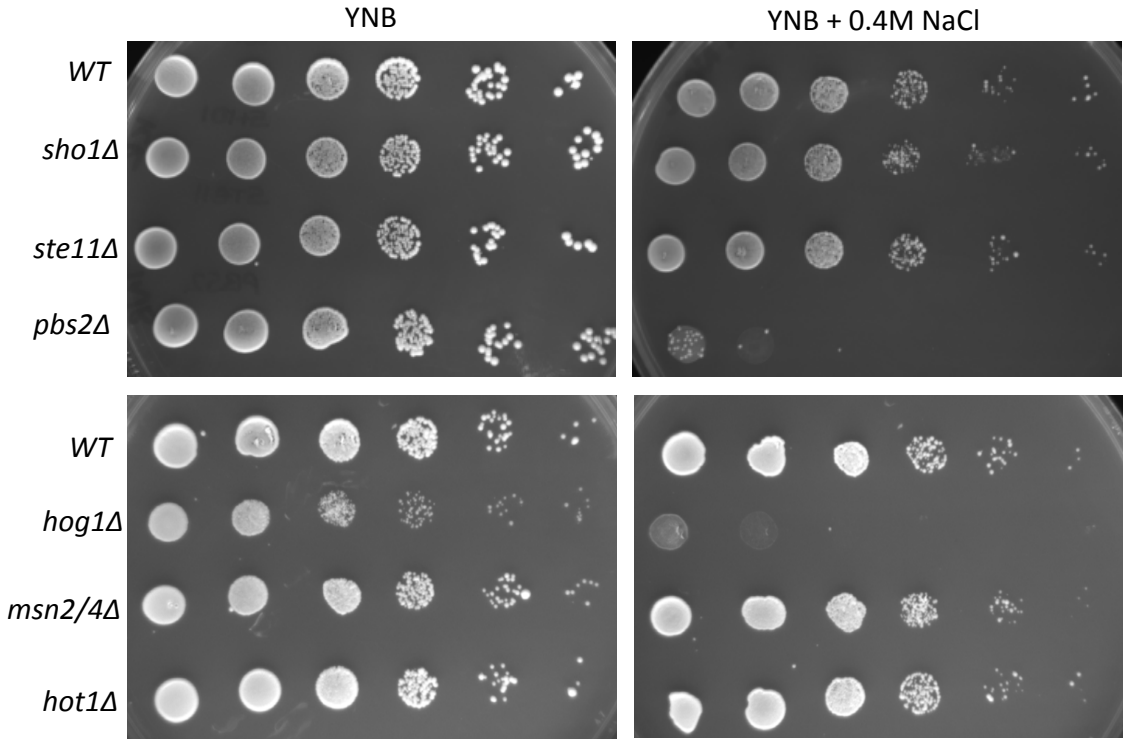


**Figure 4.27: Spot plates of *S. cerevisiae* wild type, *sho1Δ*, *ste11Δ*, *pbs2Δ*, *hog1Δ msn2/4Δ* and *hot1Δ*.** Control plates (YNB) and osmotic stress plates, YNB supplemented with 0.4M NaCl. Starting cell densities were ~2.3 x $10^7$ cells/ml before being serially diluted 1:10 across the plate down to 2.3 x $10^2$ cells/ml.

### 4.2.8 Lipid accumulation is not delayed in cells deleted for HOG1

It is known that Hog1p plays a crucial role in cell cycle control as well as in the resting exit status of cells (Escoté *et al.* 2011). Therefore it is important to determine whether the lipid phenotype observed in the *hog1* delete was the result of delayed accumulation either from delayed cell cycle progression in G1 (which has been shown to occur in *HOG1* deleted cells under stress) or from delayed resting exit resulting from resuspension of cells into YNB medium.

To determine if lipid accumulation was reduced or rather delayed in the *hog1Δ,* a time course was conducted and lipid levels determined in wild type and *hog1Δ* cells. Samples were harvested at 5, 8, 12, 18, 24, 48 and 72 hrs post resuspension so that lipid accumulation at each stage of growth could be assessed via the Nile red fluorescence method. The 72 hr time point was chosen as this is the stage where a reduction in lipids is expected to be observed due to β-oxidation (Beopoulos *et al.* 2011).

As shown in Figure 4.28, wild type cells began to gradually accumulate neutral lipids as growth progresses, with maximum levels reached after 24hrs, as cells enter stationary phase. From 48 hrs onwards, a decrease in neutral lipids was then observed. Initial neutral lipid levels in the *hog1Δ* are comparable to those found in wild type cells. However, as the growth curve progressed *hog1Δ* cells failed to accumulate neutral lipids at the level seen in wild type cells. In stationary phase (after 12 hrs) significant decreases in lipid accumulation, of between 1.3 and 1.6 fold were observed at each time point in the *hog1Δ* compared to wild type, consistent with previous stationary phase data derived for the *hog1Δ* in this chapter.

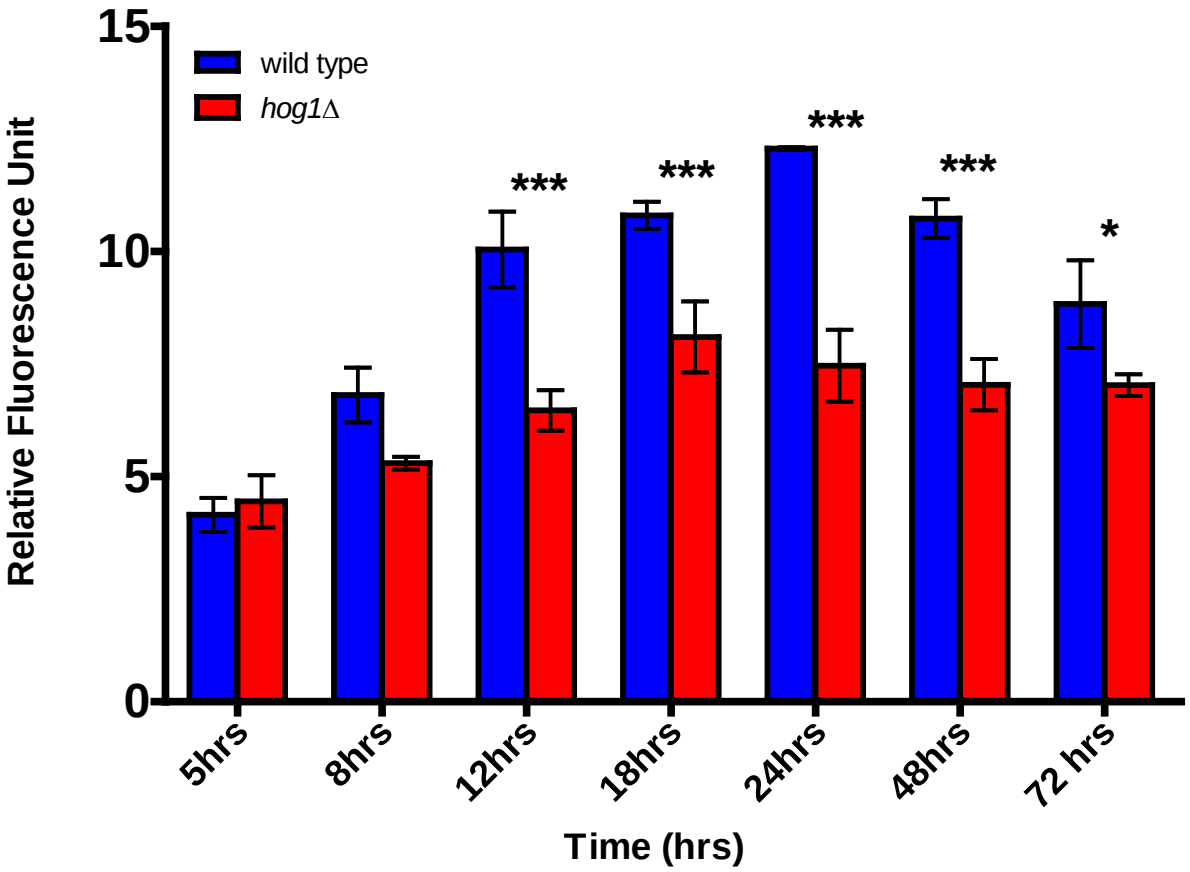


**Figure 4.28: Nile Red neutral lipid fluorescence intensity over time of *S. cerevisiae* wild type and *hog1Δ*.** Cells were harvested at 5, 8, 12, 18, 24, 48 and 72 hours post resuspension in YNB. Cells were washed twice in PBS before adjusting to a cell density of 2 x $10^7$ cells/ml. 5 x $10^6$ cells were transferred to the wells of black 96-well plates in triplicate. 25µl PBS/DMSO (1:1 v/v) and 5µg/ml Nile red were added to each sample. Plates were screened using the wavelengths: excitation 485nm, emission 535nm. Cultures were incubated for the time course at 30°C, 180rpm in YNB medium until the time points illustrated on the graph. Significant differences between wild type and the *hog1Δ* at each stage of the time course indicated by ***p≤0.001, *p≤0.05. Data analysed by one way ANOVA with Tukey *post hoc* test.

For polar lipids again the *hog1Δ* failed to accumulate lipid to a comparable level of the wild type strain after the early exponential phase 5 hr time point. Significant decreases of between 1.2 and 1.4 fold were observed at each point after 8 hours and thereafter until late stationary phase at 24 hrs, consistent with previous polar lipid related fluorescence data obtained for *hog1Δ* cells in this chapter. As expected with the 48 and 72 hr time points, a decrease in both neutral and phospholipids was observed in both wild type and *hog1* deleted cells (Figure 4.29).

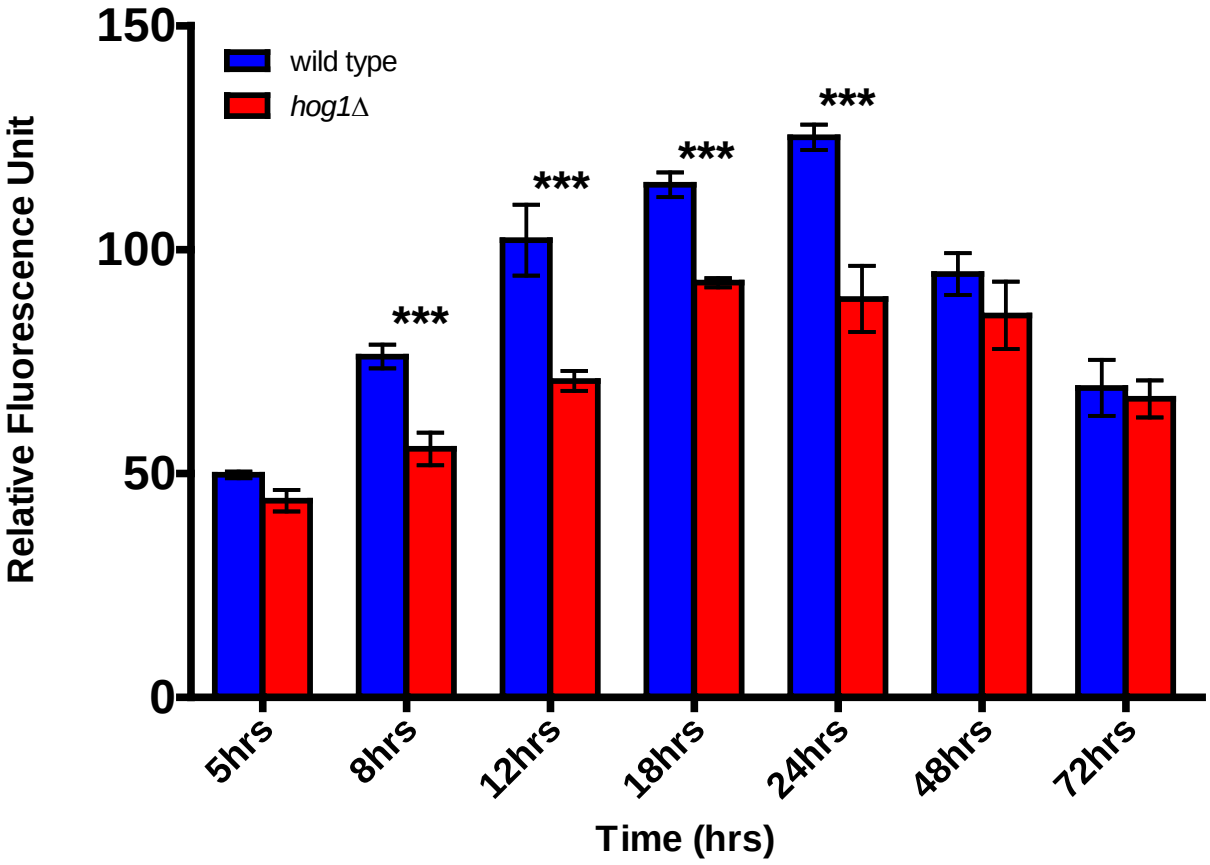


**Figure 4.29: Nile Red polar lipid fluorescence intensity over time of *S. cerevisiae* wild type and *hog1Δ*.** Cells were harvested at 5, 8, 12, 18, 24, 48 and 72 hours post resuspension in YNB. Cells were washed twice in PBS before adjusting to a cell density of 2 x $10^7$ cells/ml. 5 x $10^6$ cells were transferred to the wells of black 96-well plates in triplicate. 25µl PBS/DMSO (1:1 v/v) and 5µg/ml Nile red were added to each sample. Plates were screened using the wavelengths: excitation 535nm, emission 590nm. Cultures were incubated for the time course at 30°C, 180rpm in YNB medium until the time points illustrated on the graph. Significant differences between wild type and the *hog1Δ* at each stage of the time course indicated by ***p≤0.001. Data analysed by one way ANOVA with Tukey *post hoc* test.

This data demonstrated that the attenuated lipid accumulation phenotype seen when screening cells in mid stationary phase, 18 hrs, was not as a result of delayed accumulation in cells lacking *HOG1.*

### 4.2.9 Hog1p is dually phosphorylated as cells begin to accumulate lipid

To determine whether Hog1 is dually phosphorylated and activated at the initiation of lipid accumulation processes, which would imply a role for Hog1p in regulating lipid levels, protein samples were prepared from wild type cells at hourly time intervals from early exponential phase (5 hrs) until late exponential phase (9/10 hrs). The resultant Western blot was probed with antibodies to detect the dual phosphorylation status, α-P-p38 and total levels of Hog1p, α-Hog1.

As shown by Figure 4.30, Hog1p was phosphorylated at lag phase (5 hrs) and early exponential phase (7 hrs), which aligned with the transition of cells from lag to the exponential phase of growth.

Phosphorylation did not occur at the 8 hr time period, aligning with exponential growth, before becoming apparent again at 9 hrs. The dual phosphorylation of Hog1p at 9 hrs aligned with cells in late exponential/early stationary phase of growth and after the point at which wild type *S. cerevisiae* began to accumulate lipid, as demonstrated in Figure 4.28 (8-12 hrs). After 10 hrs phosphorylation of Hog1p was once again not observed.

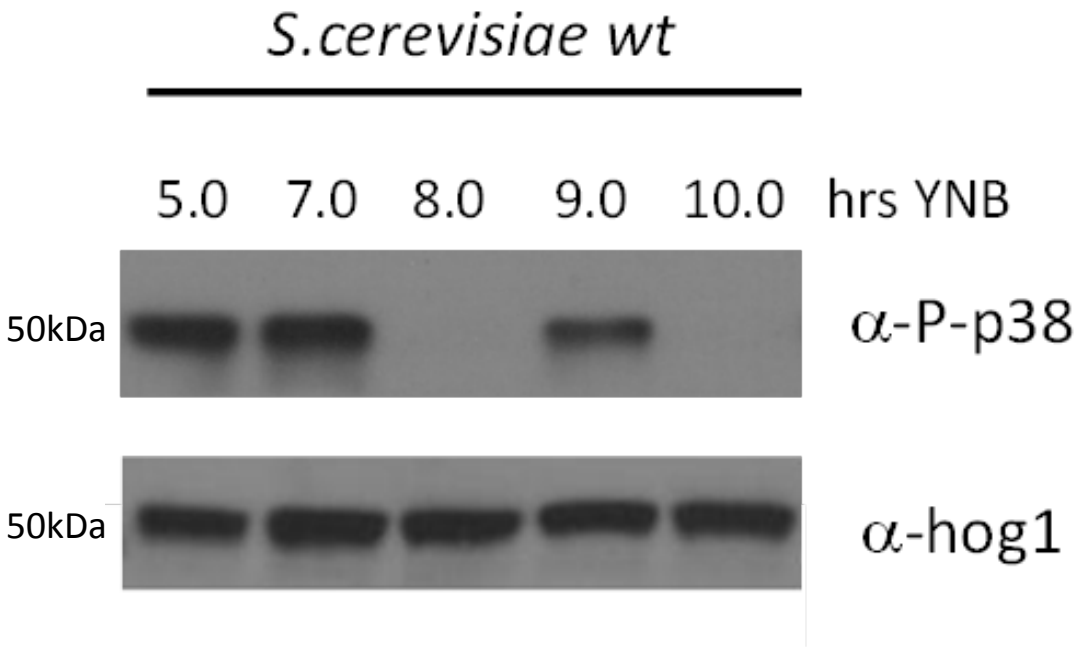


**Figure 4.30: Western blots of *S. cerevisiae* Hog1 phosphorylation status in wild type cells over time.** Time in hours indicates time protein sample was harvested post resuspension in YNB medium. α-P-p38: phosphorylated Hog1p. α-hog1: total Hog1 protein levels.

To further dissect the phosphorylation status of Hog1p, protein samples were harvested at half hourly intervals from 6 hrs until 9.5 hrs. As shown in Figure 4.31, phosphorylation of Hog1p was again observed at 7 hrs consistent with Figure 4.30. After this point Hog1p phosphorylation was again reduced until being observed again at 9 and 9.5 hrs.

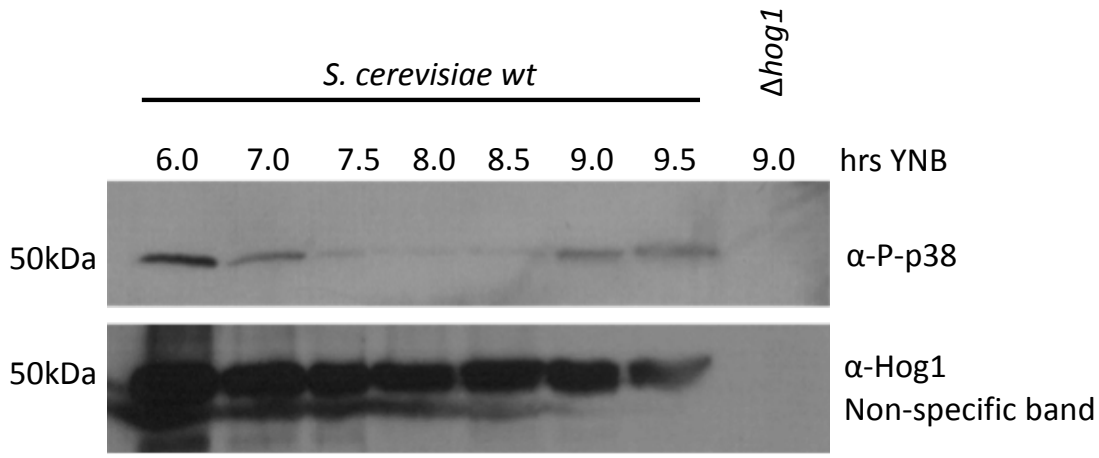


**Figure 4.31: Western blots of *S. cerevisiae* Hog1 phosphorylation status in wild type cells at half hourly intervals.** Time in hours indicates time protein sample was harvested post resuspension in YNB medium. α-P-p38: phosphorylated Hog1p. α-hog1: total Hog1 protein levels.

From this it can be concluded that Hog1p was dually phosphorylated between 9 and 9.5 hrs post resuspension in YNB and that this phosphorylation aligned with the point at which cells entered the late exponential/early stationary phase of growth, as well as aligning with increased cellular lipid accumulation in *S. cerevisiae.*

#### 4.2.9.1 Nutrient limitation as an activator of Hog1p

It has been previously reported that Hog1p is dually phosphorylated in response to nitrogen limitation (-N) (Aoki Y. *et al.* 2011b). Nutrient limitation is a natural consequence of growth as yeast cells enter late exponential/early stationary phase. In this study by Aoki *et al.* (2011) dual phosphorylation of Hog1p was observed at 3 hrs post resuspension of cells from YPD medium to YNB plus NaCl and YNB – N.

To determine whether the phosphorylation observed in Figures 4.30 and 4.31 could be as a result of nutrient limitation the experiment was repeated with some adaptations. Firstly YNB pre-cultures were employed instead of YPD, cells were resuspended either into complete YNB medium or YNB minus carbon source (-C) to assess the effect of carbon limitation. Further to this YNB –N and lacking amino acids was employed as it was unclear from the study by Aoki *et al.* (2011) whether YNB –N contained amino acids. Samples were harvested at 3 hrs post resuspension and the resulting protein samples were analysed with antibodies to detect the dually phosphorylated Hog1p and total Hog1p protein levels, as with the previous experiment.

As shown by Figure 4.32, 3 hrs post resuspension in YNB complete medium low levels of Hog1p phosphorylation were observed. Phosphorylation was increased in cells subjected to treatment with 0.4M NaCl, as expected and consistent with the observation by Aoki *et al.* (2011). However, no phosphorylation was observed when cells were transferred from YNB to medium lacking nitrogen plus amino acids, nitrogen or carbon sources.

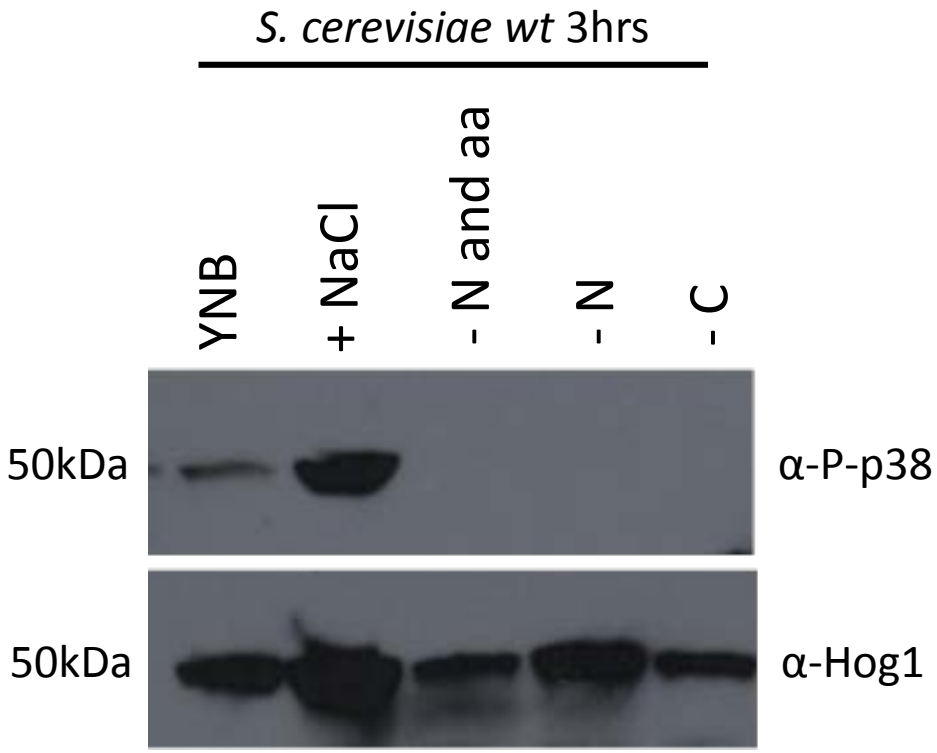


**Figure 4.32: Western blots of *S. cerevisiae* Hog1 phosphorylation status under nutrient starvation.** YNB: Yeast nitrogen base complete medium, +NaCl: Yeast nitrogen base complete medium supplemented with 0.4M NaCl, -N and aa: Yeast nitrogen base medium minus nitrogen and amino acid source, -N: Yeast nitrogen base medium minus nitrogen source, -C: Yeast nitrogen base medium minus carbon source. α-P-p38: phosphorylated Hog1p. α-hog1: total Hog1 protein levels.

This suggested that nutrient starvation, both nitrogen and carbon, did not result in the dual phosphorylation of Hog1p at 3 hrs post resuspension in starvation medium.

### 4.2.9.2 Observed phosphorylation of Hog1p appears to be Pbs2 dependant

As described previously, Hog1p is dually phosphorylated in response to stress on Thr174 and Ty176 residues by its upstream MAPKK Pbs2. However, lipid accumulation data suggests that Pbs2 was not involved at the lipogenic switch. To assess whether Hog1p phosphorylation observed in Figures 4.30 and 4.31 was Pbs2 dependant, protein samples were harvested from the *pbs2* deletion strain at 6 hrs and half hourly intervals thereafter, before probing the resultant Western blot with antibodies to detect phosphorylated and total levels of Hog1p. As shown by Figure 4.33, no phosphorylation was found to be present at any point during the time course.

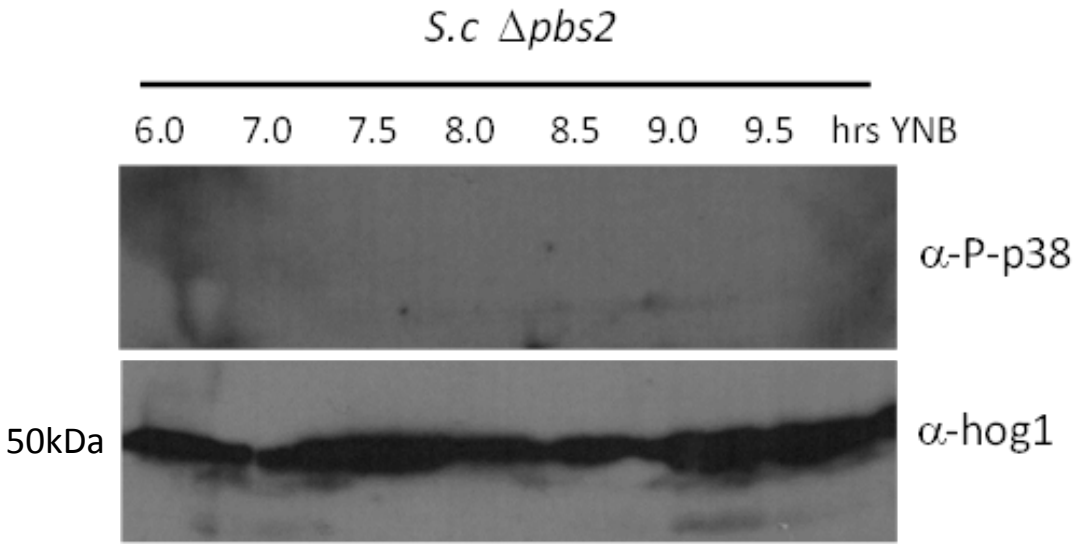


**Figure 4.33: Western blots of *S. cerevisiae* Hog1 phosphorylation status in *pbs2Δ* cells at half hourly intervals.** Time in hours indicates time protein sample was harvested post resuspension in YNB medium. α-P-p38: phosphorylated Hog1p. α-hog1: total Hog1 protein levels.

Therefore, the results of the time course conducted with the *pbs2Δ* suggested that the phosphorylation observed in Figures 4.30 and 4.31 was dependent on the MAPKK Pbs2.

### 4.2.9.3 Potential Pbs2-independent phosphorylation of Hog1

To further investigate the phosphorylation status of Hog1p in both wild type and *pbs2Δ* cells, a Phos-tag gel of protein samples utilised in Section 4.2.9 was undertaken (Figure 3.3.4. Phosphorylated proteins are bound within an SDS-PAGE gel by Phos-tag, as such the migration speed of proteins which are phosphorylated is decreased compared to non-phosphorylated proteins.

As demonstrated by Figure 4.34, at 7.5 hrs where little dual phosphorylation was observed, bands for both wild type and the *pbs2Δ* appeared to migrate to an equivalent level. At 8.5 hrs, where very little dual phosphorylation of Hog1p was detected in Figure 4.31, an upshift of the hog1 band was observed both in wild type and *pbs2Δ* samples. This is indicative of protein phosphorylation and suggested that Hog1p is further phosphorylated at this point, independently of Pbs2. At 9 hrs there appeared to be an additional upshift of the wild type sample, which is suggested to be as a result of Hog1p dual phosphorylation by Pbs2.

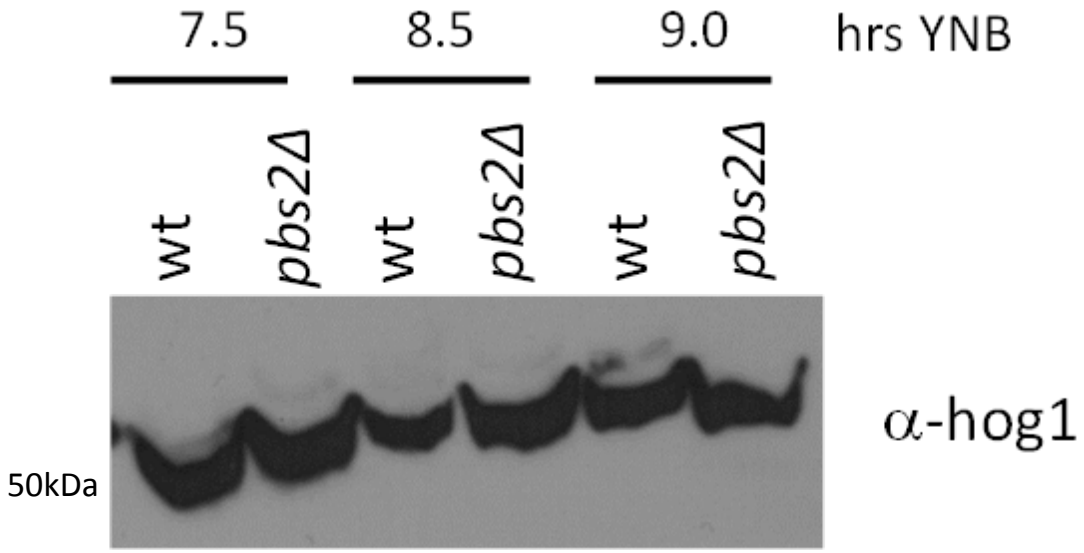


**Figure 4.34: Phos-tag Western blot of *S. cerevisiae* Hog1 in wild type and *pbs2Δ* cells.** Time in hours indicates time protein sample was harvested post resuspension in YNB medium. α-hog1: total Hog1 protein levels.

The results of the Phos-tag gel suggested that Hog1p was additionally phosphorylated in a Pbs2 independent manner at 8.5 hrs. This 8.5 hr time point precedes the point where *S. cerevisiae* displays a marked increase in accumulated lipids post resuspension in YNB, as shown previously by Figure 4.28 (8 to 12 hrs).

## 4.3 Regulation of lipid synthesis by Hog1

It has been demonstrated in this chapter that Hog1p appears to play a role in the accumulation of lipids in *S. cerevisiae* along with its downstream target Msn2/4. Utilising bioinformatics, potential targets of Hog1 and Msn2/4 that are involved in the regulation of lipid homeostasis were identified.

### 4.3.1 Potential MAPK phosphorylation sites on lipid regulatory proteins

Hog1 phosphorylates target proteins on conserved serine and threonine resides which are followed by a proline residue. Selected key lipid regulatory proteins were identified via bioinformatics analysis to contain potential MAPK phosphorylation sites.

Dga1p, a major protein involved in TAG synthesis, can be localised to the ER or present on lipid droplets within the cytoplasm. After analysis of the protein sequence via UniProt, it was found that Dga1p has four potential MAPK phosphorylation sites within the N terminus of the protein sequence (Figure 4.35).


**Figure 4.35: The protein sequence of Dga1p contains potential MAPK phosphorylation sites.** Identification of potential MAPK phosphorylation sites within the N terminus of Dga1p. Phosphorylation sites are indicated on the graphical diagram in red and yellow within the protein sequence. Phosphorylation sites were determined from data curated by Uniprot and *Saccharomyces* genome database.

Lro1p, another contributor to TAG synthesis by an acyl-CoA independent pathway, contains two potential MAPK sites at residues 475 and 586 (Figure 4.36).

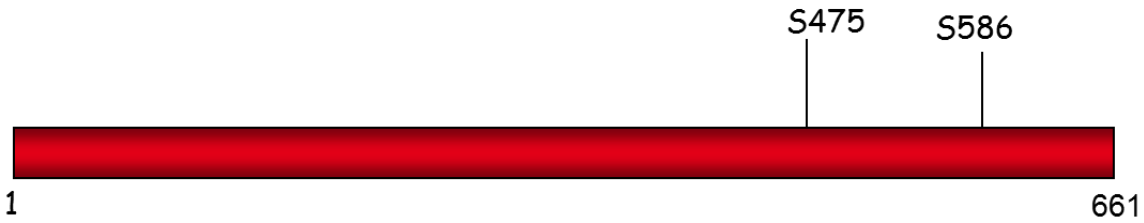


MGTLFRRNVQNQKSDSDENNKGGSVHNKRESRNHIHHQQGLGHKRRRGISGSAKRNERGK
DFDRKRDGNGRKRWRDSRRLIFILGAFLGVLLPFSFGAYHVHNSDSDLFDNFVNFDSLKV
YLDDWKDVLPQGISSFIDDIQAGNYSTSSLDDLSENFAVGKQLLRDYNIEAKHPVVMVPG
VISTGIESWGVIGDDECDSSAHFRKRLWGSFYMLRTMVMDKVCWLKHVMLDPETGLDPPN
FTLRAAQGFESTDYFIAGYWIWNKVFQNLGVIGYEPNKMTSAAYDWRLAYLDLERRDRYF
TKLKEQIELFHQLSGEKVCLIGHSMGSQIIFYFMKWVEAEGPLYGNGGRGWVNEHIDSFI
NAAGTLLGAPKAVPALISGEMKDTIQLNTLAMYGLEKFFSRIERVKMLQTWGGIPSMLPK
GEEVIWGDMKSSSEDALNNNTDTYGNFIRFERNTSDAFNKNLTMKDAINMTSISPEWLQR
RVHEQYSFGYSKNEEELRKNELHHKHWSNPMEVPLPEAPHMKIYCIYGVNNPTERAYVYK
EEDDSSALNLTIDYESKQPVFLTEGDGTVPLVAHSMCHKWAQGASPYNAGINVTIVEMKH
QPDRFDIRGGAKSAEHVDILGSAELNDYILKIASGNGDLVEPRQLSNLSQWVSQMPFPM

**Figure 4.36: The protein sequence of Lro1p contains potential MAPK phosphorylation sites.** Phosphorylation sites are indicated on the graphical diagram in red and yellow within the protein sequence. Phosphorylation sites were determined from data curated by Uniprot and *Saccharomyces* genome database.

With regards to the regulation of phospholipids, one potential MAPK site was found at position 157 in the protein sequence of Cho1, an outer mitochondrial membrane protein involved in the synthesis of PS (Figure 4.37).

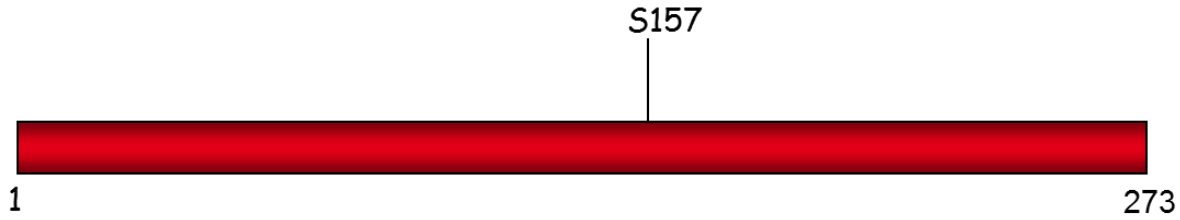


MTDSSATGFSKHQESAIVSDSEGDAIDSELHMSANPPLLRRSSSLFSLSSKDDLPKPDSK
EYLKFIDDNRHFSMIRNLHMADFITLLNGFSGFYSIISCLRYTLTGQTHYVQRAHFFILL
GLFFDFFDGRVARLRNKSSLMGQELDSLADLVSFGVSPATIAFAIGFRTTVDVLFLAFWV
LCGLTRLARFNISVNNIPKDKHGKSQYFEGLPIPTNLFWVGFMALLVYKDWIHDNLPFGI
VFQDTSFEFHLVTIGFVLQGCAEISKSLKIPKP

**Figure 4.37: The protein sequence of Cho1p contains potential MAPK phosphorylation sites.** Phosphorylation sites are indicated on the graphical diagram in red and yellow within the protein sequence. Phosphorylation sites were determined from data curated by Uniprot and *Saccharomyces* genome database.

Further to this, a further 6 potential MAPK sites were identified within sequence of the ER protein Cho2, which catalyses the first step in the phosphatidylethanolamine to phosphatidylcholine conversion (Figure 4.38).

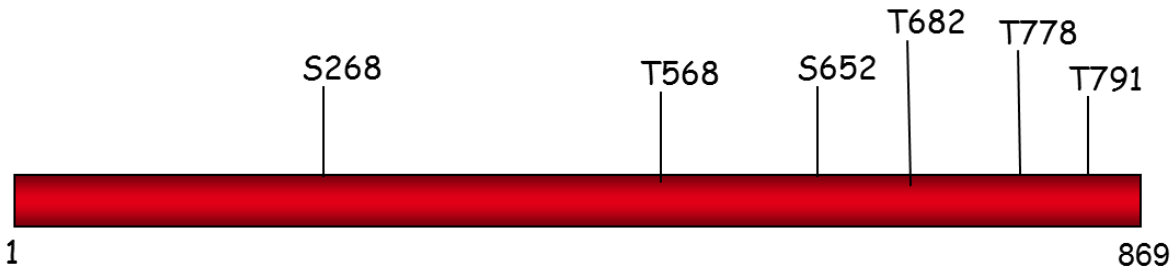


MSSCKTTLSEMVGSVTKDRGTINVEARTRSSNVTFKPPVTHDMVRSLFDPTLKKSLLEKC
IALAIISNFFICYWVFQRFGLQFTKYFFLVQYLFWRIAYNLGIGLVLHYQSHYETLTNCA
KTHAIFSKIPQNKDANSNFSTNSNSFSEKFWNFIRKFCQYEIRSKMPKEYDLFAYPEEIN
VWLIFRQFVDLILMQDFVTYIIYVYLSIPYSWVQIFNWRSLLGVILILFNIWVKLDAHRV
VKDYAWYWGDFFFLEESELIFDGVFNI**S**PHPMYSIGYLGYYGLSLICNDYKVLLVSVFGH
YSQFLFLKYVENPHIERTYGDGTDSDSQMNSRIDDLISKENYDYSRPLINMGLSFNNFNK
LRFTDYFTIGTVAALMLGTIMNARFINLNYLFITVFVTKLVSWLFISTILYKQSQSKWFT
RLFLENGYTQVYSYEQWQFIYNYYLVLTYTLMIIHTGLQIWSNFSNINNSQLIFGLILVA
LQTWCDKETRLAISDFGWFYGDFFLSNYISTRKLTSQGIYRYLNHPEAVLGVVGVWGTVL
MTNFAVTNIILAVLWTLTNFILVKFIE**T**PHVNKIYGKTKRVSGVGKTLLGLKPLRQVSDI
VNRIENIIIKSLVDESKNSNGGAELLPKNYQDNKEWNILIQEAMDSVATRL**S**PYCELKIE
NEQVETNFVLP**T**PVTLNWKMPIELYNGDDWIGLYKVIDTRADREKTRVGSGGHWSATSKD
SYMNHGLRHKESVTEIKATEKYVQGKVTFDTSLLYFENGIYEFRYHSGNSHKVLLIS**T**PF
EISLPVLNTT**T**PELFEKDLTEFLTKVNVLKDGKFRPLGNKFFGMDSLKQLIKNSIGVELS
SEYMRRVNGDAHVISHRAWDIKQTLDSLA

**Figure 4.38: The protein sequence of Cho2p contains potential MAPK phosphorylation sites.** Potential phosphorylation sites are indicated on the graphical diagram in red and yellow within the protein sequence. Phosphorylation sites were determined from data curated by Uniprot and *Saccharomyces* genome database.

Potential MAPK phosphorylation sites were also found in all four of the SREBP-like proteins of *S. cerevisiae* Mga2, Spt23, Ecm22 and Upc2. All are intracellular membrane proteins which translocate to the nucleus upon requirement and are involved in the transcription of lipid regulatory genes.

In the protein sequences of Ecm22 and Upc2 multiple potential MAPK sites were found throughout the protein sequences (Figures 4.39 and 4.40). Of those identified in the sequence of Ecm22p amino acids 431, 445 and 464 have been assigned as phosphoserines via multidimensional chromatography analysis (Albuquerque *et al.* 2008).

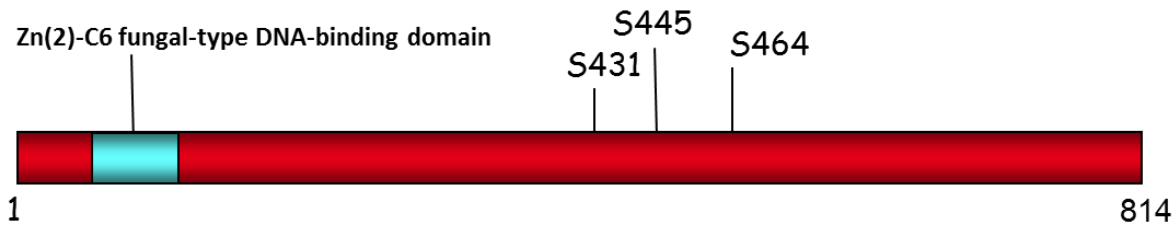


MTSDDGNAGQEREKDAELIEVGGKKVSKTSTGKRKFHNKSKTGCDNCKRRRVKCDEGKPF
CKKCTNMKLDCVYSPIQPRRRKDSSSSKFASAVHDRVGKKNLSDNAIMLQQQQQQLHHQQ
EQQFRQQQQVQLQQQLLPHVGTDEQSNSPNSVPPSVSNNMENLLLPHLLASLVNNTSNST
NSSANGAEAHNNITQTAPSSMINNNHPNMALPGNSPLSIPITPSFQSTAMNLSSSLNGLL
SPGRLNSVTNGLQQPQLQQQNQQIPQQQGTQSPFSNIPFDQLAQLNKMGLNFNMKSFNTL
FPYGAANGMASEFQELFGLGKFATSNNRAIKVSTAEEALANMQQEQEDKNKQFTKNPLDN
TKTDAVNSGNNPLNGNENKVTASDILSHNKNLIIDNTGLTISPPHTLSKPSIDQNIASPS
TGVSNVTSTKSLLSIPDNRTALGNSPTLKTSPMGDLLSNSEALSPRSSNSHTQQQSSPHS
NASSASRLVPELVGLSRKSNLNLIDLKLFHHYCTDVWHTITEAGISGPEVWSTYIPDLAF
HFPFLMHTILAFSATHLSRTEAGLDNYVSSHRLEALRLLREAVLEISDDNTDALVASALI
LILDSLANASSSSPTAWIFHVKGAVTILTAVWPLSETSKFYNLISVDLSDLGEAVINQSN
HNNDNDNSNNGDGNNNNTISELVCFDESIADLYPVEIDSPYLITLAYLDKLHREKNQLDF
MLRVFSFPALLDRTFLALLMTGDLGAMRIMRSYYTLLRGYTTEIKDKVWFLDSVSQVLPQ
DVDEYSGGGGMHMMLDFLGGGLPSMTTTNFSAFM

**Figure 4.39: The protein sequence of Ecm22p contains potential MAPK phosphorylation sites.** Phosphorylation sites that have been assigned phosphoserine status are indicated on the graphical diagram in red and yellow within the protein sequence. Phosphorylation sites were determined from data curated by Uniprot and *Saccharomyces* genome database.

Similarly for Upc2 amino acid residues 122, 519 and 522 have been assigned phosphothreonine and phosphoserine sites (Figure 4.40). Additionally, residues 520-523 have been assigned as a MAPK/ERK site (Albuquerque *et al.* 2008), demonstrating a potential interaction of MAPKs and SREBP-like proteins.

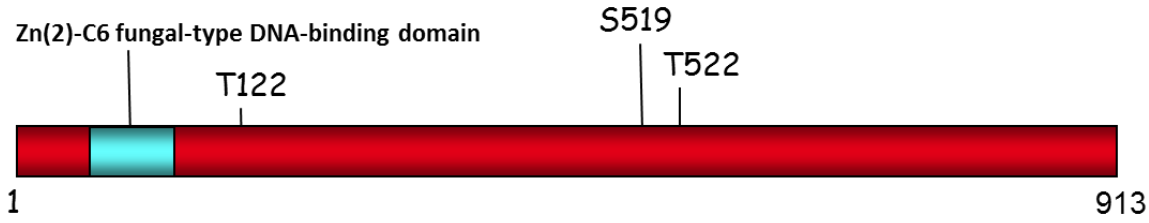


MSEVGIQNHKKAVTKPRRREKVIELIEVDGKKVSTTSTGKRKFHNKSKNGCDNCKRRRVK
CDEGKPACRKCTNMKLECQYTPIHLRKGRGATVVKYVTRKADGSVESDSSVDLPPTIKKE
QTPFNDIQSAVKASGSSNDSFPSSASTTKSESEEKSSAPIEDKNNMTPLSMGLQGTINKK
DMMNNFFSQNGTIGFGSPERLNSGIDGLLLPPLPSGNMGAFQLQQQQQVQQQSQPQTQAQ
QASGTPNERYGSFDLAGSPALQSTGMSLSNSLSGMLLCNRIPSGQNYTQQQLQYQLHQQL
QLQQHQQVQLQQYQQLRQEQHQQVQQQQQEQLQQYQQHFLQQQQQVLLQQEQQPNDEEGG
VQEENSKKVKEGPLQSQTSETTLNSDAATLQADALSQLSKMGLSLKSLSTFPTAGIGGVS
YDFQELLGIKFPINNGNSRATKASNAEEALANMQEHHERAAASVKENDGQLSDTKSPAPS
NNAQGGSASIMEPQAADAVSTMAPISMIERNMNRNSNISPSTPSAVLNDRQEMQDSISSL
GNLTKAALENNEPTISLQTSQTENEDDASRQDMTSKINNEADRSSVSAGTSNIAKLLDLS
TKGNLNLIDMKLFHHYCTKVWPTITAAKVSGPEIWRDYIPELAFDYPFLMHALLAFSATH
LSRTETGLEQYVSSHRLDALRLLREAVLEISENNTDALVASALILIMDSLANASGNGTVG
NQSLNSMSPSAWIFHVKGAATILTAVWPLSERSKFHNIISVDLSDLGDVINPDVGTITEL
VCFDESIADLYPVGLDSPYLITLAYLDKLHREKNQGDFILRVFTFPALLDKTFLALLMTG
DLGAMRIMRSYYKLLRGFATEVKDKVWFLEGVTQVLPQDVDEYSGGGGMHMMLDFLGGGL
PSMTTTNFSDFSL

**Figure 4.40: The protein sequence of Upc2p contains potential MAPK phosphorylation sites.** Phosphorylation sites that have been assigned phosphoserine or phosphothreonine status are indicated on the graphical diagram in red and yellow within the protein sequence. Phosphorylation sites were determined from data curated by Uniprot and *Saccharomyces* genome database.

In Spt23 and Mga2 the potential MAPK sites are highlighted in Figures 4.41 and 4.42 respectively. Out of all of the phosphorylation sites present within the protein sequences of Spt23 and Upc2, only residue 468 of Spt23 has been assigned as a phosphoserine by quantitative mass spectrometry *(Holt et al. 2009)*.

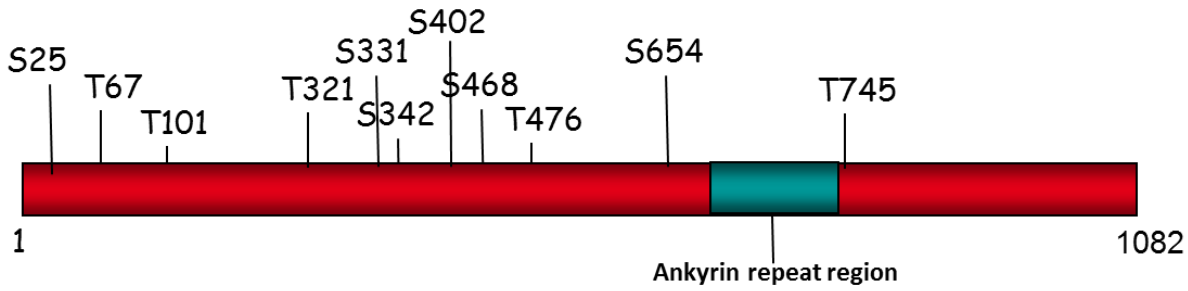


MMSGTGNVSSMLHSYSANIQHNDGSPDLDLLESELLDIALLNSGSSLQDPGLLSLNQEKM
ITAGTTTPGKEDEGELRDDIASLQGLLDRHVQFGRKLPLRTPYANPLDFININPQSLPLS
LEIIGLPKVSRVETQMKLSFRIRNAHARKNFFIHLPSDCIAKDKFFTSSDDPTNLTIPNR
DINERTLFLDAFLLCASNNNSNNFKQTYVCNRCINREKRRASRRKSGLNDNSIWQNNENK
RAIIFNSKQLFIISNNGLSGNSNCINFDLPTRIVCYCRHHKATNGFVVLFLLRDHNGDIL
AKTITDPIMIMDKKNASNTTTPTSTSNAQVSPMTNDTRSFSSPQSDLNFPSEFPLPSNSK
NFVISTNCMLDSNCNNNNNDNDNKNNIKTNTAMMNNNRHFPSPNSSSEDSNHSFSDIHFS
NNNDNNLHRSLDSWSSTGFNSSSNPALTTLTSDFSAASARHTGKRQRSVNEPFMSTPNTF
SRLPQKFIDSSKDISNHNSVPVALNNKPSIQRVIPAQGSINGGIEVTLLGSKFKQGLIIK
FGENIALSSQCWNESTMVTYLPPSSKPGPVLVTIVDPSETSMRNNSNSSVSTSNSTNDIL
HLNKYTGEKAIFTYVDDTDRQLIELALQIVGLKMNGKLEDARNIAKRIVGSDSSPSNNNA
GLHSQNSSLNSYTNMMRNINDEQLITEVIKSFKRNNNLSTVNLSMCDVRGRTLLHLAAFN
NWYSLVSLLIKYGSHLNDQDLFGFTPLHMACINGDLRIIRLLLECNVNIMKKTRNGFIAK
QFFLMNYTVNKTRYSNYETSLFDDILTRLTKNTTGSSDTQPFERNVSQSSFNSSLFDDDD
ADHDYVQERKYLLADSAALAPEQSNCNDNTSFSILDSDSGYDISDCESSSDEIALEFFNT
HKIKDFSSKPNEIPKTTKTSIEPDGSLWNRMLTRLNDELPKYEDLFPKKPKNWELGSKSV
EIGPDNSAQMTVDDSQTSSEDDELEALQVGFNTIFSKKQNFQNDKMLLFFWIPLTLVLLL
CFTLSNLGKDDDMFHNLSKIVQEYLRIGLAKVLLGNERMKTSFKMQLSKFQNNNILNDMR
VN

**Figure 4.41: The protein sequence of Spt23p contains potential MAPK phosphorylation sites.** Phosphorylation site that has been assigned phosphoserine is indicated on the graphical diagram in red and yellow within the protein sequence. Phosphorylation sites were determined from data curated by Uniprot and *Saccharomyces* genome database.

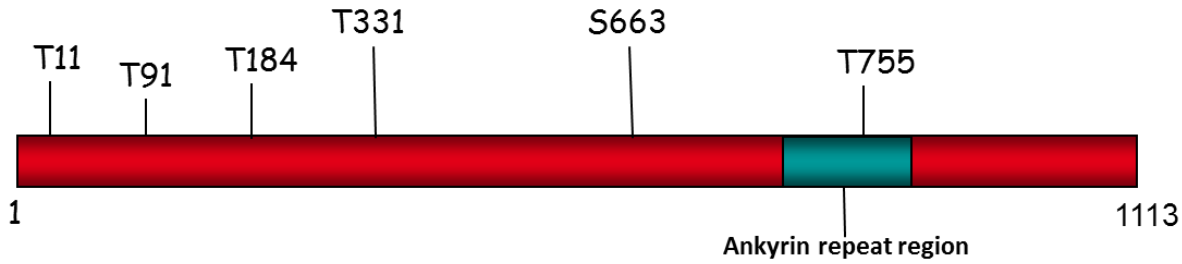


MQQNSEFLTE**T**PGSDPHISQLHANSVMESQLLDDFLLNGSPMYQDDSMAHININEGANFQ
NFIKTDEGDSPNLLSFEGIGNNTHVSQNVS**T**PLEEEMESNRALKEEEEDEHENKVFNEKN
IGNPAHDEIVFGRKETIQSVYINPLDYLKVNAAQLPLDVEVSGLPQVSRVENQLKLKVKI
TSE**T**PLNQSMLYLPSDSISREKFYLKKNIEDFSEDFKKNLLYINAFVLCAVSNRTTNVCT
KCVKREQRRAARRKSGIADNLLWCNNINRRLVVFNNKQVFPIMKTFDNVKEFELTTRLVC
YCRHHKANNGFVILFTITDWQNRLLGKFTT**T**PIMITDRKPANMDTTKFNNTTTSSRRQLT
EEESTTEYYSTDNNQLSKDENMPFQYTYQHNPYDNDSQMNNIPLKDKNVPFPYSISQQTD
LLQNNNLSLNLSLPNQHIPSPTSMSEEGSESFNYHHRDNDNPVRTISLTNIEQQSQLNQR
KRARNNLENDIGKPLFKHSFSNSISATNTMNPALHSMQDFSMKNNNNNLPSINRVIPSQG
PINGGIEVTLLGCNFKDGLSVKFGSNLALSTQCWSETTIVTYLPPAAYAGQVFVSITDTN
NENNNDDLPQEIEINDNKKAIFTYVDDTDRQLIELALQIVGLKMNGKLEDARNIAKRIVG
ND**S**PDSGTNGNSCSKSTGPSPNQHSMNLNTSVLYSDEVLIQKVIKSLNINSNISICDSLG
RTLLHLACLKNYSSLVYTLIKKGARVNDIDSFGL**T**PLHFACISGDPKIIKMLLNCKVNYS
LRSHNGLTAREVFIANHIHSEEVDKKQENRDNHKFVHNDTYISEVLSLFEEFQNGTKFTD
SVETDSNYSISRKYSQSSFNSSLLDNESLNENLFESQSMINPTSMEIQHPTLQLFENSSY
SEYDQSDFEEDGDEDLFVTDEVEKPGVACREEQSELLDIGSSANEPEEDNGSTSLWNRVL
HRINDDLPKYEDLFPLSWGKDDKLKTTNQDSIVEQSASNIENSENSEEEDYEEEEEFLKK
QFNRFFQNKQNFRNDKMLIFFWIPLTLLLLTWFIMYKFGNQDSSINHISELISEYLRIAL
AKFLLGNERMKTAFRSKLSNLQTTRMLNDLIVS

**Figure 4.42: The protein sequence of Mga2p contains potential MAPK phosphorylation sites.** Phosphorylation sites are indicated on the graphical diagram and in red and yellow within the protein sequence. Phosphorylation sites were determined from data curated by Uniprot and *Saccharomyces* genome database.

### 4.3.2 Msn2/4 as a regulator of SREBP-like protein activity

Hog1p has a number of downstream targets including the transcription factors Msn2/4. This study has demonstrated a neutral lipid phenotype associated with deletion of these genes. SREBP-like proteins are important in the transcriptional regulation of lipid homeostasis, as such bioinformatics analyses were undertaken to elucidate whether SREBP-like proteins are potential transcriptional targets of Msn2/4.

Msn2/4 bind to stress response elements (STRE) within the promoter regions of target genes in order to regulate their expression. STRE elements identified that are bound by Msn2/4 are 5'-CCCCT-3' and 5'-AGGGG-3' (Grably *et al.* 2002). It was found that both *ECM22* contained a full STRE element within its promoter region at position -238, whereas *UPC2* contained PDS elements (Figure 4.43).

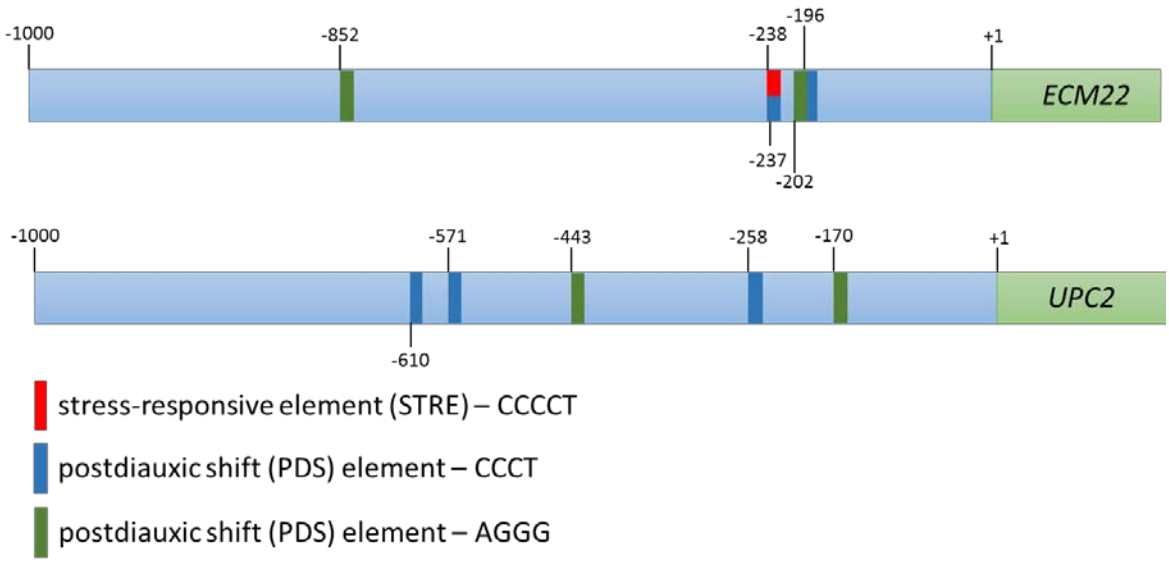


**Figure 4.43: The promoter regions of *ECM22* and *UPC2* contain STRE and PDS elements.** Promoter regions, 1000 bp upstream of the ORF were analysed for the presence of STRE and PDS elements. Sequence positions within the promoter are indicated STRE (red), PDS CCCT (blue) and PDS AGGG (green).

On analysis of the promoter regions of *SPT23* and *MGA2,* it was found that *MGA2* contained a full STRE element at position -62, and *SPT23* contained PDS elements (Figure 4.44).

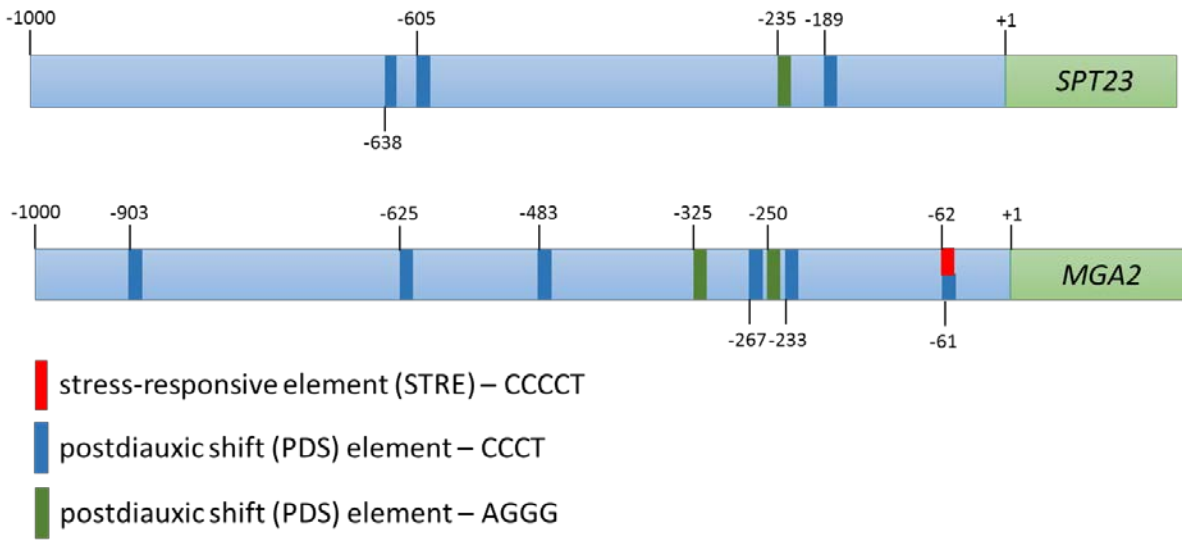


**Figure 4.44: The promoter regions of *SPT23*and *MGA2* contain STRE and PDS elements.** Promoter regions, 1000 bp upstream of the ORF were analysed for the presence of STRE and PDS elements. Sequence positions within the promoter are indicated STRE (red), PDS CCCT (blue) and PDS AGGG (green).

From analyses of the bioinformatics data collated it is suggested that the MAPK pathway of *S. cerevisiae* may regulate components important in the metabolism of lipids.

## 4.4 Lipid phenotypes observed in S. cerevisiae are conserved in the fission yeast S. pombe at the level of the MAPK

The fission yeast *S. pombe* has been used extensively as a model eukaryote in human disease research and additionally has been found to be more similar to human cells in cell cycle regulation and stress responses. As *S. pombe* cells are as divergent from *S. cerevisiae* as they are mammalian cells, the study was extended to elucidate whether the Sty1 MAPK pathway of *S. pombe* was also involved in regulating lipid homeostasis. A strain containing a deletion of the upstream MAPKK, *wis1* was screened along with a *sty1* deletion strain and a Sty1 Kinase dead mutant which is able to be phosphorylated and translocate to the nucleus. However, once in the nucleus the kinase dead mutant is unable to activate its downstream targets (Reiter *et al.* 2008). Deletions in two of the main downstream targets of Sty1p in the stress response, *atf1* and *pap1* were also screened to elucidate whether downstream members of this stress response pathway were involved in the regulation of lipid accumulation.

### 4.4.1 Lipid accumulation is attenuated upon deletion of sty1 and its upstream MAPKK wis1

The *S. pombe* MAPK protein Sty1p has been well characterised and is well conserved to both *S. cerevisiae* Hog1p and the mammalian p38 MAP Kinase. To determine if the Sty1 MAPK pathway in *S. cerevisiae* has a role in lipid accumulation, neutral and polar lipid levels were examined in *wis1* and *sty1* deletion strains along with a *sty1-KD* mutant using the Nile red assay.

Growth curves were conducted to ensure samples from wild type, *wis1Δ, sty1Δ* and *sty1-KD* strains had comparable growth phases. As shown in Figure 4.45, cells deleted for *wis1* had a longer lag phase than wild type cells. Wild type cells typically entered exponential growth 10 hrs post resuspension in EMM, whereas *wis1* deleted cells lag for approximately a further 3 hrs before entering the exponential phase. Although the *wis1Δ* entered stationary phase at a similar cell density and at the same point as wild type cells, at 24 hrs, it is important to note that up until stationary phase cells lacking *wis1* failed to reach an equivalent cell density to that of wild type cells.

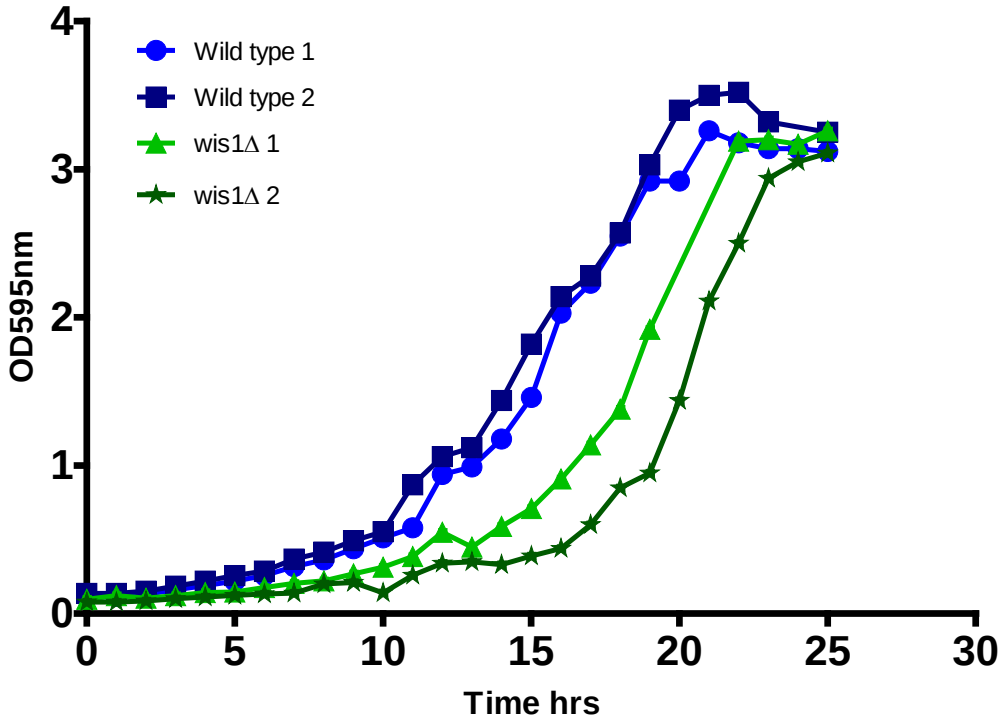


**Figure 4.45: Growth curve of *S. pombe* wild type and *wis1Δ* under normal conditions in Edinburgh minimal medium (EMM).** Cultures were diluted to 2 x $10^6$ cells ($OD_{595}$ ~0.1) and incubated with shaking, duplicate, at 30°C. Optical density readings were taken hourly until stationary phase was reached. Growth curves were conducted in duplicate (culture 1 and culture 2 for both WT and deletion strain) showing growth patterns observed for two distinct colonies of the same strain.

In cells lacking *sty1*, Figure 4.46, exponential growth began at an equivalent time point to wild type cells at 10 hrs. Although the *sty1Δ* also failed to reach an equivalent cell density until the point of stationary phase at 24 hrs, the growth defect observed was not as severe as that of the *wis1Δ* strain.

The *sty1*-kinase dead mutant displayed a similar growth pattern to that of cells deleted for *sty1*, although reached a lower cell density during exponential growth until stationary phase was achieved at 24 hrs (Figure 4.47).

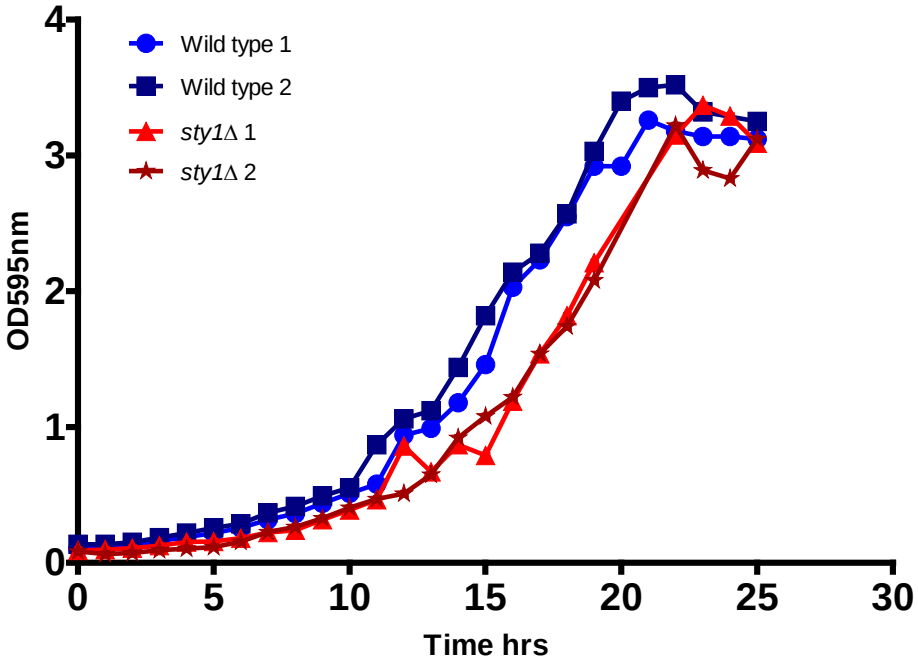


**Figure 4.46: Growth curve of *S. pombe* wild type and *sty1Δ* under normal conditions in Edinburgh minimal medium (EMM).** Cultures were diluted to 2 x $10^6$ cells ($OD_{595}$ ~0.1) and incubated with shaking, duplicate, at 30°C. Optical density readings were taken hourly until stationary phase was reached. Growth curves were conducted in duplicate (culture 1 and culture 2 for both WT and deletion strain) showing growth patterns observed for two distinct colonies of the same strain.

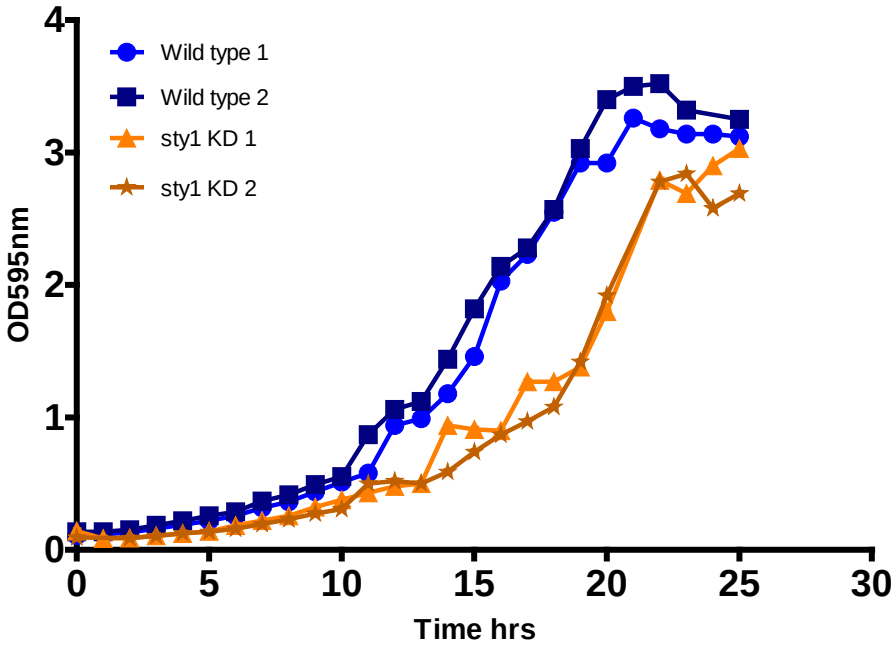


**Figure 4.47: Growth curve of *S. pombe* wild type and Sty1 kinase dead mutant under normal conditions in Edinburgh minimal medium (EMM).** Cultures were diluted to 2 x $10^6$ cells ($OD_{595}$ ~0.1) and incubated with shaking, duplicate, at 30°C. Optical density readings were taken hourly until stationary phase was reached. Growth curves were conducted in duplicate (culture 1 and culture 2 for both WT and deletion strain) showing growth patterns observed for two distinct colonies of the same strain.

The results of Nile red screening to infer the neutral lipid status at early stationary phase demonstrated that neutral lipid accumulation was significantly perturbed in both the *wis1* and *sty1* deletion strains. The *wis1Δ* exhibited a 2 fold decrease and the *sty1Δ* a 1.9 fold decrease compared to wild type cells. The *sty1-KD* mutant also accumulated significantly lower levels of neutral lipids, 1.3 fold decrease, compared to the wild type strain although the phenotype observed was not as severe as in the *sty1* deletion strain (Figure 4.48).

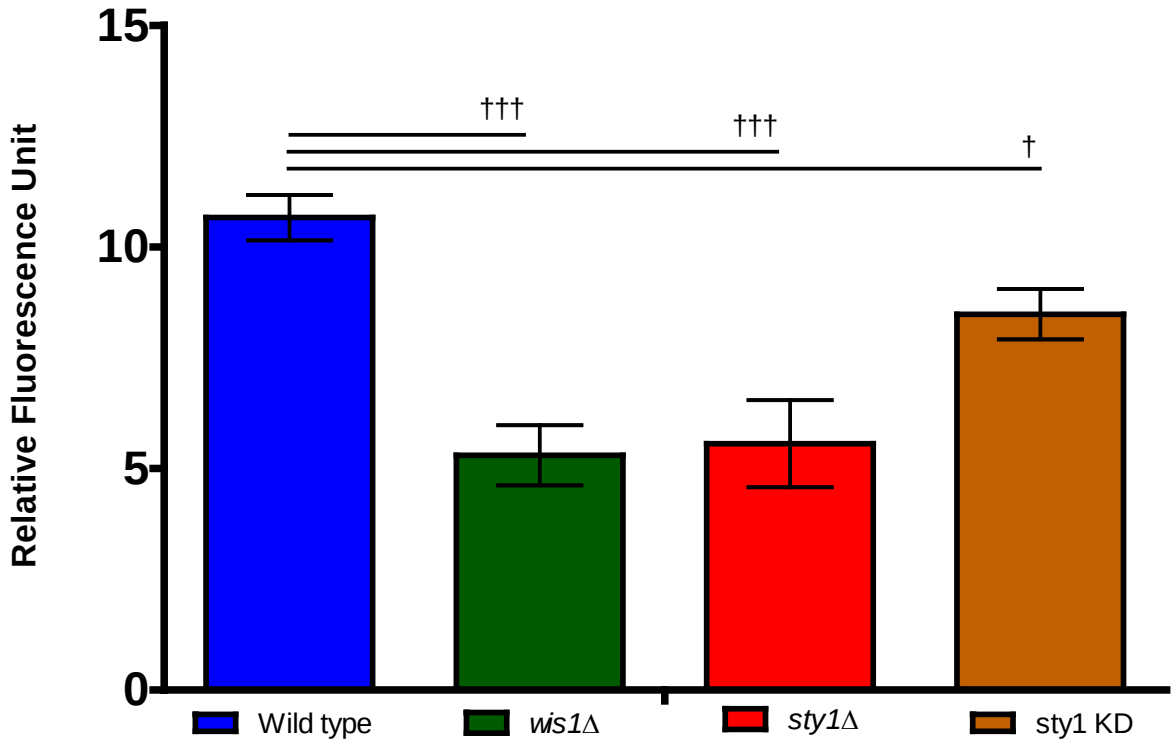


**Figure 4.48: Neutral lipid fluorescence intensity of Nile red stained *S. pombe* wild type and MAPK pathway mutants.** Cells were harvested at 24 hrs post resuspension in EMM. Cells were washed twice in PBS before adjusting to a cell density of 2 x $10^7$ cells/ml. 5 x $10^6$ cells were transferred to the wells of black 96-well plates in triplicate. 25µl PBS/DMSO (1:1 v/v) and 5µg/ml Nile red were added to each sample. Plates were screened using the wavelengths: excitation 485nm, emission 535nm. Data shown as means of triplicates ±SD. Significance between strains is indicated by solid black lines † $p<0.05$, ††† $p\leq0.001$. Data analysed by one way ANOVA with Tukey *post hoc* test.

For screening to identify more polar lipid subtypes accumulation was similarly attenuated in both the *wis1* and *sty1* deletion strains with both displaying a 1.8 fold decrease. Although a reduction of 1.3 fold was observed for the *sty1-KD* mutant, this failed to reach significance when compared to wild type cells (Figure 4.49).

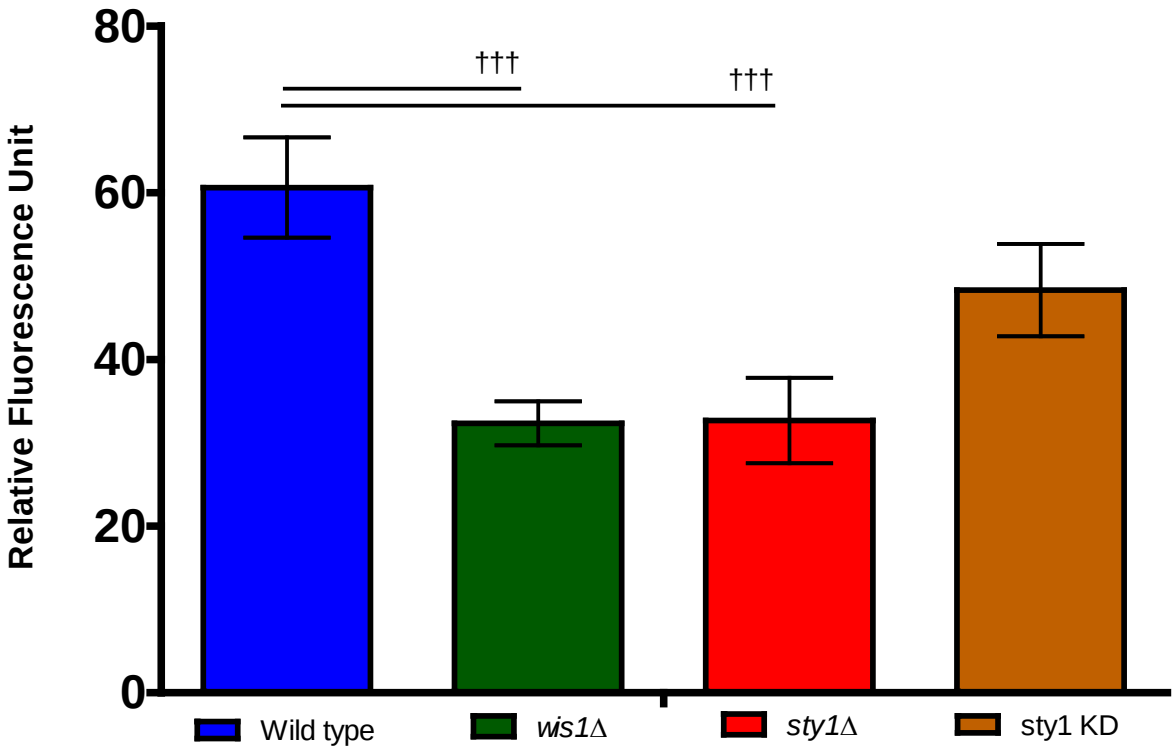


**Figure 4.49: Polar lipid fluorescence intensity of Nile red stained *S. pombe* wild type and MAPK pathway mutants.** Cells were harvested at 24 hours post resuspension in EMM for early stationary phase samples. Cells were washed twice in PBS before adjusting to a cell density of 2 x $10^7$ cells/ml. 5 x $10^6$ cells were transferred to the wells of black 96-well plates in triplicate. 25µl PBS/DMSO (1:1 v/v) and 5µg/ml Nile red were added to each sample. Plates were screened using the wavelengths: excitation 535nm, emission 590nm. Data shown as means of triplicates ±SD. Significance between strains is indicated by solid black lines ††† p≤0.001. Data analysed by one way ANOVA with Tukey *post hoc* test.

### 4.4.1.1 Viability of S. pombe MAPK deletions at stationary phase

It is reported that Sty1p is required for entry into stationary phase and mutants in Sty1 MAPK pathway lose viability at stationary phase (Shieh *et al.* 1998). As such, viability of cells deleted for *wis1* and *sty1* were determined at the 24hr time point by methylene blue on duplicate cultures.

Figure 4.50 shows the results of cell viability in early stationary phase, determined from methylene blue staining. Wild type cells had an average of 98% viability at the 24hr stationary phase time point. Samples from cultures of the *sty1* deleted strain had percentage viability within 10% of that of wild type cells at 91.5% (93% and 90%). However, the viability of cultures where cells were deleted for *wis1* was less clear. The average viability of these samples was 86% with one sample being found 81% viable and the other 91% viable.

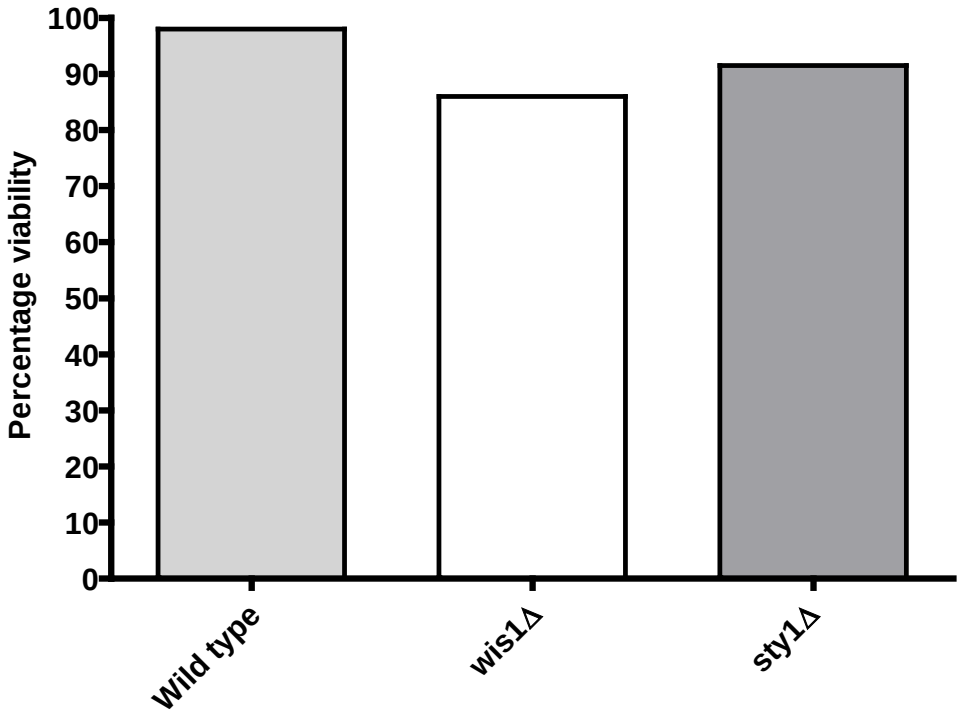


**Figure 4.50: Percentage viability of *wis1* and *sty1* deleted cells compared to cells from wild type cultures.** Samples were harvested at the 24 hr time point utilised for Nile red screening. Methylene blue stain was added to cultures at a 1:1 ratio and incubated for 5 minutes at room temperature. Cells were counted on a haemocytometer. Cells stained blue were counted as non-viable cells. Average percentage viability is displayed as means from duplicate cultures.

### 4.4.2 The stress response of S. pombe aligns with altered lipid phenotypes

As the (Sty1) MAPK pathway is involved in the response of cells to conditions of stress, a stress experiment was conducted of upstream components of the MAPK pathway. This was undertaken to assess whether the lipid phenotypes of cells deleted for *wis1* and *sty1* could potentially have resulted as a consequence of the stress response.

It has been previously shown that strains deleted for *wis1* and *sty1* are sensitive to oxidative stress ($H_20_2$). Figure 4.51 shows that cells lacking *wis1* and *sty1* were more sensitive to oxidative stress when compared to wild type. It is further demonstrated that the *sty1-KD* mutant displayed increased resistance compared to the *sty1Δ* in the presence of oxidative stress. From this it can be concluded that the stress sensitivity of these mutants did align with the lipid phenotypes observed. This is in contrast to *S. cerevisiae*, where it was shown that the stress response of deletion mutants did not align with the observed lipid phenotypes.

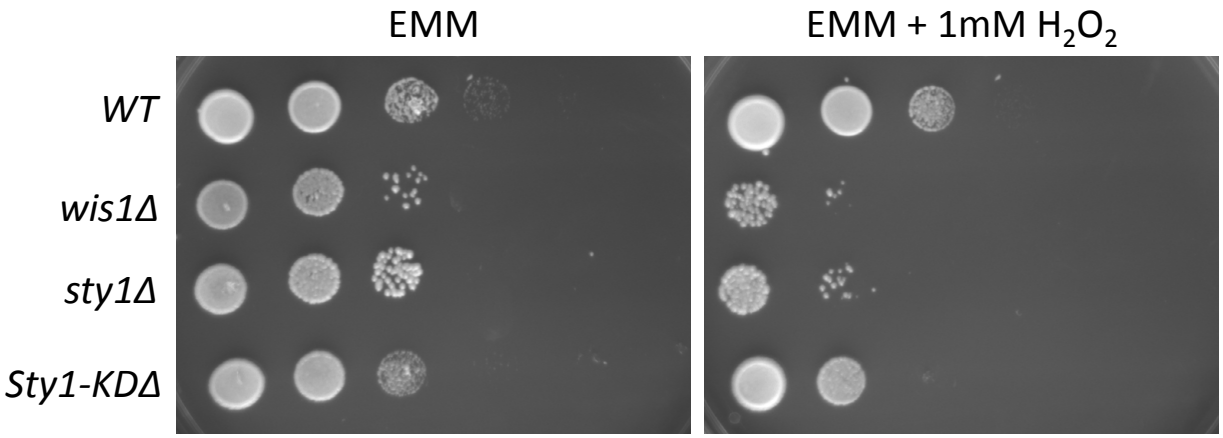


**Figure 4.51: Spot plates of *S. pombe* wild type, *wis1Δ*, *sty1Δ* and Sty1-KD.** Control plates (EMM) and oxidative stress plates, EMM supplemented with 1mM hydrogen peroxide ($H_2O_2$). Starting cell densities were ~2.3 x $10^7$ cells/ml before being serially diluted 1:10 across the plate down to 2.3 x $10^2$ cells/ml.

### 4.4.3 Atf1 and Pap1, downstream targets of Sty1, do not play a significant role in lipid accumulation

To characterise whether the lipid accumulation phenotypes extend downstream of the MAPK Sty1, the Nile red assay was performed on downstream targets of Sty1p to assess whether the transcription factors Aft1 and Pap1 contributed to the accumulation of lipids. Growth curves were conducted to ensure cells were in a comparable phase of growth before performing Nile red (Figures 4.52 and 4.53).

As demonstrated by Figures 4.52 and 4.53, after an initial lag phase of 10 hrs the deletion strains and wild type cells entered exponential growth, until early stationary phase was achieved at 24 hrs.

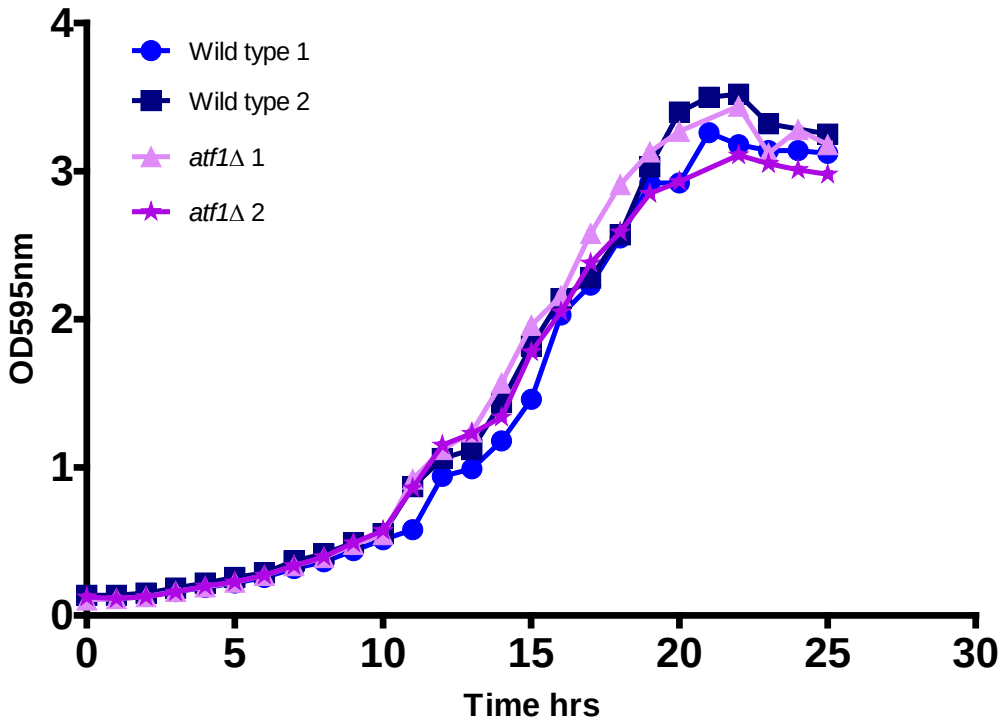


**Figure 4.52: Growth curve of *S. pombe* wild type and *aft1Δ* under normal conditions in Edinburgh minimal medium (EMM).** Cultures were diluted to 2 x $10^6$ cells ($OD_{595}$ ~0.1) and incubated with shaking, duplicate, at 30°C. Optical density readings were taken hourly until stationary phase was reached. Growth curves were conducted in duplicate (culture 1 and culture 2 for both WT and deletion strain) showing growth patterns observed for two distinct colonies of the same strain.

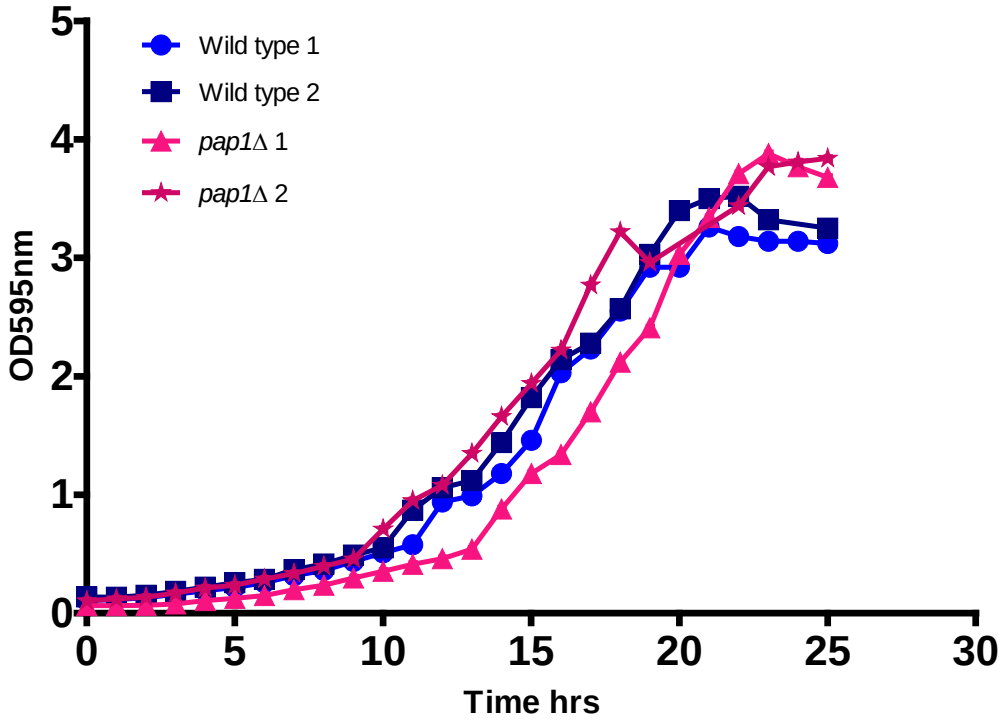


**Figure 4.53: Growth curve of *S. pombe* wild type and *pap1Δ* under normal conditions in Edinburgh minimal medium (EMM).** Cultures were diluted to 2 x $10^6$ cells ($OD_{595}$ ~0.1) and incubated with shaking, duplicate, at 30°C. Optical density readings were taken hourly until stationary phase was reached. Growth curves were conducted in duplicate (culture 1 and culture 2 for both WT and deletion strain) showing growth patterns observed for two distinct colonies of the same strain.

Figure 4.54 shows the results of the Nile red assay to assess neutral lipid status. Although changes failed to reach significance when compared to wild type, the *atf1Δ* displayed a 1.2 fold decrease and *pap1Δ* cells a 1.1 fold decrease in fluorescence intensity.

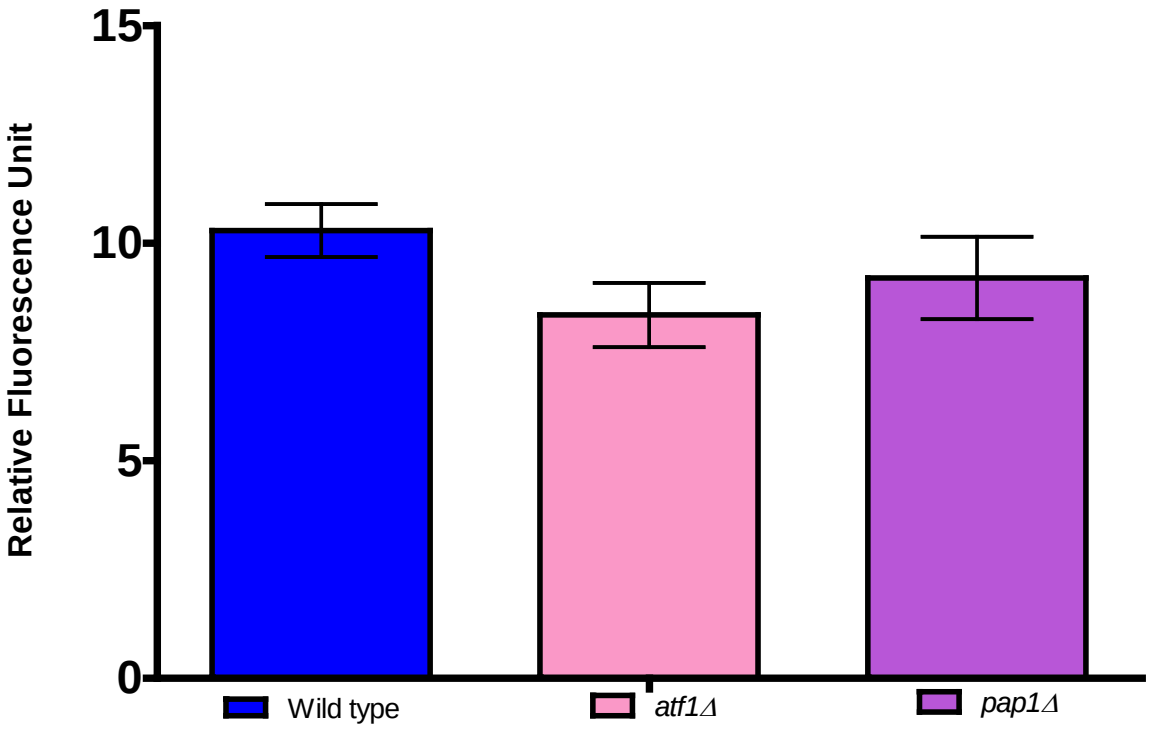


**Figure 4.54: Neutral lipid fluorescence intensity of Nile red stained *S. pombe* wild type and transcription factor mutants.** Cells were harvested at 24 hours post resuspension in EMM for early stationary phase samples. Cells were washed twice in PBS before adjusting to a cell density of 2 x $10^7$ cells/ml. 5 x $10^6$ cells were transferred to the wells of black 96-well plates in triplicate. 25µl PBS/DMSO (1:1 v/v) and 5µg/ml Nile red were added to each sample. Plates were screened using the wavelengths: excitation 485nm, emission 535nm. Data shown as means of triplicates ±SD. Data analysed by one way ANOVA with Tukey *post hoc* test.

In cells lacking *aft1* and *pap1* significant differences were detected when samples were screened using the wavelength attributed to more polar lipids by Nile red. (Figure 4.55).

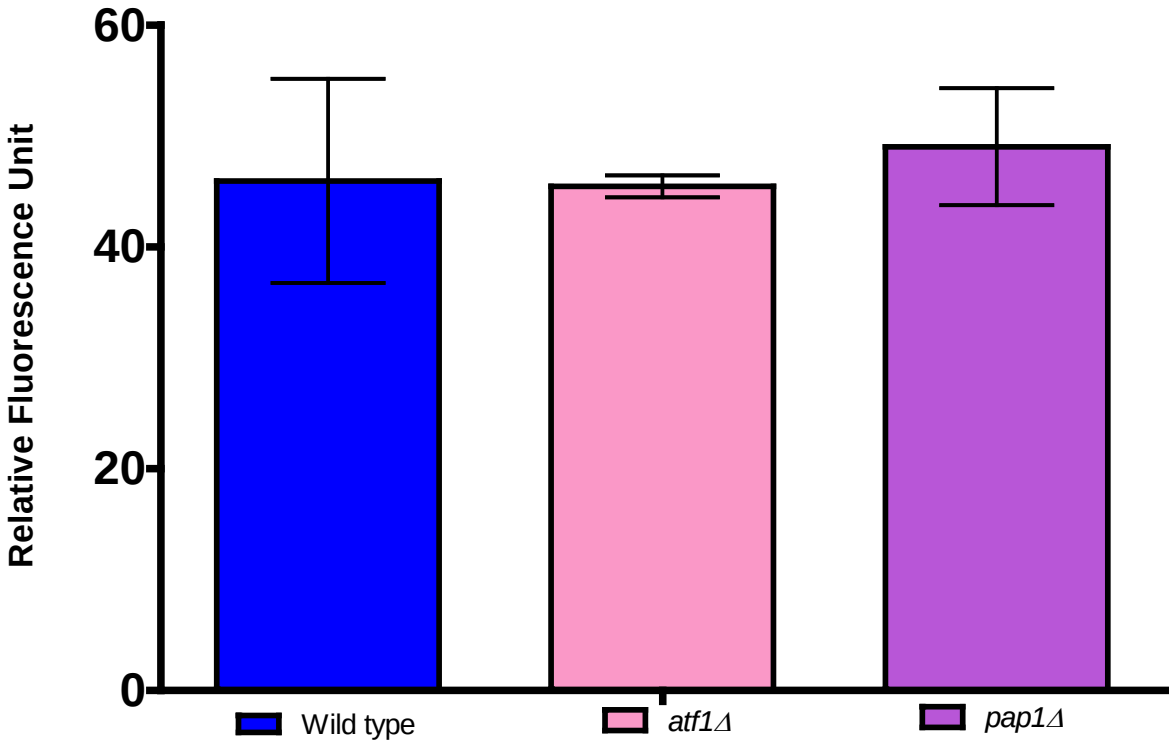


**Figure 4.55: Polar lipid fluorescence intensity of Nile red stained *S. pombe* wild type and transcription factor mutants.** Cells were harvested at 24 hours post resuspension in EMM for early stationary phase samples. Cells were washed twice in PBS before adjusting to a cell density of 2 x $10^7$ cells/ml. 5 x $10^6$ cells were transferred to the wells of black 96-well plates in triplicate. 25µl PBS/DMSO (1:1 v/v) and 5µg/ml Nile red were added to each sample. Plates were screened using the wavelengths: excitation 535nm, emission 590nm. Data shown as means of triplicates ±SD. Data analysed by one way ANOVA with Tukey *post hoc* test.

This data suggests that the downstream Sty1 targets, Atf1 and Pap1, did not hold a significant role in the regulation of lipid accumulation in *S. pombe.*

### 4.4.4 Potential MAPK sites on S. pombe lipid regulatory proteins is conserved to that of S. cerevisiae

To elucidate whether the potential MAPK sites identified for *S. cerevisiae* were conserved in *S. pombe,* Uniprot was utilised to search for potential MAPK sites with *S. pombe* protein sequences. After analysis of the protein sequences via UniProt, it was found that Dga1p has one potential MAPK phosphorylation sites within the N terminus of the protein sequence, Figure 4.56.


MSEETSIPGIIAS**T**PPISKDSRRNVSHWLQALAVFLHSVSLTLTASWYTVLWAFLPFWPF
LIVYLIWLIYDDGFVTGKDRQKRWLRNAPPYRWFCHYFPIRLHKTTELDSEKNYIFGYHP
HGIISLGAFGGFASEGADFSKLFPGINVSVLTLNSNFYVPVYRDYLMALNINSVSKKSCV
SILSRKPGDSVLIVIGGAQESLLSRPGQNNLVLKKRFGFVKLAFLTGSSLVPCFAFGESD
IFEQVDNNPRTRIYKFQEIVKKIAGFTVPFFYGRGLLNKTFGLMPWRKPINIVVGEPIDV
PKKSHPTNQEIYEVHEEYIRRLEGLWNKYKDVFLPNRISELKLSA

**Figure 4.56: The protein sequence of Dga1p contains a potential MAPK phosphorylation site.** Identification of a potential MAPK phosphorylation site within the N terminus of Dga1p. Phosphorylation sites are indicated on the graphical diagram and in yellow within the protein sequence. Phosphorylation sites were determined from data curated by Uniprot and PomBase genome database.

The Lro1p homologue in *S. pombe,* Plh1 was found to contain two potential phosphorylation sites within the N terminus of the protein sequence (Figure 4.57).


MASSKKSKTHKKKKEVKSPIDLPNSKKPTRALSEQPSASETQSVSNKSRKSKFGKRLNFI
LGAILGICGAFFFAVGDDNAVFDPATLDKFGNMLGSSDLFDDIKGYLSYNVFKDAPFTTD
KPSQSPSGNEVQVGLDMYNEGYRSDHPVIMVPGVISSGLESWSFNNCSIPYFRKRLWGSW
SMLKAMFLDKQCWLEHLMLDKKTGLDPKGIKLRAAQGFEAADFFITGYWIWSKVIENLAA
IGYEPNNMLSASYDWRLSYANLEERDKYFSKLKMFIEYSNIVHKKKVVLISHSMGSQVTY
YFFKWVEAEGYGNGGPTWVNDHIEAFINISGSLIGAPKTVAALLSGEMKDTAQLNQFSVY
GLEKFFSRSERAMMVRTMGGVSSMLPKGGDVVWGNASWAPDDLNQTNFSNGAIIRYREDI
DKDHDEFDIDDALQFLKNVTDDDFKVMLAKNYSHGLAWTEKEVLKNNEMPSKWINPLETS
LPYAPDMKIYCVHGVGKPTERGYYYTNNPEGQPVIDSSVNDGTKVENGIVMDDGDGTLPI
LALGLVCNKVWQTKRFNPANTSITNYEIKHEPAAFDLRGGPRSAEHVDILGHSELNEIIL
KVSSGHGDSVPNRYISDIQEIINEINLDKPRN

**Figure 4.57: The protein sequence of Plh1p contains potential MAPK phosphorylation sites.** Identification of potential MAPK phosphorylation sites within the N terminus of Plh1p. Phosphorylation sites are indicated on the graphical diagram and in yellow within the protein sequence. Phosphorylation sites were determined from data curated by Uniprot and PomBase genome database.

*S. pombe* Pps1p (Cho1p homologue) was found to contain 4 potential phosphorylation sites (Figure 4.58).

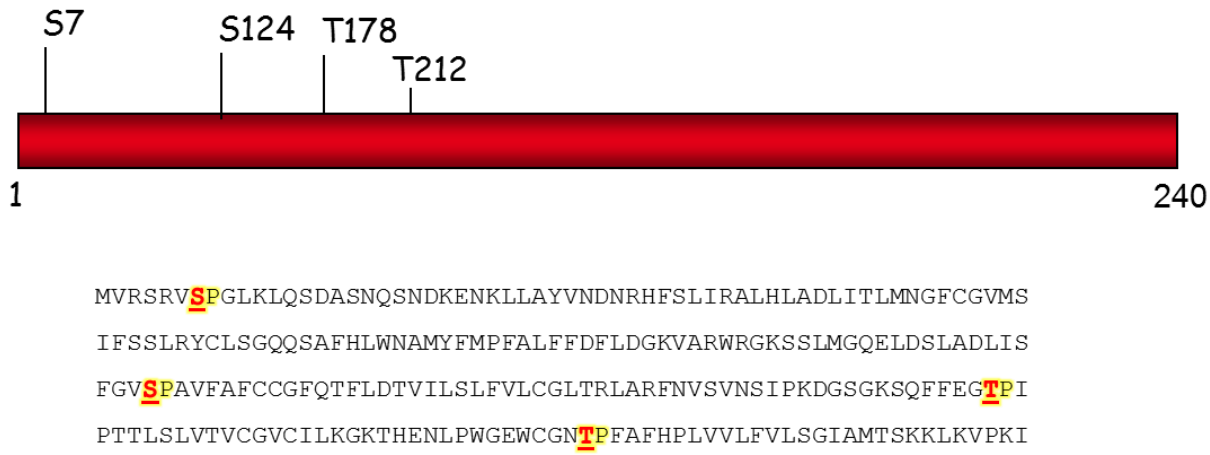


**Figure 4.58: The protein sequence of Pps1p contains potential MAPK phosphorylation sites.** Identification of potential MAPK phosphorylation sites within the protein sequence of Pps1p. Phosphorylation sites are indicated on the graphical diagram and in yellow within the protein sequence. Phosphorylation sites were determined from data curated by Uniprot and PomBase genome database.

The SREBP homologues of *S. pombe* were found to contain multiple potential MAPK phosphorylation sites throughout their protein sequences. The N terminus of Sre1p was found to be more enriched with sites than the C terminal region (Figure 4.59).


MQSSIPSVSVSVASPAMETPTKASPDSKSPNSVGAIPSSSPLASSTKASTSTPFVENCSN
LLCDLASIVEDSPPTLTNTSLSPHSFSLSDMESSMSNWLNPFAFDNTMNSAPPLFTSTNM
GSPNSLENSTNPLLSNCGSPNSFQNETFTGPSLNEFDADDKIQRQMKILHSVDTIDPSTV
QNYPSADMSNPEVKLKTEEIITPMDTTCKPEPSAKKIKLSPSSEDSCSIPETLPFSAPKS
RGSLSPSETPDFVAGPGGKPKKTAHNMIEKRYRTNLNDRICELRDAVPSLRAAAALRCGN
SLDDEDLGGLTPARKLNKGTILAKATEYIRHLEAKNKELQKTNKQLSDRLAFYEDPSMAP
PSNDTRAVNSVNVVSSSDYSVHQSSRPNLTQRAFTSPTLNTMGRTALNGMVGLGLFNYFG
NDSSQSVYGLFALPPFLMSPFTGTVLFNMLKIGVVLLGLFYLLHDNSLFKGFKGEKKSKV
STRSSMSPSSILFRKTVFEKYCLLDHSTSTISLFFGLLIFTLKSAYGYLTHRLSALYTSS
ENWVYSEQQLAEVRNMEKLLDAQLMGGDAKVDRLRLLMVFASSFSLPPSSHTCALQAMYC
QLIFSNTSVPSAIVSKCVAFFWNAAKKQHSKSSVHAELRELPECTANLIENSHADDVFSP
NMVERLWVLAKCTRDSAQMSDSIISSLSDVLVLSPLEVLASWYAADLLDALLMESLSRKV
EISEIEEIISLCPKNSSIIRHALLAKLVLFPENTADSLNEVLAAYKNTLDLCSQDKRKQS
SVLKINLSKLFTLHSCLSLALQRLGYGDVSKRMYQEIFVPDSDADITPLSFIISWTALNT
FAPICTSPKENDVVEKMAMYVRTAIGTLKIQDLKLSRKLINSCIDIGSRLQEDLGYVSSA

**Figure 4.59: The protein sequence of Sre1p contains potential MAPK phosphorylation sites.** Identification of potential MAPK phosphorylation sites within the protein sequence of Sre1p. Phosphorylation sites are indicated on the graphical diagram and in yellow within the protein sequence. Phosphorylation sites were determined from data curated by Uniprot and PomBase genome database.

As shown by Figure 4.60, the protein sequence of Sre2p also contained multiple potential MAPK sites, although not as many in comparison to Sre1 (19 sites versus 12 sites).

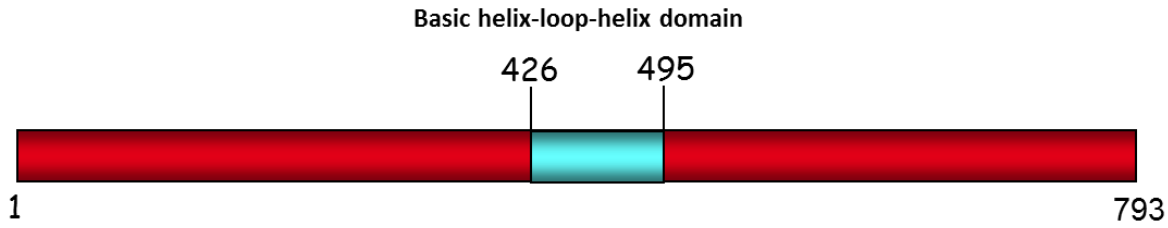


MCPSQHSSLKDIHRQLENTAISNPTENADPSSYVDGSNIMDFKHPSIVSSSASSSYPISH
VPSVGTRGIPRSYSMASAYPYQVNSNSMDASTAFNLNQDVADKPMLARNSIDSSINTELG
PLESNHWFTQAQDHSRQYSSSWDPSIDPFEVKNSLHDSTDLSITHHPHLPINHQGNTWKH
ANESLQSNQGPVPNTKFVGLETTQTDSYQQSSVNSVVKIEEADATYALREESGQFNTFTG
AENPSISPHSLNPNFPQYTEKPALTLLQSPKQNSNYDTSNFQNSVSDSSMQFTNEGMPSP
VKGIMSSDDAVAFNFSQYSTVYPQNAPENGNEFETPNKLKRTVSSPCASISSKRSYGDIA
QDCSYISSKTNGGGPSDSPSSSSTSVRGSVNDSNSPISSSATFAIQSNGVEPVGLSTQEQ
NLSPLSKRSAHNMIEKRYRSNLNDKIAELRDAVPTLRSGYNSTTADELKGTYVPLSRKLN
KATILSKATEYIKSLQSKNKKLIEENKILQKRLSEYTSVIQASLTAPSQPASLSLLGPPG
NTPGHRNVPPILKRSSIGTPSQQAYFPDAPHNCHSVPQNSSYPRPPMQVNRSPIDSMQTI
PHANFNEMHNAYSSRYPLKYSKSCNAVSHTSMMHPQEYGGSLPSSTVPSDYNQPQLVSPR
AQADQQGLSYKNVGRAVLNGLVGLETVHMLTNPDDAGSSNRFSMSVLPISPSLHSILRFL
LLLLAFLCFAMHILLTPEATLRKWASSIYLSFRLECVFISFLIFSVPIYDWGNYLNLRGK
LLSELNLESGVAT

**Figure 4.60: The protein sequence of Sre2p contains potential MAPK phosphorylation sites** Identification of potential MAPK phosphorylation sites within the protein sequence of Sre2p. Phosphorylation sites are indicated on the graphical diagram and in yellow within the protein sequence. Phosphorylation sites were determined from data curated by Uniprot and PomBase genome database.

From analysis of the protein sequences indicating potential MAPK phosphorylation sites, it may be suggested that the potential targets of Hog1p in the regulation of lipid accumulation are similarly conserved in *S. pombe*.

## 4.5 Discussion

In this chapter the aim was to elucidate whether the p38 MAP Kinase pathway, which is also commonly de-regulated in cancer and highly conserved in yeast, could play a role in mediating cancer-related *de novo* lipogenesis. Nile red screening was initially conducted on deletions from the TOR pathway, as mTORC1 has been demonstrated to be a key upstream regulator of the synthesis of lipid in mammalian cells. mTORC1 signalling, driven by Akt, results in upregulation of SREBP-1 activity contributing to the synthesis of lipids (Laplante and Sabatini 2009b). In a study by Portsmann *et al.* (2008) it was found that inhibition of mTORC1, blocked Akt induced nuclear localisation of SREBP-1, indicating that SREBP activation is dependent on mTORC1 activity (Porstmann *et al.* 2008).

The Nile red screening conducted on *S. cerevisiae* Tor component deletions showed that levels of lipid, particularly neutral lipids, were reduced in the *tor1* deletion strain (Figures 4.44 and 4.45). This highlighted a role for Tor1p in lipid synthesis in *S. cerevisiae*, which is consistent with the observation in mammalian cells that mTORC1 regulates the synthesis of lipids (Porstmann *et al.* 2008). Although not significant, an increased neutral lipid phenotype was also observed when the Tor1 complex was deleted for Tco89 (Figure 4.44). Tco89p has been shown to be involved in the packaging of enzymes/proteins into vacuoles for subsequent degradation. One such enzyme is fructose 1,6-biphosphatase (FBPase), a key enzyme of the gluconeogenic pathway. It has been described that Tco89p presence is essential for vacuole import and degradation of FBPase (Yan and Kang 2010). Therefore inefficient degradation of FBPase may contribute to increased lipid accumulation through production of glycolytic intermediates (Ros and Schulze 2013). Tor2p has not been demonstrated to play a significant role in the synthesis of lipids. The results of the Nile red assay confirmed this, demonstrating that deletion of *AVO2* did not result in a significantly different lipid phenotype from that of wild type cells (Figures 4.44 and 4.45).

Using the Nile red assay it was established that neutral and phospholipid phenotypes could be distinguished between when screening deletions of Tor components based on the fluorescence values obtained of the deletion strains compared to wild type cells.

To assess whether the HOG MAPK pathway of *S. cerevisiae* was also involved in regulation of lipid homeostasis, wild type and *hog1Δ* strains were screened via Nile red. The Nile red screening of the MAP kinase from the HOG pathway in *S. cerevisiae* revealed a decreased neutral and phospholipid phenotype of the *hog1Δ* compared to wild type (Figures 4.7 and 4.8). Upon complementation of *hog1* deleted cells with pRS315*HOG1* the stress sensitive phenotype of the *hog1Δ* to NaCl was recovered to that of wild type levels (Figure 4.9). However, upon transferring transformed cells to culture in order to assess if the lipid phenotype could be restored the Nile red data was inconsistent. In the case of the *hog1Δ* transformed with empty vector, pRS315, a significantly increased lipid phenotype was observed (Figures 4.10 and 4.11). As inconsistencies persisted, even after re-transformation of the cells (Figures 4.12 and 4.13), it was suggested that the lipid phenotype was the result of the pRS315 leucine based vector. This was further supported by the work of Kamisaka *et al.* (2007), in which a similar phenomenon occurred in the *S. cerevisiae snf2Δ* strain. When cells deleted for *snf2* were transformed with an empty leucine vector they displayed significantly increased lipid accumulation of ~1.3 fold, which was not seen in cells transformed with an empty vector containing the *URA3* marker. The phenotype observed with the empty *LEU2* vector could also be replicated by adding large amounts of leucine to the growth medium of *snf2Δ* cultures. It was found that the exogenous leucine initially acted to increase cellular weight prior to accumulation of lipid and so confirmed that leucine biosynthesis, as a consequence of *LEU2* expression from pRS315, caused enhanced lipid accumulation (Kamisaka *et al.* 2007).

The impact of leucine expression on lipid accumulation may be explained via two mechanisms. Firstly it is suggested that excessive leucine expression may impact on and subsequently upregulate TOR signalling, as TOR serves as a nutrient and amino acid sensor (Gran and Cameron-Smith 2011). Secondly, expression of leucine may serve to increase levels of glutamate production in *S. cerevisiae* (Kohlhaw 2003) which may serve to stimulate lipid accumulation via glycolysis (Dang 2012, Pellerin and Magistretti 1994).

The pRS315 vector was subsequently replaced with pRS313, which contains histidine as the selectable marker. There is no literature to suggest that the expression of *HIS3* would affect the lipid phenotype of the cell. After transformation of wild type and *hog1Δ* cells with pRS313 and pRS313*HOG1*, the stress phenotype of the *hog1Δ* strain was recovered to that of wild type levels (Figure 4.14). After transferring to culture, the results of the

Nile red screen showed that the lipid phenotype of the *hog1Δ* strain containing the empty vector remained low compared to that of wild type cells (Figures 4.16 and 4.17). Wild type cells which were transformed with pRS313*HOG1*, displayed levels of lipid comparable to that of wild type cells containing pRS313. This is likely due to feedback mechanisms in wild type cells transformed with pRS313*HOG1* to ensure Hog1p is not overexpressed, which results in lethality of *S. cerevisiae* cells (Wurgler-Murphy *et al.* 1997). This confirmed that the reduction in lipids compared to wild type cells was as a consequence of the loss of Hog1, and suggested that Hog1 function is required for cellular lipid homeostasis in *S. cerevisiae*. In addition, from this data, it can also be concluded that expression of *HIS3* does not impact on lipid accumulation in *S. cerevisiae.*

The Nile red data for components of the MAPK pathway upstream of Hog1 demonstrated that deletions in *SHO1*, *STE11*, and *PBS2* did not produce a significant change in neutral levels of lipid nor phospholipids (Figures 4.21 and 4.22). This suggested that upstream components of the HOG pathway did not play a key role in the accumulation of lipids in *S. cerevisiae.* Pbs2p is required for dual phosphorylation and thus activation of Hog1p. As the levels of lipid in the *pbs2Δ* appeared unaffected it is unlikely that Pbs2p holds a major role in regulating lipid accumulation.

It has been reported recently, via a large scale lipidomic study which utilised monitoring mass spectrometry for sphingolipid/phospholipid analysis coupled with GC-MS for sterol analysis, that both *pbs2* and *hog1* deleted cells have increased levels of sphingolipids and ceramides, which are both minor lipid components of cell walls and membranes (da Silveira Dos Santos *et al.* 2014). However, the samples in the aforementioned study were harvested in early exponential phase. As an absence of *HOG1* results in a delayed resting exit compared to wild type cells (Escoté *et al.* 2011), this means that wild type and mutant cells may not have been harvested at comparable points and the *hog1Δ* may have induced an accumulation of such lipid classes due to delayed active exponential division. Similarly, resting exit delays have also been observed in cells lacking *PBS2* (Escoté *et al.* 2011). Furthermore, as ceramide and sphingolipids represent a relatively minor proportion of cellular lipid, any increase of these lipid classes would likely be beyond the limits of detection of the Nile red assay employed by the present study.

Of the downstream targets of Hog1p, the *hot1* deletion strain did not display an altered lipid accumulation phenotype for neutral or phospholipids; this suggested that the transcription factor Hot1p was not involved in regulation of lipid homeostasis (Figures 4.25 and 4.26). Conversely, a neutral lipid phenotype was seen in the *msn2/4*Δ and suggested that Msn2/4p was involved in neutral lipid accumulation, potentially through Hog1p mediated signalling (Figure 4.25). No significantly altered phospholipid phenotype was observed in the *msn2/4* mutant, which demonstrated that synthesis of neutral lipids by the HOG pathway may proceed via the transcription factors Msn2/4 (Figure 4.26). This implied that Msn2 and Msn4 may specifically regulate the production of neutral lipids. It is unknown whether Msn2/4 are directly activated by Hog1 to drive the accumulation of neutral lipid species, however, as Msn2/4 shuttle between the cytoplasm and nucleus it is possible that Hog1 could activate Msn2/4 localised within the cytoplasm.

It is well characterised that *HOG1* deleted cells are sensitive to osmotic stress conditions (Kim Sungjoon and Shah 2007). The data presented in Section 4.2.7 proposed that the lipid phenotypes observed in both the *hog1Δ* and *msn2/4Δ* were not a consequence of the stress response (Figure 4.27). Specifically, the *msn2/4Δ* was not sensitive to osmotic stress when compared with wild type, yet exhibited a significant reduction in the amount of neutral lipids accumulated. Additionally when cells were deleted for *pbs2*, they exhibited equal osmotic stress sensitivity to cells that were deleted for *HOG1,* yet were able to accumulate wild type levels of lipid. This suggested that regulation of lipid accumulation via the Hog1 pathway in *S. cerevisiae* was independent from the stress response.

It is reported that *HOG1* deleted cells do not lose viability in stationary phase (Escoté *et al.* 2011). However, as cells lacking *HOG1* display a delay in exiting from the resting state compared to wild type cells, a delayed lipid accumulation response was ruled out by conducting a time course of lipid accumulation across all growth phases. This data demonstrated that lipid accumulation was not delayed in the *hog1*Δ strain. At each point from 8hrs post resuspension until late stationary phase, the *hog1Δ* failed to accumulate lipid in amounts comparable to that of wild type cells. Although cells deficient for *HOG1* failed to accumulate equivalent levels of lipid to that of wild type cells, the general trend of increased lipid amounts into stationary phase before a decrease at late stationary phase was conserved (Figures 4.28 and 4.29).

Activation of Hog1 via the canonical route requires dual phosphorylation on Threonine-174 and Tyrosine-176 residues by Pbs2 (Alonso *et al.* 2007). Dually phosphorylated Hog1p was present at 6 and 7 hrs post resuspension in YNB medium (Figure 4.31). It is suggested that this is due to cells undergoing the transition from lag phase into exponential phase, as growth phase-dependent activation of Hog1 has been documented (Escoté *et al.* 2011). *S. cerevisiae* showed a marked increase in the accumulation of lipid after 8 hrs post resuspension in YNB (Figure 4.28), indicating that if Hog1 activation is required for lipid accumulation it may occur between 8 and 12 hrs.

The dually phosphorylated form of Hog1 was observed at 9 hrs by Western blot analysis; as such this activation may be concomitant with the point of the lipogenic switch (Figure 4.31). However, it is also possible that this activation is attributed to the cells response to a change in growth phase or nutrient limitation at the onset of stationary phase. This is suggested as Pbs2 did not appear to be involved in the accumulation of lipid. This idea is further supported as it has been documented in both *S. cerevisiae* and *S. pombe* that nutrient limitation induces dual phosphorylation of both Hog1p and Sty1p (Aoki Yoshimasa *et al.* 2011a, Smith *et al.* 2002, Zuin *et al.* 2010a).

Data within this chapter suggested that nutrient starvation, both nitrogen and carbon, did not result in the dual phosphorylation of Hog1p, as phosphorylation of Hog1 was not detected under starvation conditions (Figure 4.32). However, it is possible that, due to the rapid and often transient nature of Hog1p phosphorylation that the response was missed in the present study. It has been reported more recently that glucose limitation, and additionally glucose stimulation, results in activation of Hog1p which is Snf1 dependent (Piao *et al.* 2012). The role and phosphorylation status of Hog1p preceding entry into stationary phase, where lipid accumulation begins to occur, is not well defined. Due to these inconsistencies a definitive conclusion on the effect of nutrient starvation and onset of stationary phase on the activation of Hog1p cannot be reached. Furthermore, the experiment conducted by Aoki *et al.* (2011), to assess the effect on Hog1p phosphorylation under nitrogen starvation is synthetic and did not allow for assessment of phosphorylation as a natural consequence of nutrient depletion during the course of normal growth conditions.

It is reported in the literature that the upstream MAPKK Pbs2p is the only known route for activation of Hog1p. The localisation of Hog1p in response to phosphorylation by Pbs2p can vary significantly and is dependent on the type of stress (Bicknell *et al.* 2010). Although Hog1p, activated by osmotic stress, rapidly translocates to the nucleus to enhance transcription of target genes, it has been described that Hog1 can activate several responses on differing time frames. For example, rapid non-transcriptional responses of Hog1p within the cytoplasm have been suggested prior to the transcriptional responses modulated by nuclear translocation (Geijer *et al.* 2013). Upon cell wall stress Hog1p is activated by dual phosphorylation and instead of being imported to the nucleus, remains in the cytoplasm where it is still able to regulate gene expression (Garcia *et al.* 2004). This highlights a Hog1 response that is distinct from that of osmotic stress. Additionally, a further differential response pattern of Hog1 has been identified following ER stress. Under conditions of ER stress, Hog1p is phosphorylated and translocates to the nucleus to activate nuclear targets. Phosphorylated Hog1p can then re-enter the cytoplasm, highlighting the potential for further activation of cytoplasmic targets (Bicknell *et al.* 2010).

To further dissect the phosphorylation status of Hog1p during the lipogenic switch, further analysis was undertaken using Phos-tag. A Phos-tag gel, which helps determine phosphorylation patterns of proteins (Ha *et al.* 2014, Lee Yong Jae *et al.* 2012) was employed to determine whether there was any evidence of Pbs2 independent Hog1p phosphorylation. The results of the Phos-tag gel in this chapter suggested that Hog1p was phosphorylated independently of Pbs2 at 8.5hrs (Figure 4.34). No dual phosphorylation of Hog1 was detected at this time point using the α-P-p38 antibody. This suggested that Hog1p may have been phosphorylated on sites other than those previously characterised.

Recent evidence has suggested that Hog1p is able to autophosphorylate, independently of Pbs2, in response to severe osmotic stress (Maayan *et al.* 2012). However this phosphorylation was detected using the antibody specific to the dual phosphorylation status of Hog1p. Due to this the possibility of autophosphorylation on a single tyrosine or threonine residue in response to nutrient limitation, or crosstalk from neighbouring pathways, resulting in Hog1p activation in a Pbs2 independent manner cannot be ruled out. Taken together this highlighted that the regulation of lipid accumulation by the HOG pathway in *S. cerevisiae* could function independently of the classical route of Hog1p

activation as well as being distinct from osmotic and nutrient stress responses. In order to confirm Pbs2 independent phosphorylation of residues on Hog1, mass spectrometry (MS) of purified Hog1p at different stages of the time course could be employed. Further approaches include MS, such as stable isotope labelling by amino acids in cell culture (SILAC), which allows simultaneous quantification of all phosphorylation events. Furthermore employment of selective reaction monitoring MS (SRM-MS) phosphorylation kinetics of individual sites may also be determined (Reiter *et al.* 2012).

It was demonstrated in this study that activation of Hog1p is important for lipid accumulation in *S. cerevisiae*; potential targets of Hog1 were inferred by bioinformatics analysis and included key components in both neutral and polar lipid synthesis. It is known that phosphorylation can result in a number of outcomes for the target protein including direct/indirect activation or inhibition of protein activity, a change in the subcellular localisation of the protein as well as affecting protein stability.

It is suggested that Hog1p may interact either directly or indirectly with a number of proteins involved in lipid accumulation. As Dga1 catalyses the terminal step in TAG formation it was speculated that the similar decrease observed for neutral lipids may indicate an interaction between Hog1 and Dga1. The consensus sequence which Hog1 recognises is highly conserved, (a serine or threonine residue followed by a proline residue) (Roux and Blenis 2004). Upon analysis of the protein sequence of Dga1, potential MAP kinase binding sites were found, indicating the possibility that Hog1 could phosphorylate Dga1 to regulated neutral lipid accumulation (Figure 4.35).

Two of the identified potential MAPK sites were at the N terminus of the protein, S17 and T53. It has been identified in a study by Lui *et al.* (2011) that the C terminus of Dga1 may have a more important role in maintenance of the enzyme activity. However, upon deletion of residues 1-62 (N1) of the proteins N terminus a significant reduction in the amount of TAG detected by Nile red screening was observed. Similarly when residues 1-33 (N2) of the N terminus were disrupted TAG levels were also reduced, although not to the extent seen with the N1 disruption (Liu Qin *et al.* 2011b). As two of the potential MAPK sites fall within these regions of the N terminus it may be postulated that the loss of activity in these N terminal mutants could be as a result of Hog1p being unable to phosphorylate Dga1p at these sites.

In order to determine if Dga1 is phosphorylated, a genomically tagged Dga1 strain could be utilised in a protein time course and a Phos-tag experiment conducted to see if an upshift in the molecular weight of Dga1 occurs. This experiment could then be conducted in cells deleted for *HOG1*, whereby it could be determined if any phosphorylation events of Dga1 appear to be Hog1 specific. Further to this, in order to confirm a Hog1/Dga1 interaction at the point of phosphorylation an immunoprecipitation experiment could be performed to see if Hog1 is bound to Dga1.

Two additional potential MAPK sites were found to be located at the C terminus of Lro1p, however these residues are present at the portion of the protein that is predicted to be embedded in the lumen of the ER (Figure 4.36). As such, this suggested that these sites would not be accessible for phosphorylation by Hog1.

A number of potential MAPK sites have been identified within the protein sequences of all four *S. cerevisiae* SREBP-like proteins (Figures 4.39, 4.40, 4.41 and 4.42). It is possible that Hog1p may activate SREBP-like proteins via phosphorylation in the cytoplasm to promote their cleavage and nuclear translocation. This concept is supported by evidence that the mammalian p38 MAPK directly phosphorylates aiding activation of SREBP-1a *in vitro* in hepatic cells, linking stress response pathways with cellular metabolism and supporting sterol independent activation of SREBPs (Kotzka *et al.* 2012).

Known and extensively studied targets of Hog1p are the transcription factors Msn2 and Msn4. Data presented within this chapter suggests that these transcription factors are involved in the regulation of neutral lipid accumulation in *S. cerevisiae* (Figure 4.25). As referred to previously, Msn2/4 are localised to the cytoplasm and translocate to the nucleus under conditions of stress, before undergoing periodical nucleocytoplasmic shuttling (Jacquet *et al.* 2003). Activation of Hog1 may activate Msn2/4 resulting in their relocation to the nucleus for gene transcription, however, it should also be noted that not all Msn2/4 dependent genes require active Hog1 for their regulation.

As previously described, Msn2/4p bind to conserved sequences known as STREs within gene promoters, in order to drive transcription (Grably *et al.* 2002). A complete STRE element (5'CCCCT3') has been identified in the promoter regions of both *MGA2* and *ECM22* (Figure 4.43). Additionally, PDS elements (both 5'CCCT3' and 5'AGGG3') which may also be bound by Msn2/4 have been identified in the promoter regions of *SPT23*,

*MGA2, UPC2* and *ECM22* (Figures 4.43 and 4.44) (Grably *et al.* 2002, Orzechowski Westholm *et al.* 2012). This suggests that Msn2/4 may drive the synthesis of neutral lipids via a SREBP dependent mechanism.

It is not yet known whether Msn2, Msn4 or even both proteins function in the regulation of lipid accumulation. Data within this chapter has shown that the double deletion results in a significantly altered neutral, but not polar, lipid phenotype (Figure 4.25). In order to elucidate whether one or both components are required each would need to be complemented in turn to assess the impact of the expression of each protein on lipid levels compared to wild type cells. Furthermore, to identify whether binding the promoters of SREBP like proteins is required, further work could seek to mutate STRE and PDS elements present in the promoter regions of SREBP like proteins to evaluate whether the lipid phenotype is altered. Additionally chromatin immunoprecipitation (ChIP) could be conducted utilising genomically tagged Msn2/4 strains to identify whether they are bound to the promoter regions of SREBP-like proteins.

With respect to the altered phospholipid phenotype of *hog1Δ* cells, it is not known whether this is as a consequence of Hog1 regulating accumulation of phospholipids or due to cells deleted for *HOG1* bearing altered membrane permeability to that of wild type cells (Escoté *et al.* 2011). Potential MAPK binding sites have been identified in Cho1 and Cho2 protein sequences, which regulate the synthesis of phospholipids (Figures 4.37 and 4.38). However, altered membrane permeability cannot be ruled out as a contributor to the reduced phospholipid phenotype of the *HOG1* deletion strain. Although the polar lipid phenotype was recovered in the *hog1Δ* following transformation with pRS313*HOG1*, it is not clear whether the more permeable membrane of *HOG1* deleted cells would also be restored. To distinguish altered membrane permeability from requirement in lipid accumulation, strains of *S. cerevisiae* other than *hog1Δ* which display altered membrane permeability, such as *ERG* mutants (Iwaki *et al.* 2008) and potentially stressed wild type cells (Davey and Hexley 2011), could be screened for polar lipids via Nile red.

The scope of potential Hog1 targets is vast due to its ability to regulate both cytoplasmic and nuclear targets along with differing dynamics and localisation which is dependent on the stimulus. Therefore it is possible that Hog1 could regulate both cytoplasmic (Dga1, Cho1, Cho2, SREBPs) targets as well as nuclear targets (including Msn2/4) in order to drive transcription of lipid regulatory genes. It is also suggested that Hog1 may have a mode of

activation and localisation dynamic that is distinct to that observed in osmotic and cell wall stress. This could be subsequently dissected by analysis of a *HOG1* GFP tagged strain over the range of growth phases where it is suggested Hog1 activity is required for lipid accumulation.

For a more in depth investigation, to identify key regulatory components in the accumulation of lipids which is specific to the HOG pathway, microarray analyses could be performed. In this case, wild type cells would be analysed, along with the *hog1Δ* and *msn2/4Δ* strains before, during and after lipid accumulation is observed. This would provide comprehensive information of genes that are activated and repressed during the lipogenic phase along with which components are dependent on the presence of functional Hog1 and Msn2/4.

The data within this chapter demonstrates that lipid accumulation is similarly perturbed in mutants within the Sty1 MAPK pathway of *S. pombe*. As demonstrated with the deletion of *HOG1,* deletion of *sty1* also results in attenuated neutral and polar lipid accumulation (Figures 4.48 and 4.49). In a study by Grimard *et al.* (2008) it was demonstrated via Nile red microscopy that cells deleted for *sty1* had increased lipid levels compared to wild type cells (Grimard *et al.* 2008). This is in contravention with results obtained in the present study. However, as the microscopy data presented by Grimard *et al.* (2008) shows *sty1Δ* cells that do not appear to be elongated, it is suggested that the cells were utilised in exponential phase growth. As shown in Chapter 3, *S. pombe* accumulates increased levels of lipids in exponential phase and as such, the *sty1Δ* may accumulate comparable levels in early exponential phase. In order to investigate this, a time course of lipid accumulation should be conducted for wild type *S. pombe* compared to cells lacking *sty1.*

Interestingly the upstream MAPKK of Sty1, Wis1, also displays an altered neutral and polar lipid phenotype (Figures 4.48 and 4.49). This observation may mean that, unlike the HOG pathway in *S. cerevisiae,* lipid accumulation could be regulated further upstream of the MAPK in *S. pombe*. However, the *wis1Δ* displayed a significant growth defect in comparison to wild type and *sty1Δ* cells, along with markedly decreased cell viability (Figures 4.45 and 4.50). As such, altered viability coupled with the growth defect cannot be ruled out as contributing factors to the lipid phenotype observed.

The results of screening with the *sty1-KD* mutant revealed a significantly altered neutral, but not polar, lipid phenotype compared to wild type cells (Figures 4.48 and 4.49). However, the reduction in neutral lipids observed was found not to be as severe as in the *sty1* deletion strain, 1.9 fold (*sty1Δ*) vs 1.3 fold (*sty1*-KD) (Figure 4.48). As previously described, the kinase dead mutant can be dually phosphorylated by Wis1 and can translocate to the nucleus. Along with phosphorylation of target proteins, Sty1 also has a role in the recruitment of RNA Polymerase II to the promoters of genes to activate transcription (Reiter *et al.* 2008). However, the kinase dead mutant is unable to phosphorylate downstream targets nor is it able to bind promoters of stress induced genes without its kinase activity (Reiter *et al.* 2008). The limited reduction in neutral lipids observed in the *sty1-KD* mutant compared to *sty1Δ* suggests that Sty1 has limited importance in the expression of lipid regulatory genes. However, recruitment of Sty1 to promoters may be required for some target genes as the level of lipid seen is *sty1-KD* does not reach that of wild type cells. Although Sty1-KD is unable to be recruited to the promoters of genes involved in the stress response, it may be possible that the Sty1-KD mutant is able to bind promoter regions of other genes. It has been demonstrated that in *S. cerevisiae* a *hog1-KD* mutant can be recruited to gene promoters, although at a reduced efficiency to wild type cells (Reiter *et al.* 2008), as such it may be informative to assess lipid accumulation in a *hog1-KD* mutant. Once downstream target genes of Sty1 that may play a role in lipid accumulation have been identified, binding at the promoter regions of both *sty1* and *sty1-KD* would need to be confirmed by chromatin immunoprecipitation (ChIP).

As lipid accumulation in the *sty1-KD* mutant is less severely perturbed compared to *sty1Δ*, it suggests that phosphorylation of Sty1 targets is not required for the response to lipid accumulation. Therefore, lipogenic targets which may be activated via the Sty1 pathway may only require interaction with Sty1 for their activity. It is possible that the interaction of Sty1 with a target protein could serve to change its subcellular localisation or stabilise it to some extent, preventing its degradation. It has been demonstrated that physical interactions occur between translation factors and Sty1, which could aid protein synthesis (Asp *et al.* 2008). As, such, the association of *sty1-KD* with lipid regulatory proteins could result in a small increase in protein levels and therefore lipid accumulation. It is further suggested that if Sty1 was able to phosphorylate such a target protein, rather than just interact, much higher levels of the target protein would result therefore increasing the

accumulation of lipids. This is supported by data in *S. pombe* that the levels of Aft1p are not only regulated by Sty1 phosphorylation but also by its interaction with Pcr1 (Lawrence C.L. *et al.* 2007).

An alternative possibility is that Sty1 may bind an inhibitor of a target lipogenic protein in the nucleus. Under normal conditions Sty1 would phosphorylate the inhibitory protein, therefore removing its inhibitory effect on the target protein. In the *sty1*-KD mutant this removal of inhibition would be unable to happen. However, the inhibitory effect may be "diluted" to some extent by interaction of Sty1-KD.

In contrast to *S. cerevisiae,* the stress response of Sty1 pathway *S. pombe* mutants aligned with the lipid accumulation phenotypes observed (Figure 4.51). Consistent with previously published observations, deletions of *wis1* and *sty1* resulted in reduced sensitivity to oxidative stress when compared to wild type cells (Rodríguez-Gabriel and Russell 2005). The *sty1-KD* mutant showed similar stress sensitivity to *sty1* deleted cells (Reiter *et al.* 2008).

No significant lipid phenotypes were observed upon deletion of the Sty1 downstream targets *aft1* and *pap1*, suggesting that Aft1 and Pap1 are not involved in the regulation of lipid accumulation (Figures 4.54 and 4.55). Potential cytoplasmic lipid regulatory targets of Sty1 were identified by bioinformatics analyses, the proteins identified which harbour potential MAPK sites, are conserved with those identified in *S. cerevisiae.* However, as with *S. cerevisiae* further investigation of cytoplasmic and downstream targets of the Sty1 pathway would need to be conducted, especially in order to elucidate the involvement of downstream targets in regulating lipid accumulation. It is suggested that once the point at which Sty1 is required for lipid accumulation is deduced, microarray analyses could be performed in both wild type, *sty1Δ* and *sty1-KD* strains to identify potential targets of the Sty1 pathway that are required for lipid accumulation based on their levels of expression compared to wild type cells.

Data within this chapter has demonstrated a novel role for the HOG and Sty1 MAPK pathways within yeast in regulating cellular neutral and polar lipid accumulation. For *S. cerevisiae* this role converges at the point of the MAPK, whereas regulation may occur further upstream at the level of the MAPKK in *S. pombe.* Although the major downstream targets of Sty1, Aft1 and Pap1, appeared to have no significant role in lipid accumulation,

downstream targets of Hog1p, Msn2/4 are suggested to play a role in the accumulation of neutral lipids. This suggests that regulation of lipid accumulation may also extend to downstream targets in *S. pombe.* Furthermore, a potential Pbs2 independent mechanism of Hog1 phosphorylation in *S. cerevisiae* has been suggested to occur preceding the point where increased cellular lipid accumulation occurs. This demonstrates that the role of the MAPK pathway in the regulation of lipid accumulation may be distinct to that observed under osmotic stress conditions.

# Chapter V *Lipomyces starkeyi* as a metabolic model for lipogenesis

## 5.1 Introduction

*Lipomyces starkeyi* is one of many species of oleaginous yeasts that are intensively employed in the biotechnology industry for the production of biofuels due to its ability to accumulate up to 70% of their dry cells mass as lipids (Lin *et al.* 2011).

It is suggested that *L. starkeyi* would serve as a favourable model organism for research into lipogenesis, not only owing to its lipid production, but also as it converts citrate to oxaloacetate and acetyl CoA via ATP-citrate lyase, a phenomenon not observed in the budding yeast *S. cerevisiae*. The presence and activity of ATP-citrate lyase is typically what distinguishes oleaginous species from non-oleaginous yeasts (Ratledge C. 2002, Walker 1998).

The utilisation of the genetically well characterised species *S. cerevisiae* and *S. pombe,* along with development of *L. starkeyi* as a model organism, may enable a better understanding of the mechanisms underlying eukaryotic lipid accumulation.

The major drawback for the use of oleaginous yeast species as model organisms for human disease is that the plethora of genetic tools, accompanying the well characterised models *S. cerevisiae* and *S. pombe,* are not available for *L. starkeyi.* The oleaginous yeast *Yarrowia lipolytica* is one of the most studied non-conventional yeast with a range of molecular tools available (Nicaud 2012). In addition, the usefulness of utilising non-conventional yeast species for human disease research is further supported by the use of *Y. lipolytica* in research on mitochondrial disorders (Kerscher *et al.* 2004).

Genetic techniques available in *S. cerevisiae* and *S. pombe* include the ability to transform cells, in order to create null strains by homologous recombination and cloning of genes for genetic complementation (Forsburg 2001). Furthermore, protein-protein and protein-DNA interactions can be readily elucidated via co-immunoprecipitation and chromatin immunoprecipitation (ChIP) techniques (Ezhkova and Tansey 2006, Geva and Sharan 2011).

The employment of *L. starkeyi* in biotechnology has fuelled interest into the development of molecular platforms, especially with regards to creation of null strains and protein overexpression (Calvey *et al.* 2014). Such platforms would enable *L. starkeyi* to be

engineered metabolically in order to enhance lipid production and improve the economic viability of biofuels derived from micro-organisms (Calvey *et al.* 2014).

The draft assembly of the *L. starkeyi* genome was published in 2011 by the Department of Energy (DOE) and Joint Genome Institute (JGI) after the course of initial work conducted in this chapter. However, very little work had been done on annotation and no work had been completed on the proteome (Liu Hongwei *et al.* 2011a).

In this chapter it has been demonstrated that *L. starkeyi* displayed a growth phenotype similar to that of *S. cerevisiae* when exposed to both osmotic and oxidative stress. Along with this, successful amplification and cloning of the MAPK homologue in *L. starkeyi* has been demonstrated for the first time. It has also been shown that the antibody recognising the dually phosphorylated MAPK in *S. cerevisiae* could potentially be utilised in *L. starkeyi*. Additionally, it has been highlighted that alternative strategies from those utilised in *S. cerevisiae* and *S. pombe* are required for genetic transformation of both plasmids and integrating cassettes into *L. starkeyi*. Finally, from bioinformatics analysis, it has been demonstrated that *L. starkeyi* appears to have a conserved MAPK pathway to that of *S. cerevisiae* and *S. pombe.*

## 5.2 Results

From the data shown in Chapter 4, it is proposed that the Hog1/Sty1 MAPK pathways are involved in the regulation of lipid accumulation. This suggests that the MAPK homologue in *L. starkeyi* may also have a similar role in mediating lipogenesis.

### 5.2.1 Characterisation of the stress response of wild type L. starkeyi

One of the main roles of the MAPK pathway in yeast is the regulation of the stress response. There is limited information on the genome of *L. starkeyi*. Furthermore there has been no characterisation conducted of this yeast species with regards to the stress response. Enhancing the knowledge of yeast physiological response is not only important to identify the role of *L. starkeyi* in the response to stress, but it is also important in biotechnology for subsequent industrial exploitation of yeast (Walker 2011). Yeasts are subjected to numerous stressors not only in the laboratory environment, but also when grown in industrial fermenters (Walker 1998), utilised in both the brewing industry and for production of biofuel. As this study is interested specifically in MAPK pathways, experiments were conducted to see if wild type *L. starkeyi* had similar stress sensitivity to *S. cerevisiae* and *S. pombe* wild type cells. Two types of cellular stressors, osmotic (NaCl) and oxidative ($H_2O_2$), were used as they are known to elicit a stress response via MAPK pathways in budding and fission yeast (Asp *et al.* 2008).

Osmotic stress results in the efflux (hyperosmotic) or influx (hypo osmotic) of water into the cell. Hyperosmotic stress is characterised by cell shrinkage, whereas hypo osmotic stress results in swelling of the cells. In response to osmotic stress yeast cells initiate a complex adaptive response resulting in temporary arrest of the cell cycle, altered transcriptional and translation and synthesis of the osmolyte glycerol. The osmoadaptation of yeasts is highly dependent on the activation of the stress-activated protein kinase (SAPK) pathway (de Nadal E. *et al.* 2002).

Oxidative stress results in the accumulation of reactive oxygen species, which can result in damage to proteins and lipids along with DNA damage and mutations (Ikner and Shiozaki 2005). In response to oxidative stress yeast *S. cerevisiae* and *S. pombe* Hog1/Sty1 pathways mediate a response to upregulate or repress transcription of genes in order to mediate antioxidant defence (Farrugia and Balzan 2012).

By comparison of *L. starkeyi* with the well characterised yeast species *S. cerevisiae* and *S. pombe,* establishment of whether the response of *L. starkeyi* to stress is conserved can be assessed. As demonstrated by Figure 5.1, wild type *S. cerevisiae* was able to grow at all concentrations of osmotic stress tested, with growth only being slightly reduced at the maximum NaCl concentration of 1.0 M. Conversely, *S. pombe* was unable to grow under osmotic stress conditions beyond a concentration of 0.4 M. In the case of *L. starkeyi* reduced growth was observed at a NaCl concentrations of 0.4 M-0.6 M (Figure 5.1).

In response to oxidative stress *S. cerevisiae* exhibited reduced growth at 6mM $H_2O_2$ with growth being abolished at a concentration of 8mM. Wild type *S. pombe* was found to be display reduced growth on plates containing 2mM $H_2O_2$ with no growth observed at 4mM. In response to oxidative stress, *L. starkeyi* growth was perturbed at a concentration of 4mM (Figure 5.2). From the stress experiments it can be concluded that *L. starkeyi,* for both osmotic and oxidative stressors, has a response which is intermediate compared to the responses displayed by *S. cerevisiae* and *S. pombe*.

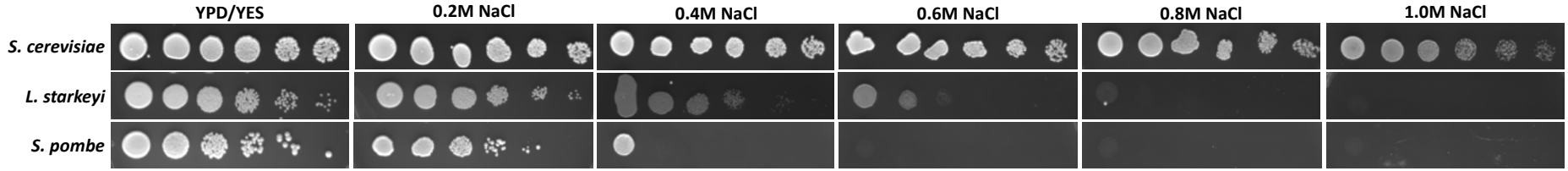


**Figure 5.1: Spot plates of wild type *S. cerevisiae*, *S. pombe* and *L. starkeyi* showing response to osmotic stress.** Control plates (YPD/YES) and osmotic stress plates, YPD/YES supplemented with NaCl. Starting cell densities were ~2.3 x $10^7$ cells/ml before being serially diluted 1:10 across the plate down to 2.3 x $10^2$ cells/ml.

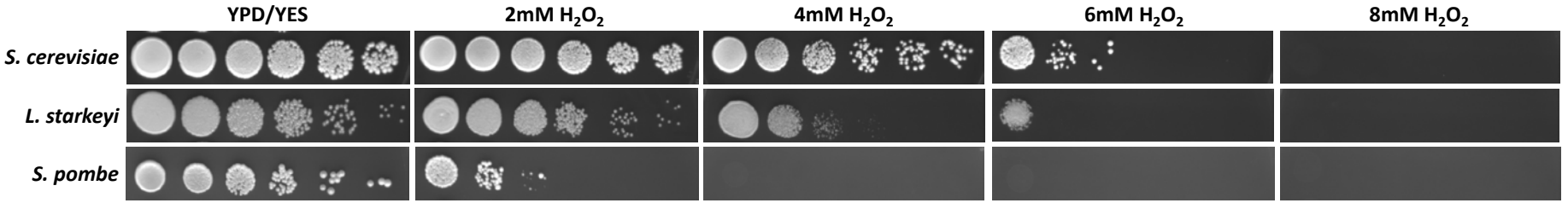


**Figure 5.2: Spot plates of wild type *S. cerevisiae*, *S. pombe* and *L. starkeyi* showing response to oxidative stress.** Control plates (YPD/YES) and oxidative stress plates, YPD/YES supplemented with $H_2O_2$. Starting cell densities were ~2.3 x $10^7$ cells/ml before being serially diluted 1:10 across the plate down to 2.3 x $10^2$ cells/ml.

As previously described the stress response of *S. cerevisiae* and *S. pombe* is largely regulated by Hog1 and Sty1 MAPK pathways which are well conserved both structurally and functionally to the p38 MAP kinase of mammalian cells.

By alignment of MAPK protein sequences from yeast species compared to mammalian p38, the percentage similarity was calculated using Clustal Omega from the European Bioinformatics Institute (EBI). Table 5.1 depicts the percentage similarity of the mammalian p38 protein sequence to corresponding MAP Kinases present in yeast. It is demonstrated that *S. cerevisiae* and *S. pombe* MAPK homologues display 50.28% AND 53.16% similarity respectively to that of mammalian p38. Further to this, the oleaginous yeast species *Y. lipolytica* p38 homologue also displays 50.14% similarity. This highlights that oleaginous yeasts may be valuable in studying the role of the MAPK pathway.

**Table 5.1: Percentage identity showing similarities between mammalian p38 and yeast p38 MAPK homologue protein sequences.** Percentage identity matrix was compiled by multiple sequence alignment using Clustal Omega from the European Bioinformatics institute (EBI).

| | | | | |
|---|---|---|---|---|
| **p38: *Homo sapiens*** | **100** | **50.28** | **53.16** | **50.14** |
| **Hog1: *S. cerevisiae*** | **50.28** | **100** | **80.52** | **78.59** |
| **Sty1: *S. pombe*** | **53.16** | **80.52** | **100** | **83.09** |
| **Hog1: *Y. lipolytica*** | **50.14** | **78.59** | **83.09** | **100** |

The phylogenetic relationship inferred from protein sequence alignments demonstrates that all yeast MAPK homologues are equally as divergent from mammalian p38 (Figure 5.3). Further, the MAP kinases of *S. pombe* and *Y. lipolytica* have been grouped as the MAPK sequences are more evolutionarily conserved between them than of the other groups.

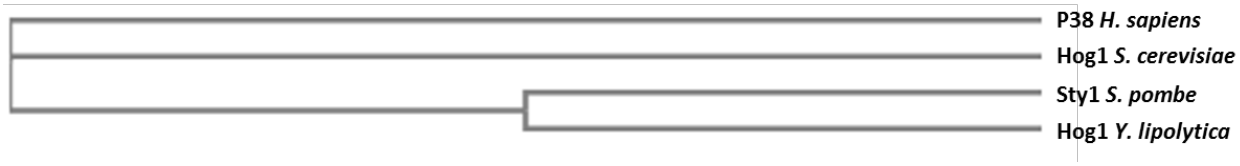


**Figure 5.3: Phylogram indicating evolutionary relationships based on MAPK protein sequence alignments.** Phylogenetic tree generated from protein sequence alignments by Clustal Omega from the European Bioinformatics Institute.

## 5.3. Amplification of the L. starkeyi p38 homologue by the polymerase chain reaction

As the *S. cerevisiae* (Hog1) and *S. pombe* (Sty1) MAP kinase proteins are well conserved and characterised (80% similar, Table 5.1) (Dinér *et al.* 2011, Sansó *et al.* 2011), amplification of the *L. starkeyi MAPK* open reading frame from genomic DNA was attempted. If successful amplification is achieved this would facilitate the creation of a MAPK null strain along with cloning of the gene for heterologous expression studies.

Before conducting any amplification of the gene by PCR, samples of *L. starkeyi* genomic DNA were extracted as detailed in Chapter 2 and run on a 0.8% agarose gel (Figure 5.4). Using an established genomic yeast DNA extraction technique detailed in Section 2.3, DNA was purified from *L. starkeyi* cultures, utilising *S. pombe* and *S. cerevisiae* as positive controls.

As the agarose gel in Figure 5.4 shows, two distinct bands were observed in lanes 1 and 2 corresponding to genomic DNA from *S. cerevisiae* and *S. pombe* at ~1.0 and ~1.5 kb respectively. Smearing on the gel also indicates the presence of genomic DNA as genomic DNA contains fragments of DNA comprising different molecular weights. Similar bands were obtained in lane 3 for the *L. starkeyi* sample indicating that the genomic DNA extraction had been successful.

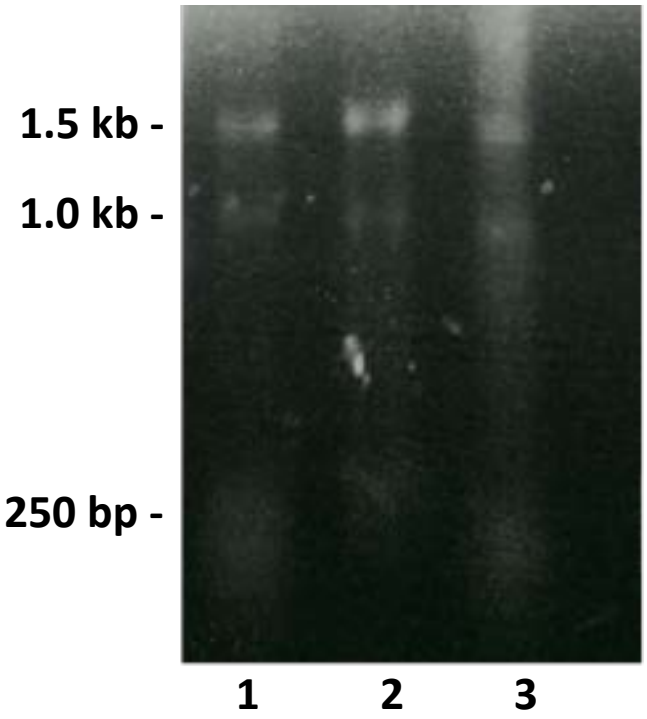


**Figure 5.4: Agarose gel showing successful extraction and presence of genomic DNA from *L. starkeyi*.** Lane 1: *S. cerevisiae*. Lane 2: *S. pombe*. Lane 3: *L. starkeyi*. DNA bands can be seen for all three species at approximately 1.5Kb, 1.0Kb and 250bp.

Following successful genomic DNA extraction, DNA sequence data from the well characterised yeast species *S. cerevisiae* and *S. pombe* was analysed. Conserved regions were identified by aligning the nucleotide sequences utilising the Kalign multiple sequence alignment tool from EBI. With no genomic sequence information available at the time for *L. starkeyi,* primers specific to *HOG1* (CLL001/002) and primers against a conserved region found in the genes *HOG1* and *sty1* (CLL003/004) were designed. The primers specific to *HOG1* were utilised to act as a positive control for the PCR reaction and the conserved primers to attempt amplification of the *L. starkeyi* p38 homologue. This was based on the assumption that similar regions between the three yeast species would be conserved. Figure 5.5 shows the aligned sequences and where the primers were designed to.

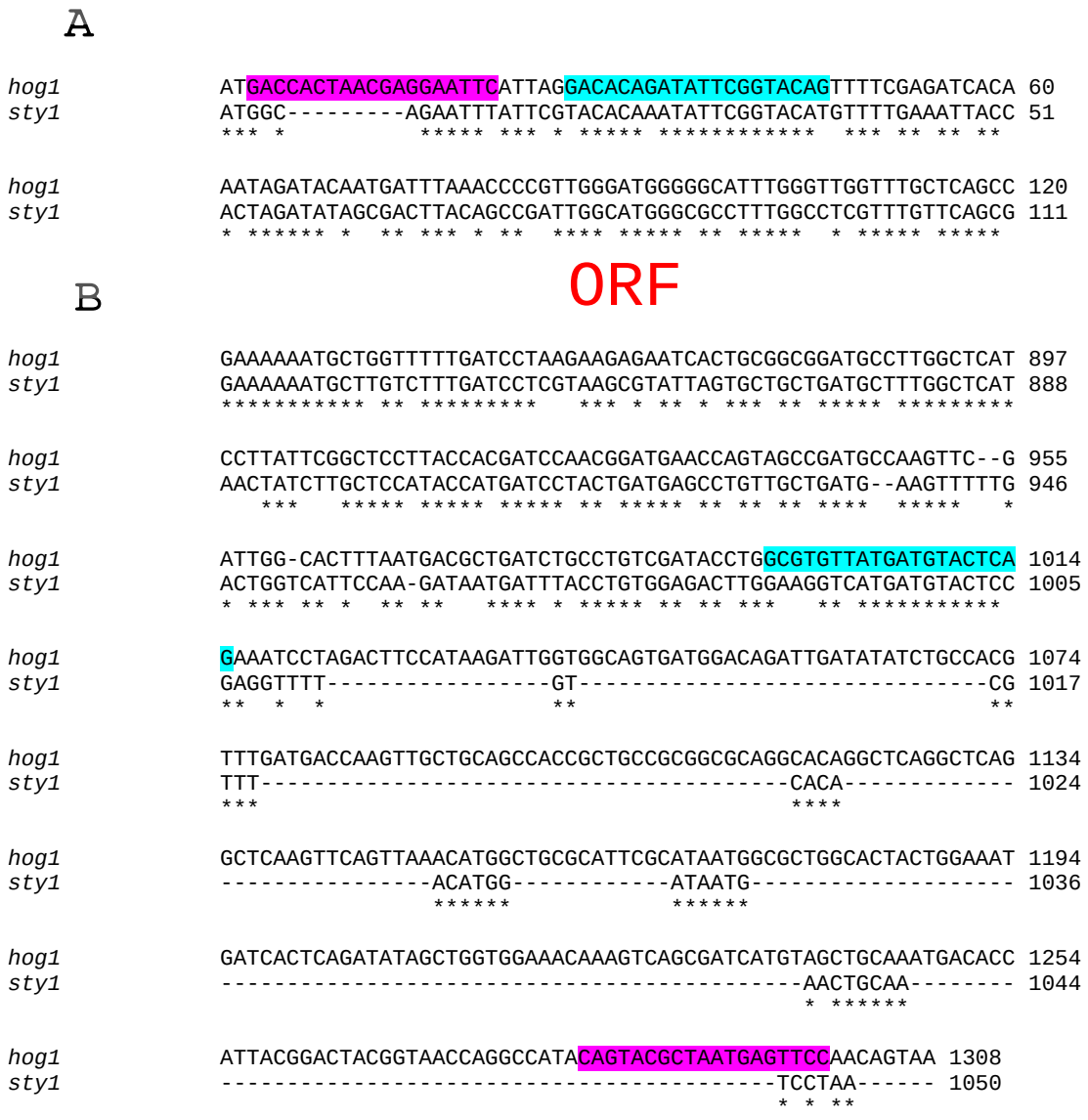


**Figure 5.5: Sequence data showing rationale behind conserved MAP Kinase primers.** Primers specific to *HOG1* are highlighted in pink (CLL001/002), Section A: forward primers and Section B: reverse primers. Highlighted in blue are the conserved primers designed to amplify *S. pombe sty1* and *L. starkeyi MAPK* homologues (as no sequence information was available at the time) (CLL003/004). The conserved primers were designed to regions of the *HOG1* and *sty1* nucleotide sequences that were well conserved, as indicated by the asterisks (*) which show where the sequences between the two species are identical.

Following PCR amplification with the standard annealing temperature of 45 °C, *S. cerevisiae HOG1* was successfully amplified using both specific (~1.3 kb) (lane 2) and conserved primers (~1 kb) (lane 6). No amplification products were observed for *S. pombe* or *L. starkeyi* (lanes 3-4 and 7-8 respectively) (Figure 5.6). The expected size of *S. pombe sty1* is ~1.0 kb with the expected size of *L. starkeyi* MAPK being ~1.4 kb.

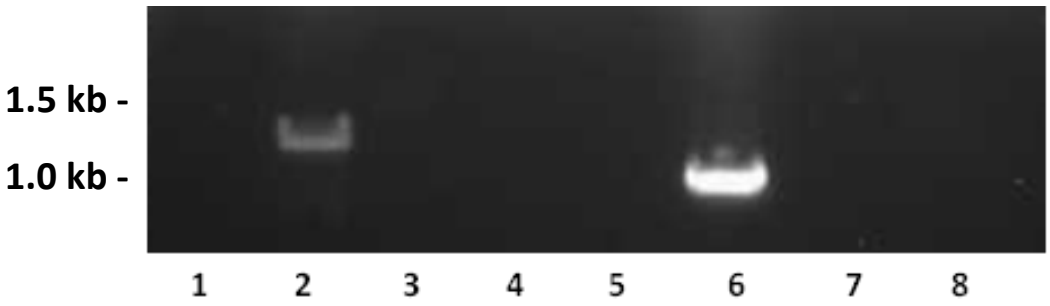


**Figure 5.6: Agarose gel showing amplification products obtained from all three yeast species using specific and conserved primers.** Lane 1: negative control, lane 2: SC with *HOG1* primers (positive control), lanes 3 and 4: *S. pombe* and *L. starkeyi* with *HOG1* primers, lane. Lane 5: negative control, lane 6: *S. cerevisiae* with conserved primers, lanes 7 and 8: *S. pombe* and *L. starkeyi* with conserved primers.

As no PCR products were observed for *S. pombe* or *L. starkeyi*, the experiment was repeated utilising a lower annealing temperature of 42 °C, as decreasing the annealing temperature results in less specific primer binding. This again produced amplification of *HOG1* in the positive control but gave no amplification products from either *S. pombe* or *L. starkeyi*. The annealing temperature was then dropped further to 40 °C, again only amplification was observed for *HOG1* positive control (data not shown).

A ramp PCR was then carried out using the conserved primers with an annealing temperature of 40 °C, 41 °C and 42 °C for 10 cycles each, the resultant agarose gel again showed only successful amplification of *HOG1* from *S. cerevisiae* using the conserved primers.

After dropping the annealing temperature further to 35 °C, amplification products were again observed corresponding to *S. cerevisiae HOG1* (lane 1). Bands were also observed for *S. pombe* and *L. starkeyi* (lanes 2 and 3 respectively), however, due to the size of the

bands these were deemed the result of non-specific amplification due to the low annealing temperature used and that products of the expected size were absent (Figure 5.7).

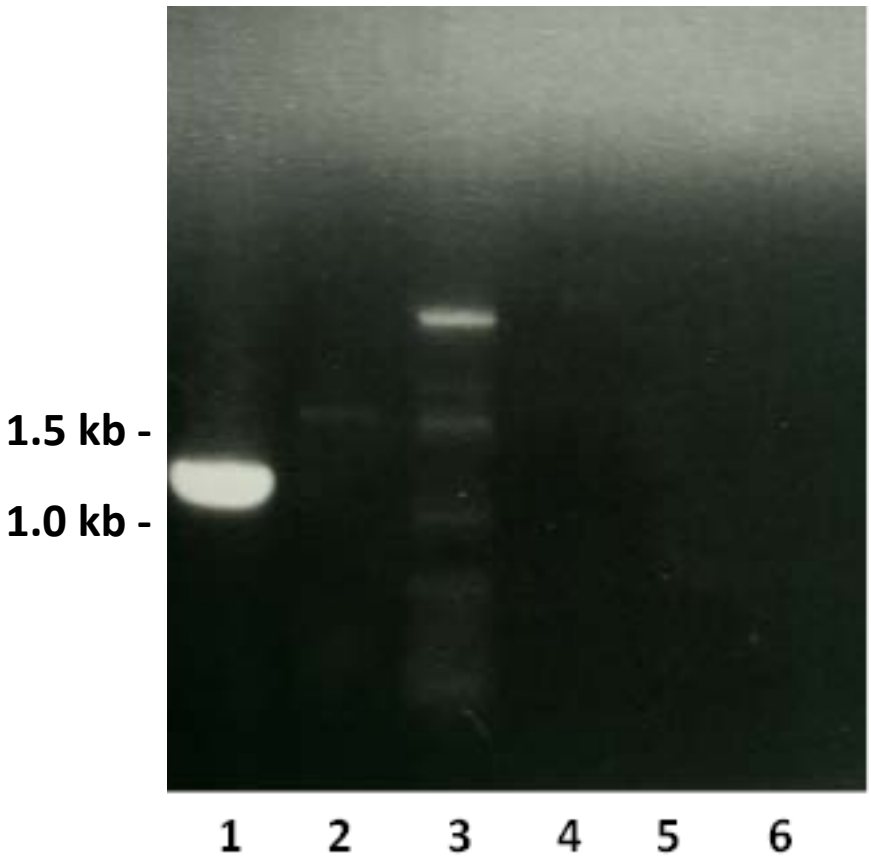


**Figure 5.7: Agarose gel showing successful amplification of *S. cerevisiae HOG1* using conserved primers.** Lane 1: *S. cerevisiae HOG1*, Lanes 2 and 3: non-specific amplification products from *S. pombe* and *L. starkeyi* respectively. Lanes 4, 5 and 6 negative controls containing no *Taq* polymerase for *S. cerevisiae, S. pombe* and *L. starkeyi* respectively.

It was determined from these results that amplification of the *L. starkeyi* MAP Kinase utilising primers conserved to *S. cerevisiae* and *S. pombe* was not a viable approach. At the time it was known that the genome of *L. starkeyi* was undergoing sequencing, however, numerous scaffolds had yet to be annotated. As such, amplification of the ORF was conducted once annotated information became available.

In 2011 92% of the *L. starkeyi* genome, which was partially annotated, became available having been sequenced in collaboration with the Department of Energy and Joint Genome Institute's Fungal Genomics Program (JGI). The nucleotide sequence for the *L. starkeyi* p38 MAPK homologue was obtained and aligned from the ATG codon, to those of *S. cerevisiae HOG1* and *S. pombe sty1* using the Kalign alignment tool from European Bioinformatics Institute (EBI) to show sequence similarity (Appendix I, Figure A8). The alignment showed that the nucleotide sequence was ~80% conserved between *L. starkeyi* and the other two yeast species (81.09% similarity to *HOG1* and 80.33% similarity to *sty1*).

Primers were then designed specifically to the ORF of *L. starkeyi* MAPK and PCR carried out for *L. starkeyi* p38 homologue (primers CLL005/006) using PCR parameters described in Chapter 2. *S. cerevisiae HOG1* (primers CLL001/002) and *S. pombe sty1* (primers CLL007/008) were utilised as positive controls for the PCR reaction.

Figure 5.8 shows successful amplification of *S. cerevisiae HOG1* (lane 1, ~1.3 kb), *S. pombe sty1* (lane 2, ~1.0 kb) and a putative *L. starkeyi* MAPK gene, (lane 3 ~1.4 kb). This is the first time that a MAPK gene has been shown to be amplified from the yeast species *L. starkeyi*.

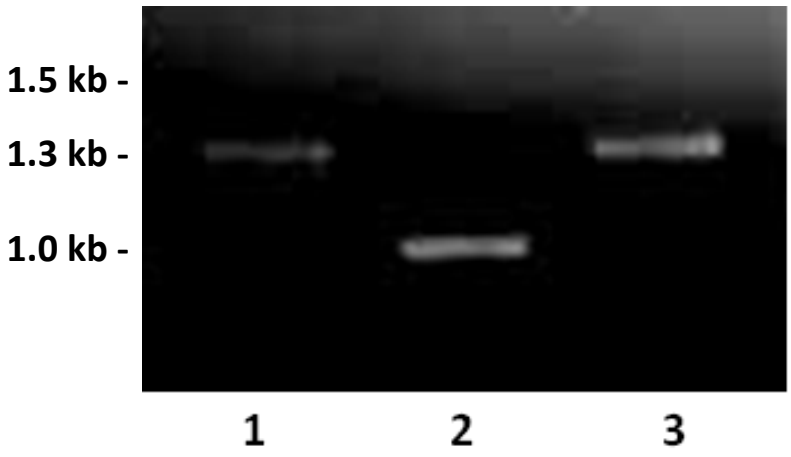


**Figure 5.8: Agarose gel showing successful amplification of *HOG1* (lane1), *sty1* (lane 2) and the p38 *MAPK* homologue of *L. starkeyi* (lane 3).** Bands were observed at ~1.3Kb, ~1.0Kb and ~1.4Kb respectively corresponding to the expected sizes of *S. cerevisiae*, *S. pombe* and *L. starkeyi* respectively.

## 5.4 Use of α-P-p38 and α-Hog1 antibodies for the detection of L. starkeyi MAPK protein

Proteomic analysis in 2010 highlighted that most proteins in mammalian cells are phosphorylated (Olsen *et al.* 2010). Phosphorylation can produce a wide range of biological effects serving to regulate a plethora of cellular processes. Phosphorylation events can serve to activate a protein, either directly, or by removing its association with an inhibitory complex. In other cases phosphorylation can inhibit the activity of a protein by mechanisms including masking of the active domain. Furthermore phosphorylation can also occur where the subcellular localisation of a protein can be altered. Additionally phosphorylation may not affect protein activity but produce a binding site to facilitate protein-protein interactions (Nishi *et al.* 2014). Phosphorylation is an important regulatory mechanism for MAPKs and is important for them to become activate. Active MAPKs are then able to activate/inhibit other proteins along with expression of genes under various cellular conditions including stress.

Due to the high conservation of mammalian p38 and yeast homologues, the dually phosphorylated status of Hog1 and Sty1 proteins can be detected with the same α-P-p38 antibody used for dually phosphorylated mammalian p38 (Bell Michal and Engelberg 2003). Similarly the α-Hog1p antibody utilised in this study is also utilised in the detection of total *S. pombe* Sty1p (Hartmuth and Petersen 2009).

Due to the high level of conservation of the MAPK across species, it was postulated that the *L. starkeyi* MAPK will also be conserved at the protein level. As such, an alignment of the three yeast species protein sequences was undertaken using the Clustal 2.1 alignment tool from EBI. This identified high levels of conservation between the three yeast species (Figure 5.9).


**Figure 5.9: Sequence alignment showing conservation of p38 homologues for all three yeast species at the protein level.** Colours that are the same indicate either identical or similar amino acids between all 3 yeast species. Carried out using Clustal 2.1 programme for multiple sequence alignment (MSA). (MSA infers sequence homology and therefore evolutionary relationships). Letters that are the same show identical amino acid sequences between the three species of yeast. Same colours but differing sequence refers to amino acids that have similar properties. Red: small, hydrophobic. Blue: Acidic. Magenta: Basic. Green: Hydroxyl + sulfhydryl + amine + G. *amino acids the same : indicates a conserved substitution and . a semi conserved substitution.

In addition to the visual alignment (Figure 5.9), the percentage identity between the protein sequences was also determined (Table 5.2).The MAPK protein sequence of *L. starkeyi* was found to be 82.05% similar to Hog1 and 83.95% similar to Sty1. The percentage conservation of *L. starkeyi* relative to *S. cerevisiae* and *S. pombe* is greater than the level of conservation seen between Hog1 and Sty1 sequences, which are 80.52% similar to one another. Additionally the percentage identity between mammalian p38 and *L. starkeyi* protein sequences was determined to be 51.14% which is greater than the homology between mammalian p38 and *S. cerevisiae* Hog1p (50.28%), but not as homologous as *S. pombe* Sty1p (53.16%) (data not shown). This indicates that antibodies available to detect dually phosphorylated MAPK and total MAPK levels may also work for *L. starkeyi* MAPK.

**Table 5.2: Percentage identity of *S. cerevisiae, S. pombe* and *L. starkeyi* protein sequences.** Percentage identity matrix was compiled by multiple protein sequence alignment using Clustal Omega from the European Bioinformatics institute (EBI).

| | | | |
|---|---|---|---|
| **Hog1: *S. cerevisiae*** | **100** | **80.52** | **82.05** |
| **Sty1: *S. pombe*** | **80.52** | **100** | **83.95** |
| **MAPK: *L. starkeyi*** | **82.05** | **83.95** | **100** |

The protein sequences of *S. cerevisiae, S. pombe* and *L. starkeyi* were further inspected to identify the residues recognised by the α-P-p38 antibody, along with the epitope recognised by the Hog1p antibody.

As shown in Figure 5.10 the Thr174 and Tyr176 phosphorylation sites (indicated in yellow) of *S. cerevisiae* and *S. pombe* are present at conserved regions within the protein sequence of *L. starkeyi*. This suggests that the P-p38 antibody should recognise these sites if they become dually phosphorylated.


**Figure 5.10: Conservation of phosphorylation sites recognised by α-P-p38 antibody.** Protein sequence alignment for *S. cerevisiae* Hog1, *S. pombe* Sty1 and a putative *L. starkeyi* MAPK were aligned using Clustal Omega from EBI. Yellow highlights show conserved Thr174 and Tyr176 residues. Conservation of the recognition motif of the antibody T-G-Y is indicated by the red box.

In the case of the antibody used to detect total Hog1 and Sty1 protein levels, the C terminal sequence that is recognised by the antibody was aligned to the corresponding region of the *L. starkeyi* protein sequence.

Figure 5.11 shows percentage identity of the C terminus alignment and highlights high levels of conservation between the sequences of *S. cerevisiae, S. pombe* and *L. starkeyi.* Although there are regions of sequence where the *L. starkeyi* sequence does not correspond to the other sequences, these are mostly regions where *S. cerevisiae* and *S. pombe* also differ, for example at position 260. Overall the degree of confirmation of the region recognised by the Hog1/Sty1 antibody is high, suggesting the Hog1 antibody should recognise the MAPK protein in *L. starkeyi*.

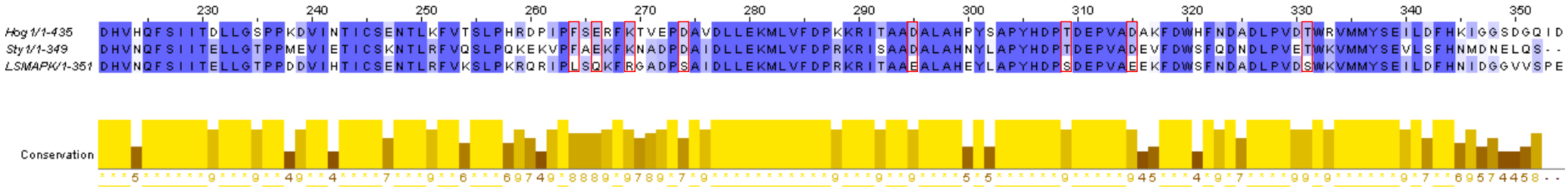


**Figure 5.11: Percentage identity and conservation of epitope region recognised by α-Hog1 in *S. cerevisiae* and *S. pombe* compared to the corresponding region of *L. starkeyi* protein sequence.** Similarity index and degree of conservation were derived from Jalview after protein sequence alignment using Clustal Omega from EBI. The strength of the colour on the sequence indicates the degree of similarity between protein sequences only, ranging from dark blue: >80% down to white: <40%. Regions where L. starkeyi sequence is not conserved to those of S. cerevisiae or S. pombe is indicated by red boxes. Degree of confirmation is shown below the sequence in yellow with the height of boxes corresponding to the similarity of the sequence.

To determine whether the antibodies utilised for detection of phosphorylated and total *S. cerevisiae* Hog1p and *S. pombe* Sty1p could also recognise the putative *L. starkeyi* MAPK, a stress experiment was conducted utilising *S. cerevisiae* as a positive control.

Wild type *S. cerevisiae* and *L. starkeyi* cultures were exposed to osmotic stress in YPD culture, utilising 0.4M NaCl. Samples were harvested at 10 minutes after exposure to stress, as it is known that *S. cerevisiae* Hog1p will be activated under this condition (de Nadal Eulalia *et al.* 2004). As *L. starkeyi* has a slower growth rate than *S. cerevisiae* and the response to stress in liquid culture is unknown for this species, further samples were harvested at 20 minutes. Protein was extracted from cells and a Western blot performed as described in Section 2.51 and 2.53.

As shown in Figure 5.12, with the α-P-p38 antibody no band was observed in non-stressed *S. cerevisiae* and a band corresponding to phosphorylated Hog1p was observed at 50 kDa. Bands were also observed for stressed *L. starkeyi* at both 10 and 20 minutes consistent with size of the *L. starkeyi* MAPK at ~40 kDa. However, a band at the same position was also observed for non-stressed *L. starkeyi*.

Using the Hog1 antibody to detect total Hog1 protein, bands at 50 kDa were observed for *S. cerevisiae* corresponding to the Hog1 protein, however, no bands were observed for *L. starkeyi* (Figure 5.12).

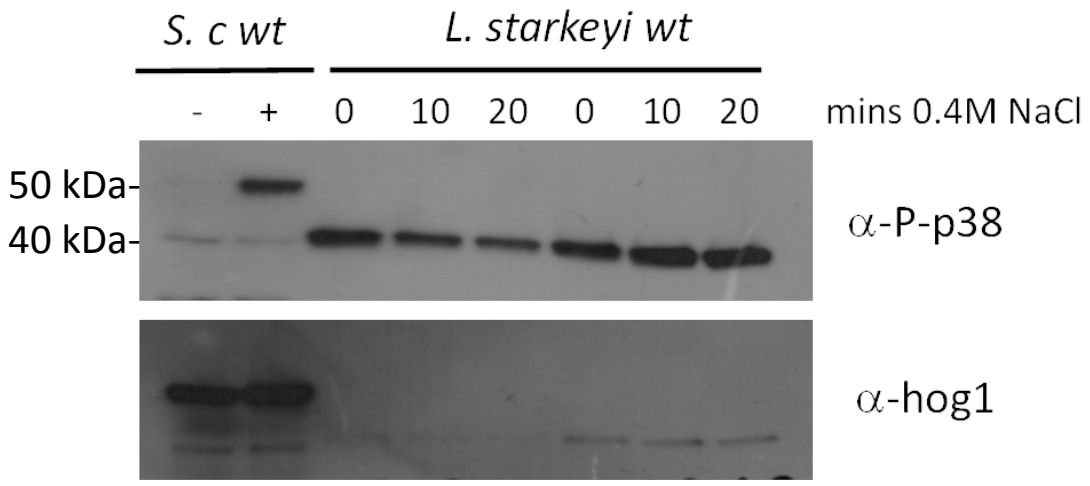


**Figure 5.12: Western blot of *S. cerevisiae* and *L. starkeyi* under non-stressed and stressed conditions.** *S. cerevisiae* non-stressed is indicated by – and stressed *S. cerevisiae* exposed to 0.4 M NaCl for 10 mins +. *L. starkeyi* 0: non stressed, 10: exposed to 0.4 M NaCl for 10 mins 20: exposed to 0.4 M Nacl for 20 mins. Phosphorylated was detected using α-P-p38 and total protein with α-Hog1.

These results suggest that the antibody used to detect the dually phosphorylated MAPK may recognise the active form of the putative *L. starkeyi* MAPK protein as bands were observed at the expected size for *L. starkeyi* MAPK. As no bands were observed when utilising the antibody to detect total MAPK protein, it is concluded that the antibody is unable detect the putative *L. starkeyi* MAPK.

## 5.5 Genomic gene deletion using homologous recombination in L. starkeyi

In order to characterise the role of the putative *L. starkeyi* MAPK in the stress response and the accumulation of cellular lipids, experiments were conducted in order to produce a MAPK null strain.

Prior to April 2014 there was no published information or methodologies for the transformation and integration of DNA into the genome of *L. starkeyi.* As such, an *S. pombe* methodology was first utilised, as described by Bahler *et al.* (1998), as this yeast species appears to be more similar at the nucleotide level to *L. starkeyi* than *S. cerevisiae.*

This methodology was used as a platform in order to optimise the DNA transformation methodology in *L. starkeyi*. Specific deletion primers (CLL009/010) were designed to the *KanMX* module of pFA6a-*KanMX6* (Bahler *et al.* 1998) vector. These primers contained flanking regions corresponding to 100 bp upstream and downstream of the *L. starkeyi* open reading frame. Kanamycin was utilised as the selectable marker as it is a commonly used antibiotic marker for gene disruption in yeast.

The deletion primers used in this study are 4 nmol Ultramer Oligos with standard desalting (CLL009/010). The primer concentration required to produce sufficient transforming DNA, according to Bahler *et al.* (1998), is high (1.2 µM). Due to this, PCR reactions were conducted to assess the lowest concentration of primers that could be utilised to generate the required MAPK deletion cassette. Following PCR DNA bands were observed at ~1.6 kb (~1.4 kb *KanMX* and 200 bp flanking region), corresponding to the expected size of the deletion cassette (Figure 5.13).

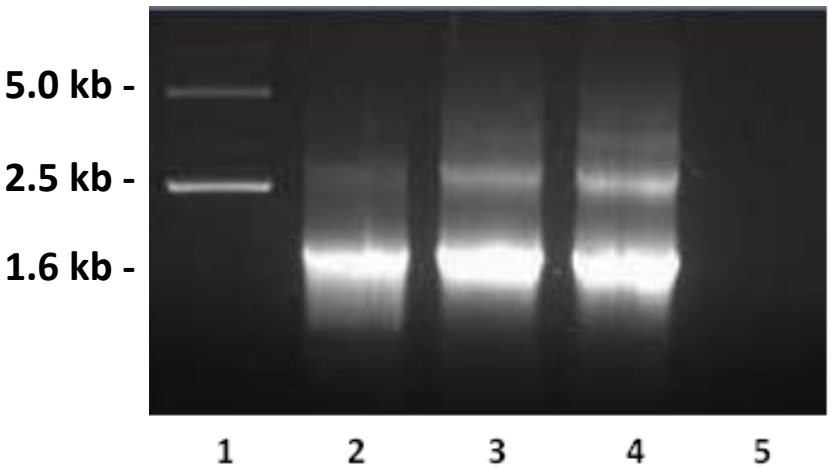


**Figure 5.13: Agarose gel showing amplification of the *MAPK* homologue deletion cassette for *L. starkeyi*.** Lane 1: Plasmid, PFA6a-*kanMX6*, lane 2: reaction using 1.2 µM, lane 3: using 0.8 µM, lane 4: using 0.4 µM of primers and lane 5: no *Taq* control. As the agarose gel shows, PCR product is still generated using a third of the recommended primer concentration.

It was determined, following successful amplification of the deletion cassette, that a primer concentration of 0.4 µM could be used (lane 4) rather than 1.2 or 0.8 µM (lanes 2 and 3). This is a more cost effective option whilst the methodology is being optimised for deleting the putative *L. starkeyi* p38 homologue.

### 5.5.1 Yeast transformation utilising S. pombe methodology

Initial transformation experiments were carried out using a method for *S. pombe*, the lithium acetate (LiAc) method described by Bahler *et al.* (1998). Cells ($5.2 \times 10^8$) from an exponentially growing culture ($2.6 \times 10^7$cells/ml) were used for each transformation. Cultures were centrifuged at 492 g for 2 minutes before washing cells with an equal amount of sterile water. Cells were then resuspended in 1ml 0.1 M LiAc/TE, centrifuged for 2 minutes at 1500 rpm before resuspending in 200µl 0.1 M LiAc/TE giving an approximate cell number of $5.2 \times 10^{10}$. Cells were mixed with 2 µg salmon sperm DNA and ~10-20 µg transforming DNA (with the appropriate volume of sterile water was added for the control) and incubated at room temperature for 10 minutes before adding 260 µl 40%PEG/LiAc/TE, mixing and incubating at 30°C for 1 hour. 43 µl DMSO was then added and the cells heat shocked for 5 minutes at 42°C before centrifugation at 1500 rpm for 2 mins. The cell pellet was washed in sterile water, before being resuspended in 2 ml of rich medium, YPD, and incubated overnight with shaking at 30 °C before plating out on YPD

agar supplemented with 400 µg/ml of G418 sulphate. After 2 weeks incubation at 30 $^{o}$C no colonies were formed on the selection plates. Although this initial transformation experiment was unsuccessful, this was used as the basis to develop a modified transformation protocol for *L. starkeyi*.

#### 5.5.1.1 Optimisation of G418 concentration

A number of conditions were identified that may influence the efficiency of yeast transformation, including concentration of the selection antibiotic, amount of transforming DNA, transforming solutions and time of heat shock.

The first was the concentration of the drug used for selection, in this case the antibiotic G418. For *S. pombe* a concentration of 200-400 µg/ml of G418 is used for selection of *KanMX* transformed cells. There is no published information on the expression of the *KanMX* gene in *L. starkeyi* or the G418 concentration at which growth of transformants may be seen. As such the concentration of G418 was reviewed and a lower concentration of 100 µg/ml G418 was used. Following a repeat of the *S. pombe* transformation method, no yeast colonies were observed on plates containing the reduced antibiotic concentration after a 2 week incubation period.

#### 5.5.1.2 Assessment of URA3 as a suitable selectable marker

In order to determine if the kanamycin selective marker was the limiting factor in the transformations, cells were transformed with pKS-URA (Bahler *et al.* 1998), a non-integrating plasmid containing uracil (URA) as the selective marker. A non-integrating plasmid was utilised to assess whether the previous transformation was unsuccessful due to failed integration of the cassette. The protocol detailed above was repeated and cells plated out onto yeast nitrogen base (YNB) agar -URA. After less than one week of incubation, yeast colonies were observed on all plates, including the control. From this it was inferred that *L. starkeyi* does not require external sources of uracil for growth and as a result URA cannot be used as a selectable marker. As such, the *KanMX* cassette continued to be utilised for further transformation protocols.

#### 5.5.1.3 Optimisation of chemical transformation reagents

In order to determine the effect of transforming DNA concentration the method was further optimised by increasing the concentration of the transforming DNA deletion cassette from 10 ng to 20 ng. This would increase the amount of transforming DNA available to be taken up by the yeast cell and potentially increase the DNA cassette transported to the nucleus of the cell, thereby increasing the chance of homologous recombination. However, this modification resulted in no visible growth following 2 weeks incubation at 30 $^{o}$C.

As a chemical transformation protocol is being employed, reagents and their proportions are one of the critical factors for yielding good transformation efficiencies. It is widely documented that the presence of polyethylene glycol (PEG) is critical for transformation of yeast cells (Ito *et al.* 1983, Kawai S. *et al.* 2010). It has been suggested that the role of PEG in transformation is to disrupt the membrane as well being essential for the attachment of DNA. Therefore too high a PEG concentration could be detrimental to yeast cells and too low a concentration not able to permeabilise the membrane sufficiently to allow transformation. As such, PEG was prepared fresh without autoclaving before use in each transformation protocol, as evaporation of water during autoclaving can increase its final concentration (Gietz and Schiestl 2007).

It has been reported that LiAc is important for passage of DNA into the cell (Kawai S. *et al.* 2010). As no colonies were observed when utilising fresh PEG, other solutions required for chemical transformation (LiAc and TE) were also prepared fresh and filter sterilised instead of autoclaving. Further to this half of the control sample, containing no transforming DNA, was plated onto YPD agar to ensure that the transformation procedure was not lethal to the cells. After 3 days of incubation at 30 $^{o}$C colonies were present on the YPD control plate showing that the transformation procedure was not lethal and cells were still viable.

### 5.5.1.4 Effect of extending heat shock

The act of heat shocking cells after the addition of carrier DNA, transforming DNA and chemical solutions is executed in order to decrease membrane fluidity via the release of lipids, which in turn open up the "pores" created by the chemical solutions used. Heat shock also promotes passage of DNA into the cell and although the optimum time for cells to be exposed to heat-shock varies with yeast species (Gietz and Schiestl 2007) between 5 and 15 mins at 42 $^{o}$C is generally utilised for most strains (Knop *et al.* 1999).

No published data on the temperature sensitivity at 42 $^{o}$C of *L. starkeyi* is available; therefore a cell viability experiment at this temperature was undertaken. Samples of *L. starkeyi* cells were harvested and exposed to 42 $^{o}$C heat for 15, 30, 45 and 60 minutes before plating out onto YPD agar. After one week of incubation at 30 $^{o}$C yeast colonies were observed on all plates, with little reduction in viability after a heat shock of 60 minutes compared to non-heat shocked control cells.

Based on the above data, the *L. starkeyi* transformation was repeated using fresh transformation chemicals with heat shock at 42 $^{o}$C for 50 minutes and selection on YPD agar supplemented with 100 µg/ml G418. A longer heat shock was utilised based on the transformation of oleaginous yeast by (Chen D.C. *et al.* 1997).

After 2 weeks of incubation at 30 $^{o}$C, a single colony was observed on one of the experimental plates (the control plate remained free of growth), suggesting genomic integration of the *KanMX* deletion cassette. To confirm a stable integration into the genome, cells transferred to YPD alone before colonies were transferred back to YPD agar supplemented with 100 µg/ml G418. To determine if the *KanMX* gene had integrated and displaced the *L. starkeyi* genomic MAPK, the cells were tested for both phenotype and genotype. If the *L. starkeyi* MAPK holds a role similar to that in *S. cerevisiae* and *S. pombe*, the gene deletion would be expected to show sensitivity to $H_2O_2$ at a lower concentration compared to that of wild type cells. To determine stress sensitivity, cells were patched onto YPD supplemented with 6 mM and 4 mM hydrogen peroxide.

Colonies were found to be more sensitive to 6mM and 4mM $H_2O_2$, indicated by inhibition of growth on YPD/$H_2O_2$ plates in comparison to the wild type strain. To determine whether this stress sensitivity was due to deletion of the MAPK a genomic DNA extraction was undertaken, as detailed in section 2.3, and a PCR carried out utilising primers specific

to the ORF of the *L. starkeyi* MAPK (CLL005/006). The resultant PCR products were compared to that amplified from wild type *L. starkeyi* genomic DNA on a 0.8% agarose gel. The agarose gel showed a clear band in the test strain at the same position as the wild type sample (~1.4 Kb) corresponding to the MAPK of *L. starkeyi*. If *KanMX* had integrated and displaced *L. starkeyi* MAPK, no PCR product at 1.4 Kb would have been expected. As the colony produced from the transformation was found to not contain the desired deletion it was concluded that either: the transforming DNA had randomly integrated into the genome allowing growth on G418 or that upon plating out the cells mutations had arisen as a result of a stress response, giving rise to cells with some resistance to G418.

#### 5.5.1.5 S. cerevisiae transformation method

As *S. pombe* methodology was unsuccessful, alternative transformation protocols were tested. The transformation method utilised for *S. cerevisiae* was also tested with *L. starkeyi*, as described in Chapter 2. As with previously utilised methods, no *L. starkeyi* colonies were observed on G418 plates after a 2 week incubation period.

#### 5.5.1.6 Yarrowia lipolytica transformation method

As neither the *S. pombe* nor *S. cerevisiae* transformation methods produced successful transformants in *L. starkeyi*, a transformation protocol for the oleaginous yeast species *Y. lipolytica* was next utilised. The transformation method used was a modified one-step method, carried out according to Chen *et al.* (1997), where transformation efficiency was reported to be ~1 x $10^4$ for integrative vectors (Chen D.C. *et al.* 1997). Liquid cultures were harvested and cells resuspended in 100 µl one step buffer [45% PEG4000, 0.1 M LiAc pH 6.0, 25 µg carrier DNA, 100 mM dithiothreitol]. 10-20 ng of transforming DNA was then added before thoroughly vortexing and incubating at 39 $^{o}$C for 60 minutes. Cells were then spread directly onto a well dried YPD plate supplemented with 100 µg/ml G418 and incubated at 30 $^{o}$C. No growth of *L. starkeyi* was observed following a 2 week incubation period.

#### 5.5.1.7 Bahler-Chen hybrid method

As no colonies were observed using the method of Chen *et al.* (1997) further transformations were carried out using the previously described modified method of Bahler *et al.* (1998) (fresh solutions, reduced G418 plate concentration and increased DNA) along with some of the principles of the method by Chen *et al.* (1997). The

principles taken from the latter paper which were then incorporated into the modified Bahler protocol were: no washing of cells in water as there is a suggestion that competent cells may be osmosensitive, longer heat shock (60 minutes) at a lower temperature (39 $^{o}$C), well dried selective plates as wet plates were found to critically affect the efficiency of transformations and finally increased the concentration of PEG4000 (45% rather than 40%). This protocol produced a single colony on one experimental plate (the control plate, YPD supplemented with 100 µg/ml G418, remained free of growth). Upon PCR of the resultant colony, the band corresponding to *L. starkeyi* MAPK was found to still be present.

#### 5.5.1.8 Lipomyces transformation protocol published by Calvey et al. 2014

In April 2014, an optimised transformation method for *L. starkeyi*, using native promoters and terminators, was published (Calvey *et al.* 2014). This protocol recommended: harvesting cells at 3 x $10^7$ cells/ml before addition of 86 mM LiAc, 240 µl 50% PEG, 30 µg ssDNA and 15 µl transforming DNA. Incubation at 30 $^{o}$C for 3 hrs and 5 minute heat shock at 42 $^{o}$C, before removal of supernatant, addition of YPD and further incubation at 30 $^{o}$C for 4 hrs. After 4 hrs of recovery at 30 $^{o}$C cells were plated onto 30 µg/ml clonNAT (Calvey *et al.* 2014).

The main differences between protocols tested in the present study and the published optimised method were: use of cells at a density of 3 x $10^7$ cells/ml, 30 $^{o}$C incubation for 3 hrs, 5 minute heat shock at 42 $^{o}$C, the further 4 hr recovery period and utilisation of nourseothricin (clonNAT) as a selectable marker. Increased cell number utilised may serve to enhance transformation efficiency by increasing the number of cells available for DNA uptake. Additionally it is reported by Calvey *et al.* (2014) that *L. starkeyi* has a low tolerance to extensive high temperature exposure, which may have affected previous transformation experiments utilising a longer heat shock at 42 $^{o}$C. Furthermore, as this species of yeast has a reduced rate of growth compared to *S. cerevisiae* and *S. pombe* the longer incubation period before heat shock and subsequent recovery period may serve to allow more efficient transformation.

Transformation was carried out as detailed by Calvey *et al.* (2014) and plates incubated at 30 $^{o}$C for 1 week. After 1 week, no colonies were observed. Following on from this, the standard protocol was repeated along with additional reactions whereby 10% DMSO was

added prior to heat shock and cells were allowed a final recovery overnight before plating onto selective medium. After 1 week of incubation at 30 $^{o}$C no colonies resulted from utilisation of the standard protocol or additional reactions containing DMSO nor those that were subjected to an overnight recovery.

## 5.6 Cloning of L. starkeyi MAPK for heterologous protein expression

As the method development for the transformation of *L. starkeyi* did not result in production of a MAPK null strain, the MAPK gene from *L. starkeyi* was amplified by PCR and cloned into pRS315 for heterologous expression studies in *S. cerevisiae.* If the MAPK of *L. starkeyi* has a similar role to that of *HOG1* in *S. cerevisiae* it might be expected that the stress sensitive phenotype of the *hog1Δ* would be recovered. The *L. starkeyi* MAPK ORF plus promoter region (1 kb upstream) was amplified by PCR using primers CLL026/028. The resulting PCR product was then digested along with pRS315 using *Xba*I and *Sac*I restriction enzymes, before ligation and transformation into *E. coli* DH5α. Resultant colonies were screened by colony PCR before mini-prep and digestion of positive colonies.

Digestion of mini-prepped plasmids with *Xba*I and *Sac*I produced fragments at 6.0 kb, corresponding to pRS315, and 2.4 kb corresponding to the *L. starkeyi* MAPK ORF plus 1 kb of upstream sequence (Figure 5.14).

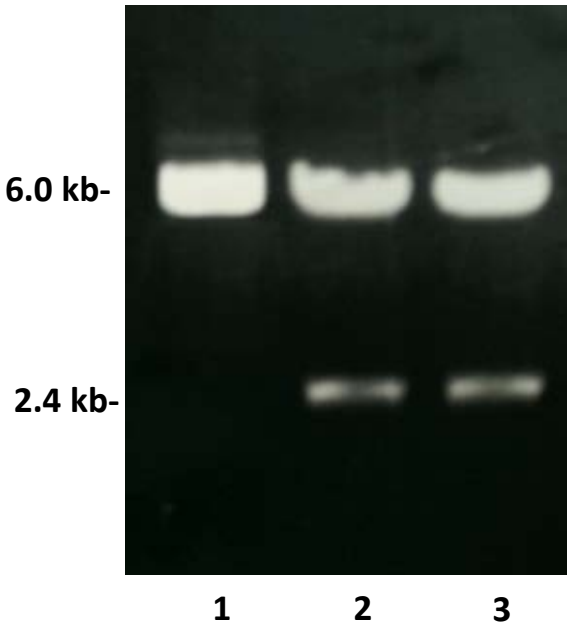


**Figure 5.14: Agarose gel of digested pRS315 and pRS315*LSMAPK.*** 0.8% agarose gel. Lane 1: Digested vector, pRS315 using *Xba*I and *Sac*I restriction enzymes, lanes 2 and 3: Digested pRS315*LSMAPK* using *Xba*I and *Sac*I restriction enzymes showing 6.0 kb band corresponding to pRS315 and ~2.4 kb band corresponding to putative *L. starkeyi* MAPK plus 1 kb promoter region.

pRS315 and pRS315*LSMAPK* were then transformed into *S. cerevisiae* wild type and cells deleted for *HOG1*, as described in Chapter 2. Transformants were transferred to YNB medium lacking leucine to select for cells containing empty vector and the constructed plasmid. To test if *L. starkeyi* MAPK recovered the osmotic stress sensitive phenotype of the *hog1Δ,* cells were transferred to YNB agar and YNB agar plus 0.4 M NaCl.

As shown in Figure 5.15, the phenotype of cells lacking *HOG1* subjected to osmotic stress was not recovered upon transformation with pRS315*LSMAPK.*

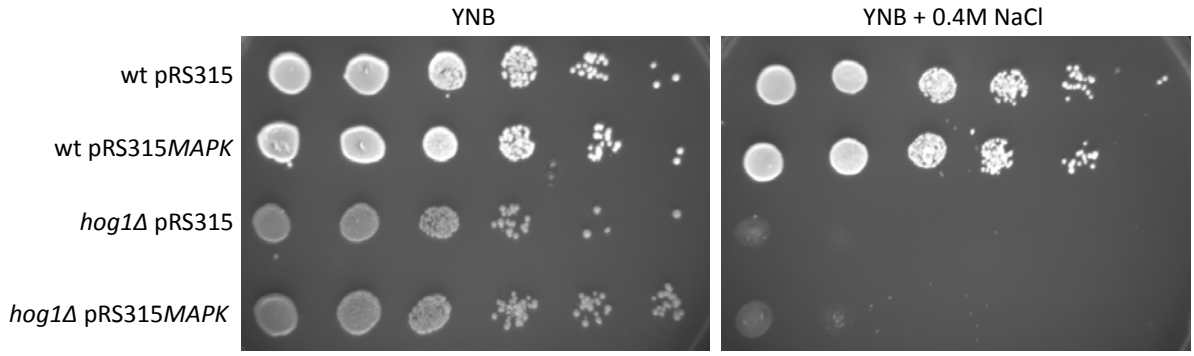


**Figure 5.15: Spot plates of *S. cerevisiae* wild type and *hog1Δ* transformed with pRS315 and pRS315*LSMAPK.*** Control plates (YNB) and osmotic stress plates, YNB supplemented with 0.4 M NaCl. Starting cell densities were ~2.3 x $10^7$ cells/ml before being serially diluted 1:10 across the plate down to 2.3 x $10^2$ cells/ml.

## 5.7 Identification of components of the MAPK pathway in L. starkeyi using bioinformatics tools

A p38/Hog1/Sty1 homologue has been identified in *L. starkeyi* suggesting that *L. starkeyi* may have a functional MAPK pathway, analogous to those of *S. cerevisiae* and *S. pombe*.

BLAST protein-protein searches were performed on the JGI database utilising protein sequences of *S. cerevisiae* and *S. pombe* MAPK components. The results, shown in Table 5.3 indicate that *L. starkeyi* contains homologues of all components of the HOG and Sty1 pathways. The MAPKKK identified, protein 42041, showed 33% similarity to that of *S. cerevisiae* Ste11 and 35% similarity to Win1 in *S. pombe.* The MAPKK, protein: 4347, was also found to be ~62% identical to Pbs2 and Wis1. As demonstrated earlier the MAPK, protein 106427, is ~82/83% similar to Hog1 and Sty1 proteins.

**Table 5.3: MAPK components of *L. starkeyi* are conserved with those in *S. cerevisiae* and *S. pombe*.** Components of the *S. cerevisiae* HOG pathway and *S. pombe* Sty1 pathway compared to homologues identified via sequences searches. Sequences were obtained from the *L. starkeyi* JGI genome portal using BLAST protein searches. Protein ID is given for *L. starkeyi* and percentage similarity of MAPKKKs, MAPKKs and MAPKs to *S. cerevisiae* shown in bold.

| Component | *S. cerevisiae* | *S. pombe* | *L. starkeyi* (% identity) |
|---|---|---|---|
| MAPKKK | **Ste11** | Win1 | **42041 (33%)**/4347 (35%) |
| MAPKK | **Pbs2** | Wis1 | 4347 (**63%**/62%) |
| MAPK | **Hog1** | Sty1 | 106427 (**82.05%**/83.95%) |
| TFs *S. cerevisiae* | Msn2/4 | ----- | 2854 (57%) |
| TFs *S. pombe* | ----- | Atf1/Pap1 | 6160 (27%)/5850 (24%) |

*L. starkeyi* also contains MAPK targets including an Msn2/4 like protein (protein 2854) which shares 57% homology to Msn2/4 of *S. cerevisiae.* Furthermore Aft1 and Pap1 like proteins (6160/5850) were also found which confer 27% and 24% similarity respectively.

## 5.8 Discussion

In this study the aim was to develop molecular techniques in the oleaginous yeast species *L. starkeyi* for use as a metabolic model to study the regulation of lipogenesis. This was required to assess whether the role of this yeast MAPK was similar to that of *S. cerevisiae* and *S. pombe* in the regulation of both the stress response and lipid accumulation.

As described in Chapter 1, the MAPK pathway is important in the response of cells to various stresses including osmotic and oxidative stress. In order to characterise the MAPK of *L. starkeyi* the responses of *L. starkeyi* to stresses was determined for comparison with those known for *S. cerevisiae* and *S. pombe*.

Results of the spot plates determined that *L. starkeyi* had a response to osmotic and oxidative stress in between those displayed by *S. cerevisiae* and *S. pombe,* most resembling that of *S. cerevisiae* (Figures 5.1 and 5.2). Although *L. starkeyi* did not grow as well as *S. cerevisiae* at higher levels of stress, this could be due to the reduced growth rate of *L. starkeyi* compared to *S. cerevisiae*. This could potentially be determined by repeating the experiment at a reduced growth temperature for *S. cerevisiae*.

Amplification of *L. starkeyi* MAPK from genomic DNA using conserved primers was not successful (Figure 5.6). This suggested the *L. starkeyi* nucleotide sequence was not well conserved to that of *S. cerevisiae* and *S. pombe*. No amplified products were yielded for *S. pombe* whilst utilising the conserved primers. This demonstrated that amplification of the MAPK genes using a conserved primer approach was not viable as no specific products for *L. starkeyi* were yielded (Figure 5.6). Amplified DNA products were observed once the annealing temperature had been dropped to 35 $^{o}$C (Figure 5.7). However, during PCR conducted below the optimal annealing temperature, the primers hybridize non-specifically to the template strand due to weak interactions caused by the lower annealing temperature. This results in amplification of non-specific products by *Taq* polymerase (Bell D. A. and DeMarini 1991). Due to this it is suggested that most of the bands observed for *S. pombe* and *L. starkeyi* in this case were likely due to non-specific binding of primers to template genomic DNA.

A further approach that could be utilised with conserved primers to amplify *L. starkeyi* MAPK, would be a touch down PCR program. With a touch down program, the annealing temperature starts 10 degrees higher than the optimal annealing temperature of the primers. The annealing temperature is then decreased by 1 degree per cycle for 10 cycles, followed by a further 10-15 cycles at the optimal annealing temperature. It is suggested that this approach may have been a more viable means of obtaining specific products from conserved PCR as it has been shown to reduce the amount of non-specific product yield (Korbie and Mattick 2008).

After obtaining sequence data from the Joint Genome Institute (JGI), the MAPK homologue gene in *L. starkeyi* was amplified successfully utilising a standard PCR program. This is the first time that amplification of the *L. starkeyi* MAPK ORF has been demonstrated (Figure 5.8). On subsequent alignment of all three nucleotide sequences it was found that regions at the beginning and end of the open reading frame of *L. starkeyi MAPK* were not well conserved to those of *S. cerevisiae* and *S. pombe* (Appendix I, Figure A8). As such, the low level conservation of the nucleotide sequences at the extremities of the ORF explains why the conserved primer PCR was unsuccessful for amplification of the *L. starkeyi* MAPK.

Upon alignment of the protein sequences from the three yeast species utilised it was found that the MAPK protein sequence of *L. starkeyi* was highly homologous to both *S. cerevisiae* and *S. pombe* (Figure 5.9).

The antibody used to detect total Hog1p detected total Hog1p for *S. cerevisiae* samples but did not produce any bands for *L. starkeyi* (Figure 5.12). This was not expected as the C terminal epitope recognised by the antibody is highly conserved between *L. starkeyi*, *S. cerevisiae* and *S. pombe* (Figure 5.11). This could suggest that residues of the *L. starkeyi* sequence that differ from both *S. cerevisiae* and *S. pombe,* such as residues 260, 270, 300 and 350, could be pivotal to recognition of the epitope by the antibody. Alternately the conformation of *L. starkeyi* MAPK may differ from that of *S. cerevisiae* and *S. pombe*, and so the epitope may be masked by differential folding of *L. starkeyi* MAPK.

Protein analysis also suggests that the commercially available P-p38 antibody would recognise the dually phosphorylated form of *L. starkeyi* MAPK due to the conserved residues being analogous to those in Hog1 and Sty1 (Figure 5.10). Western blot analysis of

*L. starkeyi* protein extracts utilising the α-P-p38 antibody suggested that the antibody may recognise dually phosphorylated *L. starkeyi* MAPK. However, no band was observed for stressed *S. cerevisiae* whereas bands were observed in the non-stressed samples where, following evidence from other yeast MAPK, dual phosphorylation would not be expected (Figure 5.12). This could be due to non-specific bands, or could demonstrate there is a basal level of MAPK dual phosphorylation in *L. starkeyi.* As sections of the nucleotide sequence are significantly different in *L. starkeyi* than in *S. cerevisiae* and *S. pombe*, due to the high conservation observed at the protein level, this suggests that the codon usage is different. This would explain the differences in nucleotide sequence yet similar protein sequence observed.

In order to determine if the band present in the *L. starkeyi* samples are as a result of phosphorylation, alkaline phosphatase treatment of native protein extracts could be employed. Alkaline phosphatase treatment would remove phosphorylation on amino acid residues of the protein, as such if the bands observed were due to phosphorylation they would be absent following treatment with alkaline phosphatase.

Transformations conducted to produce an *L. starkeyi MAPK* null strain, which would serve to characterise the role of the *MAPK* homologue in both the stress response and lipid accumulation, were unsuccessful. In initial experiments conducted utilising *S. pombe* methodology, no colonies resulted from transformations. After identification of a number of factors which may influence transformation efficiency, modifications to the protocol were made to see if successful integration resulted. Lowering the concentration of G418 did not result in efficient colony formation after transformation. As the toxicity of G418 to *L. starkeyi* cells is unknown, a toxicity assay should be performed in order to identify the minimum inhibitory concentration of G418 before further employment of *KanMX* as a selectable marker. Furthermore, as there is no published information on the expression of *KanMX* from an *S. pombe* based vector in *L. starkeyi,* it was equally possible that it might not be expressed in *L. starkeyi.*

It was also determined that *L. starkeyi* is able to grow without an exogenous source of uracil. In order to overcome this and utilise uracil as a selectable marker a URA- mutant could be developed from wild type cells. This could be achieved by spreading mature cultures into 5-FOA plates which is toxic to cells that are able to metabolise uracil.

As it has been suggested that DNA attached to the cell wall enters the cells during transformation (Kawai S. *et al.* 2010), the concentration of transforming DNA was increased as this may increase the chance of DNA attachment/entry into the cell and subsequent integration. However, it is not known whether the failure to transform *L. starkeyi* was as a result of the transforming DNA being unable to enter the cell or failure to integrate into the genome. In order to elucidate the fate of the transforming DNA, a GFP tagged DNA cassette could be utilised for transformation and assessment of DNA entry into the cell assessed via fluorescence microscopy.

A published protocol for *L. starkeyi* by Calvey *et al.* (2014) was reported to yield transformation efficiencies of >8000 transformants/µg DNA for the integrative vector used. Although modifications were made, such as addition of DMSO and an overnight recovery period, viable transformants were not yielded. Addition of DMSO to transformation mixtures was conducted prior to heat shock as it has been reported to affect the permeability of cell membranes facilitating DNA uptake (Murata *et al.* 2003). The recovery period was also increased as extended recovery periods were reported to improve the efficiency of transformation (Calvey *et al.* 2014). However, the method was not reproducible in the present study utilising a deletion cassette. The integrative vector used contained native *L. starkeyi* promoters and terminators for nourseothricin expression. In this study the *NAT* deletion module was produced using an *S. pombe* vector, which contained *S. pombe* transcriptional regulatory elements (Bahler *et al.* 1998). As such, it is possible that there was no transcription of the *S. pombe* selection marker in *L. starkeyi*. Therefore, the deletion cassette may have integrated into the genome, but it was unable to growth on the selection antibiotic.

As described earlier within this chapter, the protein sequences of *L. starkeyi* and *S. cerevisiae* are well conserved. Therefore, to study the role of the *L. starkeyi* MAPK protein, it was cloned and expressed in an *S. cerevisiae* cells deleted for *HOG1*. Recovery of the osmostress phenotype associated with the deletion of *HOG1* by the *L. starkeyi* MAPK would suggest it had a similar role in the osmostress response of the cell. Heterologous expression of mammalian MAPK proteins in *S. cerevisiae* has demonstrated the ability of p38 and JNK to recover osmosensitivity of *HOG1* deleted cells (Galcheva-Gargova *et al.* 1994, Saito and Posas 2012). On transforming *S. cerevisiae hog1Δ* with pRS315*LSMAPK* it was observed that *L. starkeyi* MAPK did not recover the osmotic stress sensitivity of the

cells (Figure 5.15). This could suggest that *L. starkeyi* MAPK does not hold a similar role to that of *S. cerevisiae* Hog1.

However, it is possible as the promoter region of *L. starkeyi* was utilised for transcription of the *L. starkeyi MAPK* within pRS315, that it was not recognised by the transcriptional machinery of *S. cerevisiae* meaning that the gene would not be transcribed. There are a number of transcription factors that regulate the expression of *HOG1* under various conditions including Hap1, Skn7 and Med2 (MacIsaac *et al.* 2006, Venters *et al.* 2011). Therefore for heterologous expression it was assumed that *L. starkeyi* would contain such transcription factor homologues. Upon analysis of the promoter regions of *L. starkeyi* and *S. cerevisiae* (1kb upstream of the ATG), they were found not to be well conserved exhibiting only 43.97% similarity (Appendix I, Figure A9). In order to overcome this, the employment of inducible promoters could be used to express *L. starkeyi* MAPK in *S. cerevisiae.* Alternately *L. starkeyi* MAPK could be cloned and placed under the control of the *HOG1* promoter.

It was demonstrated in Section 5.3.1 that the nucleotide sequence of *L. starkeyi MAPK* was 1.4 kb in length and in Section 5.4 that the mass of the protein is approximately 40 kDa. In contrast, the *S. pombe sty1* nucleotide sequence is 1.0 kb and protein 40 kDa and *S. cerevisiae* 1.3 kb and 50 kDa respectively. This demonstrated that the translated genomic DNA sequence for the *L. starkeyi* MAPK did not match with the identified size of the protein. Upon analysing the 3-frame translation of the *L. starkeyi* MAPK sequence via the genome portal of JGI it was discovered that the sequence contains 6 introns ranging between 47 and 65 base pairs long (Appendix I, Figure A10).

It has been demonstrated that another oleaginous yeast species, *Y. lipolytica,* has an intron rich genome (Mekouar *et al.* 2010). However no introns were identified within the sequence of its p38 homologue. After removal of the introns, the cDNA of *L. starkeyi MAPK* was found to be a similar length to *S. pombe sty1* at ~1.0 Kb (Appendix I, Figure A11). After analysing *S. pombe* and *S. cerevisiae sty1* and *HOG1* sequences via PomBase and the *Saccharomyces* genome database neither sequence contained introns. This suggested that the *L. starkeyi* MAPK may be transcribed in the *hog1Δ* strain, but the introns may not be spliced to form mature mRNA. This is supported by *S. cerevisiae* harbouring very simple splicing machinery, as there are only 5% of genes which contain introns in *S. cerevisiae* (Juneau *et al.* 2006). In order to confirm that the MAPK of *L.*

*starkeyi* was not expressed a Northern blot could be performed utilising the *hog1Δ* expressing *HOG1* as a positive control. If *L. starkeyi MAPK* is not found to be expressed it could be cloned utilising processed mRNA reverse transcribed to cDNA before transformation into the *S. cerevisiae hog1Δ* strain.

As a potential MAP kinase has been identified for *L. starkeyi,* it would be required to be part of a pathway in order to function. In order to identify if the potential MAPK identified had conserved upstream regulators and downstream targets, bioinformatics analyses were performed using the *Lipomyces* genome portal, JGI. After BLAST analysis of *S. cerevisiae* and *S. pombe* MAPK components using the *Lipomyces* genome database provided by JGI, MAPK protein homologues were identified in *L. starkeyi* which produced a potential MAPK cascade (Figure 5.16). All components from the MAPKKK to transcription factors were found to have homologues in *L. starkeyi* with the MAPKKs and MAPKs conferring the greatest similarity when compared to *S. cerevisiae* and *S. pombe.*

For downstream targets, homologues of *S. pombe* Aft1/Pap1 were identified but were found to only be 27% and 24% similar. In comparison for Msn2/4, homologues were identified that conferred 57% similarity, which may suggest that *L. starkeyi* is more conserved at the transcription factor level to *S. cerevisiae* than *S. pombe.*

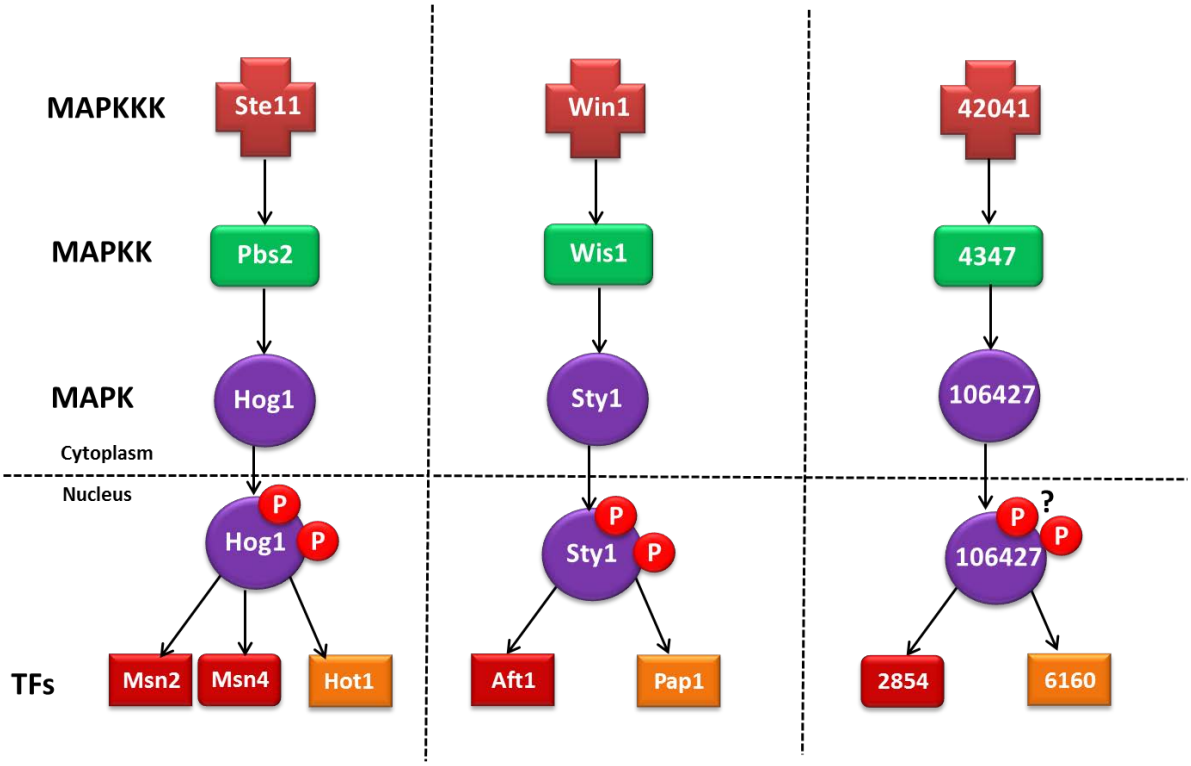


**Figure 5.16: Potential MAPK cascade identified for *L. starkeyi* via bioinformatics.** Left: *S. cerevisiae* HOG pathway. Centre: *S. pombe* Sty1 pathway. Right: potential MAPK pathway. The *L. starkeyi* MAPK pathway was constructed from searching the *Lipomyces* genome portal database, JGI using protein-protein BLAST. Searches were conducted utilising the protein sequences of MAPK components from both *S. cerevisiae* and *S. pombe*. *L. starkeyi* proteins are named based on their protein identification number obtained from JGI, TFs: Transcription factors. Protein identification; 42041: MAPKKK (Pbs2 homologue), 4347: MAPKK, 106427: MAPK, 2854: Msn2/4 homologue, 6160: Atf1 homologue.

In this chapter it has been demonstrated that the stress response of *L. starkeyi* was more similar to that of *S. cerevisiae* than *S. pombe*, suggesting that the role of the MAPK pathway in *L. starkeyi* may be conserved to this yeast species.

It has been further demonstrated that although the nucleotide sequence of the identified MAPK homologue in *L. starkeyi* is not well conserved, there is a high degree of conservation at the protein level. Further, it was been highlighted that further work is required on the development of molecular tools for *L. starkeyi,* for both transformation and detection of proteins utilising antibodies.

Finally it was shown that *L. starkeyi* may have a potentially functional MAPK pathway, from the identification of MAPK components that are homologous to those present in both *S. cerevisiae* and *S. pombe*. In conclusion, once reliable molecular tools are developed and optimised, it is expected that *L. starkeyi* would serve as an excellent complementary model organism for investigating the regulation of lipid accumulation via the MAPK pathway.

# Chapter VI Discussion

## 6.1 Discussion Summary

Since the observation by Otto Warburg in the 1920s that cancerous cells have an altered metabolic state, the regulation of tumour metabolism has become an increasingly important area of research. Although increased *de novo* lipogenesis in solid tumours has been well described, there are still many questions remaining on the impact of complex upstream signalling networks on the metabolism of lipids. As such, a greater understanding of signalling processes residing upstream of lipid regulatory proteins will ultimately aid in the development and implementation of novel therapeutic strategies. Due to the complex nature of mammalian systems, yeast have been increasingly utilised to study the regulation of lipid accumulation. This has aided the understanding of fundamental metabolic processes which are applicable to mammalian cells.

This study has focused on the regulation of lipid accumulation via the stress induced MAP kinase pathway, which is structurally and functionally conserved within yeast. A Nile red method for assessing levels of both polar and neutral lipid pools has been developed and has allowed characterisation of lipid phenotypes in yeast cells. This method has been used to demonstrate that the MAP kinase pathway plays a key role in the regulation of neutral and polar lipid accumulation. This regulation is conserved both in the budding yeast, *S. cerevisiae*, and the fission yeast, *S. pombe,* at the point of the central MAPK. The investigation has been further extended to study the use of the non-conventional yeast species, *L. starkeyi*, as a model organism. Use of this oleaginous lipid -accumulating yeast may, in future, further enhance our understanding of the role of MAP kinase and other pathways in the regulation of lipid accumulation. Ultimately, this may lead to the identification of novel targets for improved treatment of tumour-associated lipid formation.

## 6.2 Assessment of neutral and polar lipid classes utilising Nile red

As there is much unknown about the regulation of lipid accumulation an increased throughput methodology would allow components that are involved to be quickly and easily identified. Identification of novel regulatory components would increase understanding of the underlying mechanism of lipid accumulation, which would lead to an enhanced understanding of diseases including cancer. This would then lead onto facilitating the development of improved treatment strategies.

As described in Chapter 3, currently employed methodologies for the assessment of cellular lipids are often labour intensive and time consuming, involving several steps and often necessitate the use of large amounts of organic solvents. Further to this, the lipidologist must take precautions to ensure extracted lipids are not oxidised either by contaminants, such as plasticisers from plastics, or enzymes and oxygen. It is generally accepted that there is no single method of extraction that is capable of obtaining 100% lipid yield. Inherent problems with commonly used extraction methods, including those developed by Bligh and Dyer (1959) along with Folch *et al.* (1957), include inefficient cell wall breakage along with underestimates of neutral lipids in extracts comprising more than 2% lipid (Iverson *et al.* 2001).

Gas chromatography and liquid chromatography coupled with mass spectrometry are commonly utilised sensitive techniques to evaluate cellular lipids (Yang Kui and Han 2011). These techniques not only allow for assessment of cellular lipid amounts, but also allow comprehensive analysis of different lipid classes present. Due to the rapid growth of lipidomic research the development of higher throughput methodologies is being trialled. Direct infusion techniques, which do not comprise of a prior chromatographic separation, allow simultaneous analysis of multiple lipids in high throughput format. However, they have previously been shown to lack the ability to distinguish all lipid molecules present (Li Min *et al.* 2013). As such, for a more quantitative and comprehensive analysis of the lipidome, use of chromatographic separation is essential and therefore is more time consuming (Li Min *et al.* 2013). Furthermore, two separation protocols are often required in order to analyse both neutral and polar lipids which has sparked interest in the development of one step systems to analyse major components of both neutral and polar lipid pools simultaneously (Shui *et al.* 2010).

Although this highlights significant progress in the development of high throughput lipid analyses by more sophisticated means, such as GC and LC, the preparation of samples is still considered laborious and time consuming and does not allow for *in situ* measurement of cellular lipid content.

As such, screening large numbers of samples is complex and highlights the need for increased throughput methodology in order to identify key components which may then be promoted for further in-depth analyses. The Nile red fluorescence assay developed in this study (Chapter 3) allows for rapid identification of neutral and polar lipid levels *in situ*, abolishing the requirement for multiple extractions of samples which may not yield an informative phenotype.

Other dyes for assessing lipid status of cells have been described that could potentially be utilised in high throughput screening, including BODIPY, Sudan Black, LD540 and Oil Red O, which all have advantages and disadvantages in their application. However, the non-fluorescent dye Sudan Black, does not provide accurate assessment of lipid content, often producing false positive absorbance readings (Li Shi Lin *et al.* 2012). Oil red O allows fluorescent detection of neutral lipid within cells but not polar lipids and has not been utilised as extensively in yeast as Nile red. The fluorescent dye BODIPY can also be used to detect neutral lipids and has been found to have greater specificity in its detection of neutral lipid droplets. The major disadvantages of BODIPY are that it cannot be used to infer polar lipid status and its higher cost in comparison to Nile red. LD540, a fluorescent dye based on the BODIPY fluorophore shows a significant reduction in photo bleaching compared to Nile red, although under intense illumination lipid droplet fusion may be propagated by LD540 (Radulovic *et al.* 2013).

Whilst all lipophilic dyes will have their merits, Nile red is one of the most established and widely utilised. Nile red has been extensively employed in the biotechnological field as a fast, efficient lipid detection and quantification tool to identify high lipid producing microalgae and yeast species in the production of biofuels (Chen Wei *et al.* 2009, Diaz *et al.* 2008, Ren *et al.* 2013). Further to this Nile red has also been used to screen for the production of microbial biosurfactants (Castro *et al.* 2005) and has been additionally applied to detection of polyhydroxyalkanoates (PHAs). PHAs are a class of polymer produced by stressed microorganisms which may be used in the production of environmentally friendly alternatives to plastics (Zuriani *et al.* 2013).

The dual wavelength capability of Nile red has made it particularly attractive for use in the current study, allowing for analysis of neutral and polar lipid levels simultaneously with a single dye (Diaz *et al.* 2008). It has been demonstrated, for the first time, that a Nile red assay can be applied to the fission yeast *S. pombe*. This is of particular importance due to growing interest and research in the area of *S. pombe* lipid metabolism, not only for modelling mammalian lipid accumulation but also to facilitate use as a potentially relevant tool in the biotechnology industry.

As described in Chapter 3, the method is not without its limitations, namely rapid bleaching of red emission, neutral and polar lipid fluorescence values cannot be directly compared and that the assay is limited to general pools of lipids. Knowing more about the levels of individual molecular species is important to dissect the specific contribution of components in the metabolism of lipids. For example, to determine whether deletion strains differ from wild type cells in the PC composition of the polar lipid pool, rather than PS or PE. Therefore further analysis to determine changes in molecular species would need to be conducted by other means, such as gas/liquid chromatography.

However, as discussed in Chapter 3, the increased throughput nature of the Nile red assay allows for rapid identification of components that have a significant impact on the accumulation of lipids. Incorporation of the dual wavelength feature also ensures that information pertaining to carbon flux for polar lipids is not overlooked. By exploiting the dual wavelength capability of Nile red in this study, two components of the MAPK signalling pathway have been identified that have not been previously implicated in lipid biosynthesis, with one having a potential role in both neutral and polar lipid homeostasis. This emphasises the usefulness of employing both neutral and polar wavelengths when screening yeast gene deletions to assess involvement in lipogenesis.

Nile red has been extensively used both for microscopic and assay based fluorescence studies for the assessment of lipid status in numerous systems aside from yeast including *Caenorhabditis elegans* (Lemieux *et al.* 2011) (Soukas *et al.* 2013), *Drosophila* (Reis *et al.* 2010) (Liu Z. and Huang 2013), bacteria (Zuriani *et al.* 2013), zebrafish (Flynn *et al.* 2009) (Tingaud-Sequeira *et al.* 2011) and microalgae (Chen Wei *et al.* 2009, Ren *et al.* 2013). Nile red has also been utilised in staining of mammalian cells such as macrophages (Greenspan *et al.* 1985) and cell lines which include MCF-7 (breast cancer), HepG2

(hepatic cancer) (Drabsch *et al.* 2010, Yao *et al.* 2011). As such, it is possible to further develop this methodology for differential wavelength screening in a variety of model systems which are inclusive of mammalian cells.

## 6.3 Use of yeast as a model organism for lipogenesis

Previous published data and this thesis have proven that yeast systems are an excellent model system for deconstructing the regulation of lipid metabolism (Henry *et al.* 2012). Although differences exist, especially at the enzyme level, between lipid metabolism in yeast and mammalian cells the mechanisms involved in lipid accumulation are largely conserved (as described in Chapter 1). Additionally the growth of yeast in the presence of glucose is similar to that of the Warburg effect observed in cancerous cells (Vander Heiden *et al.* 2009). There are also potentially strong similarities with respect to regulation of metabolism by oncogene homologues found in yeast, as highlighted in a review by Diaz-Ruiz *et al.* (2011). Furthermore the present study has also shown that deletion of the mTORC1 homologue results in a reduced lipid phenotype (Figure 4.4 and 4.5), which is consistent with the role of mTORC1 as a positive regulator of lipid synthesis in mammalian systems.

Much of the research conducted in yeast lipid metabolism has centred on employment of the budding yeast species *S. cerevisiae*. *S. cerevisiae* has been extensively characterised owing to it being the first eukaryotic organism to have its entire genome sequenced. The conservation highlighted earlier, coupled with the simplified lipidome and ease of genetic manipulation compared to mammalian cells (Santos AXS. and Riezman 2012) placed *S. cerevisiae* as a superior model yeast for investigating the regulation of metabolic processes.

As previously described in Chapters 1 and 3, the regulation of lipid metabolism is becoming increasingly investigated due to potential exploitation in the biotechnology industry. Furthermore, *S. pombe* may prove to be a good complementary organism due to its higher degree of conservation to mammalian cells, as described previously in Chapter 1. Additionally *S. pombe* may be superior model for investigation of *de novo* lipid formation owing to the high rate of *de novo* lipid synthesis exhibited in exponential phase growth (Figure 3.49 and 3.50).

Oleaginous yeasts have been primarily employed in the biotechnology industry for production of useful products such as biofuels, biosurfactants and cocoa butter substitutes, reviewed in (Gon *et al.* 2014). It is suggested that oleaginous species, including *L. starkeyi* may prove useful as model organisms for understanding metabolic processes in human disease. It has been described previously that oleaginous species, such as *L. starkeyi,* may be more similar to humans with respect to metabolism, as they contain ATP citrate lyase (Boulton and Ratledge 1981). Furthermore, the present study has demonstrated that the MAPK of *L. starkeyi* contains introns (Appendix I, Figure A10). The human homologue also contains introns, yet *S. cerevisiae/S. pombe* Hog1/Sty1 do not further highlighting that *L. starkeyi* may be a superior model for analysis of lipid accumulation via the MAPK pathway.

The major current disadvantage in utilisation of *L. starkeyi* is the lack of robust molecular tools available for genetic manipulation along with the potential requirement for the development of antibodies. However, if the genetic tools are developed the need for antibodies for protein detection would be circumvented by the ability to genomically tag cellular components for detection. It is suggested that, until reliable molecular tools are available, *Y. lipolytica* could be utilised to offer insight into the impact of the MAPK pathway on lipid accumulation. Although less well characterised than *S. cerevisiae* and *S. pombe, Y. lipolytica* has been sequenced, utilised for human mitochondrial disorder research and has a number of molecular tools already developed. As an oleaginous yeast species it is also expected to contain ATP citrate lyase activity and furthermore contains a Hog1 homologue (Nikolaou *et al.* 2009).

## 6.4 The role of Hog1p in the regulation of lipogenesis

The data presented in Chapter 4 confirmed the involvement of the stress activated MAPK pathway in the accumulation of lipids. In *S. cerevisiae,* lipid signalling converges at the MAPK Hog1, with upstream members of the HOG pathway, Sho1, Ste11 and Pbs2, not playing a significant role in the accumulation of neutral or polar lipids. If Pbs2 was directly involved, a similar level of reduction in lipid accumulation, as seen in *HOG1* deficient cells, would be expected. As such, it is suggested that the regulation of Hog1 in the process of lipid accumulation is distinct from that of the canonical pathway, Figure 6.1.

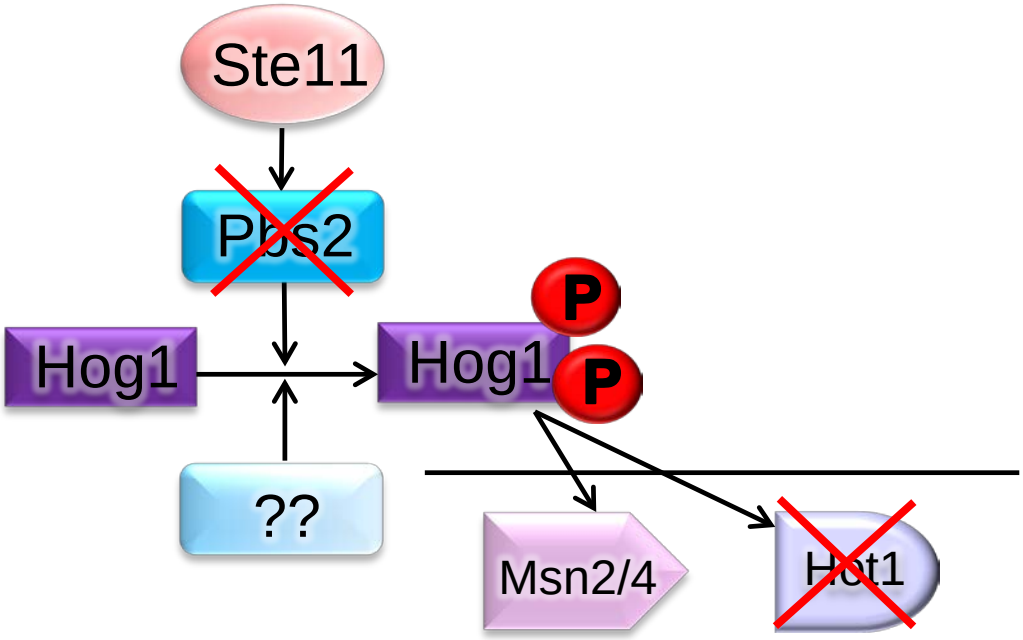


**Figure 6.1: Pbs2 independent activation of Hog1.** From Nile red screening conducted in chapter 3, Pbs2 did not appear to be involved in the accumulation of cellular lipids nor did a direct target of Hog1, Hot1p. Phos-tag suggested that a Pbs2 independent activation occurred preceding the point of increased lipid accumulation. This suggested that lipid accumulation via Hog1p did not occur as a result of activation via the canonical pathway.

Although there is no published data suggesting a direct activator of Hog1 other than Pbs2, evidence in chapter 4 suggested that Hog1 can be activated via a Pbs2 independent mechanism and this may have resulted from phosphorylation on previously undescribed residues (Figure 4.34). However, Pbs2 dependent phosphorylation of Hog1 was observed in *S. cerevisiae* in late exponential phase of growth which suggested it may play a role in activating Hog1, which is distinct from its initial activation (Figures 4.30, 4.31 and 4.33).

One potential Pbs2 independent mode of Hog1 activation in the response of *S. cerevisiae* to accumulate lipid is autophosphorylation. Hog1 autophosphorylation has been demonstrated to occur on both tyrosine and threonine residues under severe osmotic stress (Maayan *et al.* 2012). This highlighted the possibility that Hog1p could similarly be autophosphorylated on currently undescribed residues. Another possibility is the interconnection of other pathways upstream converging at the point of Hog1. Upstream signalling components that have been described to potentially influence Hog1 signalling by indirect or direct means include Tor and Sch9.

Analysis of the yeast phosphoproteome gave additional insight that Tor complex 1 is involved in the modulation of a range of glycolytic genes, not only at the transcriptional level but also at the post-translational level (Loewith 2011). It has been demonstrated in Chapter 4 that Tor1 is involved in regulating the accumulation of neutral lipids, as *TOR1* deficient cells exhibit a significant decrease of 1.3 fold in the neutral lipid pool compared to wild type (Figure 4.4). One of the major targets of Tor1 containing complex, TORC1, is the AGC protein kinase Sch9 (Urban *et al.* 2007a). Similarly in cells deleted for *SCH9,* it has been shown that the levels of TAGs and other neutral lipids were markedly reduced compared to wild type cells (Wei *et al.* 2009). This suggests that Tor1, Sch9 and Hog1 may be interconnected in the signalling mechanisms that regulate the accumulation of lipids. This is further supported by data in Chapter 4, where the neutral lipid decrease observed in *HOG1* deleted cells is 1.7 fold (Figure 4.21). The increased reduction in cells deleted for *HOG1* compared to *tor1*Δ cells, suggests Tor1 may feed into Hog1, which may hold the central role in regulating lipogenesis

Taken together, with data from the present study a two phase lipid accumulation regulatory mechanism is proposed, comprising of both Pbs2 independent and Pbs2 dependent Hog1 activation. This two phase mechanism facilitates the accumulation of

cellular lipids in *S. cerevisiae* over the course of growth from exponential to stationary phase.

In phase one (Figure 6.2) where cells are growing exponentially, potential Pbs2 independent Hog1 phosphorylation was observed 7.5hrs post resuspension in YNB (Figure 4.34). As described in Chapter 4, this was the point preceded by a marked increase in lipid accumulation in mid exponentially growing cells. In conditions where nutrient supply is favourable, as in exponential phase, Sch9 is phosphorylated and activated by Tor1 (Urban *et al.* 2007a). In addition, it has been suggested that Sch9 is activated in a Tor1 independent manner via ceramide signalling (Teixeira *et al.* 2013). Not only has Sch9 been shown to interact with Hog1 *in vitro,* Hog1 has also been shown to be a phosphorylation target of Sch9, further supporting the model of a potential Sch9 dependent Hog1 activation facilitating the accumulation of cellular lipids (Pascual-Ahuir and Proft 2007, Teixeira *et al.* 2013). Additionally, Sch9 is functionally related to PKA and has been demonstrated to share a number of phosphorylation targets, which include Hog1 (Zhu *et al.* 2000).

It is likely that at this point that the majority of Hog1 is present in the cytoplasm and is involved in the regulation of lipid regulatory proteins. It is expected that there are other potential downstream targets of Hog1 that could either be directly or indirectly activated by Hog1. Data in Chapter 3 showed that cells lacking *DGA1* had a ~1.4 fold reduction in neutral lipids compared to wild type cells (Figure 3.27). A similar reduction of ~1.6 fold in neutral lipid accumulation is observed in *HOG1* deleted cells, suggesting that Hog1 may interact directly with proteins involved in lipid accumulation. As Dga1 catalyses the terminal step in TAG formation is was speculated that this similar decrease may indicate an interaction between Hog1 and Dga1.

Upon analysis of the protein sequence of Dga1, potential MAP Kinase binding sites were found, indicating the possibility that Hog1 could phosphorylate Dga1 to regulated neutral lipid accumulation (Figure 4.35). Two of the identified potential MAPK sites in Dga1 were at the N terminus of the protein, S17, which has been assigned as a phosphoserine (Li X. *et al.* 2007), and T53, which sit on the cytoplasmic side of the ER membrane. Phosphorylation of these sites by Hog1 may result in activation of Dga1 and cause an increase in TAG levels within the cell.

Other potential targets of Hog1 include the lipid associated SREBP-like transcription factors Ecm22, Upc2, Spt23 and Mga2, which are involved in regulating the transcription of lipid biosynthetic genes. The inactive membrane bound SREBP-like proteins of *S. cerevisiae* require cleavage from the membrane in order to be activated and transported to the nucleus to facilitate transcription of lipid regulatory genes. Bioinformatics data presented within Chapter 4 depicts that several potential MAPK phosphorylation sites exist within the protein sequences of all four SREBP-like proteins. This suggests that Hog1p may promote activation and nuclear translocation of SREBP-like proteins via direct phosphorylation to support neutral lipid regulation. This concept is supported by evidence that the mammalian p38 MAPK directly phosphorylates SREBP-1a in hepatic cells, linking stress response pathways with cellular metabolism and supporting sterol independent activation of SREBPs (Kotzka *et al.* 2012). The proposal of SREBP-like protein activation via Hog1 is further supported by the suggestion of Hickmann *et al.* (2011) where it was proposed that Hog1 may interact with and activate Upc2 under conditions of hypoxia (Hickman M J. *et al.* 2011).

For more polar lipids the role of the HOG pathway as a potential regulator is unclear. Hog1 may not be involved in phospholipid synthesis as altered membrane permeability suggests that this could be the cause of reduced phospholipids. However, phospholipid regulatory elements, Cho1 and Cho2, contain potential MAPK sites (Figures 4.37 and 4.38) and so further investigation on the role of Hog1 in polar lipid accumulation is required.

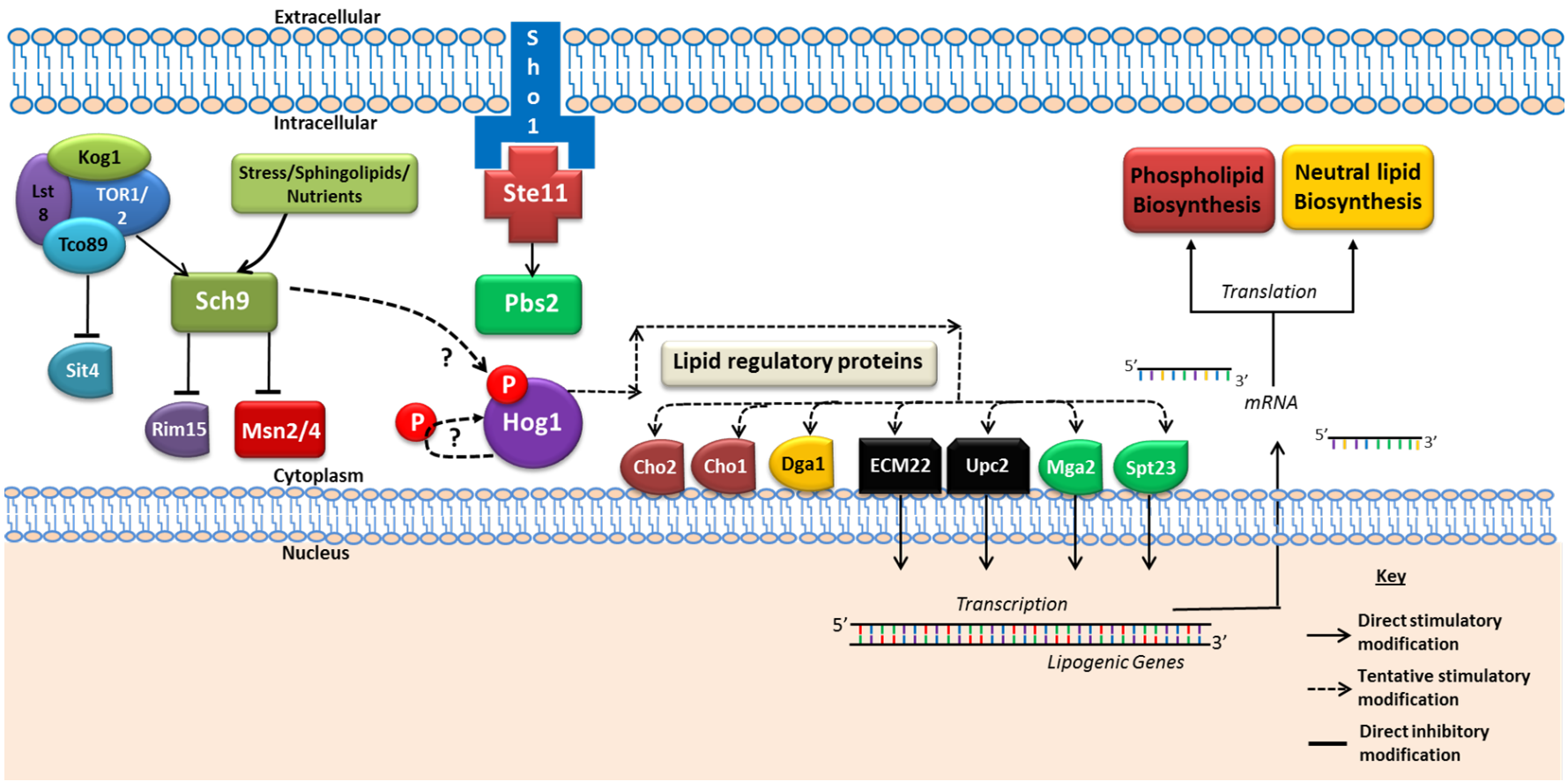


**Figure 6.2: Phase one of the proposed *Saccharomyces cerevisiae* model, Pbs2 independent regulation of lipid homeostasis by Hog1.** Under conditions where nutrients are available, the TORC1 is active, this in turn can activate the protein kinase Sch9 and inhibit the phosphatase Sit4. It is possible that Sch9 can be activated directly by an unknown mechanism, related to the lipogenic switch. Activated Sch9 inhibits Rim15 and the transcription factors Msn2/4 by retaining them in the cytoplasm, preventing nuclear accumulation. It is postulated that Sch9 may also phosphorylate Hog1 on a previously uncharacterised amino acid residue. Hog1 may also autophosphorylate itself through an unknown mechanism. Once phosphorylated, Hog1 is retained in the cytoplasm where it can potentially interact with a number of targets including lipid regulatory proteins including Cho1, Cho2, Dga1, Ecm22, Upc2, Mga2 and Spt23. The SREBP like proteins, Ecm22, Upc2, Mga2 and Spt23 may then translocate to the nucleus, where they can activate transcription of a number of lipogenic genes.

In phase 2 of the model proposed by this study, Figure 6.3, where nutrient supply becomes decreased, Pbs2 dependent dual phosphorylation of Hog1 is observed (9 hrs post resuspension YNB) (Figures 4.30 and 4.31). This dual phosphorylation of Hog1 has been previously demonstrated following nutrient limitation (Aoki Y. *et al.* 2011); however, data in Chapter 4 does not support this (Figure 4.32). It is suggested that phosphorylation of Hog1 may occur at a much earlier time point than the 3 hrs analysed in this thesis, therefore it cannot be discounted that it is involved in phase 2 activation. Dual phosphorylation of Hog1 has been linked to its translocation and accumulation in the nucleus (Ferrigno *et al.* 1998, Reiser *et al.* 1999). Previous studies have indicated a role for Sch9 in regulating cellular stress responses (Pascual-Ahuir and Proft 2007, Wei *et al.* 2009). As such, the regulation of downstream HOG pathway components could be modulated by two mechanisms. When nutrient supplies are decreased Tor1 is inhibited, which in turn leads to decreased phosphorylation of Sch9. A decrease in Sch9 activity leads to de-repression of Rim15, which is then able to translocate to the nucleus and activate the transcription factors Msn2/4 (Lee *et al.* 2013).

Additionally Sit4 phosphatase activity is increased in response to Tor inhibition which could serve to negatively regulate Hog1p. This is supported by the observation that Hog1 dual phosphorylation is increased in cells deleted for *SIT4* (Teixeira *et al.* 2013). However, in this study at the stage when decreased Tor1 is predicted to occur and in turn increased activity of Sit4, dual phosphorylation of Hog1 is observed. This suggests that Pbs2 is phosphorylating Hog1 in phase 2, additionally Sit4 could potentially facilitate the removal of the potential novel phosphorylation of Hog1 by Sch9. It is postulated that as a consequence of the signalling described in phase one, including inhibition of Rim15 which is involved in the induction of the oxidative stress response, this could result in increased levels of cellular reactive oxygen species (ROS) (Weinberger *et al.* 2010). As such, this could lead to stress related Pbs2 dependent activation of Hog1 via the canonical pathway (Smith *et al.* 2004).

Following dual phosphorylation of Hog1 by Pbs2, activated Hog1 is then able to translocate to the nucleus to drive expression of both stress responsive and potentially lipid regulatory genes via Msn2/4. It was demonstrated in chapter 4 that *S. cerevisiae* SREBPs Ecm22 and Mga2, contain full STRE elements within their promoter regions. Furthermore, Spt23 and Upc2 contain conserved regions of these STREs, PDS elements (Figures 4.43 and 4.44). This further supports a role for Msn2/4 as a key component in the transcriptional regulation of cellular lipid accumulation in *S. cerevisiae.* This suggested that Msn2/4 holds a role in regulating neutral lipid levels via driving expression of SREBPs. However, whether this regulation is dependent on Hog1p or Rim15p is unclear and would require further investigation.

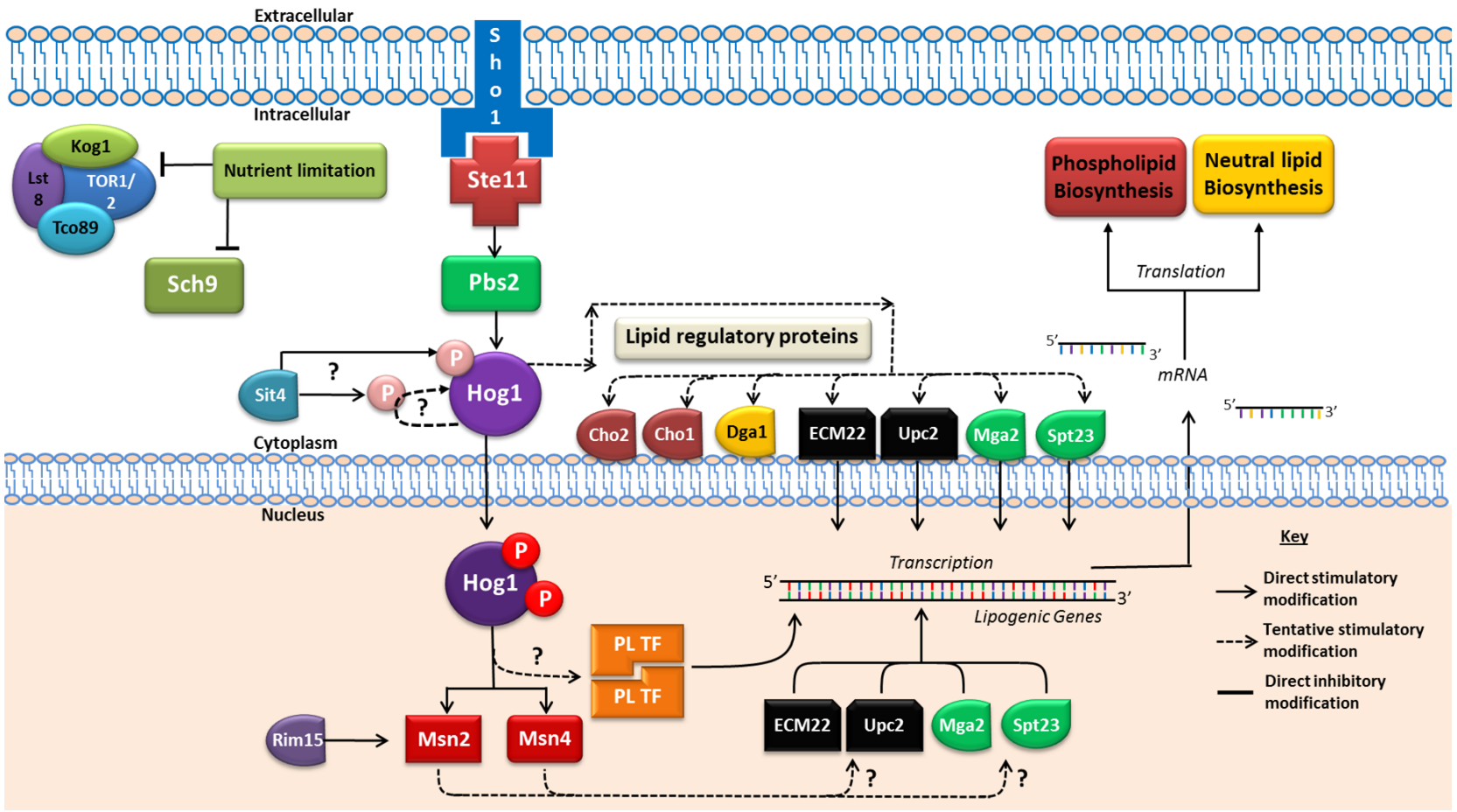


**Figure 6.3: Phase two of the proposed *Saccharomyces cerevisiae* model, Pbs2 dependent regulation of lipid homeostasis by Hog1.** As nutrients become depleted in the environment, the cell inhibits TORC1, which in turn inactivates Sch9 and activates the phosphatase Sit4. Sit4 may act directly on Hog1, dephosphorylating the novel phosphorylation added by Sch9 or its autophosphorylation. Activation of the canonical pathway, via Pbs2, results in dual phosphorylation of Hog1 which translocate to the nucleus and activates transcription both directly and indirectly via Msn2/4. Msn2/4 is also activated both directly and indirectly, by Rim15, following Sch9 inhibition.

## 6.5 The role of Sty1p in the regulation of lipogenesis

It has been demonstrated in Chapter 4 that lipid accumulation is similarly attenuated in Sty1 MAPK pathway mutants of *S. pombe,* highlighting that the regulation of lipid accumulation is conserved in *S. cerevisiae* at the point of the MAPK. Interestingly, in the case of *S. pombe* the regulation of lipid accumulation may extend further upstream to the level of the MAPKK, Wis1 as a similar decrease in lipid was also observed upon its deletion (Figure 4.48 and 4.49). Due to the extensive use of *S. pombe* as a model organism it is possible that the role of the upstream MAPKK may also be conserved in a mammalian system.

The mechanisms underlying how lipid accumulation is regulated by Sty1 are unclear in comparison to *S. cerevisiae* as there is much less known about lipid accumulation and regulation. There is a further level of complexity added as Sty1 does not only serve to regulate the response of cells to stress, but also modulates and plays an important role in other pathways including cell cycle regulation (Sturgill and Hall 2007). However, it is feasible that lipid accumulation could occur via a similar two phase system in *S. pombe.*

As described in Chapter 1 it is important to note that Tor2 in *S. pombe* is analogous to *S. cerevisiae* Tor1 (mammalian mTORC1) and *vice versa*. It has been reported that Tor2 function in *S. cerevisiae* is similarly regulated to Tor1 in *S. cerevisiae* with respect to nutrient availability which is concomitant with phase one of the proposed *S. cerevisiae* model, as discussed below.

Tor2 is activated in conditions where nutrient supply is plentiful and is inactivated in when nitrogen is restricted (Nakashima *et al.* 2010). *S. pombe* contains at least three Sch9 (S6K) homologues Sck1, Sck2 and Psk1. Although it is largely unclear whether TOR complexes in fission yeast interact with S6K homologues, it has been suggested that, in nutrient rich conditions, Tor2 phosphorylates Sck1 and Sck2 (Nakashima *et al.* 2012b). Furthermore it was demonstrated *in vitro* that Psk1 function is dependent on Tor2 phosphorylation (Nakashima *et al.* 2012b).

Taken together it is possible that Sck1, Sck2 or Psk1 could interact with and activate Sty1, as is the case with the model for *S. cerevisiae*. This connection is supported by the recent suggestion that Sck1 may elicit a biological response to nutrient availability through regulation of the Sty1 pathway in *S. pombe* (Mudge *et al.* 2014). Additionally an interaction of Sty1 with Sck2 has been suggested in connection with life span extension. Zuin *et al.* (2010) showed that lifespan promotion via deletion of *sck2* was dependent on the function of the Sty1 pathway (Zuin *et al.* 2010b). Although no evidence for an interaction with Psk1 and Sty1 has been found, these two studies demonstrate that Sty1 and S6K homologue signalling in fission yeast is interconnected, highlighting the possibility that Sty1 is a potential downstream target of S6Ks.

However, as Wis1 was also found to be involved in regulating lipid accumulation, activation of the upstream MAPKK in a S6K dependent manner could serve as an indirect means of Sty1 activation (Figure 6.3). It is unknown following the present study whether Sty1 is activated at phase 1, a similar time course experiment of Sty1 phosphorylation by Phos-tag is required to identify if there is a potential Wis1 independent activation of Sty1. Following on from this mass spectrometry of purified protein could be used to identify novel phosphorylated residues, as discussed for Hog1 in Chapter 4. Furthermore, to clarify interaction of the S6K homologues in *S. pombe* with Wis1/Sty1 immunoprecipitation could be used to determine protein-protein interactions at the point where Sty1pathway components are required. If Sck1, Sck2 or Psk1 signalling does result in activation of Sty1 in phase 1, then modulation of lipid regulatory proteins identified via bioinformatics could be Sty1 dependent. Targets identified included Dga1, Plh1 (Lro1), Pps1 (Cho) along with SREBP proteins. This highlights that the lipid regulatory targets of Hog1 and Sty1 may also be conserved.

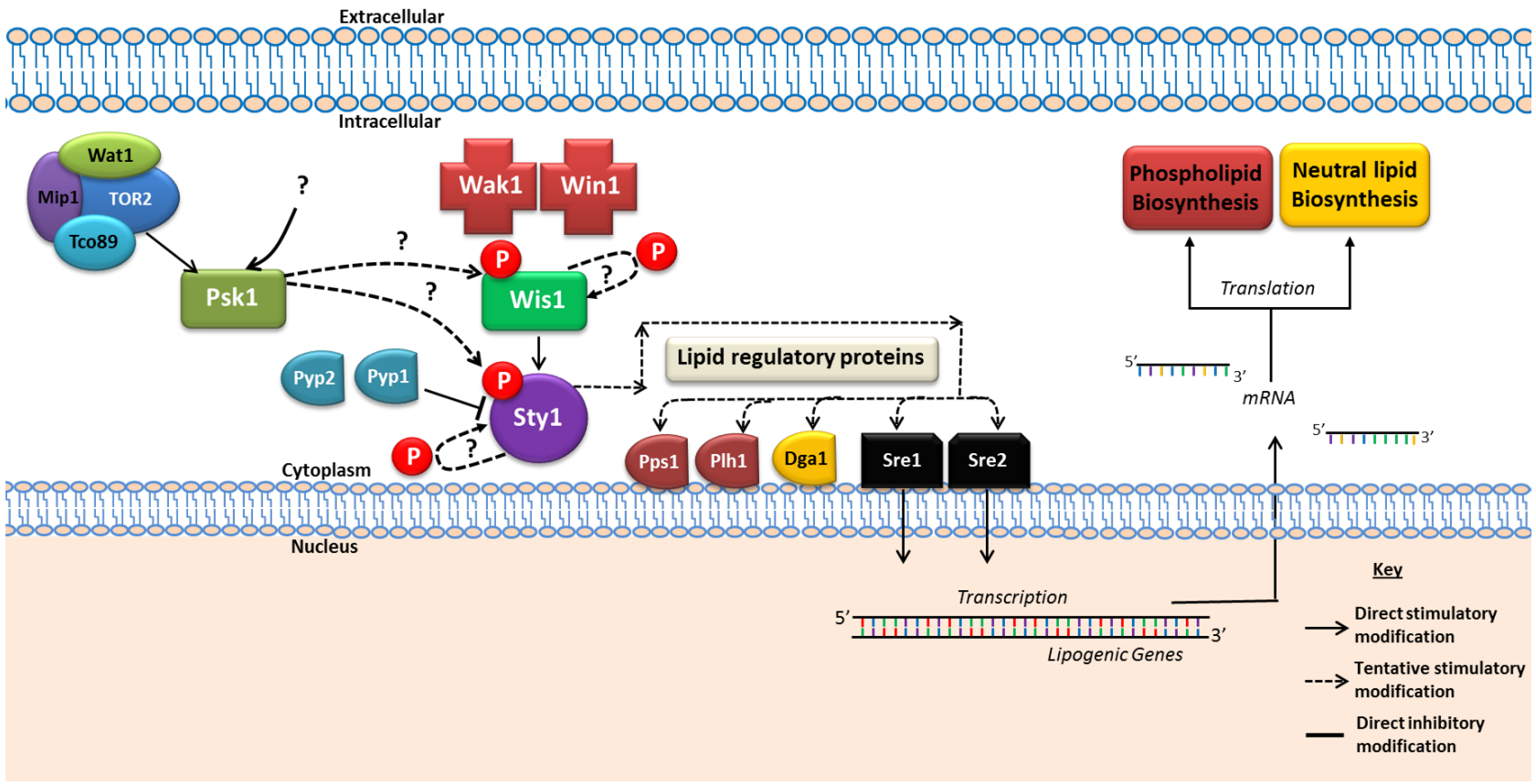


**Figure 6.4: Phase one of the proposed *Schizosaccharomyces pombe* model of regulation of lipid homeostasis by Sty1.** Under conditions where nutrients are available, the TORC2 is active, this in turn can activate the protein kinase Psk1. It is possible that Psk1 can be activated directly by an unknown mechanism, related to the lipogenic switch. It is postulated that Psk1 may phosphorylate both Wis1 and Sty1, possibly on novel residues. Wis1 and Sty1 may also autophosphorylate themselves through an unknown mechanism. Sty1 phosphorylation is also regulated via the phosphatases Pyp1 and Pyp2, possibly at the well characterised dual sites phosphorylated by Wis1, which may not be required for the lipogenic switch. Once phosphorylated, Sty1 is retained in the cytoplasm where it can potentially interact with a number of targets including lipid regulatory proteins including Pps1, Plh1, Sre1 and Sre2. The SREBP like proteins, Sre1 and Sre2 may then translocate to the nucleus, where they can activate transcription of a number of lipogenic genes.

Phase two of the proposed model for MAPK mediated regulation of lipid accumulation may also be similarly conserved (Figure 6.4). In response to decreased nitrogen Tor2 is inhibited which results in decreased phosphorylation of Psk1. The major difference between the models proposed for *S. cerevisiae* and *S. pombe* is that Sty1 is activated by dual phosphorylation in response to reduced levels of Tor2 signalling in *S. pombe* (Petersen and Nurse 2007), which occurs due to loss of Sty1 inhibition by Pyp2 and Pyp3 phosphatases. Nevertheless, this still indicates that Sty1 would be active in phase 2 conditions. As with Hog1, dually phosphorylated Sty1 is then able to translocate to the nucleus and potentially drive expression of key lipogenic genes. It has been demonstrated that phosphorylation of Hmg1, a HMG-CoA reductase which catalyses the first step in ergosterol synthesis, within the cytoplasm requires active Sty1 (Burg *et al.* 2008). This further strengthens the connections made between Sty1 and SREBP regulation made by the present study (Figures 4.59 and 4.60). Along with this it also highlights that dually phosphorylated Sty1 in phase 2 may activate cytosolic targets initially before translocation to the nucleus.

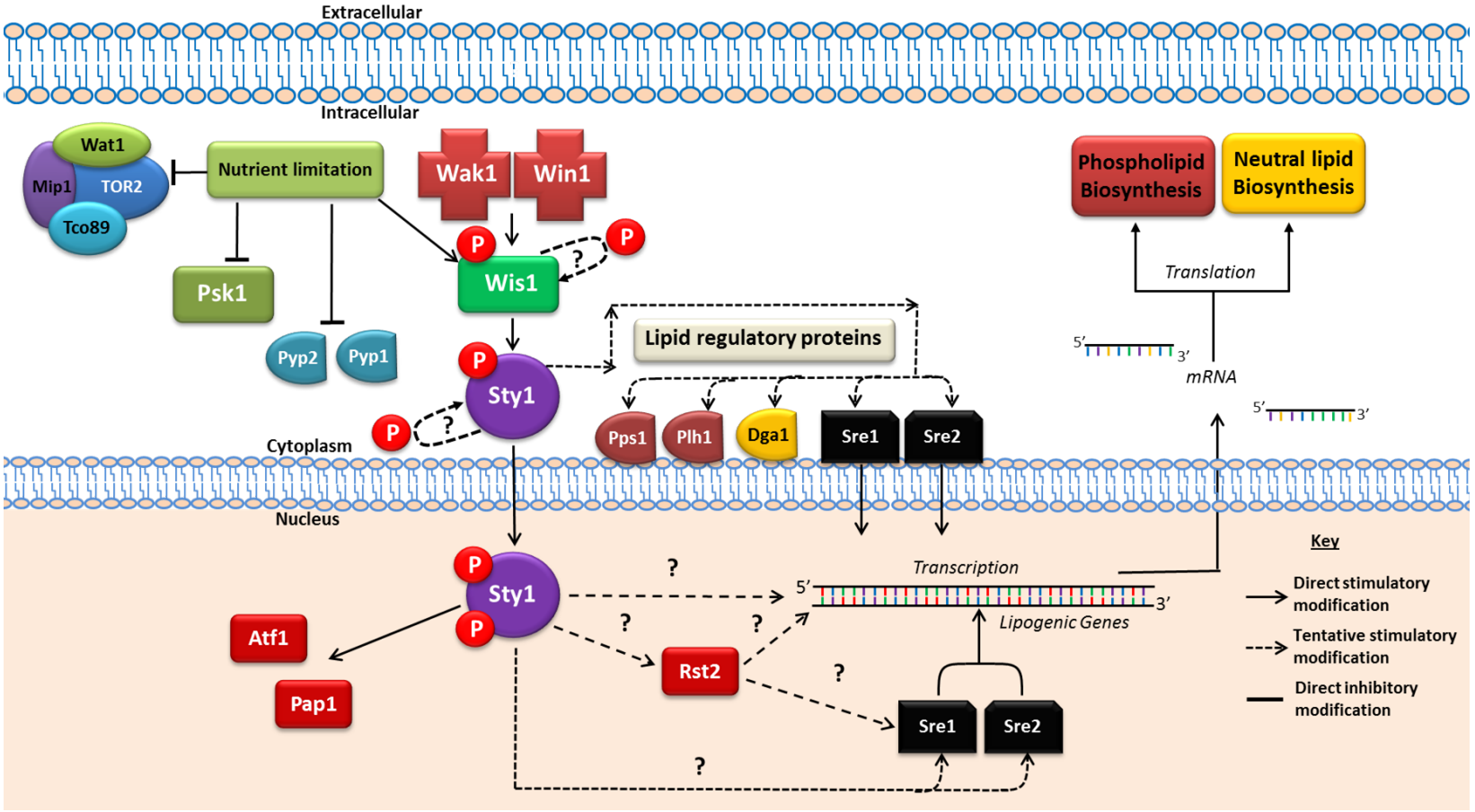


**Figure 6.5: Phase two of the proposed *Schizosaccharomyces pombe* model of regulation of lipid homeostasis by Sty1.** Under conditions of nutrient limitation, both TORC2 , Psk1, Pyp1 and Pyp2 are inhibited. Once dually phosphorylated by Wis1, Sty1 can translocate to the nucleus where it can possibly activate a number of targets both directly and indirectly, via the transcription factors Rst2, Sre1 and Sre2, including lipid regulatory proteins such as Pps1, Plh1, Sre1 and Sre2. Sty1 can also activate the transcription factors Pap1 and Atf1, but these don't appear to be important for the lipogenic switch.

Whether components downstream of Sty1 contribute to regulating lipid accumulation by the Sty1 MAPK pathway is unknown. Evidence presented in Chapter 4 suggested that direct downstream targets of Sty1, the transcription factors Atf1 and Pap1, do not play a significant role in the accumulation of cellular lipids (Figures 4.54 and 4.55). This may be due to a transcriptional response not being largely required for lipid accumulation via Sty1. As discussed in Chapter 4, the Sty1-KD mutant had an intermediate lipid phenotype, with levels determined to be between that of wild type and *Δsty1* cells (Figure 4.54 and 4.55). Although the kinase dead form of the Sty1 protein can be dually phosphorylated and translocate to the nucleus, it is unable to phosphorylate any of its targets. Further, it has been demonstrated that the Sty1-KD, following oxidative stress, cannot be recruited to the promoters of genes (Reiter *et al.* 2008). The partial effect on lipid accumulation of the Sty1-KD may suggest that Sty1 may not have a pivotal role in activating transcription in the regulation of lipid accumulation. Alternately, transcriptional activity of unknown downstream targets, other than those screened in the present study, may be required. However, this study specifically looked at recruitment of Sty1 to a limited number of stress induced gene (Reiter *et al.* 2008). Therefore, it is suggested that Sty1-KD could potentially be recruited to promoters of lipid regulatory genes but with less efficiency, as has been noted for Hog1 kinase dead mutants (Ferrigno *et al.* 1998).

To evaluate the recruitment of Sty1 to promoters of lipid regulatory genes, downstream targets of the potential S6K-Sty1 pathway via could be identified by microarray analyses in cells deleted for S6K homologues *sck1, sck2* and *psk1* along with *wis1* and *sty1.* Further, to aid in the identification of whether the main target proteins of Sty1 are in the cytoplasm or the nucleus, a mutant equivalent to that of the *S. cerevisiae NMD5* mutant, which would prevent Sty1 translocation to the nucleus (Reiser *et al.* 1999), could also be employed in the aforementioned experiment. Additionally, in order to identify whether a transcriptional response is required by the Sty1 MAPK pathway recruitment of Sty1 and Sty1-KD to promoters of downstream targets could be investigated by chromatin immunoprecipitation (ChIP) experiments.

## 6.6 Potential role for p38 signalling in tumour associated lipogenesis

Based on observations made in yeast, the effect of the p38 MAPK pathway could serve to similarly regulate lipid accumulation. It has been well described that mTOR and p38 signalling are upregulated in many cancers including glioma (Carracedo *et al.* 2008, Demuth *et al.* 2007).

As described in Chapter 1, mTORC1 is well documented in driving the accumulation of lipids contributing to the lipogenic phenotype of gliomas. Constitutively active EGFR-PI3K-Akt signalling drives mTORC1 signalling which is constitutively active irrespective of cellular nutrient levels. One of the targets of mTORC1 in mammalian cells is S6K, the mammalian equivalent to *S. cerevisiae* Sch9. Although there may be an added level of complexity in mammalian systems, it is suggested that the role of EGFR-PI3K-AKT coupled with TOR and S6K with respect to p38 signalling in lipid synthesis may be conserved to that of Hog1. Previous work has demonstrated that upregulated TOR-S6K signalling activates p21-activated kinases (PAKs) which can in turn activate p38 (Kumar *et al.* 2006, Rousseau *et al.* 2006, Zarubin and Han 2005). Specifically in the case of glioma it has been found that increased Pak1 correlates with aggressiveness and short survival (Aoki H. *et al.* 2007).

P38 signalling may be sustained even in periods where cancerous cells may switch from glycolysis to oxidative phosphorylation under conditions of lactic acidosis in solid tumours. This persistent signalling may result from increased steady state ROS levels resulting from the preceding increased glycolytic rate (El Sayed *et al.* 2013). Specifically for gliomas, this is supported by the demonstration that augmented p38 activation via ROS contributes to the tumorous capacity of glioma initiating cells (Sato *et al.* 2014).

## 6.7 Lipogenesis as a therapeutic target for cancer

Research published over the past decade demonstrates that targeting metabolic regulatory components in cancer is a potentially viable program for treatment in conjunction with other adjuvant therapy options such as chemotherapy. Furthermore lipid metabolism is becoming an emerging concept for the treatment of glioma as reviewed by (Guo D. *et al.* 2013). Some of the components regulating lipid synthesis discussed in Chapter 1, and compounds developed to potentially target them in cancer are summarised in Table 6.1.

**Table 6.1: Compounds developed to target aberrant metabolism in human disease.** Targets include glucose uptake, enzymes regulating key steps in glycolysis and fatty acid synthesis. Further targets include upstream signalling elements that impact on downstream processes, such as mTORC1.

| Target | Compound | Effect | Source |
|---|---|---|---|
| Glucose uptake | 2-deoxyglucose | Inhibitory | Simons *et al.*2007 |
| Fatty acid synthase | Cerulenin | Inhibitory | Wang *et al.* 2005 |
| ATP citrate lyase | SB-204990 | Inhibitory | Hatzivassiliou *et al.* 2005 |
| PDK1 | Dichloroacetate | Inhibitory | Bonnet *et al.* 2007 |
| HIF-1α | α -ketoglutarate derivatives | Inhibitory | Mackenzie *et al.* 2007 |
| eIF4E | Antisense oligonucleotide | Inhibitory | Graff *et al.* 2007 |
| Reactive oxygen species | N-acetylcysteine, vitamin C | Neutralisation | Gao *et al.* 2007 |
| Acetyl-CoA carboxylase | Soraphen A | Inhibitory | Beckers *et al.* 2007 |
| AMPK | Metformin | Activating | Evans *et al.* 2006 |
| mTOR | Rapamycin/Rapalogs | Inhibitory | Various |
| c-Myc | Quarofloxin | Inhibitory | Brooks and Hurley 2010 |
| p38? | ? | Inhibitory | Present study |

The TOR pathway has presented an attractive target for the treatment of gliomas. Despite the central role of the mTOR pathway in driving gliomagenesis, inhibitors including rapamycin, in clinical trials have generally presented inadequate efficacy. This is likely due to the fact that rapamycin cannot inhibit all downstream mTORC1 activity (Cloninger *et al.* 2011). Simultaneous inhibition of downstream lipid regulatory elements in conjunction with mTORC1 may be a good additional therapeutic strategy. However, it is suggest that this may be a rather paradoxical approach due to the large number of substrates that may be activated by upstream oncogenic signalling. Additionally, due to the inherent ability of cancerous cells to adapt to changes in their environment, they similarly may reprogram their metabolism to evade downstream blockades. Further to this it was demonstrated that inhibition of TOR upregulates ERK signalling (Akhavan *et al.* 2010), suggesting the potential that p38 could also be similarly upregulated. This is supported as it has been shown more recently that inhibition of mTORC1 through the use of rapalog RAD001, increases the activation of p38 in glioma cells (Grzmil *et al.* 2014). Furthermore, in glioblastoma where patients were treated with lapatinib to inhibit constitutively active EGF, enhance cleavage and nuclear translocation of SREBP-1 was found to be induced. Although this response was suggested to be mediated via Akt signalling it was found to be independent of mTORC1. This serves as an explanation as to why rapamycin inhibition was ineffective in these tumours (Guo D. *et al.* 2009a), but also highlights that another pathway is driving lipid synthesis, possibly via a p38 dependent mechanism.

As described in Chapter 1, p38 can act as an oncogene and tumour suppressor dependent on stress signal received and the type of cell in which it is expressed, presenting the dilemma of inhibition or enhancement for cancer treatment (Sui *et al.* 2014). It has been demonstrated that p38 activation in many solid tumours, especially in pancreatic tumours, mediates a pro-apoptotic response. However, in glioma cells it was found that enhanced susceptibility to cytotoxicity via temozolomide treatment was enhanced by p38 inhibition (Stupp *et al.* 2005). It was also shown that p38 may be a prognostic marker for high grade gliomas correlating immunohistochemical nuclear and cytoplasmic staining with a worse prognosis (Sooman *et al.* 2013).

Taken together, it is suggested that inhibition of mTORC1 in glioblastoma would be ineffective due to persistent signalling via MAPK pathways, including p38. Therefore inhibition of mTORC1 and p38, along with surgery and chemotherapeutic treatment, may be a more effective strategy for the treatment of glioma, particularly those exhibiting a lipogenic phenotype. In agreement with the present study, it is starting to emerge that dual inhibition of mTORC1 and p38 or its downstream targets is indeed a viable treatment option for glioma (Grzmil 2014, Cloninger 2011).

## 6.8 Conclusions

Since the elucidation that upstream oncogenic signalling contributed significantly to downstream processes including tumour associated lipid formation, much work has sought to identify potential upstream lipid regulatory mechanisms. Knowledge of what is regulating downstream processes involved in lipid accumulation not only results in a better understanding of lipid synthesis regulation, but also facilitates production of novel therapeutic strategies. Such treatment options will ultimately serve to ameliorate the aggressiveness of lipogenic solid tumours, including glioma. Utilisation of yeast as a model organism allows rapid assessment of regulation of processes via signalling pathways. Further, many components de-regulated in cancer, such as mTORC1 and lipid metabolism, are largely conserved from yeast to mammalian systems.

The present study has also highlighted that employment of oleaginous yeast species may be a good complementary strategy for the investigation of lipid accumulation via stress-activated MAPK pathways. Owing to their ability to accumulate large amounts of lipid and their apparent possession of functional MAPK pathways and ATP citrate lyase activity.

Through the use of an optimised Nile red assay, a novel role for HOG and Sty1 stress response pathways in lipid accumulation has been determined in *S. cerevisiae* and *S. pombe.* It has been further demonstrated in *S. cerevisiae* that the activation of Hog1 in response to the requirement to accumulate lipid, may be distinct from the canonical activation step of the HOG pathway by Pbs2.

The regulation in *S. pombe* appears to be largely conserved to that of *S. cerevisiae* although further work is required to identify the role of Wis1 and potential downstream components. Although Hog1 and Sty1 are evolutionarily distant from mammalian p38,

there is a high level of structural and functional conservation between them. The involvement of Hog1 and Sty1 in lipid accumulation demonstrates that the potential mechanisms highlighted in this study may be similarly conserved in mammalian cells. Therefore, treatment of lipogenic glial tumours may be improved via conventional chemotherapeutic and surgical intervention, coupled with the combined inhibition of mTORC1 and p38.

# 7.0 References


Akhavan D, Cloughesy TF, Mischel PS. (2010). mTOR signaling in glioblastoma: lessons learned from bench to bedside. *Neuro-Oncology* **12**:882-889.

Alepuz PM, de Nadal E, Zapater M, Ammerer G, Posas F. (2003). Osmostress-induced transcription by Hot1 depends on a Hog1-mediated recruitment of the RNA Pol II. *EMBO J* **22**:2433-2442.

Alepuz PM, Jovanovic A, Reiser V, Ammerer G. (2001). Stress-induced map kinase Hog1 is part of transcription activation complexes. *Mol Cell* **7**:767-777.

Aoki H, Yokoyama T, Fujiwara K, Tari AM, Sawaya R, Suki D, Hess KR, Aldape KD, Kondo S, Kumar R, Kondo Y. (2007). Phosphorylated Pak1 level in the cytoplasm correlates with shorter survival time in patients with glioblastoma. *Clin Cancer Res* **13**:6603-6609.

Aoki Y, Kanki T, Hirota Y, Kurihara Y, Saigusa T, Uchiumi T, Kang D. (2011). Phosphorylation of Serine 114 on Atg32 mediates mitophagy. *Mol Biol Cell* **22**:3206-3217.

Athenstaedt K. (2010). Neutral Lipids in Yeast: Synthesis, Storage and Degradation. Pages 471-480 in Timmis K, ed. Handbook of Hydrocarbon and Lipid Microbiology, Springer Berlin Heidelberg.

Athenstaedt K. (2011). YALI0E32769g (DGA1) and YALI0E16797g (LRO1) encode major triacylglycerol synthases of the oleaginous yeast *Yarrowia lipolytica*. *Biochim Biophys Acta* **1811**:587-596.

Athenstaedt K, Daum G. (2005). Tgl4p and Tgl5p, two triacylglycerol lipases of the yeast *Saccharomyces cerevisiae* are localized to lipid particles. *Journal of Biological Chemistry* **280**:37301-37309.

Athenstaedt K, Daum G. (2006). The life cycle of neutral lipids: synthesis, storage and degradation. *Cell Mol Life Sci* **63**:1355-1369.

Avruch J, Khokhlatchev A, Kyriakis JM, Luo Z, Tzivion G, Vavvas D, Zhang XF. (2001). Ras activation of the Raf kinase: tyrosine kinase recruitment of the MAP kinase cascade. *Recent Prog Horm Res* **56**:127-155.

Bandhakavi S, Xie H, O'Callaghan B, Sakurai H, Kim D-H, Griffin TJ. (2008). Hsf1 Activation Inhibits Rapamycin Resistance and TOR Signaling in Yeast Revealed by Combined Proteomic and Genetic Analysis. *PLoS ONE* **3**:e1598.

Banuett F. (1998). Signalling in the yeasts: an informational cascade with links to the filamentous fungi. *Microbiol Mol Biol Rev* **62**:249-274.

Bauer D, Hatzivassiliou G, Zhao F, Andreadis C, Thompson CB. (2005). ATP citrate lyase is an important component of cell growth and transformation. *Oncogene* **24**:6314-6322.

Bauer F, Pretorius IS. (2002). Pseudohyphal and Invasive Growth in *Saccharomyces cerevisiae*. Pages 109-133 in Durieux A, Simon J, eds. Applied Microbiology, vol. 2 Springer Netherlands.

Bebek G, Yang J. (2007). PathFinder: mining signal transduction pathway segments from protein-protein interaction networks. *BMC Bioinformatics* **8**:335.

Becker GW, Lester RL. (1977). Changes in phospholipids of *Saccharomyces cerevisiae* associated with inositol-less death. *Journal of Biological Chemistry* **252**:8684-8691.

Beller M, Thiel K, Thul PJ, Jäckle H. (2010). Lipid droplets: A dynamic organelle moves into focus. *FEBS Letters* **584**:2176-2182.

Beopoulos A, Mrozova Z, Thevenieau F, Le Dall M-T, Hapala I, Papanikolaou S, Chardot T, Nicaud J-M. (2008). Control of Lipid Accumulation in the Yeast *Yarrowia lipolytica*. *Applied and Environmental Microbiology* **74**:7779-7789.

Beopoulos A, Nicaud J-M, Gaillardin C. (2011). An overview of lipid metabolism in yeasts and its impact on biotechnological processes. *Applied Microbiology and Biotechnology* **90**:1193-1206.

Berlanga JJ, Rivero D, Martín R, Herrero S, Moreno S, de Haro C. (2010). Role of Mitogen-Activated Protein Kinase Sty1 in Regulation of Eukaryotic Initiation Factor 2α Kinases in Response to Environmental Stress in *Schizosaccharomyces pombe*. *Eukaryotic Cell* **9**:194-207.

Bien CM, Espenshade PJ. (2010). Sterol Regulatory Element Binding Proteins in Fungi: Hypoxic Transcription Factors Linked to Pathogenesis. *Eukaryotic Cell* **9**:352-359.

Bligh EG, Dyer WJ. (1959). A rapid method of total lipid extraction and purification. *Canadian Journal of Biochemistry and Physiology* **37**:911-917.

Botstein D, Fink G. (1988). Yeast: an experimental organism for modern biology. *Science* **240**:1439-1443.

Botstein D, Fink GR. (2011). Yeast: An Experimental Organism for 21st Century Biology. *Genetics* **189**:695-704.

Boulton CA, Ratledge C. (1981). ATP: Citrate Lyase - the regulatory enzyme for lipid biosynthesis in *Lipomyces starkeyi*? *Journal of General Microbiology* **127**:423-426.

Buller CL, Loberg RD, Fan MH, Zhu Q, Park JL, Vesely E, Inoki K, Guan KL, Brosius FC. (2008). A GSK-3/TSC2/mTOR pathway regulates glucose uptake and GLUT1 glucose transporter expression. *Am J Physiol Cell Physiol* **295**:C836-843.

Burg JS, Powell DW, Chai R, Hughes AL, Link AJ, Espenshade PJ. (2008). Insig regulates HMG-CoA reductase by controlling enzyme phosphorylation in fission yeast. *Cell Metab* **8**:522-531.

Burger P, Scheithauer B, Paulus W, *et al.* (2000). Pilocytic astrocytoma. *In: Kleihues P, Cavenee WK, (eds). Pathology and Genetics of Tumours of the Nervous System. Lyon, France: International Agency for Research on Cancer, pp 45-51.*

Cargnello M, Roux PP. (2011). Activation and function of the MAPKs and their substrates, the MAPK-Activated protein kinases. *Microbiology and Molecular Biology Reviews* **75**:50-83.

Carman GM, Henry SA. (2007). Special issue: Regulation of lipid metabolism in yeast. *Biochim Biophys Acta* **1771**:239-240.

Carracedo A, Ma L, Teruya-Feldstein J, Rojo F, Salmena L, Alimonti A, Egia A, Sasaki AT, Thomas G, Kozma SC, Papa A, Nardella C, Cantley LC, Baselga J, Pandolfi PP. (2008). Inhibition of mTORC1 leads to MAPK pathway activation through a PI3K-dependent feedback loop in human cancer. *J Clin Invest* **118**:3065-3074.

Castro G, Larson B, Panilaitis B, Kaplan D. (2005). Emulsan quantitation by Nile red quenching fluorescence assay. *Applied Microbiology and Biotechnology* **67**:767-770.

Cavaliere R, Lopes MB, Schiff D. (2005). Low-grade gliomas: an update on pathology and therapy. *Lancet Neurol* **4**:760-770.

Certik M, Megova J, Horenitzky R. (1999). Effect of nitrogen sources on the activities of lipogenic enzymes in oleaginous fungus *Cunninghamella echinulata*. *The Journal of General and Applied Microbiology* **45**:289-293.

Chabner BA, Roberts TG. (2005). Chemotherapy and the war on cancer. *Nat Rev Cancer* **5**:65-72.

Chellappa R, Kandasamy P, Oh CS, Jiang Y, Vemula M, Martin CE. (2001). The membrane proteins, Spt23p and Mga2p, play distinct roles in the activation of *Saccharomyces cerevisiae* OLE1 gene expression. Fatty acid-mediated regulation of Mga2p activity is independent of its proteolytic processing into a soluble transcription activator. *J Biol Chem* **276**:43548-43556.

Chen D, Wilkinson CR, Watt S, Penkett CJ, Toone WM, Jones N, Bahler J. (2008). Multiple pathways differentially regulate global oxidative stress responses in fission yeast. *Mol Biol Cell* **19**:308-317.

Chen M-T, Weiss R. (2005). Artificial cell-cell communication in yeast *Saccharomyces cerevisiae* using signaling elements from Arabidopsis thaliana. *Nat Biotech* **23**:1551-1555.

Chen R, Thorner J. (2007). Function and regulation in MAPK signaling pathways: lessons learned from the yeast *Saccharomyces cerevisiae*. *Biochim Biophys Acta* **1773**:1311-1340.

Chen W, Zhang C, Song L, Sommerfeld M, Hu Q. (2009). A high throughput Nile red method for quantitative measurement of neutral lipids in microalgae. *Journal of Microbiological Methods* **77**:41-47.

Cheung R, Espenshade PJ. (2013). Structural Requirements for Sterol Regulatory Element-binding Protein (SREBP) Cleavage in Fission Yeast. *Journal of Biological Chemistry* **288**:20351-20360.

Chishty IA, Rafique MZ, Hussain M, Akhtar W, Ahmed MN, Sajjad Z, Ali SZ. (2010). MRI Characterization and Histopathological Correlation of Primary Intra-axial Brain Glioma. *JLUMHS* **9**:64.

Choe G, Horvath S, Cloughesy TF, Crosby K, Seligson D, Palotie A, Inge L, Smith BL, Sawyers CL, Mischel PS. (2003). Analysis of the phosphatidylinositol 3'-kinase signaling pathway in glioblastoma patients in vivo. *Cancer Res* **63**:2742-2746.

Choi H-S, Sreenivas A, Han G-S, Carman GM. (2004). Regulation of Phospholipid Synthesis in the Yeast cki1Δ eki1Δ Mutant Defective in the Kennedy Pathway: The CHO1-encoded phosphatidylserine synthase is regulated by mRNA stability. *Journal of Biological Chemistry* **279**:12081-12087.

Choi JY, Martin CE. (1999). The *Saccharomyces cerevisiae* FAT1 gene encodes an acyl-CoA synthetase that is required for maintenance of very long chain fatty acid levels. *J Biol Chem* **274**:4671-4683.

Chou S, Lane S, Liu H. (2006). Regulation of mating and filamentation genes by two distinct Ste12 complexes in *Saccharomyces cerevisiae*. *Mol Cell Biol* **26**:4794-4805.

Chumnanpuen P, Nookaew I, Nielsen J. (2013). Integrated analysis, transcriptome-lipidome, reveals the effects of INO-level (INO2 and INO4) on lipid metabolism in yeast. *BMC Systems Biology* **7**:S7.

Cloninger C, Bernath A, Bashir T, Holmes B, Artinian N, Ruegg T, Anderson L, Masri J, Lichtenstein A, Gera J. (2011). Inhibition of SAPK2/p38 enhances sensitivity to mTORC1 inhibition by blocking IRES-mediated translation initiation in glioblastoma. *Mol Cancer Ther* **10**:2244-2256.

Clotet J, Posas F. (2007). Control of cell cycle in response to osmostress: lessons from yeast. *Methods Enzymol* **428**:63-76.

Colditz GA. (2009). Cancer and the Environment: The American Cancer Society Prevention Priorities. *CA: A Cancer Journal for Clinicians* **59**:341-342.

Coleman RA, Lee DP. (2004). Enzymes of triacylglycerol synthesis and their regulation. *Prog Lipid Res* **43**:134-176.

Crespo J, Powers T, Fowler B, Hall MN. (2002). The TOR-controlled transcription activators GLN3, RTG1, and RTG3 are regulated in response to intracellular levels of glutamine. *Proceedings of the National Academy of Sciences* **99**:6784-6789.

Crespo JL, Hall MN. (2002). Elucidating TOR signaling and rapamycin action: lessons from *Saccharomyces cerevisiae*. *Microbiol Mol Biol Rev* **66**:579-591, table of contents.

Cromie G, Smith GR. (2008). Meiotic Recombination in *Schizosaccharomyces pombe*: A Paradigm for Genetic and Molecular Analysis. *Genome Dyn Stab* **3**:195.

Cuadrado A, Nebreda AR. (2010). Mechanisms and functions of p38 MAPK signalling. *Biochem J* **429**:403-417.

Dann SG, Thomas G. (2006). The amino acid sensitive TOR pathway from yeast to mammals. *FEBS Letters* **580**:2821-2829.

Davies BS, Rine J. (2006). A role for sterol levels in oxygen sensing in *Saccharomyces cerevisiae*. *Genetics* **174**:191-201.

Davies BS, Wang HS, Rine J. (2005). Dual activators of the sterol biosynthetic pathway of *Saccharomyces cerevisiae*: similar activation/regulatory domains but different response mechanisms. *Mol Cell Biol* **25**:7375-7385.

Davis RJ. (2000). Signal transduction by the JNK group of MAP kinases. *Cell* **103**:239-252.

DeBerardinis R, Lum JJ, Thompson CB. (2006). Phosphatidylinositol 3-Kinase-dependent Modulation of Carnitine Palmitoyltransferase 1A Expression Regulates Lipid Metabolism during Hematopoietic Cell Growth. *Journal of Biological Chemistry* **281**:37372-37380.

DeBerardinis R, Sayed N, Ditsworth D, Thompson CB. (2008a). Brick by brick: metabolism and tumor cell growth. *Current Opinion in Genetics and Development* **18**:54-61.

DeBerardinis RJ, Lum JJ, Hatzivassiliou G, Thompson CB. (2008b). The biology of cancer: metabolic reprogramming fuels cell growth and proliferation. *Cell Metab* **7**:11-20.

Demuth T, Reavie LB, Rennert JL, Nakada M, Nakada S, Hoelzinger DB, Beaudry CE, Henrichs AN, Anderson EM, Berens ME. (2007). MAP-ing glioma invasion: Mitogen-

activated protein kinase kinase 3 and p38 drive glioma invasion and progression and predict patient survival. *Molecular Cancer Therapeutics* **6**:1212-1222.

Di Paolo G, Kim TW. (2011). Linking lipids to Alzheimer's disease: cholesterol and beyond. *Nat Rev Neurosci* **12**:284-296.

Diaz G, Melis M, Batetta B, Angius F, Falchi AM. (2008). Hydrophobic characterization of intracellular lipids in situ by Nile Red red/yellow emission ratio. *Micron* **39**:819-824.

Dowd SR, Bier ME, Patton-Vogt JL. (2001). Turnover of Phosphatidylcholine in *Saccharomyces cerevisiae* : The role of the CDP-choline pathway. *Journal of Biological Chemistry* **276**:3756-3763.

Downward J. (2003). Targeting RAS signalling pathways in cancer therapy. *Nat Rev Cancer* **3**:11-22.

Drabsch Y, Ramsay R, Gonda T. (2010). MYB suppresses differentiation and apoptosis of human breast cancer cells. *Breast Cancer Research* **12**:R55.

Du W, Hálová L, Kirkham S, Atkin J, Petersen J. (2012). TORC2 and the AGC kinase Gad8 regulate phosphorylation of the ribosomal protein S6 in fission yeast. *Biology Open*.

El Sayed SM, Mahmoud AA, El Sawy SA, Abdelaal EA, Fouad AM, Yousif RS, Hashim MS, Hemdan SB, Kadry ZM, Abdelmoaty MA, Gabr AG, Omran FM, Nabo MMH, Ahmed NS. (2013). Warburg effect increases steady-state ROS condition in cancer cells through decreasing their antioxidant capacities (Anticancer effects of 3-bromopyruvate through antagonizing Warburg effect). *Medical Hypotheses* **81**:866-870.

Engelhard HH, Stelea A, Mundt A. (2003). Oligodendroglioma and anaplastic oligodendroglioma: clinical features, treatment, and prognosis. *Surg Neurol* **60**:443-456.

Esechie A, Du G. (2009). Increased lipogenesis in cancer. *Communicative & Integrative Biology* **2**:545-548.

Espenshade P, Hughes A. (2007). Regulation of Sterol Synthesis in Eukaryotes. *Annual Review of Genetics* **41**:401-427.

Faubert B, Boily G, Izreig S, Griss T, Samborska B, Dong Z, Dupuy F, Chambers C, Fuerth Benjamin J, Viollet B, Mamer Orval A, Avizonis D, DeBerardinis Ralph J, Siegel Peter M,

Jones Russell G. (2013). AMPK Is a negative regulator of the Warburg effect and suppresses tumor growth *in vivo*. *Cell Metab* **17**:113-124.

Fei W, Shui G, Gaeta B, Du X, Kuerschner L, Li P, Brown AJ, Wenk MR, Parton RG, Yang H. (2008). Fld1p, a functional homologue of human seipin, regulates the size of lipid droplets in yeast. *J Cell Biol* **180**:473-482.

Fei W, Zhong L, Ta MT, Shui G, Wenk MR, Yang H. (2011). The size and phospholipid composition of lipid droplets can influence their proteome. *Biochemical and Biophysical Research Communications* **415**:455-462.

Ferrigno P, Posas F, Koepp D, Saito H, Silver PA. (1998). Regulated nucleo/cytoplasmic exchange of HOG1 MAPK requires the importin beta homologs NMD5 and XPO1. *EMBO J* **17**:5606-5614.

Feyer P, Kleeberg UR, Steingraber M, Gunther W, Behrens M. (2008). Frequency of side effects in outpatient cancer care and their influence on patient satisfaction--a prospective survey using the PASQOC questionnaire. *Support Care Cancer* **16**:567-575.

Flynn EJ, 3rd, Trent CM, Rawls JF. (2009). Ontogeny and nutritional control of adipogenesis in zebrafish (Danio rerio). *J Lipid Res* **50**:1641-1652.

Folch J, Lees M, Sloane Stanley GH. (1957). A simple method for the isolation and purification of total lipides from animal tissues. *J Biol Chem* **226**:497-509.

Françoise F. (1997). Human genetic diseases: a cross-talk between man and yeast. *Gene* **195**:1-10.

Furnari FB, Fenton T, Bachoo RM, Mukasa A, Stommel JM, Stegh A, Hahn WC, Ligon KL, Louis DN, Brennan C, Chin L, DePinho RA, Cavenee WK. (2007). Malignant astrocytic glioma: genetics, biology, and paths to treatment. *Genes Dev* **21**:2683-2710.

Garcia R, Bermejo C, Grau C, Perez R, Rodriguez-Pena JM, Francois J, Nombela C, Arroyo J. (2004). The global transcriptional response to transient cell wall damage in *Saccharomyces cerevisiae* and its regulation by the cell integrity signaling pathway. *J Biol Chem* **279**:15183-15195.

Gardocki ME, Jani N, Lopes JM. (2005). Phosphatidylinositol biosynthesis: Biochemistry and regulation. *Biochimica et Biophysica Acta (BBA) - Molecular and Cell Biology of Lipids* **1735**:89-100.

Godfraind C. (2009). Classification and controversies in pathology of ependymomas. *Child's Nervous System* **25**:1185-1193.

Gon E, Colen G, Takahashi JA. (2014). *Yarrowia lipolytica* and Its Multiple Applications in the Biotechnological Industry. *The Scientific World Journal* **2014** (art. 476207):14.

Goodison S, Sun Y, Urquidi V. (2010). Derivation of cancer diagnostic and prognostic signatures from gene expression data. *Bioanalysis* **2**:855-862.

Greenspan P, Mayer EP, Fowler SD. (1985). Nile red: a selective fluorescent stain for intracellular lipid droplets. *The Journal of Cell Biology* **100**:965-973.

Grillitsch K, Connerth M, Kofeler H, Arrey TN, Rietschel B, Wagner B, Karas M, Daum G. (2011). Lipid particles/droplets of the yeast *Saccharomyces cerevisiae* revisited: lipidome meets proteome. *Biochim Biophys Acta* **1811**:1165-1176.

Grzmil M, Huber RM, Hess D, Frank S, Hynx D, Moncayo G, Klein D, Merlo A, Hemmings BA. (2014). MNK1 pathway activity maintains protein synthesis in rapalog-treated gliomas. *J Clin Invest* **124**:742-754.

Guo D, Bell EH, Chakravarti A. (2013). Lipid metabolism emerges as a promising target for malignant glioma therapy. *CNS Oncol* **2**:289-299.

Guo D, Prins RM, Dang J, Kuga D, Iwanami A, Soto H, Lin KY, Huang TT, Akhavan D, Hock MB, Zhu S, Kofman AA, Bensinger SJ, Yong WH, Vinters HV, Horvath S, Watson AD, Kuhn JG, Robins HI, Mehta MP, Wen PY, DeAngelis LM, Prados MD, Mellinghoff IK, Cloughesy TF, Mischel PS. (2009a). EGFR signaling through an Akt-SREBP-1-dependent, rapamycin-resistant pathway sensitizes glioblastomas to antilipogenic therapy. *Sci Signal* **2**:ra82.

Guo Y, Cordes KR, Farese RV, Walther TC. (2009b). Lipid droplets at a glance. *Journal of Cell Science* **122**:749-752.

Haidinger M, Poglitsch M, Geyeregger R, Kasturi S, Zeyda M, Zlabinger GJ, Pulendran B, Hörl WH, Säemann MD, Weichhart T. (2010). A Versatile Role of Mammalian Target of

Rapamycin in Human Dendritic Cell Function and Differentiation. *The Journal of Immunology* **185**:3919-3931.

Hanahan D, Weinberg Robert A. (2011). Hallmarks of Cancer: The Next Generation. *Cell* **144**:646-674.

Hao N, Zeng Y, Elston TC, Dohlman HG. (2008). Control of MAPK specificity by feedback phosphorylation of shared adaptor protein Ste50. *J Biol Chem* **283**:33798-33802.

Hara K, Yonezawa K, Weng QP, Kozlowski MT, Belham C, Avruch J. (1998). Amino acid sufficiency and mTOR regulate p70 S6 kinase and eIF-4E BP1 through a common effector mechanism. *J Biol Chem* **273**:14484-14494.

Hay N, Sonenberg N. (2004). Upstream and downstream of mTOR. *Genes Dev* **18**:1926-1945.

Heitman J, Movva NR, Hall MN. (1991). Targets for cell cycle arrest by the immunosuppressant rapamycin in yeast. *Science* **253**:905-909.

Henry SA, Kohlwein SD, Carman GM. (2012). Metabolism and regulation of glycerolipids in the yeast *Saccharomyces cerevisiae*. *Genetics* **190**:317-349.

Hermansson M, Hokynar K, Somerharju P. (2011). Mechanisms of glycerophospholipid homeostasis in mammalian cells. *Progress in Lipid Research* **50**:240-257.

Hickman M, Winston F. (2007). Heme Levels Switch the Function of Hap1 of *Saccharomyces cerevisiae* between Transcriptional Activator and Transcriptional Repressor. *Mol Cell Biol* **27**:7414-7424.

Hickman MJ, Spatt D, Winston F. (2011). The Hog1 mitogen-activated protein kinase mediates a hypoxic response in *Saccharomyces cerevisiae*. *Genetics* **188**:325-338.

Hirschhaeuser F, Sattler UGA, Mueller-Klieser W. (2011). Lactate: A Metabolic Key Player in Cancer. *Cancer Research* **71**:6921-6925.

Hishikawa D, Hashidate T, Shimizu T, Shindou H. (2014). Diversity and function of membrane glycerophospholipids generated by the remodeling pathway in mammalian cells. *J Lipid Res* **55**:799-807.

Holland EC. (2000). Glioblastoma multiforme: the terminator. *Proc Natl Acad Sci U S A* **97**:6242-6244.

Horie T, Tatebayashi K, Yamada R, Saito H. (2008). Phosphorylated Ssk1 prevents unphosphorylated Ssk1 from activating the Ssk2 mitogen-activated protein kinase kinase kinase in the yeast high-osmolarity glycerol osmoregulatory pathway. *Mol Cell Biol* **28**:5172-5183.

Hou LC, Veeravagu A, Hsu AR, Tse VCK. (2006). Recurrent glioblastoma multiforme: a review of natural history and management options. *Neurosurgical Focus* **20**:E5.

Houten SM, Wanders RJ. (2010). A general introduction to the biochemistry of mitochondrial fatty acid beta-oxidation. *J Inherit Metab Dis* **33**:469-477.

Hsu PP, Kang SA, Rameseder J, Zhang Y, Ottina KA, Lim D, Peterson TR, Choi Y, Gray NS, Yaffe MB, Marto JA, Sabatini DM. (2011). The mTOR-regulated phosphoproteome reveals a mechanism of mTORC1-mediated inhibition of growth factor signaling. *Science* **332**:1317-1322.

Huang J, Wu S, Wu C-L, Manning BD. (2009). Signaling events downstream of mammalian target of Rapamycin complex 2 are attenuated in cells and tumors deficient for the tuberous sclerosis complex tumor suppressors. *Cancer Research* **69**:6107-6114.

Hughes AL, Stewart EV, Espenshade PJ. (2008). Identification of twenty-three mutations in fission yeast Scap that constitutively activate SREBP. *J Lipid Res* **49**:2001-2012.

Hughes AL, Todd BL, Espenshade PJ. (2005). SREBP Pathway Responds to Sterols and Functions as an Oxygen Sensor in Fission Yeast. *Cell* **120**:831-842.

Hughes B, Espenshade PJ. (2008). Oxygen-regulated degradation of fission yeast SREBP by Ofd1, a prolyl hydroxylase family member. *EMBO J* **27**:1491-1501.

Hutchins PM, Barkley RM, Murphy RC. (2008). Separation of cellular nonpolar neutral lipids by normal-phase chromatography and analysis by electrospray ionization mass spectrometry. *J Lipid Res* **49**:804-813.

Ihermann-Hella A, Lume M, Miinalainen IJ, Pirttiniemi A, Gui Y, Peränen J, Charron J, Saarma M, Costantini F, Kuure S. (2014). Mitogen-Activated Protein Kinase (MAPK) Pathway Regulates Branching by Remodeling Epithelial Cell Adhesion. *PLoS Genet* **10**:e1004193.

Iverson S, Lang SC, Cooper M. (2001). Comparison of the bligh and dyer and folch methods for total lipid determination in a broad range of marine tissue. *Lipids* **36**:1283-1287.

Jackowski S, Wang J, Baburina I. (2000). Activity of the phosphatidylcholine biosynthetic pathway modulates the distribution of fatty acids into glycerolipids in proliferating cells. *Biochim Biophys Acta* **1483**:301-315.

Jiang Y, Wang M. (2010). Personalized medicine in oncology: tailoring the right drug to the right patient. *Biomarkers in Medicine* **4**:523-533.

Jung US, Levin DE. (1999). Genome-wide analysis of gene expression regulated by the yeast cell wall integrity signalling pathway. *Mol Microbiol* **34**:1049-1057.

Jung US, Sobering AK, Romeo MJ, Levin DE. (2002). Regulation of the yeast Rlm1 transcription factor by the Mpk1 cell wall integrity MAP kinase. *Mol Microbiol* **46**:781-789.

Kamisaka Y, Noda N, Tomita N, Kimura K, Kodaki T, Hosaka K. (2006). Identification of genes affecting lipid content using transposon mutagenesis in *Saccharomyces cerevisiae*. *Biosci Biotechnol Biochem* **70**:646-653.

Kamisaka Y, Tomita N, Kimura K, Kainou K, Uemura H. (2007). DGA1 (diacylglycerol acyltransferase gene) overexpression and leucine biosynthesis significantly increase lipid accumulation in the Deltasnf2 disruptant of *Saccharomyces cerevisiae*. *Biochem J* **408**:61-68.

Kandasamy P, Vemula M, Oh C-S, Chellappa R, Martin CE. (2004). Regulation of Unsaturated Fatty Acid Biosynthesis in Saccharomyces: The Endoplasmic Reticulum protein, Mga2p, a transcriptional actovator of the OLE1 gene, regulates the stability of the OLE1 mRNA through exosome-mediated mechanisms. *Journal of Biological Chemistry* **279**:36586-36592.

Kapteyn JC, ter Riet B, Vink E, Blad S, De Nobel H, Van Den Ende H, Klis FM. (2001). Low external pH induces HOG1-dependent changes in the organization of the *Saccharomyces cerevisiae* cell wall. *Mol Microbiol* **39**:469-479.

Karin M, Lawrence T, Nizet V. (2006). Innate Immunity Gone Awry: Linking Microbial Infections to Chronic Inflammation and Cancer. *Cell* **124**:823-835.

Kaserer AO, Andi B, Cook PF, West AH. (2009). Effects of osmolytes on the SLN1-YPD1-SSK1 phosphorelay system from *Saccharomyces cerevisiae*. *Biochemistry* **48**:8044-8050.

Kawai M, Nakashima A, Ueno M, Ushimaru T, Aiba K, Doi H, Uritani M. (2001). Fission yeast tor1 functions in response to various stresses including nitrogen starvation, high osmolarity, and high temperature. *Curr Genet* **39**:166-174.

Kerscher S, Grgic L, Garofano A, Brandt U. (2004). Application of the yeast *Yarrowia lipolytica* as a model to analyse human pathogenic mutations in mitochondrial complex I (NADH:ubiquinone oxidoreductase). *Biochim Biophys Acta* **1659**:197-205.

Kim L, Hoe K-L, Yu YM, Yeon J-H, Maeng PJ. (2012). The Fission Yeast GATA Factor, Gaf1, Modulates Sexual Development via Direct Down-Regulation of ste11 Expression in Response to Nitrogen Starvation. *PLoS ONE* **7**:e42409.

Kim S-K, Kim H, Yang Y-R, Suh P-G, Chang J-S. (2011). Phosphatidylinositol phosphates directly bind to neurofilament light chain (NF-L) for the regulation of NF-L self assembly. *Exp Mol Med* **43**:153-160.

Kleihues P, Burger PC, Collins VP ea. (2000a). Glioblastoma. *In: Kleihues P, Cavenee WK, (eds). Pathology and Genetics of Tumours of the Nervous System. Lyon, France: International Agency for Research on Cancer*:pp 29-39.

Kleihues P, Davis RL, Coons SW ea. (2000b). Anaplastic astrocytoma. *In: Kleihues P, Cavenee WK, (eds). Pathology and Genetics of Tumours of the Nervous System. Lyon, France: International Agency for Research on Cancer.*

:pp 27-28.

Klig LS, Homann MJ, Carman GM, Henry SA. (1985). Coordinate regulation of phospholipid biosynthesis in *Saccharomyces cerevisiae:* pleiotropically constitutive opi1 mutant. *J Bacteriol* **162**:1135-1141.

Kohlwein SD, Veenhuis M, van der Klei IJ. (2013). Lipid Droplets and Peroxisomes: Key Players in Cellular Lipid Homeostasis or A Matter of Fat—Store 'em Up or Burn 'em Down. *Genetics* **193**:1-50.

Kotzka J, Knebel B, Haas J, Kremer L, Jacob S, Hartwig S, Nitzgen U, Muller–Wieland D. (2012). Preventing phosphorylation of sterol regulatory element-binding protein 1a by MAP-Kinases protects mice from fatty liver and visceral obesity. *PLoS ONE* **7**:e32609.

Krauss G. (2008). Biochemistry of signal transduction and regulation. *Wiley*:448-455.

Kumar R, Gururaj AE, Barnes CJ. (2006). p21-activated kinases in cancer. *Nat Rev Cancer* **6**:459-471.

Kyriakis JM, Avruch J. (2012). Mammalian MAPK signal transduction pathways activated by stress and inflammation: A 10-year update.

Lacob G, Dinca EB. (2009). Current data and strategy in glioblastoma multiforme. *J Med Life* **2**:386-393.

Lamson RE, Winters MJ, Pryciak PM. (2002). Cdc42 regulation of kinase activity and signaling by the yeast p21-activated kinase Ste20. *Mol Cell Biol* **22**:2939-2951.

Land SC, Tee AR. (2007). Hypoxia-inducible factor 1alpha is regulated by the mammalian target of rapamycin (mTOR) via an mTOR signaling motif. *J Biol Chem* **282**:20534-20543.

Laplante M, Sabatini D. (2009a). mTOR signaling at a glance. *Journal of Cell Science* **122**:3589-3594.

Laplante M, Sabatini DM. (2009b). An Emerging Role of mTOR in Lipid Biosynthesis. *Current Biology* **19**:R1046-R1052.

Lawrence CL, Botting CH, Antrobus R, Coote PJ. (2004). Evidence of a new role for the high-osmolarity glycerol mitogen-activated protein kinase pathway in yeast: regulating adaptation to citric acid stress. *Mol Cell Biol* **24**:3307-3323.

Lawrence CL, Maekawa H, Worthington JL, Reiter W, Wilkinson CRM, Jones N. (2007). Regulation of *Schizosaccharomyces pombe* Atf1 protein levels by Sty1-mediated phosphorylation and heterodimerization with Pcr1. *Journal of Biological Chemistry* **282**:5160-5170.

Lee P, Kim MS, Paik S-M, Choi S-H, Cho B-R, Hahn J-S. (2013). Rim15-dependent activation of Hsf1 and Msn2/4 transcription factors by direct phosphorylation in *Saccharomyces cerevisiae*. *FEBS Letters* **587**:3648-3655.

Leelahavanichkul K, Amornphimoltham P, Molinolo AA, Basile JR, Koontongkaew S, Gutkind JS. (2014). A role for p38 MAPK in head and neck cancer cell growth and tumor-induced angiogenesis and lymphangiogenesis. *Molecular Oncology* **8**:105-118.

Lemieux GA, Liu J, Mayer N, Bainton RJ, Ashrafi K, Werb Z. (2011). A whole-organism screen identifies new regulators of fat storage. *Nat Chem Biol* **7**:206-213.

Levin DE. (2005). Cell wall integrity signaling in *Saccharomyces cerevisiae*. *Microbiol Mol Biol Rev* **69**:262-291.

Li M, Yang L, Bai Y, Liu H. (2013). Analytical methods in lipidomics and their applications. *Analytical Chemistry* **86**:161-175.

Li S, Ault A, Malone CL, Raitt D, Dean S, Johnston LH, Deschenes RJ, Fassler JS. (1998). The yeast histidine protein kinase, Sln1p, mediates phosphotransfer to two response regulators, Ssk1p and Skn7p. *EMBO J* **17**:6952-6962.

Li SL, Lin Q, Li XR, Xu H, Yang YX, Qiao DR, Cao Y. (2012). Biodiversity of the oleaginous microorganisms in Tibetan Plateau. *Brazilian Journal of Microbiology* **43**:627-634.

Li X, Gerber SA, Rudner AD, Beausoleil SA, Haas W, Villen J, Elias JE, Gygi SP. (2007). Large-scale phosphorylation analysis of alpha-factor-arrested *Saccharomyces cerevisiae*. *J Proteome Res* **6**:1190-1197.

Liang J, Mills GB. (2013). AMPK: A contextual oncogene or tumor suppressor? *Cancer Research* **73**:2929-2935.

Lim SK, Llaguno SR, McKay RM, Parada LF. (2011). Glioblastoma multiforme: a perspective on recent findings in human cancer and mouse models. *BMB Rep* **44**:158-164.

Lisi L, Laudati E, Navarra P, Dello Russo C. (2014). The mTOR kinase inhibitors polarize glioma-activated microglia to express a M1 phenotype. *J Neuroinflammation* **11**:125.

Liu L, Rezvani HR, Back JH, Hosseini M, Tang X, Zhu Y, Mahfouf W, Raad H, Raji G, Athar M, Kim AL, Bickers DR. (2014). Inhibition of p38 MAPK signaling augments skin tumorigenesis via NOX2 driven ROS generation. *PLoS ONE* **9**:e97245.

Liu Z, Huang X. (2013). Lipid metabolism in Drosophila: development and disease. *Acta Biochim Biophys Sin (Shanghai)* **45**:44-50.

Loewith R. (2011). A brief history of TOR. *Biochem Soc Trans* **39**:437-442.

Loewith R, Jacinto E, Wullschleger S, Lorberg A, Crespo JL, Bonenfant D, Oppliger W, Jenoe P, Hall MN. (2002). Two TOR complexes, only one of which is rapamycin sensitive, have distinct roles in cell growth control. *Mol Cell* **10**:457-468.

Loewy BS, Henry SA. (1984). The INO2 and INO4 loci of *Saccharomyces cerevisiae* are pleiotropic regulatory genes. *Mol Cell Biol* **4**:2479-2485.

Long AP, Manneschmidt AK, VerBrugge B, Dortch MR, Minkin SC, Prater KE, Biggerstaff JP, Dunlap JR, Dalhaimer P. (2012). Lipid droplet de novo formation and fission are linked to the cell cycle in fission yeast. *Traffic* **13**:705-714.

Louis D, Ohgaki H, Wiestler O, Cavenee W, Burger P, Jouvet A, Scheithauer B, Kleihues P. (2007). The 2007 WHO classification of tumours of the central nervous system. *Acta Neuropathologica* **114**:97-109.

Ma XM, Blenis J. (2009). Molecular mechanisms of mTOR-mediated translational control. *Nat Rev Mol Cell Biol* **10**:307-318.

Maayan I, Beenstock J, Marbach I, Tabachnick S, Livnah O, Engelberg D. (2012). Osmostress induces autophosphorylation of Hog1 via a C-Terminal regulatory region that is conserved in p38α. *PLoS ONE* **7**:e44749.

Madrid M, Soto T, Khong HK, Franco A, Vicente J, Pérez P, Gacto M, Cansado J. (2006). Stress-induced response, localization, and regulation of the Pmk1 cell integrity pathway in *Schizosaccharomyces pombe*. *Journal of Biological Chemistry* **281**:2033-2043.

Mager WH, Winderickx J. (2005). Yeast as a model for medical and medicinal research. *Trends in Pharmacological Sciences* **26**:265-273.

Maher EA, Furnari FB, Bachoo RM, Rowitch DH, Louis DN, Cavenee WK, DePinho RA. (2001). Malignant glioma: genetics and biology of a grave matter. *Genes Dev* **15**:1311-1333.

Mao L, Yuan L, Slakey L, Jones F, Burow M, Hill S. (2010). Inhibition of breast cancer cell invasion by melatonin is mediated through regulation of the p38 mitogen-activated protein kinase signaling pathway. *Breast Cancer Research* **12**:R107.

Marques JM, Rodrigues RJ, de Magalhães-Sant'Ana AC, Gonçalves T. (2006). *Saccharomyces cerevisiae* Hog1 Protein Phosphorylation upon Exposure to Bacterial Endotoxin. *Journal of Biological Chemistry* **281**:24687-24694.

Martin S, Parton RG. (2006). Lipid droplets: a unified view of a dynamic organelle. *Nat Rev Mol Cell Biol* **7**:373-378.

Martinkova J, Gadher SJ, Hajduch M, Kovarova H. (2009). Challenges in cancer research and multifaceted approaches for cancer biomarker quest. *FEBS Letters* **583**:1772-1784.

Masui K, Cloughesy TF, Mischel PS. (2011). Review: Molecular pathology in adult high-grade gliomas: from molecular diagnostics to target therapies. *Neuropathology and Applied Neurobiology* **38**:(Epub ahead of print).

Mattison CP, Ota IM. (2000). Two protein tyrosine phosphatases, Ptp2 and Ptp3, modulate the subcellular localization of the Hog1 MAP kinase in yeast. *Genes Dev* **14**:1229-1235.

Mora G, Scharnewski M, Fulda M. (2012). Neutral lipid metabolism influences phospholipid synthesis and deacylation in *Saccharomyces cerevisiae*. *PLoS ONE* **7**:e49269.

Morrison DK. (2012). MAP kinase pathways. *Cold Spring Harb Perspect Biol* **4**.

Mudge DK, Yang F, Currie BM, Kim JM, Yeda K, Bashyakarla VK, Ivey FD, Hoffman CS. (2014). Sck1 negatively regulates Gpa2-mediated glucose signaling in *Schizosaccharomyces pombe*. *Eukaryot Cell* **13**:202-208.

Mukaiyama H, Kajiwara S, Hosomi A, Giga-Hama Y, Tanaka N, Nakamura T, Takegawa K. (2009). Autophagy-deficient *Schizosaccharomyces pombe* mutants undergo partial sporulation during nitrogen starvation. *Microbiology* **155**:3816-3826.

Nakashima A, Otsubo Y, Yamashita A, Sato T, Yamamoto M, Tamanoi F. (2012a). Psk1, an AGC kinase family member in fission yeast, is directly phosphorylated and controlled by TORC1 and functions as S6 kinase. *Journal of Cell Science* **125**:5840-5849.

Nakashima A, Otsubo Y, Yamashita A, Sato T, Yamamoto M, Tamanoi F. (2012b). Psk1, an AGC kinase family member in fission yeast, is directly phosphorylated and controlled by TORC1 and functions as S6 kinase. *J Cell Sci* **125**:5840-5849.

Nakashima A, Sato T, Tamanoi F. (2010). Fission yeast TORC1 regulates phosphorylation of ribosomal S6 proteins in response to nutrients and its activity is inhibited by rapamycin. *J Cell Sci* **123**:777-786.

Nelson D, Cox M. (2008). Principles of Biochemistry. W.H. Freeman, pp: 806-807.

Nielsen J. (2009). Systems biology of lipid metabolism: From yeast to human. *FEBS Letters* **583**:3905-3913.

Nikolaou E, Agrafioti I, Stumpf M, Quinn J, Stansfield I, Brown A. (2009). Phylogenetic diversity of stress signalling pathways in fungi. *BMC Evolutionary Biology* **9**:44.

O'Rourke SM, Herskowitz I, O'Shea EK. (2002). Yeast go the whole HOG for the hyperosmotic response. *Trends Genet* **18**:405-412.

Oelkers P, Cromley D, Padamsee M, Billheimer JT, Sturley SL. (2002). The DGA1 gene determines a second triglyceride synthetic pathway in yeast. *Journal of Biological Chemistry* **277**:8877-8881.

Oelkers P, Tinkelenberg A, Erdeniz N, Cromley D, Billheimer JT, Sturley SL. (2000). A lecithin cholesterol acyltransferase-like gene mediates diacylglycerol esterification in yeast. *J Biol Chem* **275**:15609-15612.

Ohgaki H, Dessen P, Jourde B, Horstmann S, Nishikawa T, Di Patre PL, Burkhard C, Schuler D, Probst-Hensch NM, Maiorka PC, Baeza N, Pisani P, Yonekawa Y, Yasargil MG, Lutolf UM, Kleihues P. (2004). Genetic pathways to glioblastoma: a population-based study. *Cancer Res* **64**:6892-6899.

Ohgaki H, Kleihues P. (2007). Genetic pathways to primary and secondary glioblastoma. *Am J Pathol* **170**:1445-1453.

Ohgaki H, Kleihues P. (2009). Genetic alterations and signaling pathways in the evolution of gliomas. *Cancer Science* **100**:2235-2241.

Oresic M, Simell S, Sysi-Aho M, Nanto-Salonen K, Seppanen-Laakso T, Parikka V, Katajamaa M, Hekkala A, Mattila I, Keskinen P, Yetukuri L, Reinikainen A, Lahde J, Suortti T, Hakalax J, Simell T, Hyoty H, Veijola R, Ilonen J, Lahesmaa R, Knip M, Simell O. (2008). Dysregulation of lipid and amino acid metabolism precedes islet autoimmunity in children who later progress to type 1 diabetes. *J Exp Med* **205**:2975-2984.

Otsubo Y, Yamamato M. (2008). TOR Signaling in Fission Yeast. *Critical Reviews in Biochemistry and Molecular Biology* **43**:277-283.

Papadakis MA, Workman CT. (2004). Oxidative stress response pathways: Fission yeast as archetype. *Critical Reviews in Microbiology* **0**:1-16.

Park J-S, Steinbach SK, Desautels M, Hemmingsen SM. (2009). Essential role for *Schizosaccharomyces pombe* pik1 in septation. *PLoS ONE* **4**:e6179.

Pascual-Ahuir A, Proft M. (2007). The Sch9 kinase is a chromatin-associated transcriptional activator of osmostress-responsive genes. *EMBO J* **26**:3098-3108.

Petersen J, Nurse P. (2007). TOR signalling regulates mitotic commitment through the stress MAP kinase pathway and the Polo and Cdc2 kinases. *Nat Cell Biol* **9**:1263-1272.

Peterson TR, Sengupta SS, Harris TE, Carmack AE, Kang SA, Balderas E, Guertin DA, Madden KL, Carpenter AE, Finck BN, Sabatini DM. (2011). mTOR complex 1 regulates lipin 1 localization to control the SREBP pathway. *Cell* **146**:408-420.

Petranovic D, Tyo K, Vemuri GN, Nielsen J. (2010). Prospects of yeast systems biology for human health: integrating lipid, protein and energy metabolism. *FEMS Yeast Research* **10**:1046-1059.

Pfeiffer T, Schuster S, Bonhoeffer S. (2001). Cooperation and competition in the evolution of ATP-producing pathways. *Science* **292**:504-507.

Ploegh HL. (2007). A lipid-based model for the creation of an escape hatch from the endoplasmic reticulum. *Nature* **448**:435-438.

Poli JS, Lutzhoft HC, Karakashev DB, Valente P, Angelidaki I. (2014). An environmentally-friendly fluorescent method for quantification of lipid contents in yeast. *Bioresour Technol* **151**:388-391.

Porstmann T, Santos CR, Griffiths B, Cully M, Wu M, Leevers S, Griffiths JR, Chung YL, Schulze A. (2008). SREBP activity is regulated by mTORC1 and contributes to Akt-dependent cell growth. *Cell Metab* **8**:224-236.

Quinn J, Findlay VJ, Dawson K, Millar JB, Jones N, Morgan BA, Toone WM. (2002). Distinct regulatory proteins control the graded transcriptional response to increasing H(2)O(2) levels in fission yeast *Schizosaccharomyces pombe*. *Mol Biol Cell* **13**:805-816.

Radulovic M, Knittelfelder O, Cristobal-Sarramian A, Kolb D, Wolinski H, Kohlwein SD. (2013). The emergence of lipid droplets in yeast: current status and experimental approaches. *Curr Genet* **59**:231-242.

Rajakumari S, Daum G. (2010a). Janus-faced enzymes yeast Tgl3p and Tgl5p catalyze lipase and acyltransferase reactions. *Mol Biol Cell* **21**:501-510.

---. (2010b). Multiple functions as lipase, steryl ester hydrolase, phospholipase, and acyltransferase of Tgl4p from the yeast *Saccharomyces cerevisiae*. *J Biol Chem* **285**:15769-15776.

Rajakumari S, Grillitsch K, Daum G. (2008). Synthesis and turnover of non-polar lipids in yeast. *Progress in Lipid Research* **47**:157-171.

Rajakumari S, Rajasekharan R, Daum G. (2010). Triacylglycerol lipolysis is linked to sphingolipid and phospholipid metabolism of the yeast *Saccharomyces cerevisiae*. *Biochim Biophys Acta* **1801**:1314-1322.

Ratledge C. (1982). Microbial oils and fats: an assessment of their commercial potential. *Prog Ind Microbiol*:119-206.

Reifenberger G, Kros JM, Burger PC ea. (2000). Oligoastrocytoma. In: Kleihues P, Cavenee WK, eds. Pathology and Genetics of Tumours of the Nervous System. 2nd ed. Lyon, France: IARC Press; :65-69.

Reis T, Van Gilst MR, Hariharan IK. (2010). A buoyancy-based screen of Drosophila larvae for fat-storage mutants reveals a role for Sir2 in coupling fat storage to nutrient availability. *PLoS Genet* **6**:e1001206.

Reiser V, Ruis H, Ammerer G. (1999). Kinase activity-dependent nuclear export opposes stress-induced nuclear accumulation and retention of Hog1 mitogen-activated protein kinase in the budding yeast *Saccharomyces cerevisiae*. *Mol Biol Cell* **10**:1147-1161.

Reiter W, Watt S, Dawson K, Lawrence CL, Bähler J, Jones N, Wilkinson CRM. (2008). Fission yeast MAP Kinase Sty1 is recruited to stress-induced genes. *Journal of Biological Chemistry* **283**:9945-9956.

Ren HY, Liu BF, Ma C, Zhao L, Ren NQ. (2013). A new lipid-rich microalga Scenedesmus sp. strain R-16 isolated using Nile red staining: effects of carbon and nitrogen sources and initial pH on the biomass and lipid production. *Biotechnol Biofuels* **6**:143.

Rice C, Cooke M, Treloar N, Vollbrecht P, Stukey J, McDonough V. (2010). A role for MGA2, but not SPT23, in activation of transcription of ERG1 in *Saccharomyces cerevisiae*. *Biochemical and Biophysical Research Communications* **403**:293-297.

Roberts PJ, Der CJ. (2007). Targeting the Raf-MEK-ERK mitogen-activated protein kinase cascade for the treatment of cancer. *Oncogene* **26**:3291-3310.

Rødkær SV, Færgeman NJ. (2014). Glucose- and nitrogen sensing and regulatory mechanisms in *Saccharomyces cerevisiae*. *FEMS Yeast Research* **14**:683-696.

Rolph C, Moreton R, Harwood J. (1989). Acyl lipid metabolism in the oleaginous yeast *Rhodotorula gracilis* (CBS 3043). *Lipids* **24**:715-720.

Rong Y, Durden DL, Van Meir EG, Brat DJ. (2006). 'Pseudopalisading' necrosis in glioblastoma: a familiar morphologic feature that links vascular pathology, hypoxia, and angiogenesis. *J Neuropathol Exp Neurol* **65**:529-539.

Roukos DH. (2011). Trastuzumab and beyond: sequencing cancer genomes and predicting molecular networks. *Pharmacogenomics J* **11**:81-92.

Rousseau S, Dolado I, Beardmore V, Shpiro N, Marquez R, Nebreda AR, Arthur JSC, Case LM, Tessier-Lavigne M, Gaestel M, Cuenda A, Cohen P. (2006). CXCL12 and C5a trigger

cell migration via a PAK1/2-p38α MAPK-MAPKAP-K2-HSP27 pathway. *Cellular Signalling* **18**:1897-1905.

Ruiz-Roig C, Noriega N, Duch A, Posas F, de Nadal E. (2012). The Hog1 SAPK controls the Rtg1/Rtg3 transcriptional complex activity by multiple regulatory mechanisms. *Molecular Biology of the Cell* **23**:4286-4296.

Saito H, Posas F. (2012). Response to hyperosmotic stress. *Genetics* **192**:289-318.

Sandager L, Gustavsson MH, Ståhl U, Dahlqvist A, Wiberg E, Banas A, Lenman M, Ronne H, Stymne S. (2002). Storage Lipid Synthesis Is Non-essential in Yeast. *Journal of Biological Chemistry* **277**:6478-6482.

Santamauro F, Whiffin FM, Scott RJ, Chuck CJ. (2014). Low-cost lipid production by an oleaginous yeast cultured in non-sterile conditions using model waste resources. *Biotechnol Biofuels* **7**:34.

Santos A, Riezman H. (2012). Yeast as a model system for studying lipid homeostasis and function. *FEBS Letters* **586**:2858-2867.

Santos C, Schulze A. (2012). Lipid metabolism in cancer. *FEBS Journal* **279**:2610-2623.

Sato A, Okada M, Shibuya K, Watanabe E, Seino S, Narita Y, Shibui S, Kayama T, Kitanaka C. (2014). Pivotal role for ROS activation of p38 MAPK in the control of differentiation and tumor-initiating capacity of glioma-initiating cells. *Stem Cell Research* **12**:119-131.

Schmidt C, Ploier B, Koch B, Daum G. (2013). Analysis of yeast lipid droplet proteome and lipidome. *Methods Cell Biol* **116**:15-37.

Schulze WX, Deng L, Mann M. (2005). Phosphotyrosine interactome of the ErbB-receptor kinase family. *Mol Syst Biol* **1**:2005 0008.

Seip J, Jackson R, He H, Zhu Q, Hong SP. (2013). Snf1 is a regulator of lipid accumulation in *Yarrowia lipolytica*. *Appl Environ Microbiol* **79**:7360-7370.

Shahidi F. (2001). Extraction and measurement of total lipids. Current Protocols in Food Analytical Chemistry, John Wiley & Sons, Inc.

Shao W, Espenshade PJ. (2014). Sterol Regulatory Element-binding Protein (SREBP) Cleavage Regulates Golgi-to-ER Recycling of SREBP Cleavage Activating Protein (SCAP). *Journal of Biological Chemistry*.

Shi S, Valle-Rodríguez JO, Khoomrung S, Siewers V, Nielsen J. (2012). Functional expression and characterization of five wax ester synthases in *Saccharomyces cerevisiae* and their utility for biodiesel production.

Shin GH, Veen M, Stahl U, Lang C. (2012). Overexpression of genes of the fatty acid biosynthetic pathway leads to accumulation of sterols in *Saccharomyces cerevisiae*. *Yeast* **29**:371-383.

Shui G, Guan XL, Low CP, Chua GH, Goh JS, Yang H, Wenk MR. (2010). Toward one step analysis of cellular lipidomes using liquid chromatography coupled with mass spectrometry: application to *Saccharomyces cerevisiae* and *Schizosaccharomyces pombe* lipidomics. *Mol Biosyst* **6**:1008-1017.

Sitepu IR, Ignatia L, Franz AK, Wong DM, Faulina SA, Tsui M, Kanti A, Boundy-Mills K. (2012). An improved high-throughput Nile red fluorescence assay for estimating intracellular lipids in a variety of yeast species. *J Microbiol Methods* **91**:321-328.

Smith D, Nicholls S, Morgan BA, Brown AJ, Quinn J. (2004). A conserved stress-activated protein kinase regulates a core stress response in the human pathogen *Candida albicans*. *Mol Biol Cell* **15**:4179-4190.

Smith D, Toone WM, Chen D, Bähler J, Jones N, Morgan BA, Quinn J. (2002). The Srk1 protein kinase is a target for the Sty1 stress-activated MAPK in fission yeast. *Journal of Biological Chemistry* **277**:33411-33421.

Sooman L, Lennartsson J, Gullbo J, Bergqvist M, Tsakonas G, Johansson F, Edqvist PH, Ponten F, Jaiswal A, Navani S, Alafuzoff I, Popova S, Blomquist E, Ekman S. (2013). Vandetanib combined with a p38 MAPK inhibitor synergistically reduces glioblastoma cell survival. *Med Oncol* **30**:638.

Soukas AA, Carr CE, Ruvkun G. (2013). Genetic Regulation of *Caenorhabditis elegans* Lysosome Related Organelle Function. *PLoS Genet* **9**:e1003908.

Stupp R, Mason WP, van den Bent MJ, Weller M, Fisher B, Taphoorn MJ, Belanger K, Brandes AA, Marosi C, Bogdahn U, Curschmann J, Janzer RC, Ludwin SK, Gorlia T, Allgeier A, Lacombe D, Cairncross JG, Eisenhauer E, Mirimanoff RO. (2005). Radiotherapy plus concomitant and adjuvant temozolomide for glioblastoma. *N Engl J Med* **352**:987-996.

Sturgill TW, Hall MN. (2007). Holding back TOR advances mitosis. *Nat Cell Biol* **9**:1221-1222.

Su X, Dowhan W. (2006). Regulation of cardiolipin synthase levels in *Saccharomyces cerevisiae*. *Yeast* **23**:279-291.

Sugawa N, Ekstrand AJ, James CD, Collins VP. (1990). Identical splicing of aberrant epidermal growth factor receptor transcripts from amplified rearranged genes in human glioblastomas. *Proc Natl Acad Sci U S A* **87**:8602-8606.

Sui X, Kong N, Ye L, Han W, Zhou J, Zhang Q, He C, Pan H. (2014). p38 and JNK MAPK pathways control the balance of apoptosis and autophagy in response to chemotherapeutic agents. *Cancer Letters* **344**:174-179.

Surma MA, Klose C, Peng D, Shales M, Mrejen C, Stefanko A, Braberg H, Gordon DE, Vorkel D, Ejsing CS, Farese R, Jr., Simons K, Krogan NJ, Ernst R. (2013). A lipid E-MAP identifies Ubx2 as a critical regulator of lipid saturation and lipid bilayer stress. *Mol Cell* **51**:519-530.

Swinnen JV, Brusselmans K, Verhoeven G. (2006). Increased lipogenesis in cancer cells: new players, novel targets. *Curr Opin Clin Nutr Metab Care* **9**:358-365.

Takada H, Nishimura M, Asayama Y, Mannse Y, Ishiwata S, Kita A, Doi A, Nishida A, Kai N, Moriuchi S, Tohda H, Giga-Hama Y, Kuno T, Sugiura R. (2007). Atf1 is a target of the mitogen-activated protein kinase Pmk1 and regulates cell integrity in fission yeast. *Mol Biol Cell* **18**:4794-4802.

Tamanoi F. (2011). Ras signaling in yeast. *Genes Cancer* **2**:210-215.

Tanimura A, Takashima M, Sugita T, Endoh R, Kikukawa M, Yamaguchi S, Sakuradani E, Ogawa J, Ohkuma M, Shima J. (2014). *Cryptococcus terricola* is a promising oleaginous

yeast for biodiesel production from starch through consolidated bioprocessing. *Sci. Rep.* **4**.

Tapia VE, Anschau A, Coradini AL, T TF, Deckmann AC. (2012). Optimization of lipid production by the oleaginous yeast *Lipomyces starkeyi* by random mutagenesis coupled to cerulenin screening. *AMB Express* **2**:64.

Tatebayashi K, Tanaka K, Yang HY, Yamamoto K, Matsushita Y, Tomida T, Imai M, Saito H. (2007). Transmembrane mucins Hkr1 and Msb2 are putative osmosensors in the SHO1 branch of yeast HOG pathway. *EMBO J* **26**:3521-3533.

Teixeira V, Medeiros TC, Vilaça R, Moradas-Ferreira P, Costa V. (2013). Reduced TORC1 signaling abolishes mitochondrial dysfunctions and shortened chronological lifespan of Isc1p-deficient cells.

Thomas CF, Limper AH. (2007). Current insights into the biology and pathogenesis of *Pneumocystis pneumonia*. *Nat Rev Micro* **5**:298-308.

Thornton TM, Rincon M. (2009). Non-classical p38 map kinase functions: cell cycle checkpoints and survival. *Int J Biol Sci* **5**:44-51.

Thun MJ, DeLancey JO, Center MM, Jemal A, Ward EM. (2010). The global burden of cancer: priorities for prevention. *Carcinogenesis* **31**:100-110.

Tingaud-Sequeira A, Ouadah N, Babin PJ. (2011). Zebrafish obesogenic test: a tool for screening molecules that target adiposity. *J Lipid Res* **52**:1765-1772.

Truman AW, Kim KY, Levin DE. (2009). Mechanism of Mpk1 mitogen-activated protein kinase binding to the Swi4 transcription factor and its regulation by a novel caffeine-induced phosphorylation. *Mol Cell Biol* **29**:6449-6461.

Trzcinska-Danielewicz J, Ishikawa T, Micialkiewicz A, Fronk J. (2008). Yeast transcription factor Oaf1 forms homodimer and induces some oleate-responsive genes in absence of Pip2. *Biochem Biophys Res Commun* **374**:763-766.

Urban J, Soulard A, Huber A, Lippman S, Mukhopadhyay D, Deloche O, Wanke V, Anrather D, Ammerer G, Riezman H, Broach JR, De Virgilio C, Hall MN, Loewith R. (2007a). Sch9 is a major target of TORC1 in *Saccharomyces cerevisiae*. *Mol Cell* **26**:663-674.

---. (2007b). Sch9 is a major target of TORC1 in *Saccharomyces cerevisiae*. *Mol Cell* **26**:663-674.

Valachovic M, Bareither BM, Shah Alam Bhuiyan M, Eckstein J, Barbuch R, Balderes D, Wilcox L, Sturley SL, Dickson RC, Bard M. (2006). Cumulative mutations affecting sterol biosynthesis in the yeast *Saccharomyces cerevisiae* result in synthetic lethality that is suppressed by alterations in sphingolipid profiles. *Genetics* **173**:1893-1908.

Valbuena N, Rozalén AE, Moreno S. (2012). Fission yeast TORC1 prevents eIF2α phosphorylation in response to nitrogen and amino acids via Gcn2 kinase. *Journal of Cell Science*.

van Meer G, Voelker DR, Feigenson GW. (2008). Membrane lipids: where they are and how they behave. *Nat Rev Mol Cell Biol* **9**:112-124.

Vance JE. (2008). Thematic Review Series: Glycerolipids. Phosphatidylserine and phosphatidylethanolamine in mammalian cells: two metabolically related aminophospholipids. *Journal of Lipid Research* **49**:1377-1387.

Vance JE, Tasseva G. (2013). Formation and function of phosphatidylserine and phosphatidylethanolamine in mammalian cells. *Biochimica et Biophysica Acta (BBA) - Molecular and Cell Biology of Lipids* **1831**:543-554.

Vander Heiden MG, Cantley LC, Thompson CB. (2009). Understanding the Warburg Effect: The Metabolic Requirements of Cell Proliferation. *Science* **324**:1029-1033.

Wachtler V, Rajagopalan S, Balasubramanian MK. (2003). Sterol-rich plasma membrane domains in the fission yeast *Schizosaccharomyces pombe*. *J Cell Sci* **116**:867-874.

Walther TC, Farese Jr RV. (2009). The life of lipid droplets. *Biochimica et Biophysica Acta (BBA) - Molecular and Cell Biology of Lipids* **1791**:459-466.

Wang CW, Miao YH, Chang YS. (2014). Control of lipid droplet size in budding yeast requires the collaboration between Fld1 and Ldb16. *J Cell Sci* **127**:1214-1228.

Warburg O. (1925). Uber den Stoffwechsel der Carcinomzelle (About the metabolism of the carcinoma cell). *Klin Wochenschr Berl* **4**:534-536.

Warburg O. (1956). On the origin of cancer cells. *Science* **123**:309-314.

Warmka J, Hanneman J, Lee J, Amin D, Ota I. (2001). Ptc1, a type 2C Ser/Thr phosphatase, inactivates the HOG pathway by dephosphorylating the mitogen-activated protein kinase Hog1. *Mol Cell Biol* **21**:51-60.

Watkins PA, Lu JF, Steinberg SJ, Gould SJ, Smith KD, Braiterman LT. (1998). Disruption of the *Saccharomyces cerevisiae* FAT1 gene decreases very long-chain fatty acyl-CoA synthetase activity and elevates intracellular very long-chain fatty acid concentrations. *J Biol Chem* **273**:18210-18219.

Wei M, Fabrizio P, Madia F, Hu J, Ge H, Li LM, Longo VD. (2009). Tor1/Sch9-regulated carbon source substitution is as effective as calorie restriction in life span extension. *PLoS Genet* **5**:e1000467.

Weigelt B, Baehner FL, Reis-Filho JS. (2010). The contribution of gene expression profiling to breast cancer classification, prognostication and prediction: a retrospective of the last decade. *The Journal of Pathology* **220**:263-280.

Weinberger M, Mesquita A, Caroll T, Marks L, Yang H, Zhang Z, Ludovico P, Burhans WC. (2010). Growth signaling promotes chronological aging in budding yeast by inducing superoxide anions that inhibit quiescence. *Aging (Albany NY)* **2**:709-726.

Weisman R. (2004). The fission yeast TOR proteins and the rapamycin response: an unexpected tale. *Curr Top Microbiol Immunol* **279**:85-95.

Weisman R, Finkelstein S, Choder M. (2001). Rapamycin blocks sexual development in fission yeast through inhibition of the cellular function of an FKBP12 homolog. *J Biol Chem* **276**:24736-24742.

Weisman R, Roitburg I, Nahari T, Kupiec M. (2005). Regulation of leucine uptake by tor1+ in *Schizosaccharomyces pombe* is sensitive to rapamycin. *Genetics* **169**:539-550.

Welch M, Lai R. (2009). Glioblastoma multiforme. *Curr Treat Options Neurol* **11**:297-305.

Wen PY, Kesari S. (2008). Malignant Gliomas in Adults. *New England Journal of Medicine* **359**:492-507.

Wild R, Patil S, Popović M, Zappi M, Dufreche S, Bajpai R. (2010). Lipids from *Lipomyces starkeyi*. *Food Technology and Biotechnology* **48**:329-335.

Wilfling F, Wang H, Haas Joel T, Krahmer N, Gould Travis J, Uchida A, Cheng J-X, Graham M, Christiano R, Fröhlich F, Liu X, Buhman Kimberly K, Coleman Rosalind A, Bewersdorf J, Farese Jr Robert V, Walther Tobias C. (2013). Triacylglycerol synthesis enzymes mediate lipid droplet growth by relocalizing from the ER to lipid droplets. *Developmental Cell* **24**:384-399.

Wilkinson MG, Millar JBA. (2000). Control of the eukaryotic cell cycle by MAP kinase signaling pathways. *The FASEB Journal* **14**:2147-2157.

Wulfkuhle J, Espina V, Liotta L, Petricoin E. (2004). Genomic and proteomic technologies for individualisation and improvement of cancer treatment. *European Journal of Cancer* **40**:2623-2632.

Wurgler-Murphy SM, Maeda T, Witten EA, Saito H. (1997). Regulation of the *Saccharomyces cerevisiae* HOG1 mitogen-activated protein kinase by the PTP2 and PTP3 protein tyrosine phosphatases. *Mol Cell Biol* **17**:1289-1297.

Xie J, Wu H, Dai C, Pan Q, Ding Z, Hu D, Ji B, Luo Y, Hu X. (2014). Beyond Warburg effect - dual metabolic nature of cancer cells. *Sci. Rep.* **4**.

Yamamoto K, Tatebayashi K, Tanaka K, Saito H. (2010). Dynamic control of yeast MAP Kinase network by induced association and dissociation between the Ste50 scaffold and the Opy2 membrane anchor. *Mol Cell* **40**:87-98.

Yang K, Han X. (2011). Accurate quantification of lipid species by Electrospray Ionization Mass Spectrometry — Meets a key challenge in lipidomics. *Metabolites* **1**:21-40.

Yang W, Tabancay AP, Jr., Urano J, Tamanoi F. (2001). Failure to farnesylate Rheb protein contributes to the enrichment of G0/G1 phase cells in the *Schizosaccharomyces pombe* farnesyltransferase mutant. *Mol Microbiol* **41**:1339-1347.

Yang W, Zheng Y, Xia Y, Ji H, Chen X, Guo F, Lyssiotis CA, Aldape K, Cantley LC, Lu Z. (2012). ERK1/2-dependent phosphorylation and nuclear translocation of PKM2 promotes the Warburg effect. *Nat Cell Biol* **14**:1295-1304.

Yang Y-A, Han WF, Morin PJ, Chrest FJ, Pizer ES. (2002). Activation of fatty acid synthesis during neoplastic transformation: Role of Mitogen-Activated Protein Kinase and Phosphatidylinositol 3-Kinase. *Experimental Cell Research* **279**:80-90.

Yao HR, Liu J, Plumeri D, Cao YB, He T, Lin L, Li Y, Jiang YY, Li J, Shang J. (2011). Lipotoxicity in HepG2 cells triggered by free fatty acids. *Am J Transl Res* **3**:284-291.

Yazawa H, Kumagai H, Uemura H. (2012). Characterization of triglyceride lipase genes of fission yeast *Schizosaccharomyces pombe*. *Applied Microbiology and Biotechnology* **96**:981-991.

Yen C-LE, Monetti M, Burri BJ, Farese RV. (2005). The triacylglycerol synthesis enzyme DGAT1 also catalyzes the synthesis of diacylglycerols, waxes, and retinyl esters. *Journal of Lipid Research* **46**:1502-1511.

Yoon DJ, Kwan BH, Chao FC, Nicolaides TP, Phillips JJ, Lam GY, Mason AB, Weiss WA, Kamei DT. (2010). Intratumoral therapy of glioblastoma multiforme using genetically engineered transferrin for drug delivery. *Cancer Research* **70**:4520-4527.

Yoshimoto K, Dang J, Zhu S, Nathanson D, Huang T, Dumont R, Seligson DB, Yong WH, Xiong Z, Rao N, Winther H, Chakravarti A, Bigner DD, Mellinghoff IK, Horvath S, Cavenee WK, Cloughesy TF, Mischel PS. (2008). Development of a real-time RT-PCR assay for detecting EGFRvIII in glioblastoma samples. *Clin Cancer Res* **14**:488-493.

Zarich N, Oliva JL, Martinez N, Jorge R, Ballester A, Gutierrez-Eisman S, Garcia-Vargas S, Rojas JM. (2006). Grb2 is a negative modulator of the intrinsic Ras-GEF activity of hSos1. *Mol Biol Cell* **17**:3591-3597.

Zarubin T, Han J. (2005). Activation and signaling of the p38 MAP kinase pathway. *Cell Res* **15**:11-18.

Zech M, Nübling G, Castrop F, Jochim A, Schulte EC, Mollenhauer B, Lichtner P, Peters A, Gieger C, Marquardt T, Vanier MT, Latour P, Klünemann H, Trenkwalder C, Diehl-Schmid J, Perneczky R, Meitinger T, Oexle K, Haslinger B, Lorenzl S, Winkelmann J. (2013). Niemann-Pick C Disease gene mutations and age-related neurodegenerative disorders. *PLoS ONE* **8**:e82879.

Zhang F, Du G. (2012). Dysregulated lipid metabolism in cancer. *World J Biol Chem* **3**:167-174.

Zhang Q, Chieu HK, Low CP, Zhang S, Heng CK, Yang H. (2003). *Schizosaccharomyces pombe* cells deficient in Triacylglycerols synthesis undergo apoptosis upon entry into the stationary phase. *Journal of Biological Chemistry* **278**:47145-47155.

Zhou X, Ma Y, Sugiura R, Kobayashi D, Suzuki M, Deng L, Kuno T. (2010). MAP Kinase Kinase Kinase (MAPKKK)-dependent and -independent Activation of Sty1 Stress MAPK in Fission Yeast. *Journal of Biological Chemistry* **285**:32818-32823.

Zhu G, Spellman PT, Volpe T, Brown PO, Botstein D, Davis TN, Futcher B. (2000). Two yeast forkhead genes regulate the cell cycle and pseudohyphal growth. *Nature* **406**:90-94.

Zitvogel L, Apetoh L, Ghiringhelli F, Kroemer G. (2008). Immunological aspects of cancer chemotherapy. *Nat Rev Immunol* **8**:59-73.

Zuin A, Carmona M, Morales-Ivorra I, Gabrielli N, Vivancos AP, Ayte J, Hidalgo E. (2010a). Lifespan extension by calorie restriction relies on the Sty1 MAP kinase stress pathway. *EMBO J* **29**:981-991.

Zuin A, Castellano-Esteve D, Ayte J, Hidalgo E. (2010b). Living on the edge: stress and activation of stress responses promote lifespan extension. *Aging (Albany NY)* **2**:231-237.

Zuriani R, Vigneswari S, Azizan MNM, Majid MIA, Amirul AA. (2013). A high throughput Nile red fluorescence method for rapid quantification of intracellular bacterial polyhydroxyalkanoates. *Biotechnology and Bioprocess Engineering* **18**:472-478.

# Appendix I

**A1. Plasmid map of pRS315**

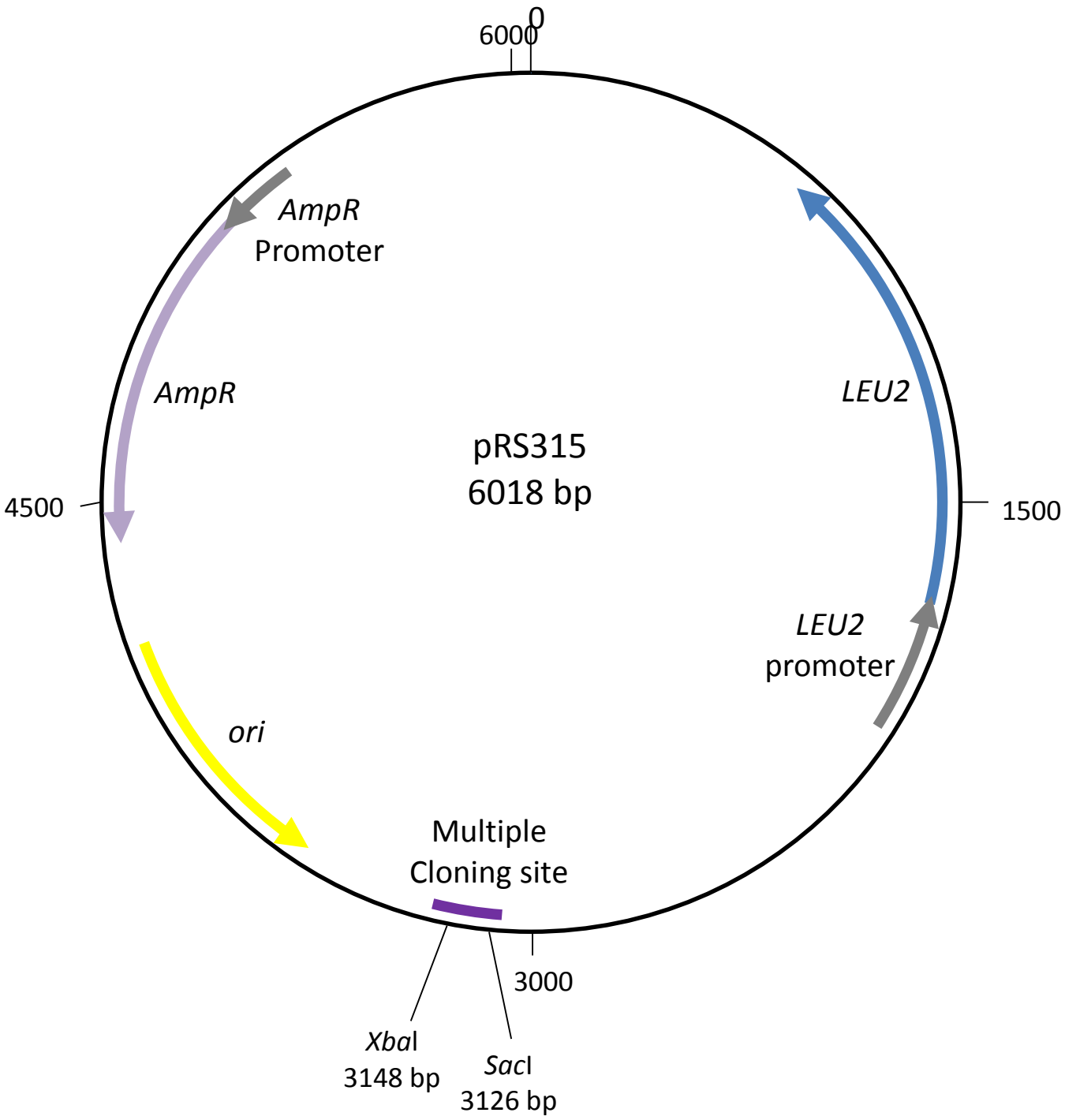

**A2. Plasmid map of CLLp001 – pRS315 HOG1 plus 1kb promoter upstream of ATG cloned into *XbaI* and *SacI* sites of pRS315 (2.3KB)**

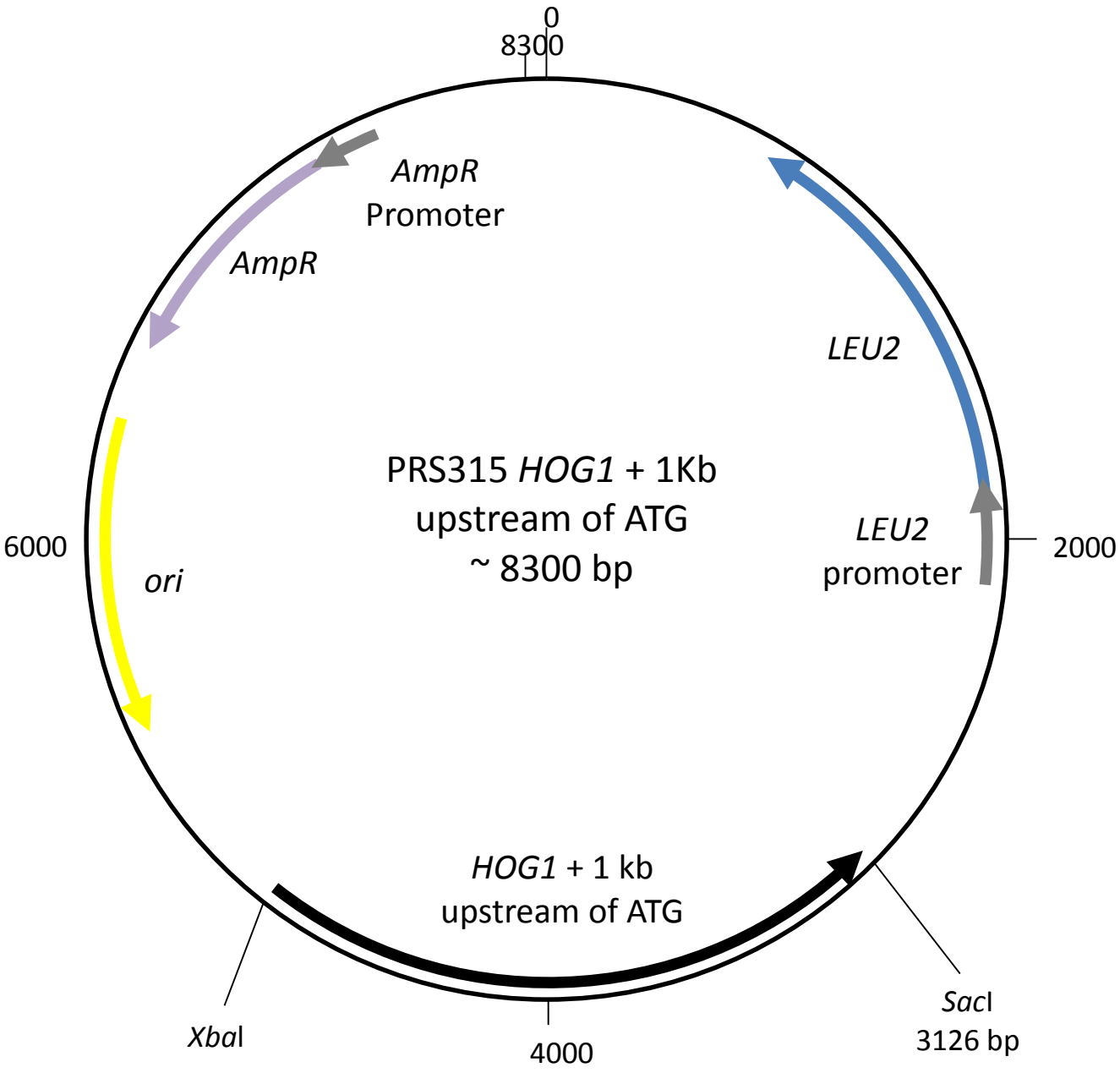

**A3. Plasmid map of CLLp002 – pRS315 *Lipomyces starkeyi* MAPK plus 1kb promoter upstream of ATG cloned into *XbaI* and *SacI* sites of pRS315.**

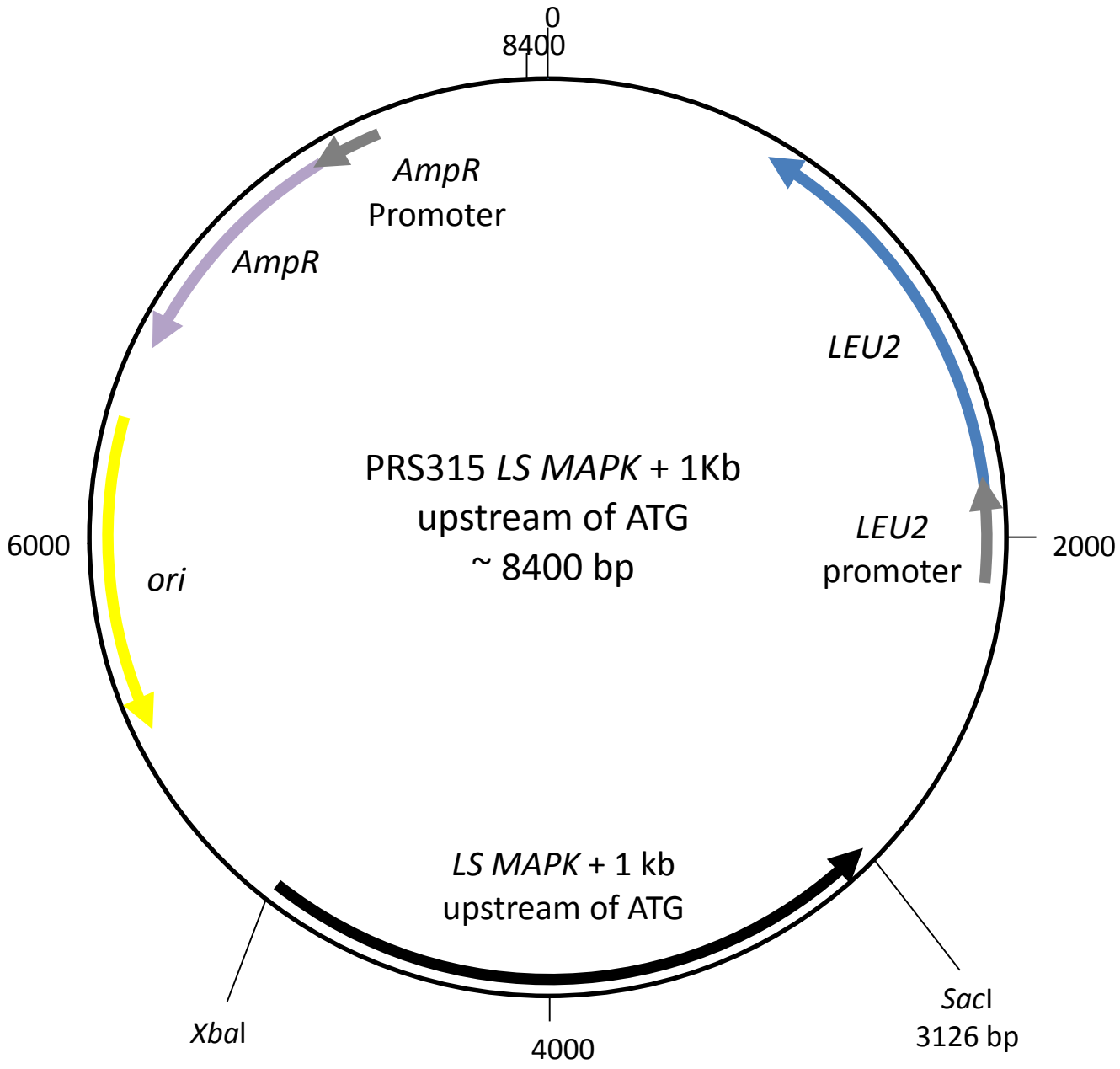

**A4. Plasmid map of pRS313**

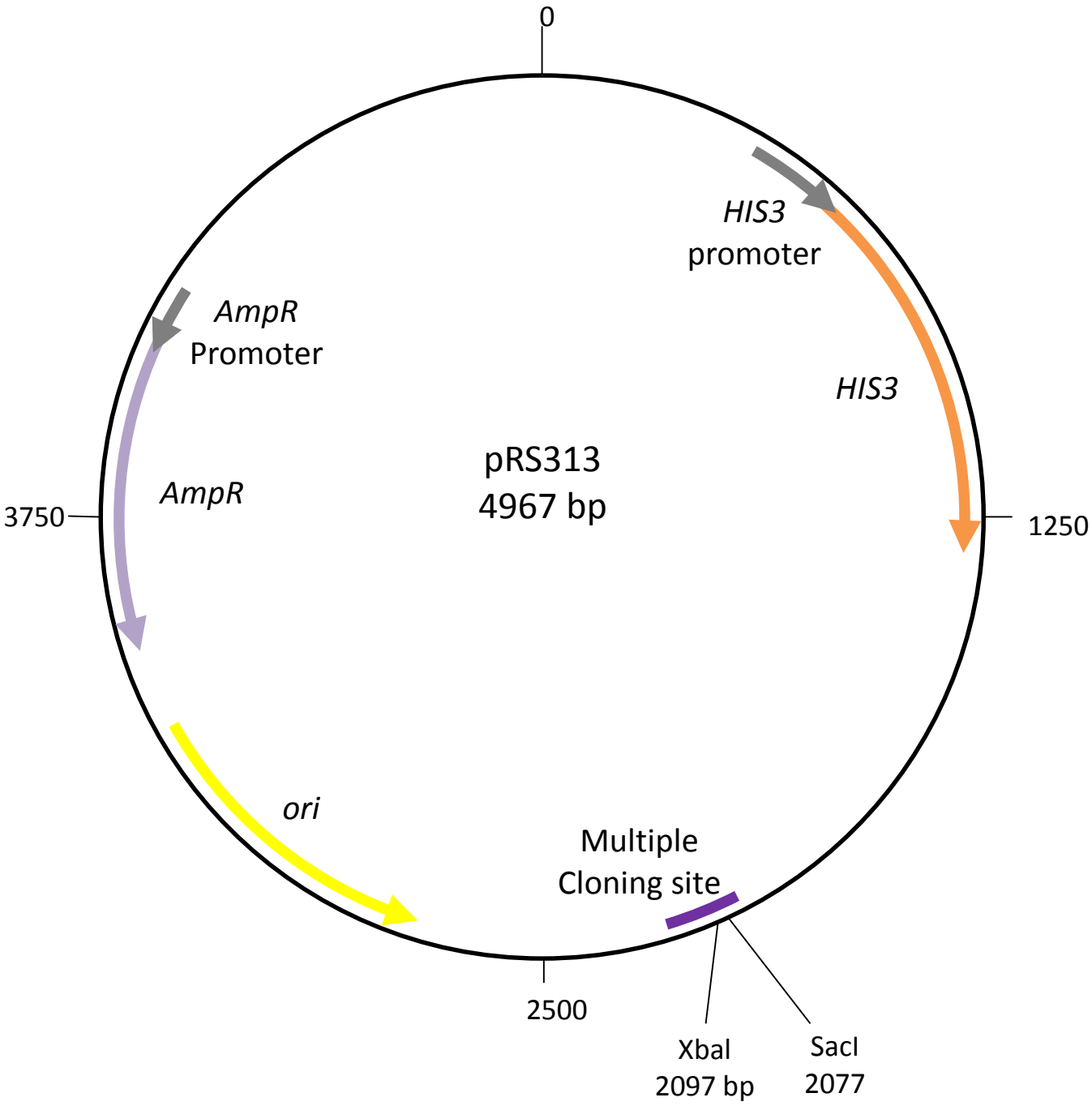

**A5. Plasmid map of pCLLp004 – pRS313 HOG1 plus 1kb promoter upstream of ATG cloned into *XbaI* and *SacI* sites of pRS313 (2.3KB)**

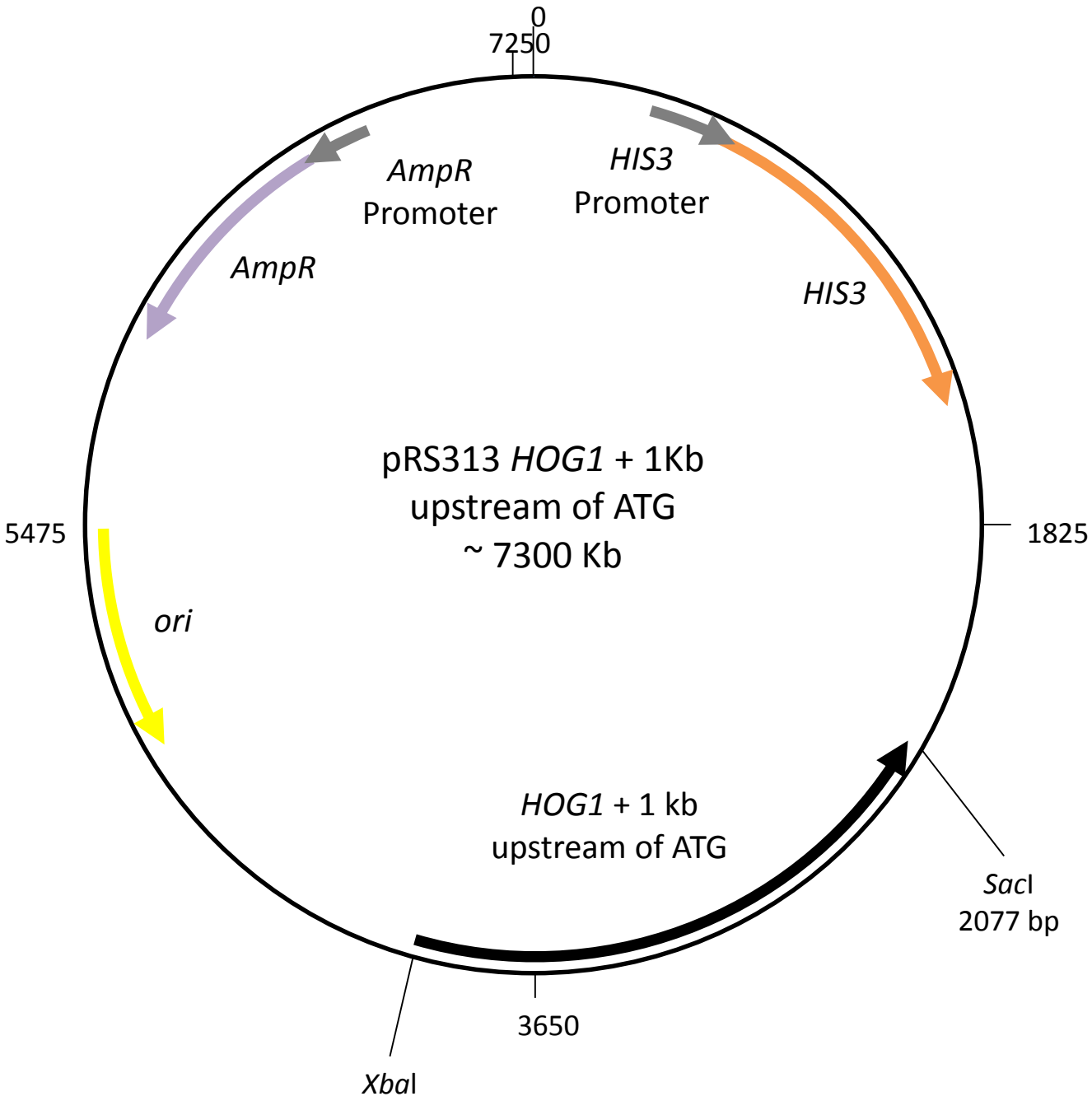

**A6. Plasmid map of pFA6a-KanMX6**

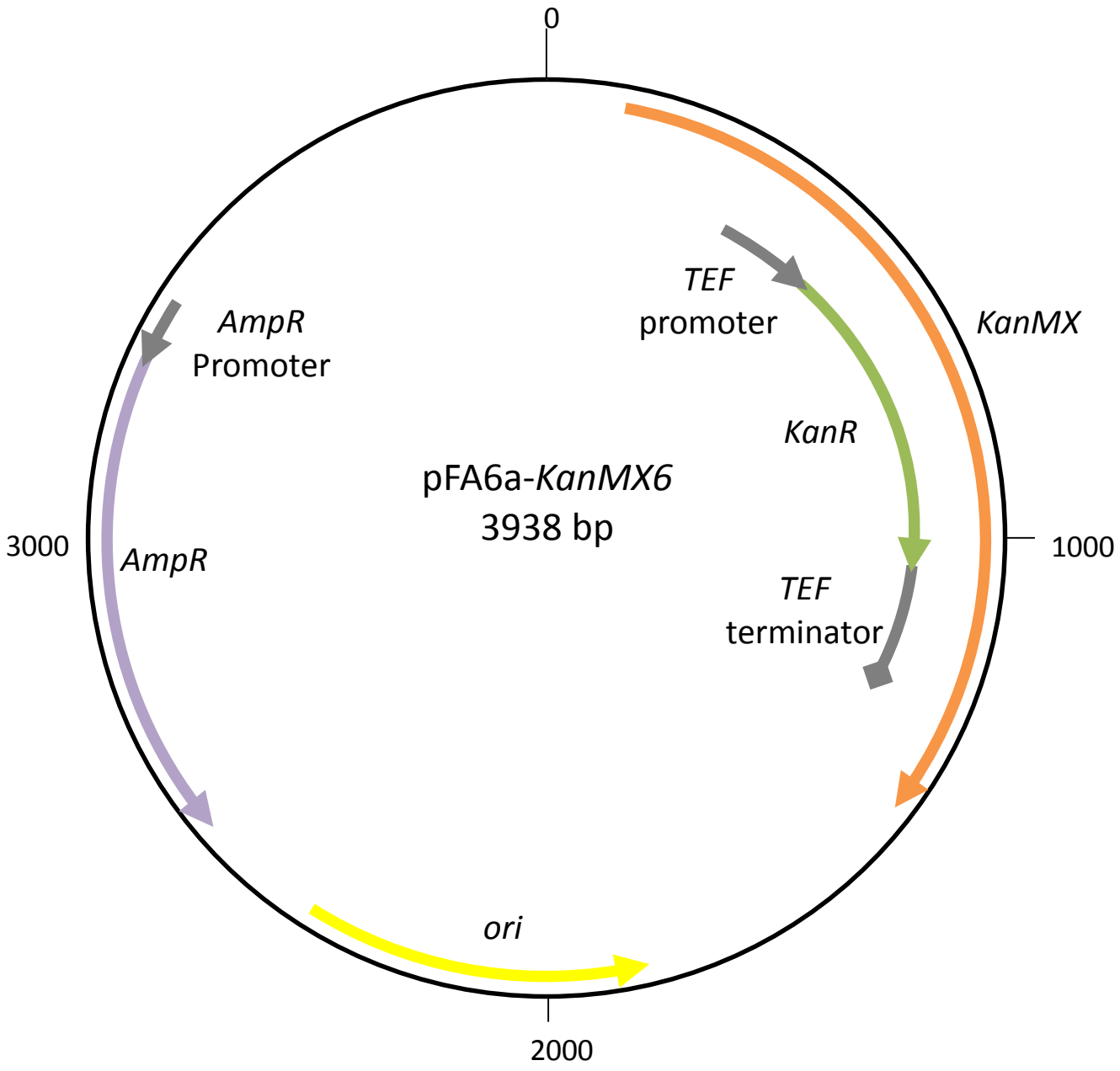

**A7. Plasmid map of pFA6a-natMX6**

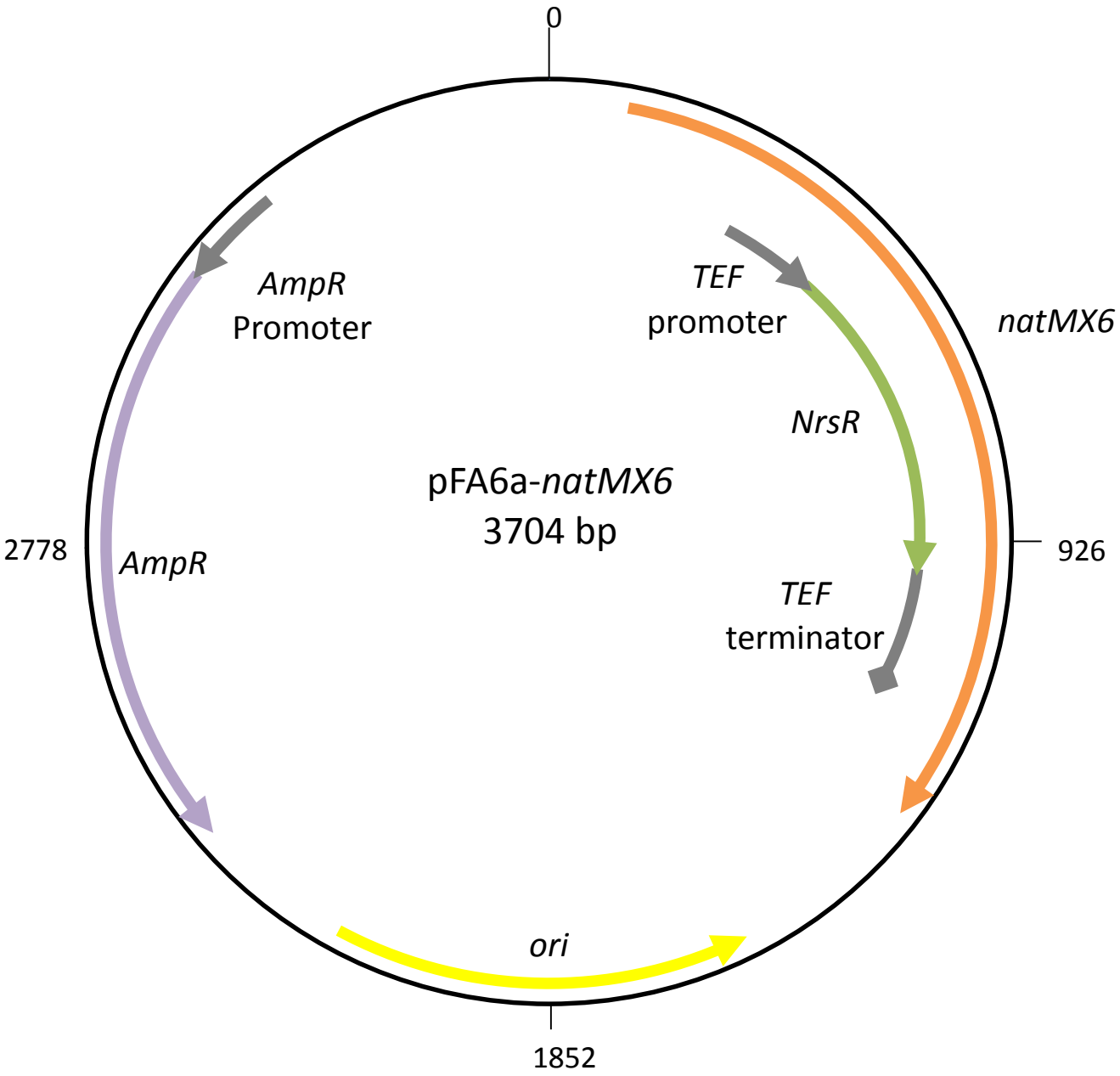

## A8. Alignment of MAPK genomic DNA sequences from *S. cerevisiae* (HOG1), *S. pombe* (sty1) and *L. starkeyi* (LSMAPK)

```
HOG1       ATGACC------ACTAACGAGGAAT----------TCAT--TAGGA--------------
sty1       ATGGC--------------AG-AAT----------TTAT--TCGTA--------------
LSMAPK     ATGGCCGATTTCA-T--C-AGGTATGTGCGTGCGGTTATCTTCGGATGCATCAGTGCTGA


HOG1       -CA-----------CAGATATTCGGTAC-------------------A-G----------
sty1       -CA-----------CAAATATTCGGTAC-------------------ATG----------
LSMAPK     CCATTGTCAGAACCCAGATCTTCGGCACCTCCTTCGAGATCACCAGCA-GGTACAACTTT


HOG1       -------TTTTC-------GAGAT---C-----ACAAA---------TAGATACAATGAT
sty1       -------TTTT--------GAAATTACC-----AC------------TAGATATAGCGAC
LSMAPK     TACATCTTTTTCCGCAATTGAGATCGCCTACTGAC--AGTAGTCGCTTAGATATGCCGAT


HOG1       TTAAACC--CCG-TTGGGATGGGGGCATTTGGGTTGGT----------------------
sty1       TTA---CAGCCGATTGGCATGGGCGCCTTTGGCCTCGT----------------------
LSMAPK     CTGAA-C--CCGGTTGGAATGGGTGCGTTCGGTTTGGTGTGGTATGTGACGGACGCCTGC


HOG1       -------------------TTGCT-------------------CAGC-------CACGGA
sty1       -------------------TTGTT-------------------CAGC-------GAAGGA
LSMAPK     ATAATACTTAGCTGTCAAGTTGTTTATTCATCTGACATCTATCCAGCTCCGCTCGA--GA


HOG1       -CA-CT---T----TGACATCTCAGCCAGTTGCCATTAAGAAAATCATGAAACCTTTT--
sty1       TCAGCTAACTGGAATGA-AT--------GTCGCTGTTAAGAAAATTATGAAACCCTTTAG
LSMAPK     TCAGCTTACCG----GA-----CAGGCAGTCGCTATTAAAAAGATCATGAAGCCGTTTAG


HOG1       TCCACTGCAGTGCTGGCCAAAA-GGACATATCGTGAACTAAAACTACTAAAACATCTAAG
sty1       T--ACTCCGGTACTGG-CAAAACGTACCTATCGGGAATTAAAACTATTAAAGCATTTAAG
LSMAPK     --CACACCAGTTTTGT-CTAAGCGAACATATAGAGAGCTGAAGTTGTTAAAGCATCTTCG


HOG1       ACACGAGAAC-TTGATTTGCCTTCAGGA-C-ATATTTCT--TTCTCCATTGGAAGATATA
sty1       GCATGAGAATATT-ATTAGC-TT---GAGCGATATTTTTATTTCTCCCTTTGAAGATATT
LSMAPK     TCACGAGAAC-GTGATTT-CCCT---GAGCGACATCTTTATTTCTCCGCTCGAAGATATC
```

```
HOG1        TATTTTGTCACGGAA-TTACAAGGAACAGAT-TTACATAGACT-CTTGCAAACA---AGA
sty1        TATTTTGTCACGGAGCTT-CTGGGAACAGATCTT-CATAGACTACTT----ACATCGCGA
LSMAPK      TACTTTGTCACGGAA-TTGCTAGGCACAGACCTT-CATCGATTGCTC----ACCTCGCGA

HOG1        CC-CTTGGAAAAGCAATTTGTTCAGTATTTCCTATACCAAATTCT---AAGGG-----GT
sty1        CC-TTTAGAGACGCAATTTATACAATACTTCTTATACCAAAT-CTTGCGAGGGCTCAAGT
LSMAPK      CCACTT-GAAAAGCAGTTTATACAATATTTCTTGTACCAGAT-ATTGC--GTG-----GT

HOG1        TTAAAATACGTTCACTCCGCGGGCGTCATTCA---TAGAGATTTGAAACCGAGCAACATT
sty1        TT-------GTTCATTCTGCCGGTGTTATTCACCGT---GATCTGAAACCCAGTAACATC
LSMAPK      TTGAAATATGTTCATTCAGCTGGCGTTATTCATCGT---GACTTAAAGCCGAGCAATATC

HOG1        CTGAT-T-AATGAAAACTGTGATTTGAAG-----------------------------
sty1        TTAAT-T-AACGAAAATTGCGATTTAAAA-----------------------------
LSMAPK      CT--TGTGAACGAGAATTGTGATTTGAAGGTATTCCTCCTCGAGTTCCAAGACTTCTGAA

HOG1        -ATTTGC-----GATTTCG----------------------GTCTAGCAAGAATTCAAGA
sty1        -ATCTGC-----GATTTCG----------------------GTTTGGCTCGTATTCAAGA
LSMAPK      CATTTGCTGATGGATTTCGACAAATTAGATTTGCGACTTTGGCTTGGCTCGTATTCAGGA

HOG1        CCCTCAAATGACAGGCTATGTTTCCACTAGATACTACAGGGCACCTGAAATCATGCTAAC
sty1        CCCTCAAATGACGGGCTATGTTTCTACTCGTTATTACCGTGCACCTGAGATTATGTTAAC
LSMAPK      TCCGCAAATGACGGGATATGTCTCCACGCGATATTATCGGGCACCAGAGATCATGCTTAC

HOG1        GTGGCAAAAATATGACGTCGAGGTCGACATTTGG--TCCGCTGGTTGTATTTTTGCCGAA
sty1        TTGGCAAAAGTACAACGTCGAAGTTGATATTTGGAGT--GCGGGTTGTATTTTTGCTGAG
LSMAPK      GTGGCAAAAGTACGACGTCGAGGTTGACATATGGAGT--GCAGGATGTATCTTTGCTGAA

HOG1        ATGATTGAA-GGTAAGCCTTTGTTCCCTGG--GAAA-GATCATGTTCACCAATTTTCGAT
sty1        ATGATTGAA-GGAAAACCCTTGTTTCCCGGCCG--A-GACCACGTTAACCAGTTTTCTAT
LSMAPK      ATG-TTGGACGGAAAGCCATTGTTTCC-AG--GAAAGGACCATGTGAATCAGTTTTCGAT

HOG1        CATCACTGACTTGTTGGGATCTCCGCCAAAG--GATGTGATAAAT----ACTATTTGTTC
sty1        AATCACGGAATTGTTGGGAACGCCGCCTATG--GAAGT----AATTGAGACGATTTG--C
LSMAPK      TATCACTGAACTCTTGGGAACTCCACC--TGACGACGT--T--ATCCACACGATTTG--C
```

```
HOG1       CG--AAAAT-----------------------------------------------AC--
sty1       AGTAAAAAC-----------------------------------------------ACAC
LSMAPK     AGCGAGAACGTGAGTCTATTTTTAATCCTTTAGTGCAATATTTTGACGACATGTAGACA-

HOG1       T---CTAAAATTTGTT--ACTTCG-TTACCACACA--GAGATCC----AA-TTCCATTTT
sty1       TTCGC-----TTTGTTCAA--TCA-TTGCCTCAAAAGGAGA-------AAGTTCC-TTTT
LSMAPK     TT-GC---GATTTGTGAAA--TCGCTT--C-CAAA--GAGA--CAGAGAA-TACCACTCT

HOG1       -CTGAAAGATTTAAAA-CAGTCGAACCT--GATGCCGTA--GACCTTTTGGAAAAAATGC
sty1       GCTGAAAAGTTCAAAAAC-GCCGATCCA--GATGC--TATTGATCTGTTAGAAAAAATGC
LSMAPK     -CCCAAAAATTTAGAGGC-GCCGATCCTCTG--GCA--ATCGACCTACTAGAAAAGATGC

HOG1       TGGTTTTTGATCCTAAG-AAGAGAATCACTGCGGCGGATGC-CTTG-GCTC----AT--C
sty1       TTGTCTTTGATCCT-CGTAAGCGTATTAGTGCTGCTGATGC-TTTG-GCTC----ATAAC
LSMAPK     TAGTATTTGACCCG-CGCAAGAGGATTACTGCTGCAGAGGCGCTTGCGCACGAGTAT--C

HOG1       ---CTTATTCGGCTCCTTACCACGATCCAACGGATGAACCAGTAGCCGATGCCAAGTTC-
sty1       TATCTT-----GCTCCATACCATGATCCTACTGATGAGCCTGTTGCTGATG--AAGTTTT
LSMAPK     TA---------GCGCCATATCACGATCCGTCTGATGAACCTGTTGCAGAGGAGAAGTTT-

HOG1       -GATTGG-CACTTTAA--TGACGCTGATCTGC-----CTGTCGATACCTGGC-GTGTTAT
sty1       TGACTGGTCATTCCAAGATAA---TGATTTAC-----CTGTGGAGACTTGGAAG-GTCAT
LSMAPK     -GATTGGTCA-TTCAA--------TGGTATACAAATGCTAT-------T------GTTAT

HOG1       -GATGTACTCAGAAATCCTAGACTTC------CATAAGATTG-GTGGCAGTGATGGACAG
sty1       -GATGTAC----------------TC------C----GA--G-GT--------T------
LSMAPK     GGATG--C-CAG---T----GATTTCAGTTTGC-TA--ATTGAGT-GC-----T----AG

HOG1       AT--TGATATATCTGCCACGTTTGATGACCAAGTTGCTGCAGCCACCGCTGCCGCGGCGC
sty1       -T--TG-------T----CGTTT-------------------------------------
LSMAPK     ATGCTG----ATCTTCCA-GTT----GA-----TT------------------------

HOG1       AGGCACAGGCTCAGGCTCAGGCTCAAGTTCAGTTAAACATGGCTGCGCATTCGCATAATG
sty1       ---CAC-----------------------------AACATGG------------ATAATG
LSMAPK     -----C---CT--------GG--------------AA---GG-TG---------ATGATG
```

```
HOG1        GCGCTGGCACTA--CTGGAAAT----GAT---CACTCAGATATAGCTGGTGGAAACAAAG
sty1        --------A--A--CTG---------------CAATC--------CT-----AA------
LSMAPK      ----------TATTCCG-AGATATTAGATTTCCA--CA-ATATAGATGGCGGA-------


HOG1        TCAGCGATCATGTAGCTGCAAATGACACCATTACGGACTACGGTAACCAGGCCATACAGT
sty1        ------------------------------------------------------------
LSMAPK      -----------GTAGTT-----T--CAC-----CGGA--A---TAA--------------


HOG1        ACGCTAATGAGTTCCAACAGTAA
sty1        -----------------------
LSMAPK      -----------------------
```

## A9. Alignment of promoter region of MAPK genomic DNA sequences from *S. cerevisiae* (HOG1) and *L. starkeyi* (LSMAPK)

Promoter regions

```
HOG1      ----GGACCCATTCCGATTTTCCCATTTGGTTCTTGCGCGTGCTGATTCCGACACGCGCG
MAPK      AAGGAGAGCAGTTCCAAGT-------CTAGTAGCTCGACCTTGTGGTTCCCACTCGCAAG
               ** *  **** * *        * **   *   * *  ** **** ** ***  *

HOG1      TCTATAAATAGCATGAAGTATCCGCACACCGCAGCGTTAGTGAGGT---------GAGGG
MAPK      ACTATCACCAGGAGGATTGTTTCCACCTACGCCTCGTGCTTGAATGACATGAAGAGTCGA
           **** *  ** * **    * *   *  ***  ***   ***           *  *

HOG1      TGGCAGCAAGCTAATTCCCGCAT-----------CTGGAATCTGAAC-------------
MAPK      TTGCACGCACTTGATTCCAAGGTCAGCTTGACGTATGACGTGTGGACTTCGAAAACGAAT
          * ***   *  * *****    *            **   * ** **

HOG1      T------GCCCCTTTTGGACTAACCGTGTGGTTCATGGGTGGGCGAAGTGCGCAACCTCG
MAPK      TTACCTTACGCCAGCGTTACGGTCCATTATGTGGACGCCGATTGGAAGTGTAAAAGGCCA
          *       * **      **   ** *   **  * *       ******   **   *

HOG1      AAGGTTTTCTTTTGCGTGTCGGATTTTACATCCGGCGGTAGCGCATGATGCCATGGCTGG
MAPK      CCTGCATTCTTTCACGT-----ATTTTCCGTATCCGCACACTGCCCAGTGCCATCAGGAC
             *  ******  ***     ***** * *        *  **    ******

HOG1      CTCCAGATACATCCTCAGGGCACCAGCATCTATAATTAGATTGGCGCAACATGGCTGGCT
MAPK      CTTGGGATTT-TGCTCGGGGGTCGACTTCTTAG-----------GGTTCCAAGTGCAAGT
          **   ***   * *** ***  * *     **            *   ** *      *

HOG1      GCACTGCTGTCTTCACTTCTTTCTTTTTCCGGCAATGAATGATGTA--TGTTTTGTGGCA
MAPK      GAATTCGAGTTTTCCCATCGCTAGTCACCGACCCGGGAAAACCGTCATTCAGTTGCGGCC
          * * *   ** *** * **  *  *   *   *   ***    **   *   *** ***

HOG1      AAAGGGTCCGCATTGTACCTGTTTACAGTTGAGATTATCGTTTTTGGTAGCCCTTCATTA
MAPK      AT----------------------ACCAAGAAGAAAACACAGTT--------CCCCGTCC
          *                       **     ***  *     **        *  * *

HOG1      CGGCATAACGTATTAAGTTTCTTTTATTTTGCTTTGCCCTGGTTTAAAAGACAATG-TCG
MAPK      GATCAACACCAGTTAAGCTTCTTTGGGCCTACTTAGTACTGCGGTGGGAGACCACGCTGG
             **  **   ***** ******     * *** *  ***   *   **** * * * *

HOG1      A-------------------------------------TTAAAAGTTAATTTTAATC
MAPK      AATCGTAGGTGCTGCAATTCCTTTTTTTGAAATTCCTACAATTTGATCTTCATGACATAA
          *                                     **  *  ** **   *
```

```
HOG1      GATTGAAGGAAATAAGAGGAATAGCGCAAGTTGTTAGGAAAGCGTTCTTTATCTCCAAGA
MAPK      TATTGGCGGATGGGCCTGTAAAGTGGCAAACTGA----------------AACCGACAGG
           ****  ***       * **    ****  **                 * *    **

HOG1      CTTTGCCCTGTATATAATTA----AACACCTCAAAGCGCTTCGTCATGGATGGAGATTA-
MAPK      ACTTTCCTTGTGAATGTGACGCTAAGCTAAGACTCGGGATTCCAAATTGCAAGAGTAACT
            ** ** ***  **         * *        * * ***   ** *   ***

HOG1      ---TTCGGCATTTTGACATACAGGAGTGCCACATGCGAAAGCGGAGTGGGCGTATTCTCT
MAPK      TTTGTTACAATCGAAACCAGTGGAAATTCCAAGTTGTTCGGACAAGGTAAACTACTGAAT
              *    **    **     * * * ***  *      *   **      ** *   *

HOG1      GGTTACCCTACATGGTCTGGCGGCGTTATTATACGGGAGGATCTTCGAAGGGAAGGAAGG
MAPK      GAT--------ATGTGTTGCCGGTCTGCGGCTCGCG----------GAGGAGAGAGAAAA
          * *        ***   ** ***  *     *   *          ** * **  ***

HOG1      AAAAAAAAAAAGAAAAGGCCAACGAAAAGCAAA-TATTATCTATCGTCGAAATTATCATA
MAPK      GTTTAGCGAAAGTTAAGGCTACGTCATGGAGCAGCCGGCTTGGAGGTCGGACCGATGCAG
              *   ****  ***** *    *  *   *      *     **** *   **

HOG1      CTATCTTACAATAAGAGTAGTA-ATTACTTTCTTGTTTGTATAGTGGAAGAGGAATTTGC
MAPK      CTAGCGCA----ACTCTTCTTTATCGAGCTTCTGGCTGCCATCACTGTCTGCAACGTACC
          *** *  *    *    *  *     *  **** * *   **    *      *  *  *

HOG1      GATAATAATAGCAAAAGTAACTAATCTCTAACAAGAAACCT--------TATTTATTTTC
MAPK      GC------TCACAAGCGAATATAATCCCCACCCATCCATCTCCACACGCTTCTACGGCTC
          *       *  ***  * *  ***** * * * *   * **        *  *     **

HOG1      TCTTTCTTCTATATTGGTAAATACTAGACTCGAAAAAAAGGAACAAAGGGAAAACAGGGA
MAPK      GCTCTGTCCCATCCATCAACACAGTATCTGT-----CTGCTCAGCAACCGTCGTCAGTGC
           ** * * * **      * * * **               *  **  *    *** *

HOG1      AAACTACAACTATCGTATATAATA
MAPK      TATTTAGTGATCTGCTAACACCA-
           *  **    * *  **
```

## A10. Genomic DNA sequence of *L. starkeyi* MAPK with six introns identified in yellow.

Genomic DNA sequence of *L. starekyi* MAPK with introns (1392bp).

ATGGCCGATTTCATCAGGTATGTGCGTGCGGTTATCTTCGGATGCATCAGTGCTGACCATTGTCAGAA
CCCAGATCTTCGGCACCTCCTTCGAGATCACCAGCAGGTACAACTTTTACATCTTTTTCCGCAATTGA
GATCGCCTACTGACAGTAGTCGCTTAGATATGCCGATCTGAACCCGGTTGGAATGGGTGCGTTCGGTT
TGGTGTGGTATGTGACGGACGCCTGCATAATACTTAGCTGTCAAGTTGTTTATTCATCTGACATCTAT
CCAGCTCCGCTCGAGATCAGCTTACCGGACAGGCAGTCGCTATTAAAAAGATCATGAAGCCGTTTAGC
ACACCAGTTTTGTCTAAGCGAACATATAGAGAGCTGAAGTTGTTAAAGCATCTTCGTCACGAGAACGT
GATTTCCCTGAGCGACATCTTTATTTCTCCGCTCGAAGATATCTACTTTGTCACGGAATTGCTAGGCA
CAGACCTTCATCGATTGCTCACCTCGCGACCACTTGAAAAGCAGTTTATACAATATTTCTTGTACCAG
ATATTGCGTGGTTTGAAATATGTTCATTCAGCTGGCGTTATTCATCGTGACTTAAAGCCGAGCAATAT
CCTTGTGAACGAGAATTGTGATTTGAAGGTATTCCTCCTCGAGTTCCAAGACTTCTGAACATTTGCTG
ATGGATTTCGACAAATTAGATTTGCGACTTTGGCTTGGCTCGTATTCAGGATCCGCAAATGACGGGAT
ATGTCTCCACGCGATATTATCGGGCACCAGAGATCATGCTTACGTGGCAAAAGTACGACGTCGAGGTT
GACATATGGAGTGCAGGATGTATCTTTGCTGAAATGTTGGACGGAAAGCCATTGTTTCCAGGAAAGGA
CCATGTGAATCAGTTTTCGATTATCACTGAACTCTTGGGAACTCCACCTGACGACGTTATCCACACGA
TTTGCAGCGAGAACGTGAGTCTATTTTTAATCCTTTAGTGCAATATTTTGACGACATGTAGACATTGC
GATTTGTGAAATCGCTTCCAAAGAGACAGAGAATACCACTCTCCCAAAAATTTAGAGGCGCCGATCCT
CTGGCAATCGACCTACTAGAAAAGATGCTAGTATTTGACCCGCGCAAGAGGATTACTGCTGCAGAGGC
GCTTGCGCACGAGTATCTAGCGCCATATCACGATCCGTCTGATGAACCTGTTGCAGAGGAGAAGTTTG
ATTGGTCATTCAATGGTATACAAATGCTATTGTTATGGATGCCAGTGATTTCAGTTTGCTAATTGAGT
GCTAGATGCTGATCTTCCAGTTGATTCCTGGAAGGTGATGATGTATTCCGAGATATTAGATTTCCACA
ATATAGATGGCGGAGTAGTTTCACCGGAATAA

Intron 1 – 49bp (+18 to +66)

Intron 2 – 58bp (+106 to +163)

Intron 3 – 65bp (+212 to +276)

Intron 4 – 59bp (+641 to +699)

Intron 5 – 47bp (+967 to +1013)

Intron 6 – 58bp (+1240 to +1297)

## A11. cDNA sequence of *L. starkeyi* MAPK

cDNA sequence of *L. starkeyi* MAPK (1056bp).

ATGGCCGATTTCATCAGAACCCAGATCTTCGGCACCTCCTTCGAGATCACCAGCAGATATGCCGATCT
GAACCCGGTTGGAATGGGTGCGTTCGGTTTGGTGTGCTCCGCTCGAGATCAGCTTACCGGACAGGCAG
TCGCTATTAAAAAGATCATGAAGCCGTTTAGCACACCAGTTTTGTCTAAGCGAACATATAGAGAGCTG
AAGTTGTTAAAGCATCTTCGTCACGAGAACGTGATTTCCCTGAGCGACATCTTTATTTCTCCGCTCGA
AGATATCTACTTTGTCACGGAATTGCTAGGCACAGACCTTCATCGATTGCTCACCTCGCGACCACTTG
AAAAGCAGTTTATACAATATTTCTTGTACCAGATATTGCGTGGTTTGAAATATGTTCATTCAGCTGGC
GTTATTCATCGTGACTTAAAGCCGAGCAATATCCTTGTGAACGAGAATTGTGATTTGAAGATTTGCGA
CTTTGGCTTGGCTCGTATTCAGGATCCGCAAATGACGGGATATGTCTCCACGCGATATTATCGGGCAC
CAGAGATCATGCTTACGTGGCAAAAGTACGACGTCGAGGTTGACATATGGAGTGCAGGATGTATCTTT
GCTGAAATGTTGGACGGAAAGCCATTGTTTCCAGGAAAGGACCATGTGAATCAGTTTTCGATTATCAC
TGAACTCTTGGGAACTCCACCTGACGACGTTATCCACACGATTTGCAGCGAGAACACATTGCGATTTG
TGAAATCGCTTCCAAAGAGACAGAGAATACCACTCTCCCAAAAATTTAGAGGCGCCGATCCTCTGGCA
ATCGACCTACTAGAAAAGATGCTAGTATTTGACCCGCGCAAGAGGATTACTGCTGCAGAGGCGCTTGC
GCACGAGTATCTAGCGCCATATCACGATCCGTCTGATGAACCTGTTGCAGAGGAGAAGTTTGATTGGT
CATTCAATGATGCTGATCTTCCAGTTGATTCCTGGAAGGTGATGATGTATTCCGAGATATTAGATTTC
CACAATATAGATGGCGGAGTAGTTTCACCGGAATAA